AN INVESTIGATION OF LANDING GEAR - SOFT SOIL INTERACTION UTILIZING THE OV-10A AIRCRAFT

FINAL TECHNICAL REPORT

JANUARY 1971

PREPARED UNDER CONTRACT N00019-69-C-0063
FOR NAVAL AIR SYSTEMS COMMAND
DEPARTMENT OF THE NAVY

COLUMBUS DIVISION OF
NORTH AMERICAN ROCKWELL CORPORATION
COLUMBUS, OHIO

Best
Available
Copy

File No.______

Report No. NR70H-570

North American Aviation/Columbus
North American Rockwell

AN INVESTIGATION OF LANDING GEAR -

SOFT SOIL INTERACTION UTILIZING

THE OV-10A AIRCRAFT

CONTRACT N00019-69-C-0063

PREPARED BY C. E. Cook
C.E. Cook, MTS
Vehicle Analysis - Loads

J. D. Gargiulo
J. D. Gargiulo, MTS
Vehicle Analysis - Loads

APPROVED BY R. R. Deakins
R. R. Deakins, MTS
Vehicle Analysis - Loads

O. G. Acker
O. G. Acker, Manager
Vehicle Design, Aircraft R&E

L. E. Kazmerzak
L. E. Kazmerzak, Manager
Vehicle Analysis

No. of Pages______

Date 15 January 1971

REVISIONS

DATE	REV. BY	PAGES AFFECTED	REMARKS

FORM 354-K REV 7-69

ABSTRACT

This report is presented in compliance with the requirements of Department of the Navy, Air Systems Command Contract N00019-69-C-0063. The results of an investigation of the interaction between landing gear and soft soil are presented. During early May of 1969, OV-10A (BuNo. 155392) was used to perform sixteen landings and takeoffs on soft unprepared terrain at Blackstone Army Air Base, Virginia. Two fifty channel oscillographs were used to measure time histories of the airplane response. Measurements were also taken of the terrain contour and static and dynamic strengths of the soil. Landings were successfully performed with soil penetrometer (static strength) readings as low as 40 for sink speeds as great as 16 feet per second. The experimental data is presented.

Equations of motion are presented for a mathematical model of the OV-10A landing and taking off from yieldable uneven terrain. This model simulates the soil-tire interactions, landing gear-airplane interactions, and the airplane dynamic response. A system of 20 non-linear, coupled second order differential equations results. Analytical determination of landing gear loads for correlation with experimental data was included in the work to be performed under this contract. However, this task could not be accomplished within the allocated funds.

Conclusions and recommendations are presented.

TABLE OF CONTENTS

Table of Contents (continued)

REFERENCES

UNCLASSIFIED
Security Classification

DOCUMENT CONTROL DATA - R & D

(Security classification of title, body of abstract and indexing annotation must be entered when the overall report is classified)

1. ORIGINATING ACTIVITY (Corporate author) Columbus Division, North American Rockwell Corporation 4300 East Fifth Avenue Columbus, Ohio 43216	2a. REPORT SECURITY CLASSIFICATION UNCLASSIFIED 2b. GROUP

3. REPORT TITLE

AN INVESTIGATION OF LANDING GEAR - SOFT SOIL INTERACTION UTILIZING THE OV-10A AIRCRAFT

4. DESCRIPTIVE NOTES (Type of report and inclusive dates)

Final Technical Report (November 1968 through January 1970)

5. AUTHOR(S) (First name, middle initial, last name)

Charles E. Cook; Joseph D. Gargiulo

6. REPORT DATE	7a. TOTAL NO. OF PAGES	7b. NO. OF REFS
15 January 1971	361	4

8a. CONTRACT OR GRANT NO. N00019-69-C-0063	9a. ORIGINATOR'S REPORT NUMBER(S) NR70H-570
b. PROJECT NO. APPROVED FOR PUBLIC RELEASE; DISTRIBUTION UNLIMITED	
c.	9b. OTHER REPORT NO(S) (Any other numbers that may be assigned this report)
d.	

10. DISTRIBUTION STATEMENT

~~THIS DOCUMENT IS SUBJECT TO SPECIAL EXPORT CONTROLS AND EACH TRANSMITTAL TO FOREIGN GOVERNMENTS OR FOREIGN NATIONALS MAY BE MADE ONLY WITH PRIOR APPROVAL OF NAVAL AIR SYSTEMS COMMAND, CODE AIR-50021.~~

11. SUPPLEMENTARY NOTES	12. SPONSORING MILITARY ACTIVITY NAVAL AIR SYSTEMS COMMAND DEPARTMENT OF THE NAVY WASHINGTON, D.C.

13. ABSTRACT

The results of an investigation of the interaction between landing gear and soft soil are presented. During early May of 1969, OV-10A (BuNo. 155392) was used to perform sixteen landings and takeoffs on soft unprepared terrain at Blackstone Army Air Base, Virginia. Two fifty channel oscillographs were used to measure time histories of the airplane response. Measurements were also taken of the terrain contour and static and dynamic strengths of the soil. Landings were successfully performed with soil penetrometer (static strength) readings as low as 40 for sink speeds as great as 16 feet per second. The experimental data is presented.

Equations of motion are presented for a mathematical model of the OV-10A landing and taking off from yieldable uneven terrain. This model simulates the soil-tire interactions, landing gear-airplane interactions, and the airplane dynamic response. A system of 20 non-linear, coupled second order differential equations results. Analytical determination of landing gear loads for correlation with experimental data was included in the work to be performed under this contract. However, this task could not be accomplished within the allocated funds.

Conclusions and recommendations are presented.

DD FORM 1 NOV 65 1473 (PAGE 1)

S/N 0101-807-6801

UNCLASSIFIED
Security Classification

14 KEY WORDS	LINK A		LINK B		LINK C	
	ROLE	WT	ROLE	WT	ROLE	WT
LANDING GEAR-SOFT SOIL INTERACTION						
OV-10A						
LANDING GEAR						
AIRCRAFT EQUIPMENT						
SOFT LANDING						
SOIL STRUCTURE						
EQUATIONS OF MOTION						
COMPUTER SYSTEMS PROGRAMS						
FLIGHT TESTING						

1.0 REFERENCES

(1) Soil Value System as Determined with a Precision Bevameter, University of Michigan, Dept. of Mechanical Engineering Report 03026-2-P, Prepared Under Contract DA-20-018-ORD-14620, October 1961, Richard Leis, (AD 420208).

(2) Aircraft Dynamic Loads From Substandard Landing Sites, Phase 1 Interim Technical Report, Prepared Under Contract AF33(615)-2563, by The Boeing Company, Renton, Washington, November 1965.

(3) Normal Stresses at the Tire-Soil Interface in Yielding Soils, Misc. Paper Nc. 4-629, U. S. Army WES, C. of E., Vicksburg, Mississippi, February 1964.

(4) NA67H-839, Statement of Work For Investigation of Aircraft Landing Characteristics On Unprepared Terrain, 25 September 1967.

INTRODUCTION

2.0 INTRODUCTION

One of the major facets in aircraft design which has been receiving increased attention recently is the military need to operate from unprepared terrain. Two basic problems have resulted from this need. First is the definition of adequate design criteria that will satisfy the above military need but will not impose excessive penalties on other operational necessities. Second is the capability on the part of the aircraft industry to satisfy such criteria in a rational manner rather than rely on a trial and error approach.

Since there is a serious lack of past experience on which to base future criteria and methods to satisfy such criteria, it was decided to utilize the OV-10A to obtain accurate and detailed data while operating from unprepared terrain. This decision was based on the knowledge that the OV-10A was designed and demonstrated to operate from terrain that included rigid 4 inch high and 10 inch long (1-cosine) bumps and 3 inch steps. Such design and test requirements provided the OV-10A with strength to obtain data on unprepared terrain at military operational levels of sink speed. In addition, OV-10A BuNo. 155392, was fully instrumented to perform a complete formal Landing and Take-off Demonstration under the basic OV-10A contract. Thus, approximately a hundred parameters were available to help develop a computer program to describe the response of an airplane during such operation.

The schedule of work to be performed under Department of the Navy, Air Systems Command Contract No. N00019-69-C-0063 was as follows:

(1) Develop a computer program for analytically simulating the applied ground loads and airplane response for take-off and landing operations from soft-soil rough-terrain sites. Include in this program the interactions between the transient motions of the airplane, landing gears, and soil for differing rough terrain contours and bearing strength of soils as well as airplane and landing gear rigid and flexible body degrees of freedom, including symmetric and anti-symmetric modes of vibration.

(2) Perform laboratory tests to determine load-deflection characteristics of the tires and load-footprint area of the tires.

(3) Perform tests to determine the impulse loading characteristics of soil samples from the selected landing sites.

(4) Perform two (2) take-off tests and ten (10) landing impact and roll-out tests with airplane model OV-10A, Bureau Number 155392, at Blackstone Army Air Base and at the following conditions:

Condition No.	Sink Speed (V -- FPS)	Horizontal Speed (V --- KNOTS)	Pitch Attitude
1	10	75-80	Tail Down
2	12	75-80	Tail Down
3	14	75-80	Tail Down
4	16	75-80	Tail Down
5	14	90-95	Tail Down
6	10	75-80	Nose Down
7	12	75-80	Nose Down
8	14	75-80	Nose Down
9	16	75-80	Nose Down
10	14	90-95	Nose Down

Also, make each landing touchdown and roll-out on a different portion of the test site, to preclude surface compacting, and make the two take-offs over the same general areas as the landing test area.

(5) Provide instrumentation for measuring time-histories of tire pressures as well as maintain the instrumentation required for the Contractor's Rough Terrain Demonstration required under Contract NOw 65-0118-f. A complete list of instrumentation is given in Paragraph 4.1.2.

(6) Determine analytically, airplane and landing-gear loads and responses for the required take-off runs and landing impact and roll-out runs from computer analyses utilizing Government furnished data on profiles and soil characteristics for each take-off and landing test.

(7) Record and read out time histories and peak values of airplane and landing gear applied loads and responses and determine the correlation between such experimental data and the analytical data. In addition, determine the correlation between the static measured and predicted terrain deflections.

Development of the computer program for analytically simulating the airplane response and loads requires a complexity greater than planned. Therefore, scheduled item (1) was not completed and item (6) was not initiated due to insufficient allocated funds. In addition, on the final landing under this contract, a failure of the nose gear occurred. Since uncommitted funds were required to return the test aircraft to flight status, additional funds were not available to complete the contract at this time. The items completed and reported herein, however, provide a basis for continuation of the program.

SOIL STUDY

3.0 SOIL STUDY

3.1 General

The objective of the following analysis is to develop a method of determining the response of an aircraft landing gear tire operating on soft unprepared terrain. The analysis of the interaction of a pneumatic tire and deformable soil may be separated into two parts. The first part presents the development of a soil model while the second part presents the mathematical model of a pneumatic tire on deformable soil.

The analytical representation of soil is presented in Paragraph 3.3. This soil model is developed by assuming that the static and dynamic strength properties of soil may be mathematically represented by a second order differential equation with variable stiffness and damping coefficients. These coefficients are determined from experimental data obtained from a penetrometer and a specially constructed cylinder drop test vehicle.

The analytical representation of a pneumatic tire on soft soil is presented in Paragraph 3.4. A method of determining the drag and vertical forces action on the tire is presented. The primary input to the analysis is the soil model representation.

Section 5.0 includes comments pertaining to the quality and range of application of the combined tire-soil analysis.

3.2 Nomenclature

List of Symbols

z	=	Sinkage depth
$\dot{z}$	=	Sinkage velocity
$\ddot{z}$	=	Sinkage acceleration
$\dot{z}_{im}$	=	Velocity of the wheel, probe, or tire at the time of soil contact
T	=	Vertical driving force
m_c	=	Mass of cylinder
m_T	=	Mass of tire
m_w	=	Mass of wheel
m_{TS}	=	Effective mass of tire-soil interface
$C(z,\dot{z},\dot{z}_{im})$	=	Soil dynamic damping coefficient as a function of sinkage depth, velocity, and soil impact velocity
$K(z)$	=	Static soil stiffness coefficient as a function of sinkage depth
$P_S(z)$	=	Static soil pressure as a function of sinkage depth
b	=	Tire width
i	=	Plate number
X_i	=	Length of plate i
t_p	=	Plate thickness
n	=	Number of cylinder plates of thickness t_p
r_m	=	Plate thickness parameter $(0 < r_m < 1)$
n_T	=	Number of tire plates of thickness t_p
Y_i	=	Tire-plate coordinate perpendicular to z axis

List of Symbols (cont.)

z_i = Plate depth below soil surface

l = Tire length dimension associated with soft soil

A_N = Tire segment area associated with rigid uneven terrain

r_T = Undeflected tire radius

δ_T = Tire deflection

X_{AD}, Z_{AD} = Coordinates of axil in deck system

$Z_{G(x)}$ = Terrain profile

$X_{(1)}, X_{(2)}$ = Intersection points of surface and tire

l_t = Total footprint length of tire

V = Tire velocity parallel to X-axis (horizontal velocity)

$\dot{\xi}$ = Tire-soil effective deformation rate

$C(z, \dot{z}, \dot{\xi})$ = Soil dynamic damping coefficient as a function of sinkage depth, velocity, and tire-soil effective deformation rate

μ = Tire drag coefficient

ρ_s = Soil density

C_{DI} = Soil inertia drag coefficient

T_R = Tire force resulting from rigid uneven terrain

T_{FX} = Conventional tire drag force associated with tire skidding, rolling, and carcass effects.

T_{SZ} = Vertical tire force resulting from the depth dependent static soil pressure acting on tire surface B

T_{RTX} = Tire drag force generated by soft soil rutting

List of Symbols (cont.)

T_{Ix} = Tire inertial resistance generated by the rut frontal area

T_{Dx} = Vertical tire force resulting from the dynamic soil strength

3.3 Analytical Soil Model

The primary assumption for the mathematical soil model is that a soil element has properties of stiffness and dynamic damping. Further, it is assumed that the soil response may be expressed as a second order differential equation of the form

$$M_c \ddot{Z} + C(z, \dot{z}, \dot{z}_{im}) \dot{Z} + K(z) Z = T \tag{3-1}$$

where $\dot{z}_{IM}$ represents the velocity of the wheel, probe, or tire at the time of soil contact.

The specific problem in formulating the soil model is determination of the stiffness and damping coefficients. Once the coefficients are determined, Equation (3-1) can be used to calculate the penetration depth of a landing gear tire in soft terrain. The driving force, T, will then represent the vertical tire load and will be the coupling term between the soil-wheel analysis and the aircraft landing gear analysis.

Preliminary studies indicated that controlled tests on the specific soil of interest could be used to determine the stiffness and damping coefficients. Specifically, an Airfield Soil Penetrometer could be used to supply data for the soil stiffness coefficient evaluation. Also, drop tests of a rigid wheel onto the soil could be used to supply data for evaluation of the soil damping coefficients.

3.3.1 Experimental Data

Experimental tests were conducted at Blackstone Army Air Base, Blackstone, Virginia. The soil type will be referred to herein as "Virginia Clay". The basic data used for the soil analysis and descriptions of the soil testing apparatus are presented in Appendix A1.

Additional data required for correlation purposes between predicted and experimental load values were obtained at each of the landing impact areas. This additional data is also presented in Appendix A1.

3.3.2 Stiffness Coefficient Analysis

The static characteristics of soil were examined to evaluate the static strength term, $[K_{(z)}]Z$, of Equation (3-1). It is possible to represent this term as the product of soil pressure integrated over the area of interest:

$$\int_0^A P_{g(z)}\, dA = [K_{(z)}]Z \qquad (3\text{-}2)$$

Where, $P_{g(z)}$ represents the soil pressure as a function of depth, Z .

Soil pressure information was obtainable from the penetrometer tests. The soil penetrometer was constructed to read the pressure required to penetrate the soil with a .5 square inch area cone as shown in the following figure.

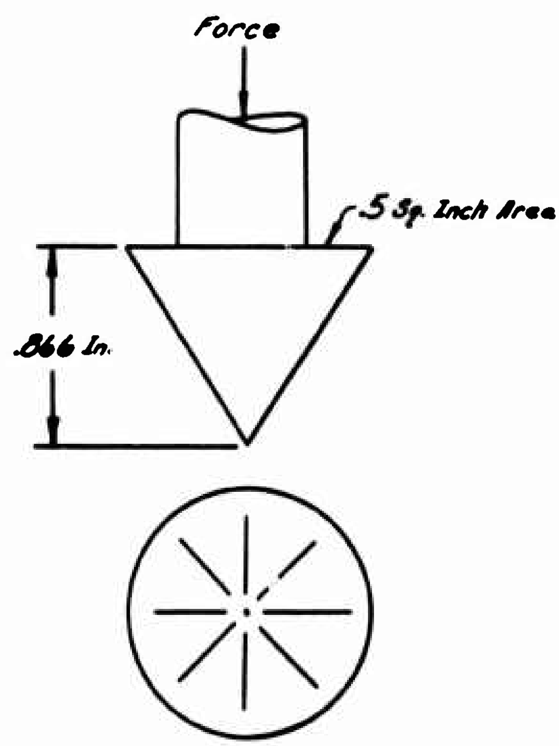

Penetrometer Cone

The penetrometer data was converted to soil pressure data by considering an idealistic method of measuring the soil pressure. The force required to penetrate a flat plate type probe into the soil at a nearly static rate was measured versus depth. This force divided by the area represents the average soil pressure. The relationship between cone penetration data and the nearly static penetration of a flat plate type probe must then be established. This problem may be separated into two basic parts. One part deals with the geometric conversion of cone probe data to flat plate probe data. The second part accounts for an eliminates the dynamic effects associated with the penetrometer data.

3.3.2.1 Geometric Conversion

A report by Richard Leis, Reference (1), is especially helpful in formulating the geometric conversion of cone probe data to flat plate probe data. Briefly, the report is a study of the relationship of pressure-sinkage characteristics between a flat plate and four other, differently shaped probes. The probes are depicted on Page 3-9. The pressure-sinkage data was obtained with a precision bevameter which is a hydraulic device that can offer a controllable constant velocity penetration of the probes. Leis penetrated the flat plate and other four probes into soil and recorded required pressure (defined as required penetration force divided by the flat base area of the particular probe) as a function of sinkage depth. The results of these tests have been reproduced from Reference (1) and are presented on Page 3-10. Leis deduced a relationship between the pressure-sinkage data of the flat plate and the other four probes. The findings may be summarized as follows. Initially, the reference point for the sinkage measurements was the initial soil contact point of each probe. As a result of the test observations, it was noted that by changing the reference point on the four general probes to an intermediate position along the probe, the pressure-sinkage curves would be shifted to match the flat plate data. Specifically, a reference point shift of 1/2 inch for probes 2, 3, and 5 and 1 inch for probe 4 would force the pressure-sinkage curves to be nearly coincident with the flat plate curve. Leis attribues the observed relationship to boundary layer effects: once the boundary layer has developed around a probe, which will occur at a specific depth depending on the probe shape, the reaction of the soil is independent of the probe shape. Thus, it was concluded that oddly shaped probes display physical properties in soil very similar to that of a flat plate probe.

Based upon these observations, it was assumed that by shifting the reference point from the tip of the penetrometer cone, the penetrometer data could be transformed into flat plate soil pressure data. Results and conclusions from Reference (1) were utilized to determine an approximate axis shift for the penetrometer cone. Considering probe bluntness and shape, and the general trends presented in Reference (1), it was concluded that a reference point shift of 75% of the cone length would modify the penetrometer data to represent that of a flat plate probe. The resulting shifted penetrometer data is presented on Page A1-57.

3.3.2.2 Penetrometer Dynamic Effects

Various soil studies such as Reference (2), have presented experimental data that show that soils exhibit an effective increase in penetration resistance as the rate of load application or penetration increases.

Based upon the penetrometer data and preliminary analysis it was determined that the average penetrometer soil penetration velocity was 1.5 inches per second. Erroneously, one might assume that at such a small penetration rate the dynamic stiffness effects of soil would be negligible. However, many studies such as Reference (2) have presented experimental data that indicate increases in soil strength as high as 90% above the static strength for plate sinkage rates as low as 0.6 inches per second. Thus, it may be assumed that the penetrometer data contains dynamic stiffness effects. In order to determine the true soil static strength the dynamic effects must be eliminated from the penetrometer data.

PROBES USED TO DETERMINE
PRESSURE SINKAGE CHARACTERISTICS

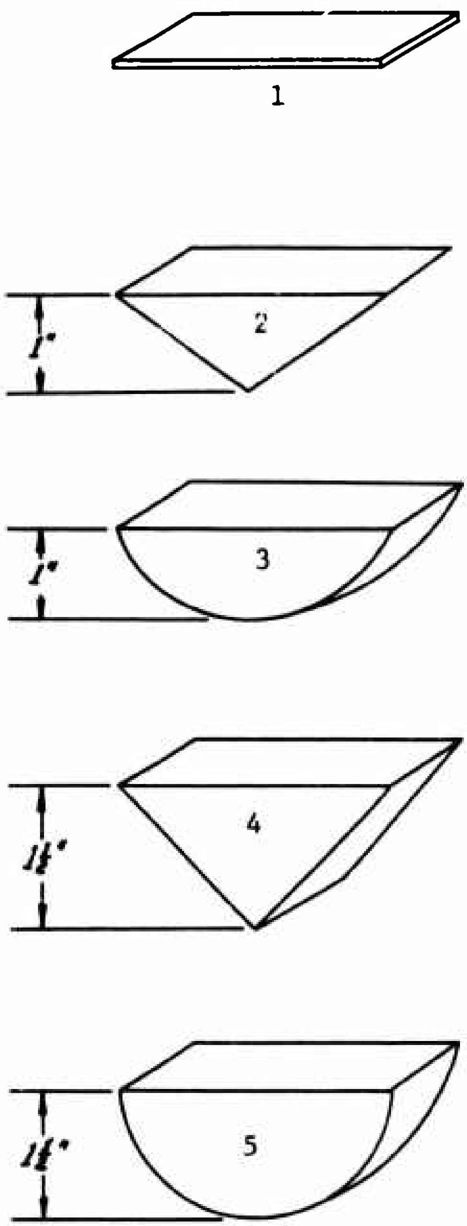

All top surfaces
3" x 1"

PRESSURE VERSUS SINKAGE DEPTH

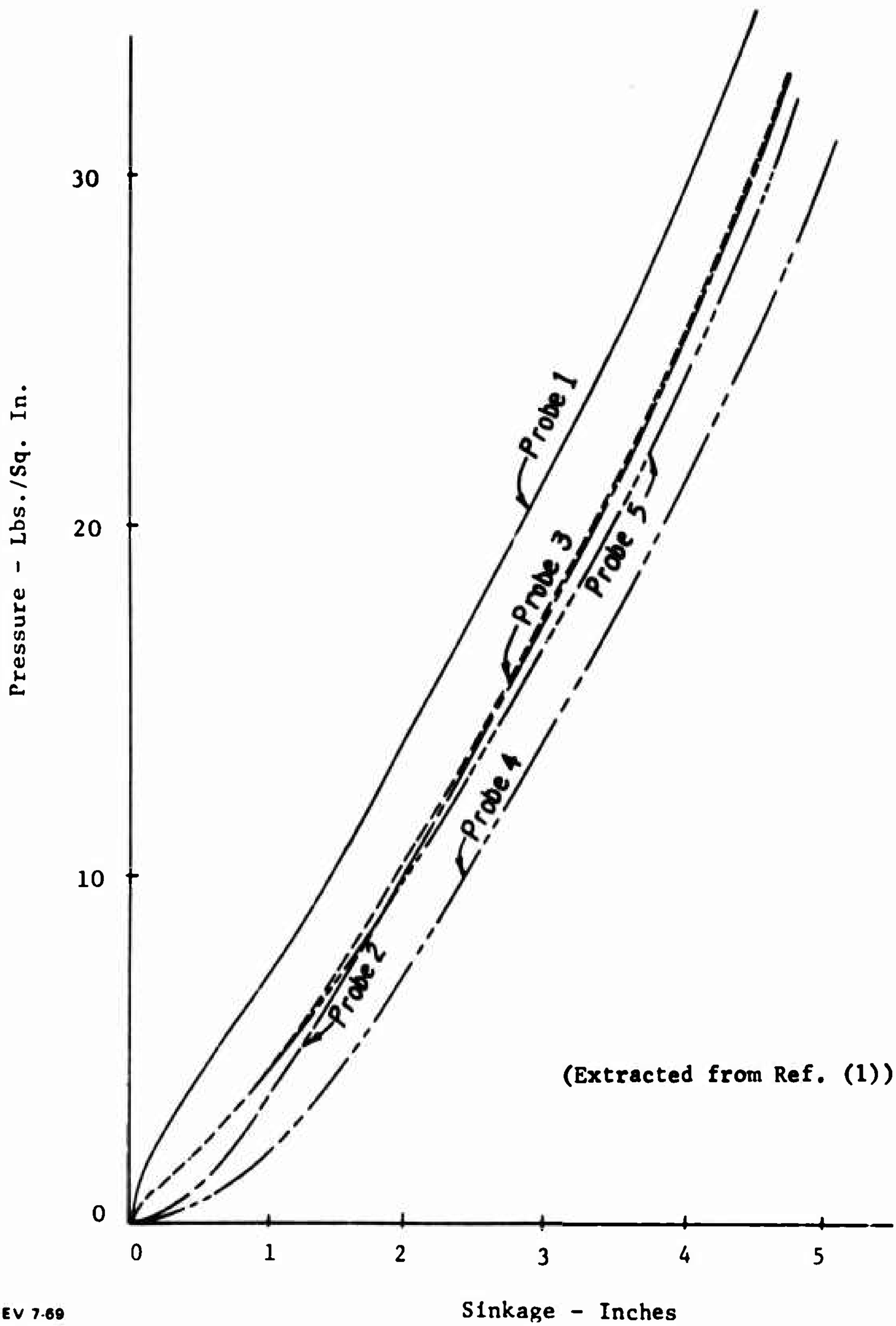

Observations of the OV-10 resting on the "Virginia Clay" indicated that the shifted penetrometer data was not representative of static soil pressure. With a main gear tire footprint area of approximately 165 square inches and vertical load of 4200 pounds, the average pressure exerted on the soil was 25 psi. The tire was observed to sink about 1 inch into the soil. However, by using the shifted penetrometer data, presented on Page A1-57, representing the softest soil (Terrain Hardness A), it can be determined that the tire would sink only 0.1 inches into the soil. Further investigation indicated that the poor correlation between the observed and calculated tire sinkage resulted from the presence of dynamic effects in the penetrometer data.

To extract the dynamic effects from the penetrometer data, it will be necessary to consider additional experimental observations. One available source is in Reference (2). The needed data from Reference (2) is presented on Page 3-13. This data was obtained from several constant rate plate sinkage tests and a very slowly loaded or static test. Though these tests were not conducted on "Virginia Clay," the general results will be used. As stated in Reference (2), it is expected that different soils will display somewhat different characteristics although the general trends from one soil to another should be similar.

By interpolation of the curves on Page 3-13, a curve representing the change in the ratio of dynamic soil pressure to static soil pressure as a function of sinkage depth for a constant probe velocity of 1.5 inches per second was obtained. This curve is presented on Page 3-14 and was used to ratio the previously modified soil pressure curves to account for and eliminate the dynamic stiffness effects. The resulting curves, on Page A1-61, show the soil penetrometer data modified to represent the static soil pressure of "Virginia Clay" hardnesses A, B, C, D, G and I.

3.3.2.3 The static soil pressure curves for various terrain hardnesses, as presented on Page A1-50, were used to evaluate the soil strength term, $[K(z)]z$, by solving the integral of Equation (3-2). These soil depth dependent static soil pressure values, $P_{g}(z)$, were integrated over the area of the probe-soil contact interface. The probe is the 6-inch steel cylinder for which experimental soil sinkage depth, velocity, acceleration, and soil hardness type are known. The data from any particular drop test of the cylinder furnishes the displacement of the wheel as a function of time. The soil-cylinder contract interface area and static soil pressure are both a function of sinkage depth. Hence, sufficient data is available to determine a value of static strength, $[K_{(z)}]Z$, as a function of time. The mathematical nature of the static soil pressure curves and the variable soil-cylinder interface area requires a numerical integration technique which is developed in Appendix A1. The resulting expression for the static strength term is:

$$[K_{(z)}]Z = 2b\left\{\sum_{i=0}^{n}\left[(X_i - X_{i-1})P_{g(z_i)}\right] + (X_{n+r_m} - X_n)P_{g(z_n+r_m)}\right\} \qquad (3\text{-}3)$$

where $P_{g(z_i)}$ and $P_{g(z_n+r_m)}$ are static soil pressure values at soil depths z_i and z_{n+r_m} which are obtained from the static soil pressure curves on Page A1-61.

Values for the stiffness coefficient, $K(z)$, could now be determined. However, it is theorized that the stiffness coefficients are not only a function of penetration depth but also a function of probe geometry. The soil damping coefficients are assumed not to be a function of geometry. Thus, when solving Equation (3-1) for tire motion of soft soil, the static strength term, $[K_{(z)}]Z$, must be re-evaluated to account for the tire geometry. Evaluating the static strength term for the rigid cylinder is only needed as an intermediate step to determine the soil damping coefficients.

3.3.3 Numerical Evaluation of the Damping Coefficient

Damping coefficients were evaluated by using Equation (3-1), the static soil pressure data, and the rigid cylinder drop test data. Equation (3-1) is rewritten as:

$$C_{(z,\dot{z},\dot{z}_{sm})} = \left\{M_c g - [K_{(z)}]Z - M_c \ddot{z}\right\}\left\{1/\dot{z}\right\} \qquad (3\text{-}4)$$

The static strength term $[K_{(z)}]Z$, evaluated as discussed in Section 3.3.2 and $\ddot{z}$ and $\dot{z}$ were obtained from appropriate rigid cylinder drop tests. To obtain sufficient accuracy in the solution of Equation (3-4), it will be necessary to use small values of plate thickness in the numerical integration of the static strength term.

Further, in order to obtain an adequate representation of the damping coefficient curve for each terrain hardness, many time slices must be examined. To facilitate the desired quality of the damping coefficient evaluation, a digital computer program was developed. The output of the program is presented in Appendix A1. Pages A1-83 through A1-88 present the damping coefficient curves as a function of time for each of the six terrain hardness types. The damping coefficient curves were reduced to eliminate time dependence and presented as a function of soil deformation rate on Pages A1-91 through A1-96 .

CONSTANT RATE PLATE-SINKAGE TESTS
BOSTON BLUE CLAY
1.5 IN. DIA. PLATE
(Extracted from Ref. (2))

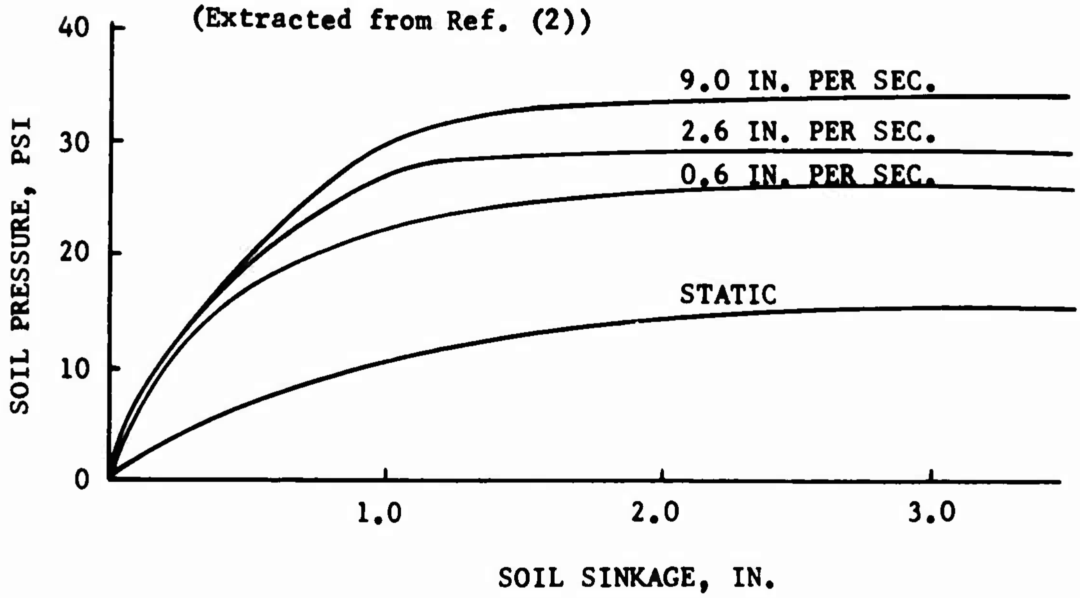

RATIO OF DYNAMIC AND STATIC

SOIL PRESSURE

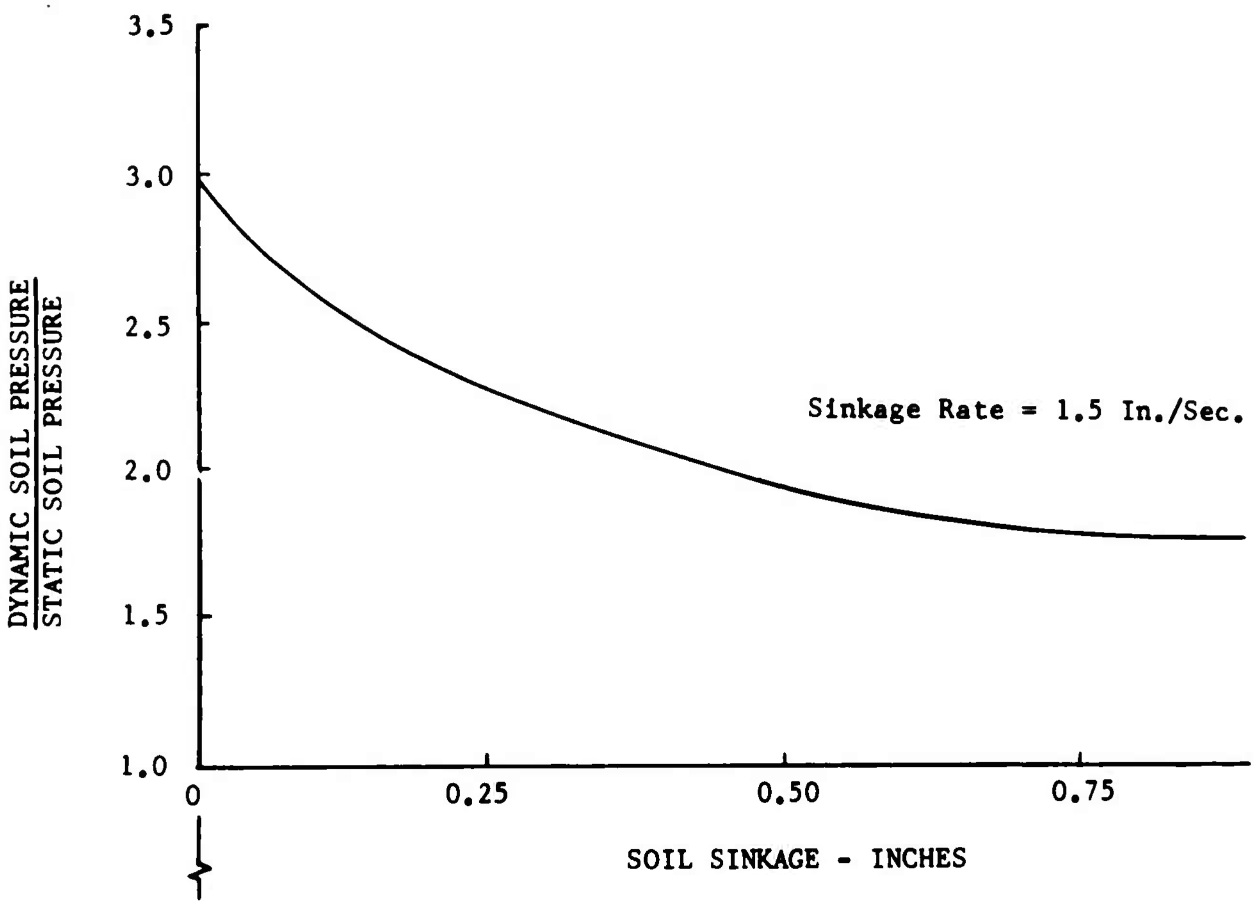

3.4 Analytical Tire-Soil Model

An analytical representation of a pneumatic tire operating on soft, uneven terrain is discussed in this section. An equation of motion representing the vertical degree of freedom of the tire-soil interface and an equation for the total drag force acting on the tire are presented. The vertical and drag forces originate from unevenness of the terrain and the yieldability of the surface. It is assumed that the condition of uneven terrain is independent of soil yieldability.

The general expressions for the vertical equation of motion of the tire-soil interface and the total tire drag force are given as:

$$m_{TS}\ddot{z} = (m_T + m_W)g = T_{Rz} - T_{Sz} - T_{Dz} \qquad (3\text{-}5)$$

$$\text{Total Tire Drag} = T_{Rx} + T_{Fx} + T_{RT_x} + T_{Ix} \qquad (3\text{-}6)$$

Forces, T_{Rx} and T_{Rz}, which are components of the force, T_R, result from the rigid, uneven characteristics of the terrain. Tire force, T_{Fx}, is the conventional drag associated with tire skidding, rolling, and carcass effects. These three tire forces are discussed in Paragraph 3.4.1. Forces T_{Sz}, T_{RT_x}, and T_{Ix} result from the yieldable characteristic of soil and are discussed in Paragraph 3.4.2. Specifically, the vertical force T_{Sz} is due to the depth dependent static soil pressure acting on the tire. T_{RT_x} is the resistance generated by soft soil rutting. T_{Ix} is the inertial resistance generated by the rut frontal area. The vertical force term, T_{Dz}, is discussed in Paragraph 3.4.3. This force represents the dynamic soil strength resulting from the resistance to motion of the soil under the tire. It is a function of the soil dynamic damping coefficients that are discussed in Section 3.3.

Paragraph 3.4.4 presents a brief summary of the soil-tire relationships.

3.4.1 Tire Reactions Resulting From Rigid Uneven Terrain

It is assumed that the tire force due to undeflected terrain is a direct function of the net area between the soil contour and the undeflected tire circumference. This area is shown as the shaded area in the sketch given below. It is also assumed that the force acts at the centroid of this area and is directed through the wheel axle.

The tire force versus area is obtained from the conventional tire force versus deflection curve using A_N versus tire force, T_R, where A_N is

$$A_N = r_T^2 \cos^{-1}\frac{r_T - \delta_T}{r_T} - (r_T - \delta_T)\sqrt{r_T^2 - (r_T - \delta_T)^2} \tag{3-7}$$

Note that the above relation is merely the relation for the area of a segment of a circle.

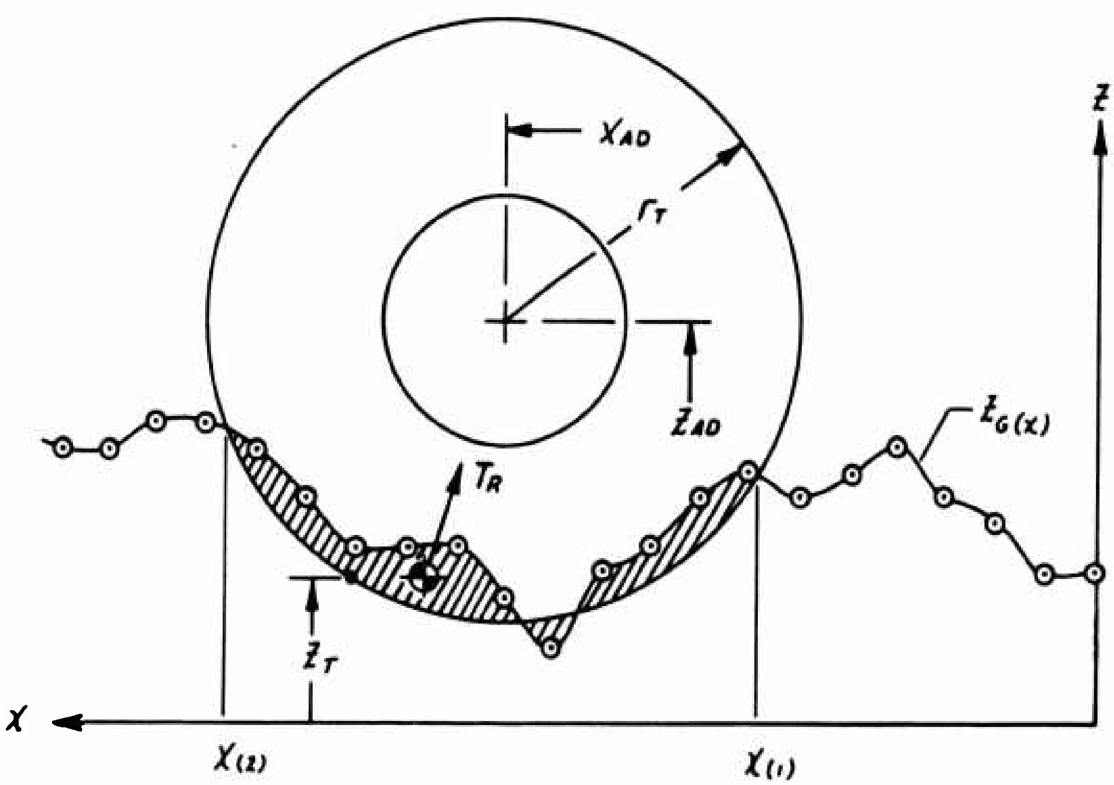

The conventional tire drag, T_{FX} , associated with tire skidding, rolling and tire carcass effects is a function of the vertical component of T_R and the tire drag coefficient, μ . This force is represented by the following relationship:

$$T_{FX} = \mu T_{RZ} \tag{3-8}$$

3.4.2 Tire Reactions Resulting From Smooth Yieldable Terrain

The terrain surface is assumed to be smooth and yieldable with soil properties and characteristics as described in Paragraph 3.3. The tire surface B shown in the sketch below is assumed to be flat.

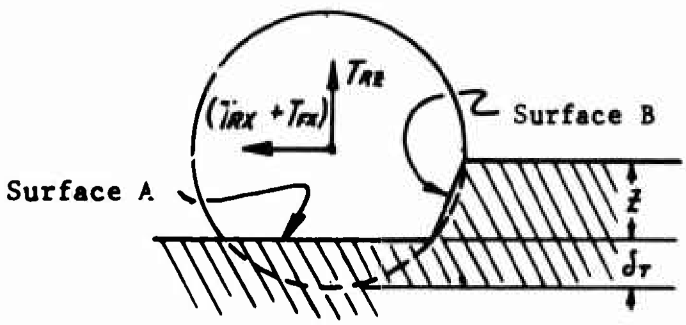

The tire forces associated with surface A are those defined in Paragraph 3.4.1 as T_R and T_{FX} . Three additional tire forces, T_{SZ} , T_{RTX} , and T_{IX} result from the soft terrain.

The vertical force T_{SZ} acts on surface B of the tire and originates from the depth dependent soil pressure. The method of determining this force is similar to the method of obtaining the static force acting on the rigid cylinder as developed in Appendix A1. Consider the following figure of the assumed tire.

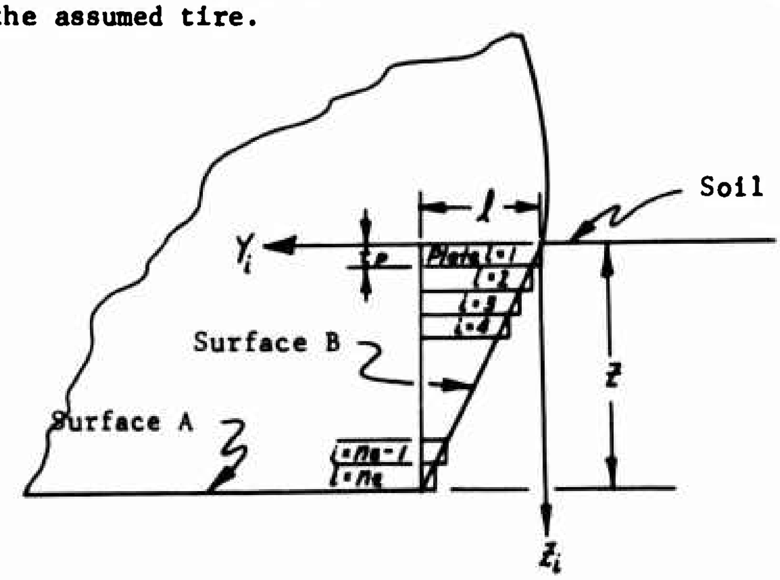

When $\ell \geq Y_i \geq 0$ and $z \geq z_i \geq 0$

Then $z_i = (z/\ell)\, Y_i$

$t_p = z/n_z$

$z_i = i\, t_p \qquad i = 1 \text{ to } n_z$

The vertical force acting on surface B is given by

$$T_{SZ} = \sum_{i=1}^{n_z} \left[(\ell b/n_z)(P_{g(z_i)}) \right] \tag{3-9}$$

The tire force T_{RT_X} is the rolling resistance generated by soft soil rutting. It has been experimentally measured by the U.S. Army Engineer Waterways Experiment Station, Corps of Engineers, Reference (3). The experimental results indicated the following expression for T_{RT_X} :

$$T_{RT_X} = (T_{RZ} + T_{SZ}) \frac{z}{\ell_t} \tag{3-10}$$

Tire force, T_{IX} , represents inertial resistance which is assumed to be proportional to the rut frontal area and the dynamic soil pressure. The following relationship for inertial resistance was developed in Reference (2).

$$T_{IX} = C_{DI} \frac{1}{2} \rho_s V^2 b z \tag{3-11}$$

The soil inertia drag coefficient, C_{DI} , must be determined experimentally since there is at present no theoretical means of determining its value.

3.4.3 Vertical Tire Force Due to Dynamic Soil Strength

Soil resistance to tire sinkage in soft terrain is known to vary with sinkage rate and the initial tire-soil impact velocity. This resistance is known as the dynamic soil strength, :

$$T_{DZ} = [C_{(z,\dot{z},\dot{\xi})}]\, \dot{z} \tag{3-12}$$

The coefficient, $C_{(z,\dot{z},\dot{\xi})}$, is the soil dynamic damping coefficient for the tire-soil interface. It is obtainable from the soil dynamic damping coefficients, $C_{(z,\dot{z},\dot{z}_{im})}$, previously determined from the static soil pressure and cylinder drop test data as discussed in Section 3.3.

The soil dynamic damping coefficient curves presented on Pages (A1-91) through (A1-96) generally indicate increased coefficient values, $C_{(z,\dot{z},\dot{z}_{IM})}$, for increased initial soil impact velocities, $\dot{z}_{IM}$, of the rigid cylinder. An identical impact effect results from the motion of a tire on yieldable terrain. This impact effect was experimentally observed and documented in Reference (2). This reference concluded that the impact type load resulting from the tire motion could be represented as increased soil resistance due to an effective increase in the soil impact deformation rate. The following equation for the effective impact deformation rate of soil under a rolling pneumatic tire was developed in Reference (2).

$$\dot{\xi} = \dot{z} + \frac{z}{(l_t/V)} \qquad (3\text{-}13)$$

Note that (l_t/V) is the impact duration, the time the soil element is under the tire. The parameter, $\dot{\xi}$, replaces the initial vertical impact velocity parameter, $\dot{z}_{IM}$, in the damping coefficient term. At the instant of tire impact $\dot{\xi} = \dot{z} = \dot{z}_{IM}$ as before. However, after initial impact, the motion of the tire influences the dynamic soil strength.

3.4.4 Summary of Soil-Tire Relationships

The following equations represent the vertical equation of motion of the tire-soil interface (surface A), and the total tire drag:

$$m_{TS}\ddot{z} = (m_w + m_T)g - T_{Rz} - \sum_{i=1}^{n_t}[(lb/n_t)(P_{g(z_i)})] - [C_{(z,\dot{z},\dot{\xi})}]\dot{z} \qquad (3\text{-}14)$$

$$\text{Total Tire Drag} = T_{Rx} + \mu T_{Rz} + \left\{T_{Rz} + \sum_{i=1}^{n_t}[(lb/n_t)(P_{g(z_i)})]\right\}\frac{z}{l_t} + C_{DI}\frac{1}{2}\rho_s V^2 b z \qquad (3\text{-}15)$$

The specific terrain contour data, Pages (A1-121) through (A1-125) are utilized along with tire position and geometry to obtain forces T_{Rx} and T_{Rz} . The soil hardness type (A, B, C, D, G or I) is used to indicate the proper dynamic damping coefficient curve, Pages (A1-91) through (A1-96), as well as the static soil pressure curve, Page (A1-61).

Tire geometry, sinkage depth, and the instantaneous vertical and horizontal velocity of the tire are used to obtain the effective impact soil deformation rate, $\dot{\xi}$, from Equation (3-13).

The instantaneous value for the coefficient, $C(z,\dot{z},\dot{\xi})$, can then be determined from the appropriate soil dynamic damping curve on Pages (A1-91) through (A1-96). The generalized mass, m_{TS}, is a combination of soil mass and the tire geometry. It represents the effective mass of the moving soil under the tire. Values for the effective mass can be obtained from correlation of theoretical tire response predictions and experimental measurements. All other parameters and terms in Equations (3-14) and (3-15) are obtainable from tire geometry, sinkage depth, instantaneous velocities, and soil pressure and dynamic coefficient curves contained in Appendix A1.

AIRPLANE STUDY

4.0 AIRPLANE STUDY

4.1 Airplane Instrumentation

4.1.1 Landing Gear Load Calibration

Strain gages were bonded on the landing gears in the locations shown by the sketches given on Pages A2-5 and A2-6. A typical strain gage bridge is also shown on Page A2-7. For calibration purposes, the landing gears were mounted inverted in a fixture with a dummy wheel installed. Loads were applied singly in the vertical, forward, aft, left, and right directions. The loads were applied at the center of the axle for vertical and drag directions and at the rolling radius of the tire for the side direction. They were applied perpendicular and parallel to the fuselage reference system with the oleo in four different positions of compression.

Strain gage outputs were recorded by a standard oscillograph and the results reduced to a unit R/Cal step and plotted against load for response analysis. These data plots are shown on Pages A2-8 thru A2-43. The resulting interaction equations are given on Pages A2-44 thru A2-49 and plotted on Pages A2-50 thru A2-61.

4.1.2 Pilot's Panel and Oscillograph Parameters

The total list of airplane parameters recorded during the tests are as follows:

Pilot's Panel

Parameter	Range
1. Airspeed	0-500 knots
2. Altitude	0-35000 feet
3. Vertical Acceleration @ C.G.	± 10 "g's"
4. Frame Counter	
5. Angle of Yaw	± 7.5 degrees

Oscillograph #1

Channel No.	Parameter	Calibration Range
1.		
2.		
3.	Altitude (Low Range)	0-3000 feet
4.	Lateral Stick Position	± 30 degrees
5.	L/H M.G. Tire Pressure	0-120 psig
6.	R/H M.G. Tire Pressure	0-120 psig
7.	Airspeed (Low Range)	0-160 knots
8.	N.G. Tire Pressure	0-160 psig
9.	R/H Boom Inbd Dorsal Attach Load	-
10.	R/H Boom Vertical Acceleration @ F.S. 380	± 50 "g's"
11.	Lateral Stick Force	± 80 lbs
12.	R/H Boom Outbd Dorsal Attach Load	-
13.	R/H Aft Inbd Vertical Spar Attach Load	-
14.		
15.	Longitudinal Stick Position	+ 26 degrees - 10 degrees
16.	Longitudinal Stick Force	± 120 lbs
17.	Cockpit Floor Vertical Acceleration	± 10 "g's"
18.	Rudder Pedal Position	± 3.25 inches
19.	Cockpit Floor Longitudinal Acceleration	± 5 "g's"
20.	Elevator Spring Tab Position	
21.	L/H Fwd Vertical Inbd Spar Attach Load	-
22.	Cockpit Floor Lateral Acceleration	± 5 "g's"
23.	R/H Engine Longitudinal Acceleration	± 15 "g's"
24.	Trace I.D.	
25.	Trace I.D.	
26.	N.G. Drag Load Fwd Link (T/M)	
27.	L/H Aft Vertical Inbd Spar Attach Load	-
28.	Pilot's Seat Longitudinal Acceleration	± 10 "g's"
29.	Elevator Position	+ 35 degrees - 25.5 degrees
30.	R/H Engine Lateral Acceleration	± 15 "g's"
31.	L/H Fwd Vertical Outbd Spar Attach Load	-
32.	Pilot's Seat Vertical Acceleration	± 10 "g's"
33.	Rudder Position	± 25 degrees
34.	L/H Engine Mount Vertical Acceleration	± 20 "g's"
35.	R/H Engine Vertical Acceleration	± 25 "g's"
36.	Pilot's Seat Lateral Acceleration	± 10 "g's"
37.	L/H Aft Outbd Spar Attach Load	-
38.	Horizontal Fwd Spar Lateral Acceleration	± 25 "g's"
39.	L/H Aileron Position	± 25 degrees

Oscillograph #1 (Cont.)

Channel No.		Calibration Range
40.		
41.	R/H Fwd Outbd Vertical Spar Attach Load	-
42.	Horizontal Fwd Spar Longitudinal Acceleration	± 50 "g's"
43.	Longitudinal Trim Actuator Position	± 1.6 inches
44.	Horizontal Fwd Spar Vertical Acceleration	± 50 "g's"
45.		
46.	R/H Aft Outbd Vertical Spar Attach Load	-
47.	Upper Right Fuselage Longitudinal Load FS 140	-
48.		
49.		
50.	Correction and Pilot Marker	

Oscillograph #2

1.	L/H Hoop Pressure	0-9000 psig
2.	R/H Hoop Pressure	0-9000 psig
3.	Angle of Bank	± 15 degrees
4.	Longitudinal Acceleration @ C.G.	± 10 "g's"
5.	L/H M.G. Vertical Acceleration @ Axle	± 250 "g's"
6.	L/H Power Lever Position	0-120 degrees
7.	Vertical Acceleration @ C.G.	± 10 "g's"
8.	R/H Power Lever Position	0-120 degrees
9.	L/H M.G. Vertical Load	+ 25000 lbs
10.	L/H M.G. Side Load	± 1000 lbs
11.	L/H M.G. Oleo Position	0-9.06 inches
12.	L/H M.G. Drag Load	± 50000 lbs
13.		
14.	L/H M.G. Trunnion Vertical Acceleration	± 25 "g's"
15.	L/H M.G. Lateral Acceleration @ Axle	± 50 "g's"
16.	L/H M.G. Longitudinal Accleration @ Axle	± 250 "g's"
17.	Angle of Sideslip (F.T. Boom)	± 15 degrees
18.		
19.		
20.	N.G. Hoop Pressure	0-25000 psig
21.	N.G. Scissors Axial Load	-
22.	Angle of Pitch	± 15 degrees
23.	N.G. Oleo Position	0-7.53 inches
24.	Trace I.D.	
25.	Trace I.D.	

Oscillograph #2 (Cont.)

Channel No.	Parameter	Calibration Range
26.		
27.	N.G. Vertical Load	+ 20000 lbs
28.	N.G. Fwd Link Drag Load	+ 60000 lbs - 30000 lbs
29.	N.G. Vertical Acceleration @ Axle	± 250 "g's"
30.	N.G. Longitudinal Acceleration @ Axle	± 250 "g's"
31.	N.G. Lateral Acceleration @ Axle	± 50 "g's"
32.	N.G. Oleo Axial Load	0-25000 lbs
33.	N.G. Side Load	± 8000 lbs
34.	R/H M.G. Side Load	+ 10000 lbs
35.	R/H M.G. Vertical Load	0-25000 lbs
36.	R/H M.G. Drag Load	± 50000 lbs
37.	R/H M.G. Oleo Position	0-9.06 inches
38.	R/H M.G. Vertical Acceleration @ Axle	± 250 "g's"
39.	R/H M.G. Trunnion Acceleration	± 25 "g's"
40.	R/H M.G. Longitudinal Acceleration @ Axle	± 250 "g's"
41.	L/H Engine Truss Diagonal Axial Strain- Upper Member	-
42.	Lateral Acceleration @ C.G.	± 3 "g's"
43.	L/H Engine Truss Diagonal Axial Strain - Lower Member	-
44.	R/H M.G. Lateral Acceleration @ Axle	± 50 "g's"
45.	Angle of Attack (F.T. Boom)	+ 50 degrees - 10 degrees
46.	L/H Engine Truss Diagonal Axial Strain - Inbd Member	-
47.	L/H Engine Truss Diagonal Axial Strain - Outbd Member	-
48.	Angle of Attack (ADD Probe)	± 25 degrees
49.	LLORI Correlation	-
50.	Correlation and Pilot Marker	-

4.2 Tire Data

Load-deflection characteristics and load-footprint areas for the tires was provided by the B. F. Goodrich Tire Company. This data is presented on pages A3-10 thru A3-13.

4.3 Airplane Mathematical Model

The minimum degrees of freedom to adequately represent the airplane response are longitudinal (X_D), vertical (Z_D), pitch (θ), roll (φ), and flexible (ξ_j) motions. The landing gears require stroking (ξ_i), fore and aft (q_{d_i}), and lateral bending, (q_{l_i}) motions. In summary form, the airplane degrees of freedom may be simply written as:

$$(m_u + \sum_i^3 m_{G_i})\ddot{X}_D = L_{XD} + D_{XD} + \sum_i^3 G_{XD_i} \tag{4-1}$$

$$(m_u + \sum_i^3 m_{G_i})\ddot{Z}_D = L_{ZD} + D_{ZD} + \sum_i^3 G_{ZD_i} \tag{4-2}$$

$$I_{YY}\ddot{\theta} + J_{XZ}\dot{\varphi}^2 = M_\theta + \sum_i^3 G_{\theta_i} \tag{4-3}$$

$$I_{XX}\ddot{\varphi} - J_{XZ}\dot{\varphi}\dot{\theta} = \sum_i^3 G_{\varphi_i} \tag{4-4}$$

$$m_j \ddot{\xi}_j + m_j c_j \omega_j \dot{\xi}_j + m_j \omega_j^2 \xi_j = \mathcal{F}_j \tag{4-5}$$

The gear motions are more complex since the equations must be written relative to moving coordinates. Using the sketch on Page 4-10, the moments about the nose gear fork pivot point may be obtained using the vector relation:

$$\Sigma \vec{M}_L = \vec{r}_{L_{CG}} \times m_L \ddot{\vec{R}}_{L_{CG}} + \frac{d}{dt}\int^L [\vec{r}_L \times (\vec{\omega}_L \times \vec{r}_L)]dm \tag{4-6}$$

Assuming the nose gear to be symmetric about its plane and applying equation (4-6), the fork pivot point moment reactions are:

$$\begin{aligned} M_{XL}' = {} & I_{XX_L}(\ddot{\varphi}C\xi + \dot{\varphi}\dot{\xi}S\xi) + (I_{YY_L} - I_{ZZ_L})(\dot{\theta} + \dot{\xi})\dot{\varphi}S\xi \\ & + Z_A[S\varphi S\xi T_{XD} + (S\theta C\varphi S\xi - C\theta C\xi)T_{YD}] - Z_S R_{YS} \end{aligned} \tag{4-7}$$

$$\begin{aligned} M_{YL}' = {} & I_{YY_L}(\ddot{\theta} + \ddot{\xi}) - (I_{ZZ_L} - I_{XX_L})\dot{\varphi}^2 S\xi C\xi + m_L l_{L_{CG}}(\ddot{r}_{XB_L}S\xi + \ddot{r}_{ZB_L}C\xi) \\ & + l_L[-(C\theta S\xi + S\theta C\varphi C\xi)T_{XD} + S\varphi C\xi T_{YD} + (C\theta C\varphi C\xi - S\theta S\xi)T_{ZD}] \\ & - Z_A(C\varphi T_{XD} - S\theta S\varphi T_{YD}) - R_{XS}[X_S S(\xi - \sigma) - Z_S C(\xi - \sigma)] \\ & - R_{ZS}[X_S C(\xi - \sigma) + Z_S S(\xi - \sigma)] - W_L l_{L_{CG}}(C\theta C\varphi C\xi - S\theta S\xi) \end{aligned} \tag{4-8}$$

$$M'_{ZL} = -I_{ZZ_L}(\ddot{\varphi}S\xi + \dot{\varphi}\dot{\xi}C\xi) - (I_{YY_L} - I_{XX_L})(\dot{\theta}+\dot{\xi})\dot{\varphi}C\xi + m_L \ell_{L_{CG}} \ddot{r}_{YB_L}$$
$$-\ell_L[S\theta S\varphi T_{XD} + C\varphi T_{YD} - C\theta S\varphi T_{ZD}] - \ell_A[S\varphi C\xi T_{XD}$$
$$+ (C\theta S\xi + S\theta C\varphi C\xi)T_{YD}] + X_S R_{YS} - W_L \ell_{L_{CG}} C\theta S\varphi \tag{4-9}$$

Similar considerations provide the following force reactions at the fork pivot point:

$$R_{XL} = m_L(-\ddot{r}_{XB_{L_{CG}}}C\xi + \ddot{r}_{ZB_{L_{CG}}}S\xi) - (S\theta C\varphi S\xi - C\theta C\xi)T_{XD} + S\varphi S\xi T_{YD}$$
$$+ (S\theta C\xi + C\theta C\varphi S\xi)(T_{ZD} - W_L) + R_{XS}C(\xi - \sigma) - R_{ZS}S(\xi - \sigma) \tag{4-10}$$

$$R_{YL} = m_L \ddot{r}_{YB_{L_{CG}}} - S\theta S\varphi T_{XD} - C\varphi T_{YD} + C\theta S\varphi(T_{ZD} - W_L) + R_{YS} \tag{4-11}$$

$$R_{ZL} = -m_L(\ddot{r}_{XB_{L_{CG}}}S\xi + \ddot{r}_{ZB_{L_{CG}}}C\xi) + (C\theta S\xi + S\theta C\varphi C\xi)T_{XD} - S\varphi C\xi T_{YD}$$
$$-(C\theta C\varphi C\xi - S\theta S\xi)(T_{ZD} - W_L) + R_{XS}S(\xi - \sigma) + R_{ZS}C(\xi - \sigma) \tag{4-12}$$

The acceleration terms in the above are derived from the vector relations:

$$\ddot{\bar{R}}_{B_{L_{CG}}} = \ddot{r}_{XB_{L_{CG}}}\bar{i}_B + \ddot{r}_{YB_{L_{CG}}}\bar{j}_B + \ddot{r}_{ZB_{L_{CG}}}\bar{k}_B \tag{4-13}$$

$$\ddot{\bar{R}}_{B_{L_{CG}}} = \ddot{\bar{R}} + \ddot{\bar{R}}_1 + \ddot{\bar{r}}_1 + \ddot{\bar{r}}_{L_{CG}} + 2(\bar{\omega}_D \times \dot{\bar{R}}) + (\dot{\bar{\omega}}_D \times \bar{R}) + \bar{\omega}_D \times (\bar{\omega}_D \times \bar{R})$$
$$+ 2(\bar{\omega}_B \times \dot{\bar{R}}_1) + (\dot{\bar{\omega}}_B \times \bar{R}_1) + \bar{\omega}_B \times (\bar{\omega}_B \times \bar{R}_1)$$
$$+ 2(\bar{\omega}_1 \times \dot{\bar{r}}_1) + (\dot{\bar{\omega}}_1 \times \bar{r}_1) + \bar{\omega}_1 \times (\bar{\omega}_1 \times \bar{r}_1)$$
$$+ 2(\bar{\omega}_L \times \dot{\bar{r}}_{L_{CG}}) + (\dot{\bar{\omega}}_L \times \bar{r}_{L_{CG}}) + \bar{\omega}_L \times (\bar{\omega}_L \times \bar{r}_{L_{CG}}) \tag{4-14}$$

$$\ddot{r}_{XB_{L_{CG}}} = \ddot{r}_{XB_L} + \ell_{L_{CG}}[(\ddot{\theta} + \ddot{\xi})S\xi + (\dot{\theta} + \dot{\xi})^2 C\xi] \tag{4-15}$$

$$\ddot{r}_{YB_{L_{CG}}} = \ddot{r}_{YB_L} - \ell_{L_{CG}}[\ddot{\varphi}S\xi + (\dot{\theta} + 2\dot{\xi})\dot{\varphi}C\xi] \tag{4-16}$$

$$\ddot{r}_{ZB_{L_{CG}}} = \ddot{r}_{ZB_L} + \ell_{L_{CG}}\{(\ddot{\theta} + \ddot{\xi})C\xi - [(\dot{\theta} + \dot{\xi})^2 + \dot{\varphi}^2]S\xi\} \tag{4-17}$$

$$\ddot{r}_{XB_L} = \ddot{r}_{XB_1} - \ell_1[(\ddot{\theta} - \ddot{\beta})S\beta - (\dot{\theta} - \dot{\beta})^2 C\beta] \tag{4-18}$$

$$\ddot{r}_{YB_L} = \ddot{r}_{YB_1} + \ell_1[\ddot{\varphi}S\beta - (\dot{\theta} - 2\dot{\beta})\dot{\varphi}C\beta] \tag{4-19}$$

$$\ddot{r}_{ZB_L} = \ddot{r}_{ZB_1} + \ell_1\{(\ddot{\theta} - \ddot{\beta})C\beta + [(\dot{\theta} - \dot{\beta})^2 + \dot{\varphi}^2]S\beta\} \tag{4-20}$$

$$\ddot{r}_{XB_1} = \ddot{X}_{BCG} + \ddot{X}_{B_1} + 2\dot{Z}_{B_1}\dot{\theta} - X_{B_1}\dot{\theta}^2 + Y_{B_1}\dot{\varphi}\dot{\theta} + Z_{B_1}\ddot{\theta} \qquad (4\text{-}21)$$

$$\ddot{r}_{YB_1} = \ddot{Y}_{BCG} + \ddot{Y}_{B_1} - 2\dot{Z}_{B_1}\dot{\varphi} + X_{B_1}\dot{\varphi}\dot{\theta} - Y_{B_1}\dot{\varphi}^2 - Z_{B_1}\ddot{\varphi} \qquad (4\text{-}22)$$

$$\ddot{r}_{ZB_1} = \ddot{Z}_{BCG} + \ddot{Z}_{B_1} + 2(\dot{Y}_{B_1}\dot{\varphi} - \dot{X}_{B_1}\dot{\theta}) - X_{B_1}\ddot{\theta} + Y_{B_1}\ddot{\varphi} - Z_{B_1}(\dot{\varphi}^2 + \dot{\theta}^2) \qquad (4\text{-}23)$$

Where: $X_{B_1} = X_{IGA} + (Z_{IGA} - Z_{REF})\sum_j^n \phi'_{x_j}\xi_j - C\sigma\phi_{IGAd_i} q_{d_i}$ (4-24)

$$Y_{B_1} = Y_{IGA} + \sum_K^m \phi_K \xi_K - (Z_{IGA} - Z_{REF})\left[\sum_j^n \phi'_{Y_j}\xi_j + \sum_K^m \phi'_{Y_K}\xi_K\right]$$

$$- (Y_{P,GA} - X_{TGA})\sum_K^m \phi'_{x_K}\xi_K + \phi_{IGA\ell_i} q_{\ell_i} \qquad (4\text{-}25)$$

$$Z_{B_1} = Z_{IGA} + \sum_j^n \phi_j \xi_j - (X_{IGA} - X_{TGA})\sum_j^n \phi'_{x_j}\xi_j + S\sigma\phi_{IGAd_i} q_{d_i} \qquad (4\text{-}26)$$

The terms $\dot{X}_{B_1}$, $\ddot{X}_{B_1}$, etc. are the scalar differentiation of the above relations.

Dynamic and kinematic constraints are acting on the nose gear. The dynamic constraint is the oleo stroking relation:

$$m_S \ddot{Z}_S = R_{ZS} - G_S + W_S \qquad (4\text{-}27)$$

With: $\ddot{Z}_S = [\ddot{r}_{XB_L} + (\ddot{\theta} + \ddot{\xi})(X_S S\xi - Z_S C\xi) + (\dot{\theta} + \dot{\xi})^2(X_S C\xi + Z_S S\xi)]S\sigma$

$$+ \{\ddot{r}_{ZB_L} + (\ddot{\theta} + \ddot{\xi})(X_S C\xi - Z_S S\xi) - [(\dot{\theta} + \dot{\xi})^2 + \dot{\varphi}^2](X_S S\xi - Z_S C\xi)\}C\sigma \qquad (4\text{-}28)$$

The torque arm kinematic constraint is:

$$\beta = COS^{-1}\left\{\frac{1}{l_1}\left[-dCH - SH(l_1^2 - d^2)^{1/2}\right]\right\} \qquad (4\text{-}29)$$

Where: $H = \sigma + \sum_j^n \phi'_{x_j}\xi_j$ (4-30)

$$d = X_S C(\xi - H) + Z_S S(\xi - H) + l_1 C(\phi'_{IGAd_i} q_{d_i}) - (\phi_{LGAd_i} - \phi_{IGAd_i}) q_{d_i} \qquad (4\text{-}31)$$

The torque arm moments and forces are:

$$M'_{X1} = -I_{XX_1}(\ddot{\varphi}C\beta - \dot{\varphi}\dot{\beta}S\beta) + (I_{ZZ_1} - I_{YY_1})(\dot{\theta} - \dot{\beta})\dot{\varphi}S\beta + M'_{XL}C(\xi + \beta) + M'_{ZL}S(\xi + \beta) \qquad (4\text{-}32)$$

$$M'_{Y1} = I_{YY_1}(\ddot{\theta} - \ddot{\beta}) + (I_{ZZ_1} - I_{XX_1})\dot{\varphi}^2 S\beta C\beta - m_1 l_{1CG}(\ddot{r}_{XB_1} S\beta - \ddot{r}_{ZB_1} C\beta)$$

$$+ l_1[R_{XL}S(\xi + \beta) - R_{ZL}C(\xi + \beta)] - W_1 l_{1CG}(S\theta S\beta + C\theta C\varphi C\beta) + M'_{YL} \qquad (4\text{-}33)$$

$$M'_{Z1} = I_{ZZ_1}(\ddot{\varphi}S\beta + \dot{\varphi}\dot{\beta}C\beta) + (I_{XX_1} - I_{YY_1})(\dot{\theta} - \dot{\beta})\varphi C\beta + m_1 l_{1CG}\ddot{r}_{YB_1} + l_1 R_{YL}$$

$$- W_1 l_{1CG} C\theta S\varphi - M'_{XL}S(\xi + \beta) + M'_{ZL}C(\xi + \beta) \qquad (4\text{-}34)$$

$$R_{X1} = -m_1(\ddot{r}_{XB_{1CG}} C\beta + \ddot{r}_{ZB_{1CG}} S\beta) + R_{XL}C(\xi + \beta) + R_{ZL}S(\xi + \beta)$$

$$+ W_1(C\theta C\varphi S\beta - S\theta C\beta) \qquad (4\text{-}35)$$

$$R_{Y1} = m_1 \ddot{r}_{YB_{1CG}} + R_{YL} - W_1 C\theta S\varphi \tag{4-36}$$

$$R_{Z1} = m_1 (\ddot{r}_{XB_{1CG}} S\beta - \ddot{r}_{ZB_{1CG}} C\beta) - R_{XL} S(\xi+\beta) + R_{ZL} C(\xi+\beta)$$
$$+ W_1 (S\theta S\beta + C\theta C\varphi C\beta) \tag{4-37}$$

Where: $$\ddot{r}_{XB_{1CG}} = \ddot{r}_{XB_1} - l_{1CG} [(\ddot{\theta}-\ddot{\beta}) S\beta - (\dot{\theta}-\dot{\beta})^2 C\beta] \tag{4-38}$$

$$\ddot{r}_{YB_{1CG}} = \ddot{r}_{YB_1} + l_{1CG} [\ddot{\varphi} S\beta - (\dot{\theta} - 2\dot{\beta})\dot{\varphi} C\beta] \tag{4-39}$$

$$\ddot{r}_{ZB_{1CG}} = \ddot{r}_{ZB_1} + l_{1CG} \{(\ddot{\theta}-\ddot{\beta}) C\beta + [(\dot{\theta}-\dot{\beta})^2 + \dot{\varphi}^2] S\beta\} \tag{4-40}$$

A summation of moments about the nose gear trunnion gives the following relation for the drag brace load:

$$R_P = l_{B_{XG}} \{ I_{YY_{GT}} \ddot{\theta} + I_{XZ_{GT}} \dot{\varphi}^2 + m_{GT} (Z_{GT_{CG}} \ddot{r}_{XB_{GT}} - X_{GT_{CG}} \ddot{r}_{ZB_{GT}}) + (l_E - S) R_{XS}$$
$$- X_1 [R_{X1} S(\beta+\sigma) + R_{Z1} C(\beta+\sigma)] - (Z_{B_{GA}} - Z_{TGA})(R_{X1} C\beta - R_{Z1} S\beta) + l_{GT_{CG}} W_{GT} (S\theta C\sigma + C\theta C\varphi S\sigma) \} \tag{4-41}$$

Where: $$l_{B_{XG}} = \frac{l_P}{X_P[(Y_{B_{GA}} - X_{BB}) S\sigma + (Z_{B_{GA}} - Z_{BB}) C\sigma] + (X_{B_{GA}} - X_{BB})(Z_{B_{GA}} - Z_{TGA})} \tag{4-42}$$

$$\ddot{r}_{XB_{GT}} = \ddot{X}_{B_{CG}} + \ddot{X}_{B_T} + 2 \dot{Z}_{B_T} \dot{\theta} - X_{B_T} \dot{\theta}^2 + Y_{B_T} \dot{\varphi}\dot{\theta} + Z_{B_T} \ddot{\theta} \tag{4-43}$$

$$\ddot{r}_{ZB_{GT}} = \ddot{Z}_{B_{CG}} + \ddot{Z}_{B_T} + 2(\dot{Y}_{B_T} \dot{\varphi} - \dot{X}_{B_T} \dot{\theta}) - X_{B_T} \ddot{\theta} + Y_{B_T} \ddot{\varphi} - Z_{B_T} (\dot{\theta}^2 + \dot{\varphi}^2) \tag{4-44}$$

Using these moments and forces the fore and aft bending equation becomes:

$$m_{d_i} \ddot{q}_{d_i} + m_{d_i} C_{d_i} \dot{q}_{d_i} + m_{d_i} \omega_{d_i} q_{d_i} = R_{XS} \phi_{LGA_{d_i}} - R_{X1} [\phi_{1GA_{d_i}} C(\beta+\sigma) + X_1 \phi'_{1GA_{d_i}} S(\beta+\sigma)]$$
$$+ R_{Z1} [\phi_{1GA_{d_i}} S(\beta+\sigma) - X_1 \phi'_{1GA_{d_i}} C(\beta+\sigma)] + \frac{R_P}{l_P} [-(C\sigma \phi_{BGA_{d_i}} + X_P S\sigma \phi'_{BGA_{d_i}})(X_{B_{GA}} - X_{BB})$$
$$+ (S\sigma \phi_{BGA_{d_i}} - X_P C\sigma \phi'_{BGA_{d_i}})(Z_{B_{GA}} - Z_{BB})] \tag{4-45}$$

Similarly the lateral bending relation is:

$$m_{l_i} \ddot{q}_{l_i} + m_{l_i} C_{l_i} \omega_{l_i} \dot{q}_{l_i} + m_{l_i} \omega_{l_i}^2 q_{l_i} = R_{YS} \phi_{LGA_{l_i}} + [\{-Z_S [S\theta S\varphi T_{XD} + C\varphi T_{YD}$$
$$- C\theta S\varphi (T_{ZD} - W_L) + R_{YL}] - Z_A [S\varphi S\xi T_{XD} + (S\theta C\varphi S\xi - C\theta C\xi) T_{YD}] + M'_{XL}\} C(\xi - \sigma)$$
$$+ \{(l_L - X_S)[S\theta S\varphi T_{XD} + C\varphi T_{YD} - C\theta S\varphi T_{ZD}] + X_S R_{YL} + Z_A [S\varphi C\xi T_{XD}$$
$$+ (C\theta S\xi + S\theta C\varphi C\xi) T_{YD}] + W_L (X_{L_{CG}} - X_S) C\theta S\varphi + M'_{ZL}\} S(\xi - \sigma)] \phi'_{LGA_{l_i}}$$
$$+ R_{Y1} \phi_{1GA_{l_i}} + [M_{X1} C(\beta+\sigma) - M_{Z1} S(\beta+\sigma)] \phi'_{1GA_{l_i}} \tag{4-46}$$

Assuming that the airplane motions are known, then the above equations result in three degrees of freedom, namely $\ddot{\xi}_i$, $\ddot{q}_{d_i}$, and $\ddot{q}_{\ell_i}$. The first two are coupled and must be solved simultaneouslv. Rewriting those equations that are functions of these degrees of freedom in functional form and noting the boundary conditions that $M_{YL}' = M_{Y1} = 0$, then the solution is as shown in the flow chart on Page 4-11 .

The remaining degree of freedom ($\ddot{q}_{\ell_i}$) may be obtained by considering the boundary condition that the torque about the oleo centerline created by the forces and moments on the fork must be reacted by the torque link. The moment about the oleo centerline due to the moments and forces acting on the fork may be written as:

$$
\begin{aligned}
M_{S_{\mathbb{C}_L}} = \{ & z_S[S\theta S\psi T_{XD} + C\psi T_{YD} - C\theta S\psi(T_{ZD} - W_L) + R_{YL}] + z_A[(S\theta C\psi S\xi - C\theta C\xi)T_{YD} \\
& + S\psi S\xi T_{XD}] - M_{XL}' \} S(\xi - \sigma) + \{(\ell_L - X_S)(S\theta S\psi T_{XD} + C\psi T_{YD} - C\theta S\psi T_{ZD}) + X_S R_{YL} \\
& + W_L(X_{L_{CG}} - X_S) C\theta S\psi + z_A[(C\theta S\xi + S\theta C\psi C\xi)T_{YD} + S\psi C\xi T_{XD}] + M_{ZL}' \} C(\xi - \sigma)
\end{aligned}
\tag{4-47}
$$

The reacting moment due to the torque link is:

$$
M_{S_{\mathbb{C}_1}} = \ell_1 R_{Y1} + M_{X1} S(\beta + \sigma) + M_{Z1} C(\beta + \sigma) \tag{4-48}
$$

Setting these two relations equal to each other and writing those equations which are a function of $\ddot{q}_{\ell_i}$ in functional form, then the solution is shown in the flow chart on Page 4-11 .

NOSE GEAR FORCE DIAGRAM

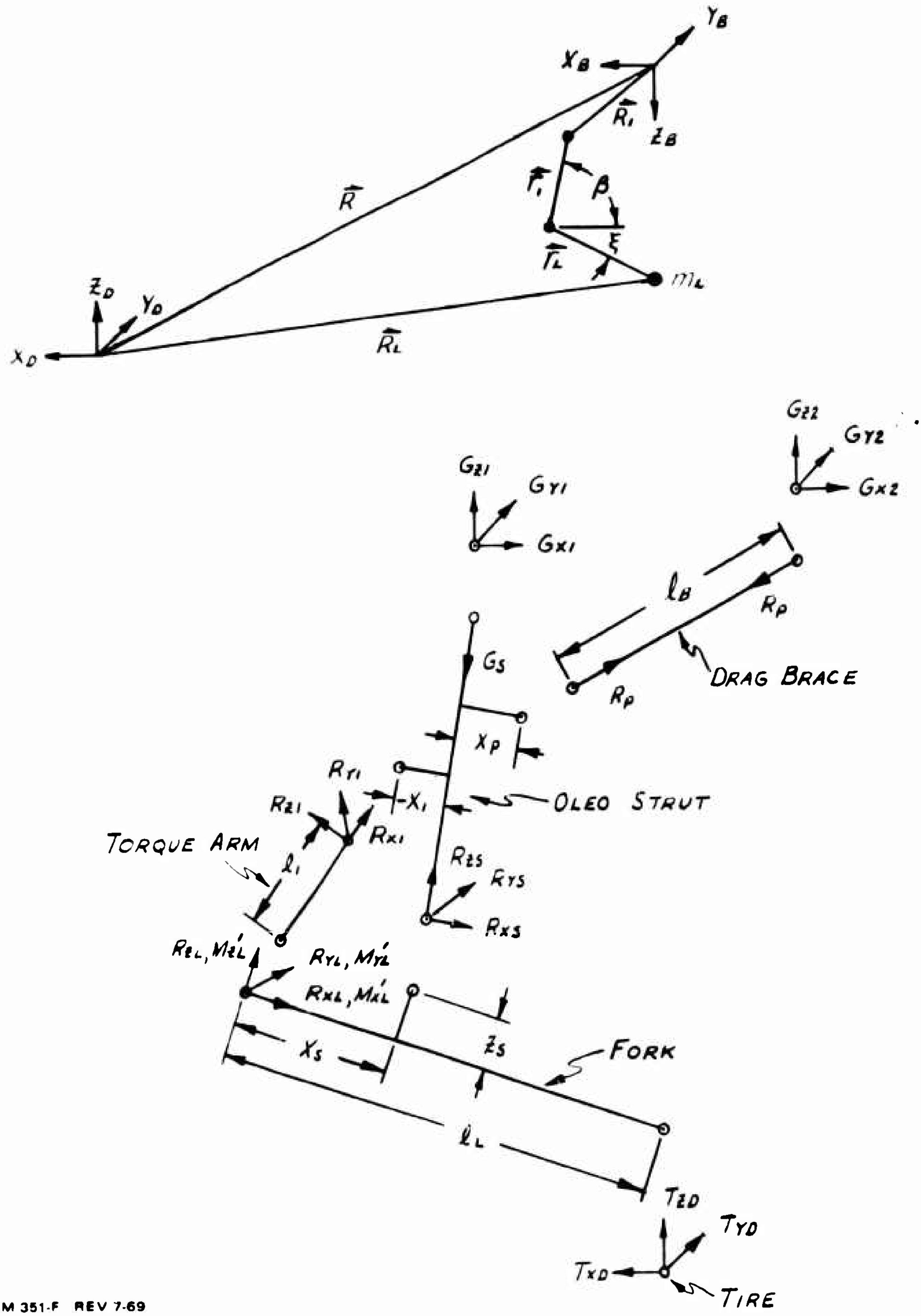

NOSE GEAR EQUATION FLOW CHART

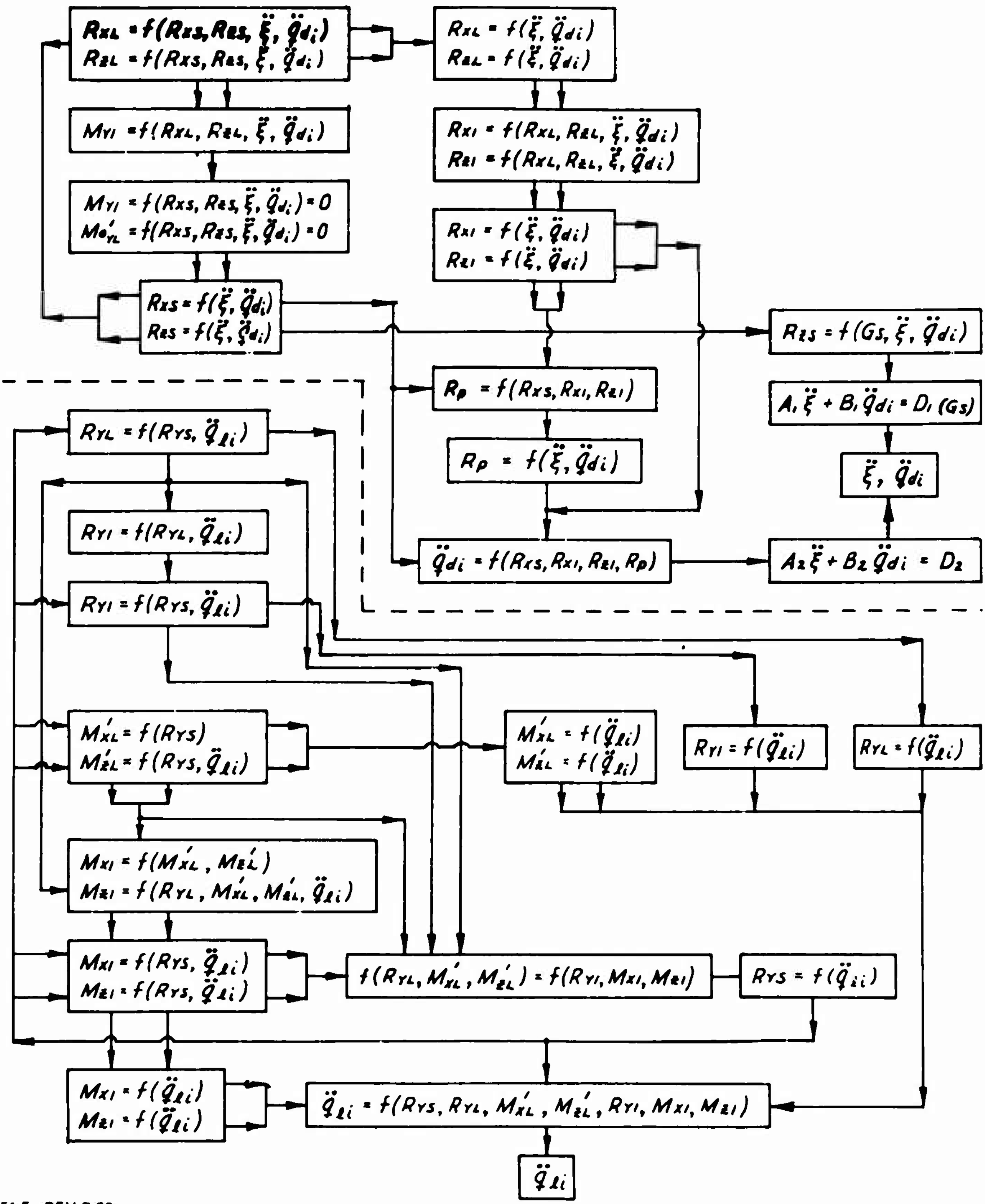

The main gear has some major differences compared to the nose gear. Among these are that the main gear cannot be considered symmetric about its XZ plane, and the oleo capsule is pin jointed at both ends such that it does not transmit any bending loads. Also the drag brace is mounted such that drag loads are reacted in tension instead of compression. Using the sketch on Page 4-15and employing the vector relations used on the nose gear, the main gear equations are:

$$\begin{aligned}
M_{XL}' = {} & I_{XX_L}(-\ddot{\varphi} C\xi + \dot{\varphi}\dot{\xi} S\xi) + (I_{YY_L} - I_{ZZ_L})(\dot{\theta}+\dot{\xi})\dot{\varphi} S\xi - I_{XY_L}(\ddot{\theta}+\ddot{\xi}-\dot{\varphi}^2 S\xi C\xi) \\
& + I_{XZ_L}[\ddot{\varphi} S\xi + (\dot{\theta}+2\dot{\xi})\dot{\varphi} C\xi] + I_{YZ_L}[(\dot{\varphi} S\xi)^2 - (\dot{\theta}+\dot{\xi})^2] - m_L Y_{L_{CG}}(\ddot{r}_{XB_L} S\xi + \ddot{r}_{ZB_L} C\xi) \\
& - Y_A[-(C\theta S\xi + S\theta C\varphi C\xi)T_{XD} + S\varphi C\xi\, T_{YD} + (C\theta C\varphi C\xi - S\theta S\xi)(T_{ZD} - W_L)] \\
& + Z_A[(S\theta C\varphi S\xi - C\theta C\xi)T_{YD} + S\varphi S\xi\, T_{XD}] - R_{ZS}[Y_S(\mu_{ZS} S\xi + \lambda_{ZS} C\xi) - Z_S \nu_{ZS}]
\end{aligned} \tag{4-49}$$

$$\begin{aligned}
M_{YL}' = {} & I_{YY_L}(\ddot{\theta}+\ddot{\xi}) - (I_{ZZ_L} - I_{XX_L})\dot{\varphi}^2 S\xi C\xi + I_{XY_L}(\ddot{\varphi} C\xi + \dot{\varphi}\dot{\theta} S\xi) + I_{XZ_L}\dot{\varphi}^2(C^2\xi - S^2\xi) \\
& + I_{YZ_L}(\ddot{\varphi} S\xi - \dot{\varphi}\dot{\theta} C\xi) + m_L X_{L_{CG}}(\ddot{r}_{XB_L} S\xi + \ddot{r}_{ZB_L} C\xi) + X_A[-(C\theta S\xi + S\theta C\varphi C\xi)T_{XD} \\
& + S\varphi C\xi\, T_{YD} + (C\theta C\varphi C\xi - S\theta S\xi)(T_{ZD} - W_L) + Z_A(S\theta S\varphi\, T_{YD} - C\varphi\, T_{XD}) \\
& - R_{ZS}[-X_S(\mu_{ZS} S\xi + \lambda_{ZS} C\xi) + Z_S(\mu_{ZS} C\xi - \lambda_{ZS} S\xi)]
\end{aligned} \tag{4-50}$$

$$\begin{aligned}
M_{ZL}' = {} & -I_{ZZ_L}(\ddot{\varphi} S\xi + \dot{\varphi}\dot{\xi} C\xi) - (I_{YY_L} - I_{XX_L})(\dot{\theta}+\dot{\xi})\dot{\varphi} C\xi + I_{XY_L}[(\dot{\theta}+\dot{\xi})^2 - (\dot{\varphi} C\xi)^2] \\
& - I_{XZ_L}[-\ddot{\varphi} C\xi + \dot{\varphi}(\dot{\theta}+2\dot{\xi}) S\xi] - I_{YZ_L}(\ddot{\theta}+\ddot{\xi}-\dot{\varphi}^2 S\xi C\xi) + m_L[X_{L_{CG}} \ddot{r}_{YB_L} \\
& + Y_{L_{CG}}(\ddot{r}_{XB_L} C\xi - \ddot{r}_{ZB_L} S\xi)] - X_A[S\theta S\varphi\, T_{XD} + C\varphi\, T_{YD} - C\theta S\varphi(T_{ZD} - W_L)] \\
& + Y_A[(S\theta C\varphi S\xi - C\theta C\xi)T_{XD} - S\varphi S\xi\, T_{YD} - (S\theta C\xi + C\theta C\varphi S\xi)(T_{ZD} - W_L)] \\
& - Z_A[(C\theta S\xi + S\theta C\varphi C\xi)T_{YD} + S\varphi C\xi\, T_{XD}] - R_{ZS}[X_S \nu_{ZS} - Y_S(\mu_{ZS} C\xi - \lambda_{ZS} S\xi)]
\end{aligned} \tag{4-51}$$

$$\begin{aligned}
R_{XL} = {} & m_L(-\ddot{r}_{XB_{L_{CG}}} C\xi + \ddot{r}_{ZB_{L_{CG}}} S\xi) + (C\theta C\xi - S\theta C\varphi S\xi)T_{XD} + S\varphi S\xi\, T_{YD} \\
& + (S\theta C\xi + C\theta C\varphi S\xi)(T_{ZD} - W_L) - R_{ZS}(\mu_{ZS} C\xi - \lambda_{ZS} S\xi)
\end{aligned} \tag{4-52}$$

$$R_{YL} = m_L \ddot{r}_{YB_{L_{CG}}} - S\theta S\psi T_{XD} - C\psi T_{YD} + C\theta S\psi (T_{ZD} - W_L) - R_{ZS}\nu_{ZS} \tag{4-53}$$

$$R_{ZL} = -m_L(\ddot{r}_{XB_{L_{CG}}} S\xi + \ddot{r}_{ZB_{L_{CG}}} C\xi) + (C\theta S\xi + S\theta C\psi C\xi)T_{XD} - S\psi C\xi T_{YD}$$
$$+ (S\theta S\xi - C\theta C\psi C\xi)(T_{ZD} - W_L) - R_{ZS}(\mu_{ZS} S\xi + \lambda_{ZS} C\xi) \tag{4-54}$$

Where the acceleration terms may be represented by the same relations as for the nose gear except that all reference to the torque arm needs to be deleted. The dynamic constraint of the oleo capsule is:

$$m_S \ddot{Z}_S = R_{ZS} - G_S + W_S \tag{4-55}$$

With: $$\ddot{Z}_S = [\ddot{r}_{XB_L} + (\ddot{\theta} + \ddot{\xi})(X_S S\xi - Z_S C\xi) + (\dot{\theta} + \dot{\xi})^2 (X_S C\xi + Z_S S\xi)]\mu_{ZS}$$
$$+ [\ddot{r}_{YB_L} - \ddot{\psi}(X_S S\xi - Z_S C\xi) - \dot{\psi}(\dot{\theta} + 2\dot{\xi})(X_S C\xi + Z_S S\xi)]\nu_{ZS}$$
$$+ \{\ddot{r}_{ZB_L} + (\ddot{\theta} + \ddot{\xi})(X_S C\xi + Z_S S\xi) - [(\dot{\theta} + \dot{\xi})^2 + \dot{\psi}^2](X_S S\xi - Z_S C\xi)\}\lambda_{ZS} \tag{4-56}$$

A summation of moments about the main gear post trunnion gives the following relation for the drag brace load:

$$R_D = l_{B_{XG}}\{I_{YY_{GT}}\ddot{\theta} - I_{XY_{GT}}\ddot{\psi} + I_{XZ_{GT}}\dot{\psi}^2 + I_{YZ_{GT}}\dot{\psi}\dot{\theta} + m_{GT}(Z_{GT_{CG}}\ddot{r}_{XB_{GT}} - X_{GT_{CG}}\ddot{r}_{ZB_{GT}})$$
$$- X_{LPA}(R_{XL} S\xi - R_{ZL} C\xi) - Z_{LPA}(R_{XL} C\xi + R_{ZL} S\xi) - G_S(-X_{SPA}\lambda_{ZS} + Z_{SPA}\mu_{ZS})$$
$$+ W_{GT}(X_{GT_{CG}} C\theta C\psi + Z_{GT_{CG}} S\theta)\} \tag{4-57}$$

Where: $$l_{B_{XG}} = \frac{l_D}{-(X_{B_{BPA}} - X_{GT})(Z_{B_{BPA}} - Z_{BB}) + (Z_{B_{BPA}} - Z_{GT})(X_{B_{BPA}} - X_{BB})} \tag{4-58}$$

$\ddot{r}_{XB_{GT}}$ and $\ddot{r}_{ZB_{GT}}$ are as the nose gear equations.

The fore and aft bending and side bending equations are:

$$m_{d_i}\ddot{q}_{d_i} + m_{d_i}C_{d_i}\omega_{d_i}\dot{q}_{d_i} + m_{d_i}\omega_{d_i}^2 q_{d_i} = [(\mu_{X_{LPA}} C\xi - \lambda_{X_{LPA}} S\xi)R_{XL} - \nu_{X_{LPA}} R_{YL}$$
$$+ (\mu_{X_{LPA}} S\xi + \lambda_{X_{LPA}} C\xi)R_{ZL}]\phi_{LPAd_i} - [(\mu_{Y_{LPA}} C\xi - \lambda_{Y_{LPA}} S\xi)M_{XL}' + (\mu_{Y_{LPA}} S\xi$$
$$+ \lambda_{Y_{LPA}} C\xi)M_{ZL}']\phi_{LPAd_i}' + G_S[(\mu_{X_{LPA}}\mu_{ZS} + \nu_{X_{LPA}}\nu_{ZS} + \lambda_{X_{LPA}}\lambda_{ZS})\phi_{SPAd_i}$$
$$- X_0(\mu_{Z_{LPA}}\mu_{ZS} + \nu_{Z_{LPA}}\nu_{ZS} + \lambda_{Z_{LPA}}\lambda_{ZS})\phi_{SPAd_i}'] + \frac{R_D}{l_D}\{[\mu_{X_{LPA}}(X_{B_{BPA}} - X_{BB})$$
$$+ \nu_{X_{LPA}}(Y_{B_{SPA}} - Y_{BB}) + \lambda_{X_{LPA}}(Z_{B_{BPA}} - Z_{BB})] - X_D[\mu_{Z_{LPA}}(X_{B_{BPA}} - X_{BB})$$
$$+ \nu_{Z_{LPA}}(Y_{B_{BPA}} - Y_{BB}) + \lambda_{Z_{LPA}}(Z_{B_{BPA}} - Z_{BB})]\phi_{BPAd_i}'\} \tag{4-59}$$

$$m_{\ell_i}\ddot{q}_{\ell_i} + m_{\ell_i} C_{\ell_i}\omega_{\ell_i}\dot{q}_{\ell_i} + m_{\ell_i}\omega_{\ell_i}^2 q_{\ell_i} = [(\mu_{Y_{LPA}} C\xi - \lambda_{Y_{LPA}} S\xi) R_{XL} - \nu_{Y_{LPA}} R_{YL}$$
$$+ (\mu_{Y_{LPA}} S\xi + \lambda_{Y_{LPA}} C\xi) R_{ZL}] \phi_{LPA\ell_i} + [(\mu_{Z_{LPA}} C\xi - \lambda_{Z_{LPA}} S\xi) M'_{XL} + (\mu_{Z_{LPA}} S\xi$$
$$+ \lambda_{Z_{LPA}} C\xi) M'_{ZL}] \phi'_{LPA\ell_i} + G_S[(\mu_{Y_{LPA}}\mu_{ZS} + \nu_{Y_{LPA}}\nu_{ZS} + \lambda_{Y_{LPA}}\lambda_{ZS})\phi_{SPA\ell_i}$$
$$+ Y_0 (\mu_{Z_{LPA}}\mu_{ZS} + \nu_{Z_{LPA}}\nu_{ZS} + \lambda_{Z_{LPA}}\lambda_{ZS})\phi'_{SPA\ell_i}] + \frac{R_P}{I_P}\{[\mu_{Y_{LPA}}(X_{B_{BPA}} - X_{B_B})$$
$$+ \lambda_{Y_{LPA}}(Z_{B_{BPA}} - Z_{B_B})]\phi_{BPA\ell_i} - Y_P[\mu_{Z_{LPA}}(X_{B_{BPA}} - X_{B_B}) + \nu_{Z_{LPA}}(Y_{B_{BPA}} - Y_{B_B})$$
$$+ \lambda_{Z_{LPA}}(Z_{B_{BPA}} - Z_{B_B})]\phi'_{BPA\ell_i}\} \tag{4-60}$$

In all of the main gear equations, the following apply:

$$\mu_{ZS} = \frac{X_{BSPA} - X_{BSLA} + X_S C\xi + Z_S S\xi}{L_E - S} \tag{4-61}$$

$$\nu_{ZS} = \frac{Y_{BSPA} - Y_{BSLA} - Y_S}{L_E - S} \tag{4-62}$$

$$\lambda_{ZS} = \frac{Z_{BSPA} - Z_{BSLA} - X_S S\xi + Z_S C\xi}{L_E - S} \tag{4-63}$$

The main gear equations result in a system of three equations in the three unknowns ξ , $\ddot{q}_{d_i}$, $\ddot{q}_{\ell_i}$ and may be solved as indicated by the flow chart on Page 4-17.

MAIN GEAR FORCE DIAGRAM

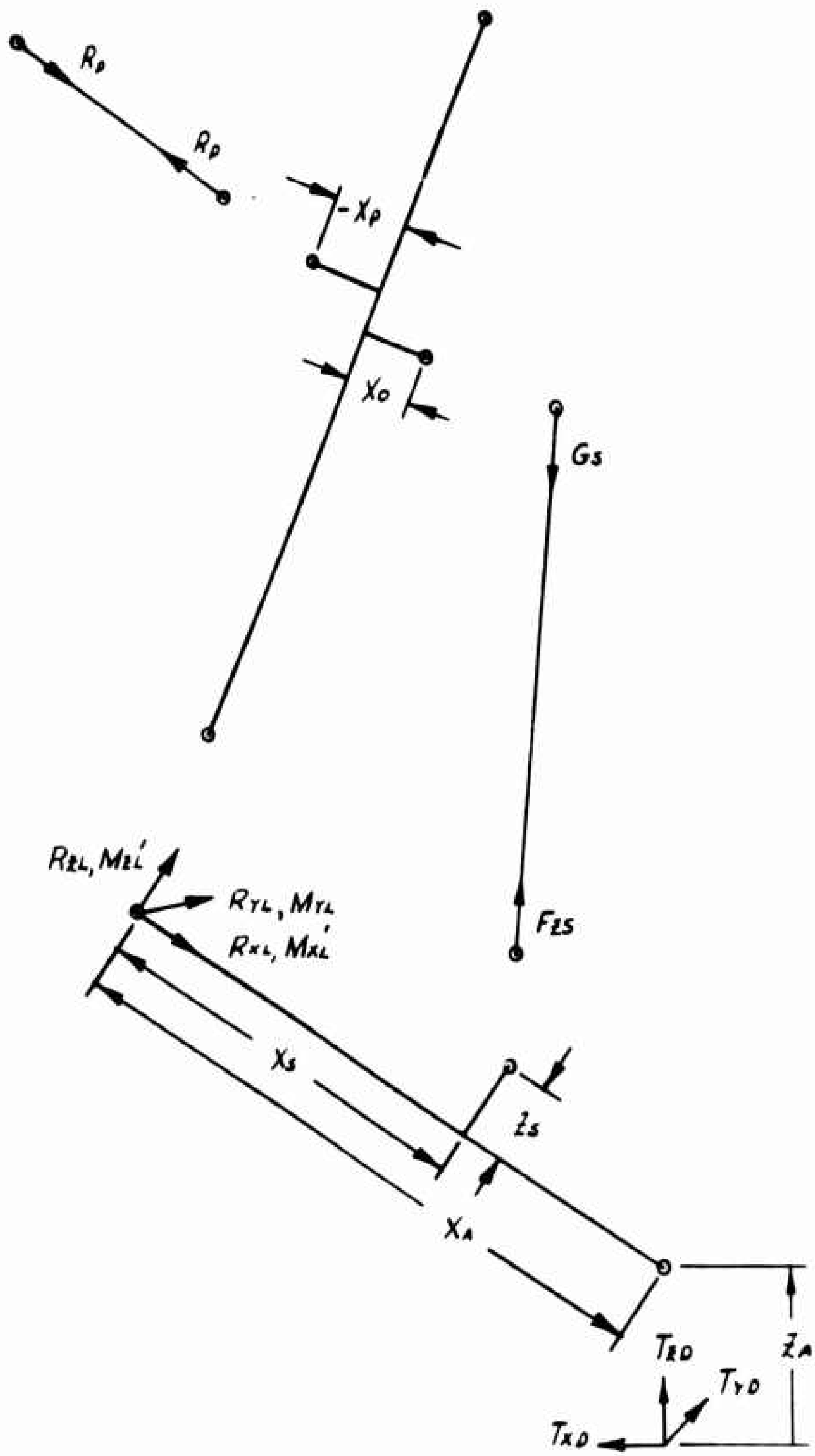

MAIN GEAR KINEMATIC DIAGRAM

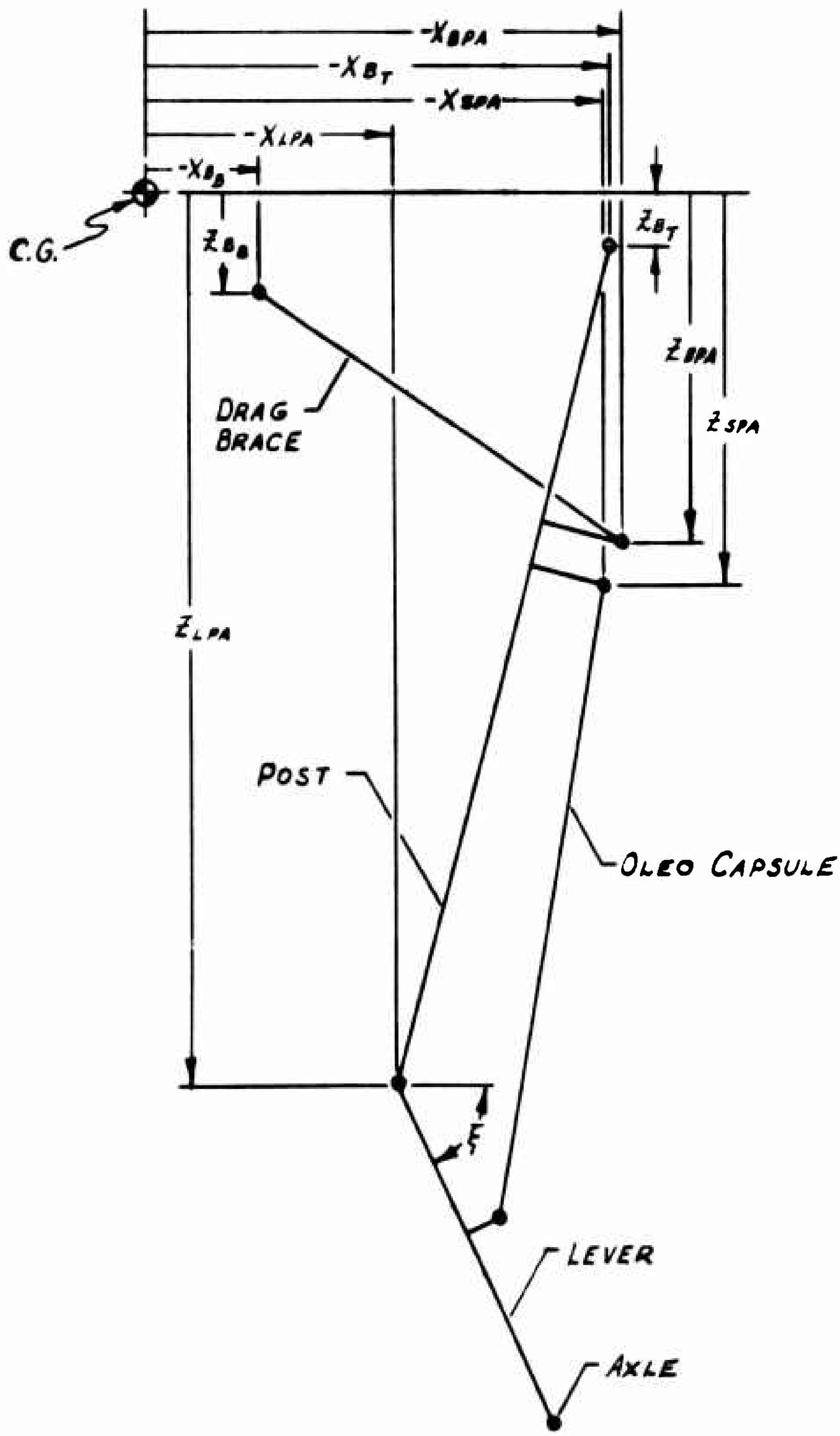

MAIN GEAR EQUATION FLOW CHART

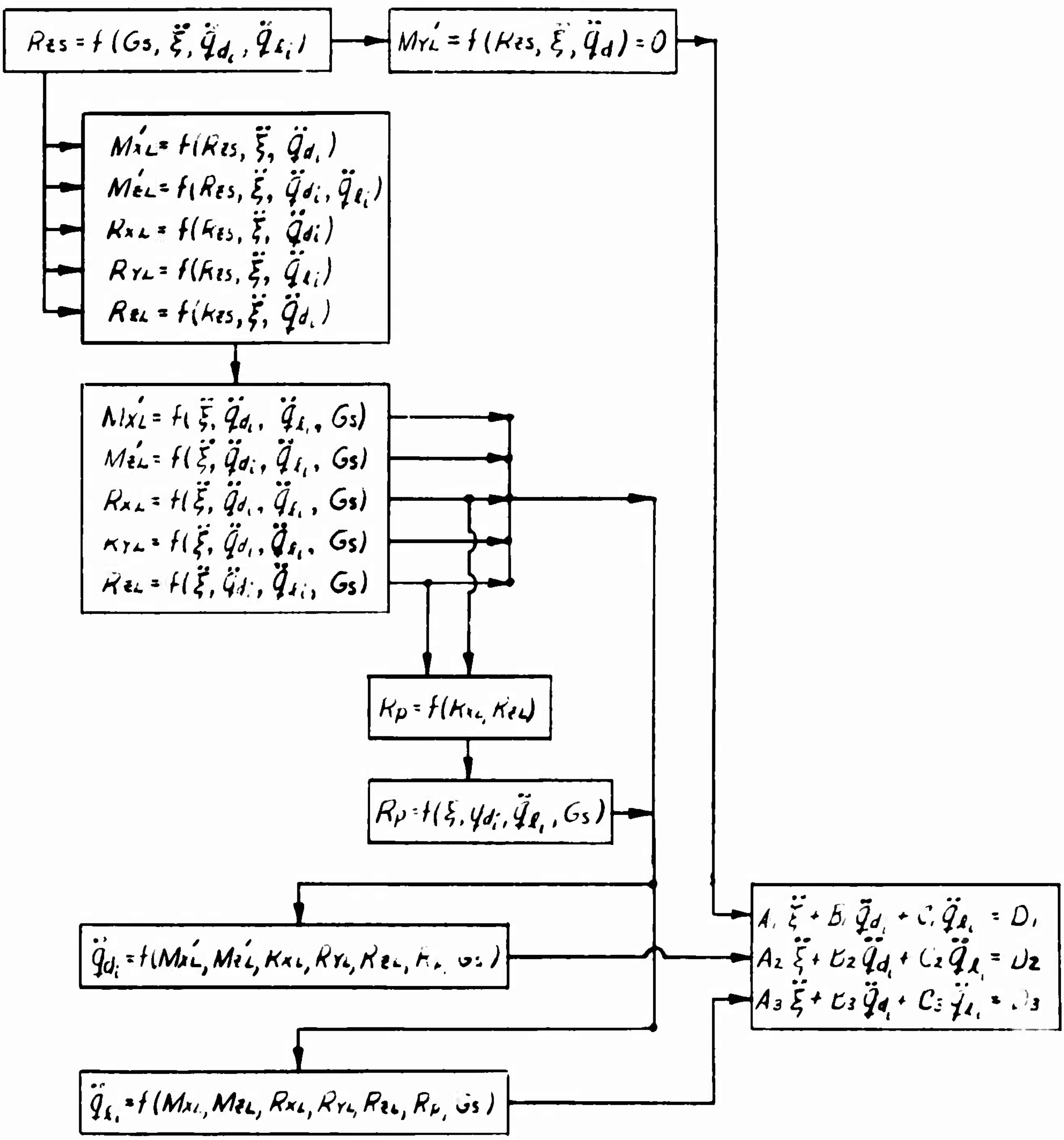

4.4 Nomenclature

Symbols:

X_D, Z_D	= Longitudinal and vertical motion of the airplane C.G., respectively
θ, φ	= Pitch and roll motion about the airplane C.G., respectively
ξ, β	= Angular motion of fork and torque arm, respectively
ξ_j, Q_{d_i}, Q_{l_i}	= Flexible motion of the airplane and landing gear in the fore and aft and lateral directions, respectively
S	= Stroking motion of the oleo capsule
$\vec{r}, \vec{\omega}, \ddot{\vec{R}}$	= Position, angular velocity, and acceleration vectors, respectively
L, D, M_θ	= Aerodynamic lift, drag, and pitching moment, respectively
$G, \mathcal{F}_j$	= Landing gear oleo and generalized force, respectively
T	= Tire force
R, M'	= Reaction forces and moments, respectively
I, J	= Moments and products of inertia, respectively
m, W	= Mass and weight, respectively
C, ω	= Structural damping coefficient and vibration frequency, respectively
ϕ, ϕ'	= Mode shape and slope of mode slope, respectively
σ	= Inclination of oleo strut with respect to a fuselage station
l	= Length along a particular landing gear component
X, Y, Z	= Particular coordinate dimensions
μ, ν, λ	= Direction cosines

Subscripts:

X, Y, Z	= Particular coordinate direction
D, L, l, S, P, A, T, O	= Parameter with respect to deck, fork, torque arm, lower oleo, drag brace, axle, strut trunnion, and upper oleo, respectively
E	= Extended
$C.G.$	= Center of gravity
j, k	= Airplane symmetric and anti-symmetric modes of vibration, respectively
i	= Nose, right, or left main gear
LGA, lGA, PGA, TGA	= Fork, torque arm, drag brace, and strut trunnion to gear attach point
B	= Parameter with respect to the body axis system
REF	= Reference plane for airplane flexibility
SPA, LPA, BPA	= Oleo, lever, and brace to post attach point
SLA	= Oleo to lever attach point

The use of $S\theta$, $C\theta$, etc. is meant to imply the normal trigometric functions sine and cosine of the respective angle. Also, the use of a single dot above a symbol is meant to imply differentiation with respect to time.

CONCLUSIONS AND RECOMMENDATIONS

5.0 CONCLUSIONS AND RECOMMENDATIONS

5.1 Conclusions

1. Penetrometer penetration rate as well as probe shape must be considered when converting penetrometer data to soil static pressure. A penetration rate as low as 0.6 inches per second can significantly alter the soil static pressure.

2. Soil dynamic strength is a function of the vertical as well as horizontal motion of the tire. For example, the OV-10A effective impact velocity is estimated to be three times the value of the maximum sink speed.

3. Due to soil dynamic strength, the OV-10A was able to taxi over and land successfully at sink speeds as great as 16 feet per second and with soil penetrometer readings as low as 40 (see Appendix A1). This static strength level is a factor of three softer than it was originally expected that the OV-10A would be able to operate satisfactorily.

4. Observations of the soil data indicated a large variation of soil strength characteristics. Thus, to adequately describe the soil static and dynamic strength, penetrometer and drop test readings should be taken at intervals no greater than the footprint length apart.

5. The inertia drag coefficient must be obtained experimentally.

6. The soil-tire and landing gear-aircraft interactions result in a system of twenty non-linear coupled second order differential equations.

5.2 Recommendations

1. Perform additional cylinder drop test data at impact velocities up to 60 feet per second to obtain a sufficient range of soil dynamic strength values.

2. Perform additional soil tests to evaluate the soil inertia drag coefficient.

3. Mechanize the soil-tire and landing gear-aircraft interaction equations on a hybrid (analog-digital) computer so that correlation between experimental and analytical aircraft response values may be attempted.

4. Perform additional study to provide data and criteria for tire selection relative to flotation based upon the dynamic influences from soft soil-tire interactions as developed in Section 3.0.

APPENDIX A1

SOIL STATIC AND DYNAMIC DATA

TABLE OF CONTENTS

List of Symbols

R = Rigid cylinder radius

b = Rigid cylinder length

z = Sinkage depth

R_v = Total static force acting on the cylinder

t_p = Plate thickness

n = Number of plates of thickness tp

r_m = Plate thickness parameter $(0 < r_m < 1)$

i = Plate number

X_i = Length of plate i

z_i = Depth of plate i

A_i = Effective area of plate i

$P_g(z_i)$ = Static soil pressure at depth z_i

R_{v_i} = Static force acting on plate i

$K(z)$ = Soil stiffness coefficient as a function of sinkage depth

$C(z,\dot{z},\dot{z}_{im})$ = Soil dynamic damping coefficient as a function of sinkage depth, penetration velocity, and the cylinder-soil impact velocity

DISCUSSION

The experimental data used in the soil study was obtained from six general test locations. The map of the Blackstone Army Air Base on Page A1-9 and the sketch of the landing site area at the apex of runways 21 and 26 presented on Page A1-10, may be used to locate the test sites. Test location number 1 was on the centerline of Site II at field station 80. Test locations number 2 and 3 were on Site II at field station 80, twenty-five feet to the right and left, respectively, of the centerline. Test locations 4, 5, and 6 were in the touchdown areas of the left main gear, right main gear, and nose gear, respectively, of the OV-10A landing number 226. The OV-10A landing points are defined on the touchdown points and terrain contour log presented on Page A-11.

Two types of experimental tests were conducted at the test locations. One test was used to indicate the static strength properties of the soil. The second test provided data that represented the dynamic characteristics of the soil. Data from both tests was utilized to determine the dynamic strength of the soil.

An airfield penetrometer (No. 6635-639-8973) provided by the U. S. Army Aviation Material Laboratories of Fort Eustis, Virginia was used to obtain data that was required to determine the soil static strength. The penetrometer, depicted on Page A1-15, indicates the pressure required to penetrate a cone-shaped probe into the soil. The depth of cone penetration (measured from the cone apex) and corresponding penetration pressure were recorded. Penetrometer data of test location number 1 was not obtained.

A special cylinder drop test apparatus, depicted on Page A1-16, was used to obtain data that represented the dynamic characteristics of soil. Instrumentation on the drop test apparatus measured the displacement, velocity, and acceleration of a rigid steel cylinder that could be set up to free fall or be accelerated onto the soil. Four 1/4 inch bungees attached to the cylinder carriage and one of six positions (holes) on the frame provided the accelerated drop tests.

The free fall drop test resulted in a soil impact velocity of 11.8 feet per second. The six accelerated drop tests with the bungees attached to hole position 1, 2, 3, 4, 5 or 6 resulted in respective soil-cylinder impact velocities of 11.1, 12.6, 14.2, 15.5, 16.7, and 17.5 feet per second. As a result of an improper bungee length, all cylinder drop test data obtained with the bungee attached at hole 1 was disregarded.

The data from each of the six test locations was obtained in a consistent manner. At the initial position of each general test location a penetrometer test and a free fall cylinder drop test (designated Hole 0) were conducted. A second penetrometer test and cylinder drop test with the bungee connected at hole 1 were performed at a position of six inches down field of the initial position. The testing process continued in the same manner at six inch intervals for each of the five remaining accelerated drop tests. The resulting raw penetrometer data is presented in tabular form on Pages A1-19 and A1-20. The pertinent cylinder drop test displacement, velocity, and acceleration data is presented on Pages A1-23 through A1-45.

The raw soil penetrometer data obtained from all the cylinder drop test sites was plotted as penetrometer pressure versus penetration depth. Nine different curves were apparent and arbitrarily identified a Terrain Hardness Curves A through I. Six of these curves all differ in ultimate hardness and shape and, thus, formed the basis for soil type differentiation. These six plots of penetrometer data are presented on Pages A1-49 through A1-54. The data for curves E, F, and H was scattered and insufficient to uniquely define a curve.

Page A1-57 presents the shifted penetrometer data curves as discussed in paragraph 3.3.2.1. Page A1-61 presents the final static soil pressure curves. These curves are a direct indication of the static load supporting ability of the soil. Corresponding values of static soil pressure and penetrometer reading may be determined for any specific soil element by correlating the selected penetrometer data, presented on Pages A1-49 through A1-54, with the static soil pressure curves, presented on Page A1-61. Consider, for example, the static load supporting ability of the soil surface of Terrain Hardness A which is representative of the softest soil on which the OV-10 operated. The average penetrometer reading over the first inch of penetration was approximately 40. The corresponding average static soil pressure value is approximately 20 psi. Thus, a surface penetrometer value of 40 is representative of a soil that can support a maximum static load of 20 pounds per square inch with some soil deformation but without vertical shearing.

The load supporting ability of the soil measured in CBR units is not available for the various Terrain Hardnesses. Soil tests to determine CBR values were not conducted and a general method of transformation between penetrometer values and CBR units does not exist.

The method for determining the static force acting on the rigid cylinder is developed on Pages A1-63 through A1-67. Application of this method along with the static soil pressure curves and cylinder drop test data are combined as discussed in paragraph 3.3.3 to determine the soil damping coefficients presented on Pages A1-71 through A1-80. Plots of the soil damping coefficients as a function of time and vertical velocity are given on Pages A1-83 through A1-88 and Pages A1-91 through A1-96, respectively.

In addition to the penetrometer data associated with the cylinder impact tests, penetrometer measurements were made at each of the OV-10A landing impact areas. This data will be required for correlation purposes between predicted and experimental load values. The data is presented on Pages A1-99 through A1-118. Specifically, the plots on Pages A1-99 and A1-100 show the effects of water added to the surface of Site II to make it softer. The tables and curves presented on Pages A1-101 through A1-106 present a general view of the soil hardness for Site II on the day of the tail down landings. Note that the symbol I used in the tables is meant to imply a reading beyond the range of the penetrometer. A value above 300 indicates essentially a rigid surface. The remaining penetrometer data presented on Pages A1-109 through A1-118 was taken after each landing at the impact points for all three landing gears. There are three readings given for each landing gear. The sketch under ℄ (i.e.,) is meant to depict the shape of the terrain lateral profile and the given dimensions apply to this sketch only. The left and right values are measured in undisturbed soil to the left and right of the tire track, while the ℄ value is measured in the compacted soil on the centerline of the tire track.

Terrain longitudinal profiles of Site II are given on Pages A1-121 through A1-125. As indicated by the graph symbol (e.g., GRAPH VII, etc.) only thirteen profiles were measured. The location of these are given by the log on Page A1-11. It was felt that these 13 profiles were adequate to describe the contour of Site II.

TEST SITE LOCATIONS

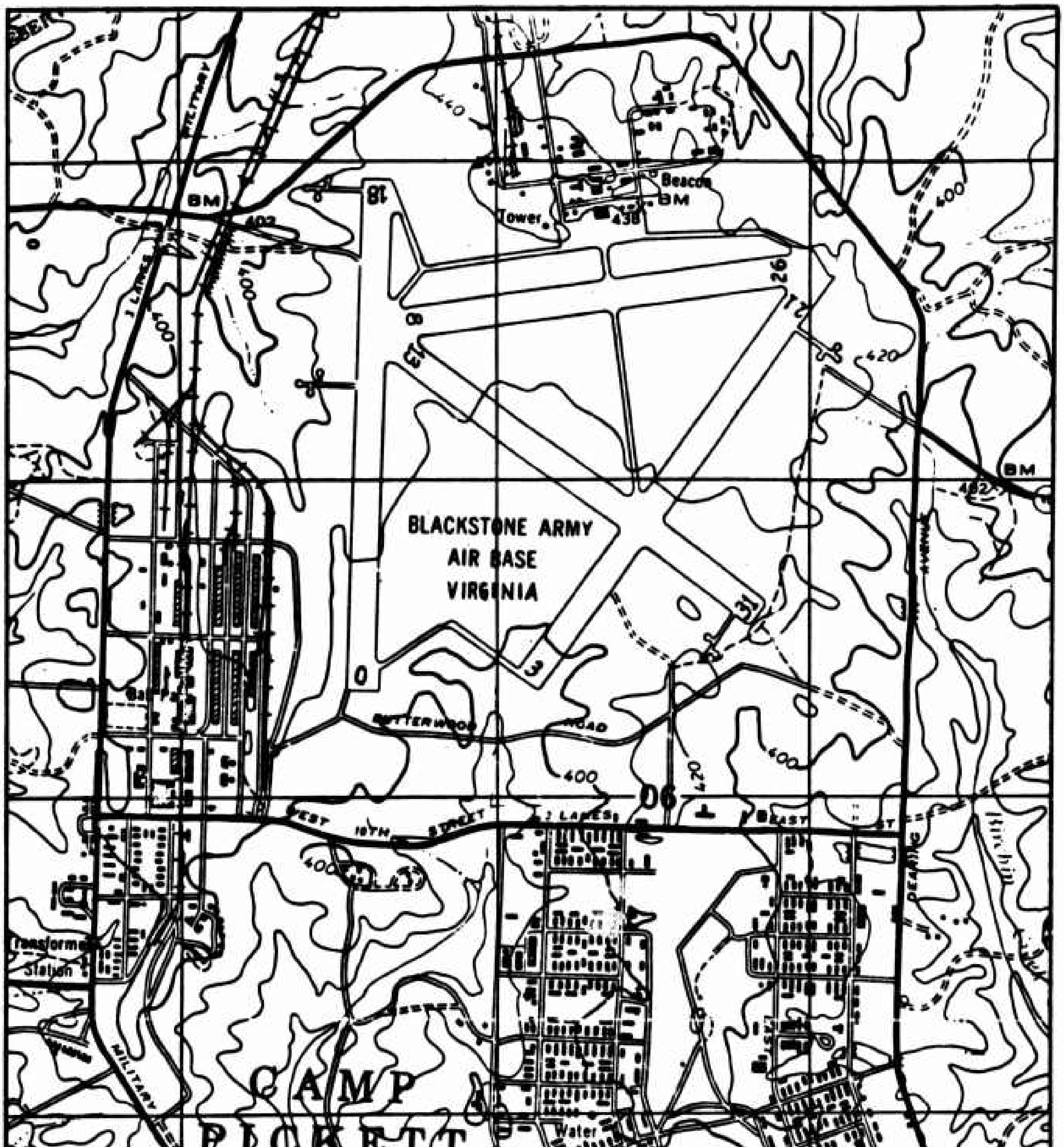

PRECEDING PAGE BLANK

LANDING SITE LOCATION

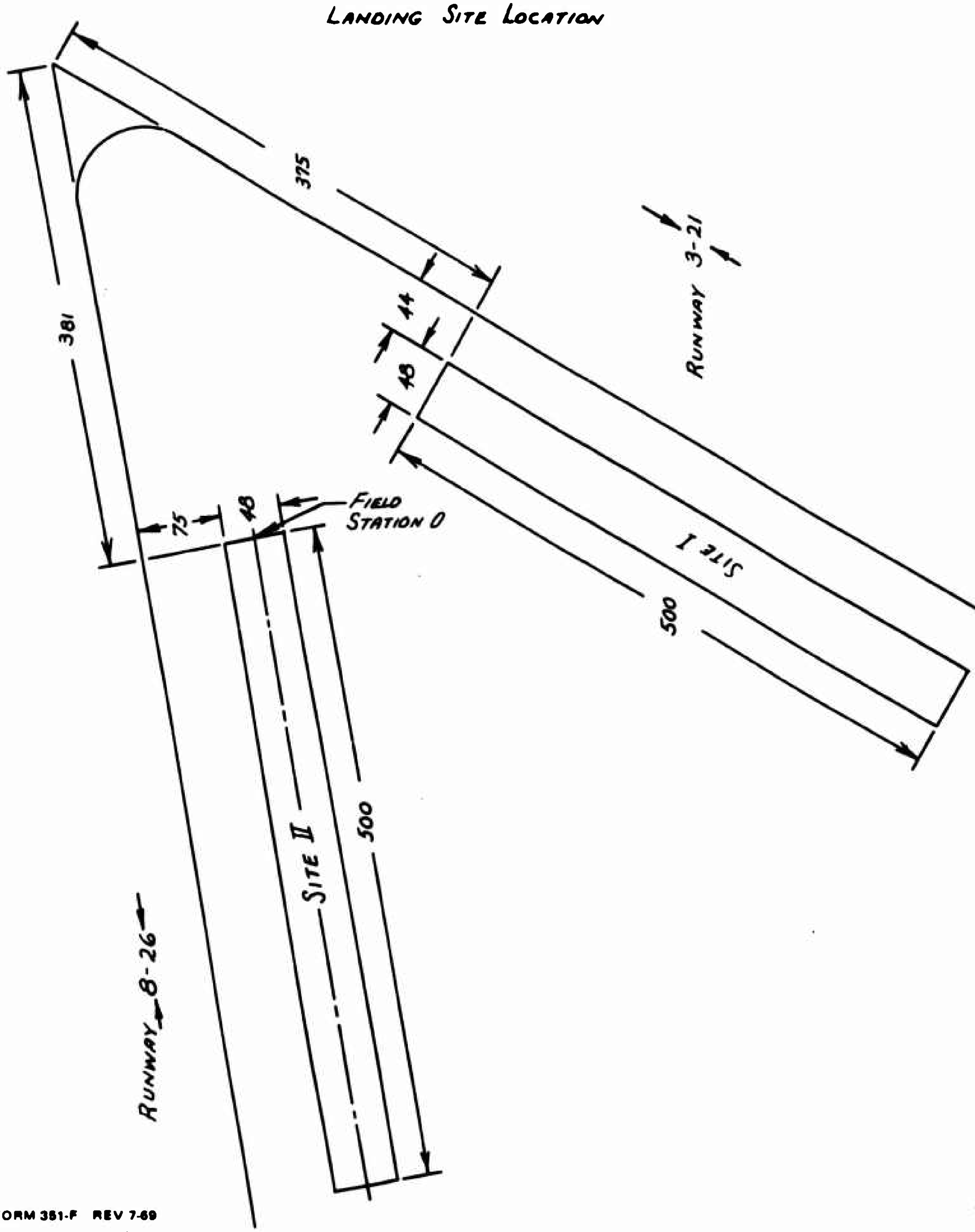

TOUCHDOWN POINTS & TERRAIN CONTOUR LOG

DATE	FLT. NO.	LEFT MAIN GEAR			NOSE GEAR			RIGHT MAIN GEAR		
		X (FROM 0 REFERENCE)	Y (FROM ₵)	GRAPH SYMBOL	X (FROM 0 REFERENCE)	Y (FROM ₵)	GRAPH SYMBOL	X (FROM 0 REFERENCE)	Y (FROM ₵)	GRAPH SYMBOL
5/7	208	0	16'11½" LT	I	0	9'6" LT	II	0	2'6" LT	III
	209	0	2'6" LT		0	4'6" RT	IV	0	11"11½" RT	V
5/10	215	25'	14' LT	VI	40'	6'6" LT	VII	25'	6" RT	
	216	38'6"	10'6" LT			3' LT		32'	4'5" RT	
	217	35'4"	8'9" LT	VIII	(SEE NOTE 3)					
	218	50'	8'5" LT		90'	5" LT		59'	6'9" RT	
	219	76'6"	19' LT		101'8"	12' LT		78'8"	4'6" LT	
	220	58'	24' LT	IX	80'	16'6" LT		58'	8'5" LT	
	221	90'	3'6" LT		112'	5' RT		88'	11'7" RT	
5/11	223	148'	9'7" LT		175'	1'5" LT		142'	5' RT	
	224	95'	22'4" LT		110'	13'10" LT	X	90'	7'6" LT	
	225	180'	2'6" LT		193'	5'6" RT		180'	12'4" RT	
	226	148'	7'5" LT	XI	152'	On ₵	XII	148'	7'5" RT	XIII

NOTES:

1. LT implies LEFT.
2. RT implies RIGHT.
3. Aircraft traveled diagonally from LT to RT across site: 90' from 0 Reference Left Main Gear was at 7'6" LT of ₵ .

SOIL TESTING APPARATUS

PRECEDING PAGE BLANK

CONE PENETROMETER

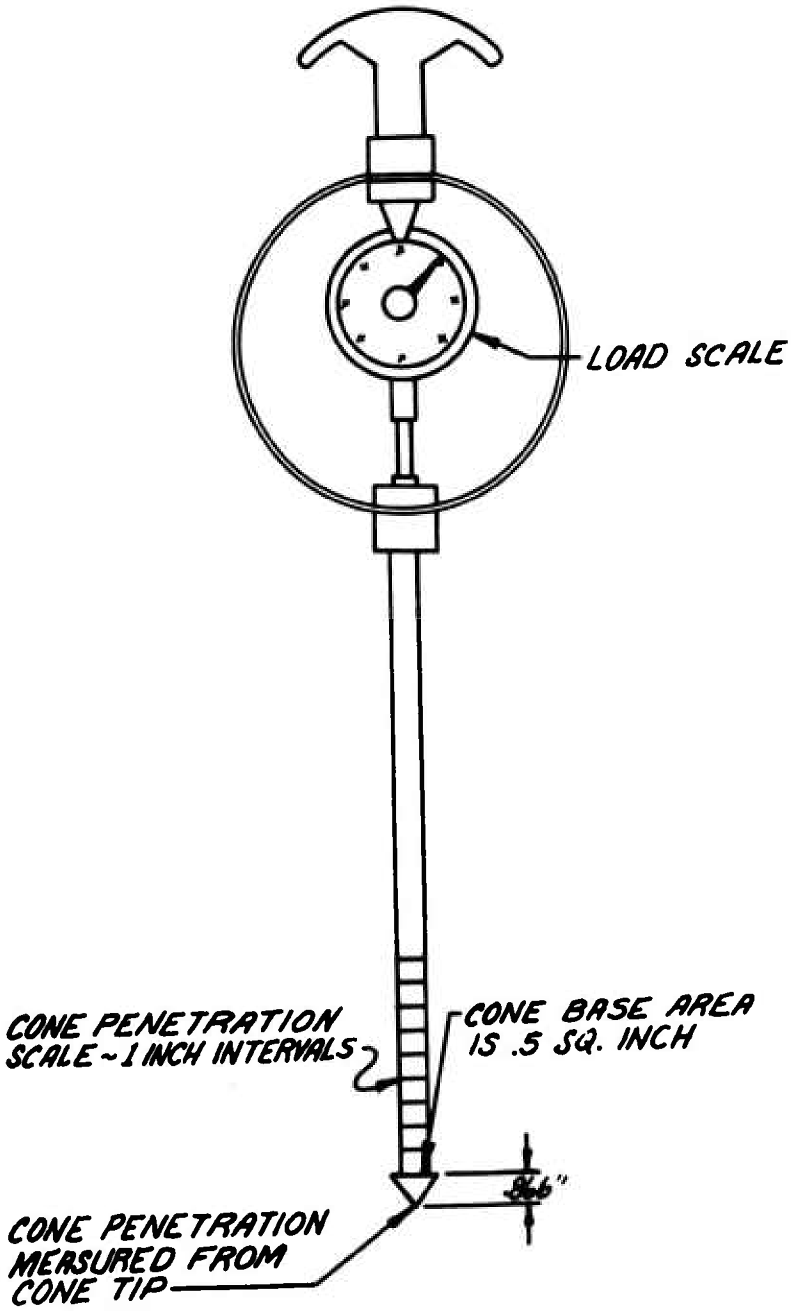

PRECEDING PAGE BLANK

CYLINDER DROP TEST APPARATUS

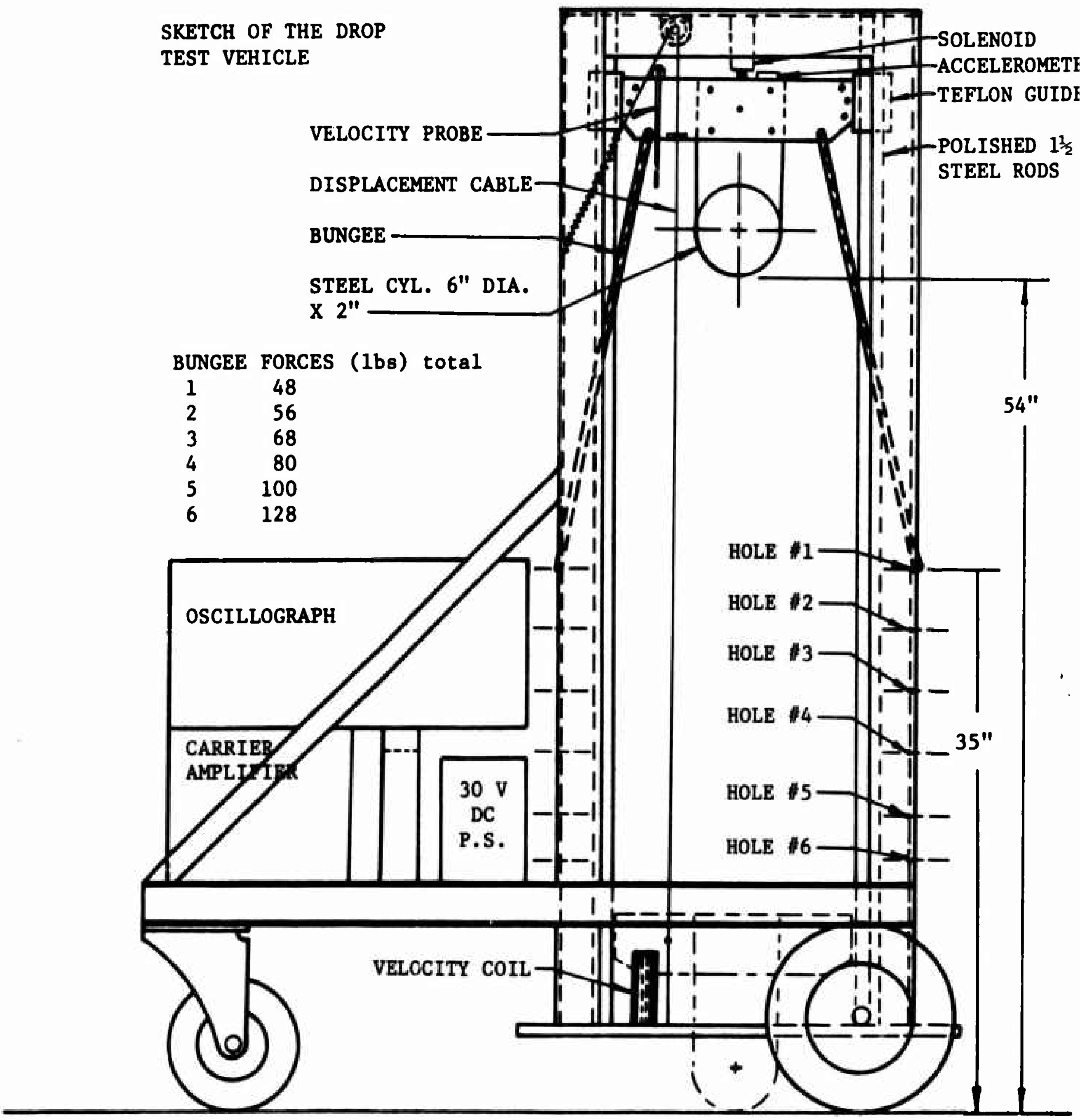

PENETROMETER DATA ASSOCIATED WITH CYLINDER DROP TESTS

PENETROMETER READINGS

TEST NO. 1 (MAY 8)
NO PENETROMETER DATA EXISTS

DEPTH (INCHES)	TEST NO. 2 (MAY 10) BUNGEE ATTACHED AT HOLE NUMBER						
	0	1	2	3	4	5	6
1	40	40	40	40	70	40	70
2	40	40	40	40	75	40	75
3	60	60	60	60	75	60	75
4	70	70	70	70	100	70	100
5	100	100	100	100	180	100	180
6	200	200	200	200	300	200	300
7	300	300	300	300		300	

DEPTH (INCHES)	TEST NO. 3 (MAY 10) BUNGEE ATTACHED AT HOLE NUMBER						
	0	1	2	3	4	5	6
1	80	40	70	80	80	40	100
2	100	40	75	100	100	40	220
3	120	60	75	120	120	60	300
4	300	70	100	300	300	70	
5		100	180			100	
6		200	300			200	
7		300				300	

PRECEDING PAGE BLANK

PENETROMETER READINGS
MAY 11
SITE NO. 2
LANDING NO. 226

DEPTH (INCHES)	LEFT MAIN GEAR - TEST NO. 4						
	BUNGEE ATTACHED AT HOLE NUMBER						
	0	1	2	3	4	5	6
1	275	270	220	175	190	185	195
2	280	260	255	165	210	205	230
3	240	240	245	175	205	210	230
4	205	185	220	205	225	180	180
5	265	220	205	215	300	160	145
6	300	265	230	230		230	190
7		300	280	300		300	300

DEPTH (INCHES)	NOSE GEAR - TEST NO. 6						
	BUNGEE ATTACHED AT HOLE NUMBER						
	0	1	2	3	4	5	6
1	200	130	135	155	165	165	150
2	165	120	130	155	145	160	160
3	230	105	135	160	150	140	140
4	300	85	160	160	155	150	150
5		185	300	155	220	220	300
6		300		300	300	300	

DEPTH (INCHES)	RIGHT MAIN GEAR - TEST NO. 5						
	BUNGEE ATTACHED AT HOLE NUMBER						
	0	1	2	3	4	5	6
1	100	120	120	120	125	80	110
2	105	120	125	115	115	85	130
3	110	140	130	110	145	75	170
4	140	190	200	300	300	65	300
5	300	300	300			180	
6						300	

CYLINDER DROP TEST DATA

CYLINDER DROP TEST DATA
TEST NO. 2, BUNGEE HOLE O
TERRAIN HARDNESS A

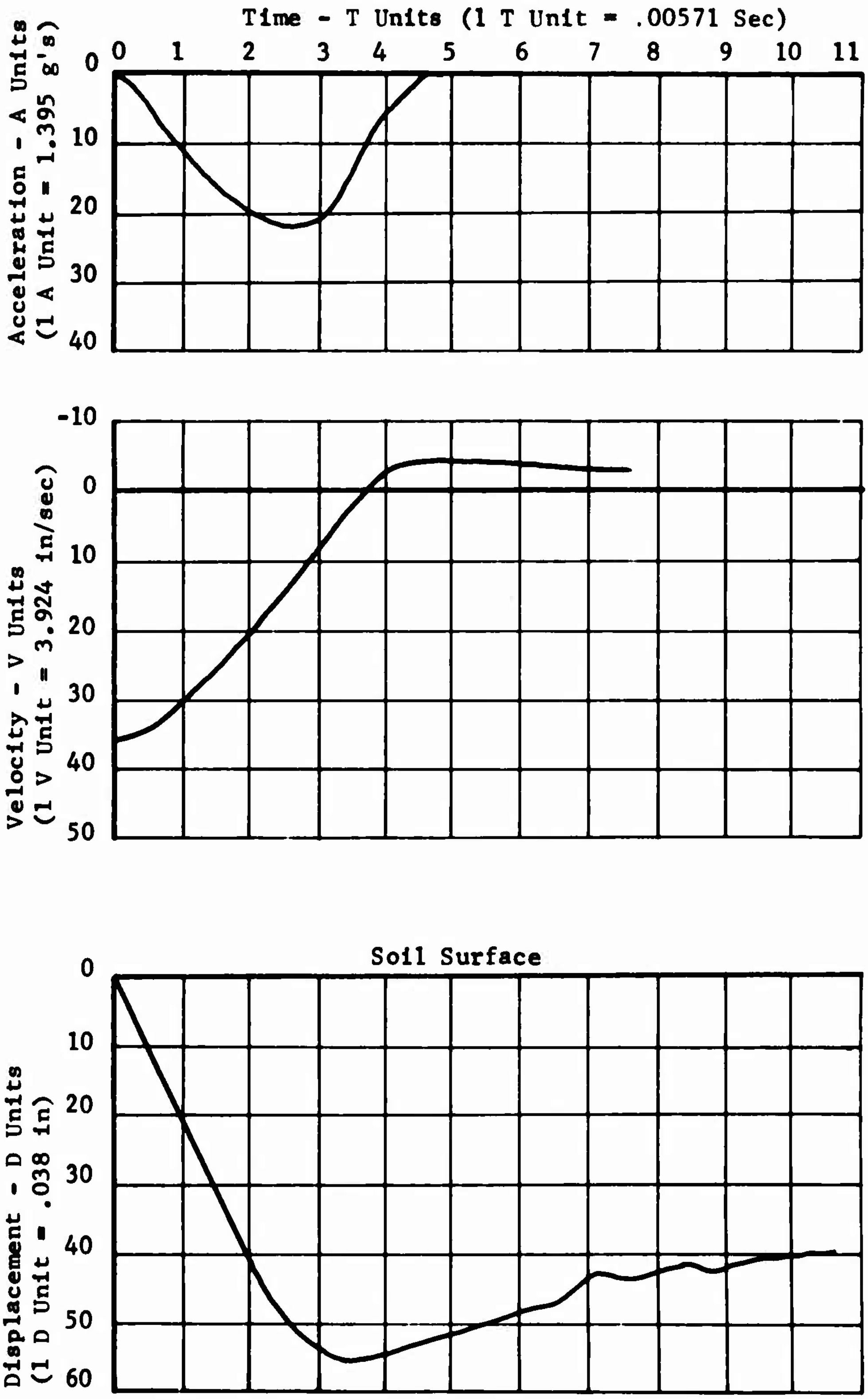

PRECEDING PAGE BLANK

CYLINDER DROP TEST DATA
TEST NO. 2, BUNGEE HOLE 2
TERRAIN HARDNESS A

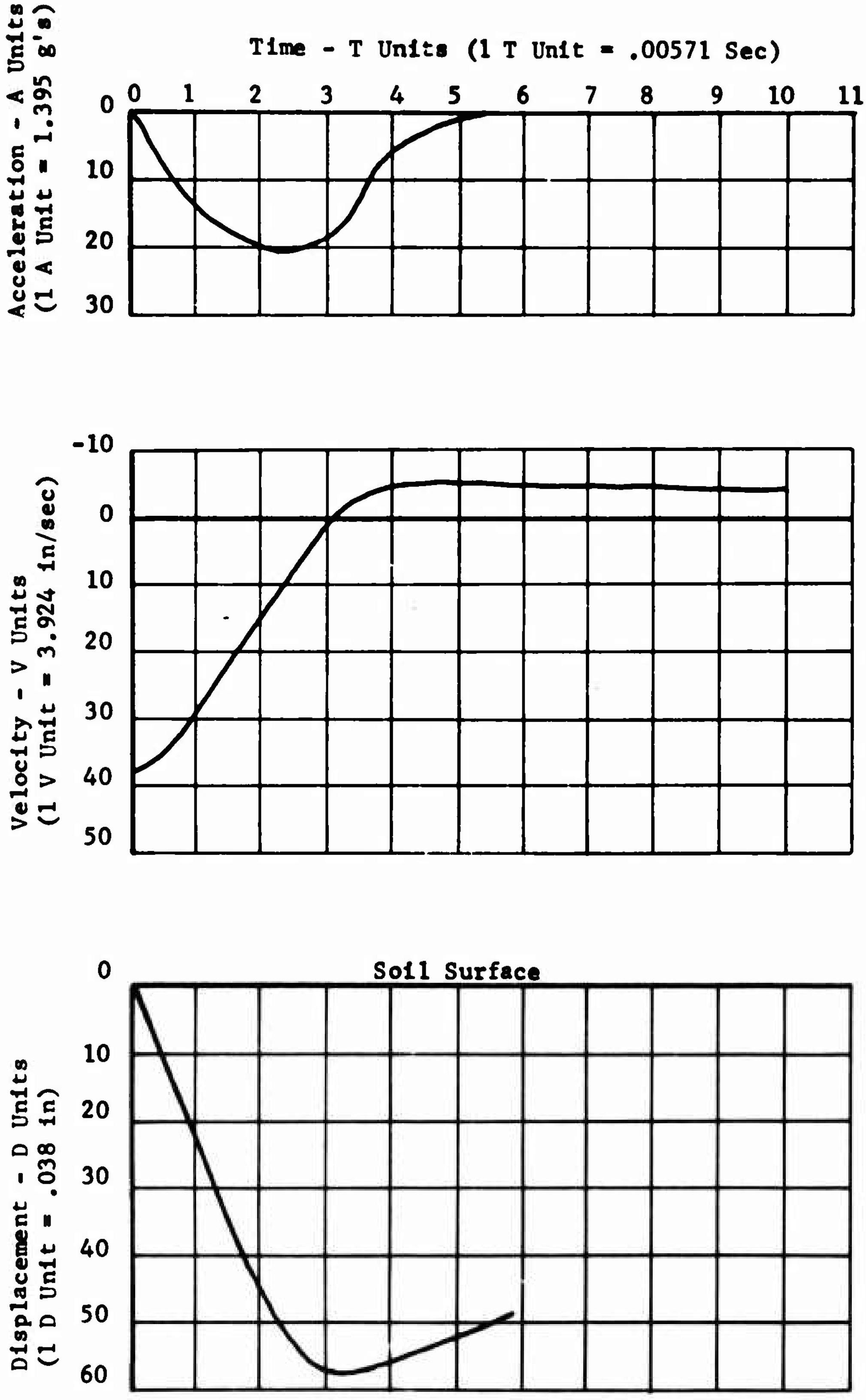

CYLINDER DROP TEST DATA
TEST NO. 2, BUNGEE HOLE 3
TERRAIN HARDNESS A

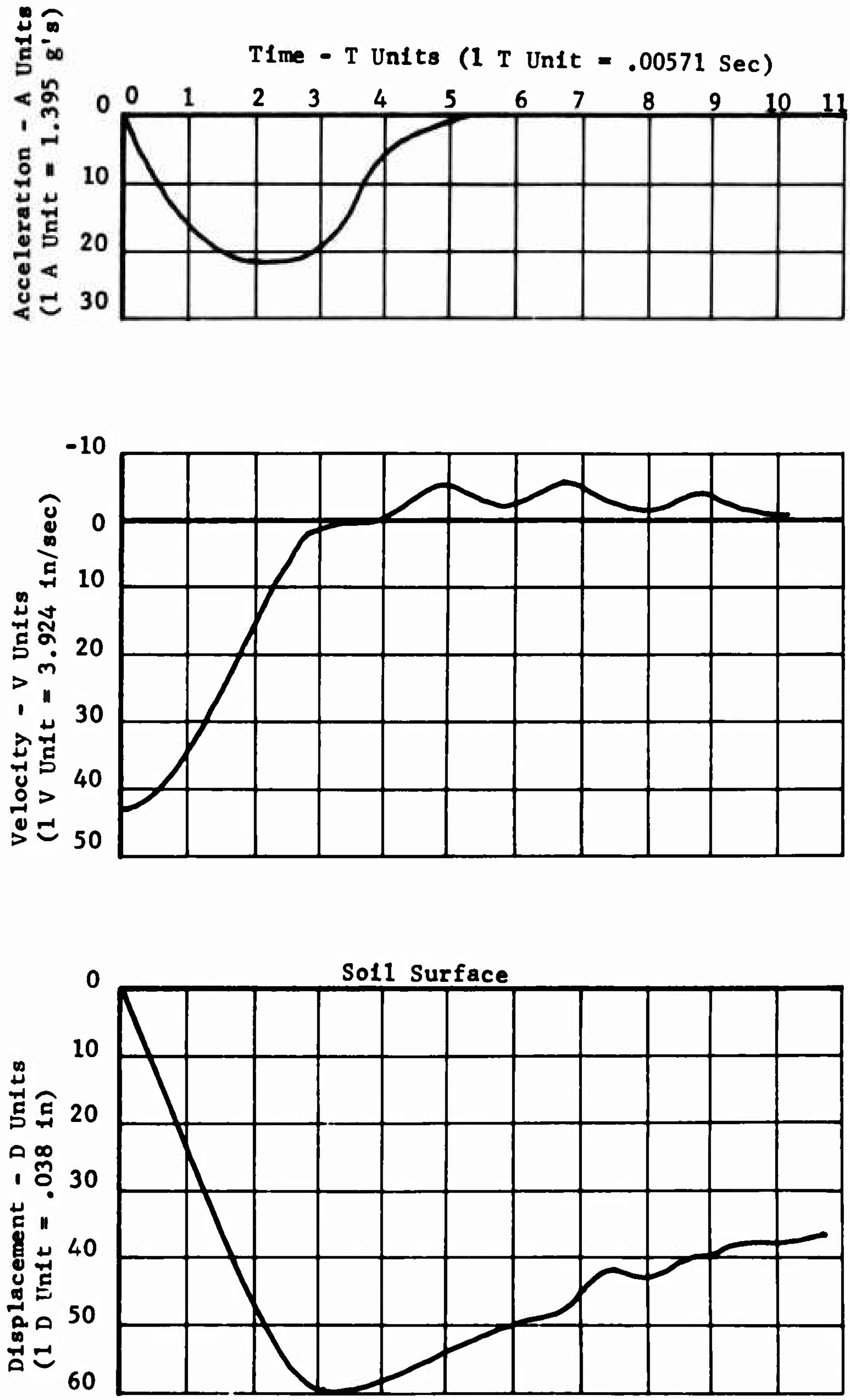

CYLINDER DROP TEST DATA
TEST NO. 2, BUNGEE HOLE 5
TERRAIN HARDNESS A

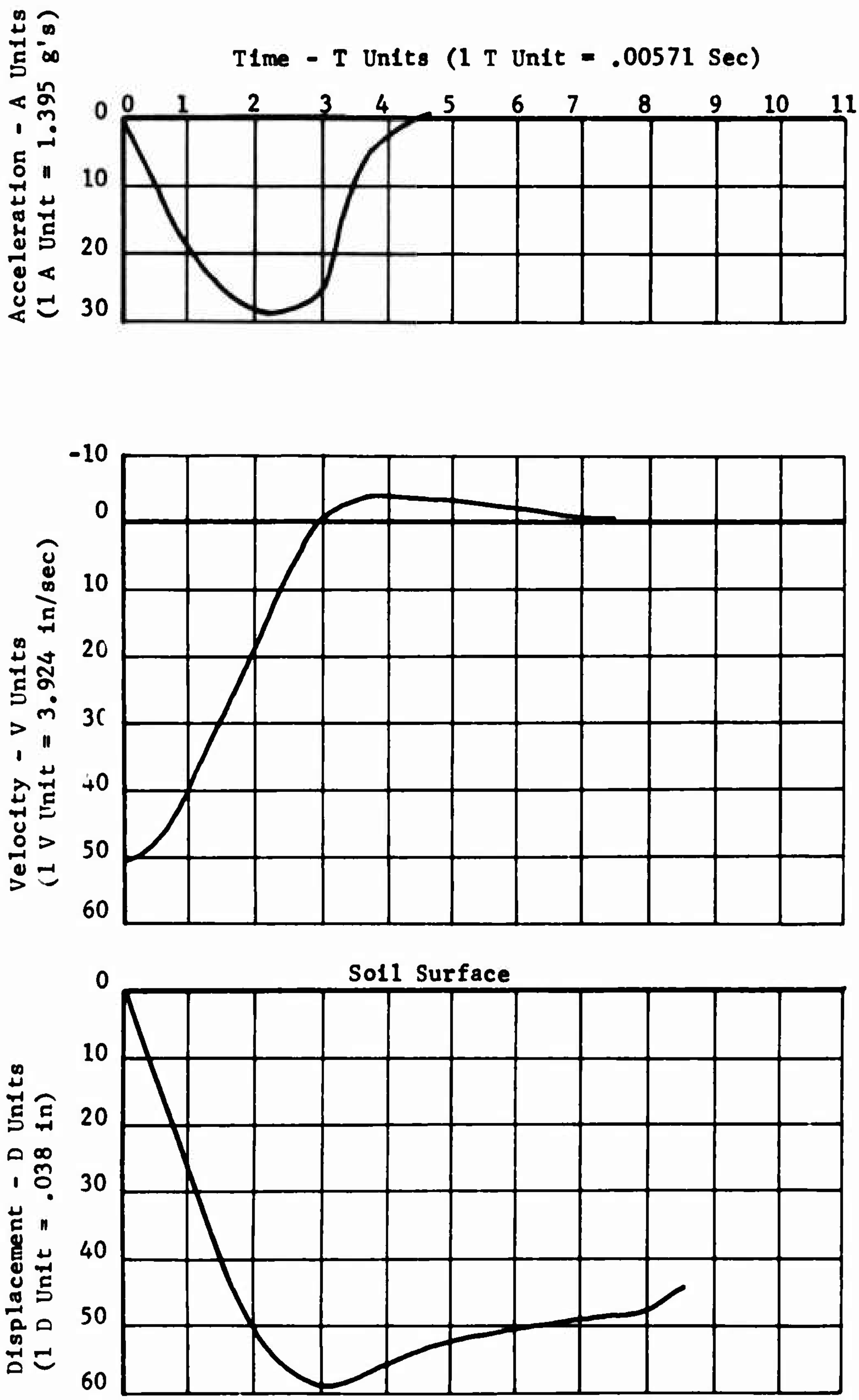

CYLINDER DROP TEST DATA
TEST NO. 3, BUNGEE HOLE 2
TERRAIN HARDNESS B

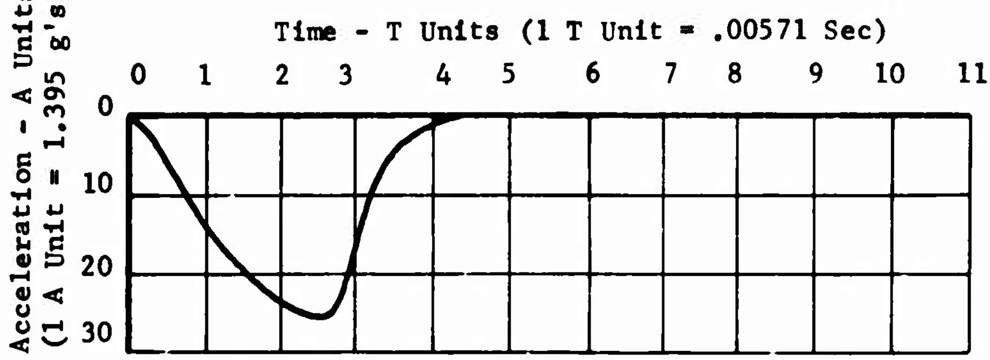

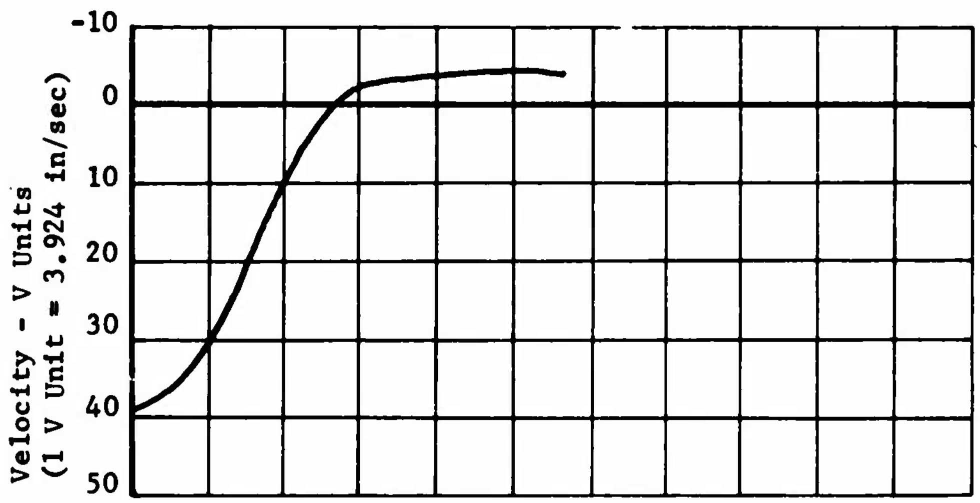

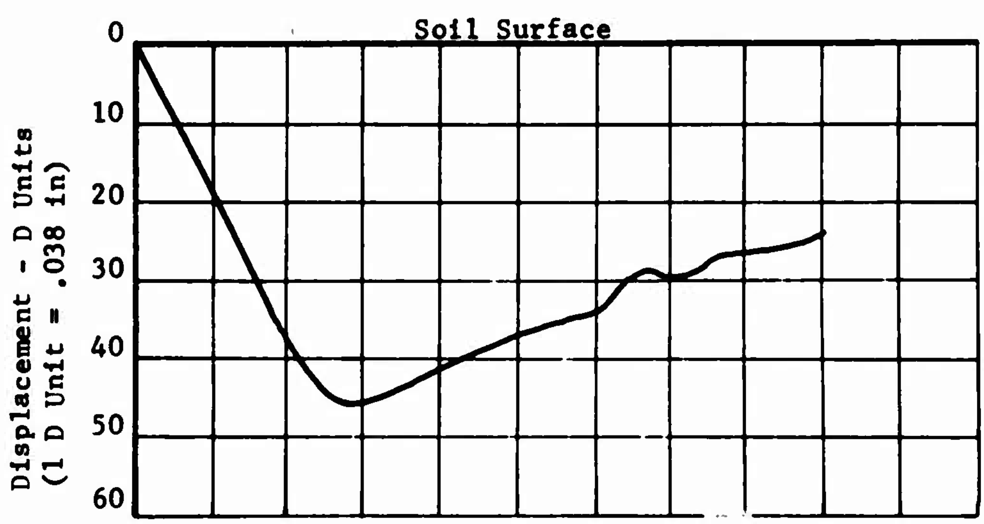

CYLINDER DROP TEST DATA
TEST NO. 2, BUNGEE HOLE 4
TERRAIN HARDNESS B

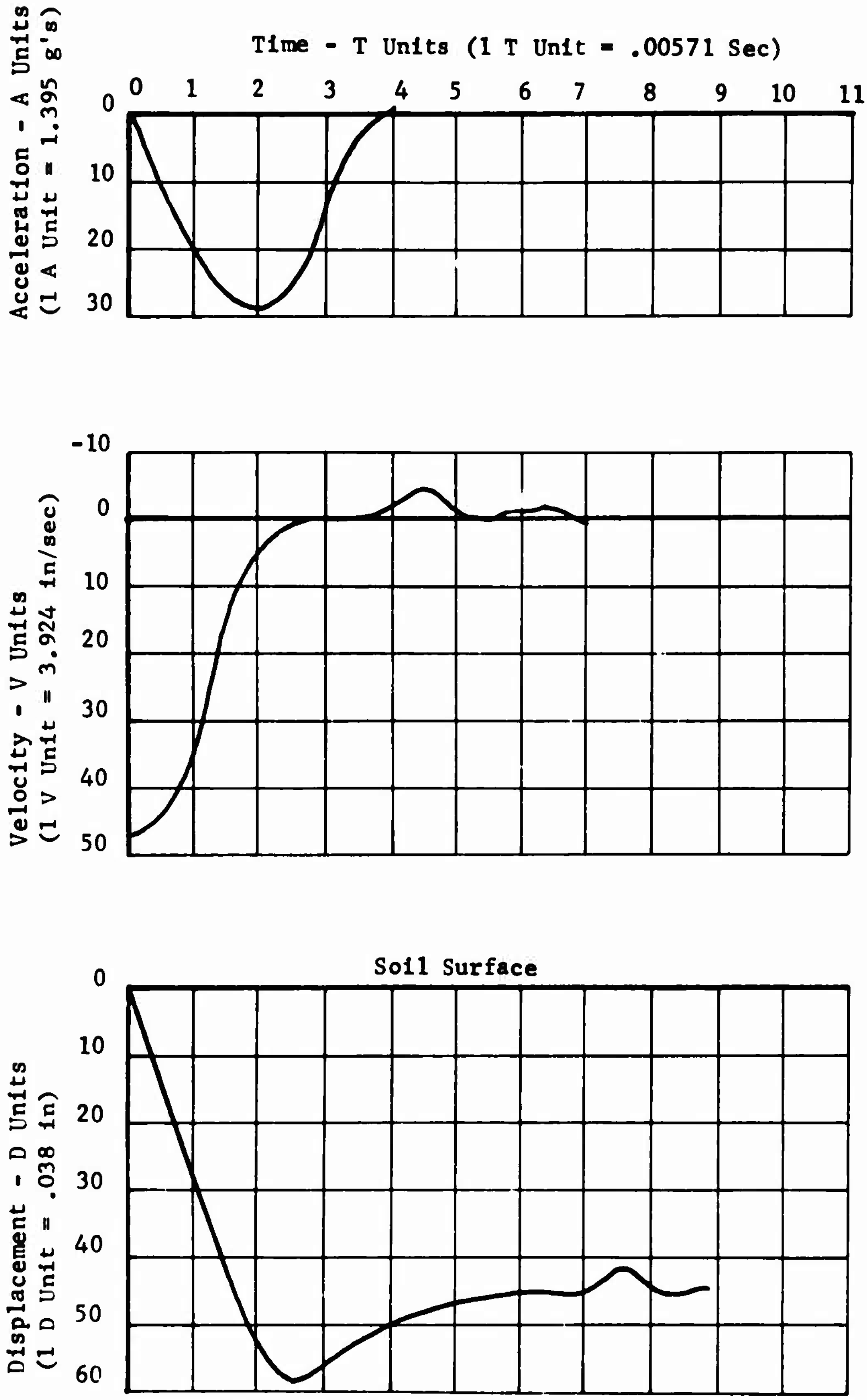

CYLINDER DROP TEST DATA
TEST NO. 2, BUNGEE HOLD 6
TERRAIN HARDNESS B

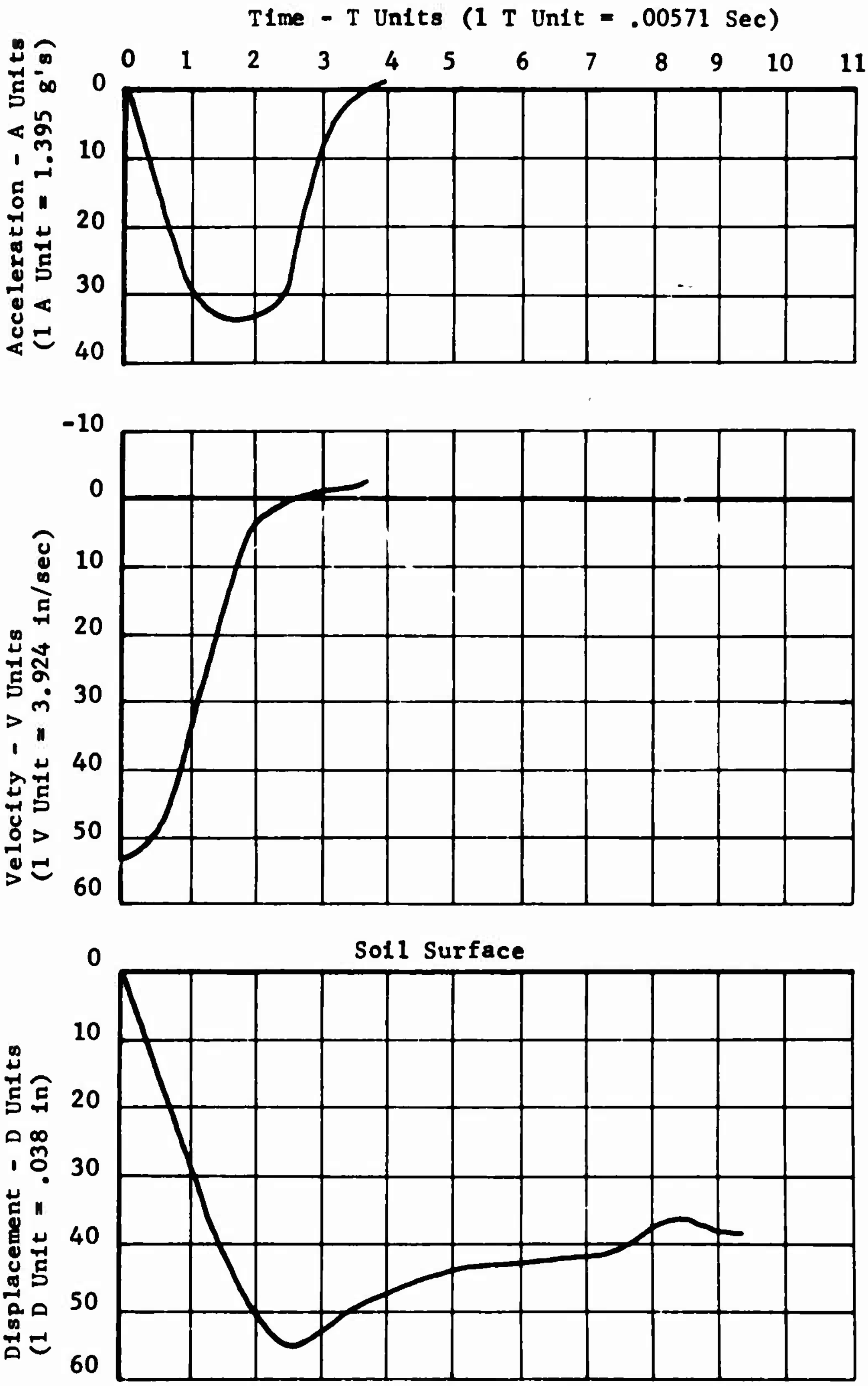

CYLINDER DROP TEST DATA
TEST NO. 6, BUNGEE HOLE 2
TERRAIN HARDNESS C

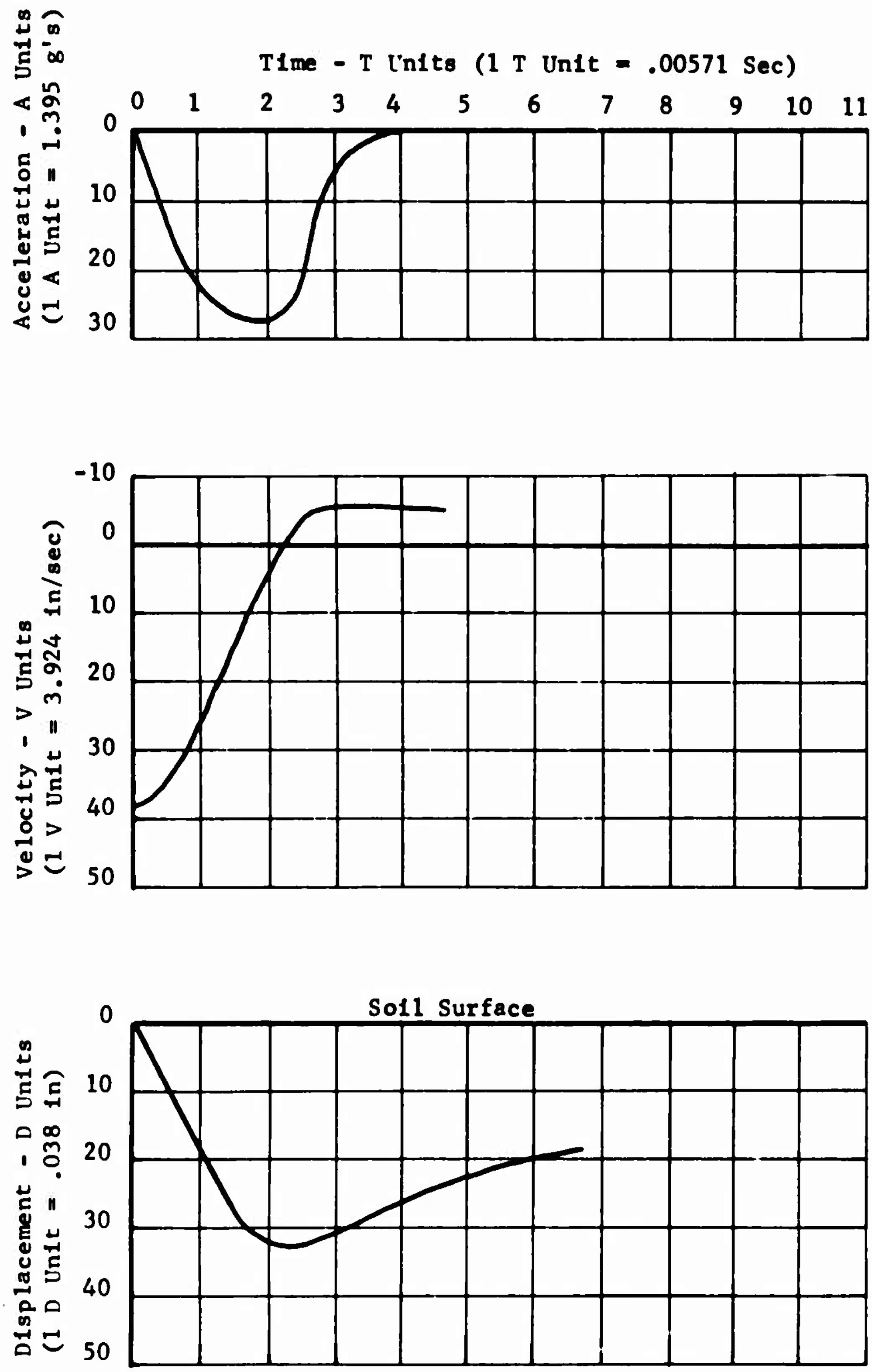

CYLINDER DROP TEST DATA
TEST NO. 6, BUNGEE HOLE 3
TERRAIN HARDNESS C

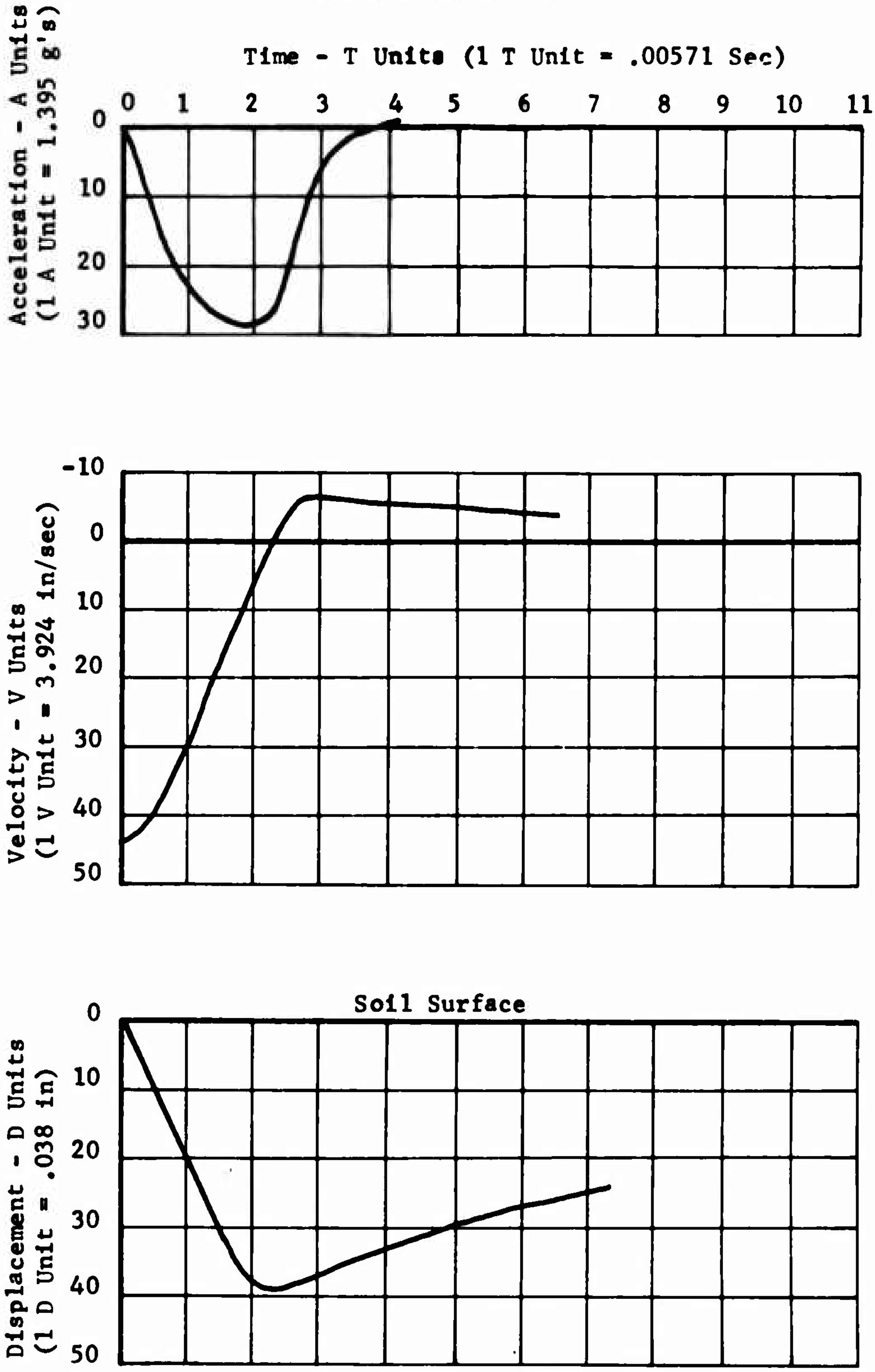

CYLINDER DROP TEST DATA
TEST NO. 6, BUNGEE HOLE 4
TERRAIN HARDNESS C

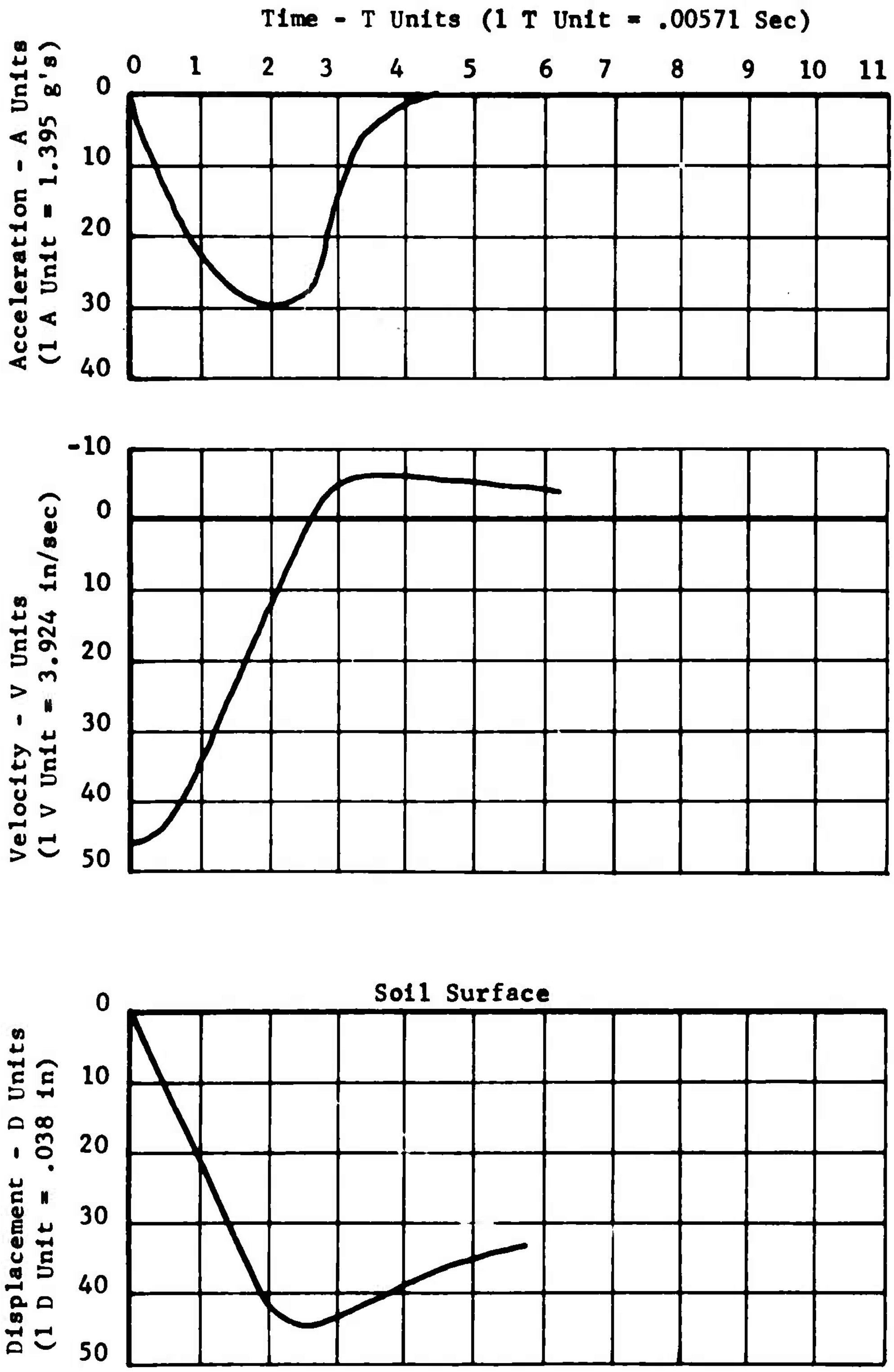

CYLINDER DROP TEST DATA
TEST NO. 6, BUNGEE HOLE 5
TERRAIN HARDNESS C

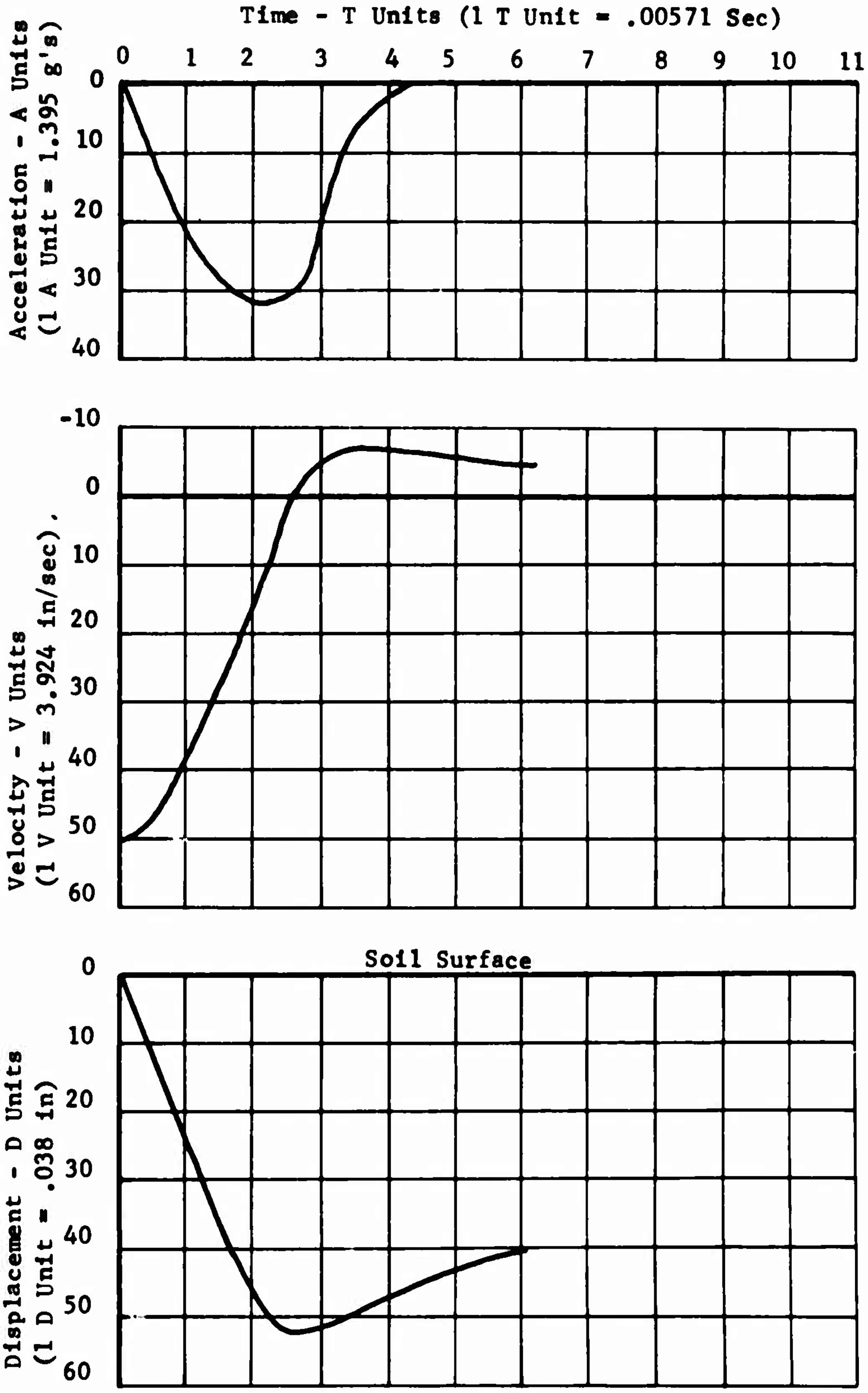

CYLINDER DROP TEST DATA
TEST NO. 5, BUNGEE HOLE O
TERRAIN HARDNESS D

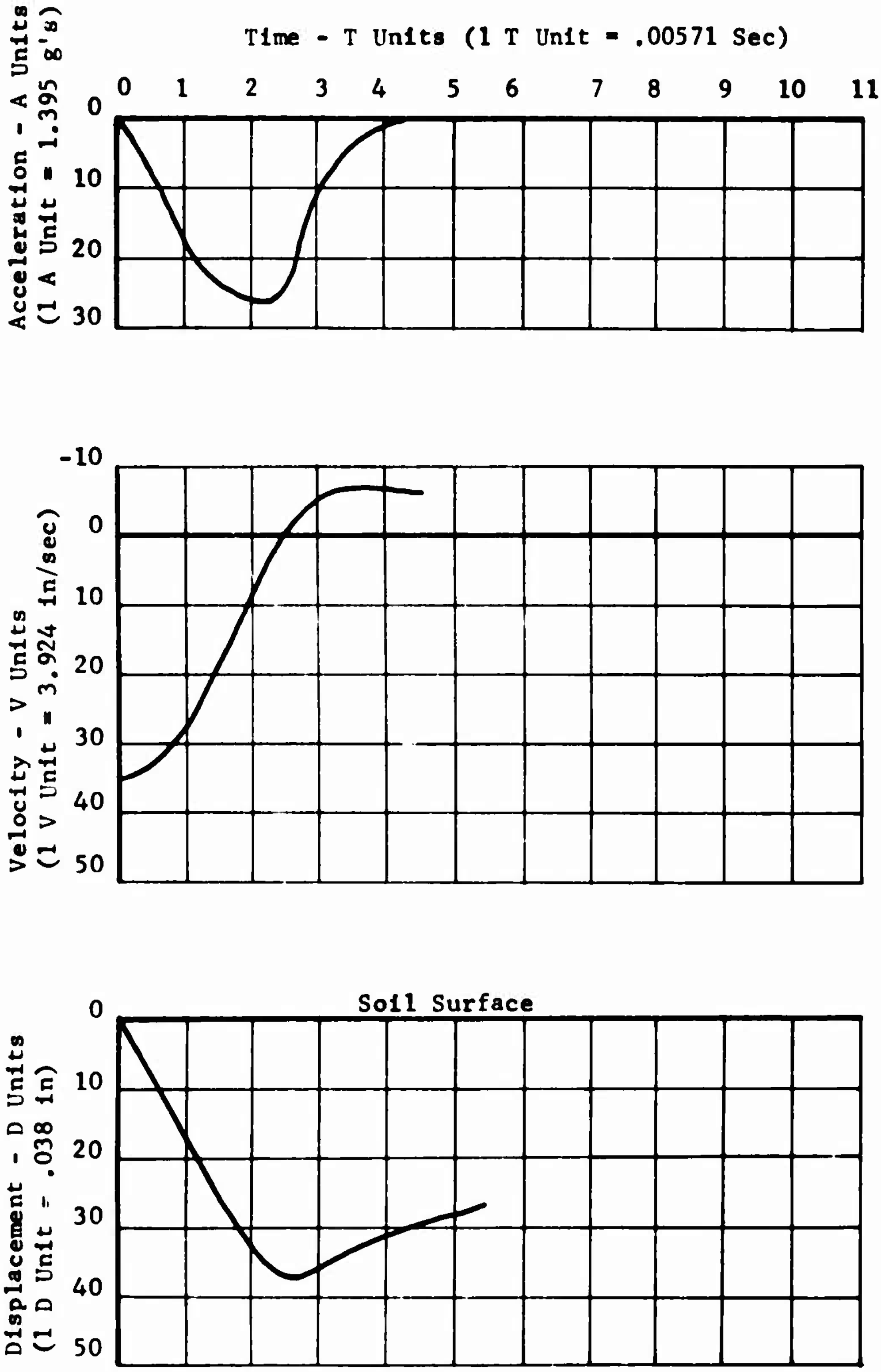

CYLINDER DROP TEST DATA
TEST NO. 5, BUNGEE HOLE 2
TERRAIN HARDNESS D

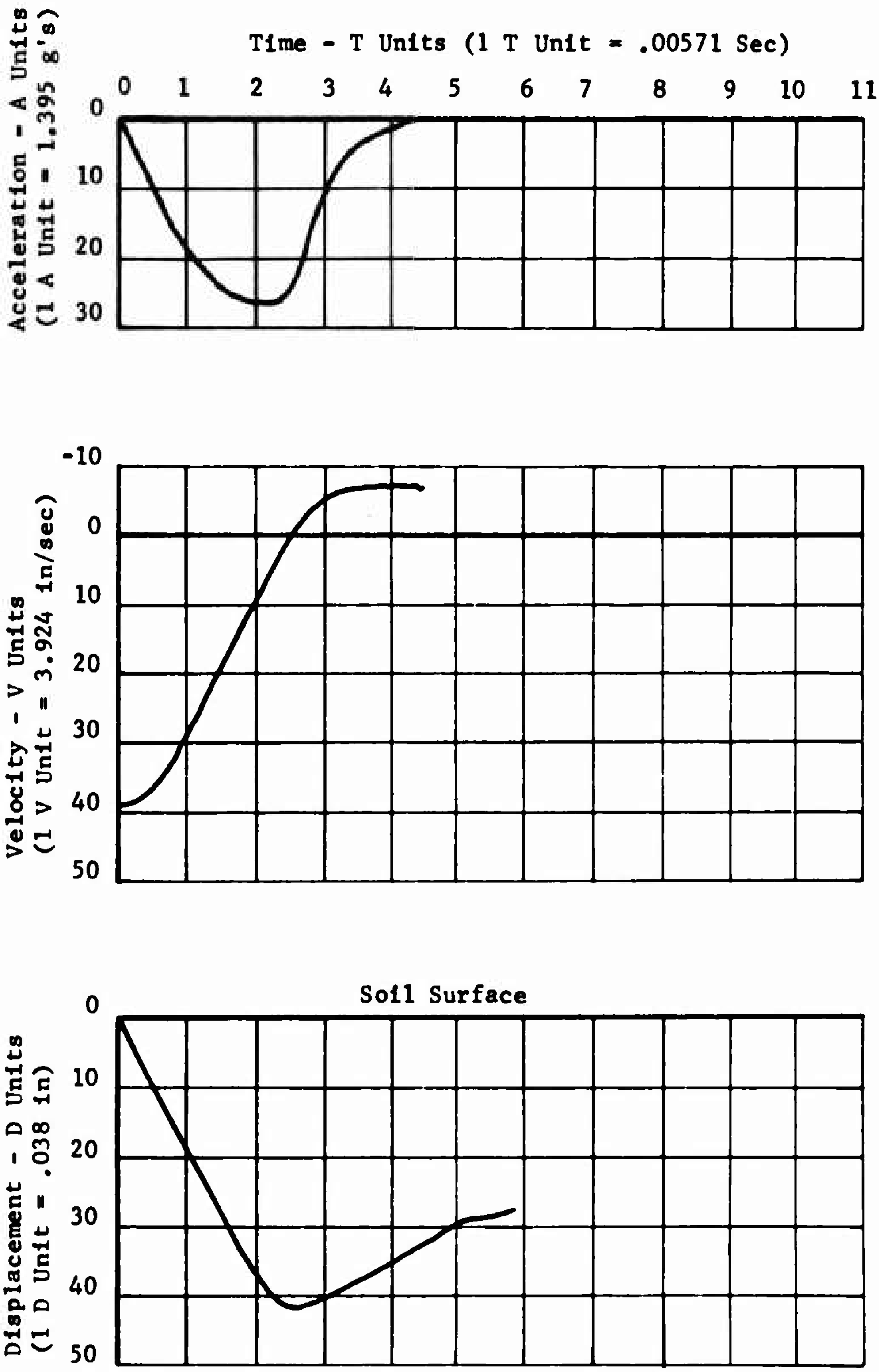

CYLINDER DROP TEST DATA
TEST NO. 5, BUNGEE HOLE 3
TERRAIN HARDNESS D

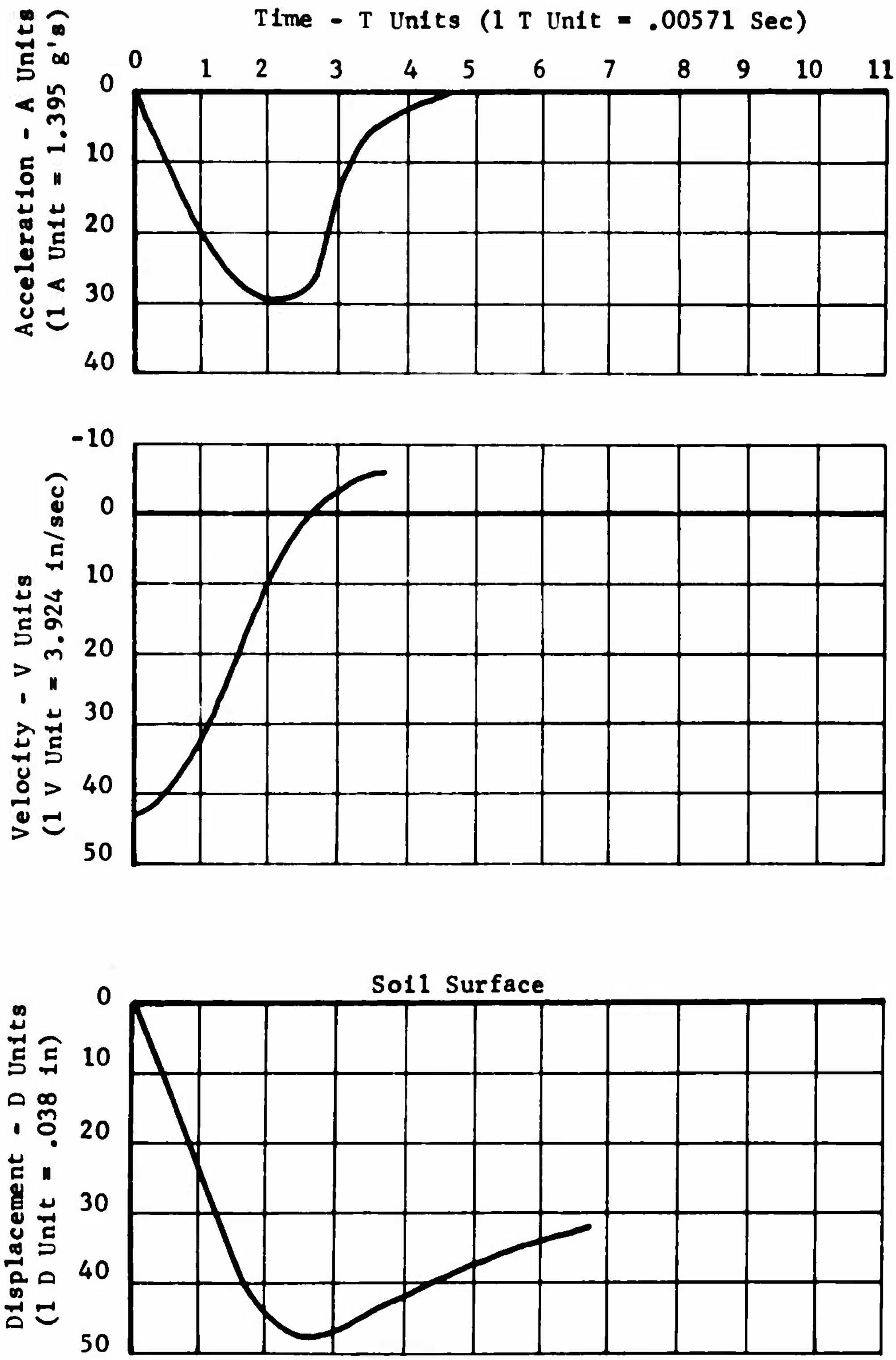

CYLINDER DROP TEST DATA
TEST NO. 5, BUNGEE HOLE 4
TERRAIN HARDNESS D

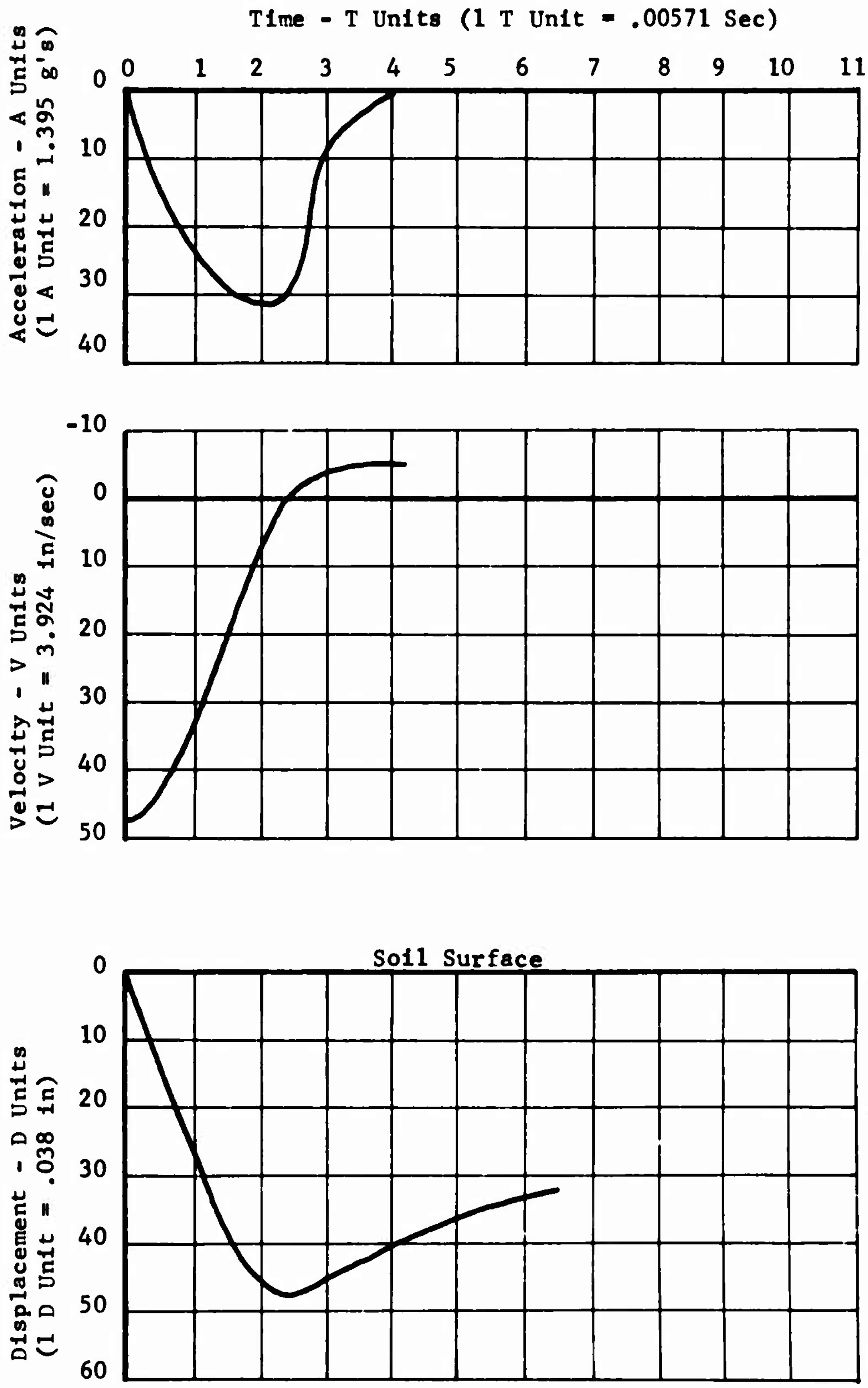

North American Aviation/Columbus
North American Rockwell

CYLINDER DROP TEST DATA
TEST NO. 5, BUNGEE HOLE 5
TERRAIN HARDNESS D

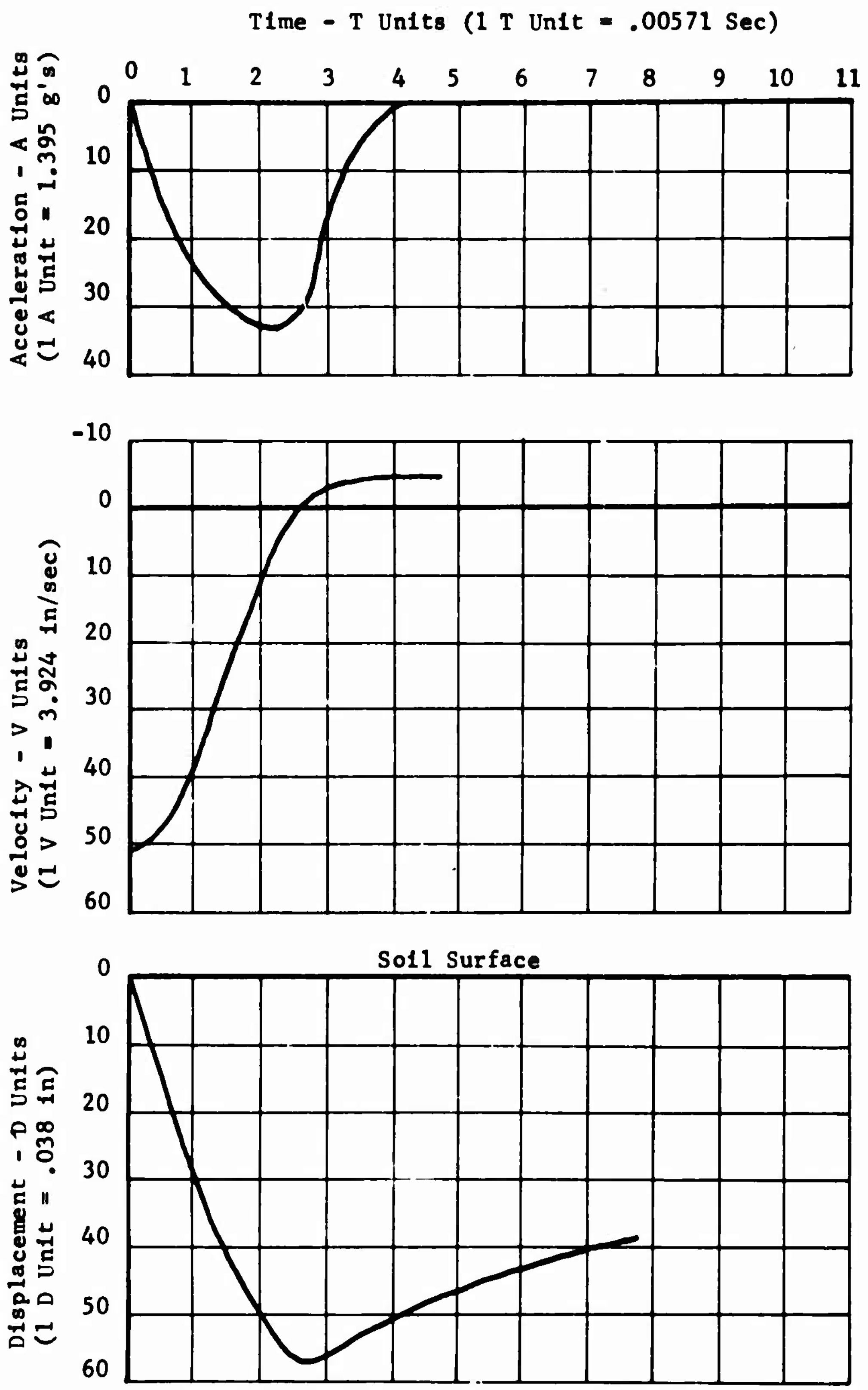

CYLINDER DROP TEST DATA
TEST NO. 4, BUNGEE HOLE 2
TERRAIN HARDNESS G

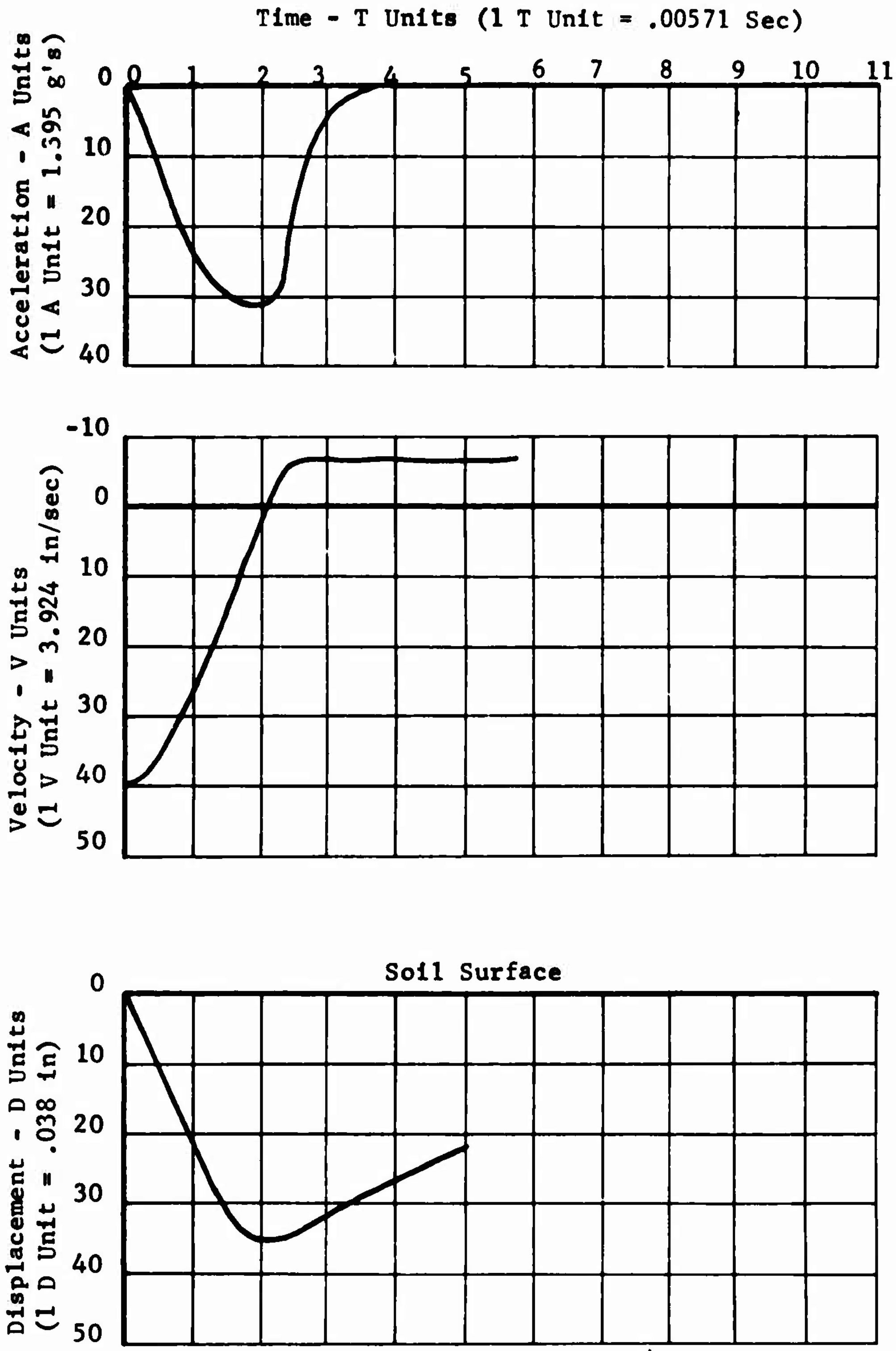

CYLINDER DROP TEST DATA
TEST NO. 4, BUNGEE HOLE 3
TERRAIN HARDNESS G

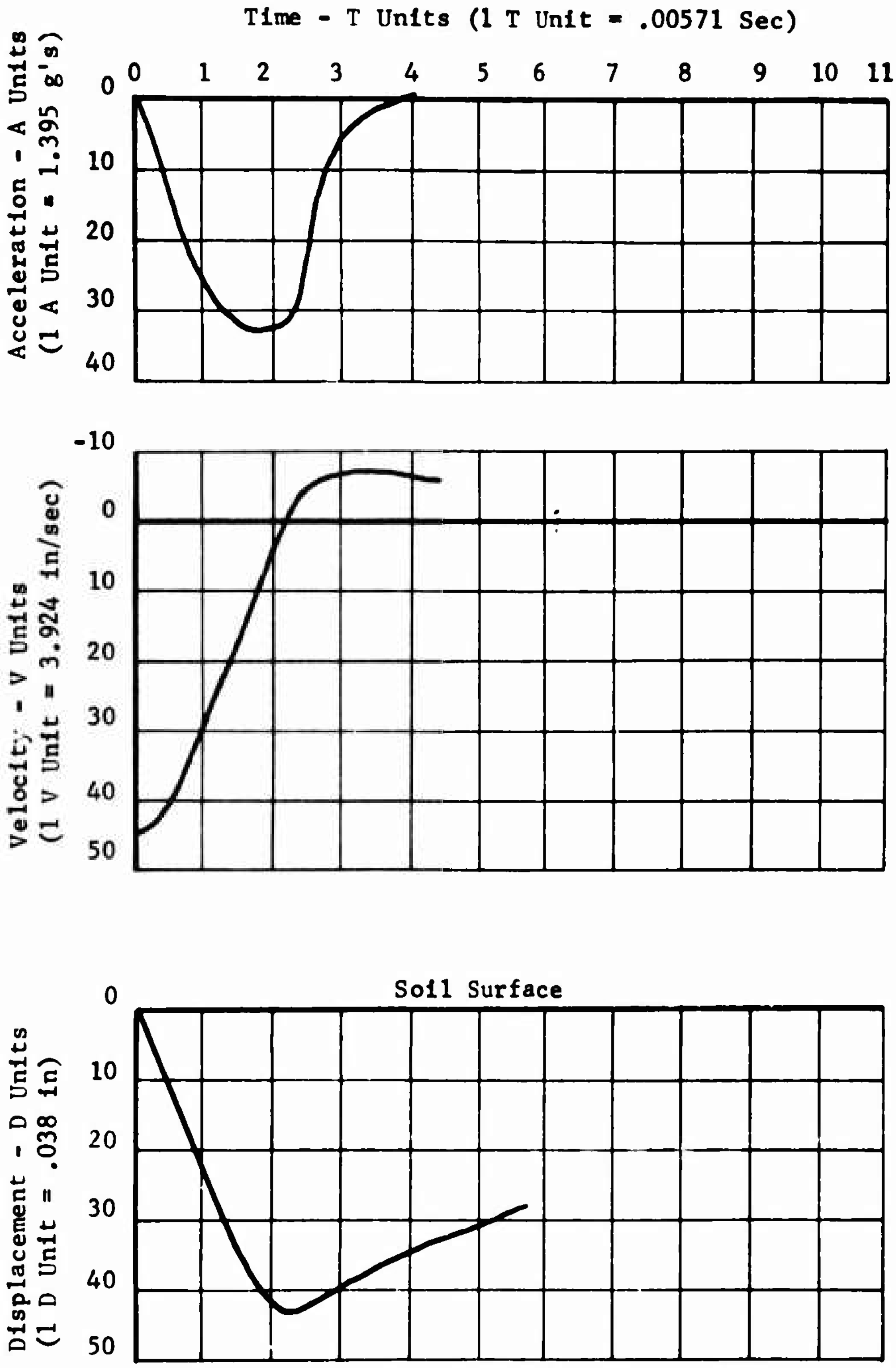

CYLINDER DROP TEST DATA
TEST NO. 4, BUNGEE HOLE 4
TERRAIN HARDNESS G

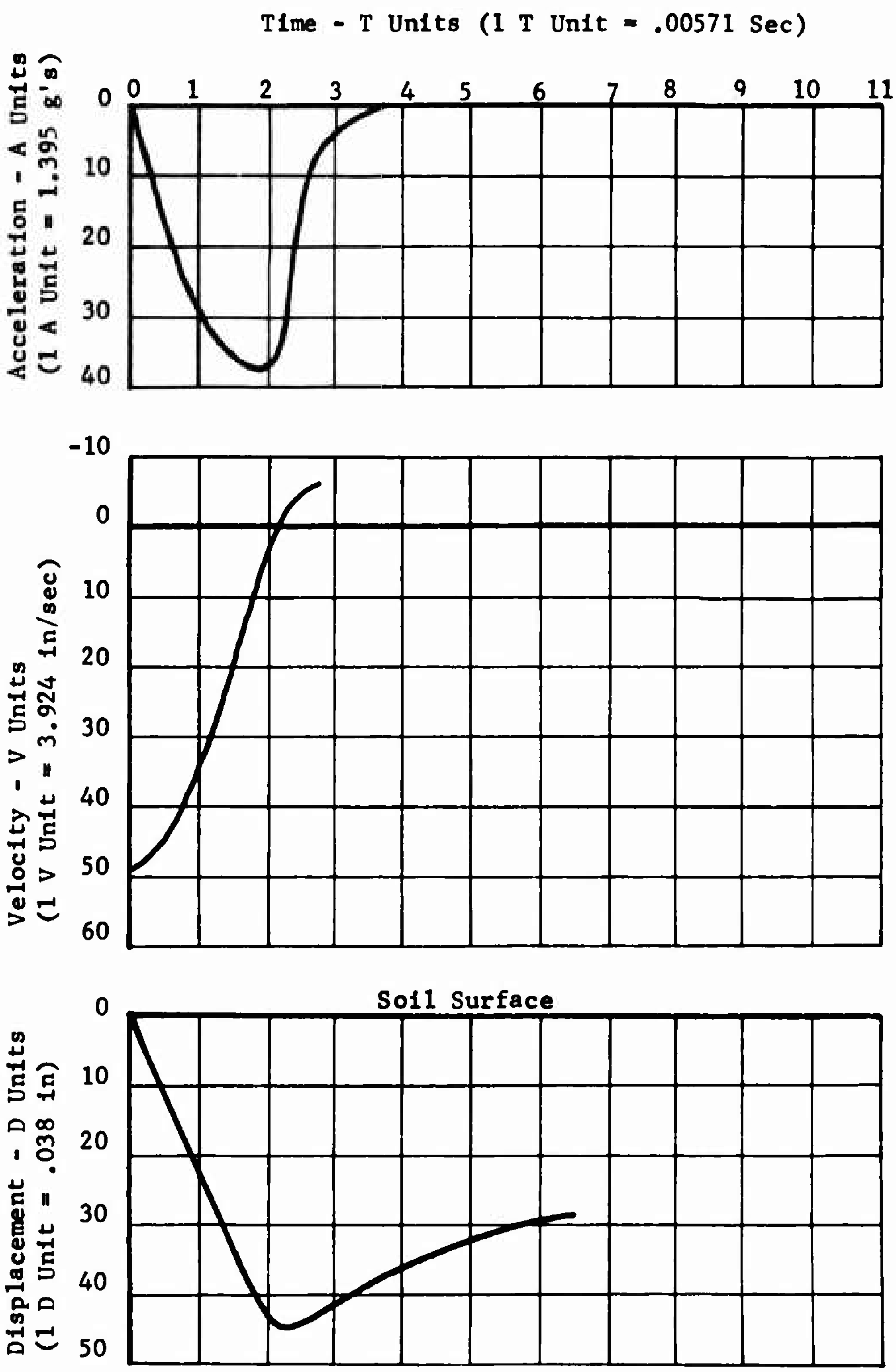

CYLINDER DROP TEST DATA
TEST NO. 4, BUNGEE HOLE 5
TERRAIN HARDNESS G

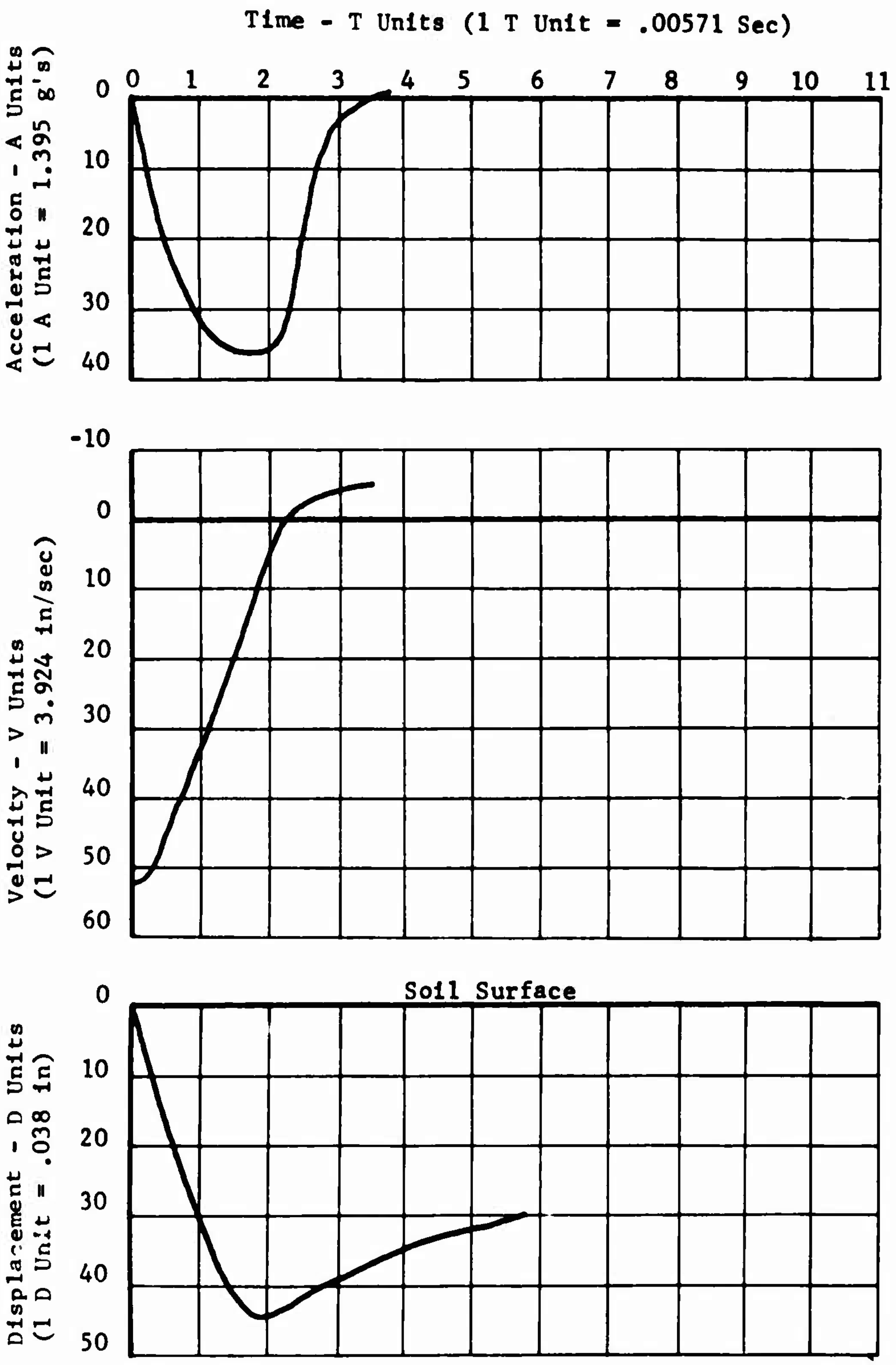

CYLINDER DROP TEST DATA
TEST NO. 3, BUNGEE HOLE 0
TERRAIN HARDNESS I

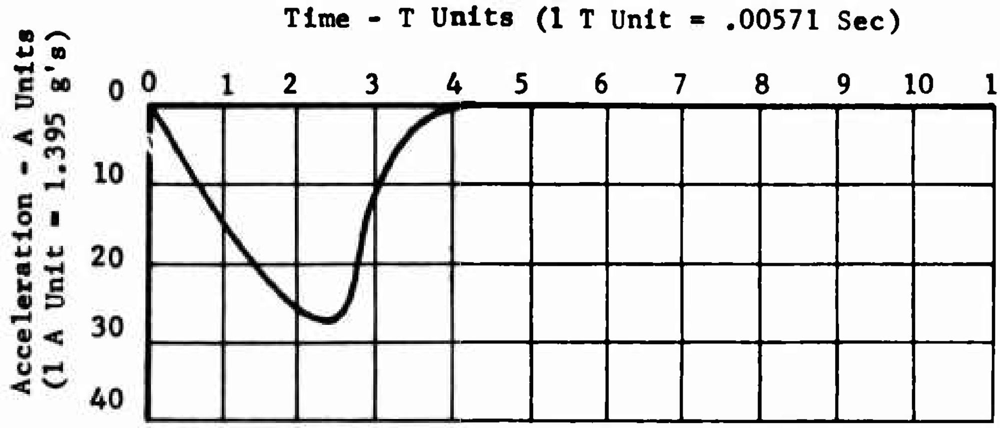

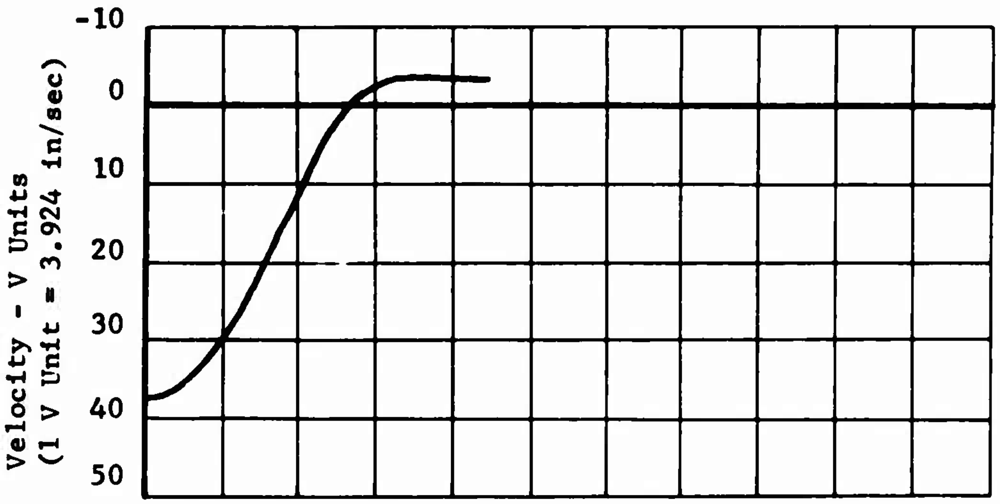

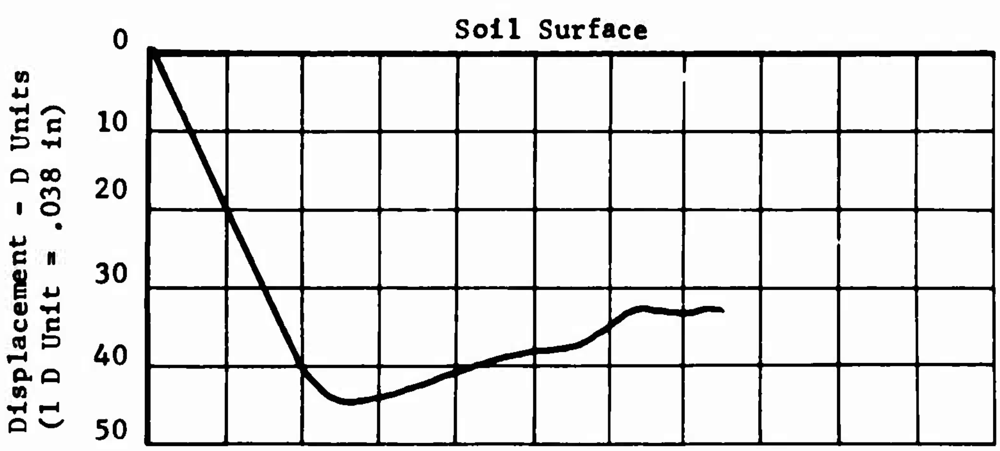

CYLINDER DROP TEST DATA
TEST NO. 3, BUNGEE HOLE 3
TERRAIN HARDNESS I

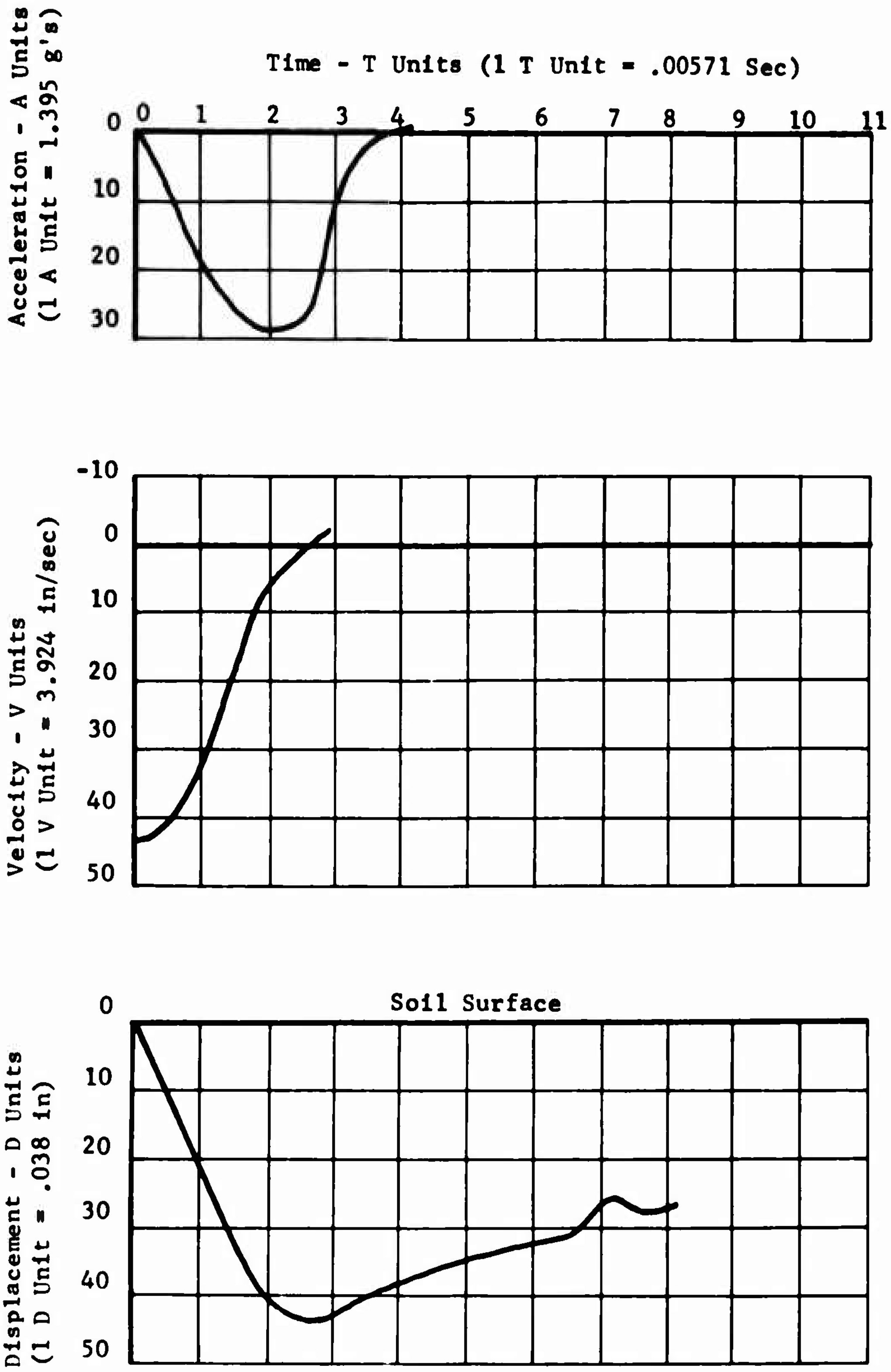

CYLINDER DROP TEST DATA
TEST NO. 3, BUNGEE HOLE 4
TERRAIN HARDNESS I

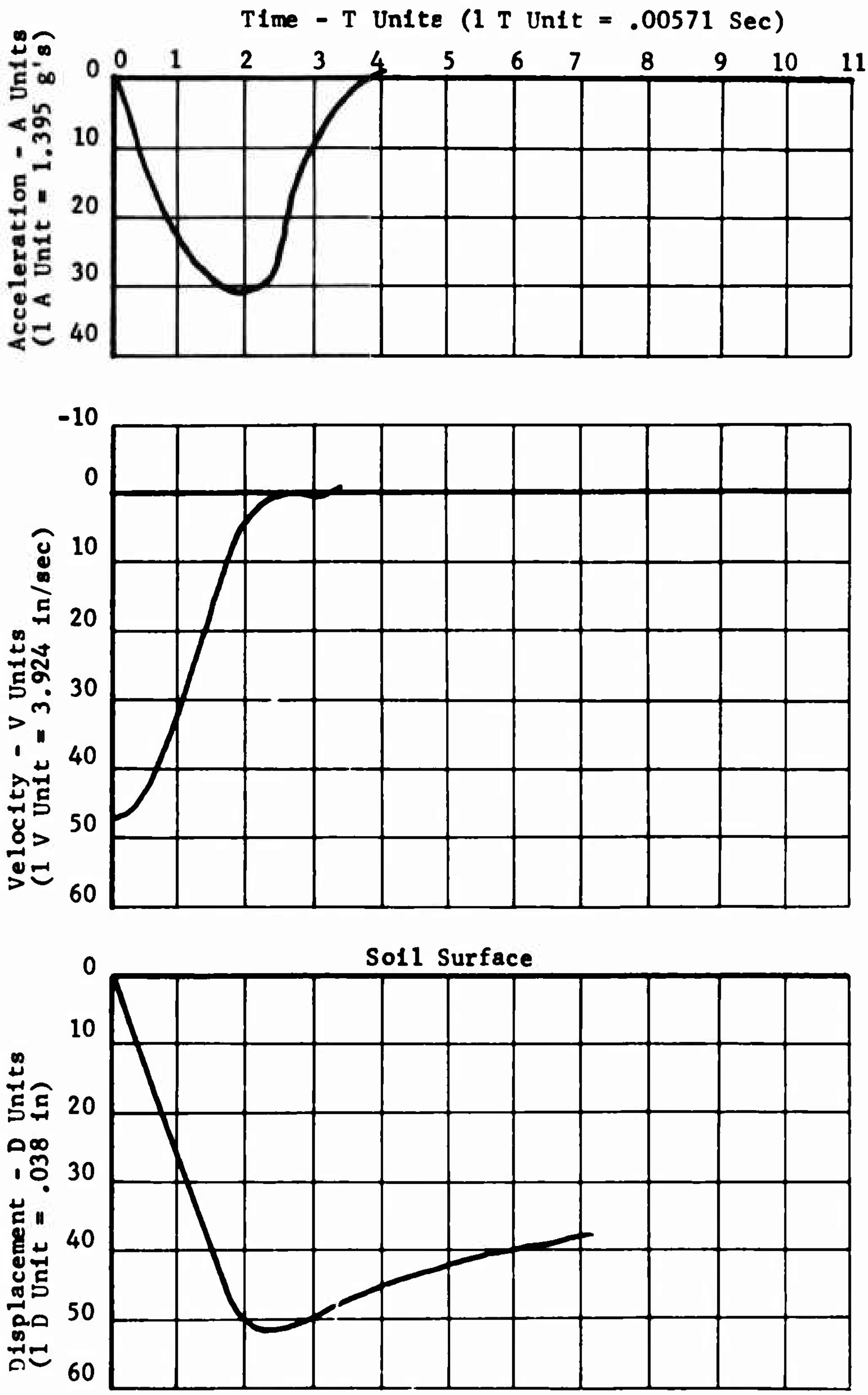

SELECTED PENETROMETER DATA

(TERRAIN HARDNESS CURVES)

PRECEDING PAGE BLANK

PENETROMETER DATA

TERRAIN HARDNESS A

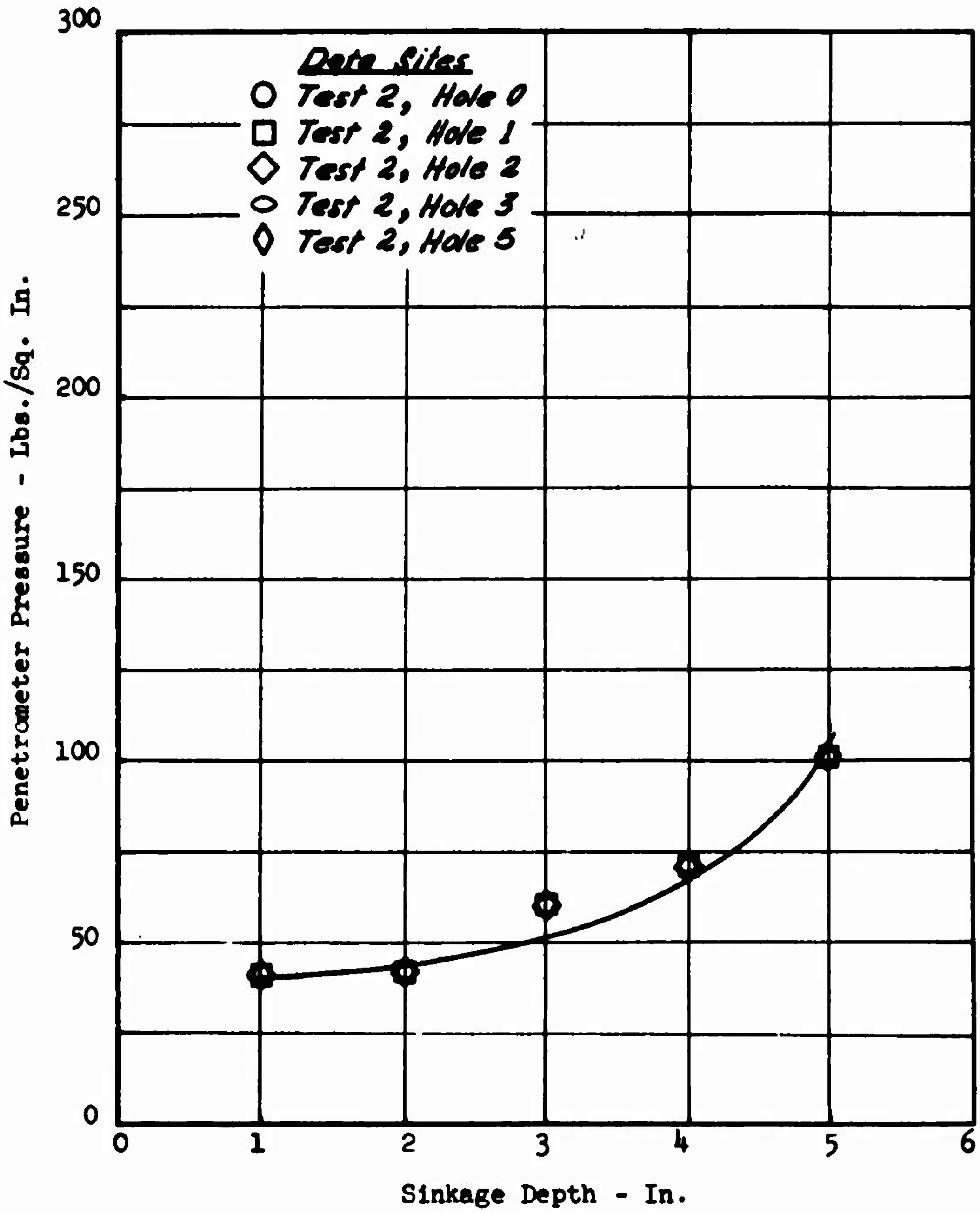

PRECEDING PAGE BLANK

PENETROMETER DATA

TERRAIN HARDNESS B

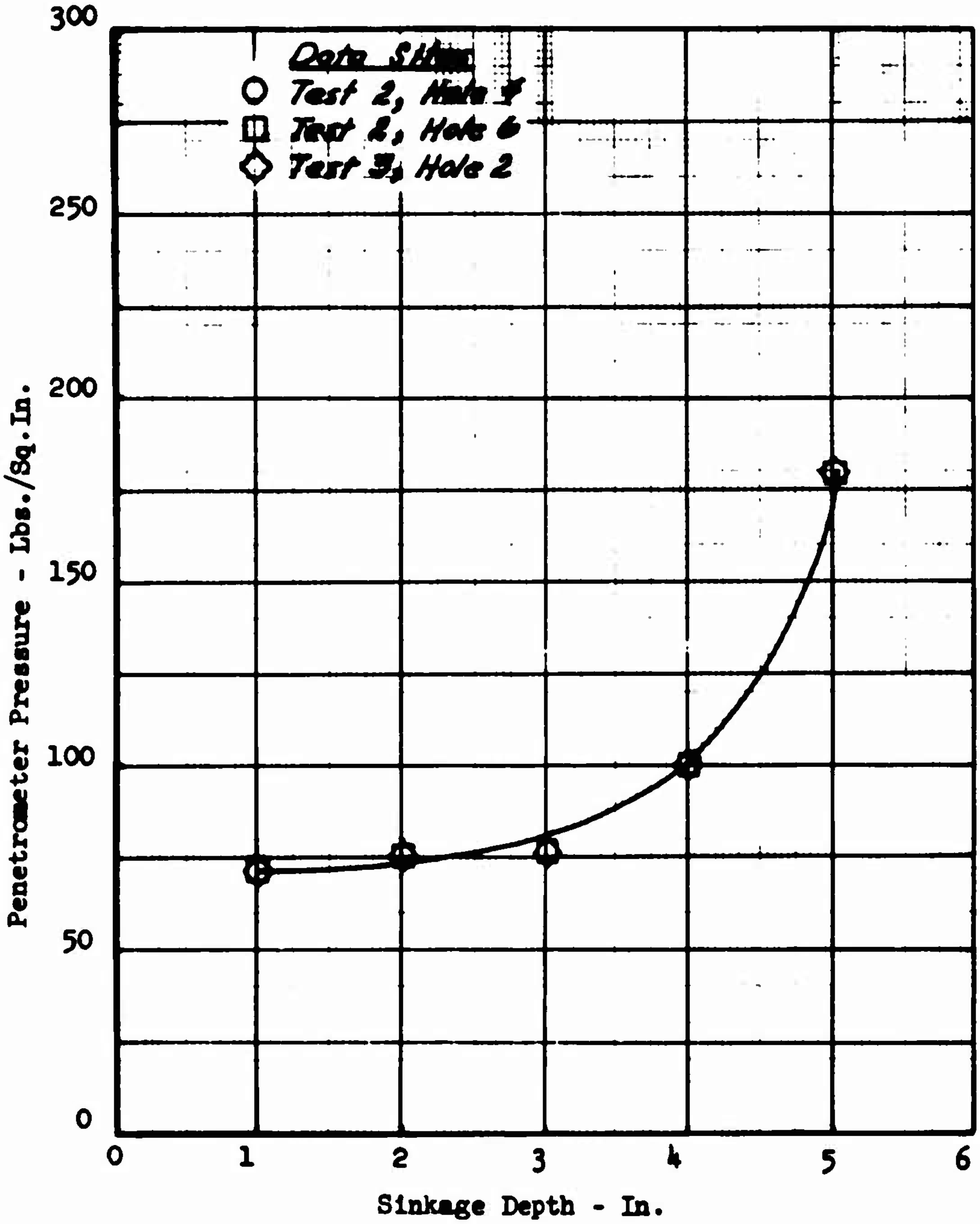

PENETROMETER DATA

TERRAIN HARDNESS C

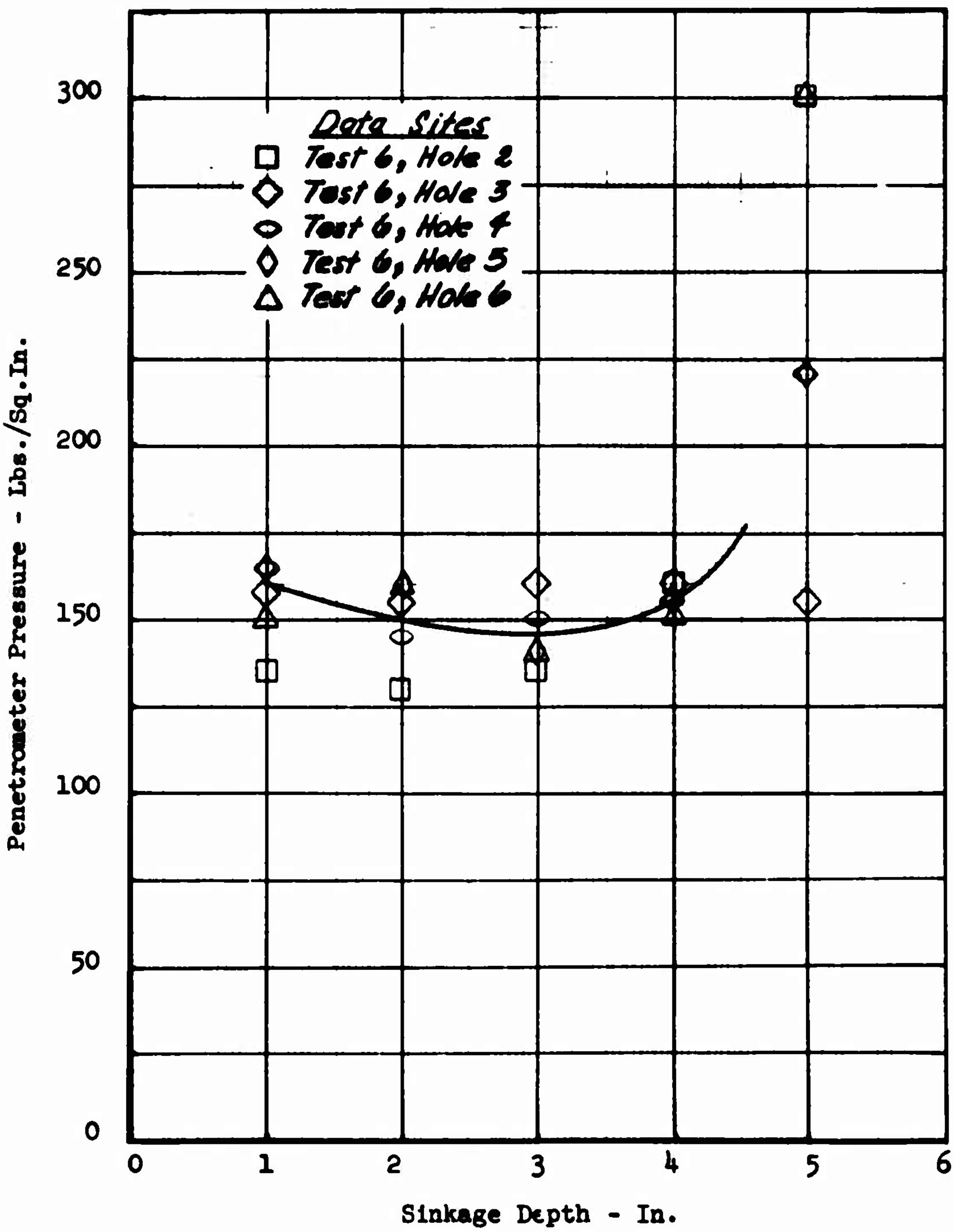

PENETROMETER DATA

TERRAIN HARDNESS D

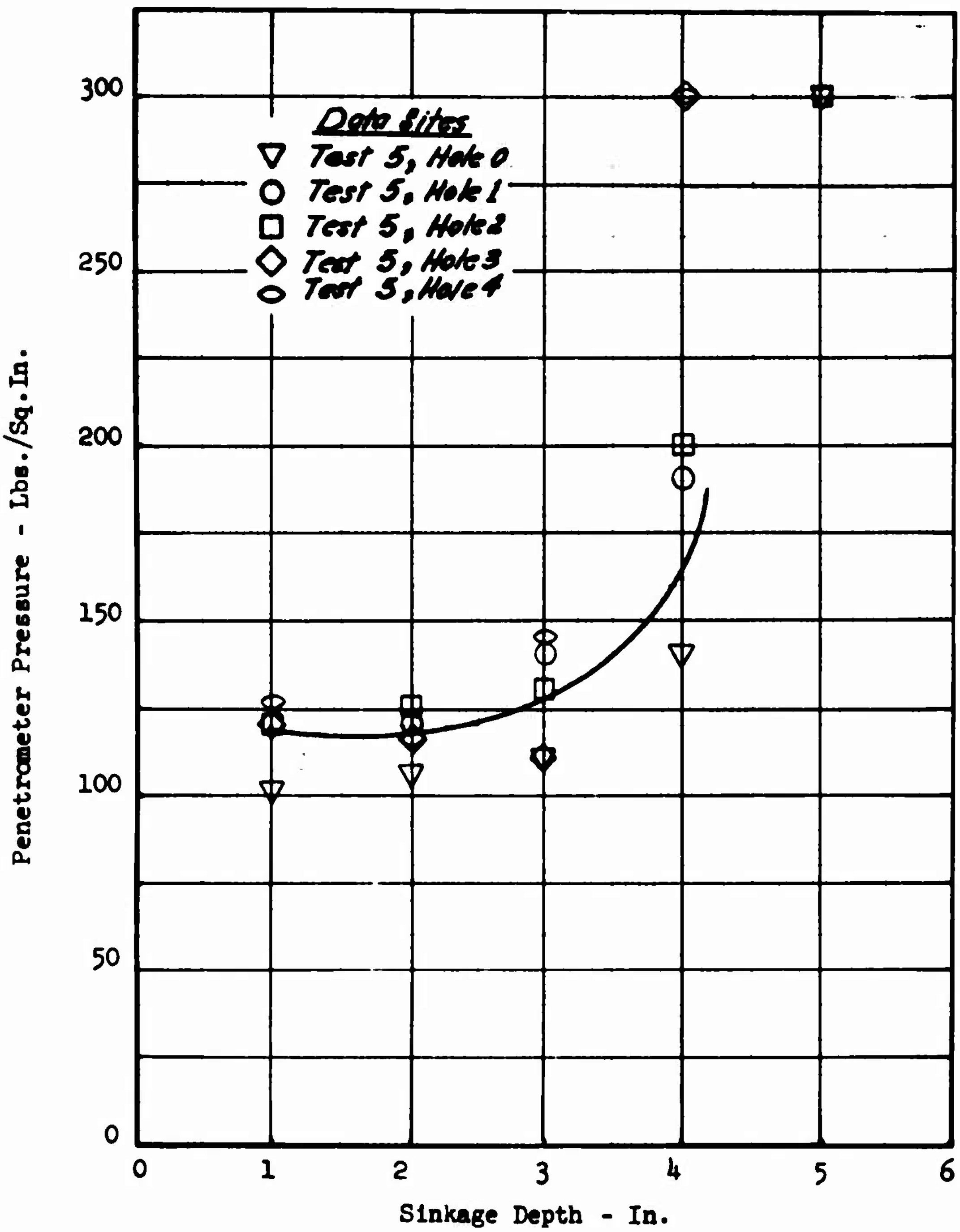

PENETROMETER DATA

TERRAIN HARDNESS G

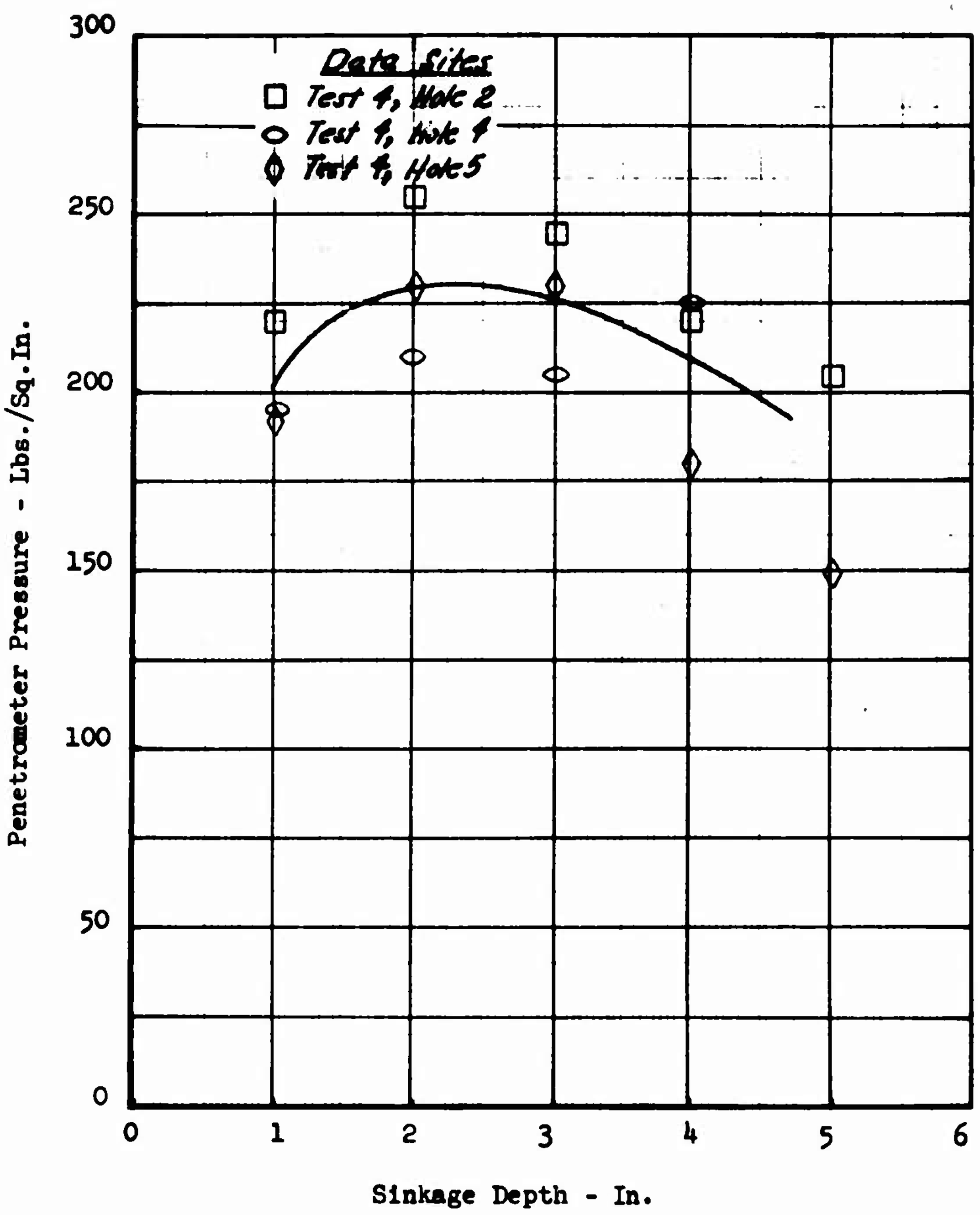

PENETROMETER DATA

TERRAIN HARDNESS I

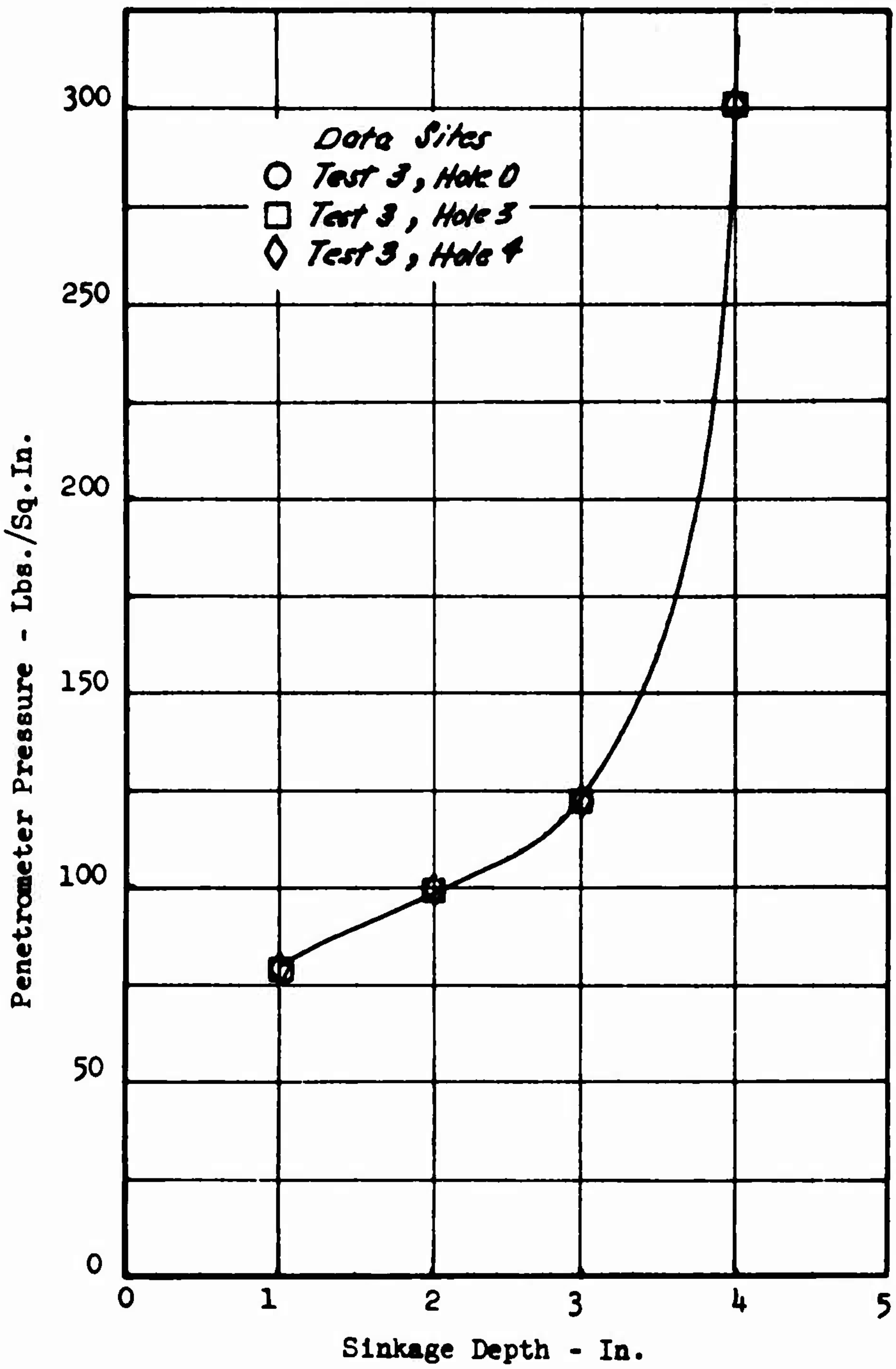

SHIFTED TERRAIN HARDNESS CURVES

SHIFTED PENETROMETER DATA

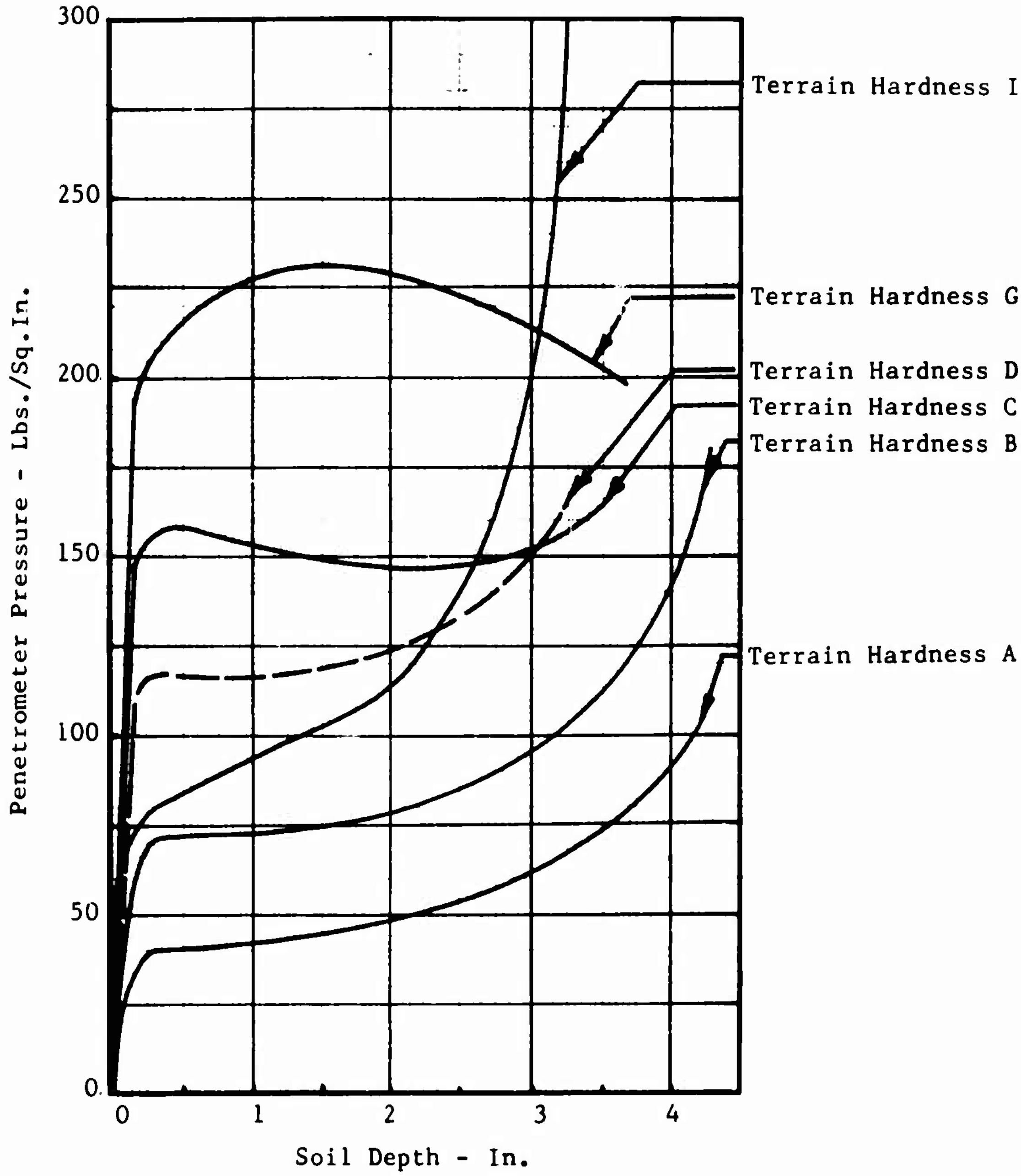

PRECEDING PAGE BLANK

STATIC SOIL PRESSURE CURVES

PRECEDING PAGE BLANK

STATIC SOIL PRESSURE CURVES

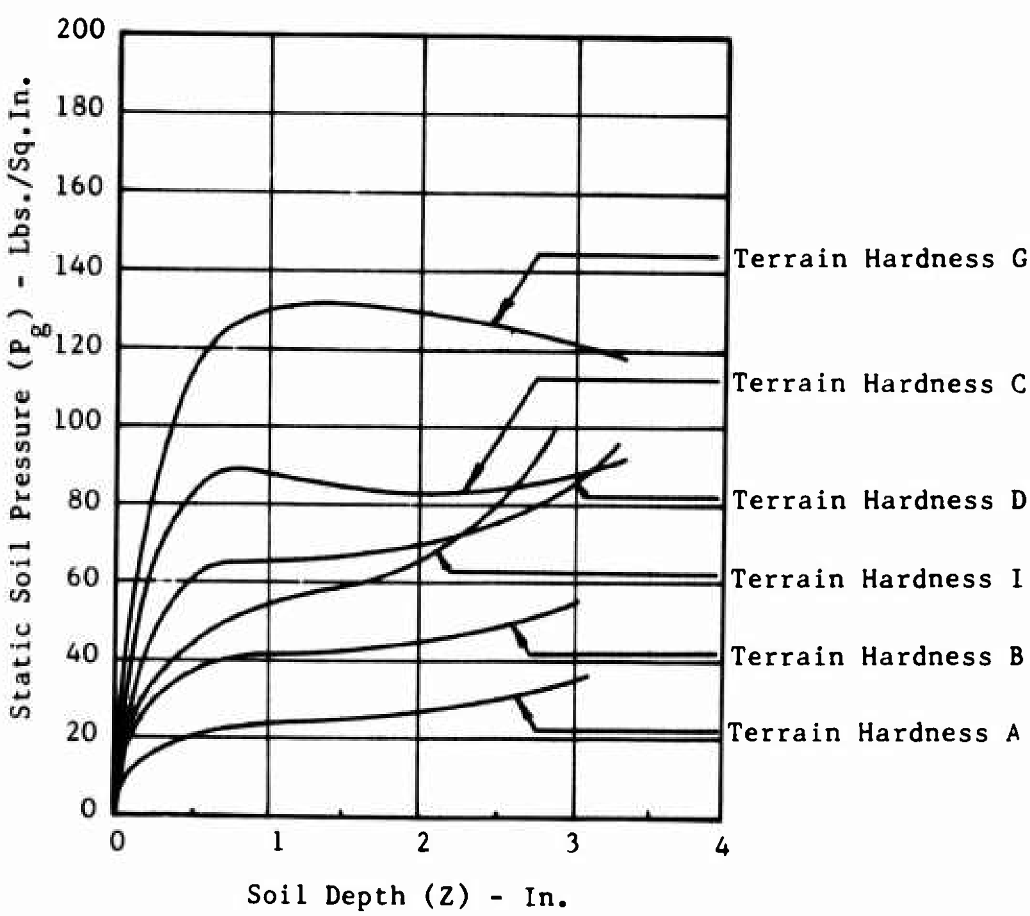

PRECEDING PAGE BLANK

<u>METHOD OF DETERMINING THE STATIC FORCE</u>

<u>ACTING ON THE RIGID CYLINDER</u>

PRECEDING PAGE BLANK

Method of Determing the Static Force Acting On the Rigid Cylinder

Depicted below is the rigid cylinder of radius R penetrated to the depth Z in soft soil. The static reactive force acting on the cylinder resulting from the depth dependent soil pressure is determined by dividing the portion of the cylinder below the surface into a series of flat plates.

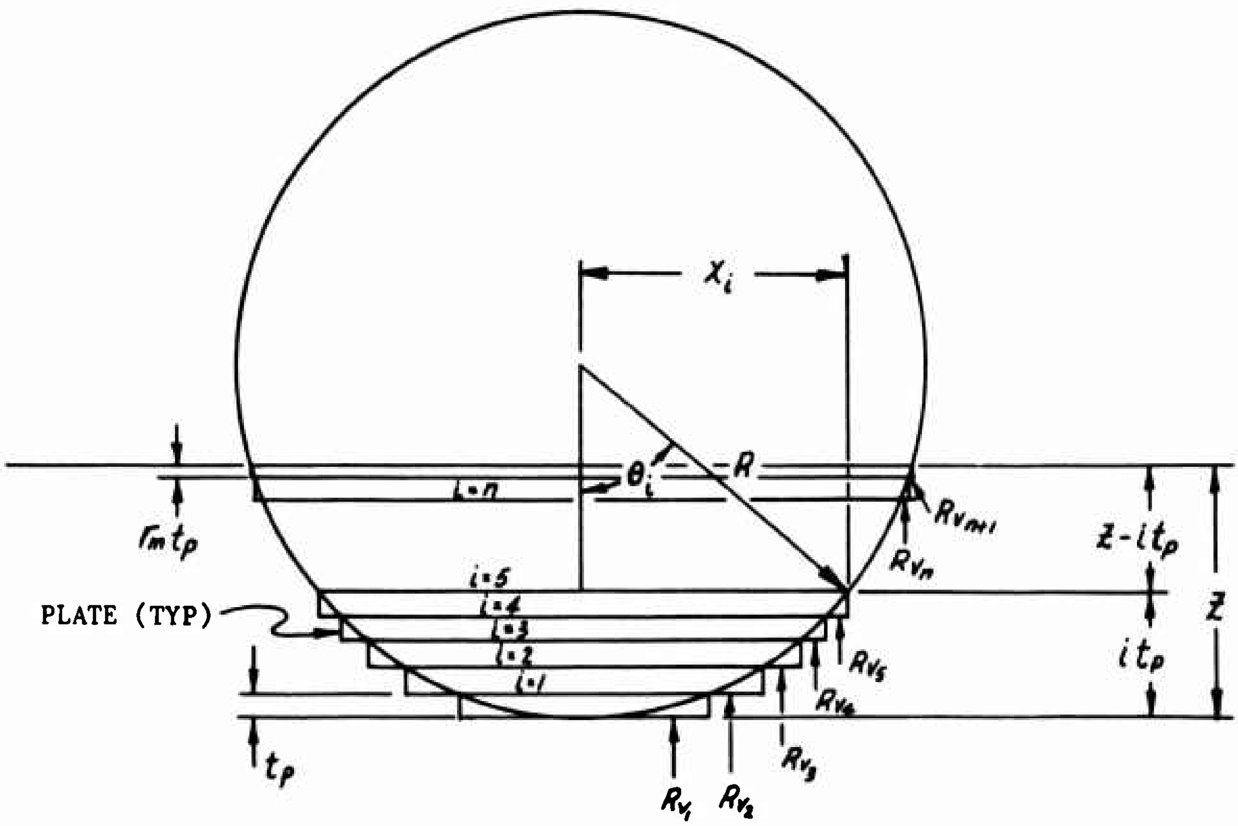

PRECEDING PAGE BLANK

The static reactive force (soil static strength) is the sum of the vertical forces acting on the effective area of each plate:

$$R_v = 2R_{v1} + 2R_{v2} + \cdots + 2R_{vn} + 2R_{vn+1} = 2\sum_{i=1}^{n+1} R_{vi} \qquad \text{(A1-1)}$$

The elemental reactive forces, R_{vi}, are a function of the effective area and the local static soil pressure. Accuracy of the total reactive force, R_v, is inversly proportional to the plate thickness t_p. Generally, there are n plates of thickness t_p, and one plate $(n+1)$ of thickness $r_m t_p$ where r_m is less than 1. Thus

$$n + r_m = \frac{z}{t_p} \qquad \text{(A1-2)}$$

The following relationships result with reference to the preceeding figure.

$$\cos\theta_i = (R - i t_p)/R \ , \ i = 1,2,\cdots,n,n+r_m \qquad \text{(A1-3)}$$

$$X_i = R(1-\cos^2\theta_i)^{1/2} \ , \ i = 1,2,\cdots,n,n+r_m \qquad \text{(A1-4)}$$

Combine Equations (A1-3) and (A1-4) to obtain the following expression.

$$X_i = \left[2R(i t_p) - (i t_p)^2\right]^{1/2} \qquad \text{(A1-5)}$$

Thus, the effective area of each plate i is

$$A_i = 2b(X_i - X_{i-1}) \ , \ i = 1,2,\cdots,n,n+r_m \qquad \text{(A1-6)}$$

Note that when $i=1$, the value of X_{i-1} is identically zero. The elemental force acting on surface A_i is given by the following expression.

$$R_{v_i} = (A_i)\left[P_g(z_i)\right] \ , \ i = 1,2,\cdots,n,n+r_m \qquad \text{(A1-7)}$$

Where $P_g(z_i)$ represents the static soil pressure of plate depth z_i.

$$z_i = z - (1 - \tfrac{1}{2}) t_p \ , \ i = 1,2,\cdots,n \qquad \text{(A1-8)}$$

$$z_i = \tfrac{1}{2} r_m t_p \ , \ i = n+r_m$$

The expression for the total static reactive force results from the combination of Equations (A1-1), (A1-6), and (A1-7):

$$R_V = 2b\left\{\sum_{i=1}^{n}\left[(X_i - X_{i-1})P_{g(z_i)}\right] + (X_{n+r_n} - X_n)P_{g(z_n+r_m)}\right\} \tag{A1-9}$$

CALCULATED SOIL DAMPING COEFFICIENTS

CALCULATED SOIL DAMPING COEFFICIENTS

Terrain Hardness A, Test No. 2, Bungee Hole 0

Z (IN)	$\dot{Z}$ (IN/SEC)	$\ddot{Z}$ (IN/SEC**2)	$K(Z)$ (LBS/IN)	$C(Z,\dot{Z},\dot{Z}_{IM})$ (LBS/IN/SEC)
0.2280	138.9096	3.0690	244.7759	0.5136
0.4180	134.2008	7.6725	231.3619	1.2988
0.6042	127.5300	11.8575	219.4047	2.1111
0.8094	118.1124	16.4610	205.1040	3.2143
0.9956	109.8720	20.0880	190.7820	4.2691
1.1970	100.0620	23.0175	177.0236	5.3832
1.3870	90.2520	25.8075	166.0537	6.7302
1.5770	78.4800	27.9000	156.8477	8.3560
1.7556	66.7080	29.9925	149.5612	10.5826
1.8696	51.0120	30.6900	145.4558	14.0823

Terrain Hardness A, Test No. 2, Bungee Hole 2

Z (IN)	$\dot{Z}$ (IN/SEC)	$\ddot{Z}$ (IN/SEC**2)	$K(Z)$ (LBS/IN)	$C(Z,\dot{Z},\dot{Z}_{IM})$ (LBS/IN/SEC)
0.2280	143.6184	5.5800	244.7759	1.0432
0.4370	137.3400	11.1600	229.6970	2.0360
0.6802	127.5300	15.3450	213.9063	2.8643
0.8740	114.1884	19.1115	200.0498	3.9727
1.0792	100.0620	21.9015	184.8101	5.1590
1.2920	87.1128	23.9940	171.2725	6.4259
1.5010	73.3788	25.8075	160.3296	8.1370
1.6910	60.8220	27.7605	152.0784	10.5488
1.8430	45.9108	28.5975	146.3790	14.2700
1.9950	32.1768	28.7370	141.3246	20.1182

PRECEDING PAGE BLANK

CALCULATED SOIL DAMPING COEFFICIENTS

Terrain Hardness A, Test No. 2, Bungee Hole 5

z (IN)	$\dot{z}$ (IN/SEC)	$\ddot{z}$ (IN/SEC**2)	K(z) (LBS/IN)	C($z,\dot{z},\dot{z}_{IM}$) (LBS/IN/SEC)
0.2090	193.8456	6.4170	244.9241	0.9316
0.4750	185.6052	15.3450	227.1854	2.1706
0.7372	174.6180	20.6460	210.1707	2.9865
0.9880	153.4284	26.6445	191.3358	4.3985
1.2540	131.4540	31.5270	173.5043	6.0774
1.4820	111.8340	34.8750	161.2414	7.8879
1.7176	92.2140	37.6650	151.0303	10.2899
1.9000	72.5940	39.1995	144.4208	13.5250
2.0330	50.6196	40.0365	140.1725	19.7042
2.1356	30.9996	39.4785	137.3735	31.3416

Terrain Hardness A, Test No. 2, Bungee Hole 3

z (IN)	$\dot{z}$ (IN/SEC)	$\ddot{z}$ (IN/SEC**2)	K(z) (LBS/IN)	C($z,\dot{z},\dot{z}_{IM}$) (LBS/IN/SEC)
0.2090	165.5928	7.6725	244.9241	1.3275
0.4560	158.9220	13.2525	228.2174	2.1477
0.6992	146.7576	18.1350	212.6431	3.0614
0.9424	133.4160	22.4595	194.7397	4.1193
1.1400	117.7200	25.3890	180.8786	5.2536
1.3680	98.1000	27.9000	167.0548	6.8766
1.5960	78.4800	29.2950	156.0274	8.8902
1.7860	59.6448	29.9925	148.4263	11.7936
1.9722	37.6704	30.1320	142.0514	18.3890
2.1204	23.5440	29.8530	137.7667	28.5438

CALCULATED SOIL DAMPING COEFFICIENTS

Terrain Hardness B, Test No. 3, Bungee Hole 2

Z (IN)	$\dot{Z}$ (IN/SEC)	$\ddot{Z}$ (IN/SEC**2)	$K(Z)$ (LBS/IN)	$C(Z,\dot{Z},\dot{Z}_{IM})$ (LBS/IN/SEC)
0.1710	149.1120	3.0690	421.0560	0.3699
0.3458	141.6564	8.3700	426.5780	1.0257
0.5510	131.4540	14.6475	401.0132	2.0389
0.7600	117.7200	19.8090	370.9373	3.1292
0.9310	100.0620	23.7150	344.9055	4.5096
1.0830	80.4420	27.2025	323.3340	6.6030
1.2730	60.8220	29.9925	299.4891	9.6555
1.4440	40.0248	32.3640	280.9567	15.9132
1.5770	21.5820	34.5960	268.1844	31.9455
1.6796	8.2404	35.4330	259.3600	85.3005

Terrain Hardness B, Test No. 2, Bungee Hole 4

Z (IN)	$\dot{Z}$ (IN/SEC)	$\ddot{Z}$ (IN/SEC**2)	$K(Z)$ (LBS/IN)	$C(Z,\dot{Z},\dot{Z}_{IM})$ (LBS/IN/SEC)
0.2470	181.2888	7.3935	432.6683	0.8573
0.5130	173.0484	15.3450	406.7348	1.7458
0.7410	158.9220	21.6225	373.3887	2.7074
1.0450	136.1628	27.6210	328.5079	4.0475
1.2920	102.0240	33.0615	297.3172	6.6679
1.5770	56.8980	36.9675	268.1844	13.4198
1.7860	33.3540	39.0600	250.9166	24.0972
1.9570	19.6200	40.3155	238.9789	41.9688
2.1090	9.8100	38.5020	229.7344	76.4452
2.2040	3.9240	34.7355	224.5795	158.4509

Terrain Hardness B, Test No. 2, Bungee Hole 6

Z (IN)	$\dot{Z}$ (IN/SEC)	$\ddot{Z}$ (IN/SEC**2)	$K(Z)$ (LBS/IN)	$C(Z,\dot{Z},\dot{Z}_{IM})$ (LBS/IN/SEC)
0.2660	202.4784	8.9280	431.8654	0.9649
0.5852	189.9216	20.9250	395.7539	2.3881
0.8550	166.3776	31.3875	356.4480	4.2515
1.1096	127.9224	40.7340	319.7728	7.4214
1.3794	94.1760	44.7795	287.6682	10.9773
1.5998	61.2144	46.4535	266.1651	17.2690
1.7860	33.3540	46.8720	250.9166	31.4164
1.9380	14.9112	46.0350	240.2215	67.3517
2.0520	6.6708	43.6635	233.0221	137.5507

CALCULATED SOIL DAMPING COEFFICIENTS

Terrain Hardness C, Test No. 6, Bungee Hole 2

Z (IN)	$\dot{Z}$ (IN/SEC)	$\ddot{Z}$ (IN/SEC**2)	$K(Z)$ (LBS/IN)	$C(Z,\dot{Z},\ddot{Z}_{IM})$ (LBS/IN/SEC)
0.1330	145.5804	6.9750	825.9881	0.9573
0.3192	136.1628	17.0190	947.8334	1.9135
0.5130	123.6060	25.3890	900.1229	2.9359
0.6954	103.9860	30.6900	835.2912	3.9376
0.8740	80.0496	34.3170	768.7070	5.3942
1.0488	58.0752	36.9675	703.8702	7.7187
1.1590	35.3160	37.8045	667.3465	12.4359
1.2160	15.3036	37.8045	649.7043	27.6144

Terrain Hardness C, Test No. 6, Bungee Hole 3

Z (IN)	$\dot{Z}$ (IN/SEC)	$\ddot{Z}$ (IN/SEC**2)	$K(Z)$ (LBS/IN)	$C(Z,\dot{Z},\ddot{Z}_{IM})$ (LBS/IN/SEC)
0.1710	165.9852	9.0675	905.8388	0.9622
0.3572	154.2132	18.1350	944.4602	1.6899
0.5510	136.1628	26.7840	886.9139	2.7875
0.7600	115.7580	32.0850	812.8718	3.5948
0.9462	92.2140	35.8515	741.0398	4.8847
1.1780	66.7080	38.0835	661.4100	6.6292
1.3186	45.5184	39.1995	619.8165	9.6432
1.4440	22.7592	39.3390	586.4443	18.1803

CALCULATED SOIL DAMPING COEFFICIENTS

Terrain Hardness C, Test No. 6, Bungee Hole 4

z (IN)	$\dot{z}$ (IN/SEC)	$\ddot{z}$ (IN/SEC**2)	$K(z)$ (LBS/IN)	$C(z,\dot{z},\dot{z}_{IM})$ (LBS/IN/SEC)
0.1976	177.7572	9.7650	928.1107	0.8608
0.3876	168.7320	18.1350	937.3486	1.3907
0.5890	154.9980	25.6680	873.3504	2.0579
0.8208	133.0236	31.3875	789.5266	2.7369
1.0070	111.8340	35.5725	718.6534	3.7485
1.2274	92.2140	38.5020	646.2257	4.7852
1.4250	67.8852	40.4550	591.3042	6.6710
1.5922	47.0880	41.1525	550.8642	9.3480
1.6454	26.6832	40.5945	539.0619	15.4725

Terrain Hardness C, Test No. 6, Bungee Hole 5

z (IN)	$\dot{z}$ (IN/SEC)	$\ddot{z}$ (IN/SEC**2)	$K(z)$ (LBS/IN)	$C(z,\dot{z},\dot{z}_{IM})$ (LBS/IN/SEC)
0.2090	194.2380	6.9750	934.0258	0.2780
0.4370	184.4280	15.3450	922.2775	0.5842
0.6802	170.6940	23.0175	840.5156	1.0477
0.9310	151.0740	29.2950	746.7410	1.6648
1.1400	131.4540	34.8750	673.9758	2.6835
1.3680	108.6948	39.0600	606.2904	3.8868
1.5656	89.0748	42.1290	556.9484	5.3418
1.7404	64.3536	43.9425	519.1006	7.7853
1.9000	38.8476	44.2215	488.0542	12.5071

CALCULATED SOIL DAMPING COEFFICIENTS

Terrain Hardness D, Test No. 5, Bungee Hole 0

z (IN)	$\dot{z}$ (IN/SEC)	$\ddot{z}$ (IN/SEC**2)	$K(z)$ (LBS/IN)	$C(z,\dot{z},\dot{z}_{IM})$ (LBS/IN/SEC)
0.1520	135.7704	4.6035	658.4164	0.5526
0.3192	130.6692	10.6020	699.6136	1.0656
0.4826	121.6440	17.4375	674.9071	2.0590
0.6536	108.3024	24.8310	635.2789	3.6195
0.8170	91.0368	29.7135	590.3985	5.2445
0.9576	71.4168	32.7825	552.3124	7.3765

Terrain Hardness D, Test No. 5, Bungee Hole 2

z (IN)	$\dot{z}$ (IN/SEC)	$\ddot{z}$ (IN/SEC**2)	$K(z)$ (LBS/IN)	$C(z,\dot{z},\dot{z}_{IM})$ (LBS/IN/SEC)
0.1748	150.6816	5.5800	675.2637	0.5813
0.3724	143.6184	13.9500	693.7287	1.4542
0.5510	129.4920	21.3435	660.3054	2.5824
0.7220	111.4416	26.6445	616.5423	3.7575
0.8968	92.6064	30.4110	568.3752	5.0955
1.0792	74.5560	33.4800	522.5076	6.8889
1.2388	56.1132	35.7120	488.0088	9.6716
1.3984	37.2780	36.4095	458.3917	14.1647
1.5200	18.8352	36.5490	438.5162	26.9103

Terrain Hardness D, Test No. 5, Bungee Hole 3

z (IN)	$\dot{z}$ (IN/SEC)	$\ddot{z}$ (IN/SEC**2)	$K(z)$ (LBS/IN)	$C(z,\dot{z},\dot{z}_{IM})$ (LBS/IN/SEC)
0.1710	167.9472	7.5330	673.6165	0.9019
0.3952	160.8840	14.6475	690.7615	1.3426
0.6536	148.7196	21.6225	635.2789	1.9616
0.8702	130.2768	27.3420	575.6015	2.9537
1.1058	107.1252	32.6430	516.4304	4.4833
1.3490	86.3280	36.6885	467.0636	6.3444
1.5466	60.8220	39.1995	434.4593	9.6067
1.6606	41.2020	40.7340	418.0357	14.8050
1.7556	21.9744	40.7340	405.4056	26.9613

CALCULATED SOIL DAMPING COEFFICIENTS

Terrain Hardness D, Test No. 5, Bungee Hole 4

z (IN)	$\dot{z}$ (IN/SEC)	$\ddot{z}$ (IN/SEC**2)	$K(z)$ (LBS/IN)	$C(z,\dot{z},\dot{z}_{IM})$ (LBS/IN/SEC)
0.2850	180.1116	11.4390	699.7260	1.0510
0.5510	169.5168	20.5065	660.3054	1.8184
0.7980	151.0740	27.2025	595.7555	2.6869
1.0070	130.2768	32.7825	539.8081	3.9310
1.2502	104.3784	37.1070	485.7162	5.5912
1.4706	78.4800	40.7340	446.3461	8.2542
1.6226	51.7968	42.6870	423.3436	13.0954
1.7290	30.9996	43.5240	408.8519	22.0800
1.7936	6.6708	42.9660	400.5906	98.2548

Terrain Hardness D, Test No. 5, Bungee Hole 5

z (IN)	$\dot{z}$ (IN/SEC)	$\ddot{z}$ (IN/SEC**2)	$K(z)$ (LBS/IN)	$C(z,\dot{z},\dot{z}_{IM})$ (LBS/IN/SEC)
0.2926	195.8076	13.1130	699.9057	1.2065
0.5434	187.5672	20.7855	662.1019	1.7114
0.8284	172.6560	28.5975	587.2099	2.5396
1.0678	151.8588	34.4565	525.1731	3.6036
1.3110	125.5680	38.7810	474.0139	4.9513
1.5276	96.1380	41.7105	437.3454	6.9339
1.7176	69.4548	44.0820	410.3511	10.1360
1.8924	43.1640	46.0350	388.6704	17.0124
2.0330	17.6580	45.7560	373.0352	39.7975

CALCULATED SOIL DAMPING COEFFICIENTS

Terrain Hardness G, Test No. 4, Bungee Hole 2

z (IN)	$\dot{z}$ (IN/SEC)	$\ddot{z}$ (IN/SEC**2)	$K(z)$ (LBS/IN)	$C(z,\dot{z},\dot{z}_{IM})$ (LBS/IN/SEC)
0.1748	151.4664	7.8120	1257.7122	0.3666
0.3800	139.3020	17.2980	1262.3202	0.6614
0.5890	122.0364	25.8075	1195.8769	1.0928
0.8056	102.0240	33.4800	1112.5554	1.7763
1.0222	81.2268	38.5020	1020.4407	2.3557
1.1818	57.6828	41.5710	958.0354	3.4349
1.2920	31.7844	42.9660	918.5979	5.8868
1.3262	7.8480	43.5240	906.7924	24.0554

Terrain Hardness G, Test No. 4, Bungee Hole 3

z (IN)	$\dot{z}$ (IN/SEC)	$\ddot{z}$ (IN/SEC**2)	$K(z)$ (LBS/IN)	$C(z,\dot{z},\dot{z}_{IM})$ (LBS/IN/SEC)
0.2090	169.5168	9.0675	1262.7587	0.2990
0.4256	158.9220	19.8090	1253.5261	0.7348
0.6422	139.3020	29.2950	1175.1572	1.3785
0.8702	117.7200	35.5725	1084.4103	1.6925
1.0754	92.2140	41.4315	998.9692	2.7294
1.2920	67.1004	44.5005	918.5979	3.5031
1.4554	41.5944	46.0350	864.1975	5.0990
1.5770	16.4808	45.3375	826.9772	8.7316

CALCULATED SOIL DAMPING COEFFICIENTS

Terrain Hardness G, Test No. 4, Bungee Hole 4

z (IN)	$\dot{z}$ (IN/SEC)	$\ddot{z}$ (IN/SEC**2)	$K(z)$ (LBS/IN)	$C(z,\dot{z},\dot{z}_{IM})$ (LBS/IN/SEC)
0.2280	186.3900	10.4625	1263.4512	0.3763
0.4560	175.7952	22.3200	1244.0681	0.9184
0.6536	156.9600	32.2245	1170.7681	1.7396
0.8740	133.0236	39.8970	1082.8311	2.4931
1.1020	103.9860	46.0350	988.4424	3.6599
1.2958	71.4168	49.9410	917.2964	5.6468
1.4858	41.5944	51.3360	854.6702	8.7904
1.6378	11.7720	50.9175	809.2273	25.2353

Terrain Hardness G, Test No. 4, Bungee Hole 5

z (IN)	$\dot{z}$ (IN/SEC)	$\ddot{z}$ (IN/SEC**2)	$K(z)$ (LBS/IN)	$C(z,\dot{z},\dot{z}_{IM})$ (LBS/IN/SEC)
0.3230	198.1620	14.6475	1265.9558	0.4041
0.6384	177.7572	27.3420	1176.7726	0.7563
0.9120	155.7828	36.5490	1066.2857	1.2900
1.1628	129.4920	43.5240	965.1322	2.0783
1.4174	102.4164	48.1275	876.3967	2.8612
1.5770	75.7332	50.0805	826.9772	3.8573
1.6720	47.8728	50.6385	799.5071	5.7846
1.6796	19.6200	49.9410	797.3847	12.8756

CALCULATED SOIL DAMPING COEFFICIENTS

Terrain Hardness I, Test No. 3, Bungee Hole 0

Z (IN)	$\dot{Z}$ (IN/SEC)	$\ddot{Z}$ (IN/SEC**2)	$K(Z)$ (LBS/IN)	$C(Z,\dot{Z},\dot{Z}_{IM})$ (LBS/IN/SEC)
0.1862	142.0488	5.5800	546.1392	0.7317
0.3724	137.3400	11.1600	498.7622	1.4145
0.5624	125.5680	16.3215	472.0180	2.1967
0.7410	114.5808	20.9250	450.4537	3.0666
0.9348	100.0620	25.3890	424.1477	4.2790
1.1362	82.7964	29.2950	398.0157	5.9724
1.3300	64.7460	32.7825	376.5626	8.5700
1.5390	45.1260	35.8515	356.4698	13.3626
1.6530	21.5820	37.6650	346.9033	29.4157

Terrain Hardness I, Test No. 3, Bungee Hole 3

Z (IN)	$\dot{Z}$ (IN/SEC)	$\ddot{Z}$ (IN/SEC**2)	$K(Z)$ (LBS/IN)	$C(Z,\dot{Z},\dot{Z}_{IM})$ (LBS/IN/SEC)
0.1710	165.9852	3.4875	549.3044	0.2790
0.3800	158.1372	11.2995	497.1833	1.2358
0.6080	144.0108	19.3905	466.5913	2.4548
0.8284	125.1756	25.8075	439.0704	3.7867
1.0108	100.0620	31.5270	413.7437	5.9789
1.2160	68.6700	36.1305	388.8013	10.0123
1.3870	35.3160	38.9205	370.7916	20.7619
1.5200	21.5820	39.7575	358.1283	33.7928
1.6074	11.7720	39.3390	350.6024	59.2113
1.6378	3.9240	37.6650	348.1042	162.6290

Terrain Hardness I, Test No. 3, Bungee Hole 4

Z (IN)	$\dot{Z}$ (IN/SEC)	$\ddot{Z}$ (IN/SEC**2)	$K(Z)$ (LBS/IN)	$C(Z,\dot{Z},\dot{Z}_{IM})$ (LBS/IN/SEC)
0.2470	181.2888	7.6725	527.5149	0.7762
0.4940	172.6560	16.8795	480.6439	1.8609
0.7334	156.9600	25.5285	451.3505	3.1728
0.9880	133.4160	31.3875	416.7961	4.4996
1.2540	102.0240	36.2700	384.6067	6.6885
1.5390	70.2396	40.4550	356.4698	10.6331
1.8050	39.2400	42.1290	335.3551	18.9211
1.9152	17.6580	42.9660	327.7252	42.2629
1.9608	7.8480	40.7340	325.1046	84.9544

SOIL DAMPING COEFFICIENTS VERSUS TIME

SOIL DYNAMIC DAMPING COEFFICIENTS
FOR TERRAIN HARDNESS A

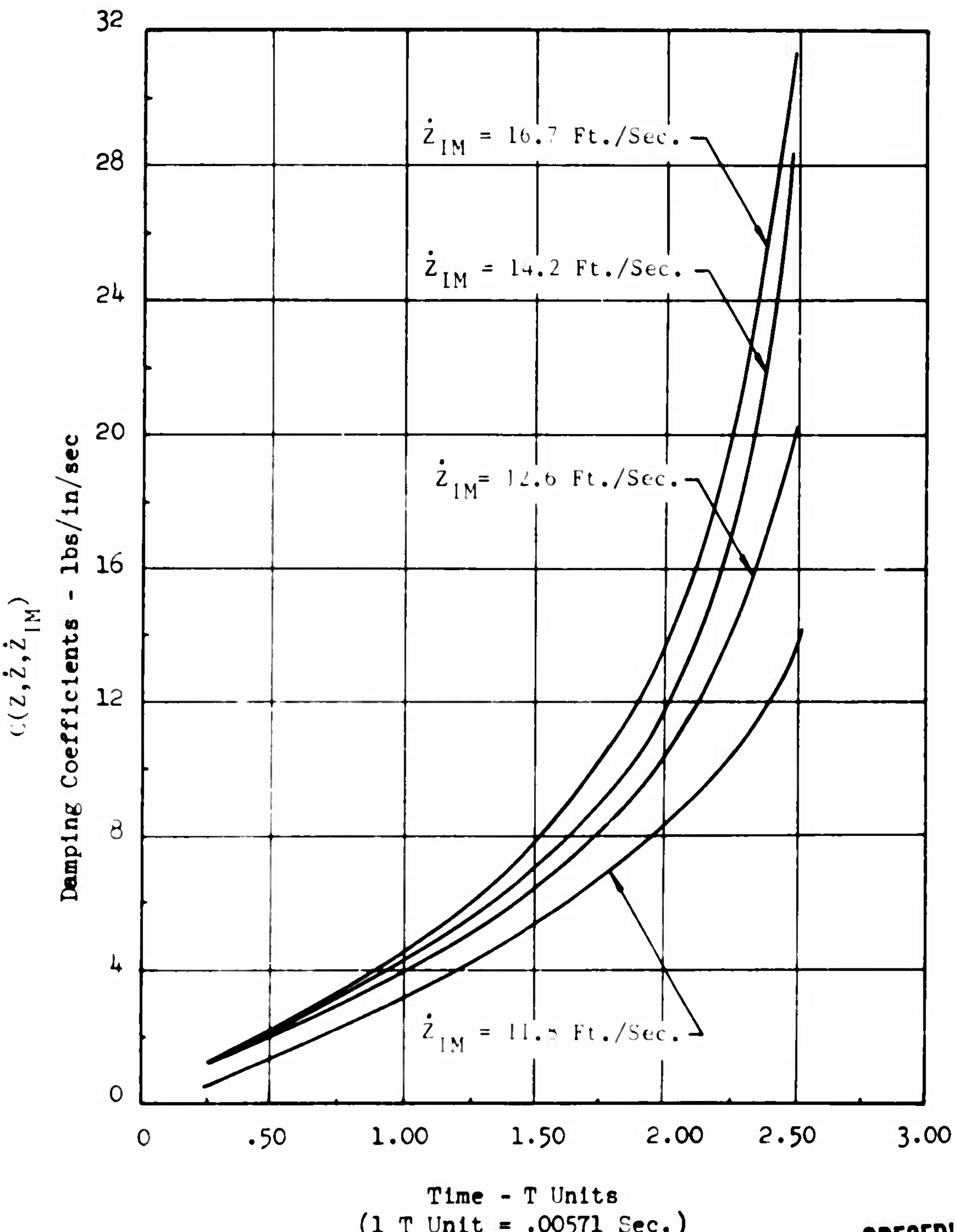

PRECEDING PAGE BLANK

SOIL DYNAMIC DAMPING COEFFICIENTS
FOR TERRAIN HARDNESS B

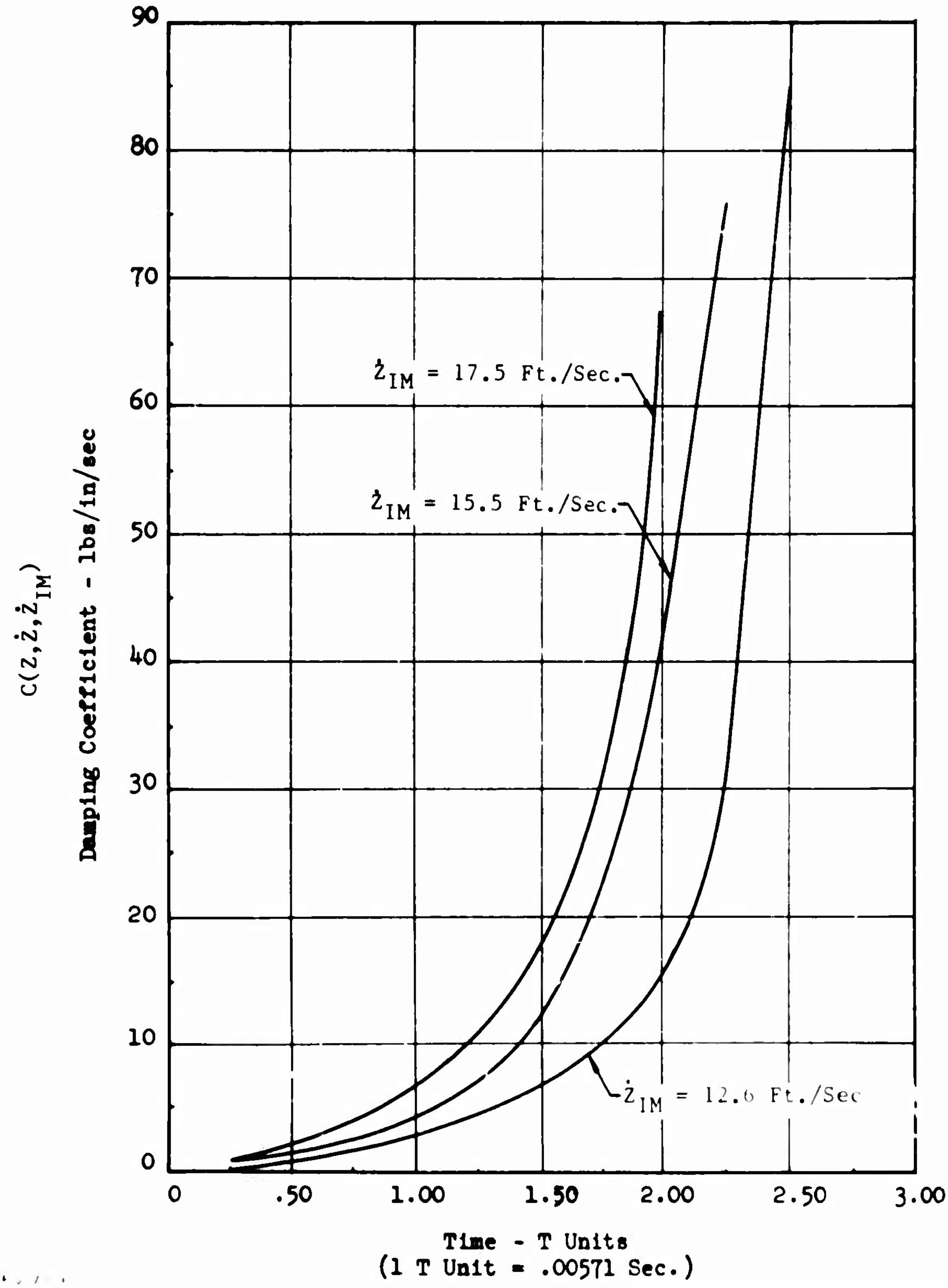

SOIL DYNAMIC DAMPING COEFFICIENTS
FOR TERRAIN HARDNESS C

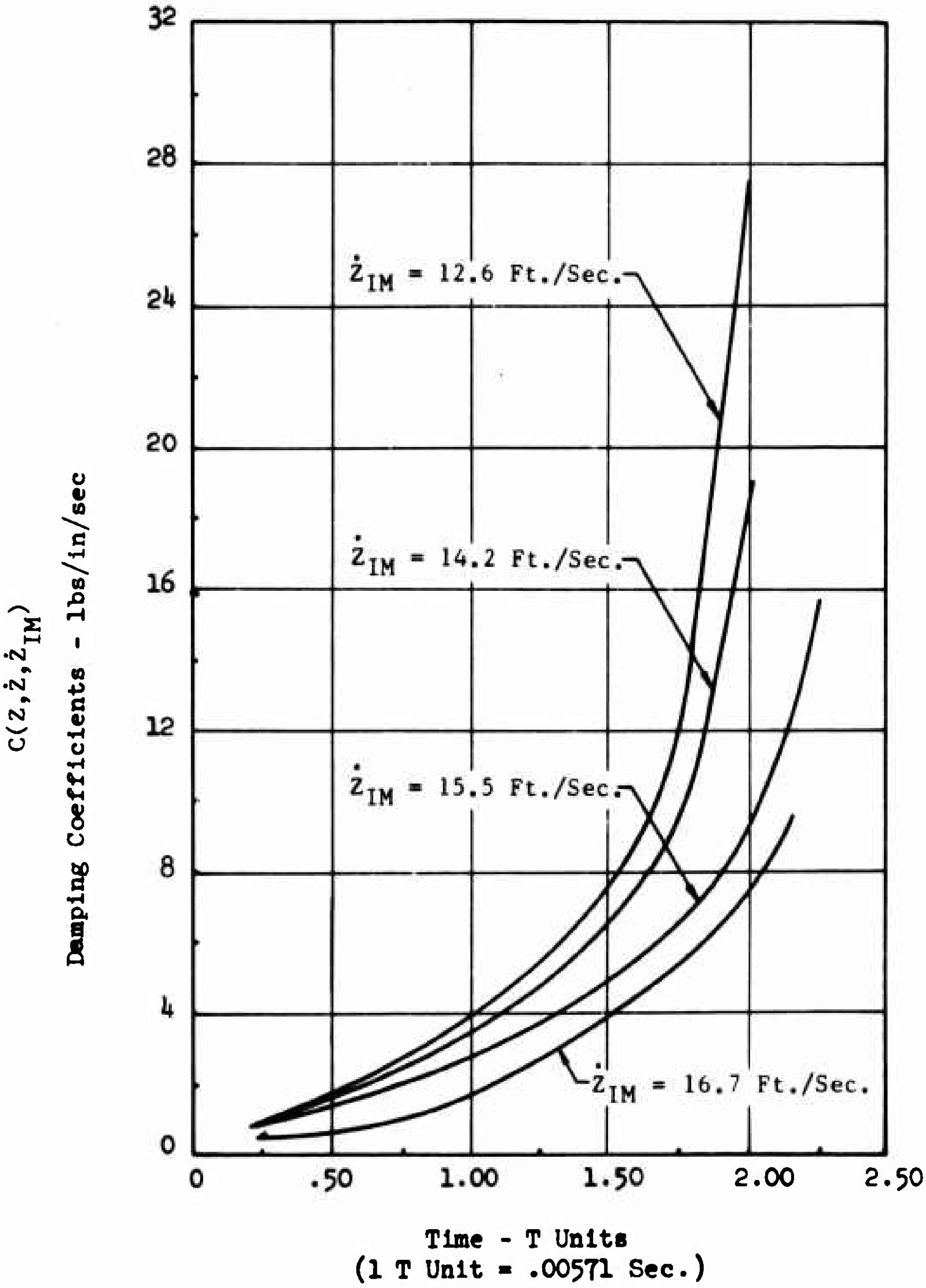

SOIL DYNAMIC DAMPING COEFFICIENTS
FOR TERRAIN HARDNESS D

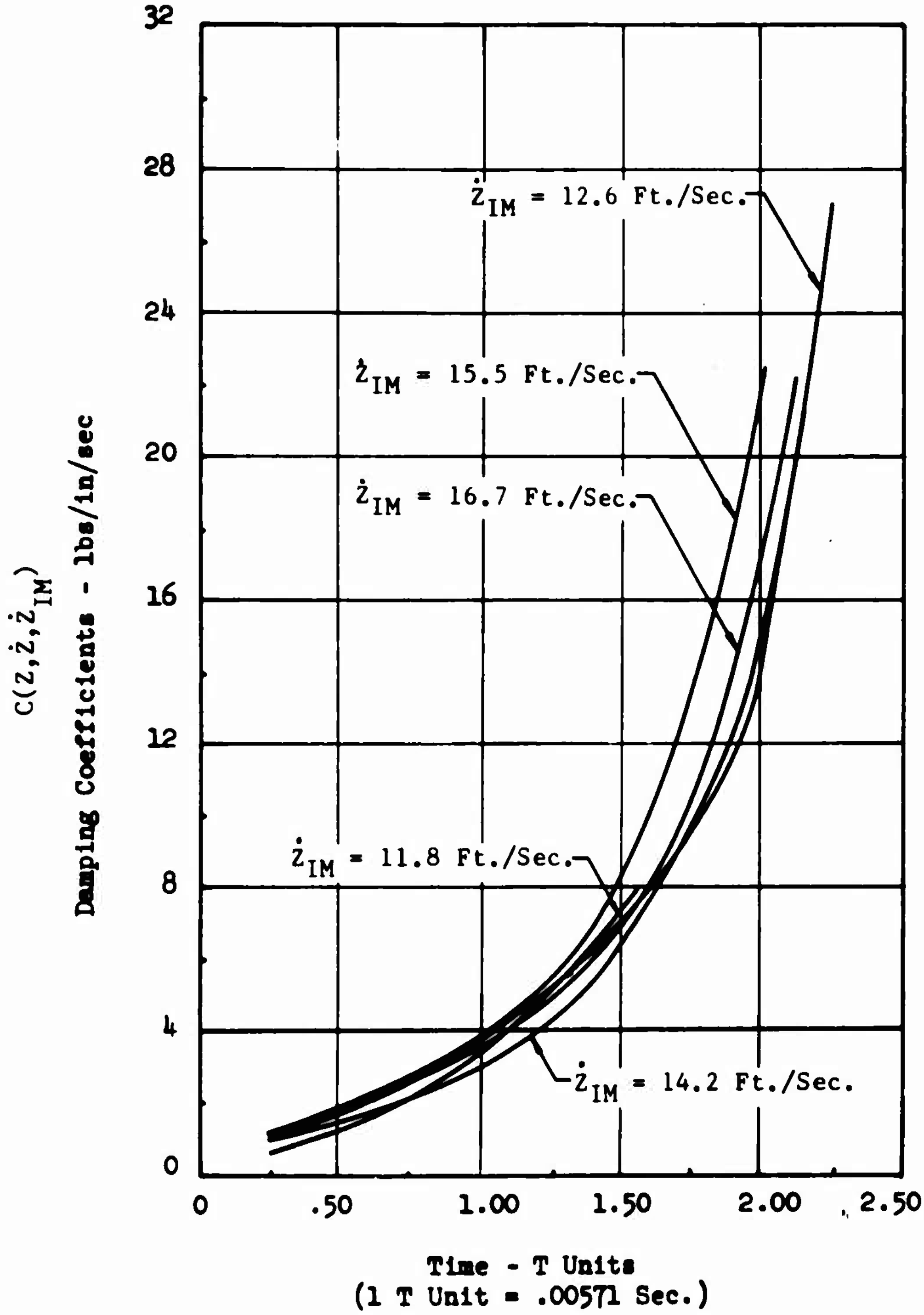

SOIL DYNAMIC DAMPING COEFFICIENTS
FOR TERRAIN HARDNESS G

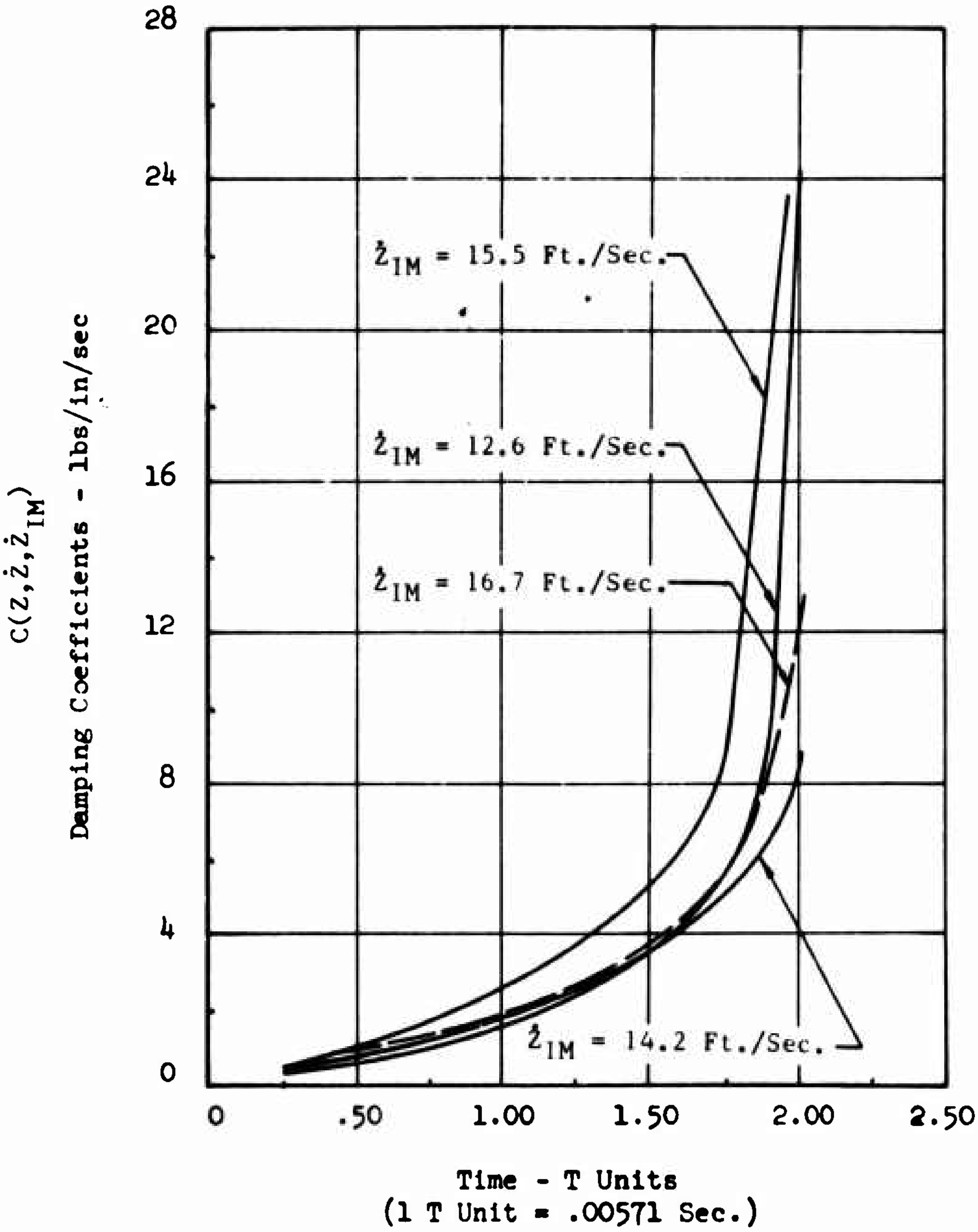

SOIL DYNAMIC DAMPING COEFFICIENTS
FOR TERRAIN HARDNESS I

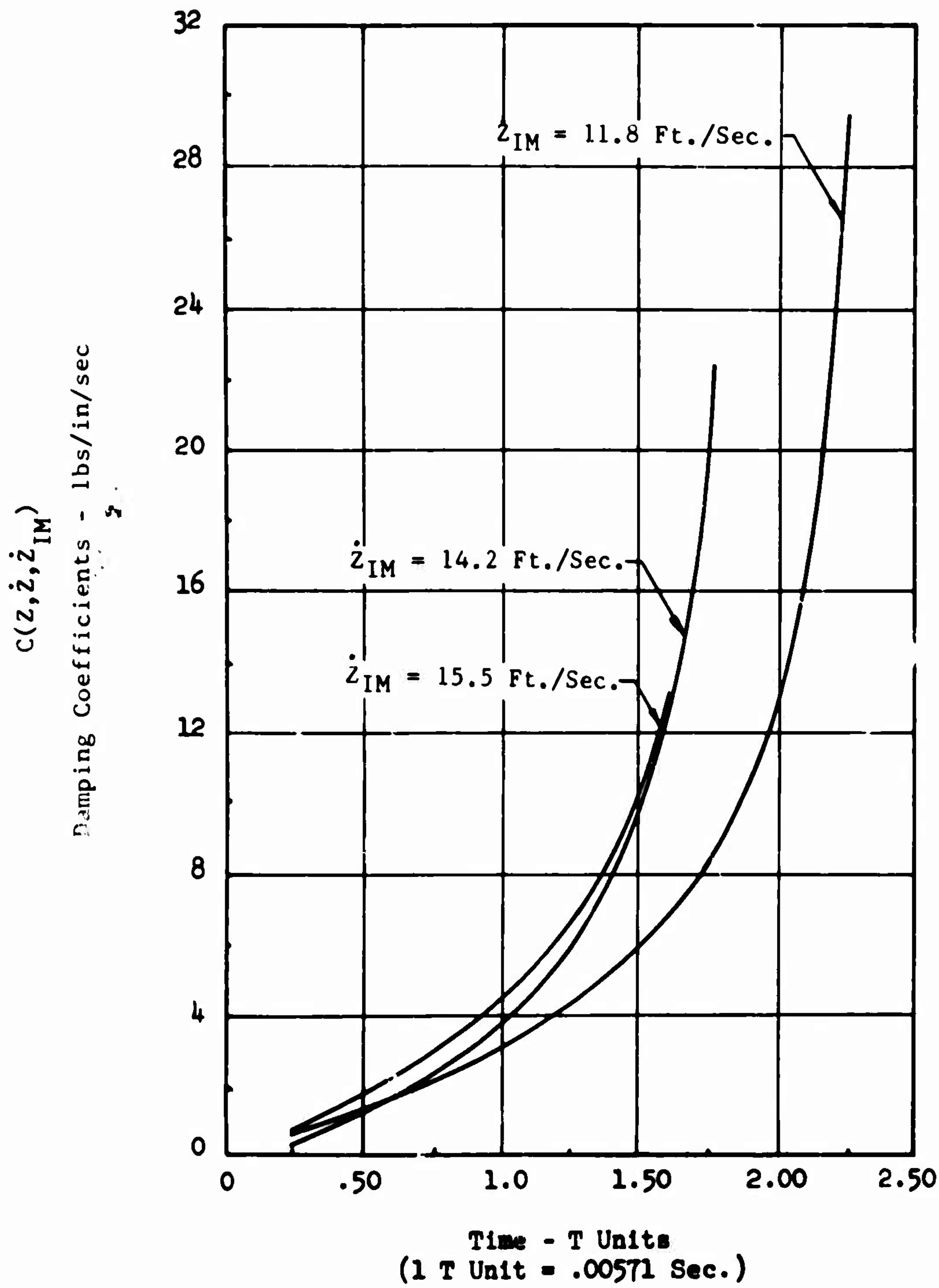

SOIL DAMPING COEFFICIENTS VERSUS VELOCITY

SOIL DYNAMIC DAMPING COEFFICIENTS
FOR TERRAIN HARDNESS A

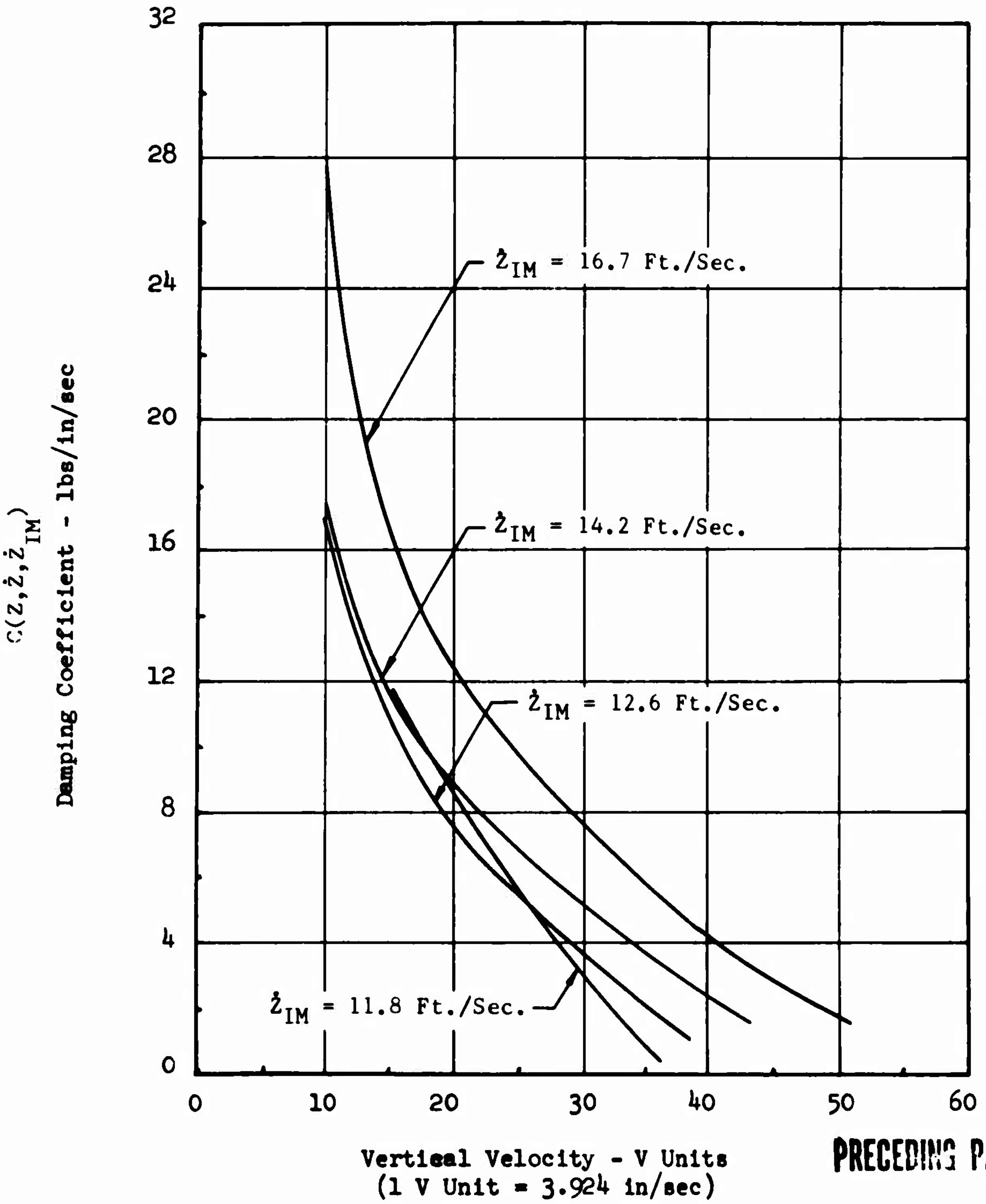

PRECEDING PAGE BLANK

SOIL DYNAMIC DAMPING COEFFICIENTS
FOR TERRAIN HARDNESS B

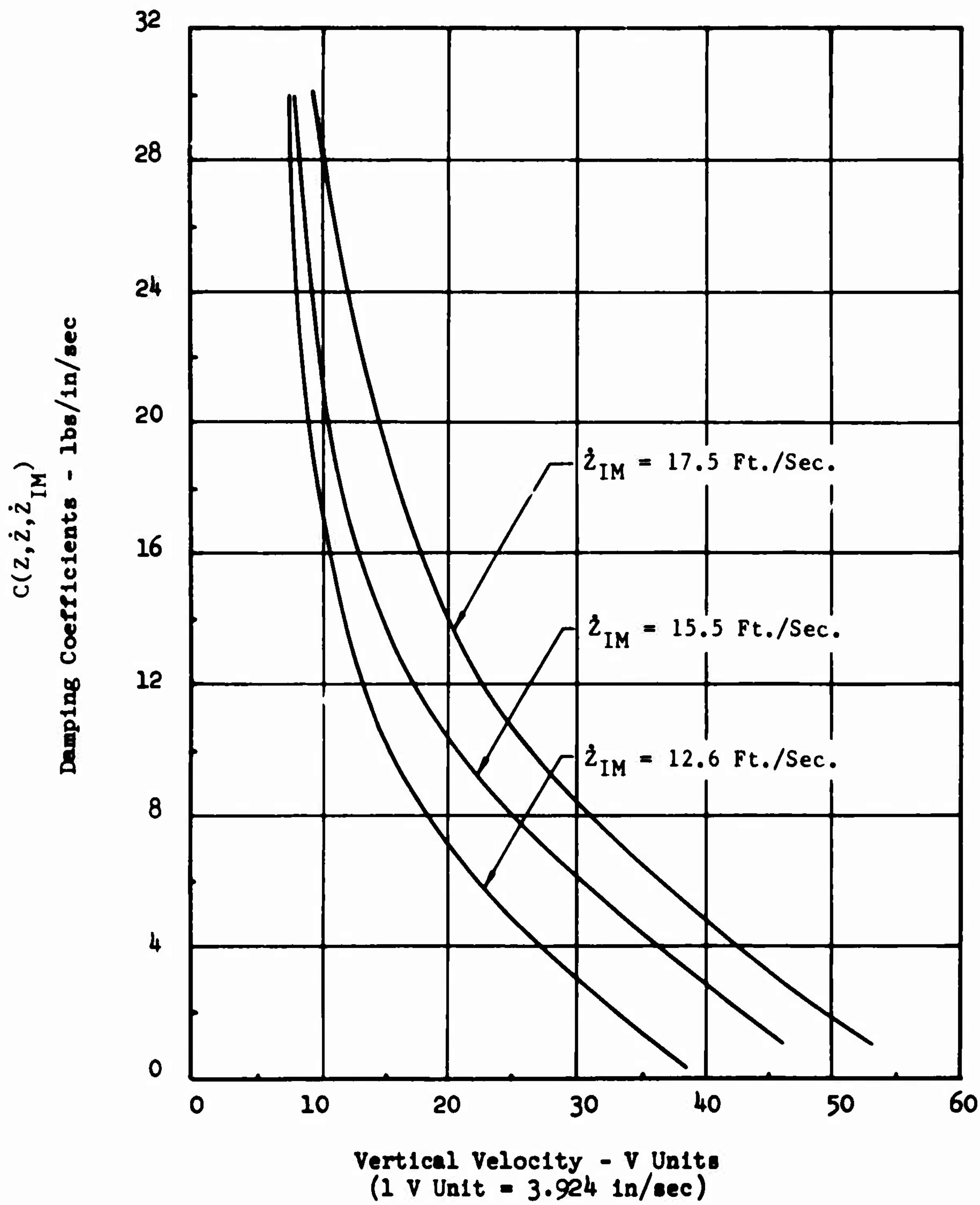

SOIL DYNAMIC DAMPING COEFFICIENTS
FOR TERRAIN HARDNESS C

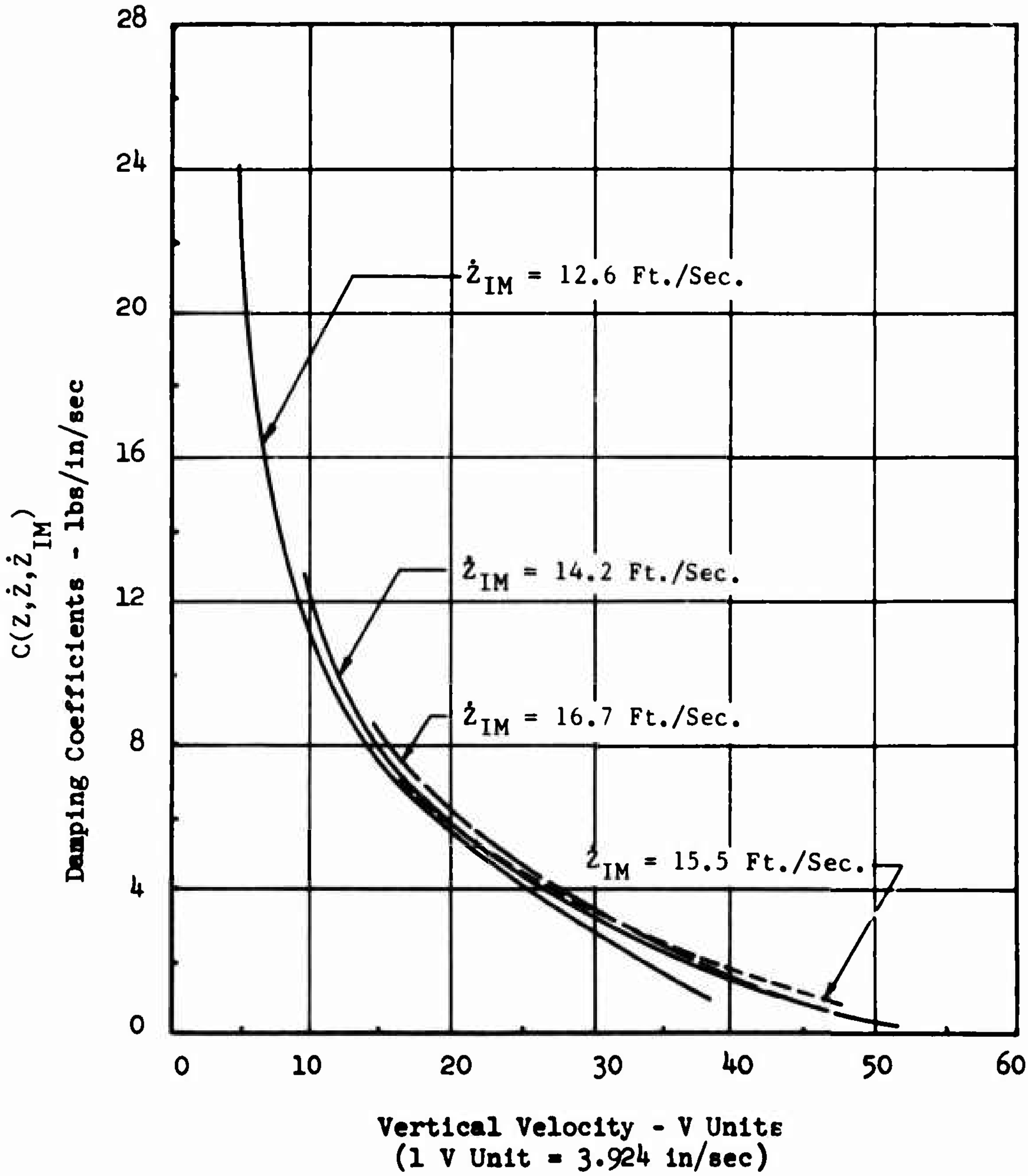

SOIL DYNAMIC DAMPING COEFFICIENTS
FOR TERRAIN HARDNESS D

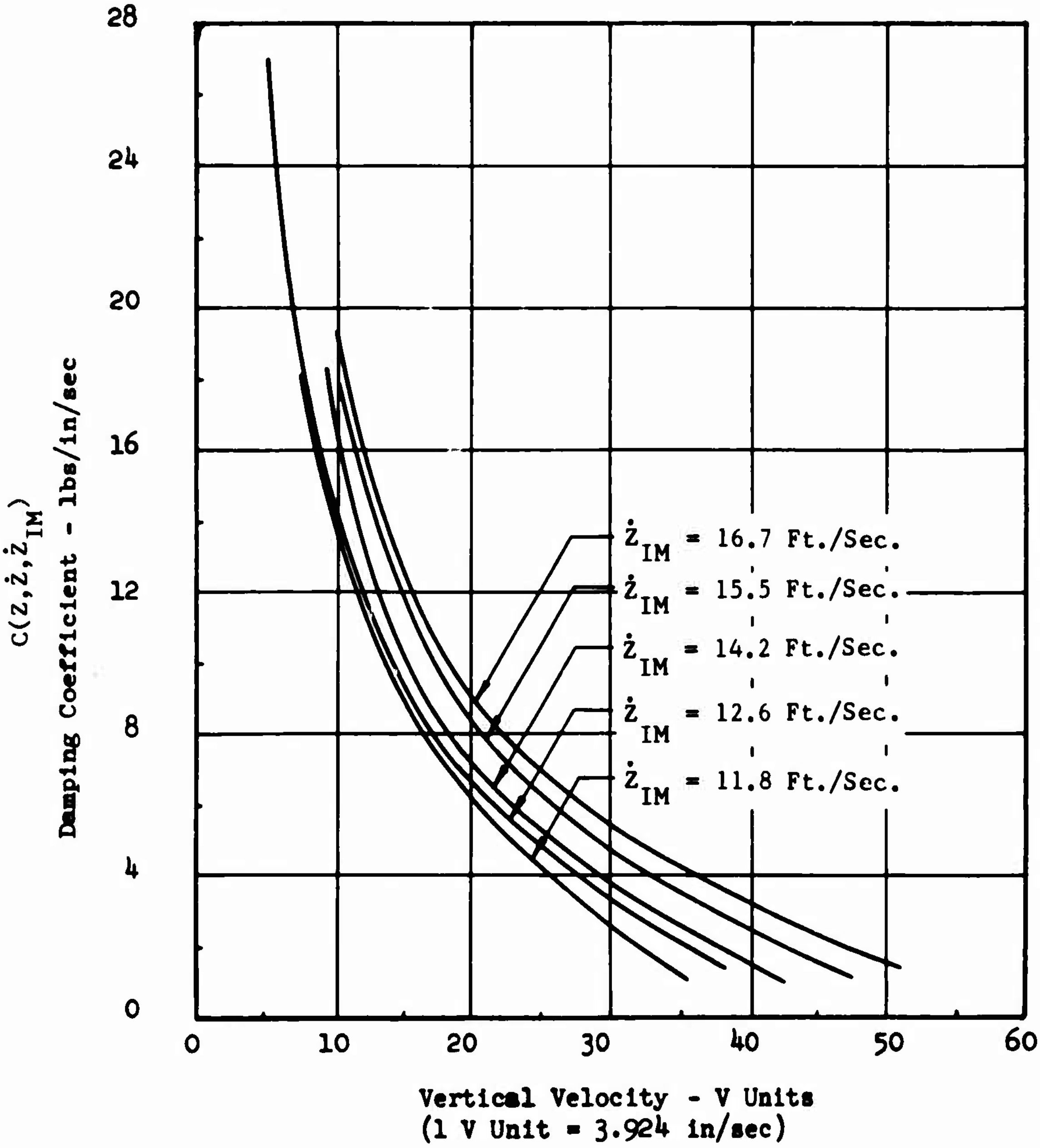

SOIL DYNAMIC DAMPING COEFFICIENTS
FOR TERRAIN HARDNESS G

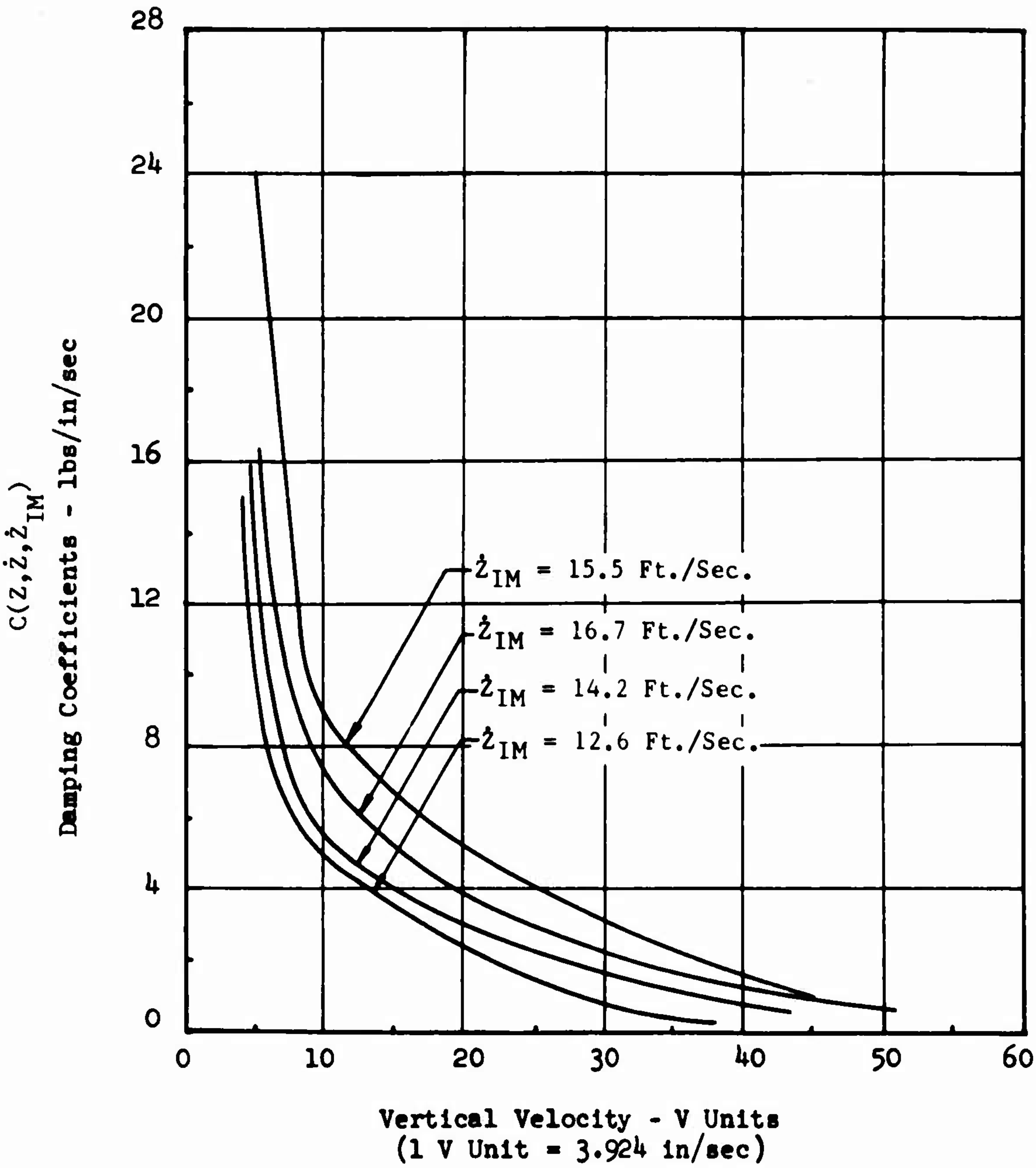

SOIL DYNAMIC DAMPING COEFFICIENTS
FOR TERRAIN HARDNESS I

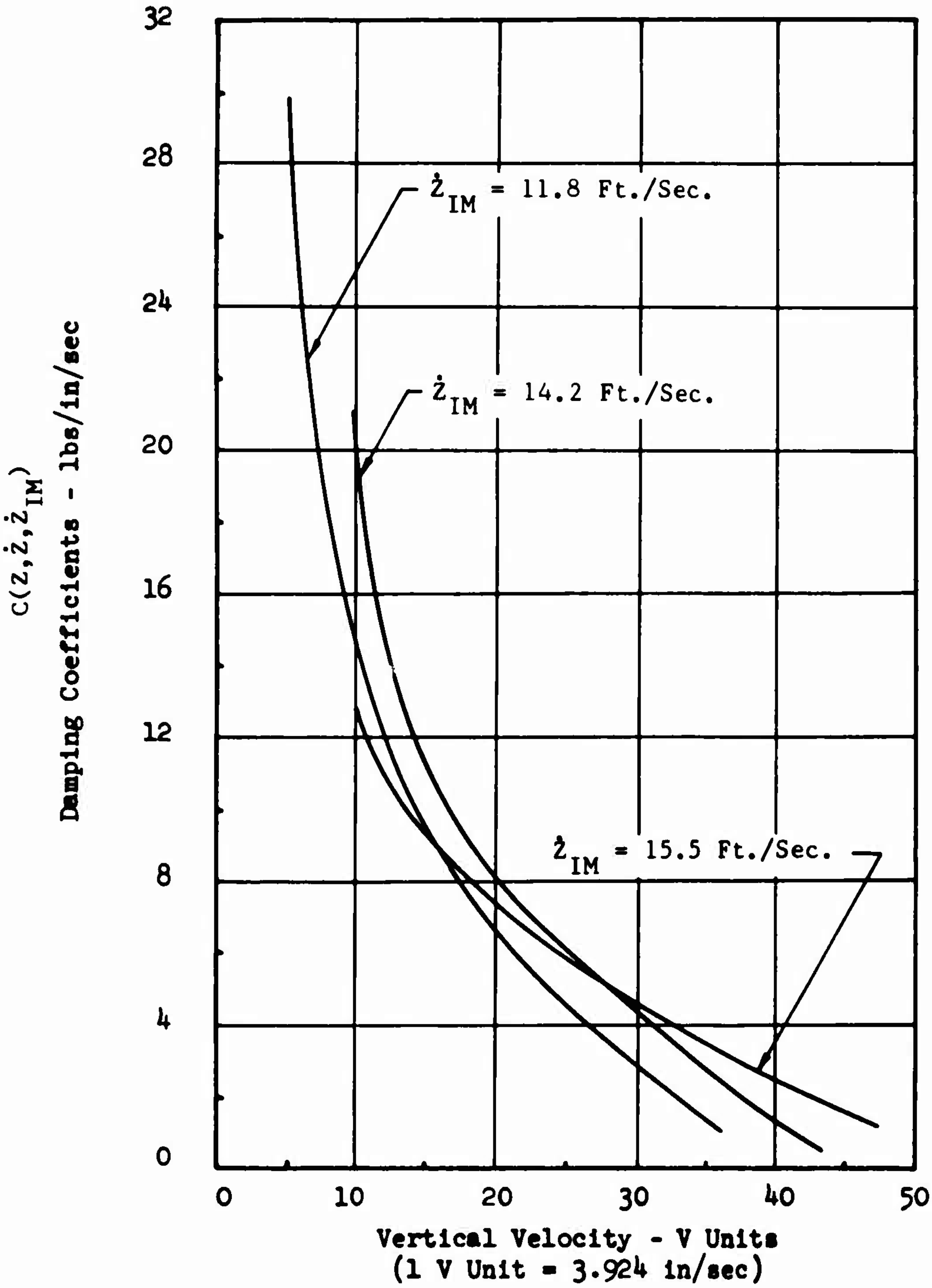

GENERAL PENETROMETER DATA

ASSOCIATED WITH LANDING

SITE II

PENETROMETER READINGS
8 MAY - A.M.
SITE NO. 2 (II)
CENTERLINE

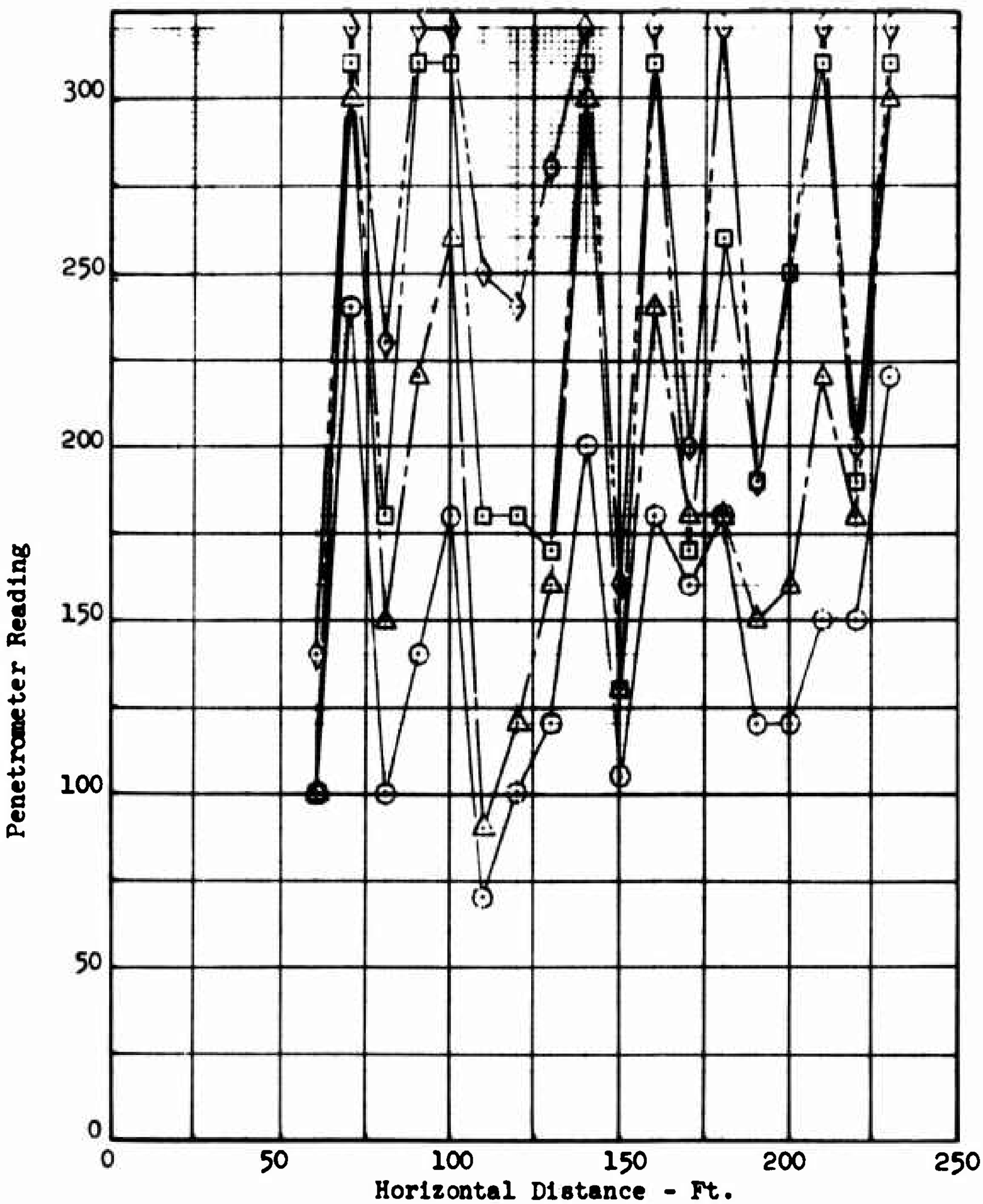

○ Implies 1 Inch Depth ——
△ Implies 2 Inch Depth —·—
□ Implies 3 Inch Depth —---
◇ Implies 4 Inch Depth ----

Values at 320 Indicate Readings Beyond Range of Penetrometer

PRECEDING PAGE BLANK

PENETROMETER READINGS
8 MAY - P.M.
SITE NO. 2 (II)
CENTERLINE

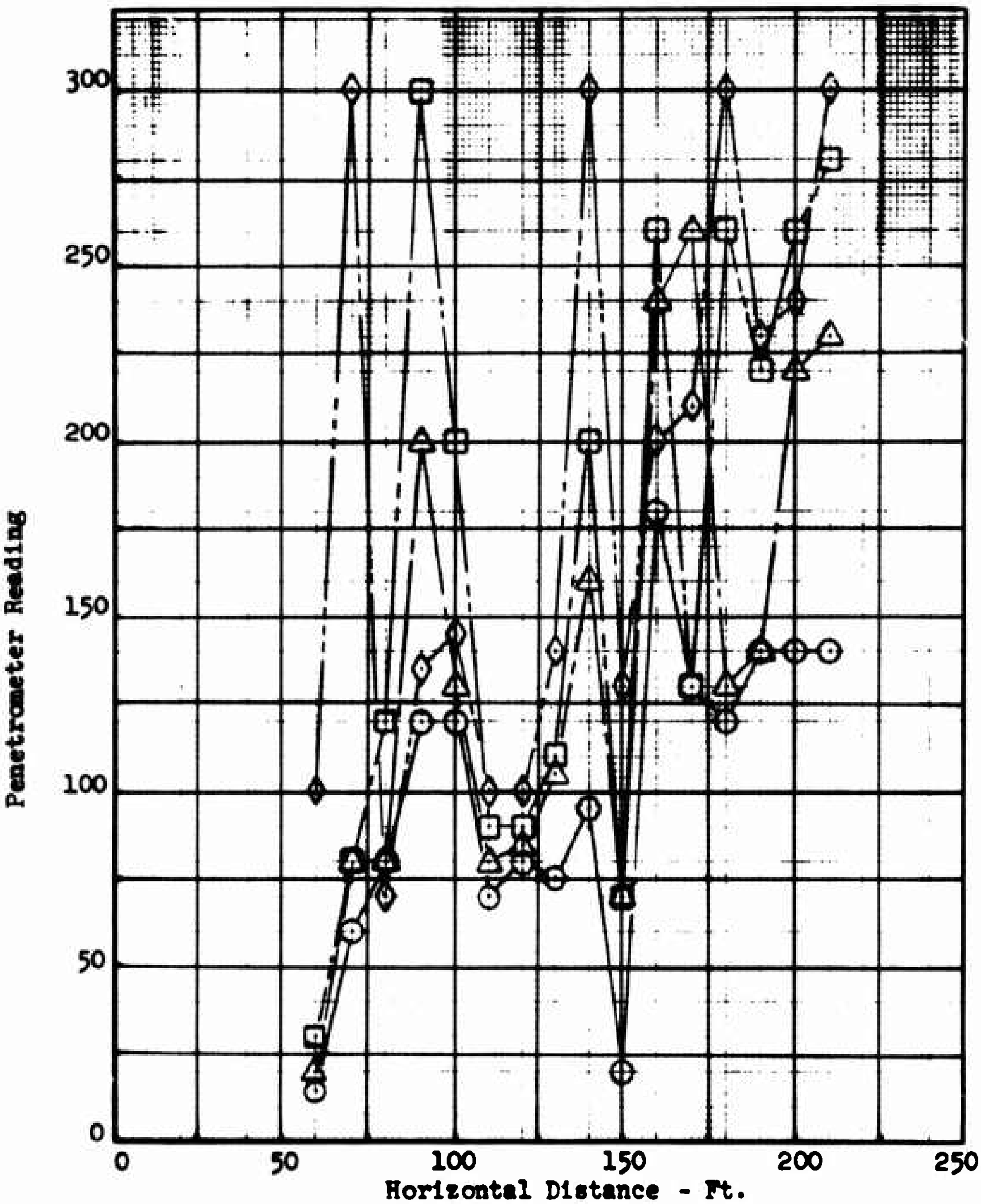

○ Implies 1 Inch Depth ———
△ Implies 2 Inch Depth —·—
□ Implies 3 Inch Depth —··—
◇ Implies 4 Inch Depth -----

PENETROMETER READINGS
May 10 - A. M.

25 Feet Left of Centerline of Site No. 2 (II)

DEPTH							HORIZONTAL DISTANCE - FEET														
(INCHES)	-60	60	70	-80	80	90	100	110	120	130	140	150	160	170	180	190	-200	200	210	220	230
1	70	90	80	70	80	60	70	60	70	110	100	110	110	90	70	120	100	100	180	300	300
2	110	120	140	100	100	80	100	70	130	150	90	120	150	110	90	150	220	110	300	I	I
3	150	130	190	110	100	90	110	110	180	220	70	130	170	130	120	180	300	140	I		
4	240	150	240	300	180	110	160	240	280	300	100	130	200	110	240	220	I	180			
5	I	130	I	I	300	110	300	300	I	I	130	160	300	120	I	260		280			
6		140			I	130	I	I			280	200	I	130		I		I			
7		130				200					I	200		200							
8		160				I						200		300							
9		250										I		I							

NOTES: 1. The negative sign preceeding the distance indicates a reading 2 inches upstream

2. Symbol I implies a reading beyond the range of the penetrometer

PENETROMETER READINGS
May 10 - A. M.

Centerline of Site No. 2 (II)

DEPTH (INCHES)	HORIZONTAL DISTANCE - FEET																			
	60	70	80	-90	90	100	-110	110	120	130	140	150	160	170	180	190	200	210	220	230
1	70	120	70	170	80	120	75	120	100	130	140	120	180	110	135	170	210	190	200	240
2	75	200	70	300	120	135	95	130	105	150	300	120	190	145	300	180	210	230	200	300
3	100	300	70	I	135	145	100	140	100	140	I	130	200	210	I	230	240	300	200	I
4	140	I	95		300	250	130	140	210	140		160	200	240		245	240	I	180	
5	180		180		I	I	300	300	300	300		160	220	250		300	240		160	
6	230		300				I	I	I	I		300	300	300		I	300		300	
7	230		I									I	I	I			I		I	
8	280																			

NOTES:

1. The negative sign preceeding the distance indicates a reading 2 inches upstream
2. Symbol I implies a reading beyond the range of the penetrometer

PENETROMETER READINGS
May 10 - A. M.

25 Feet Right of Centerline of Site No. 2 (II)

DEPTH (INCHES)	HORIZONTAL DISTANCE - FEET																						
	60	-70	70	80	90	-100	100	-110	110	-120	120	-130	130	-140	140	150	160	170	180	190	200	210	220	230
1	80	40	60	70	40	30	70	70	40	50	30	30	40	50	70	60	70	90	100	120	220	220	200	300
2	100	60	60	75	40	50	70	60	70	50	30	30	45	40	120	60	80	100	100	130	260	300	280	I
3	120	220	100	75	60	60	80	60	110	40	200	40	50	40	270	80	110	120	110	160	I	I	I	
4	300	I	300	100	70	70	120	60	180	50	300	30	120	40	I	140	130	140	110	180				
5	I		I	180	100	90	240	60	300	70	I	20	250	50		280	280	140	140	200				
6				300	200	120	I	100	I	180		60	I	300		I	I	200	300	I				
7				I	300	200		300		300		180		I				I	I					
8					I	300		I		I		300												
9						I						I												

NOTES:
1. The negative sign preceeding the distance indicates a reading 2 inches upstream
2. Symbol I implies a reading beyond the range of the penetrometer

PENETROMETER READINGS
10 MAY - A.M.
SITE NO.2 (II)
25 FEET LEFT OF CENTERLINE

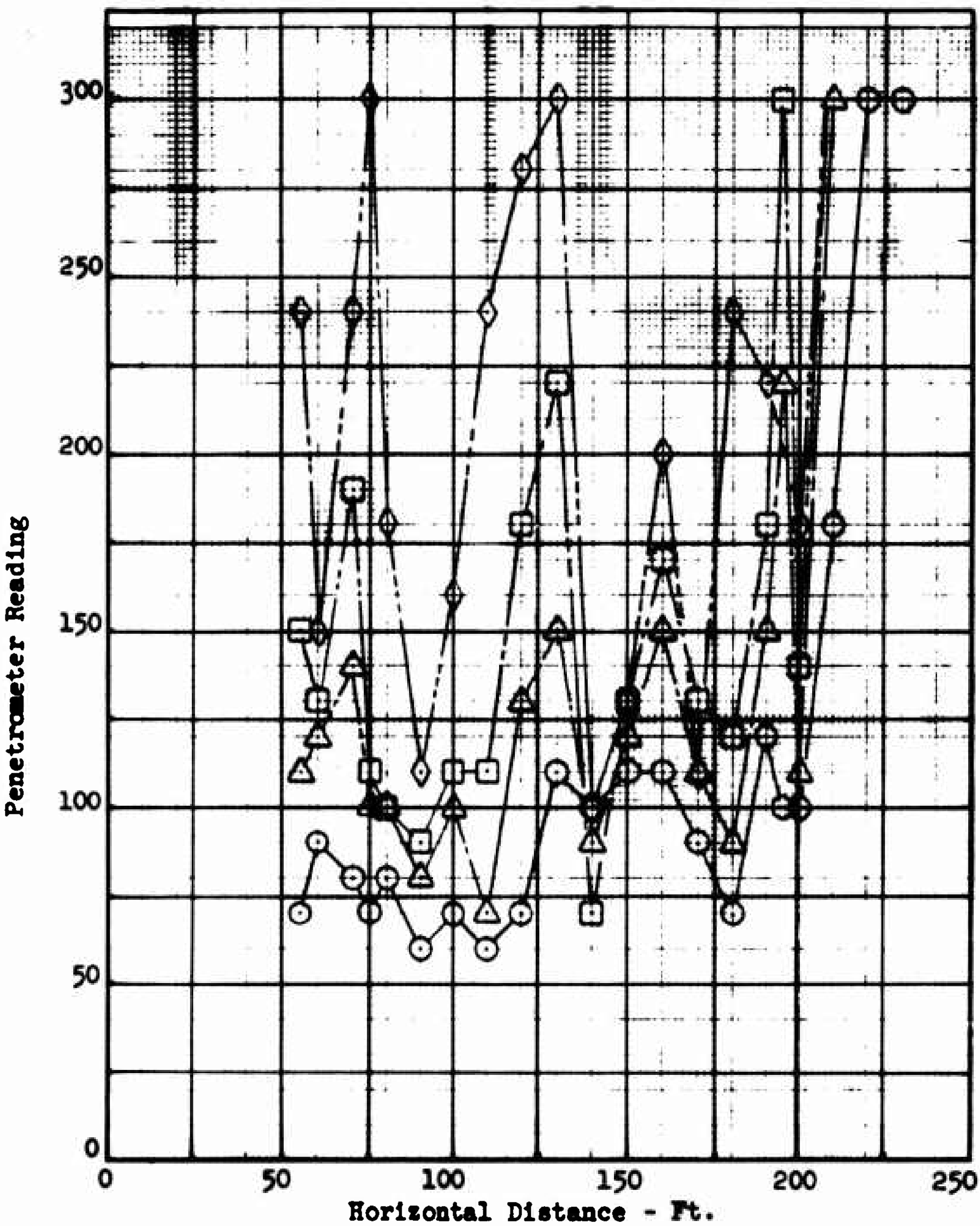

○ Implies 1 Inch Depth ———
△ Implies 2 Inch Depth —·—
□ Implies 3 Inch Depth —··—
◇ Implies 4 Inch Depth —···—

PENETROMETER READINGS
10 MAY - A.M.
SITE NO. 2 (II)
CENTERLINE

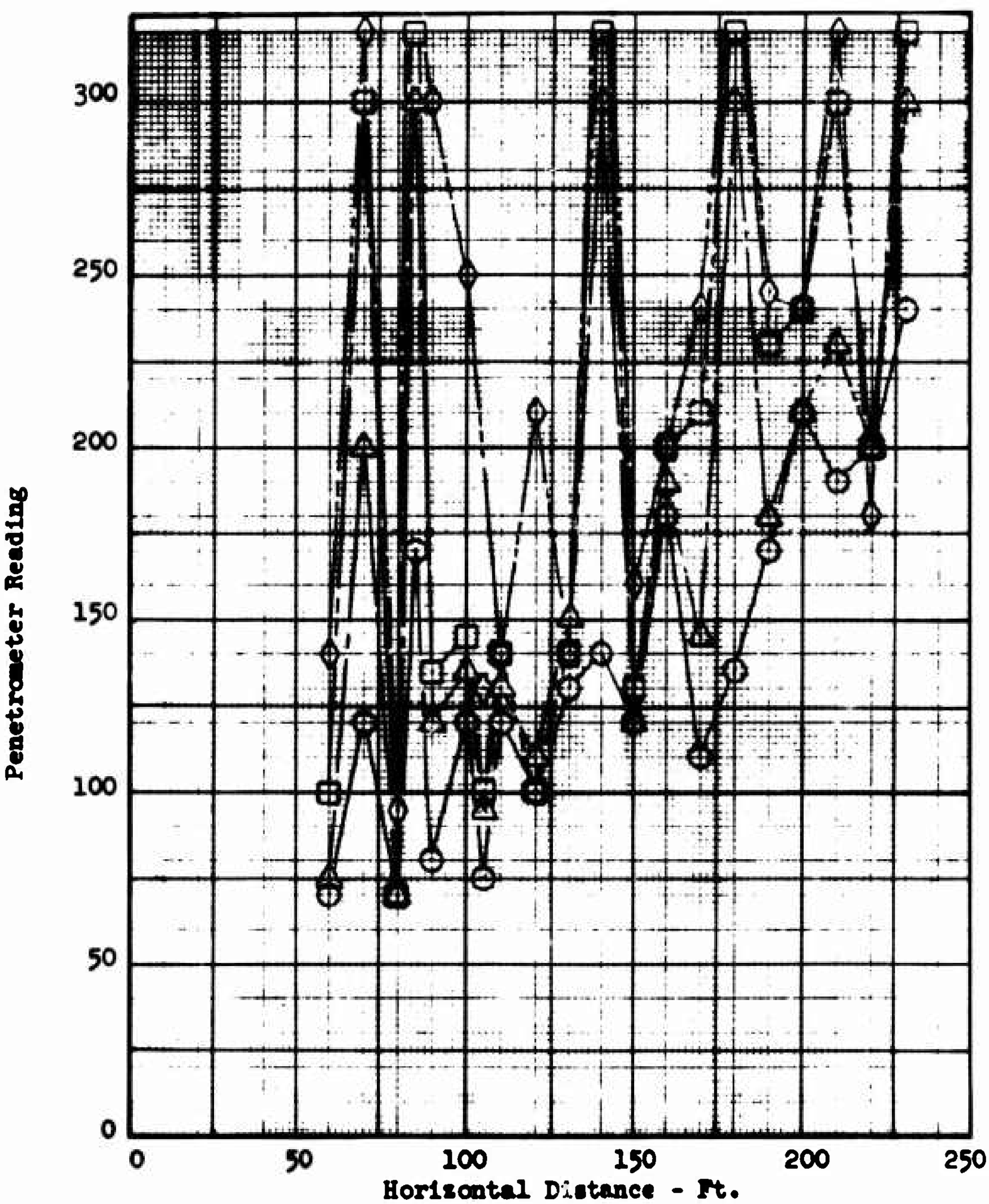

○ Implies 1 Inch Depth ——
△ Implies 2 Inch Depth -·-
□ Implies 3 Inch Depth ----
◇ Implies 4 Inch Depth -----

Values at 320 Indicate Readings Beyond Range of Penetrometer

PENETROMETER READINGS
10 MAY - A.M.
SITE NO. 2 (II)
25 FEET RIGHT OF CENTERLINE

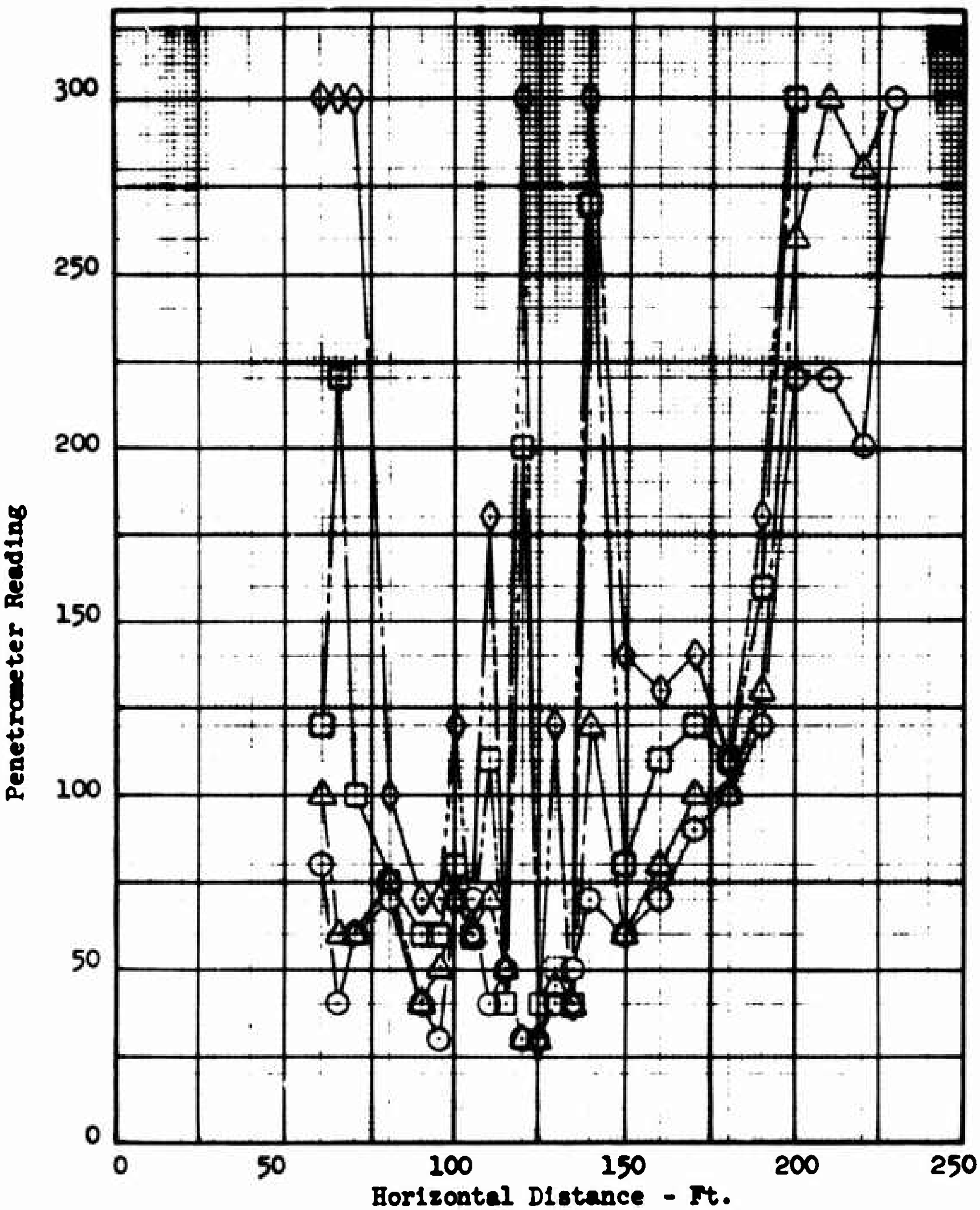

○ Implies 1 Inch Depth ——
△ Implies 2 Inch Depth —·—
□ Implies 3 Inch Depth —---
◇ Implies 4 Inch Depth —·····

PENETROMETER DATA ASSOCIATED WITH INDIVIDUAL LANDINGS

PENETROMETER READINGS
MAY 10
SITE NO. 2 (II)
LANDING NO. 215

DEPTH (INCHES)	LEFT MAIN GEAR			NOSE GEAR			RIGHT MAIN GEAR		
	LEFT	℄	RIGHT	LEFT	℄ 3" Low	RIGHT	LEFT	℄	RIGHT
1	100	80	180	75	100	55	210	220	300
2	140	150	130	110	185	75	300	300	I
3	185	200	100	180	300	150	I	I	
4	260	300	85	280	I	190			
5	I	I	105	280		280			
6			220	I		I			
7			280						
8			I						

DEPTH (INCHES)	6 FEET DOWNSTREAM LEFT MAIN GEAR			NOSE GEAR			RIGHT MAIN GEAR		
	LEFT	℄ 4" Low	RIGHT 6" Low	LEFT	℄ 2" Low	RIGHT	LEFT	℄	RIGHT
1	110	35	50	165	190	105			
2	120	55	45	260	280	215			
3	220	90	45	300	I	300			
4	240	155	50	I		I			
5	240	210	70						
6	I	300	90						
7		I	160						
8			260						
9			I						

NOTES: 1. Dimensions apply to sketch under ℄ for the gear and indicate terrain lateral profile.
2. Symbol I implies a reading beyond the range of the penetrometer.

PRECEDING PAGE BLANK

PENETROMETER READINGS
MAY 10
SITE NO. 2 (II)
LANDING NO. 216

DEPTH (INCHES)	LEFT MAIN GEAR			NOSE GEAR			RIGHT MAIN GEAR		
	LEFT	℄ 2" Low	RIGHT	LEFT	℄	RIGHT	LEFT	℄ 2" Low	RIGHT
1	115	90	120	95	85	195	75	140	90
2	110	135	115	140	230	300	130	185	145
3	125	170	125	200	I	I	170	210	260
4	185	190	190	300			205	I	I
5	210	230	245	I			235		
6	300	280	300				I		
7	I	I	I						

LANDING NO. 217

DEPTH (INCHES)	LEFT MAIN GEAR			NOSE GEAR			RIGHT MAIN GEAR		
	LEFT	℄	RIGHT	LEFT	℄ 3" LOW	RIGHT	LEFT	℄	RIGHT
1	135	120	120	75	25	80	80	55	220
2	185	140	145	100	70	95	110	60	300
3	260	190	220	115	95	110	170	95	I
4	300	300	300	140	130	110	300	130	
5	I	I	I	300	300	105	I	300	
6				I	I	150		I	
7						300			
8						I			

NOTES:
1. Dimensions apply to sketch under ℄ for the gear and indicate terrain lateral profile.
2. Symbol I implies a reading beyond the range of the penetrometer.

PENETROMETER READINGS
MAY 10
SITE NO. 2 (II)
LANDING NO. 218

DEPTH (INCHES)	LEFT MAIN GEAR			NOSE GEAR			RIGHT MAIN GEAR		
	LEFT 4" HIGH	℄	RIGHT	LEFT	℄	RIGHT	LEFT	℄ 2" LOW	RIGHT
1	80	85	45	105	160	125	115	60	80
2	80	85	80	125	300	150	170	110	80
3	185	95	125	140	I	180	210	170	115
4	160	105	165	225		300	290	280	260
5	170	100	210	300		I	300	300	300
6	175	105	180	I			I	I	I
7	190	155	300						
8	300	220	I						
9	I	300							
10		I							

1 FOOT DOWNSTREAM

DEPTH (INCHES)	LEFT MAIN GEAR		
	LEFT	℄	RIGHT
1	120	90	65
2	130	110	120
3	130	140	160
4	110	140	165
5	110	190	165
6	100	200	195
7	195	170	195
8	280	100	NB
9	I	100	
10		100	
11		100	
12		NB	

NOTES:
1. Dimensions apply to sketch under ℄ for the gear and indicate terrain lateral profile.
2. Symbol I implies a reading beyond the range of the penetrometer.

PENETROMETER READINGS
MAY 10
SITE NO. 2 (II)
LANDING NO. 219

DEPTH (INCHES)	LEFT MAIN GEAR			NOSE GEAR			RIGHT MAIN GEAR		
	LEFT	℄	RIGHT	LEFT	℄ 3" Low	RIGHT	LEFT	℄	RIGHT
1	110	100	90	90	100	40	90	260	160
2	180	160	160	90	240	90	150	300	240
3	200	230	220	140	300	140	260	I	300
4	240	300	220	290	I	240	300		I
5	300	I	260	I		300			
6	I		300			I			
7			I						

2 FEET DOWNSTREAM

DEPTH (INCHES)				
		LEFT	℄ 3" Low	RIGHT
1		80	80	60
2		100	140	90
3		120	300	160
4		160	I	300
5		300		I
6		I		

NOTES:
1. Dimensions apply to sketch under ℄ for the gear and indicate terrain lateral profile.
2. Symbol I implies a reading beyond the range of the penetrometer.

FORM 351-F REV 7-69

North American Aviation/Columbus
North American Rockwell

NR70H-570
A1-113

PENETROMETER READINGS
MAY 10
SITE NO. 2 (II)
LANDING NO. 220

DEPTH (INCHES)	LEFT MAIN GEAR			NOSE GEAR			RIGHT MAIN GEAR		
	LEFT	℄	RIGHT	LEFT	℄ 3" LOW	RIGHT	LEFT	℄ 4" Low	RIGHT
1	300	300	300	70	60	40	120	100	90
2	I	I	I	130	120	60	170	140	120
3				180	220	100	200	200	190
4				220	270	120	200	240	220
5				280	300	180	200	200	230
6				300	I	230	180	160	240
7				I		300	150	200	220
8						I	140	300	160
9							120	I	120
10							260		120
11							I		120
12									120
13									300
14									I

2½ FEET DOWNSTREAM

DEPTH (INCHES)	LEFT MAIN GEAR		NOSE GEAR			RIGHT MAIN GEAR		
	LEFT	RIGHT	LEFT 4" HIGH	℄ 3" HIGH	RIGHT	LEFT	℄ 4" LOW	RIGHT
1			50	40	60	110	110	130
2			50	80	50	110	120	180
3			40	190	50	100	160	200
4			40	240	120	100	200	200
5			100	240	180	120	180	240
6			130	230	250	200	140	270
7			180	300	300	I	130	I
8			260	I	I		150	
9			300				240	
10			I				300	
11							I	

NOTES: 1. Dimensions apply to sketch under ℄ for the gear and indicate terrain lateral profile.
2. Symbol I implies a reading beyond the range of the penetrometer.

PENETROMETER READINGS
MAY 10
SITE NO. 2 (II)
LANDING NO. 221

DEPTH (INCHES)	LEFT MAIN GEAR			NOSE GEAR			RIGHT MAIN GEAR		
	LEFT	℄	RIGHT	LEFT	℄ 2" Low	RIGHT	LEFT 3" High	℄ 2" High	RIGHT
1	180	160	200	160	70	90	60	80	100
2	240	240	300	190	120	110	70	80	120
3	300	260	I	240	260	120	80	180	180
4	I	280		300	300	200	90	300	300
5		300		I	I	300	120	I	I
6		I				I	220		
7							I		

2½ FEET DOWNSTREAM

DEPTH (INCHES)	LEFT MAIN GEAR			NOSE GEAR			RIGHT MAIN GEAR		
	LEFT	℄ 1" Low	RIGHT	LEFT	℄ 2½" Low	RIGHT	LEFT	℄ 3" Low	RIGHT
1	100	170	110	110	120	140	100	50	80
2	120	260	110	130	180	130	110	70	80
3	140	I	180	160	300	170	90	160	100
4	300		300	220	I	170	80	300	180
5	I		I	300		240	70	I	300
6				I		I	140		I
7							300		
8							I		

NOTES:
1. Dimensions apply to sketch under ℄ for the gear and indicate terrain lateral profile.
2. Symbol I implies a reading beyond the range of the penetrometer.

North American Aviation/Columbus
North American Rockwell

NR70H-570
A1-115

PENETROMETER READINGS
MAY 11
SITE NO. 2 (II)
LANDING NO. 223

DEPTH (INCHES)	LEFT MAIN GEAR			NOSE GEAR			RIGHT MAIN GEAR		
	LEFT	℄ 2" Low	RIGHT	LEFT 2" High	℄	RIGHT	LEFT	℄ 1" Low	RIGHT
1	135	120	80	180	260	200	140	100	90
2	170	120	90	300	300	150	155	125	120
3	140	100	110	I	I	165	155	160	180
4	130	110	145			220	170	255	210
5	140	130	180			245	155	300	290
6	200	200	200			230	165	I	300
7	240	300	160			300	240		I
8	300	I	180			I	260		
9	I		270				265		
10			I				300		
11							I		

2½ FEET DOWNSTREAM

DEPTH (INCHES)	LEFT MAIN GEAR			NOSE GEAR			RIGHT MAIN GEAR		
	LEFT	℄ 1" Low	RIGHT	LEFT 2" Low	℄ 4" Low	RIGHT	LEFT	℄	RIGHT
1	60	160	130	210	260	160	160	90	70
2	75	170	160	300	300	160	235	120	85
3	75	195	165	I	I	165	265	190	115
4	65	230	120			180	300	255	120
5	80	300	90			230	I	I	180
6	120	I	110			250			300
7	300		150			265			I
8	I		230			300			
9			200			I			
10			300						
11			I						

NOTES:
1. Dimensions apply to sketch under ℄ for the gear and indicate terrain lateral profile.
2. Symbol I implies a reading beyond the range of the penetrometer.

PENETROMETER READINGS
MAY 11
SITE NO. 2 (II)
LANDING NO. 224

DEPTH (INCHES)	LEFT MAIN GEAR			NOSE GEAR			RIGHT MAIN GEAR		
	LEFT	℄	RIGHT	LEFT	℄	RIGHT	LEFT	℄	RIGHT
1	300	140	220	220	110	200	105	70	110
2	I	260	220	240	195	260	190	135	145
3		300	I	280	255	300	245	210	180
4		I		300	270	I	285	280	220
5				I	300		220	300	300
6					300		220	I	I
7					I		300		
8							I		

2½ FEET DOWNSTREAM

DEPTH (INCHES)	LEFT MAIN GEAR			NOSE GEAR			RIGHT MAIN GEAR		
	LEFT	℄	RIGHT	LEFT 6" High	℄	RIGHT 3" High	LEFT 1" Low	℄	RIGHT
1	300	220	230	160	180	115	95	130	180
2	I	300	260	210	240	135	75	200	265
3		I	300	285	255	135	80	285	300
4			I	300	265	190	120	300	I
5				I	270	300	300	I	
6					270	I	I		
7					220				
8					240				
9					200				
10					200				
11					200				
12					200				
13					NB				

NOTES:
1. Dimensions apply to sketch under ℄ for the gear and indicate terrain lateral profile.
2. Symbol I implies a reading beyond the range of the penetrometer.

PENETROMETER READINGS
MAY 11
SITE NO. 2 (II)
LANDING NO. 225

DEPTH (INCHES)	LEFT MAIN GEAR			NOSE GEAR			RIGHT MAIN GEAR		
	LEFT	℄	RIGHT	LEFT	℄	RIGHT	LEFT	℄	RIGHT
1	170	90	120	240	195	205	190	100	130
2	210	140	135	280	235	200	240	165	210
3	210	280	280	300	300	220	280	300	300
4	240	300	I	300	I	250	300	I	I
5	300	I		I		300	I		
6	I					I			

2½ FEET DOWNSTREAM

DEPTH (INCHES)	LEFT MAIN GEAR			NOSE GEAR			RIGHT MAIN GEAR		
	LEFT	℄	RIGHT	LEFT	℄ 1" Low	RIGHT	LEFT	℄	RIGHT
1	250	160	160	250	300	250	190	125	185
2	300	220	220	280	I	300	240	180	300
3	I	280	300	300		I	300	260	I
4		300	I	I			I	300	
5		I						I	

NOTES:
1. Dimensions apply to sketch under ℄ for the gear and indicate terrain lateral profile.
2. Symbol I implies a reading beyond the range of the penetrometer.

PENETROMETER READINGS
MAY 11
SITE NO. 2 (II)
LANDING NO. 226

DEPTH (INCHES)	LEFT MAIN GEAR			NOSE GEAR			RIGHT MAIN GEAR		
	LEFT 1" High	℄	RIGHT	LEFT	℄ 2" Low	RIGHT	LEFT 2" High	℄	RIGHT
1	120	150	140	220	170	120	80	90	80
2	140	150	200	250	230	120	80	120	70
3	180	170	230	260	230	150	80	200	90
4	220	120	300	300	240	140	80	300	140
5	270	130	I	I	300	200	80	300	300
6	300	150			I	300	100	300	I
7	I	180				I	200	I	
8		220					I		
9		300							
10		I							

2½ FEET DOWNSTREAM

DEPTH (INCHES)	LEFT MAIN GEAR			NOSE GEAR			RIGHT MAIN GEAR		
	LEFT 3" High	℄	RIGHT	LEFT	℄ 3" Low	RIGHT	LEFT	℄ 2" Low	RIGHT
1	60	120	160	260	140	120	80	100	80
2	60	150	160	300	140	140	80	160	70
3	70	170	160	220	160	160	80	280	70
4	70	300	280	220	300	300	80	I	120
5	60	I	I	300	I	I	100		300
6	40			I			160		I
7	40						300		
8	40						I		
9	150								
10	300								
11	I								

NOTE:
1. Dimensions apply to sketch under ℄ for the gear and indicate terrain lateral profile.
2. Symbol I implies a reading beyond the range of the penetrometer.

TERRAIN CONTOUR DATA

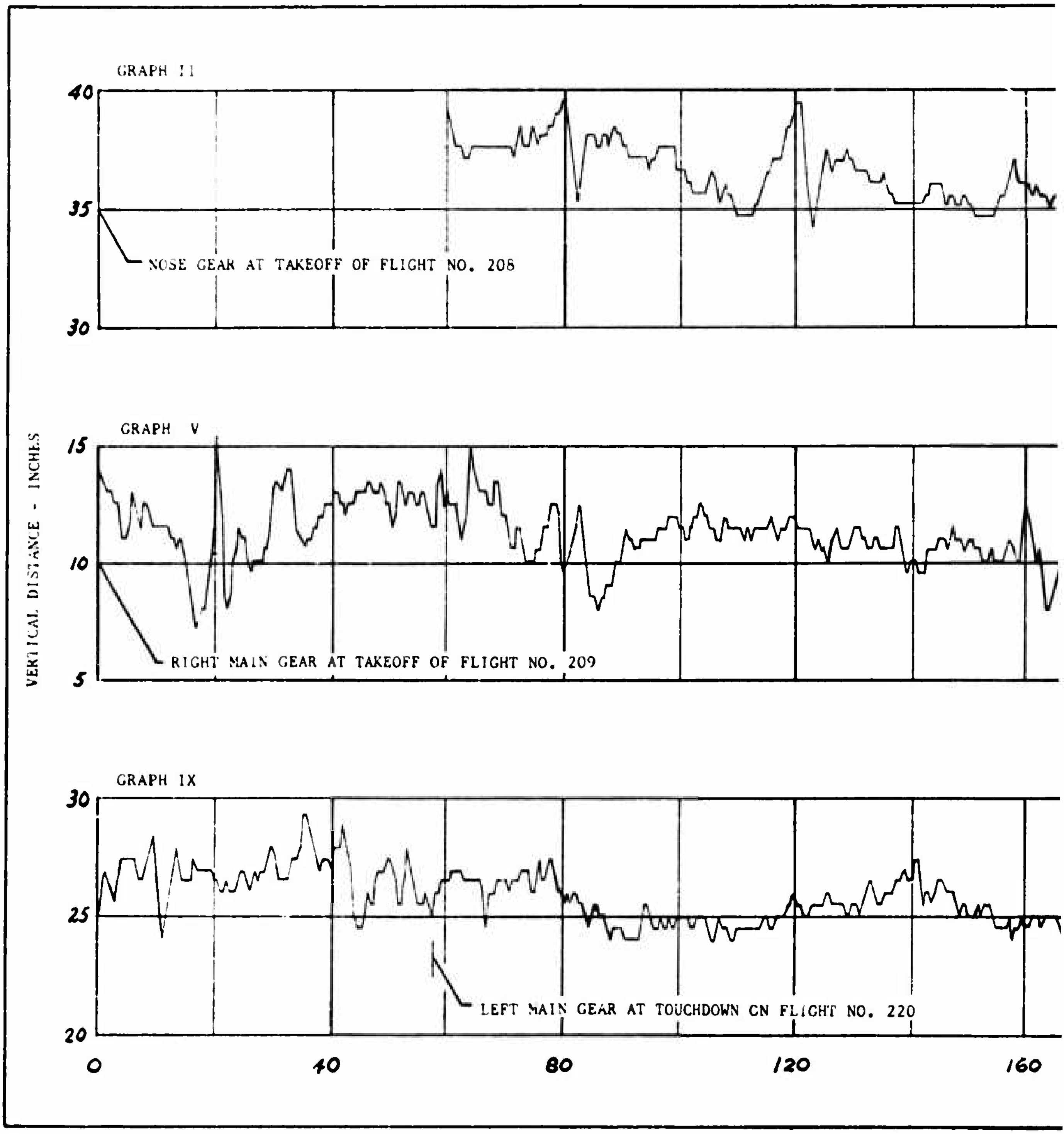

GRAPH II
NOSE GEAR AT TAKEOFF OF FLIGHT NO. 208
GRAPH V
RIGHT MAIN GEAR AT TAKEOFF OF FLIGHT NO. 209
GRAPH IX
LEFT MAIN GEAR AT TOUCHDOWN ON FLIGHT NO. 220
VERTICAL DISTANCE - INCHES
40
35
30
15
10
5
30
25
20
0
40
80
120
160

B

:ONTOUR

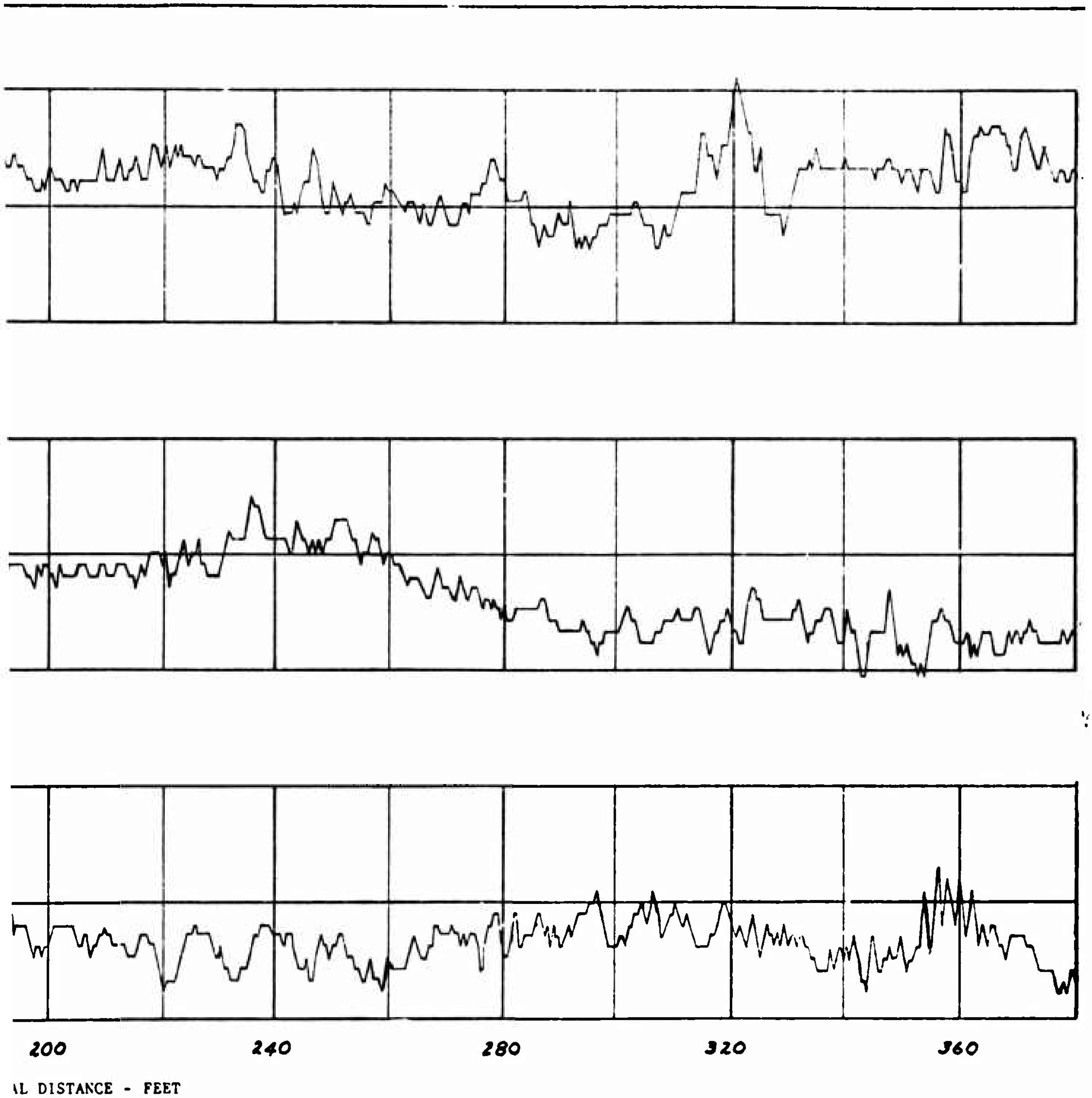

PRECEDING PAGE BLANK

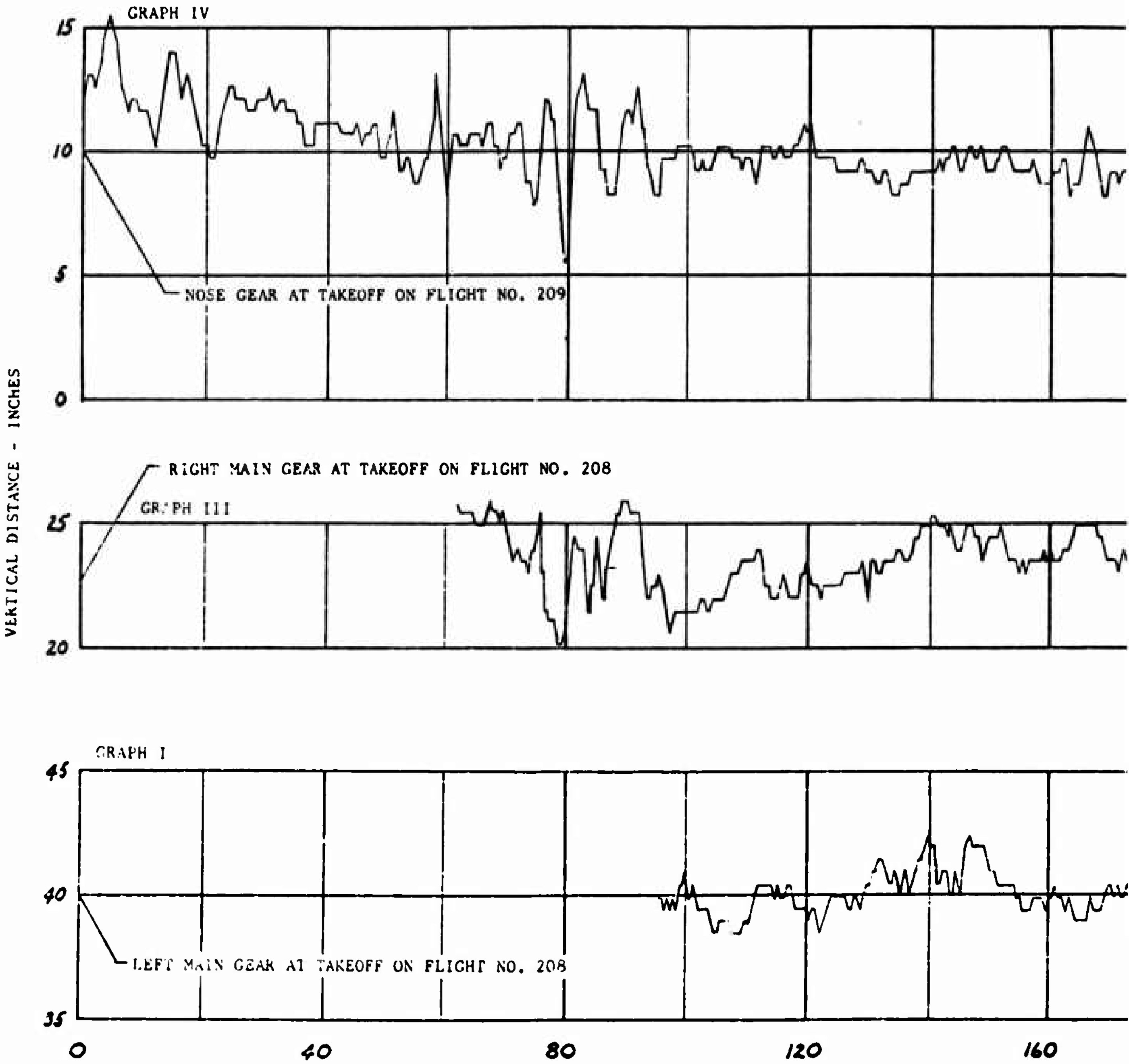
GRAPH IV
15
10
5
0
NOSE GEAR AT TAKEOFF ON FLIGHT NO. 209
VERTICAL DISTANCE - INCHES
RIGHT MAIN GEAR AT TAKEOFF ON FLIGHT NO. 208
GRAPH III
25
20
GRAPH I
45
40
35
LEFT MAIN GEAR AT TAKEOFF ON FLIGHT NO. 208
0
40
80
120
160

1 13

IN CONTOUR

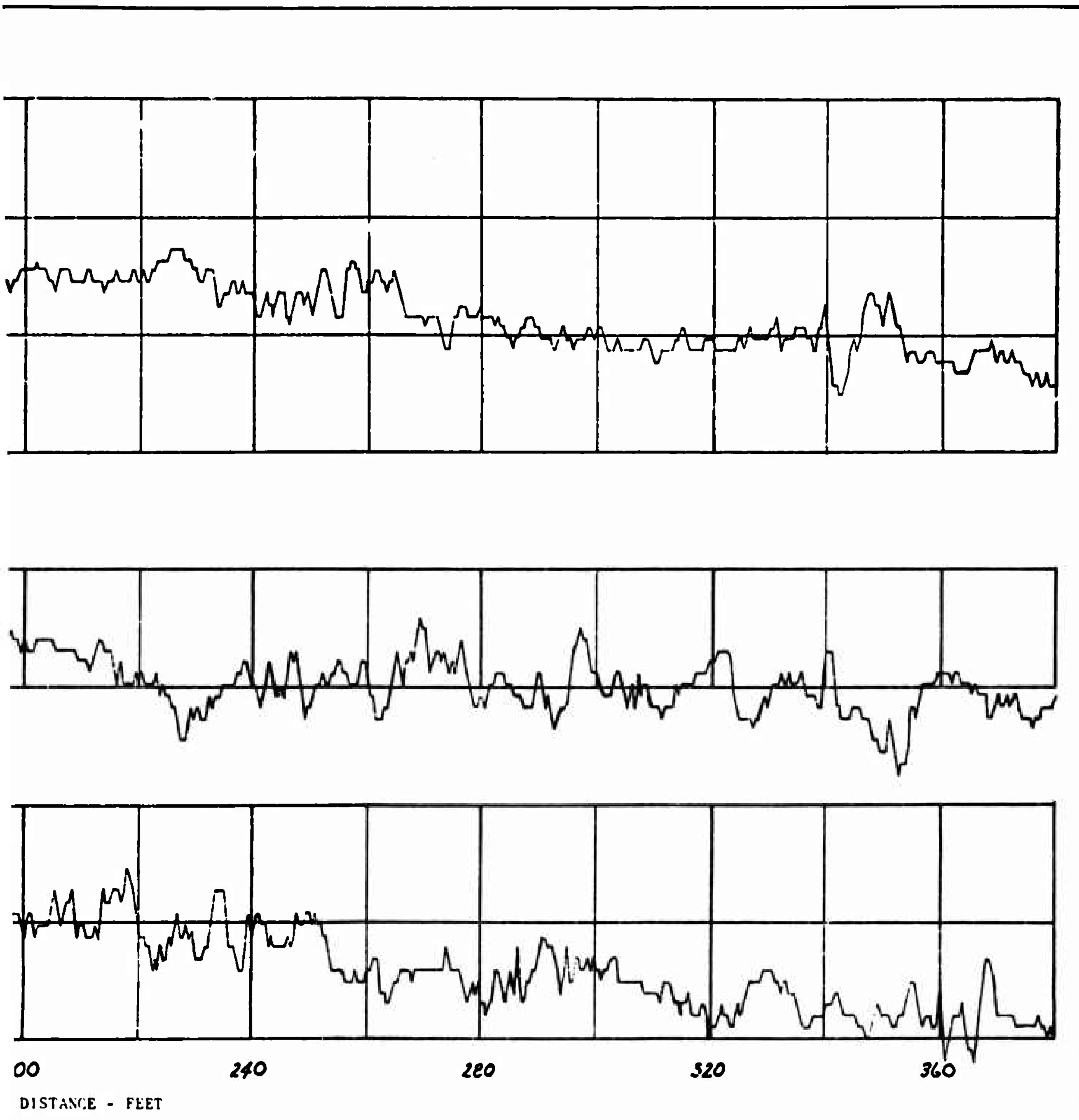

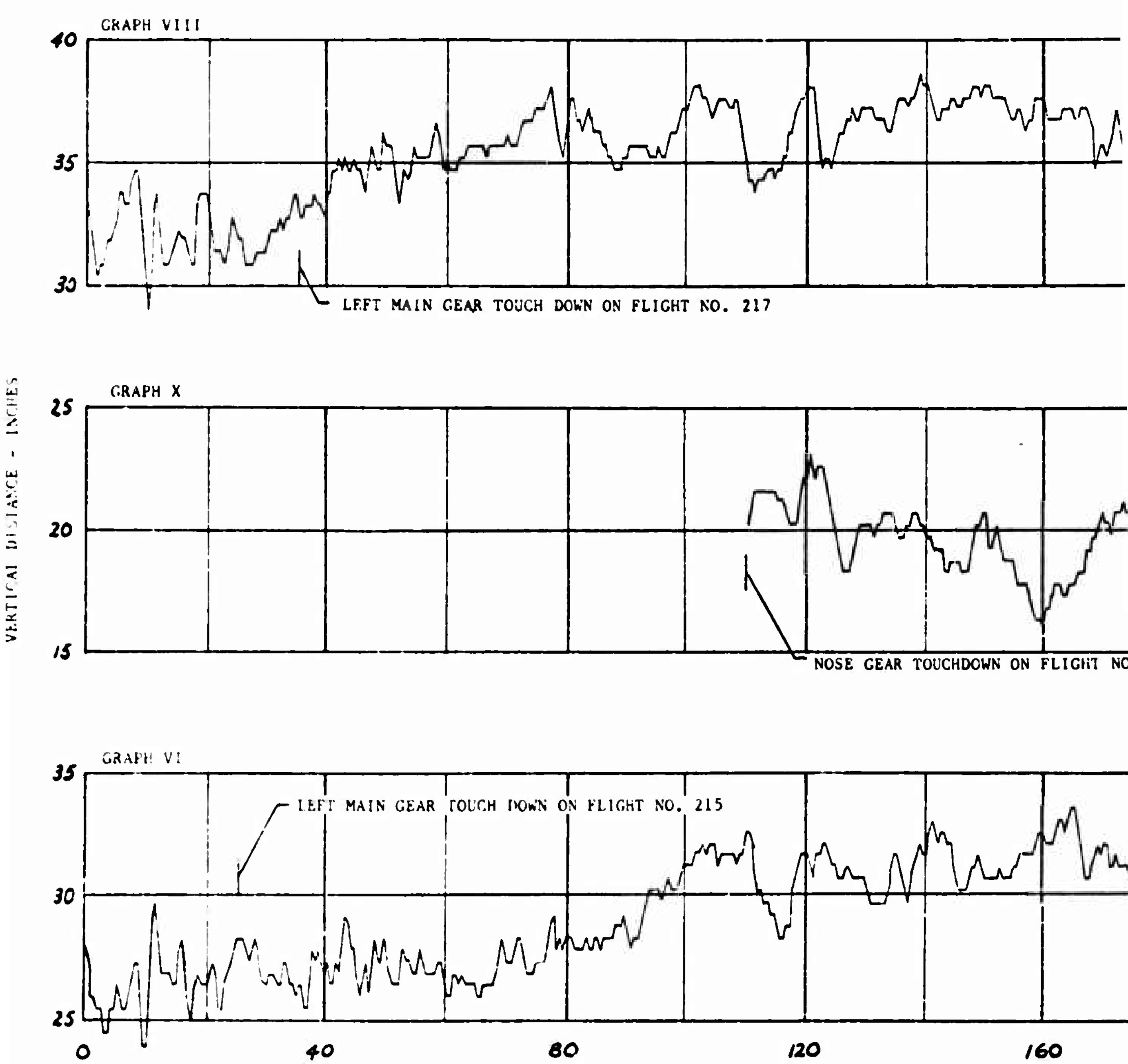

GRAPH VIII
40
35
30
LEFT MAIN GEAR TOUCH DOWN ON FLIGHT NO. 217
GRAPH X
25
20
15
NOSE GEAR TOUCHDOWN ON FLIGHT NO
GRAPH VI
35
30
25
LEFT MAIN GEAR TOUCH DOWN ON FLIGHT NO. 215
VERTICAL DISTANCE - INCHES
0
40
80
120
160

I B

CONTOUR

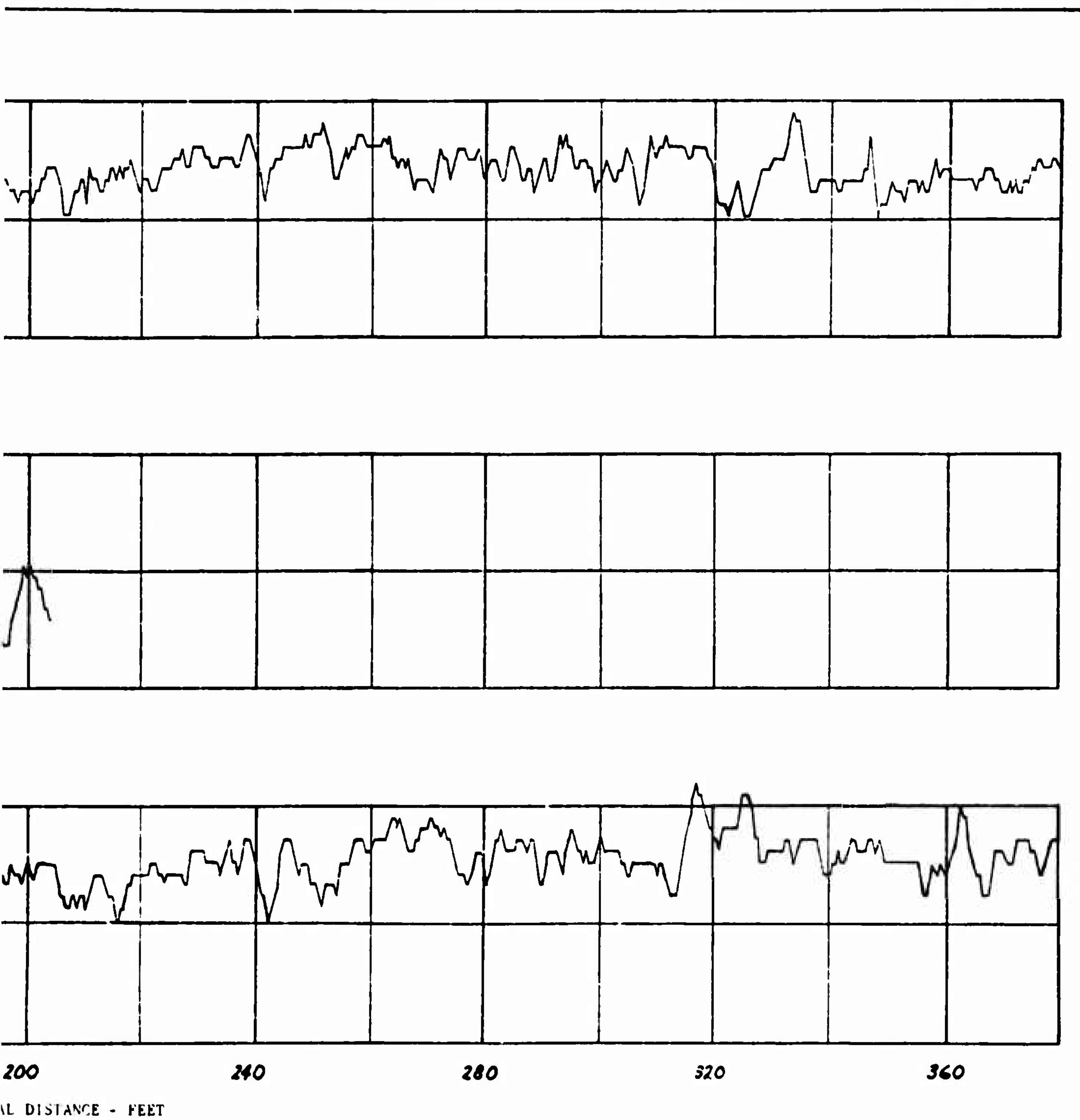

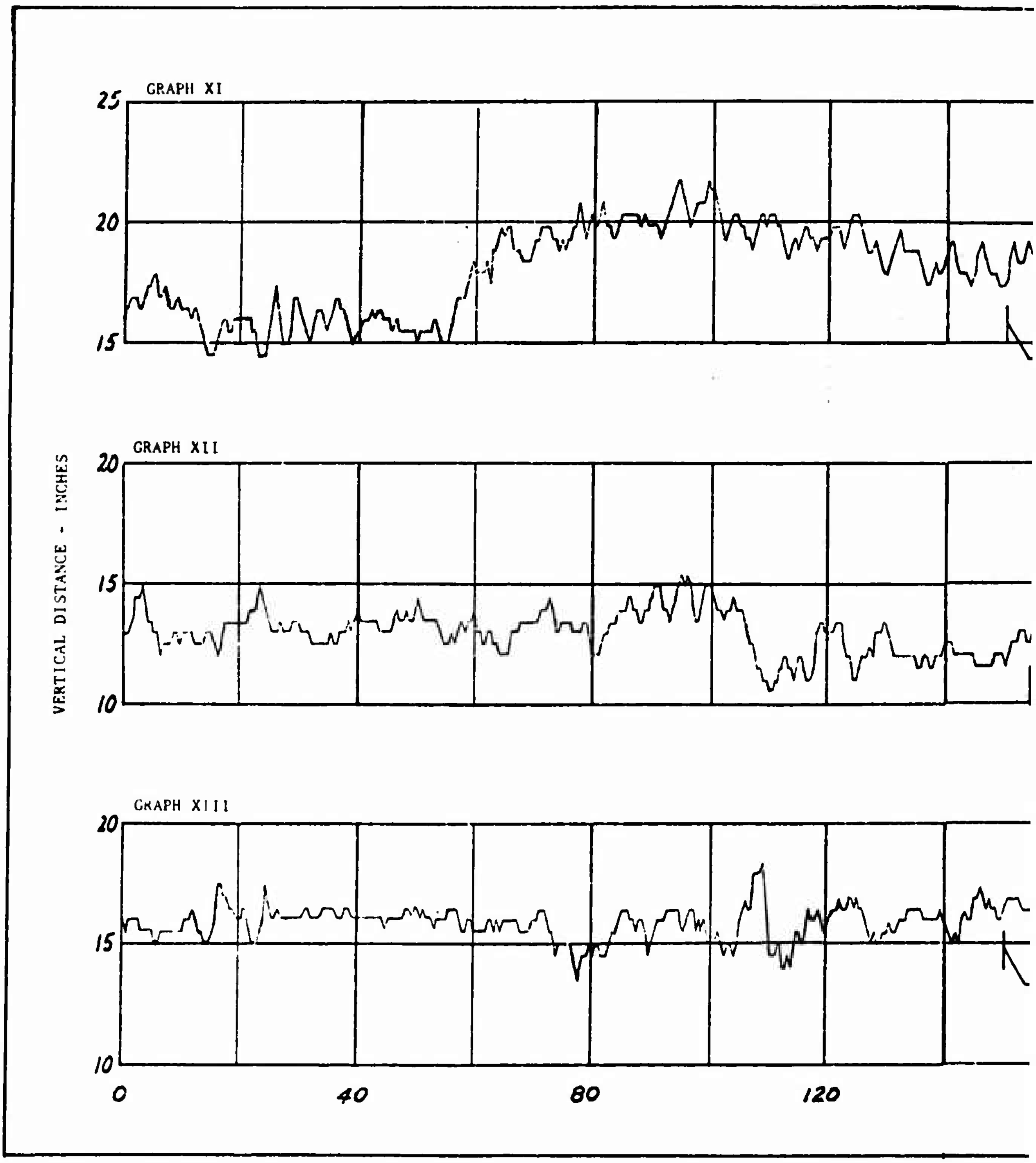
GRAPH XI
25
20
15
GRAPH XII
20
15
10
VERTICAL DISTANCE - INCHES
GRAPH XIII
20
15
10
0
40
80
120

ɴTOUR

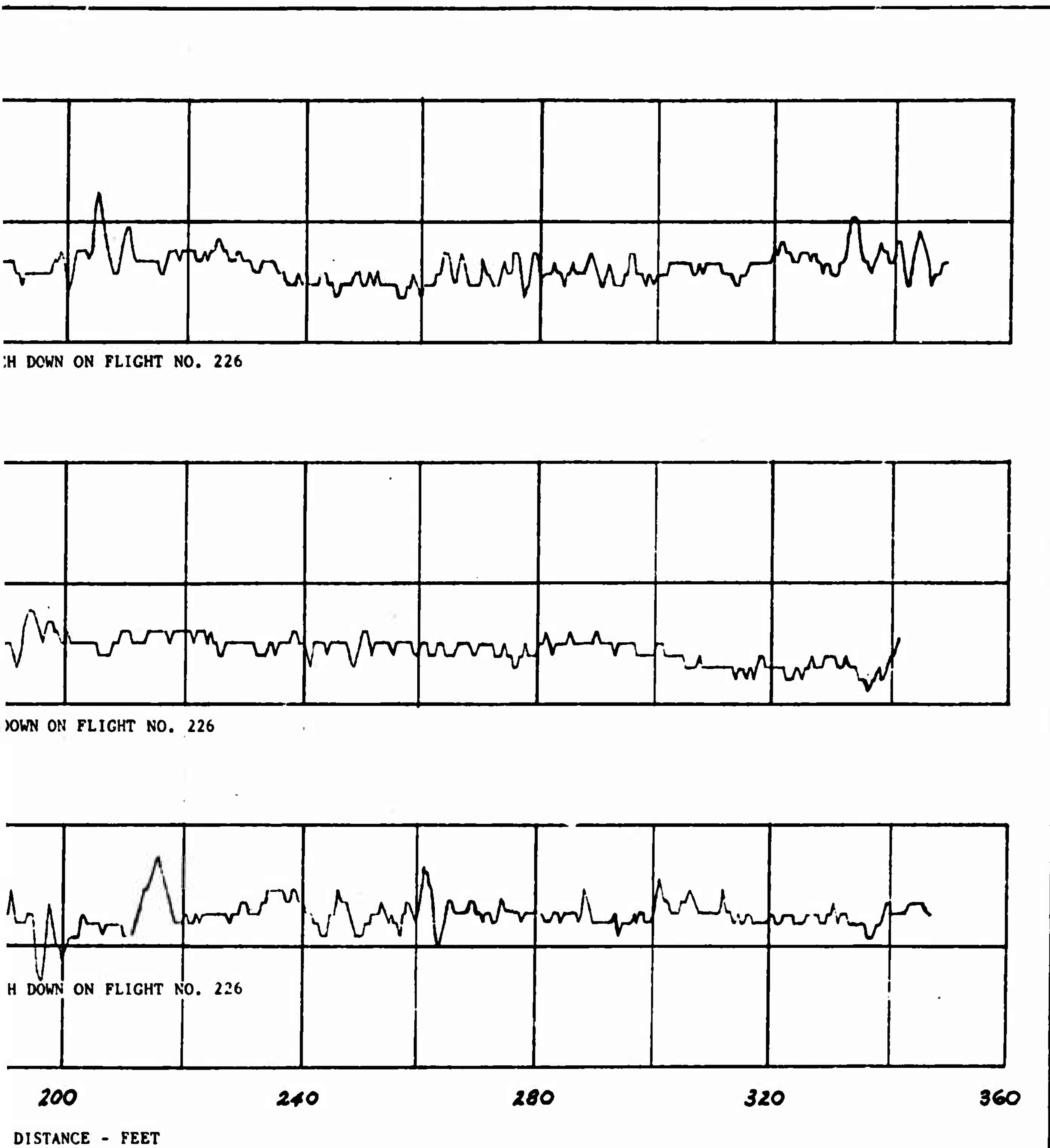

:H DOWN ON FLIGHT NO. 226
OWN ON FLIGHT NO. 226
H DOWN ON FLIGHT NO. 226
200
240
280
320
360
DISTANCE - FEET

A

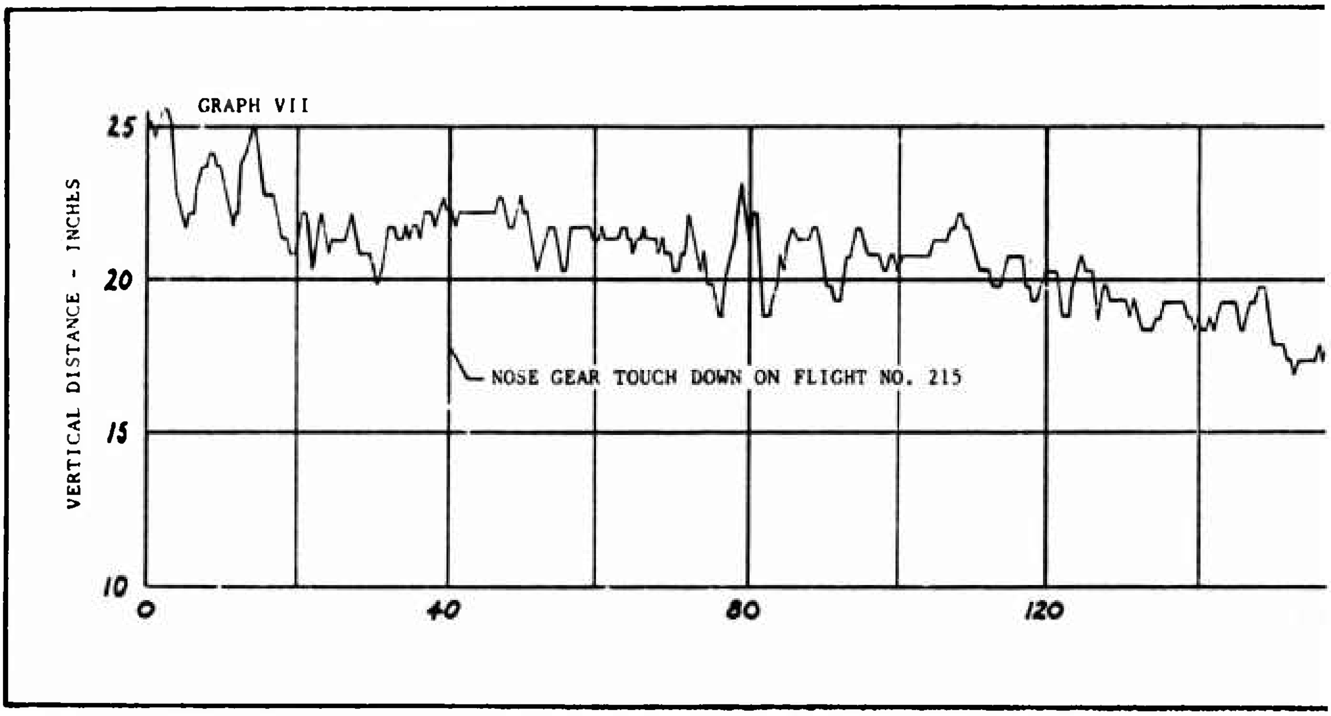
GRAPH VII
VERTICAL DISTANCE - INCHES
25
20
15
10
0
40
80
120
NOSE GEAR TOUCH DOWN ON FLIGHT NO. 215

ÀIN CONTOUR

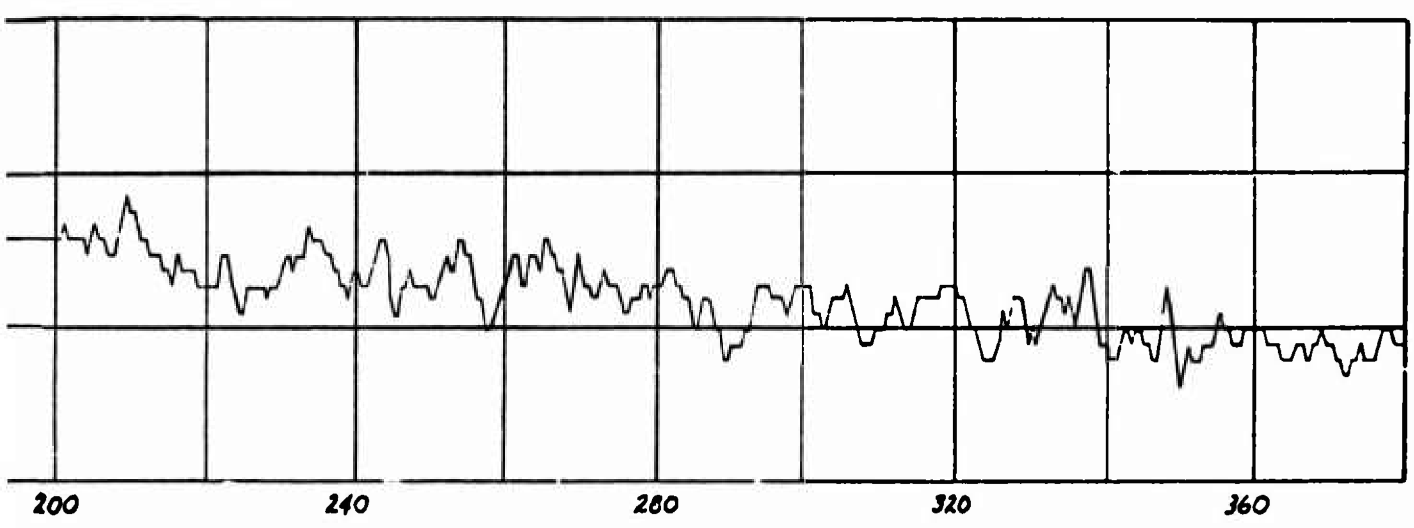

'AL DISTANCE - FEET

APPENDIX A2

LANDING GEAR CALIBRATION DATA

TABLE OF CONTENTS

List of Symbols

δ	= Corrected trace deflection to a unit R/Cal step
R/Cal	= Resistance Calibration of strain gage bridge
Δ	= Trace deflection from baseline under loaded condition
Δ_o	= Trace deflection from baseline under a no load condition
$V_v, V_d (V_D), V_s$	= Vertical bridge output due to a known vertical, drag, and side load, respectively
$D_v, D_d (D_D), D_s$	= Drag bridge output due to a known vertical, drag, and side load, respectively
$S_v, S_d (S_D), S_s$	= Side bridge output due to a known vertical, drag, and side load, respectively
$\delta_v, \delta_d, \delta_s$	= Vertical, drag, and side bridge outputs, respectively
V, D, S	= Vertical, drag, and side loads, respectively
$\left.\begin{matrix} KV_v, KV_d, KV_s \\ KD_v, KD_d, KD_s \\ KS_v, KS_d, KS_s \end{matrix}\right\}$	= Slopes of the calibration curves

Subscripts

sp	= Spare gage

Data Reduction Method

The location of strain gages on the nose and main gears, respectively, are shown on Pages A2-5 and A2-6. A typical strain gage bridge is shown on Page A2-7. As indicated in Section 4.1.1, strain gage outputs due to known singly applied loads were recorded by a standard oscillograph and the results reduced to a unit R/Cal step and plotted against load. These plots are given on Pages A2-8 thru A2-43. Mathematically, this procedure may be written as:

$$\delta = \frac{1}{R/Cal}(\Delta - \Delta_o)$$

For combined loading, the strain gage bridge outputs can be written in terms of the calibration values.

$$\delta_V = KV_V \cdot V + KV_d \cdot D + KV_s \cdot S$$

$$\delta_d = KD_V \cdot V + KD_d \cdot D + KD_s \cdot S$$

$$\delta_s = KS_V \cdot V + KS_d \cdot D + KS_s \cdot S$$

The above may be written in the form

$$\{\delta\} = [A]\{L\}$$

and solved for loads in the form

$$\{L\} = [A]^{-1}\{\delta\}$$

A sample calculation is shown below:

Nose Gear, Full Compressed Position, Positive Loadings

KV_V = 0.93/10000 = 0.93×10^{-4}
KV_d = 0.06/5000 = 0.12×10^{-4}
KV_s = 0 = 0
KD_V = 0.74/10000 = 0.74×10^{-4}
KD_d = 0.84/5000 = 1.68×10^{-4}
KD_s = 0 = 0
KS_V = 0 = 0
KS_d = 0 = 0
KS_s = 1.39/4000 = 3.475×10^{-4}

$$A = 10^{-4} \begin{vmatrix} 0.93 & 0.12 & 0 \\ 0.74 & 1.68 & 0 \\ 0 & 0 & 3.475 \end{vmatrix} = 10^{-4}(5.42934-0.30858) = 5.12076\times10^{-4}$$

$$A^T = \text{transpose of } A = 10^{-4} \begin{vmatrix} 0.93 & 0.74 & 0 \\ 0.12 & 1.68 & 0 \\ 0 & 0 & 3.475 \end{vmatrix}$$

$$C^T = \text{adjoint of } A^T = 10^{-4} \begin{vmatrix} 5.8380 & -0.4170 & 0 \\ -2.5715 & 3.23175 & 0 \\ 0 & 0 & 1.4736 \end{vmatrix}$$

$$A^{-1} = \frac{C^T}{A} = \begin{vmatrix} 1.140065 & -0.081433 & 0 \\ -0.502171 & 0.631107 & 0 \\ 0 & 0 & 0.287769 \end{vmatrix}$$

Thus: $V = 11401\,\delta_v - 814\,\delta_d$

$D = -5022\,\delta_v + 6311\,\delta_d$

$S = 2878\,\delta_s$

These relations are given on Pages A2-44 through A2-49 and plotted on Pages A2-50 through A2-61.

SKETCH OF NOSE GEAR SHOWING LOCATION OF STRAIN GAGES

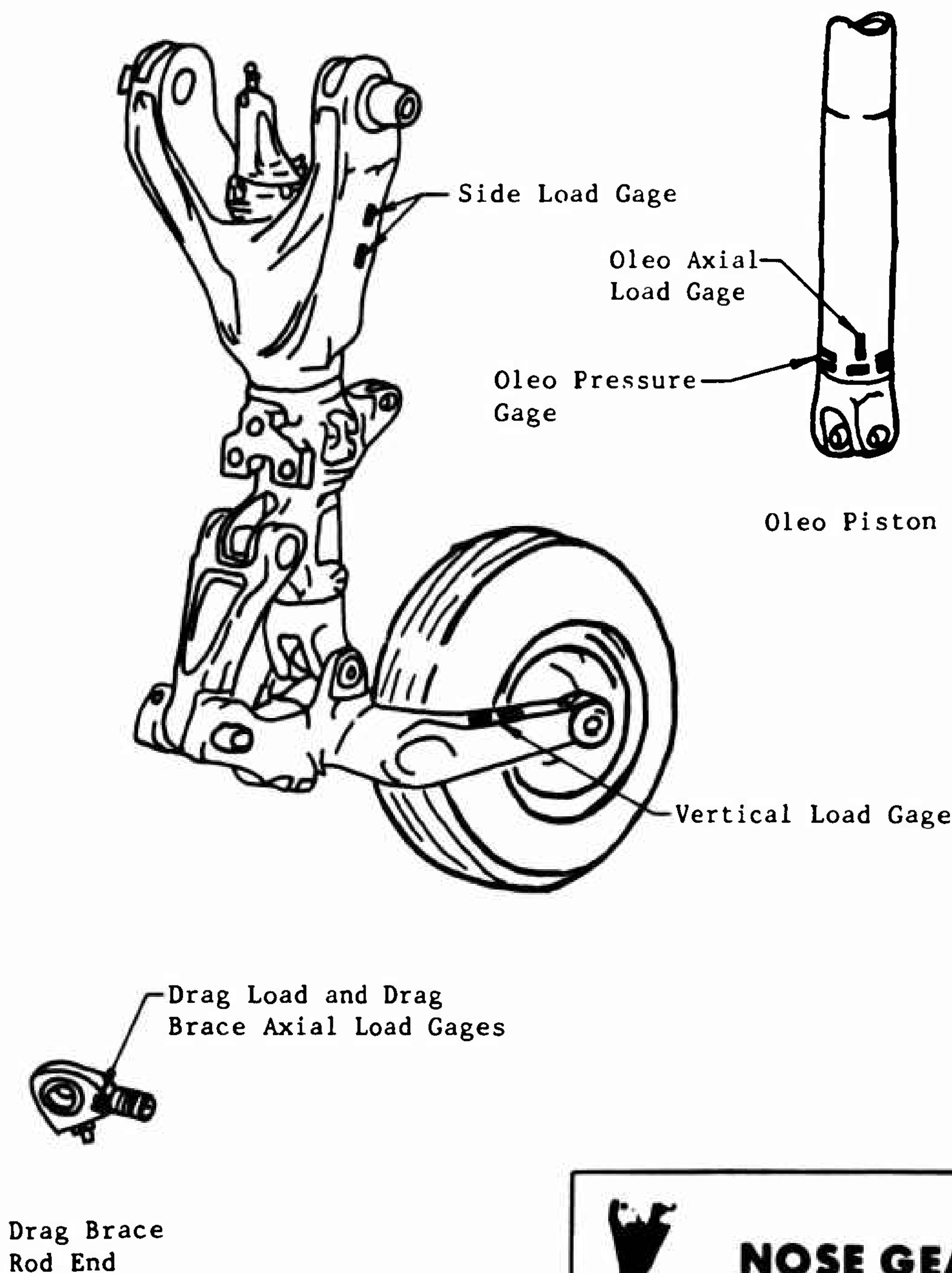

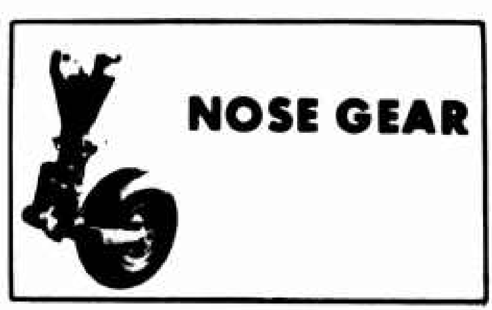

SKETCH OF MAIN GEAR SHOWING LOCATION OF STRAIN GAGES

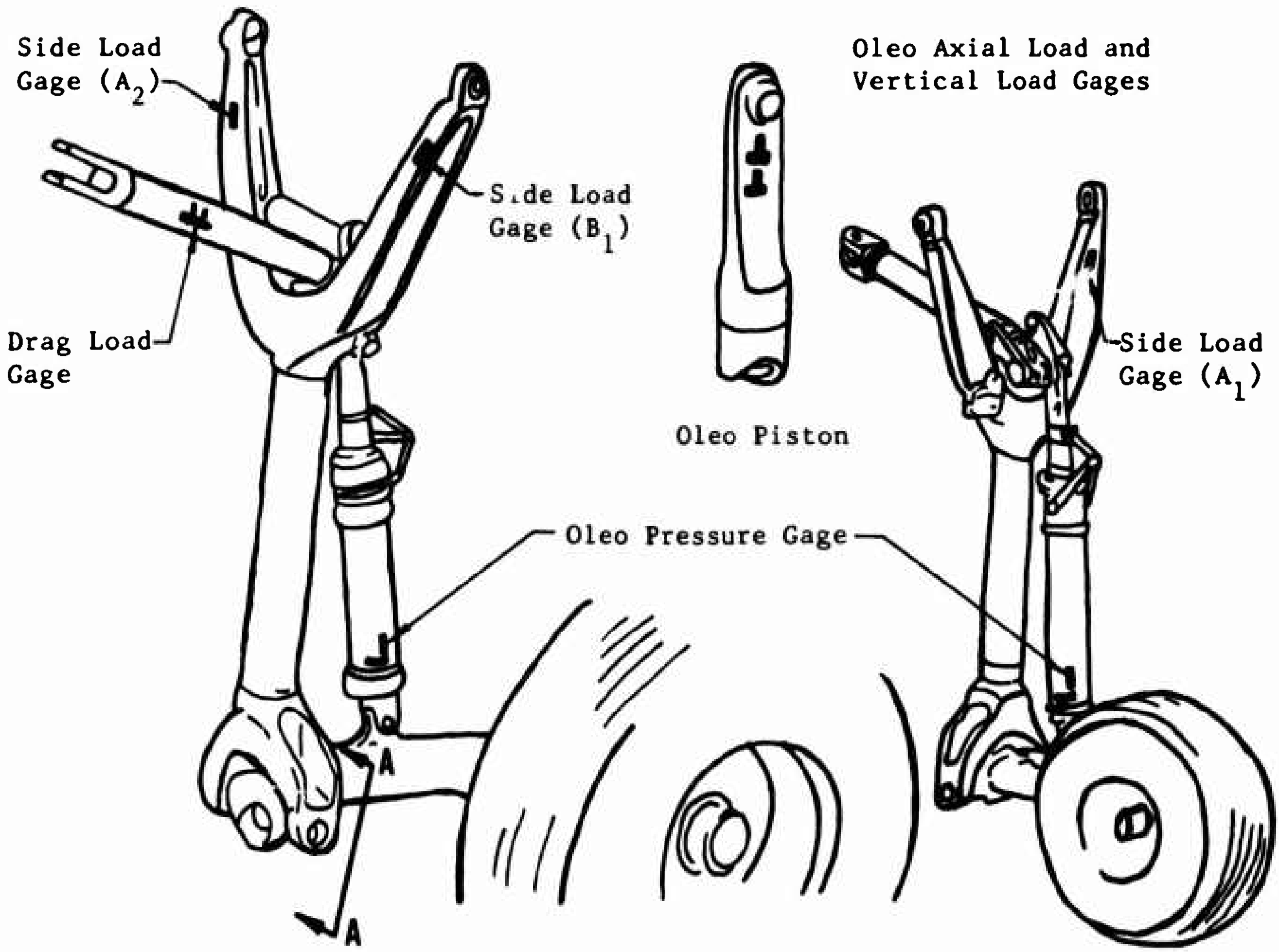

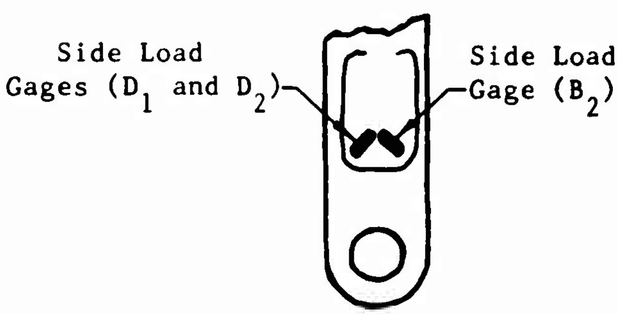

View A-A

Typical Strain Gage Bridge

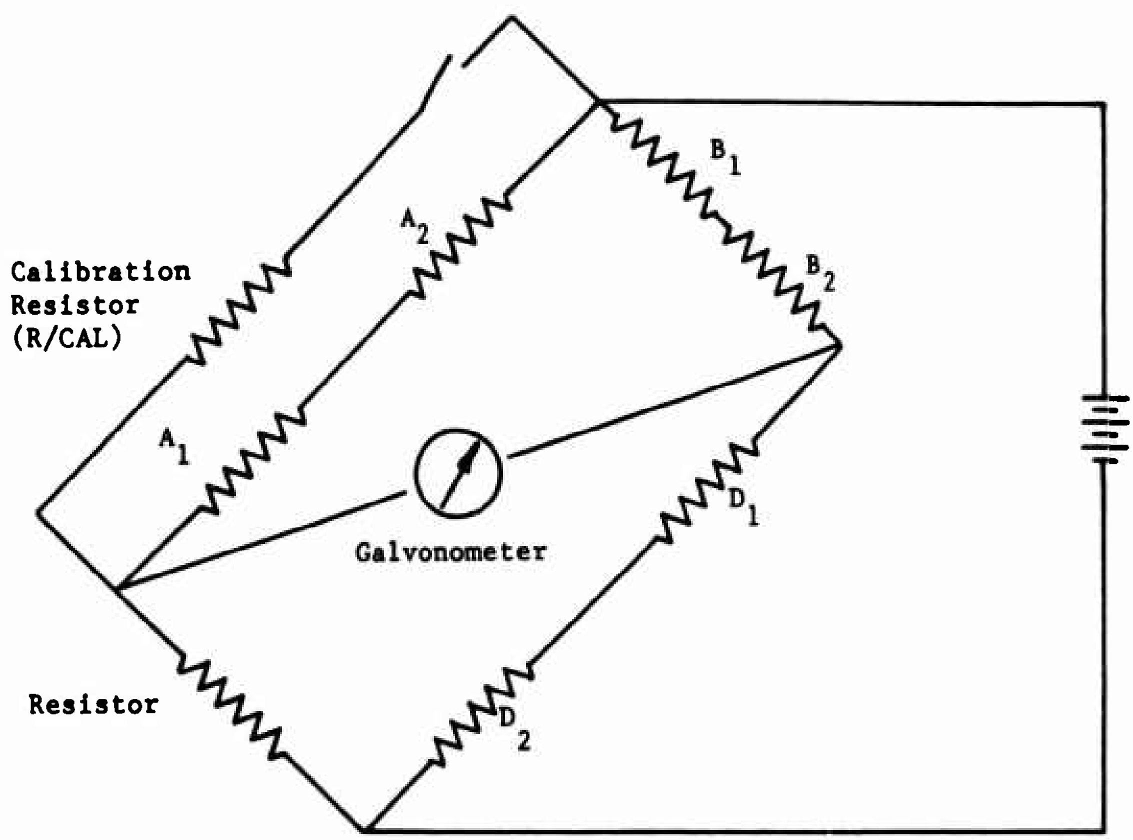

Main Gear Side Load Bridge Shown

NOSE GEAR

FULL COMPRESSED

STRAIN GAGE CALIBRATION

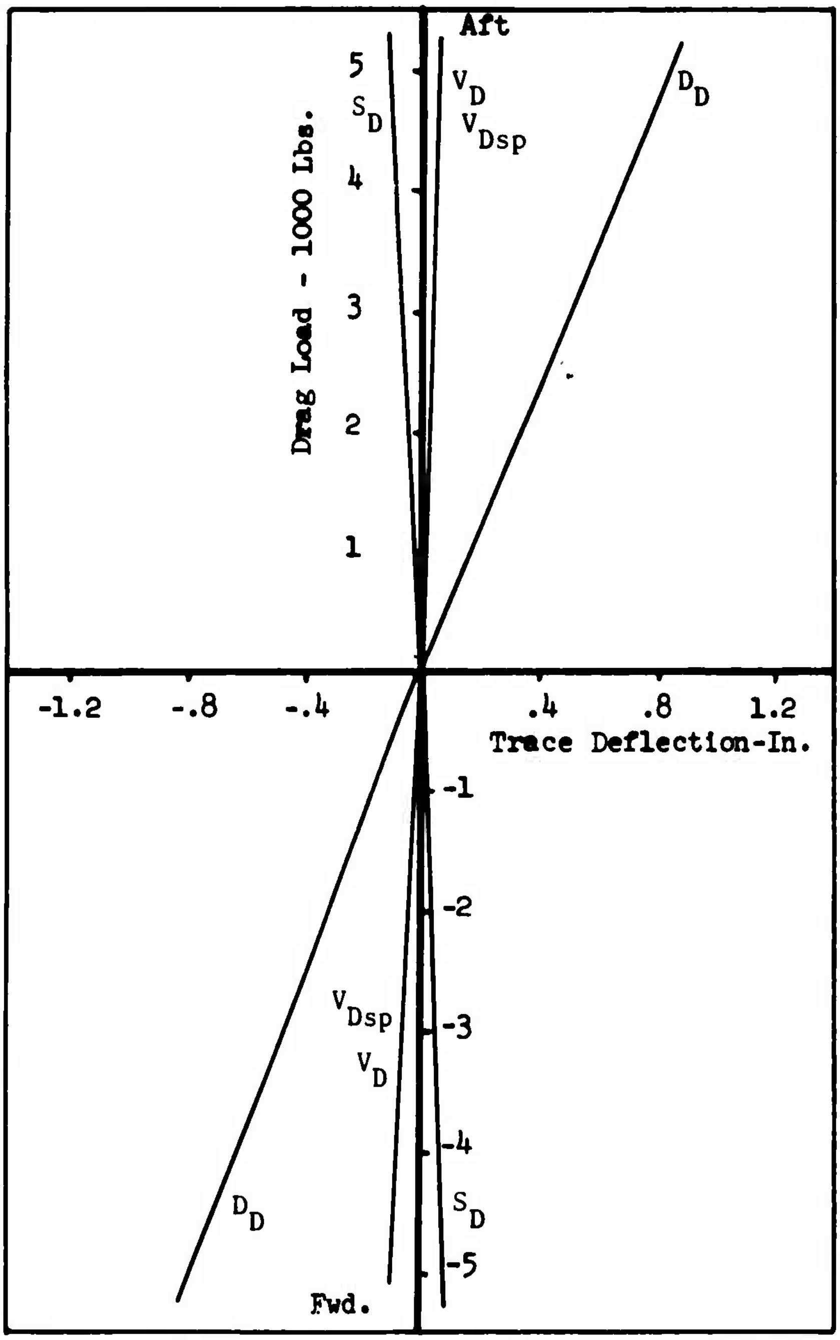

NOSE GEAR

FULL COMPRESSED

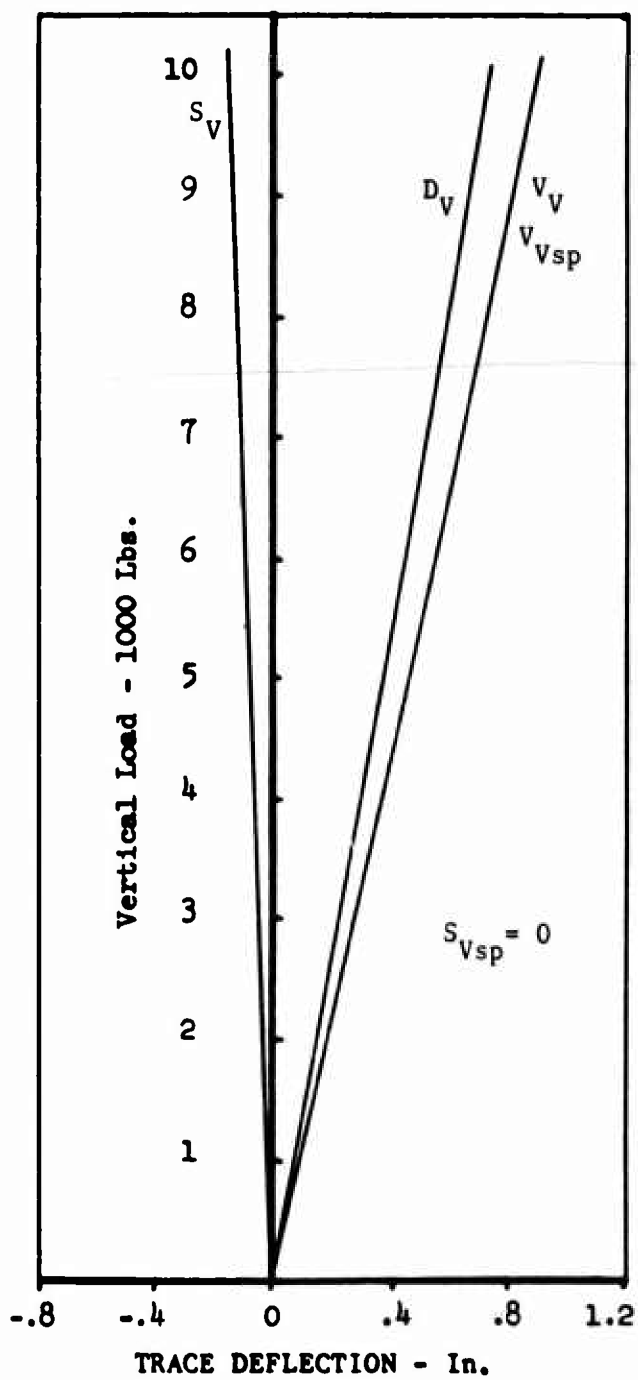

NOSE GEAR

FULL COMPRESSED

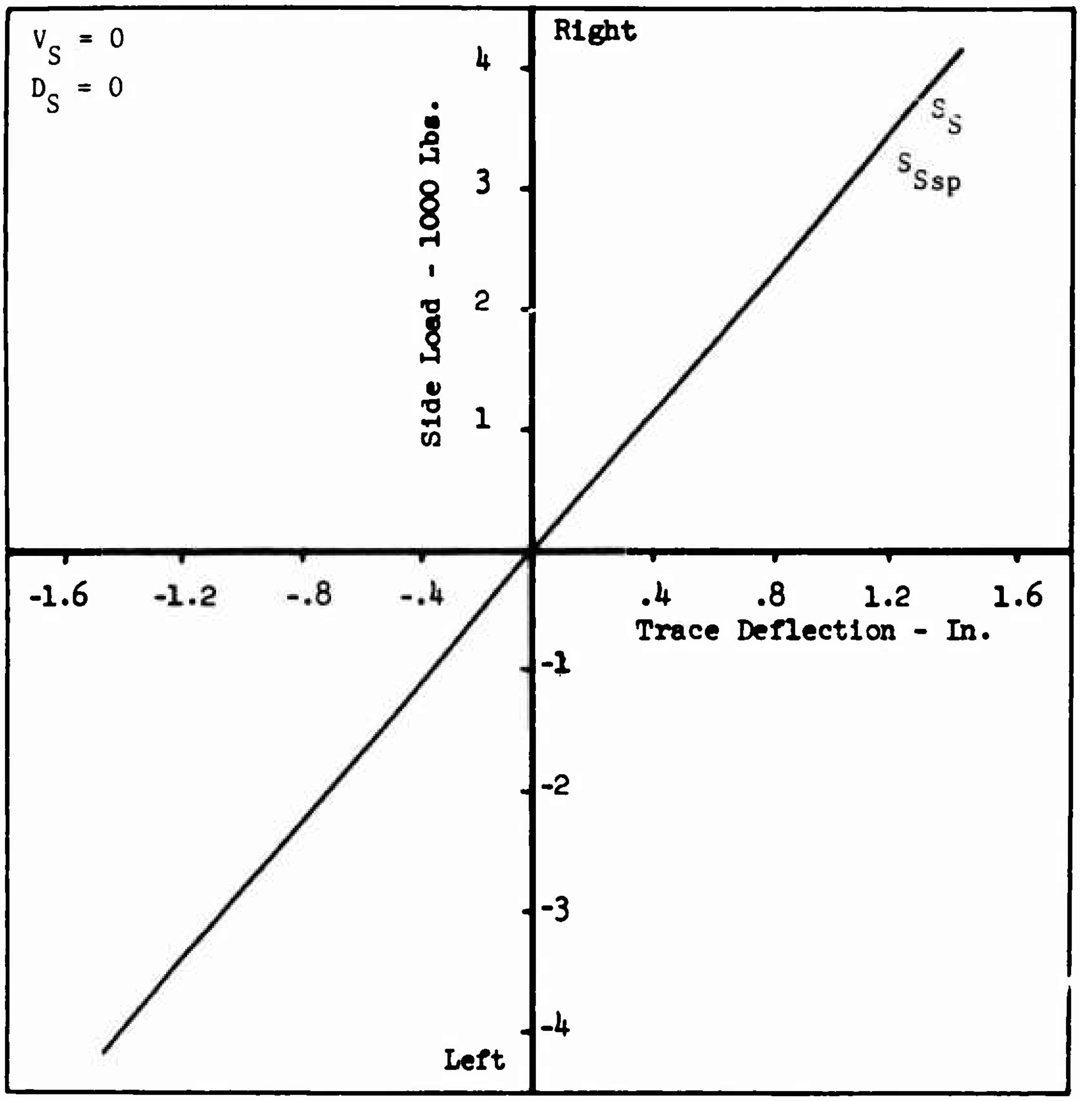

NOSE GEAR

2/3 COMPRESSED

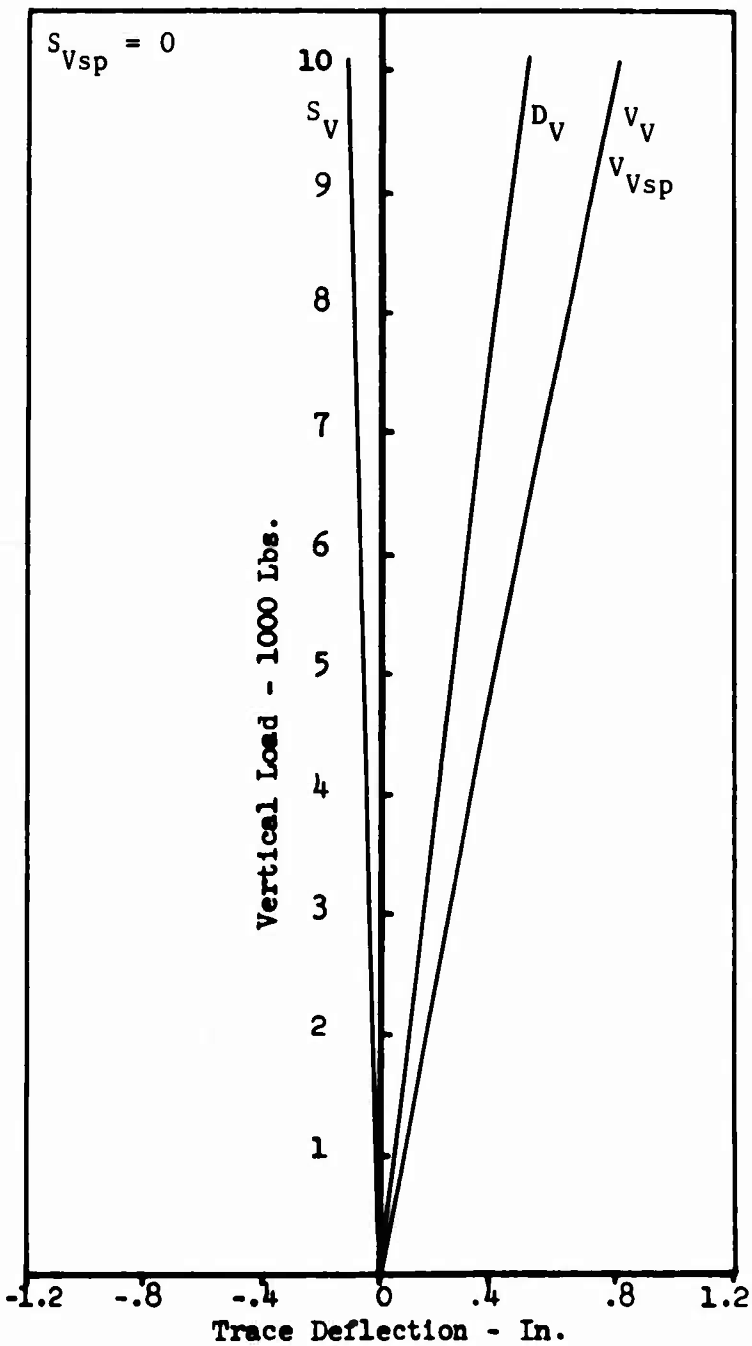

NOSE GEAR

2/3 COMPRESSED

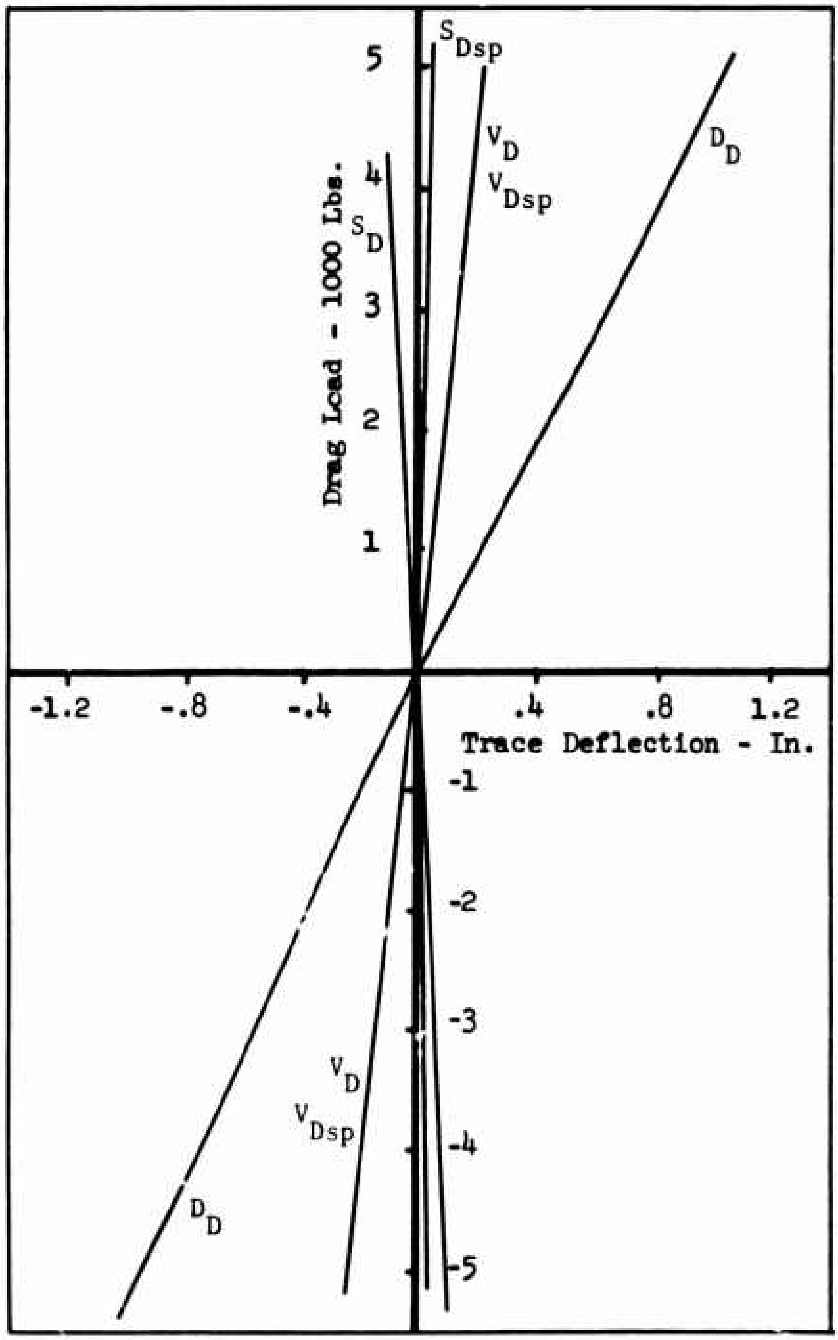

NOSE GEAR

2/3 COMPRESSED

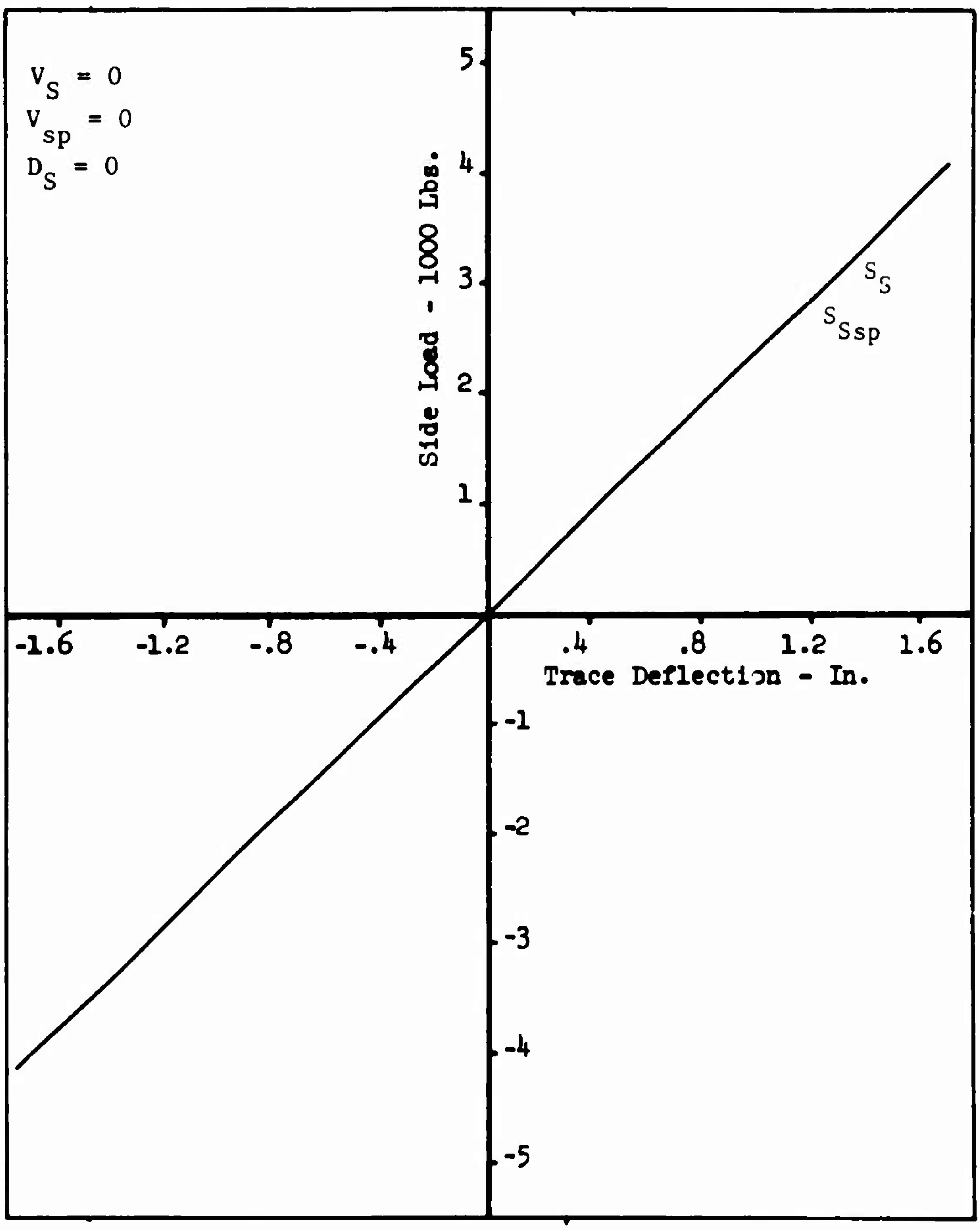

NOSE GEAR

1/3 COMPRESSED

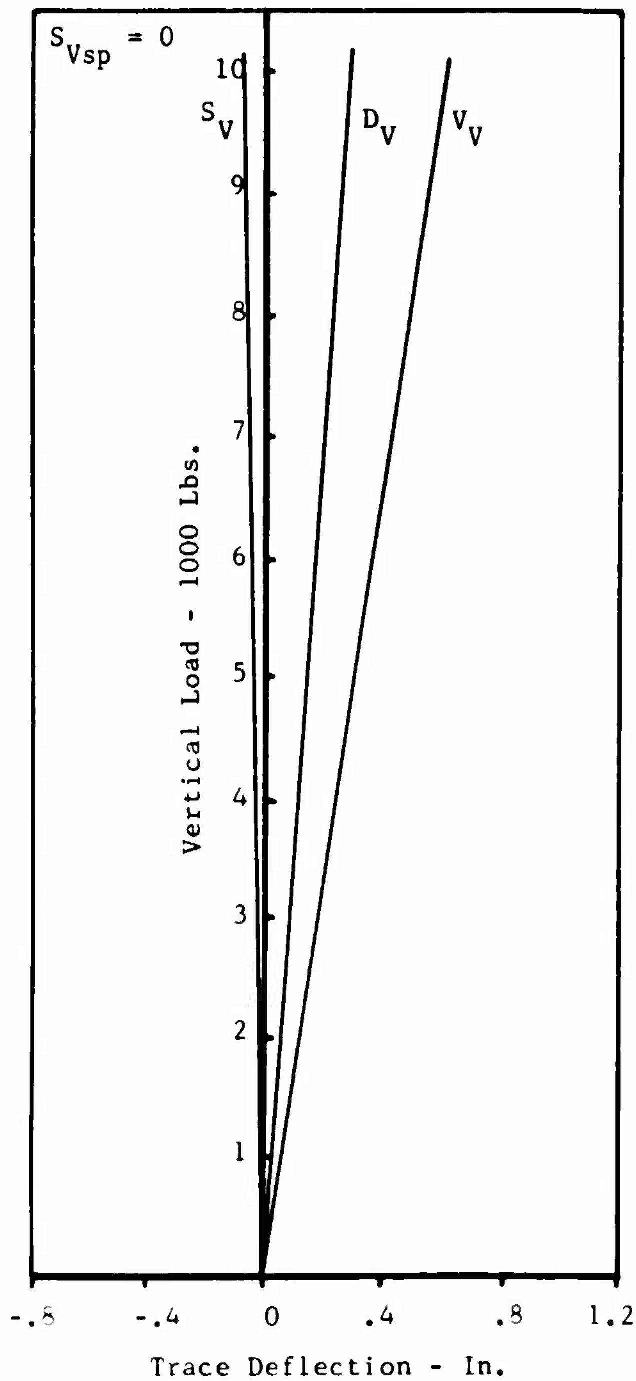

NOSE GEAR

1/3 COMPRESSED

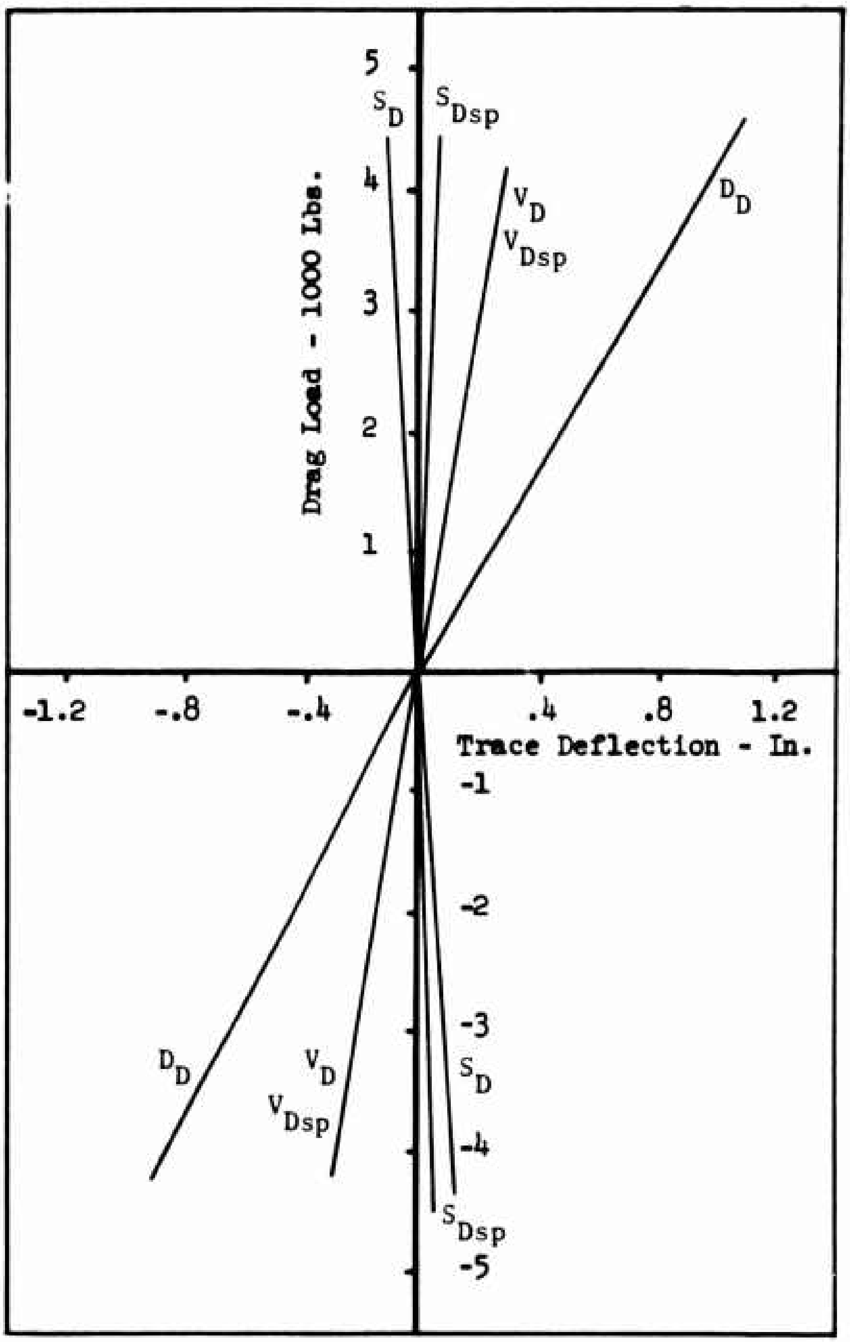

NOSE GEAR

1/3 COMPRESSED

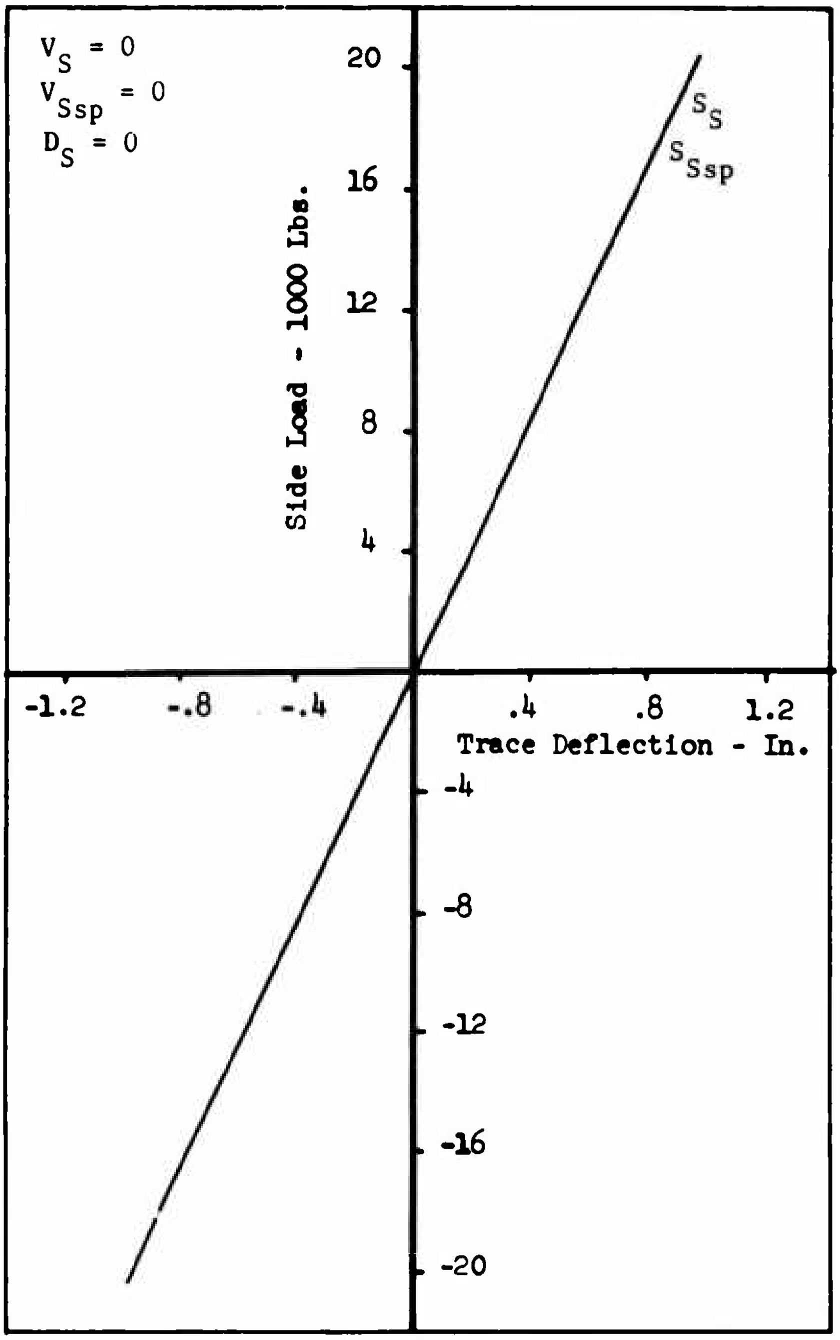

NOSE GEAR

FULL EXTENDED

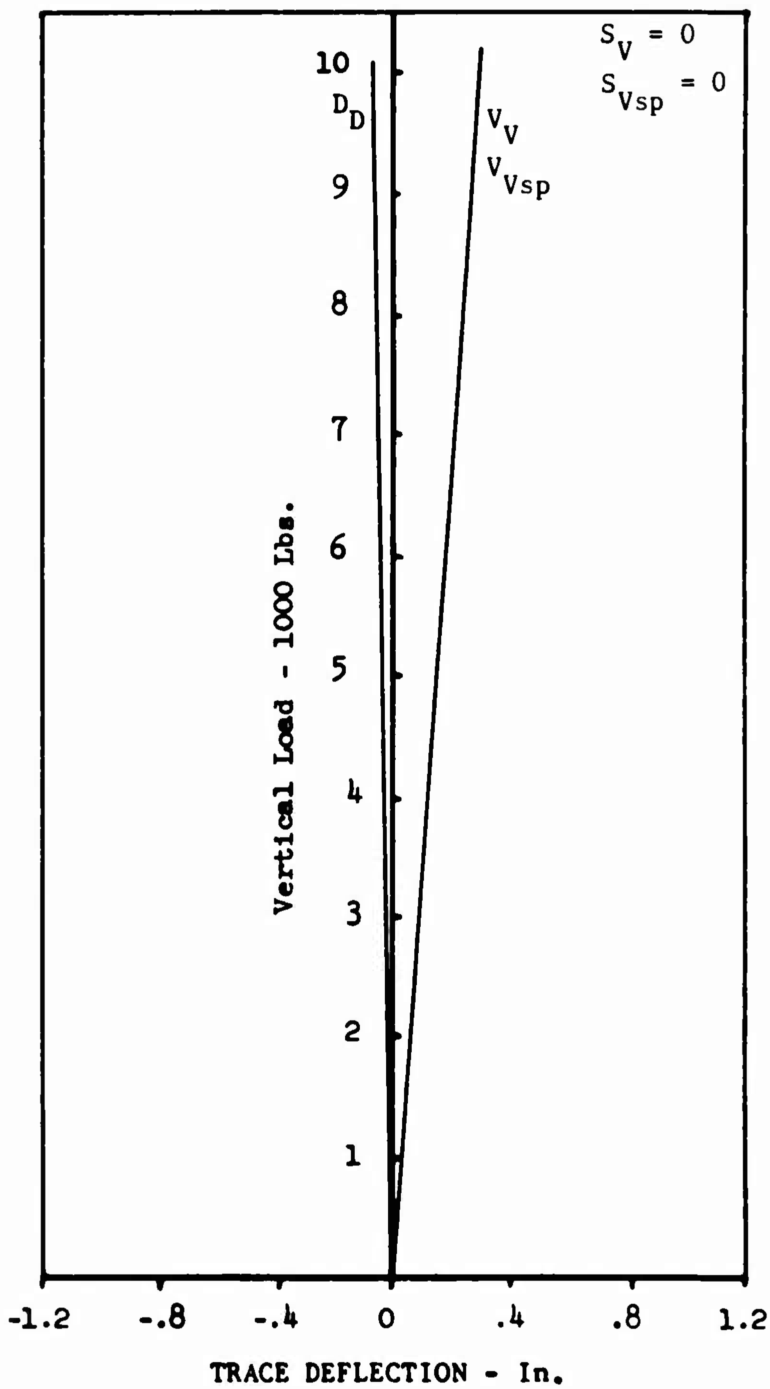

NOSE GEAR

FULL EXTENDED

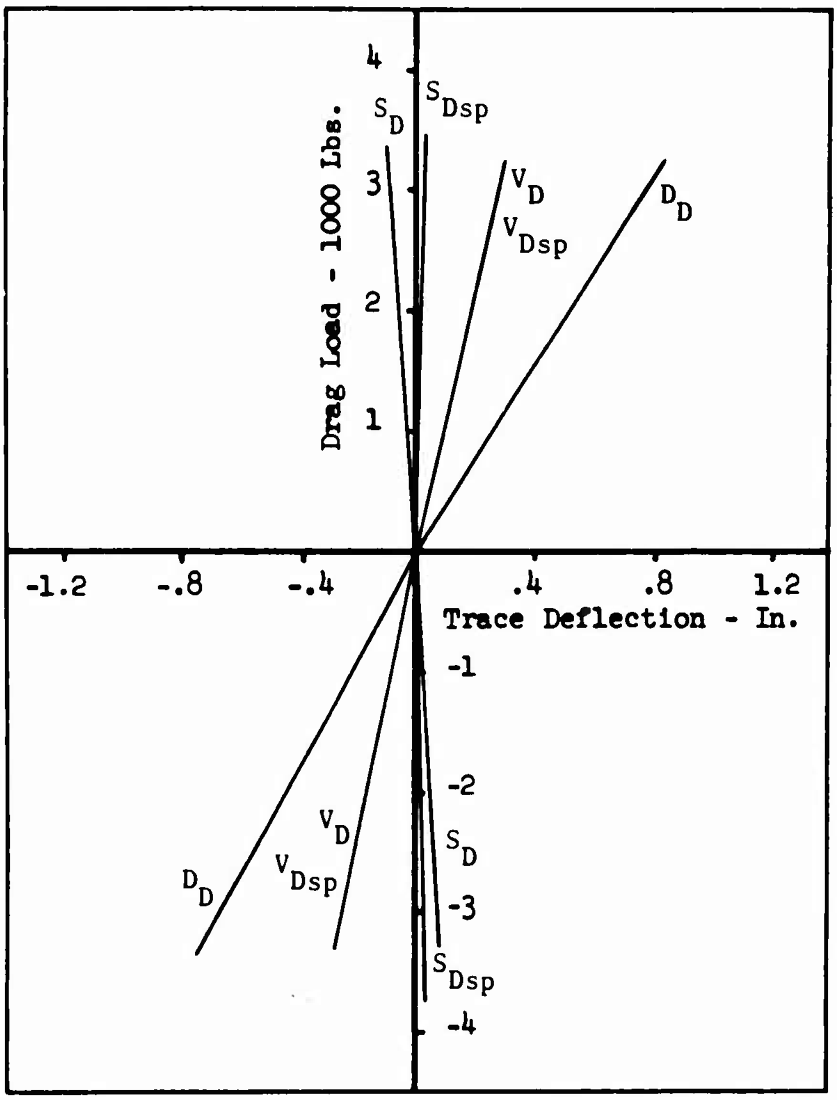

NOSE GEAR

FULL EXTENDED

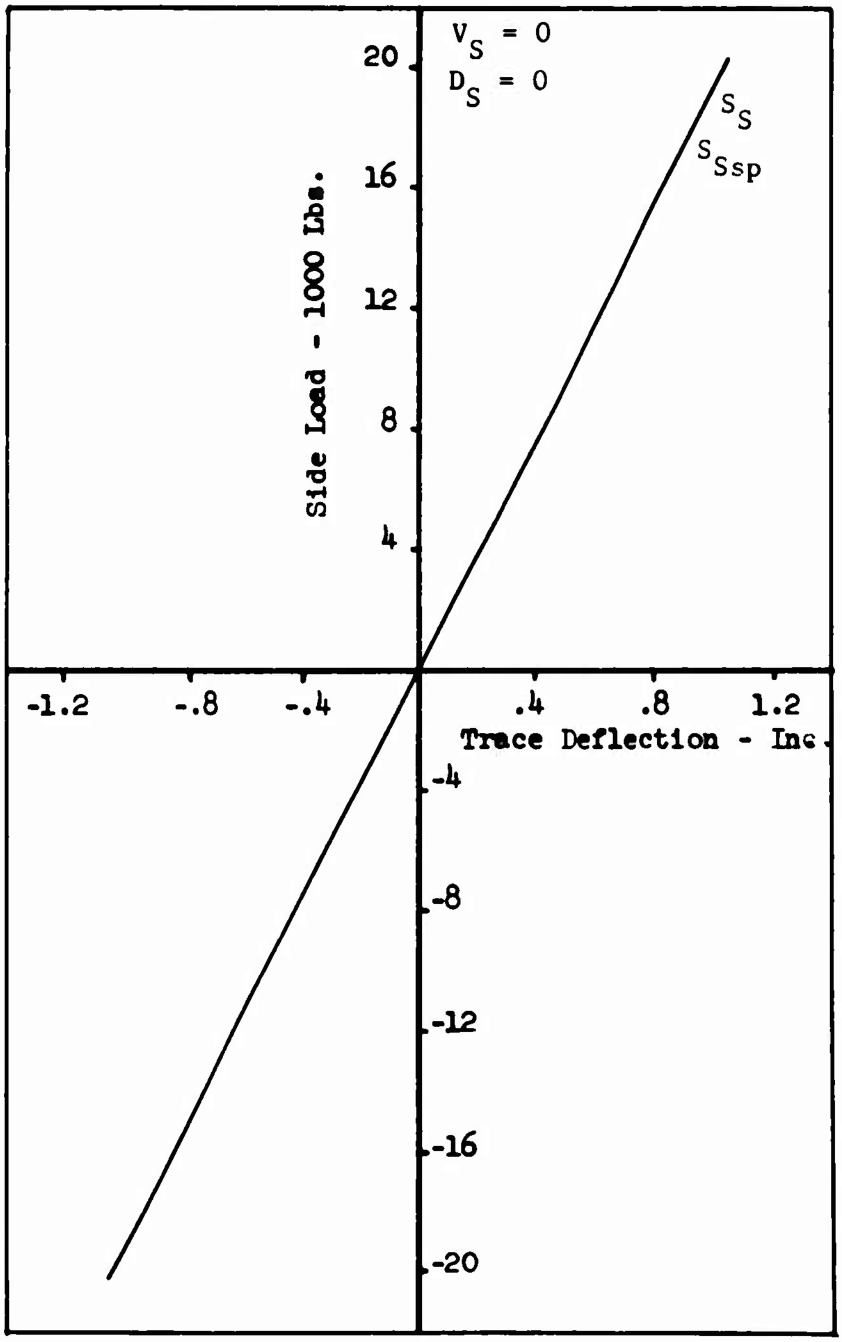

RIGHT MAIN GEAR

FULL COMPRESSED

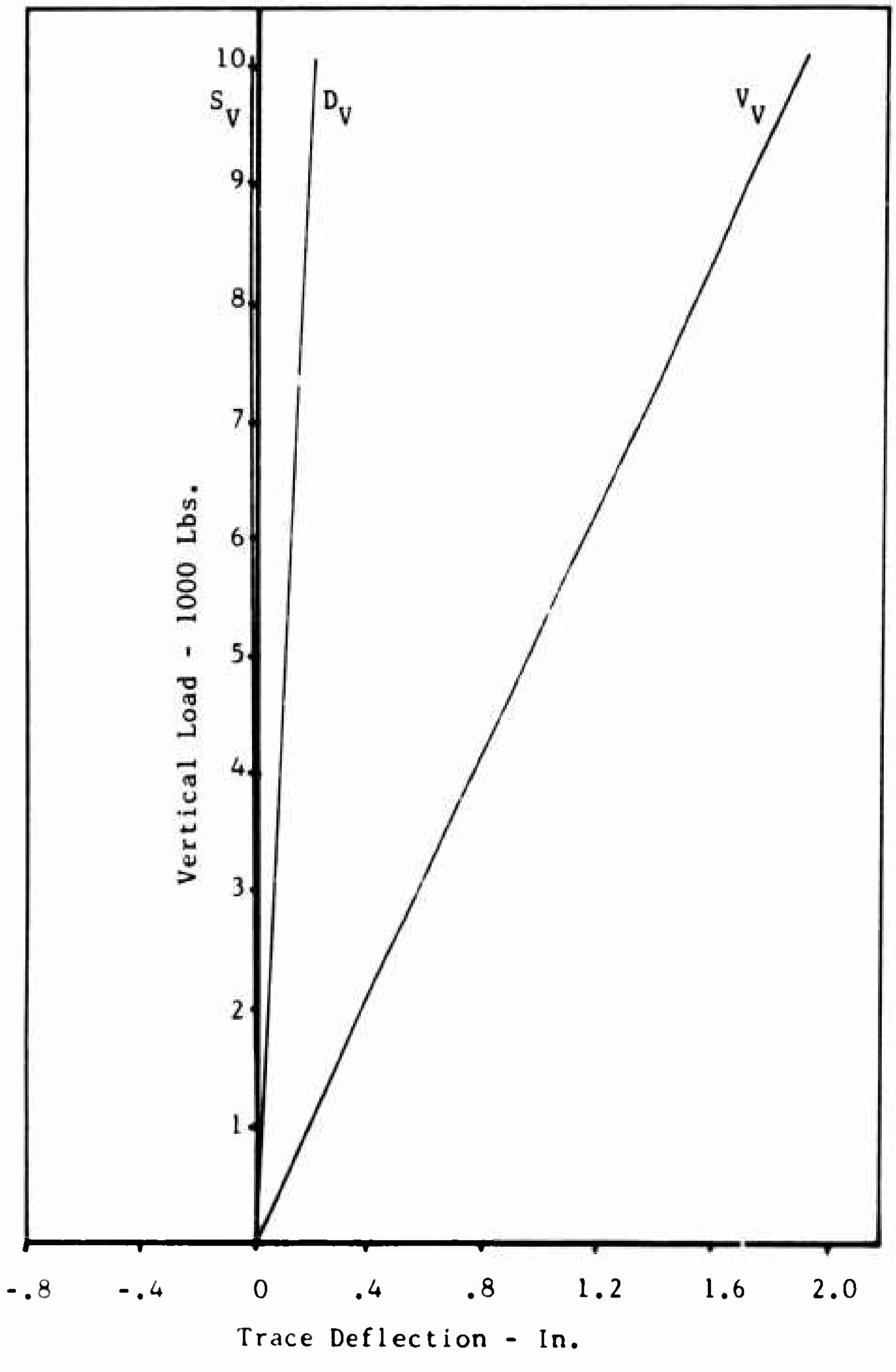

RIGHT MAIN GEAR

FULL COMPRESSED

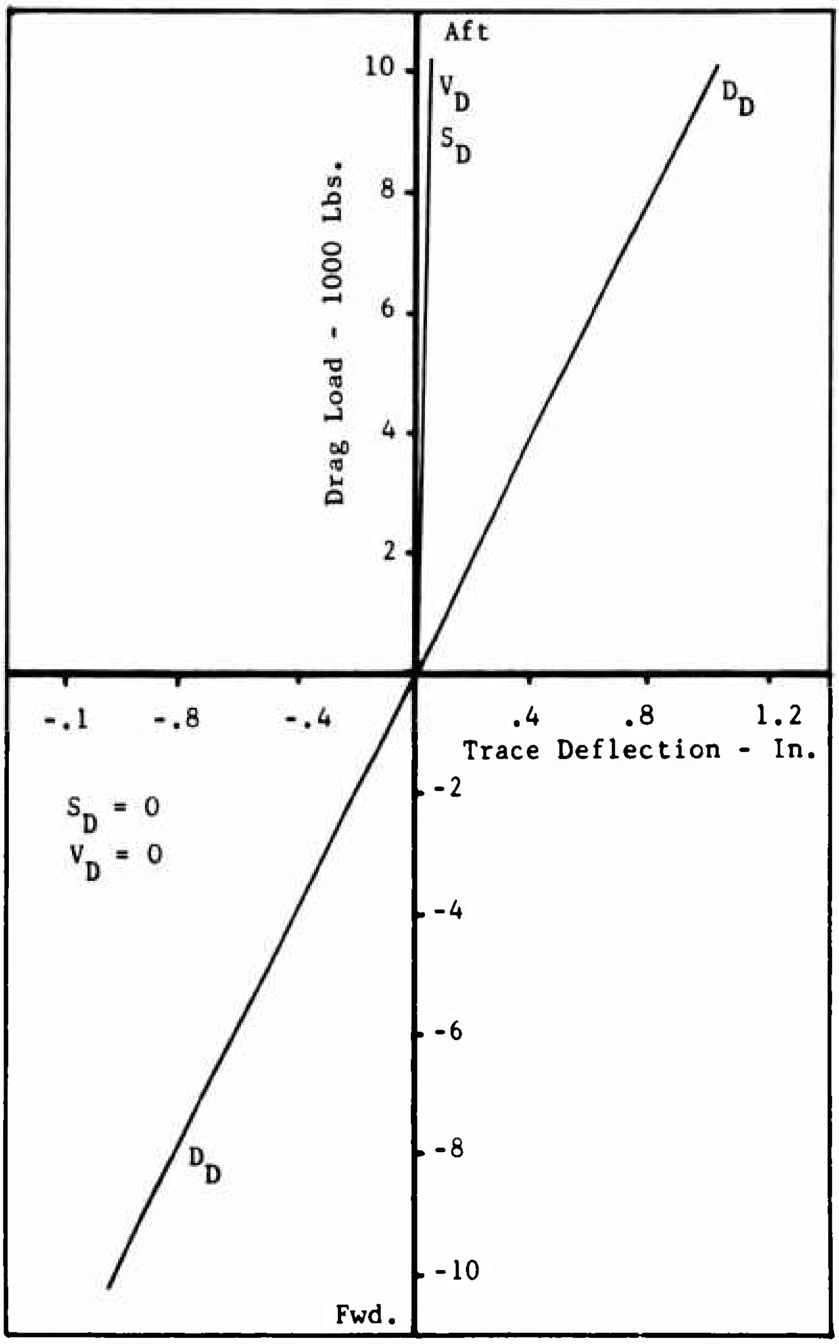

RIGHT MAIN GEAR

FULL COMPRESSED

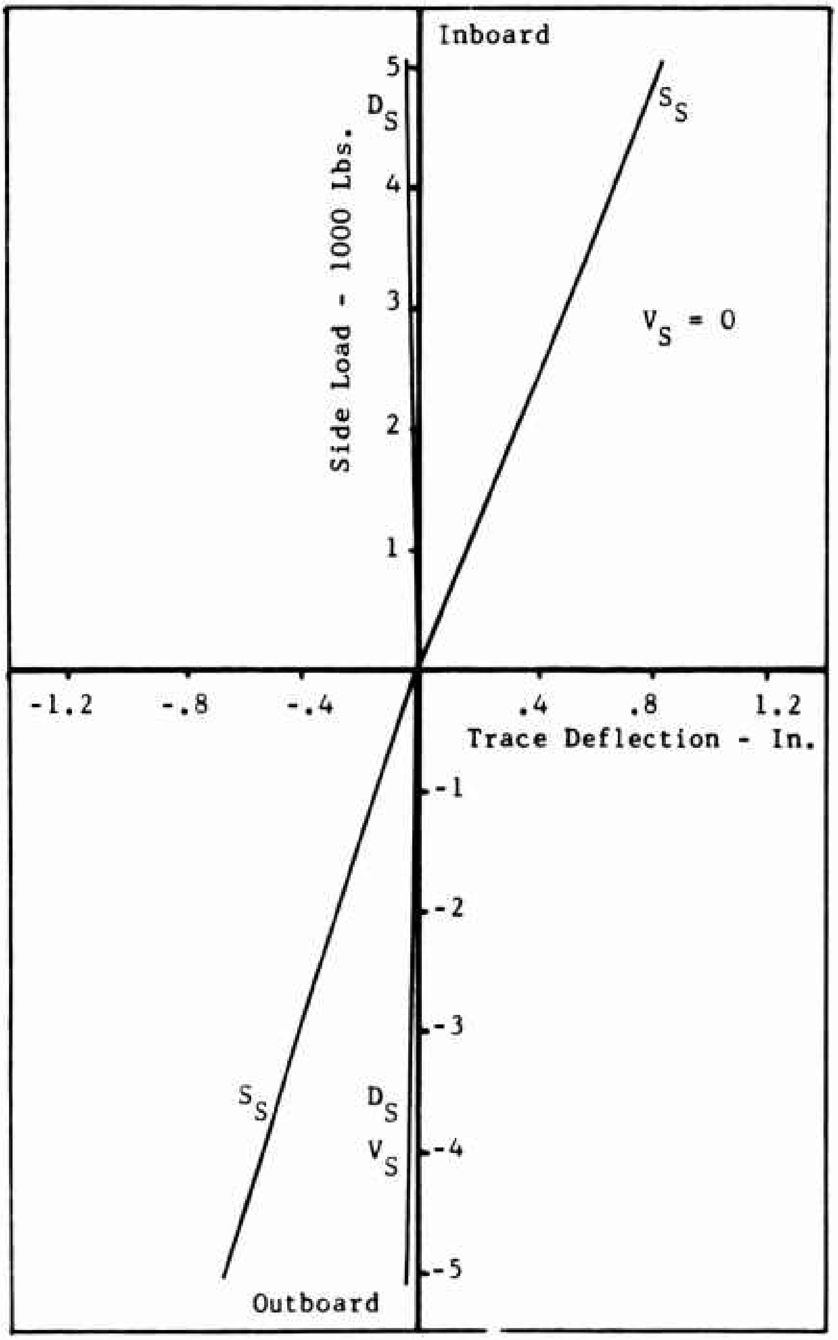

RIGHT MAIN GEAR

2/3 COMPRESSED

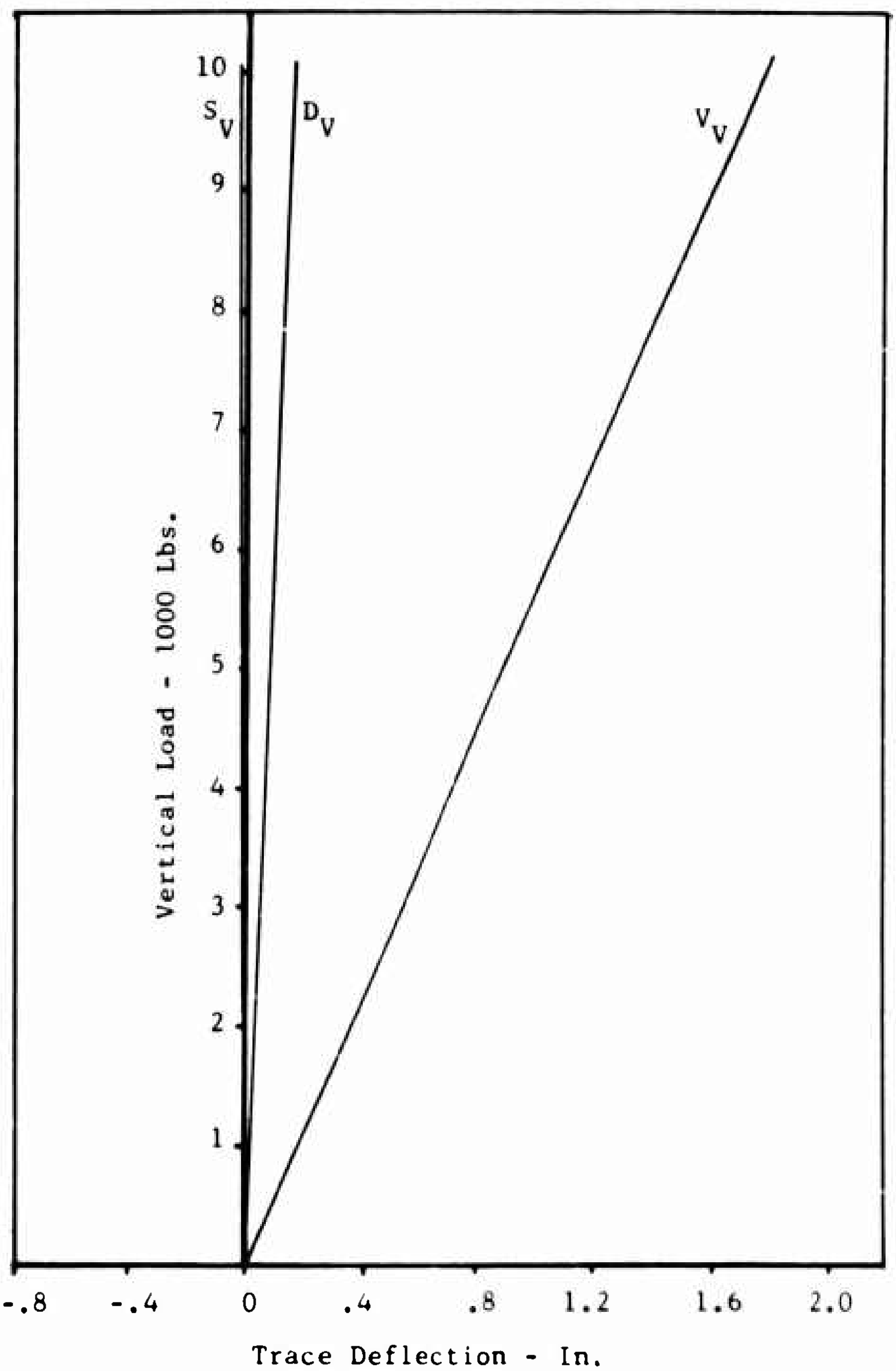

RIGHT MAIN GEAR

2/3 COMPRESSED

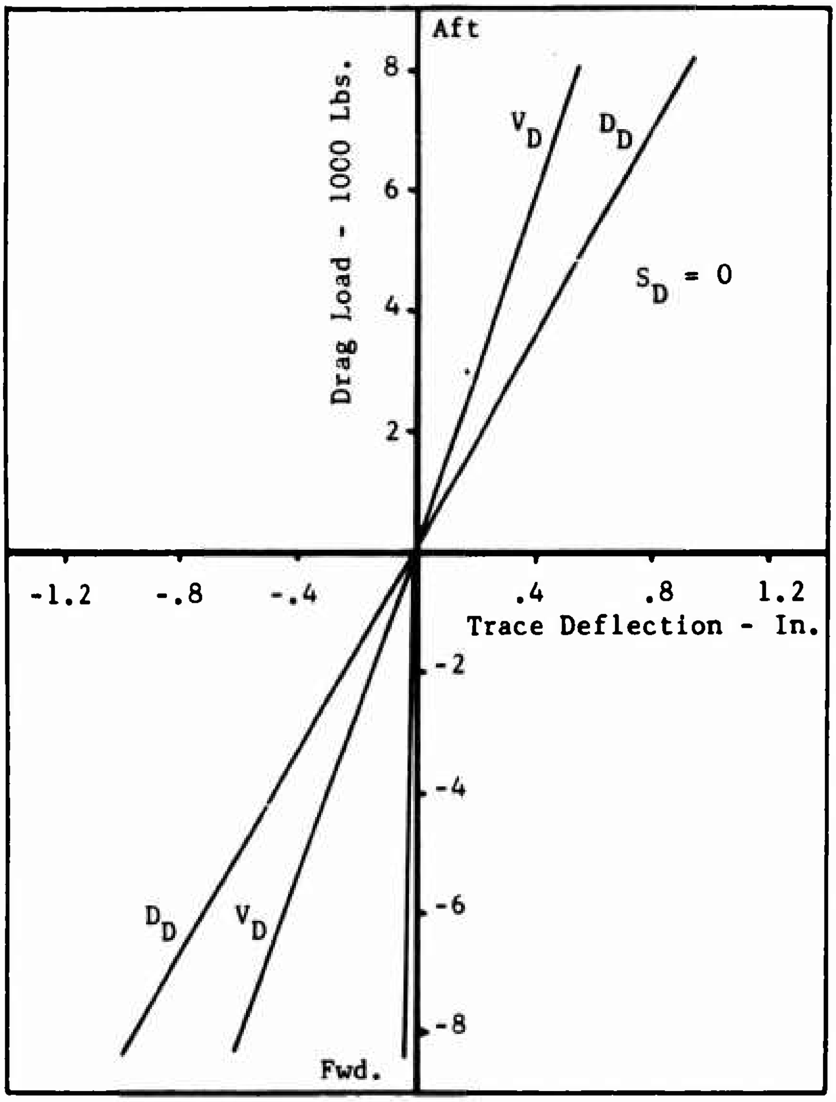

RIGHT MAIN GEAR

2/3 COMPRESSED

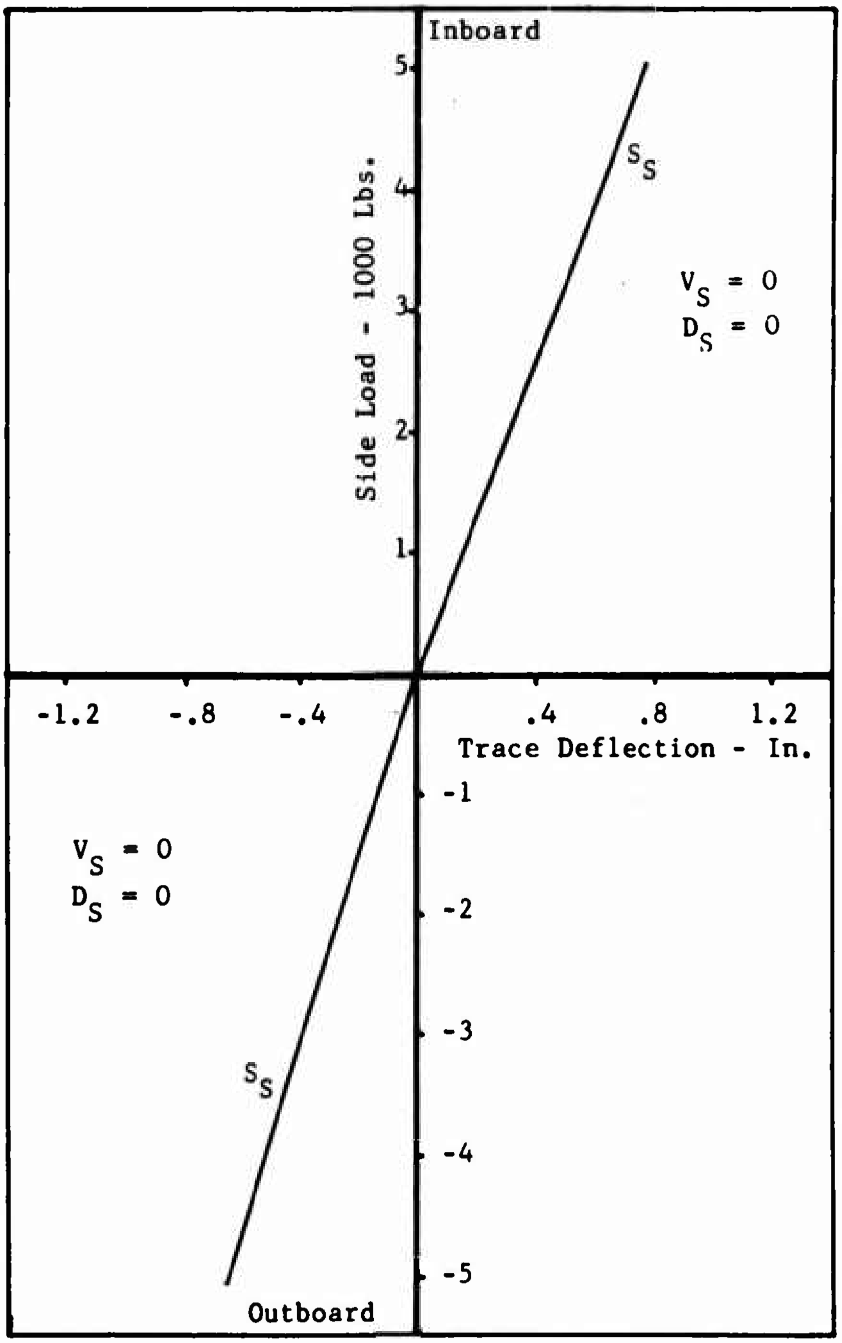

RIGHT MAIN GEAR

1/3 COMPRESSED

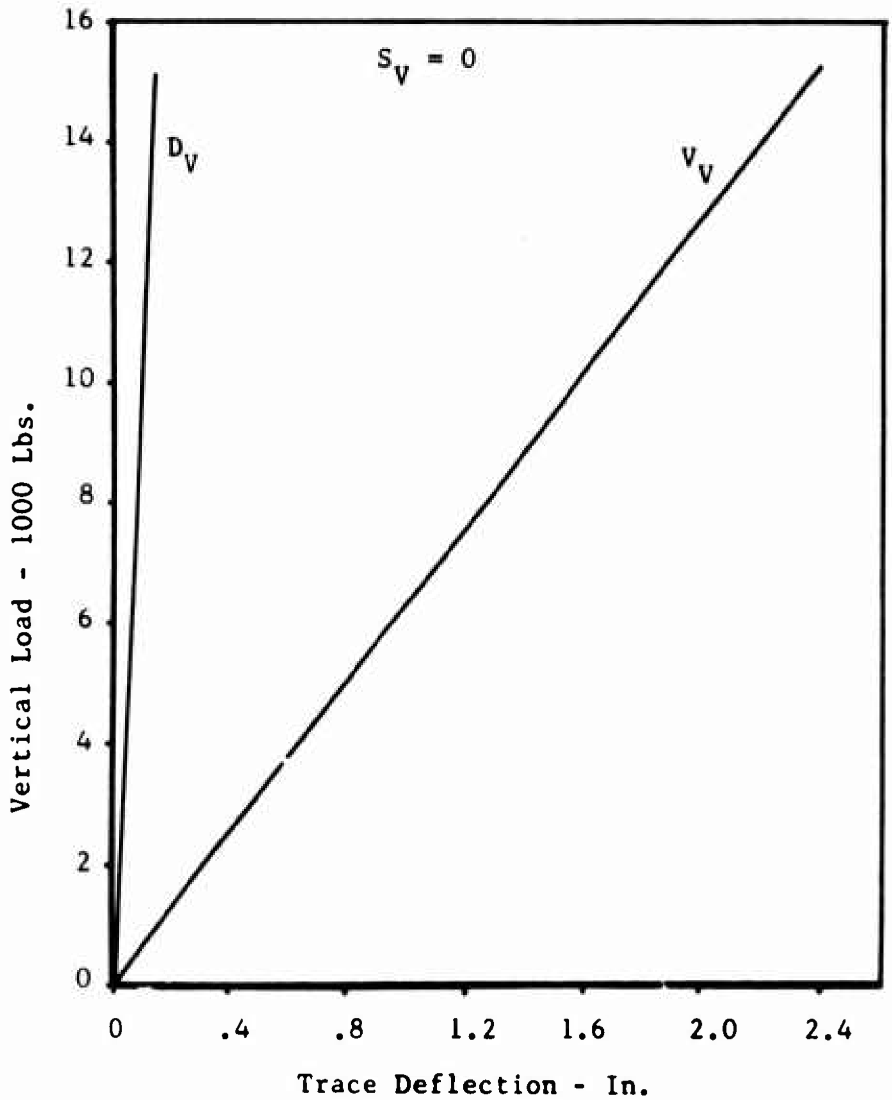

RIGHT MAIN GEAR

1/3 COMPRESSED

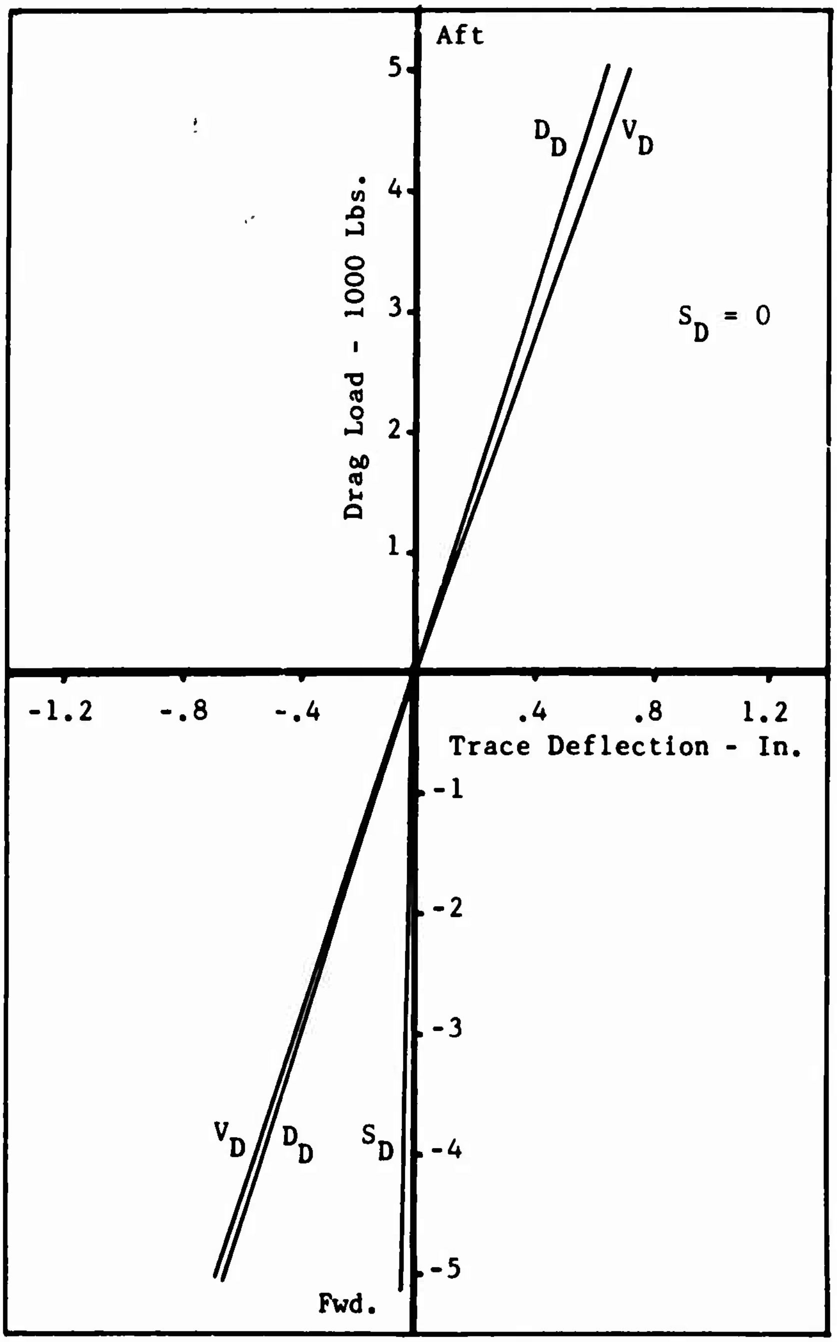

RIGHT MAIN GEAR

1/3 COMPRESSED

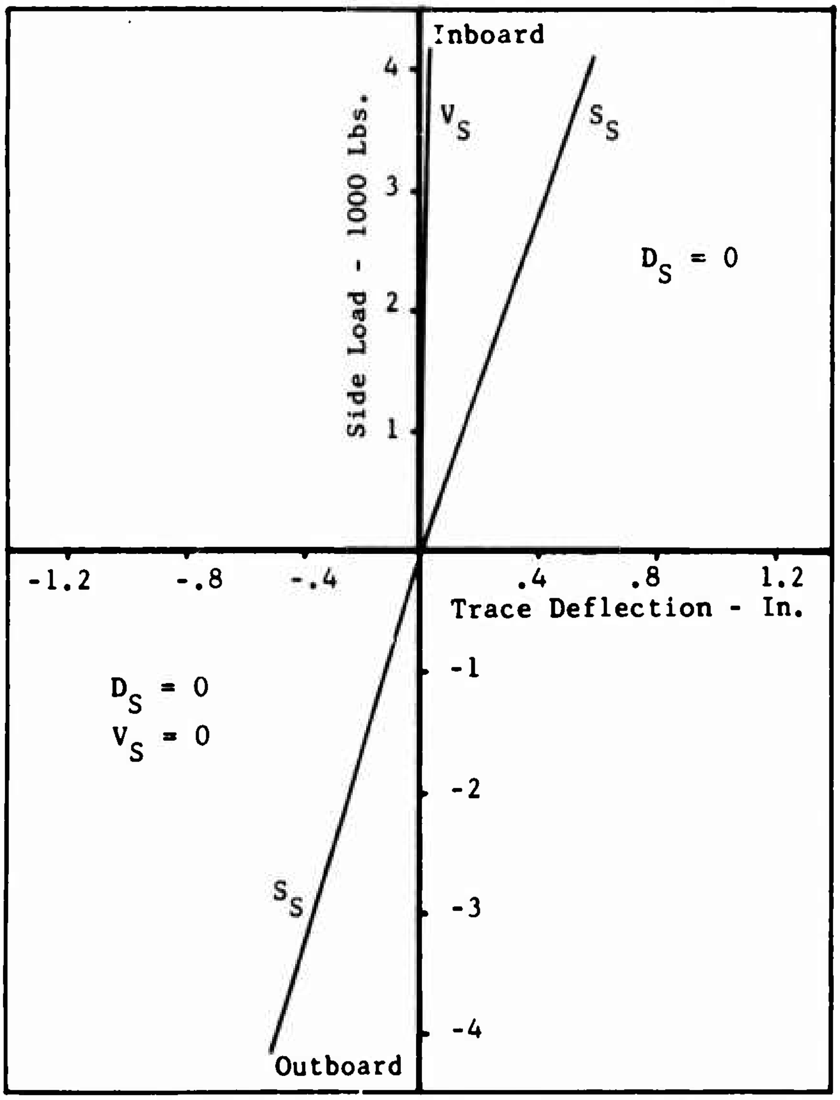

RIGHT MAIN GEAR

FULL EXTENDED

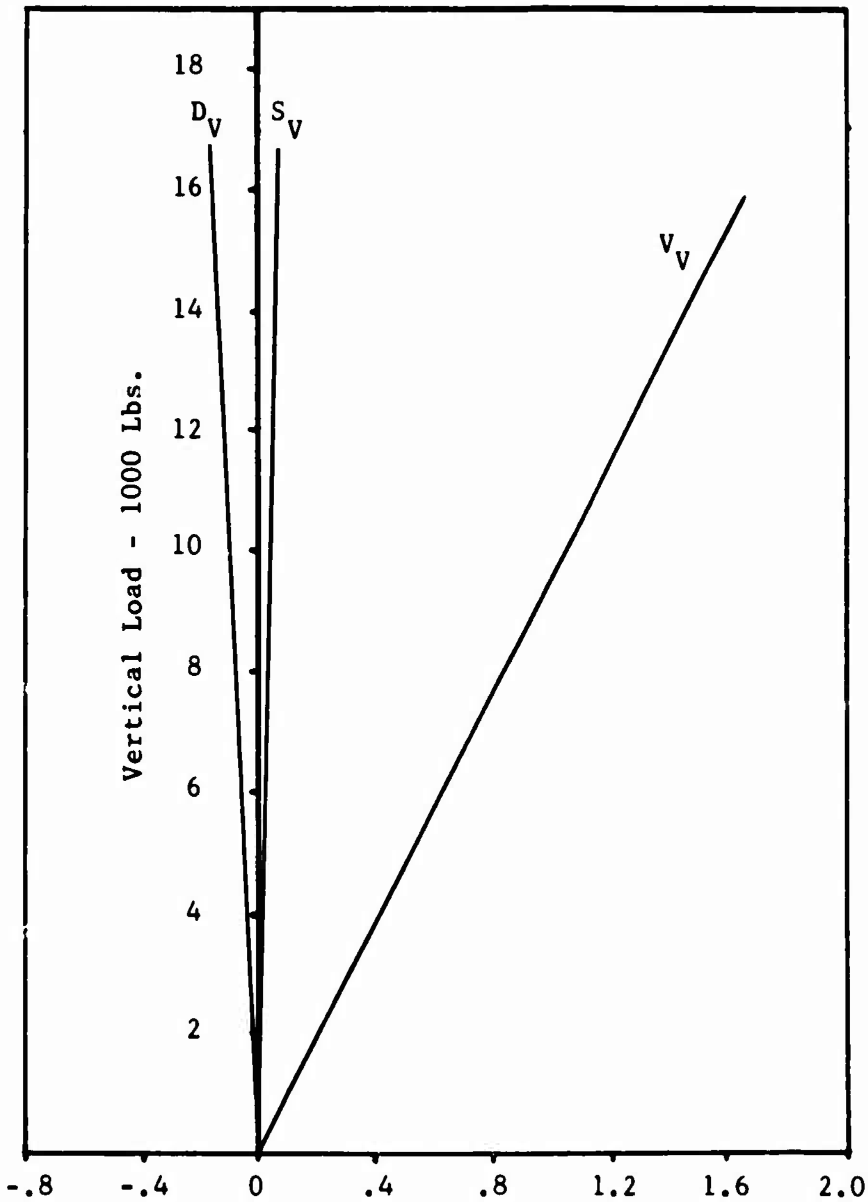

RIGHT MAIN GEAR

FULL EXTENDED

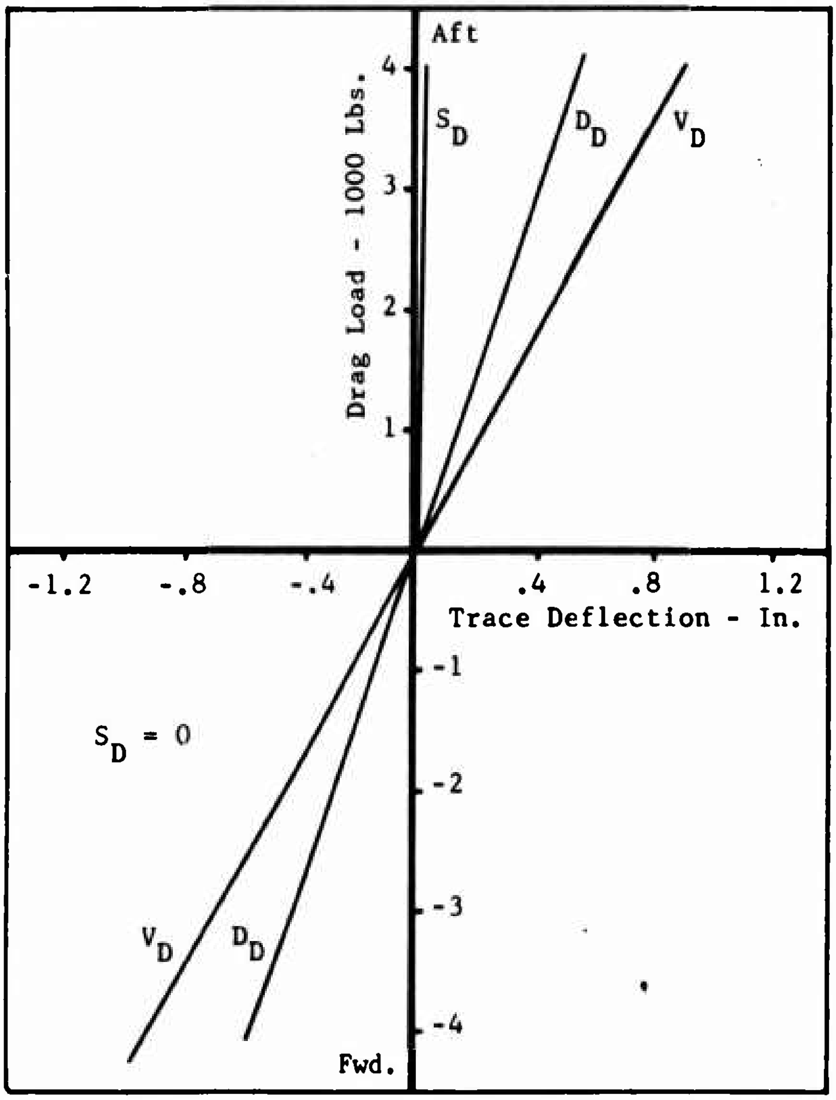

RIGHT MAIN GEAR

FULL EXTENDED

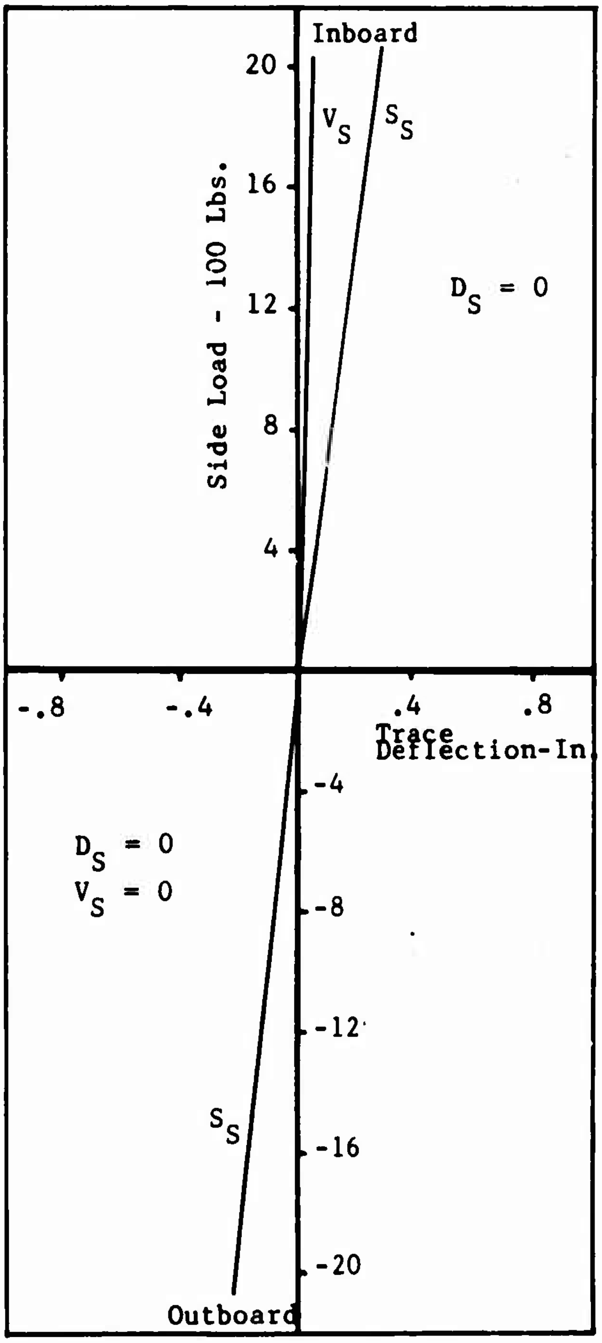

LEFT MAIN GEAR

FULL COMPRESSED

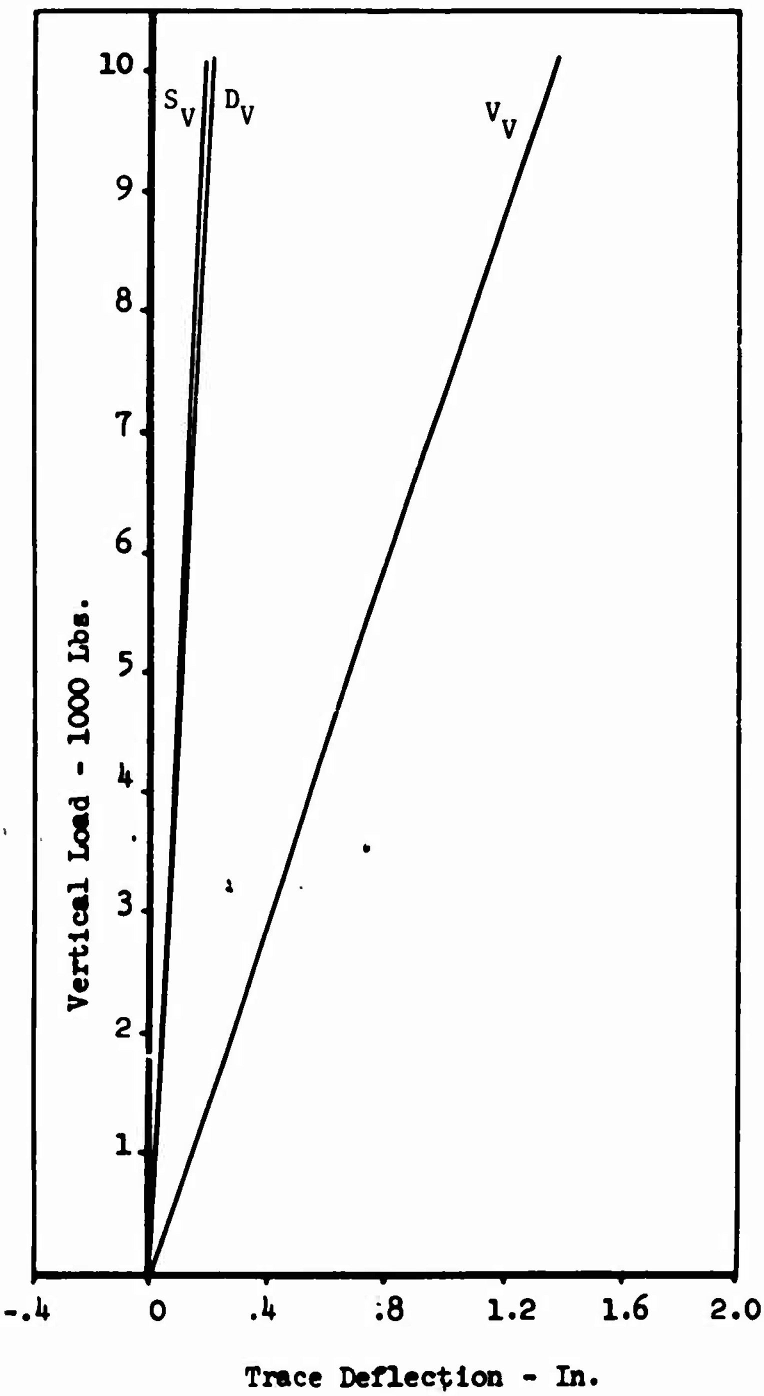

LEFT MAIN GEAR

FULL COMPRESSED

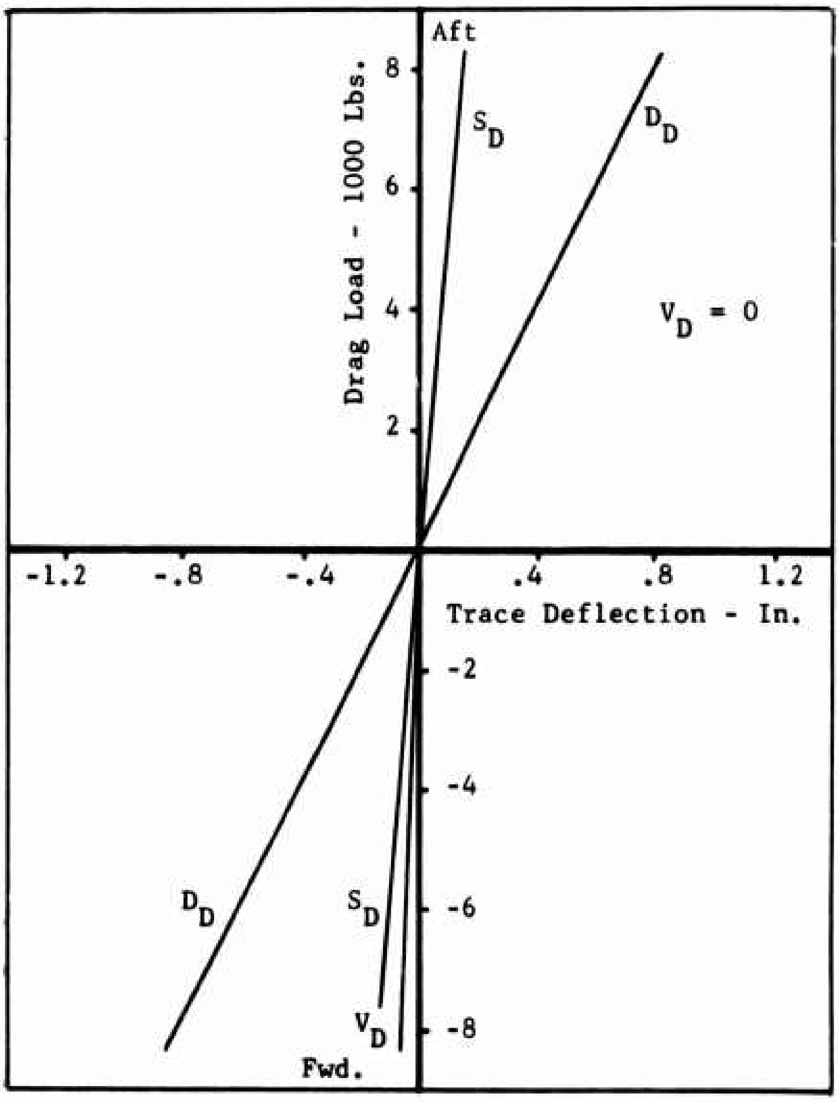

LEFT MAIN GEAR

FULL COMPRESSED

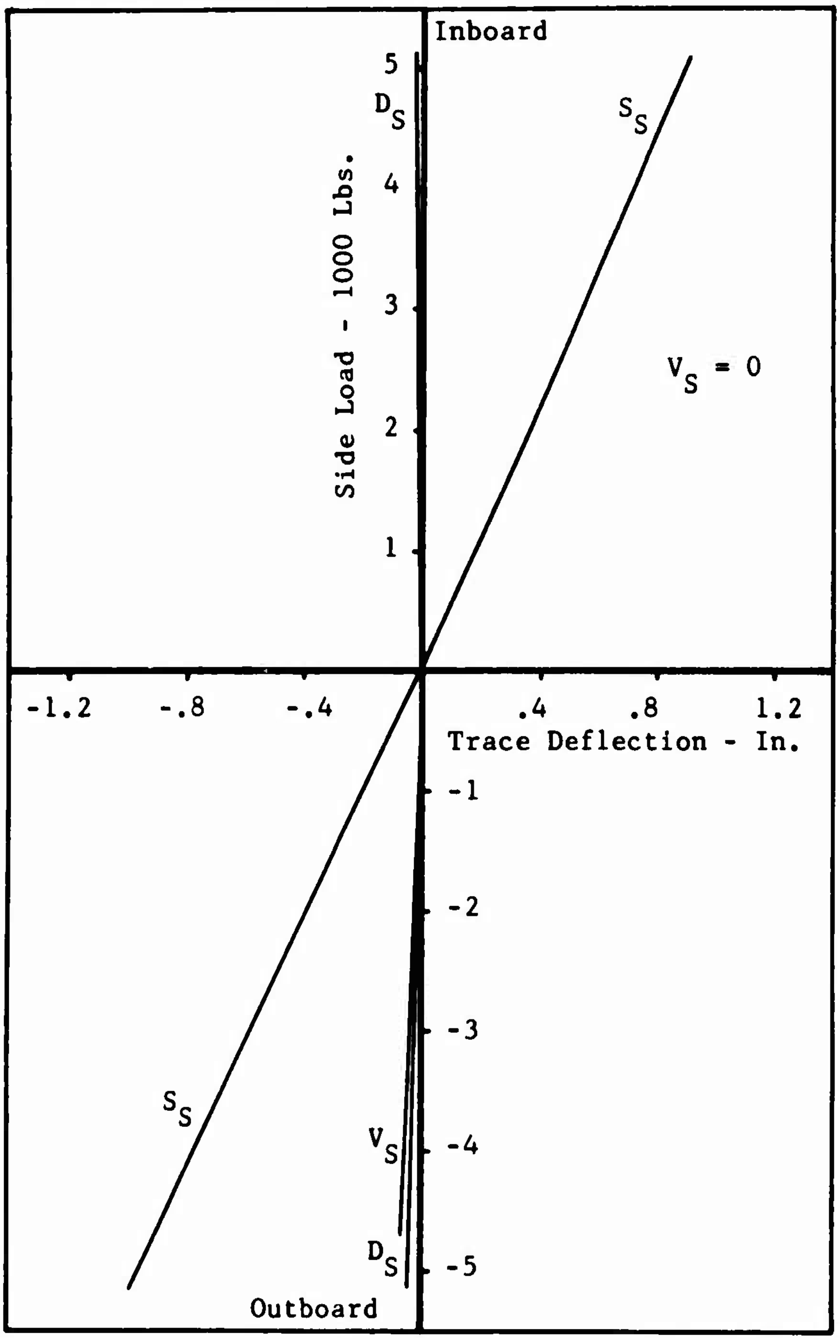

LEFT MAIN GEAR

2/3 COMPRESSED

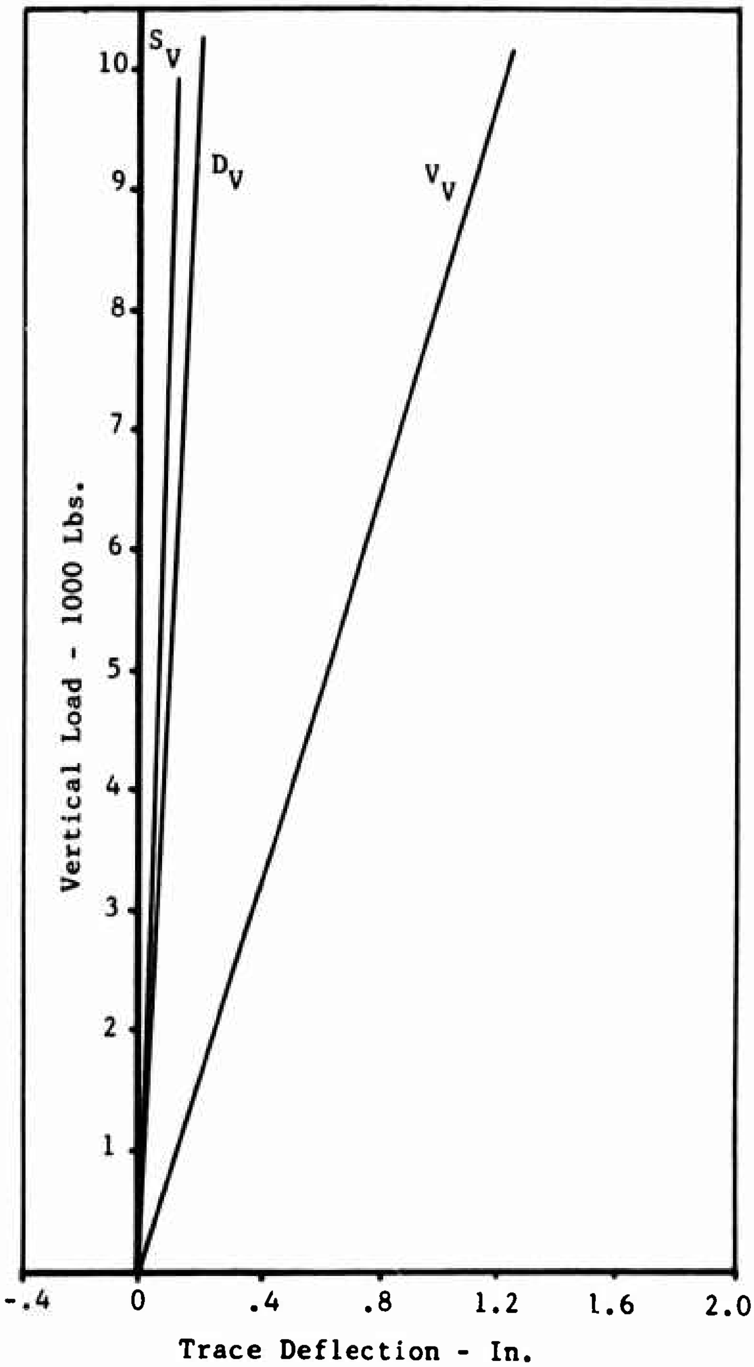

LEFT MAIN GEAR

2/3 COMPRESSED

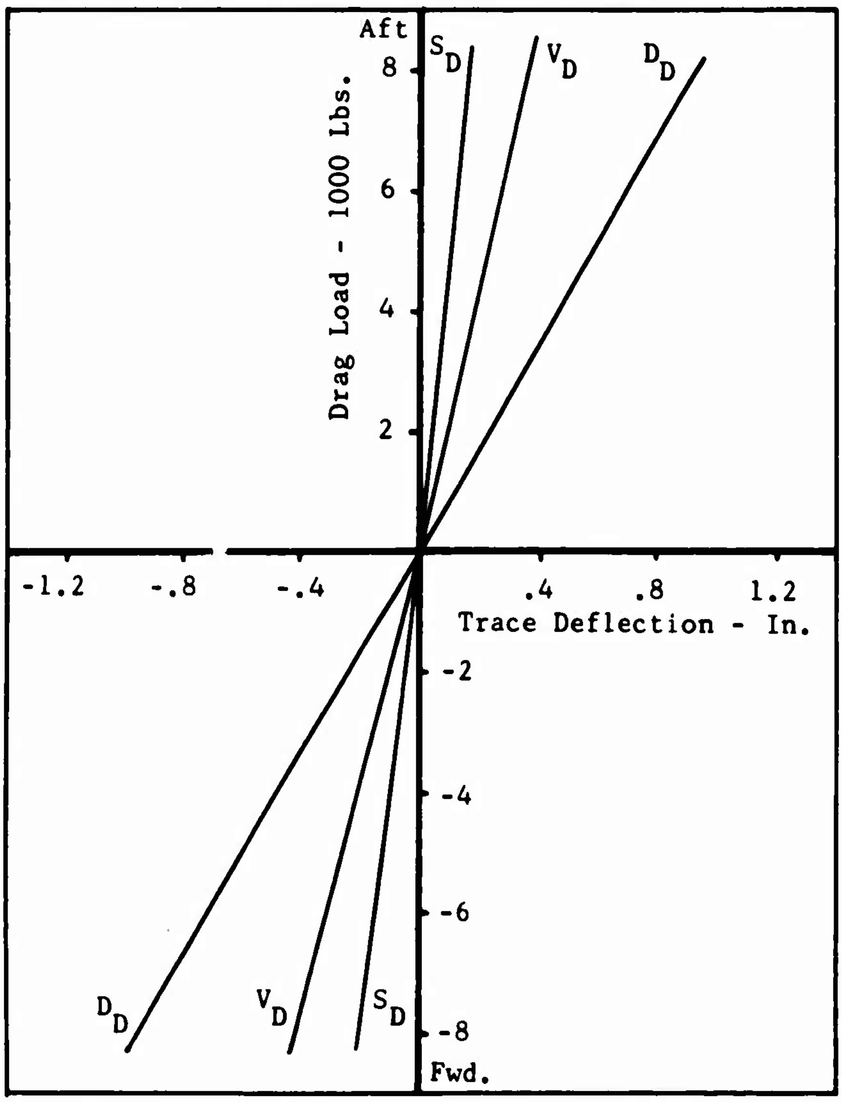

LEFT MAIN GEAR

2/3 COMPRESSED

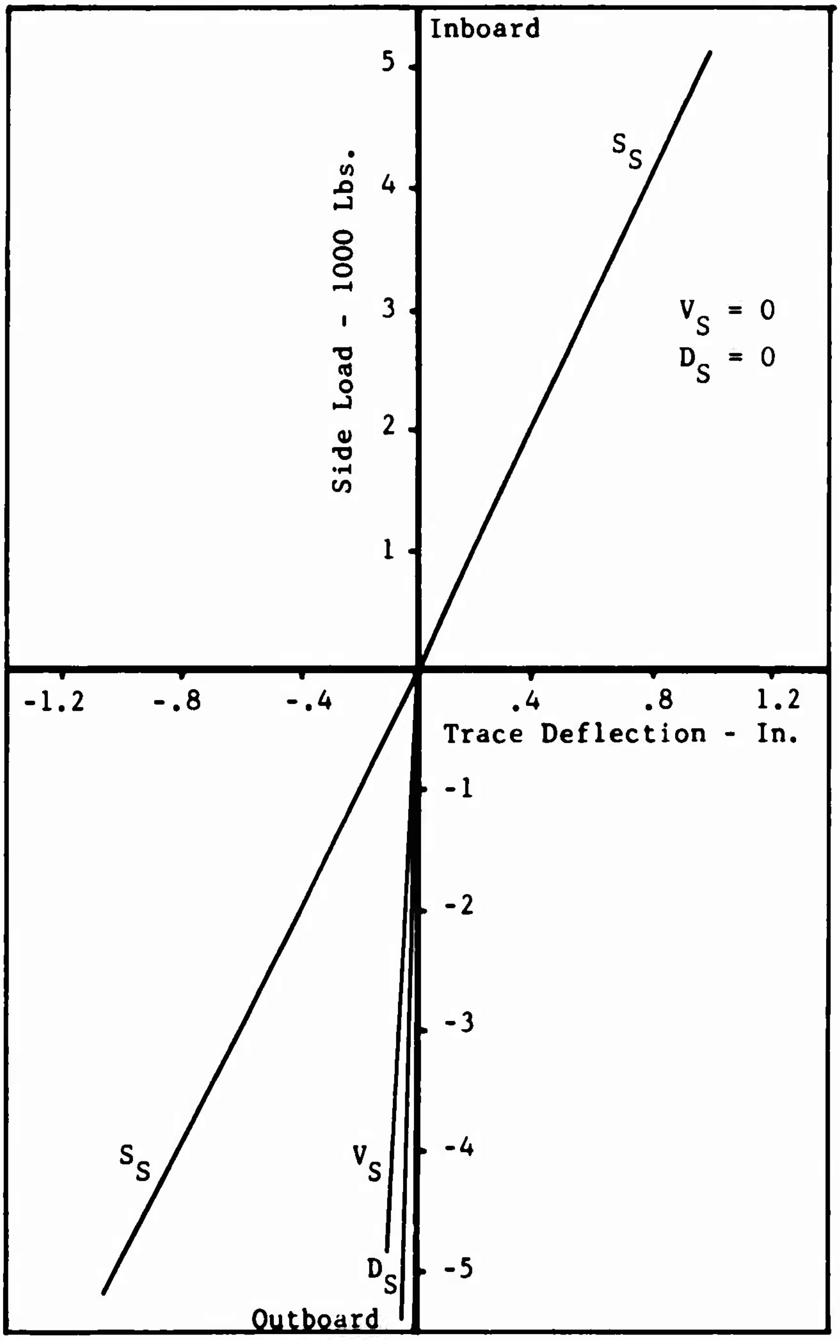

LEFT MAIN GEAR
1/3 COMPRESSED

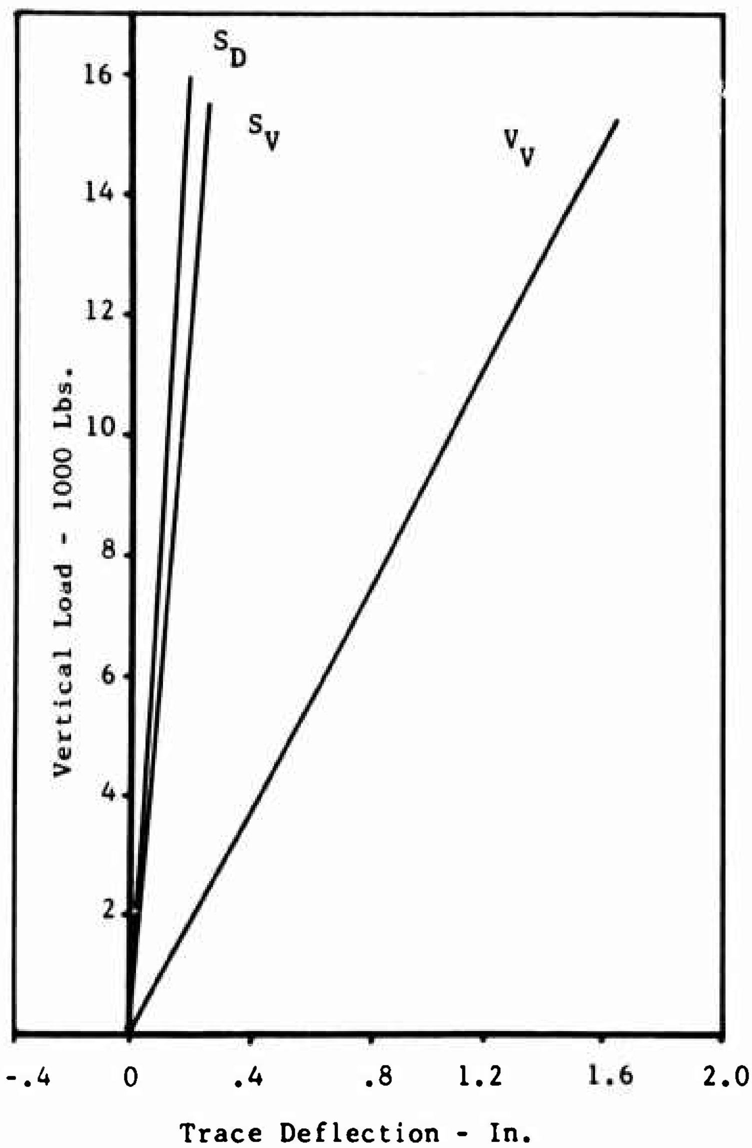

LEFT MAIN GEAR

1/3 COMPRESSED

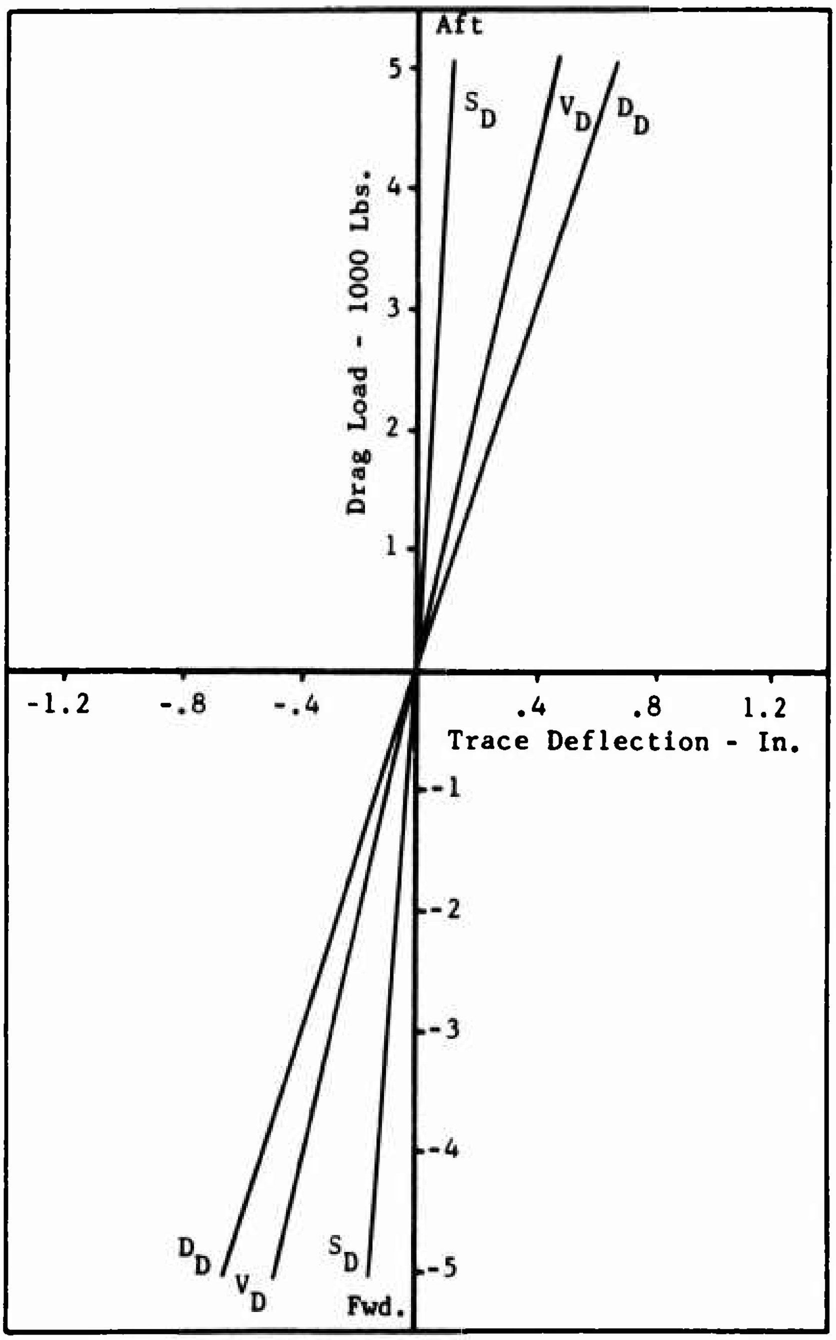

LEFT MAIN GEAR

1/3 COMPRESSED

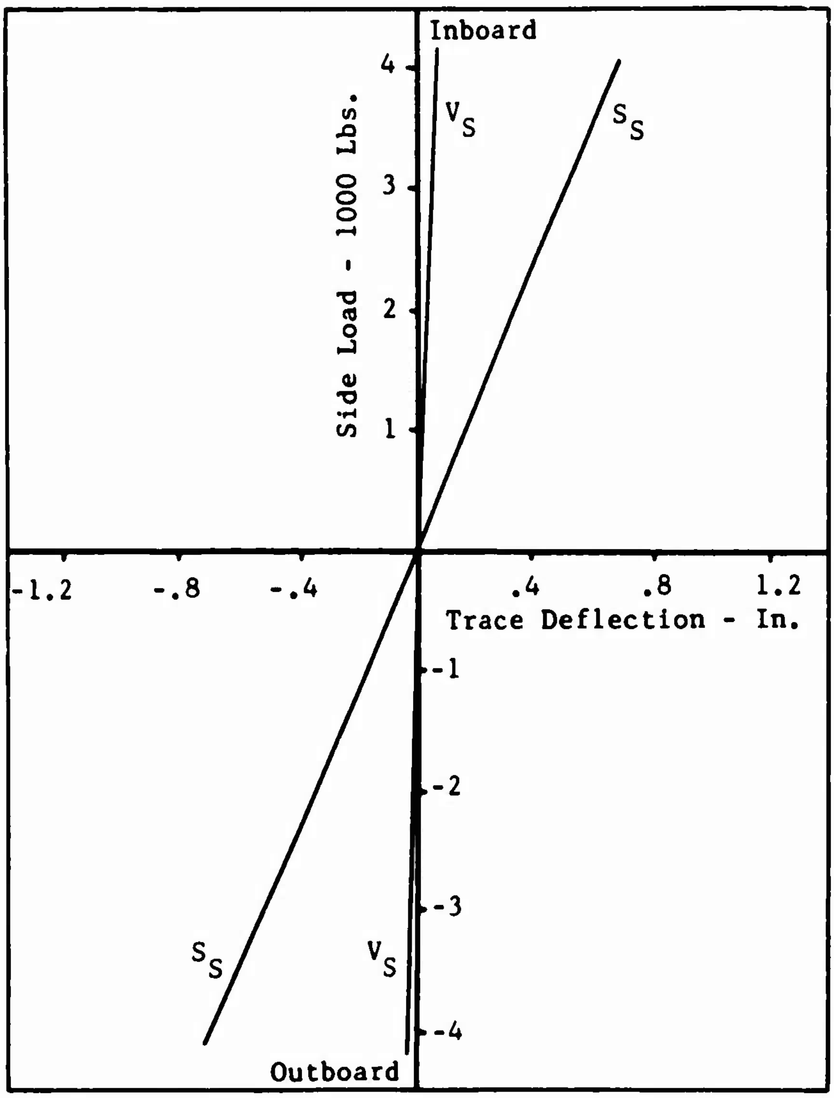

LEFT MAIN GEAR

FULL EXTENDED

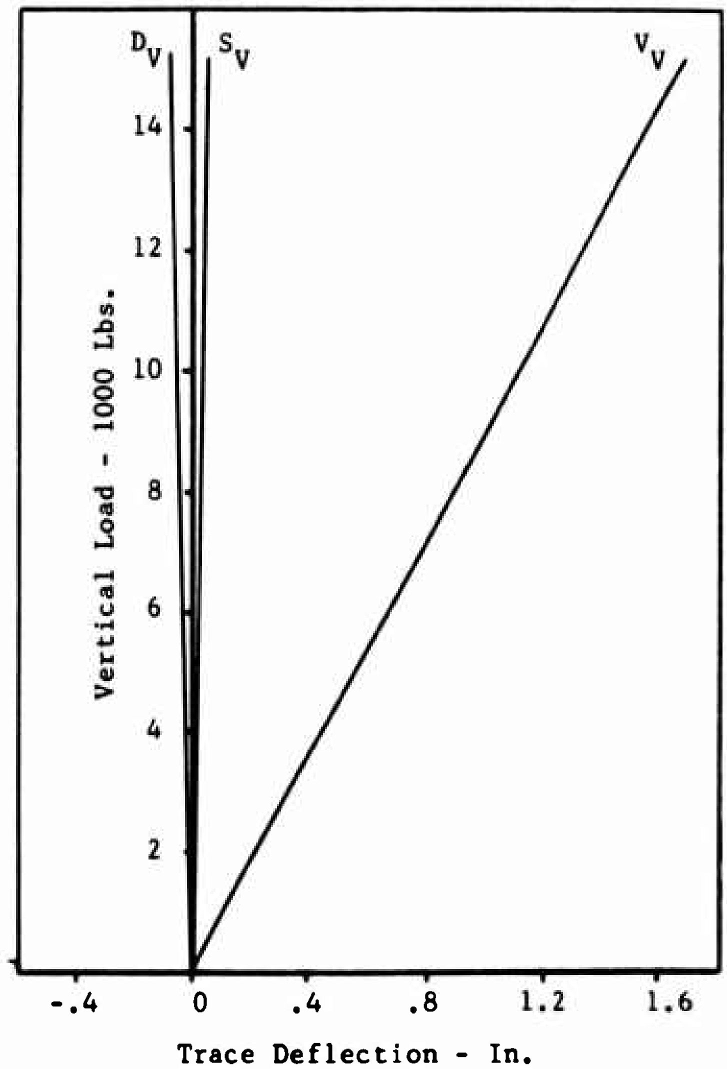

LEFT MAIN GEAR

FULL EXTENDED

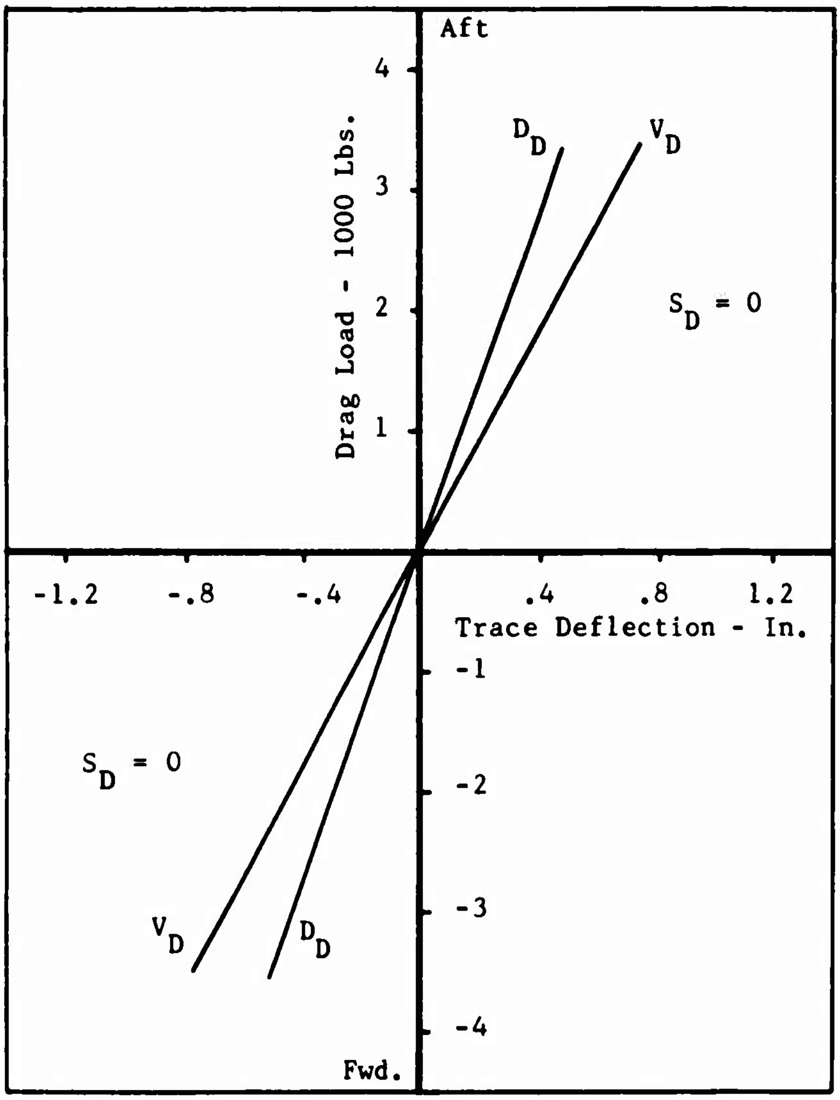

LEFT MAIN GEAR

FULL EXTENDED

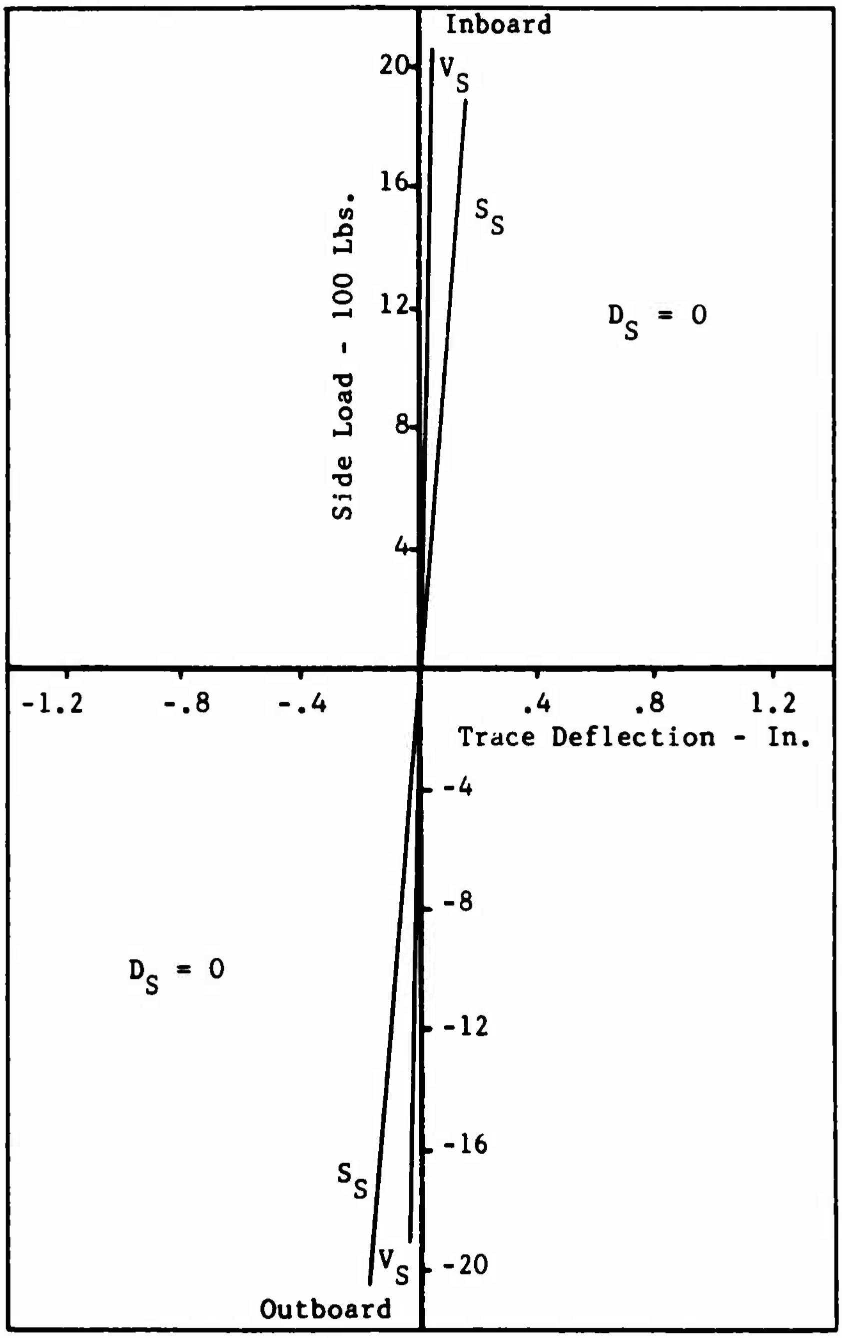

Nose Gear

Full compressed position (7.05")

Positive V, D, S

$$V = 11401\,\delta v - 814\,\delta d$$
$$D = -5022\,\delta v + 6311\,\delta d$$
$$S = 2878\,\delta s$$

Positive V, D and -5

$$V = 11401\,\delta v - 814\,\delta d$$
$$D = 5022\,\delta v + 6311\,\delta d$$
$$S = 2837\,\delta s$$

Positive V and -D, -S

$$V = 11825\,\delta v - 1347\,\delta d$$
$$D = -5538\,\delta v + 6960\,\delta d$$
$$S = 2837\,\delta s$$

$$V = 11825\,\delta v - 1347\,\delta d$$
$$D = -5538\,\delta v + 6960\,\delta d$$
$$S = 2878\,\delta s$$

Two-thirds compressed position (4.69")

Positive V, D. S

$$V = 14315\,\delta v - 3067\,\delta d$$
$$D = -3545\,\delta v + 5521\,\delta d$$
$$S = 85\,\delta v - 132\,\delta d + 2395\,\delta s$$

Positive V, D and -S

$$V = 14315\,\delta v - 3067\,\delta d$$
$$D = 3545\,\delta v + 5521\,\delta d$$
$$S = 83\,\delta v \quad 130\,\delta d + 2353\,\delta s$$

Positive V and -D, -S

$$V = 14706\,\delta v - 3676\,\delta d$$
$$D = -4025\,\delta v + 6269\,\delta d$$
$$S = -47\,\delta v + 74\,\delta d + 2353\,\delta s$$

Positive V, S and -D

$$V = 14706\,\delta v - 3676\,\delta d$$
$$D = -4025\,\delta v + 6269\,\delta d$$
$$S = 48\,\delta v + 75\,\delta d + 2395\,\delta s$$

Nose Gear

One-third compressed position (2.34")

Positive V, D, S

$$V = 19033\,\delta v - 5551\,\delta d$$
$$D = -2300\,\delta v + 4837\,\delta d$$
$$S = 71\,\delta v - 150\,\delta d + 2062\,\delta s$$

Positive V, D and -S

$$V = 19033\,\delta v - 5551\,\delta d$$
$$D = -2300\,\delta v + 4837\,\delta d$$
$$S = 72\,\delta v - 151\,\delta d + 2083\,\delta s$$

Positive V and -D, -S

$$V = 19523\,\delta v - 6583\,\delta d$$
$$D = -2633\,\delta v + 5539\,\delta d$$
$$S = -55\,\delta v + 115\,\delta d + 2083\,\delta s$$

Positive V, S, -D

$$V = 19523\,\delta v - 6583\,\delta d$$
$$D = 2633\,\delta v + 5539\,\delta d$$
$$S = -54\,\delta v + 114\,\delta d + 2062\,\delta s$$

Full extended position (0.00")

Positive V, D, S

$$V = 34360\,\delta v - 12048\,\delta d$$
$$D = 803\,\delta v + 3614\,\delta d$$
$$S = 10\,\delta v - 44\,\delta d + 1818\,\delta s$$

Positive V, D and -S

$$V = 34360\,\delta v - 12048\,\delta d$$
$$D = 803\,\delta v + 3614\,\delta d$$
$$S = -10\,\delta v - 44\,\delta d + 1818\,\delta s$$

Positive V and -D, -S

$$V = 34137\,\delta v - 13052\,\delta d$$
$$D = 904\,\delta v + 4066\,\delta d$$
$$S = 11\,\delta v + 49\,\delta d + 181\,\delta s$$

Positive V, S and -D

$$V = 34137\,\delta v - 13052\,\delta d$$
$$D = 904\,\delta v + 4066\,\delta d$$
$$S = 11\,\delta v + 49\,\delta d + 1818\,\delta s$$

Right Main Gear

Full compressed position (9.06")

Positive V, D, S

$$V = 5070\,\delta v - 186\,\delta d - 4\,\delta s$$
$$D = -1041\,\delta v + 9833\,\delta d + 237\,\delta s$$
$$S = 85\,\delta v - 224\,\delta d + 6019\,\delta s$$

Positive V, D, -S

$$V = 4068\,\delta v - 181\,\delta d - 144\,\delta s$$
$$D = -1048\,\delta v + 9852\,\delta d - 259\,\delta s$$
$$S = 103\,\delta v - 274\,\delta d + 7358\,\delta s$$

Positive V, -D, +S

$$V = 5051\,\delta v$$
$$D = -1037\,\delta v + 9804\,\delta d + 236\,\delta s$$
$$S = 61\,\delta v + 6024\,\delta s$$

Positive V, -D, -S

$$V = 5049\,\delta v - 149\,\delta s$$
$$D = -1042\,\delta v + 9804\,\delta d - 258\,\delta s$$
$$S = 74\,\delta v + 7351\,\delta s$$

Two-thirds Compressed position (6.04")

Positive V, D, S

$$V = 5838\,\delta v - 3540\,\delta d$$
$$D = -795\,\delta v + 8993\,\delta d$$
$$S = 77\,\delta v - 47\,\delta d + 6579\,\delta s$$

Positive V, D, -S

$$V = 5838\,\delta v - 3540\,\delta d$$
$$D = -795\,\delta v + 8993\,\delta d$$
$$S = 90\,\delta v - 54\,\delta d + 7692\,\delta s$$

Positive V, -D, +S

$$V = 5846\,\delta v - 3631\,\delta d$$
$$D = -788\,\delta v + 8910\,\delta d$$
$$S = 98\,\delta v - 282\,\delta d + 6579\,\delta s$$

Positive V, -D, -S

$$V = 5846\,\delta v - 3631\,\delta d$$
$$D = 788\,\delta v + 8910\,\delta d$$
$$S = 114\,\delta v - 330\,\delta d + 7692\,\delta s$$

Right Main Gear

One-third compressed position (3.02")

Positive V, D, S

$$V = 6800\,\delta v - 7437\,\delta d - 239\,\delta s$$
$$D = -531\,\delta v + 8394\,\delta d + 19\,\delta s$$
$$S = 7018\,\delta s$$

Positive V, D, -S

$$V = 6800\,\delta v - 7437\,\delta d$$
$$D = -531\,\delta v + 839\,\delta d$$
$$S = 8163\,\delta s$$

Positive V, -D, +S

$$V = 6777\,\delta v - 7070\,\delta d - 238\,\delta s$$
$$D = -513\,\delta v + 8111\,\delta d + 18\,\delta s$$
$$S = 29\,\delta v - 455\,\delta d + 7017\,\delta s$$

Positive V, -D, -S

$$V = 6778\,\delta v - 7086\,\delta d$$
$$D = -513\,\delta v + 8113\,\delta d$$
$$S = 34\,\delta v - 530\,\delta d + 8163\,\delta s$$

Full extended position (0")

Positive V, D, S

$$V = 8308\,\delta v - 13535\,\delta d - 1231\,\delta s$$
$$D = 604\,\delta v \quad 6288\,\delta d - 90\,\delta s$$
$$S = -276\,\delta v + 91\,\delta d + 7448\,\delta s$$

Positive V, D, -S

$$V = 826\,\delta v - 13520\,\delta d$$
$$D = 601\,\delta v - 6289\,\delta d$$
$$S = -353\,\delta v + 116\,\delta d + 9524\,\delta s$$

Positive V, -D, +S

$$V = 8318\,\delta v - 13426\,\delta d - 1232\,\delta s$$
$$D = 584\,\delta v + 6075\,\delta d - 86\,\delta s$$
$$S = -246\,\delta v + 398\,\delta d + 7444\,\delta s$$

Positive V, -D, -S

$$V = 8278\,\delta v - 13360\,\delta d$$
$$D = 581\,\delta v + 6080\,\delta d$$
$$S = -315\,\delta v + 509\,\delta d + 9524\,\delta s$$

Left Main Gear

Full compressed position (9.06")

Positive V, D, S

$$V = 5051\,\delta v$$
$$D = -1009\,\delta v + 9991\,\delta d + 377\,\delta s$$
$$S = 24\,\delta v - 236\,\delta d + 9425\,\delta s$$

Positive V, D, -S

$$V = 5051\,\delta v$$
$$D = -1012\,\delta v + 10022\,\delta d - 871\,\delta s$$
$$S = 28\,\delta v - 272\,\delta d + 10893\,\delta s$$

Positive V, -D, +S

$$V = 5088\,\delta v - 371\,\delta d -$$
$$D = -989\,\delta v + 9792\,\delta d + 370\,\delta s$$
$$S = 93\,\delta v - 924\,\delta d + 9399\,\delta s$$

Positive V, -D, -S

$$V = 5088\,\delta v - 376\,\delta d + 33\,\delta s$$
$$D = -1001\,\delta v + 9913\,\delta d - 862\,\delta s$$
$$S = 109\,\delta v - 1078\,\delta d + 10963\,\delta s$$

Two-thirds compressed position (6.04")

Positive V, D, S

$$V = 5885\,\delta v - 3255\,\delta d$$
$$D = -1002\,\delta v + 9065\,\delta d$$
$$S = 9375\,\delta s$$

Positive V, D, -S

$$V = 5885\,\delta v - 3255\,\delta d + 225\,\delta s$$
$$D = -1002\,\delta v + 9065\,\delta d - 625\,\delta s$$
$$S = 10{,}345\,\delta s$$

Positive V, -D, +S

$$V = 5932\,\delta v - 3684\,\delta d$$
$$D = -999\,\delta v + 9042\,\delta d$$
$$S = 47\,\delta v - 424\,\delta d + 9375\,\delta s$$

Positive V, -D, -S

$$V = 5933\,\delta v - 3696\,\delta d + 255\,\delta s$$
$$D = -1002\,\delta v + 9070\,\delta d - 626\,\delta s$$
$$S = 52\,\delta v - 469\,\delta d + 10377\,\delta s$$

Left Main Gear

One-third compressed position (3.02")

Positive V, D, S

$V = 6910\,\delta v - 6910\,\delta d - 1063\,\delta s$
$D = -645\,\delta v + 8107\,\delta d + 99\,\delta s$
$S = -133\,\delta v + 133\,\delta d + 10277\,\delta s$

Positive V, D, -S

$V = 6902\,\delta v - 6902\,\delta d - 383\,\delta s$
$D = -644\,\delta v + 8106\,\delta d + 36\,\delta s$
$S = -144\,\delta v + 144\,\delta d + 11{,}119\,\delta s$

Positive V, -D, +S

$V = 6947\,\delta v - 7368\,\delta d - 1069\,\delta s$
$D = -658\,\delta v + 8273\,\delta d + 101\,\delta s$
$S = -134\,\delta v + 142\,\delta d + 10277\,\delta s$

Positive V, -D, -S

$V = 6938\,\delta v - 7358\,\delta d - 385\,\delta s$
$D = -657\,\delta v + 8273\,\delta d + 36\,\delta s$
$S = -145\,\delta v + 153\,\delta d + 11{,}196\,\delta s$

Full extended position (0")

Positive V, D, S

$V = 8453\,\delta v - 13083\,\delta d - 1585\,\delta s$
$D = 322\,\delta v + 6644\,\delta d - 60\,\delta s$
$S = -352\,\delta v + 545\,\delta d + 12566\,\delta s$

Positive V, D, -S

$V = 8409\,\delta v - 13014\,\delta d$
$D = 320\,\delta v + 6647\,\delta d$
$S = -431\,\delta v + 667\,\delta d + 15385\,\delta s$

Positive V, -D, +S

$V = 8463\,\delta v - 12887\,\delta d - 1587\,\delta s$
$D = 308\,\delta v + 6350\,\delta d - 58\,\delta s$
$S = -353\,\delta v + 537\,\delta d + 12566\,\delta s$

Positive V, -D, -S

$V = 8418\,\delta v - 12819\,\delta d$
$D = 306\,\delta v + 6352\,\delta d$
$S = -4325\,\delta v + 657\,\delta d + 15385\,\delta s$

OV-10A #3
NOSE GEAR
PRIMARY CALIB
9-1-67

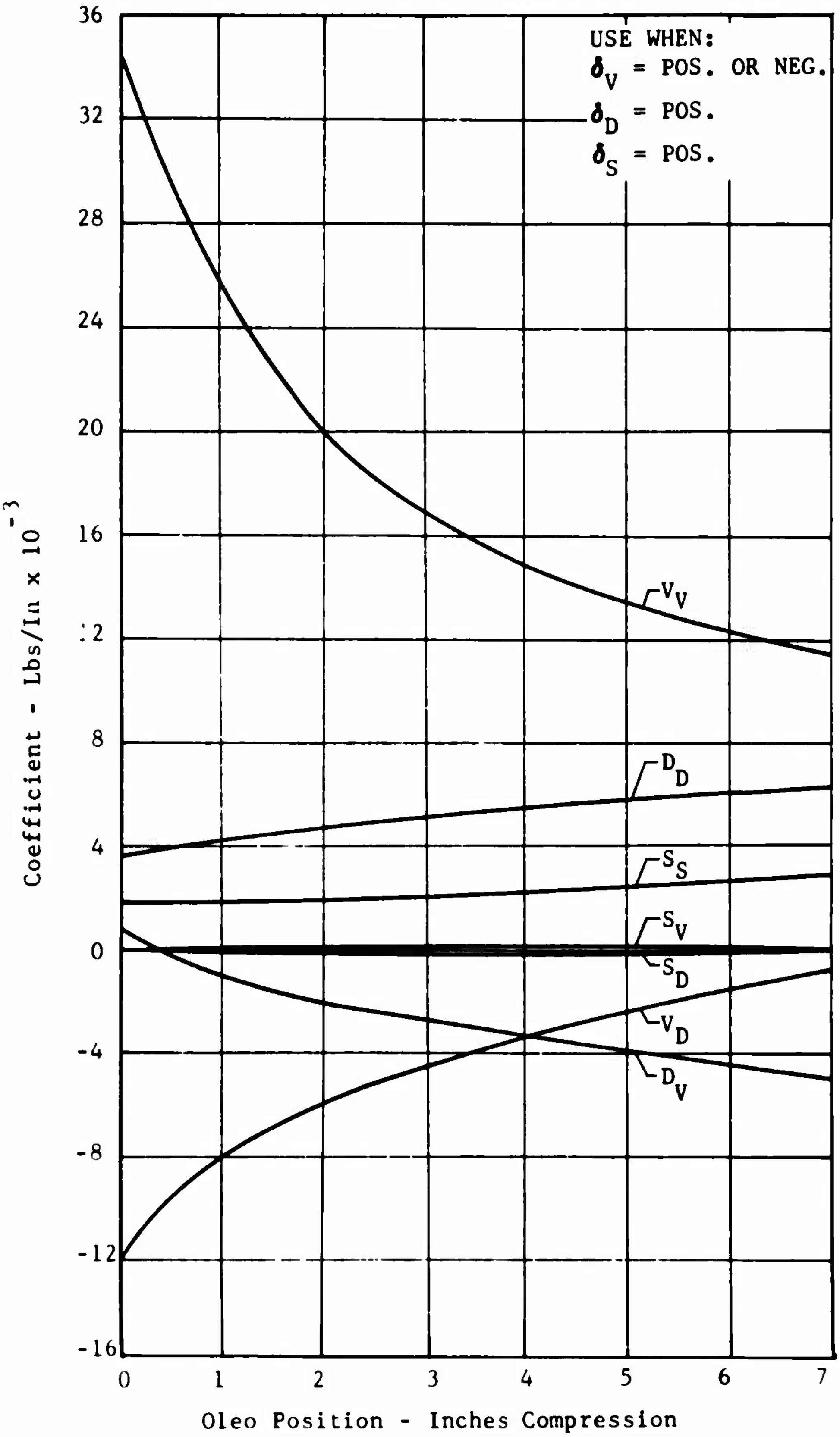

OV-10A #3
NOSE GEAR
PRIMARY CALIB
9-1-67

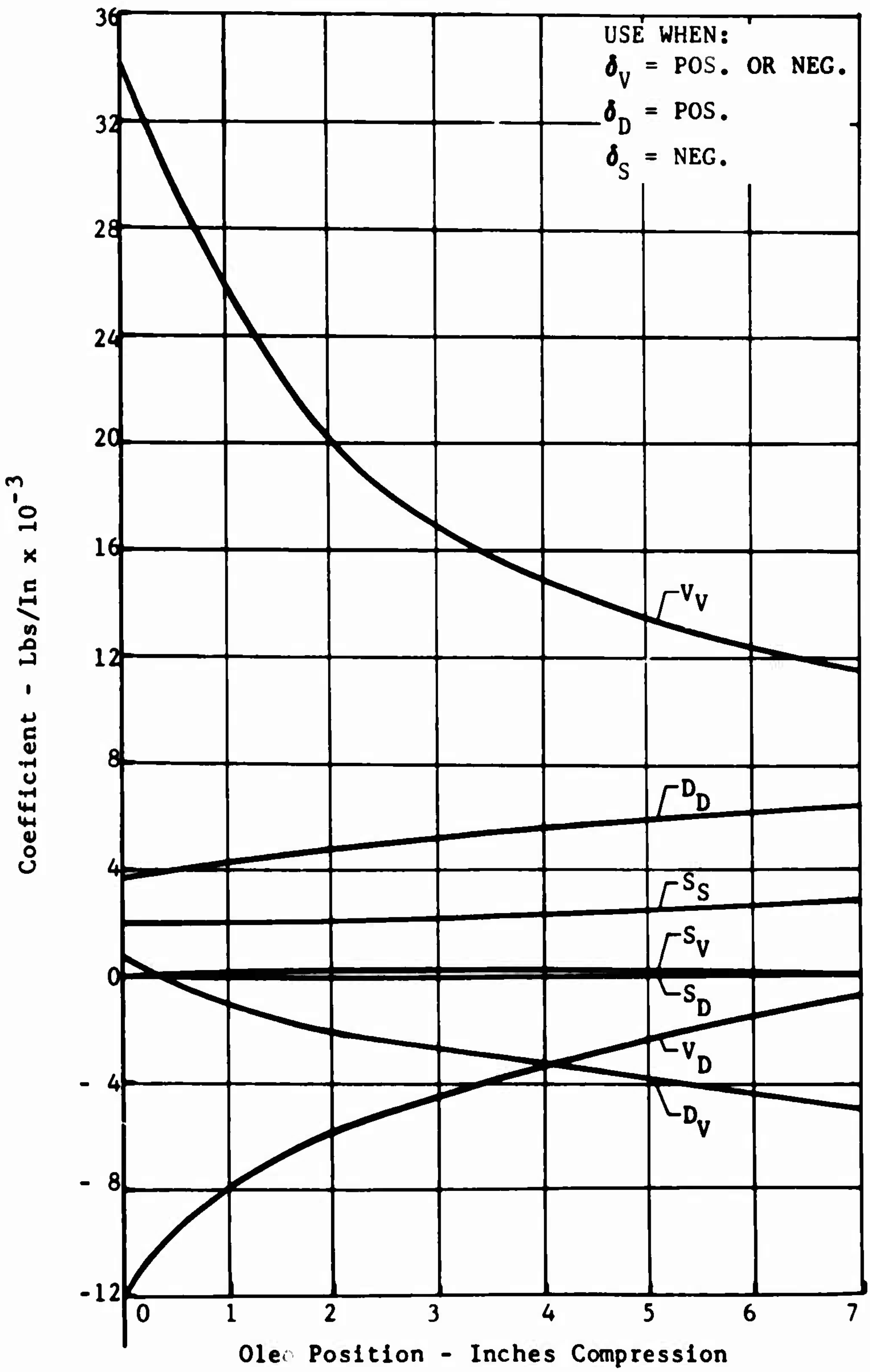

OV-10A #3
NOSE GEAR
PRIMARY CALIB
9-1-67

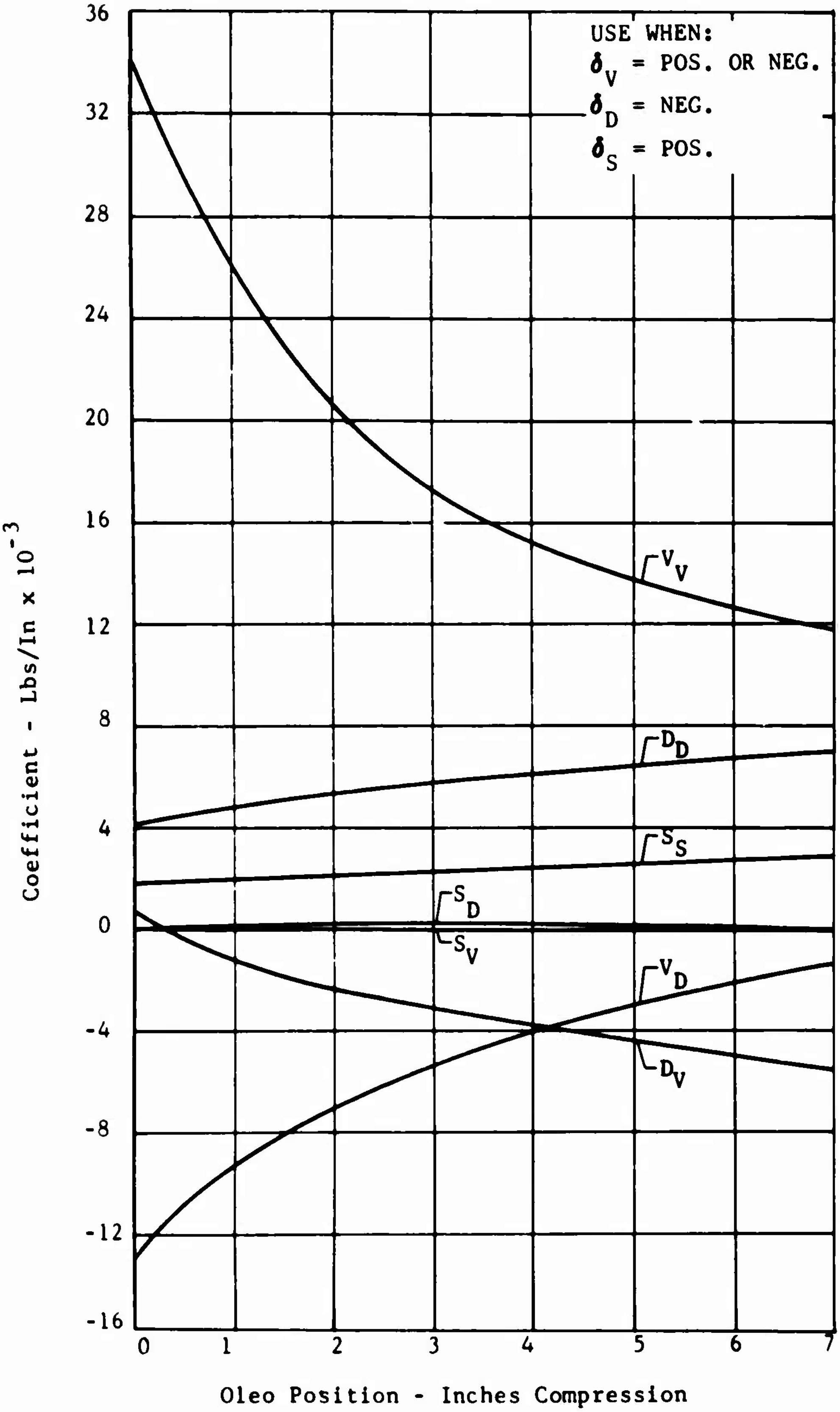

OV-10A #3
NOSE GEAR
PRIMARY CALIB
9-1-67

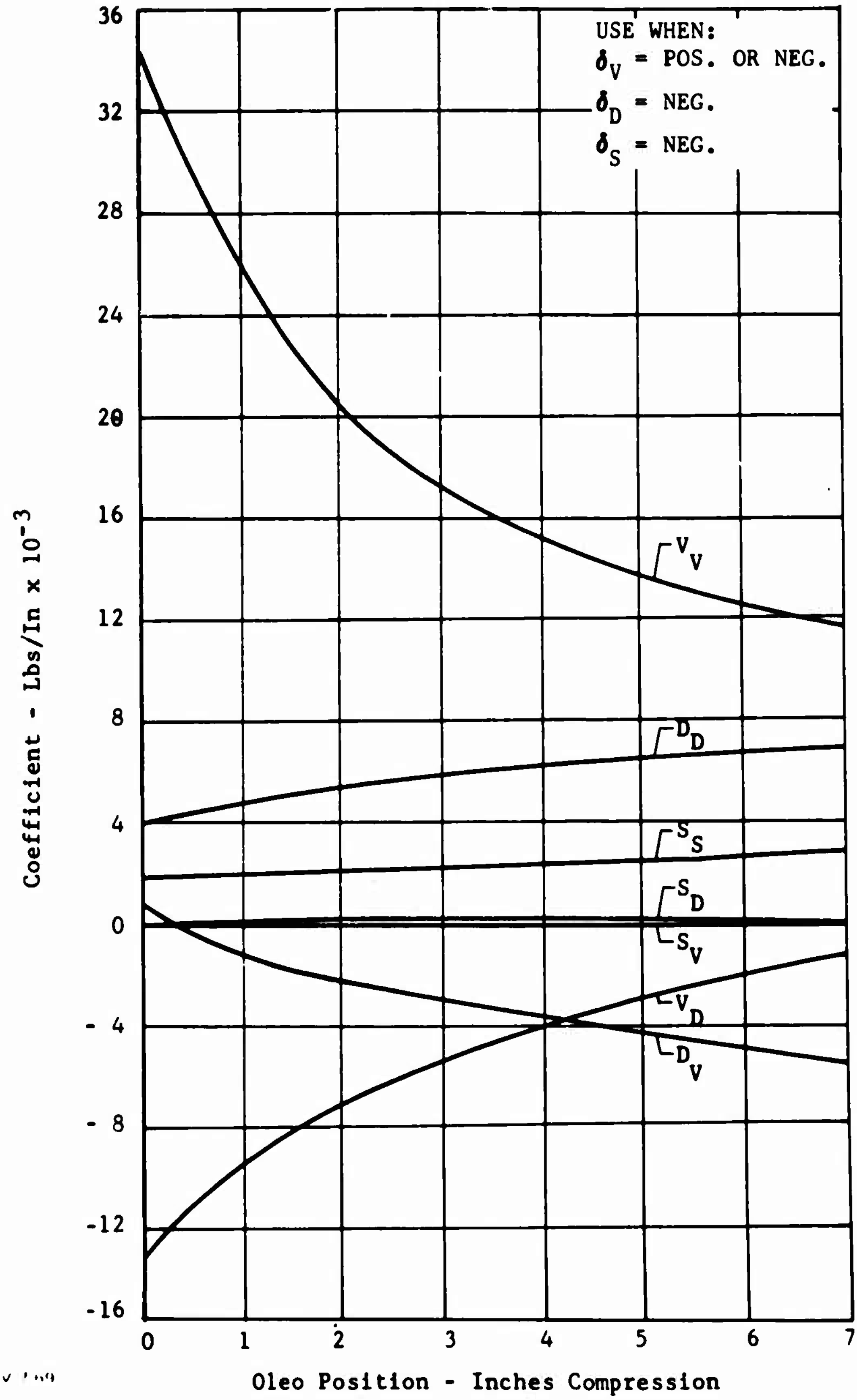

OV-10A #3
R/H MAIN GEAR
PRIMARY CALIB
8-10-67

USE WHEN:
δ_V = POS. OR NEG.
δ_D = POS.
δ_S = POS.

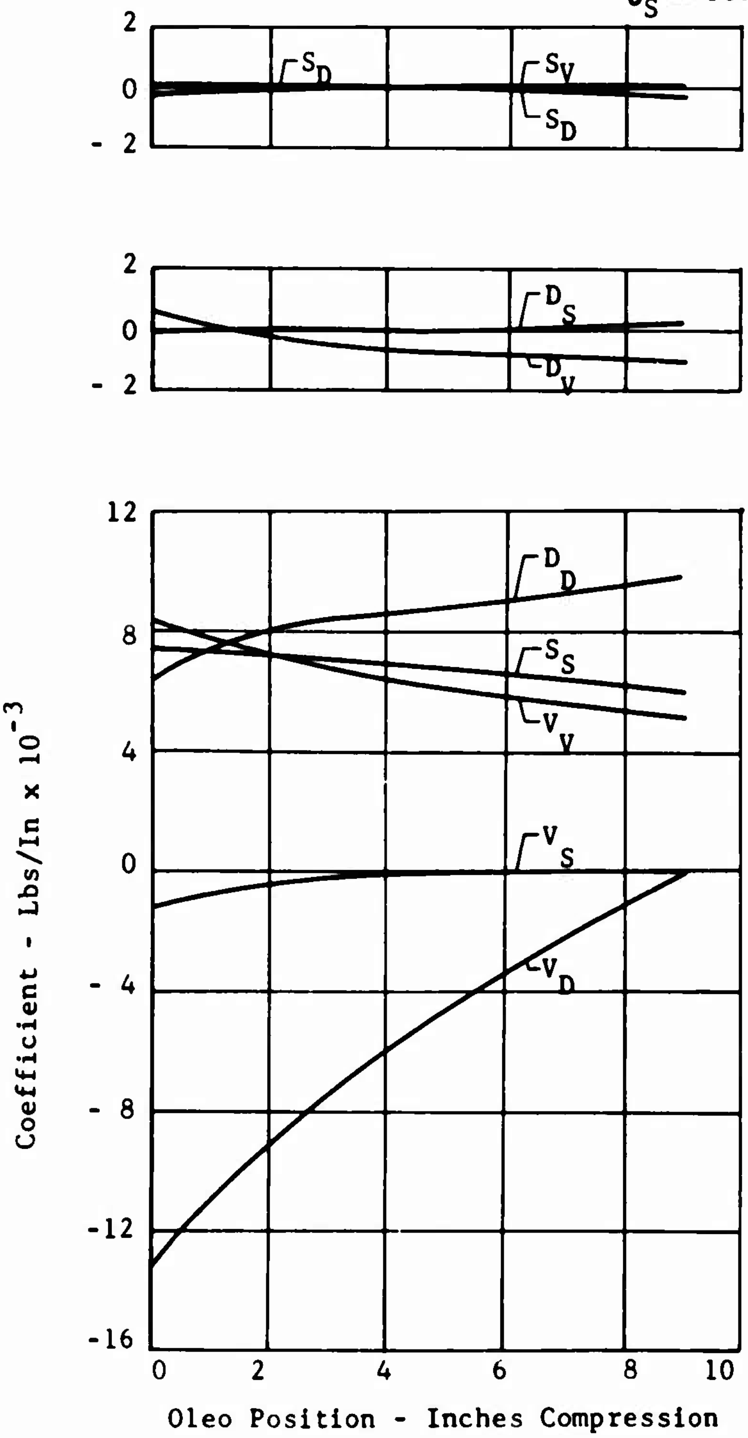

OV-10A #3
R/H MAIN GEAR
PRIMARY CALIB
8-10-67

USE WHEN:
δ_V = POS. OR NEG.
δ_D = POS.
δ_S = NEG.

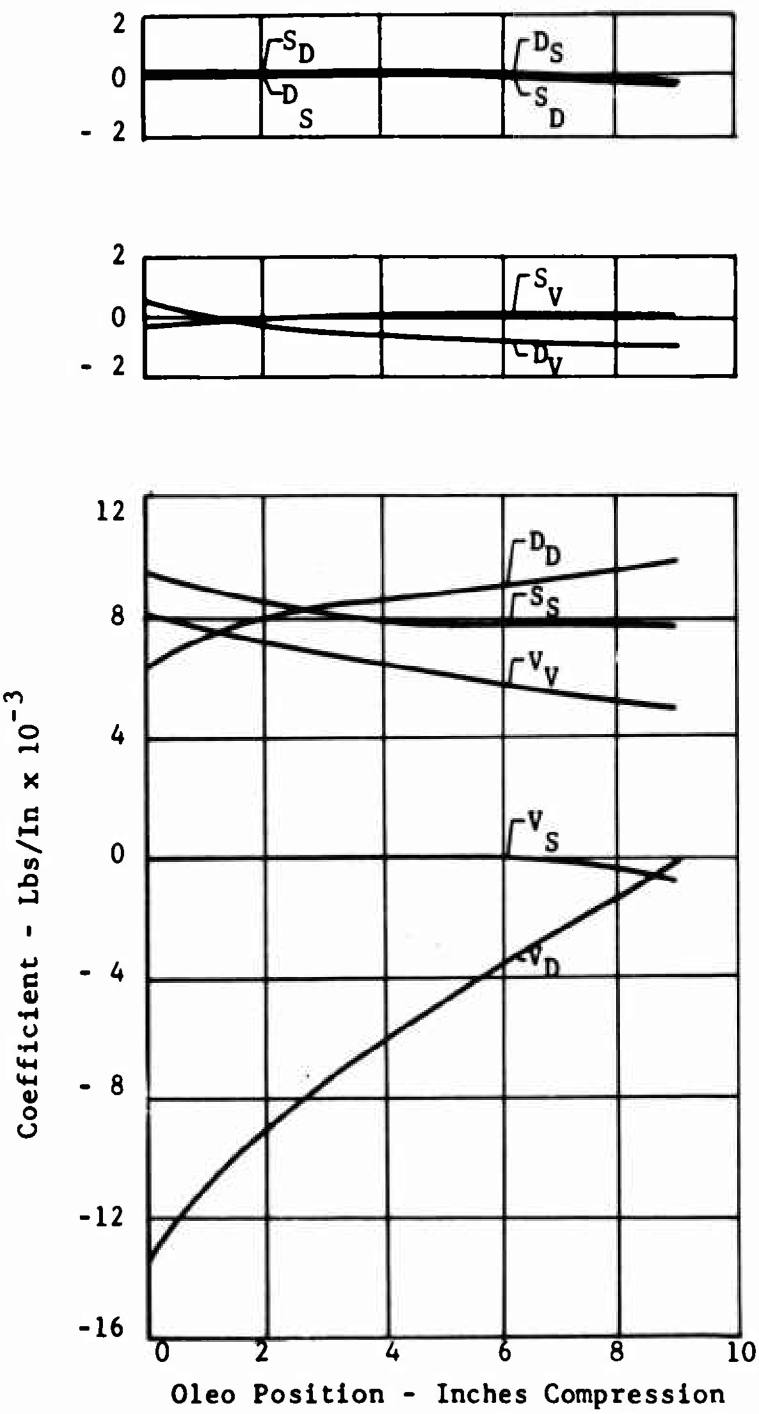

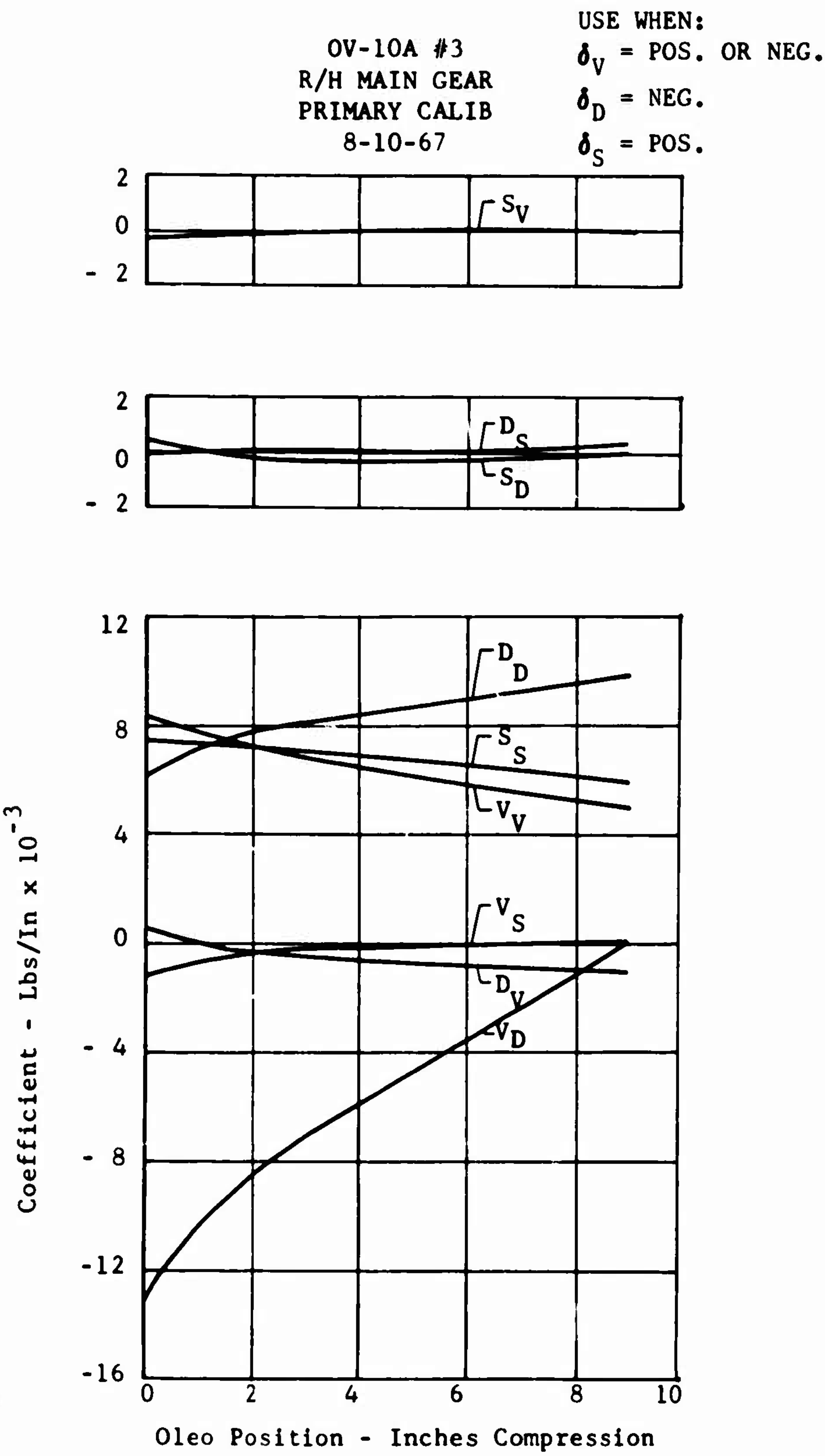
OV-10A #3
R/H MAIN GEAR
PRIMARY CALIB
8-10-67
USE WHEN:
δ_V = POS. OR NEG.
δ_D = NEG.
δ_S = POS.
S_V
D_S
S_D
D_D
S_S
V_V
V_S
D_V
V_D
Coefficient - Lbs/In x 10^{-3}
Oleo Position - Inches Compression

OV-10A #3
R/H MAIN GEAR
PRIMARY CALIB
8-10-67

USE WHEN:
δ_V = POS. OR NEG.
δ_D = NEG.
δ_S = NEG.

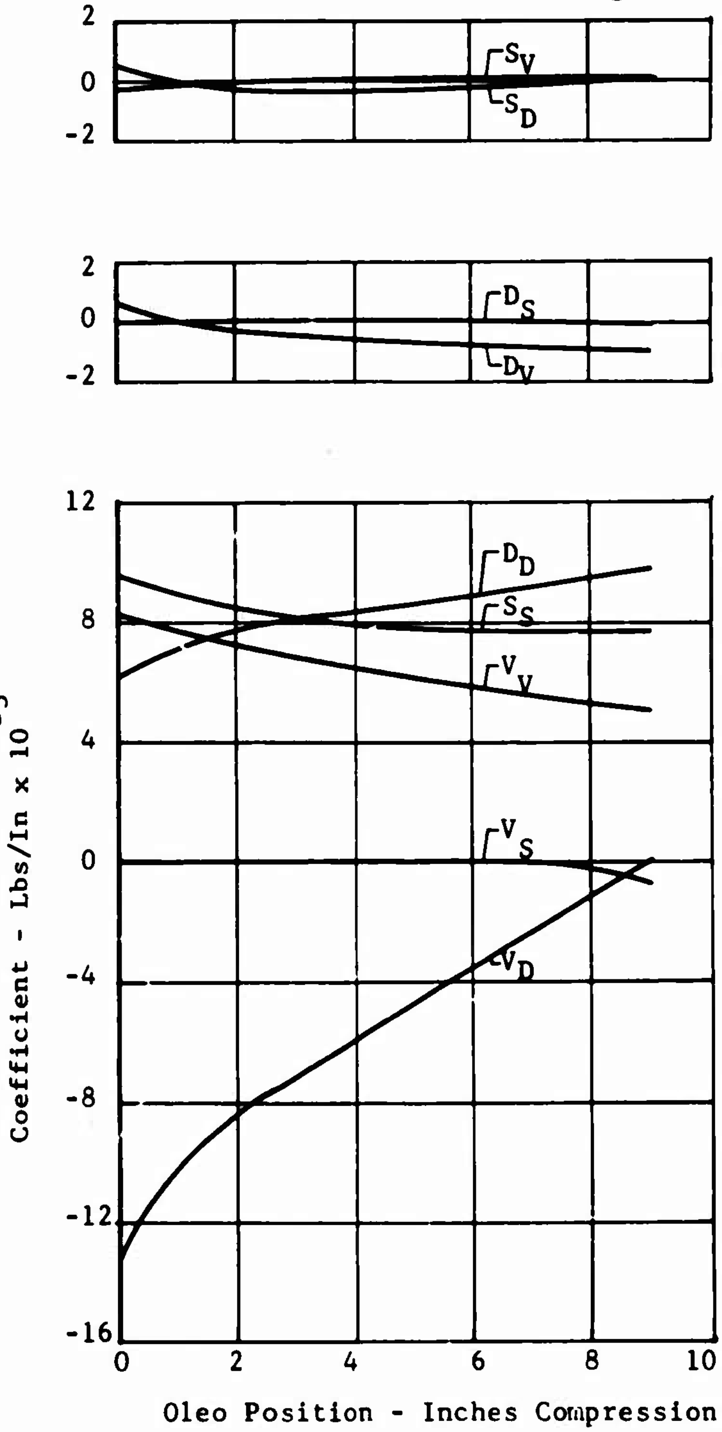

OV-10A #3
L/H MAIN GEAR
PRIMARY CALIB
9-21-67

USE WHEN:
δ_V = POS. OR NEG.
δ_D = POS.
δ_S = POS.

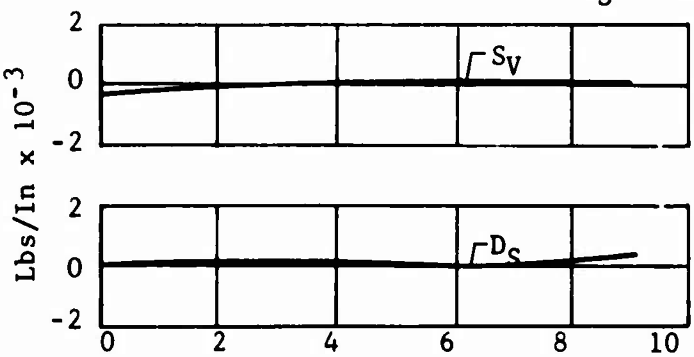

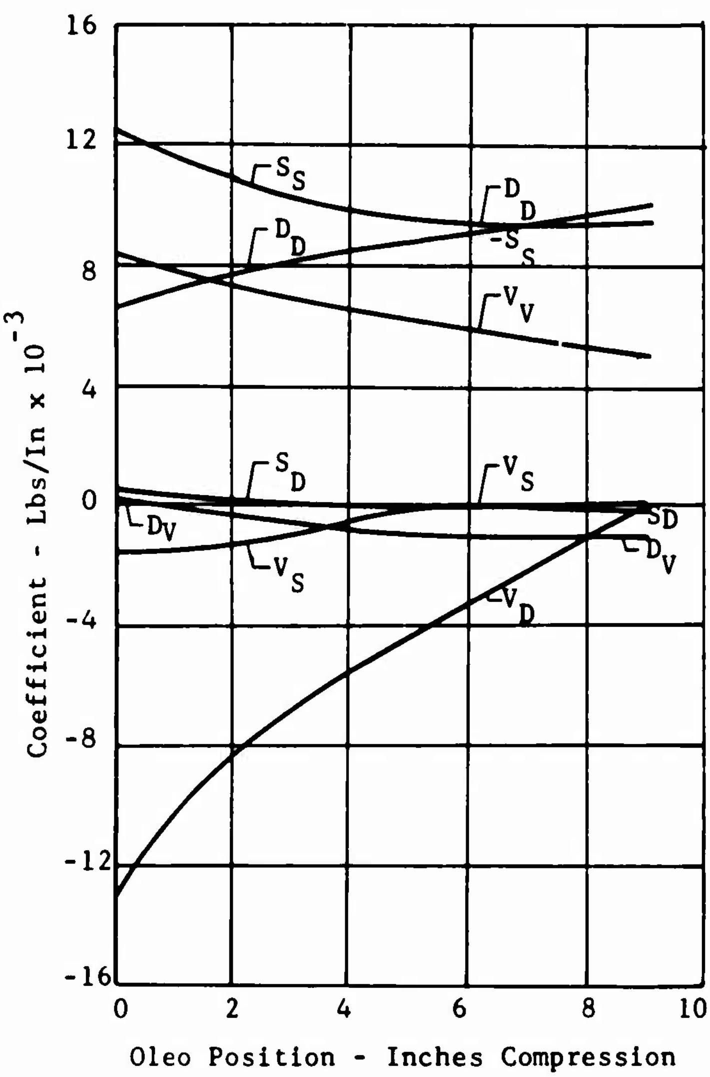

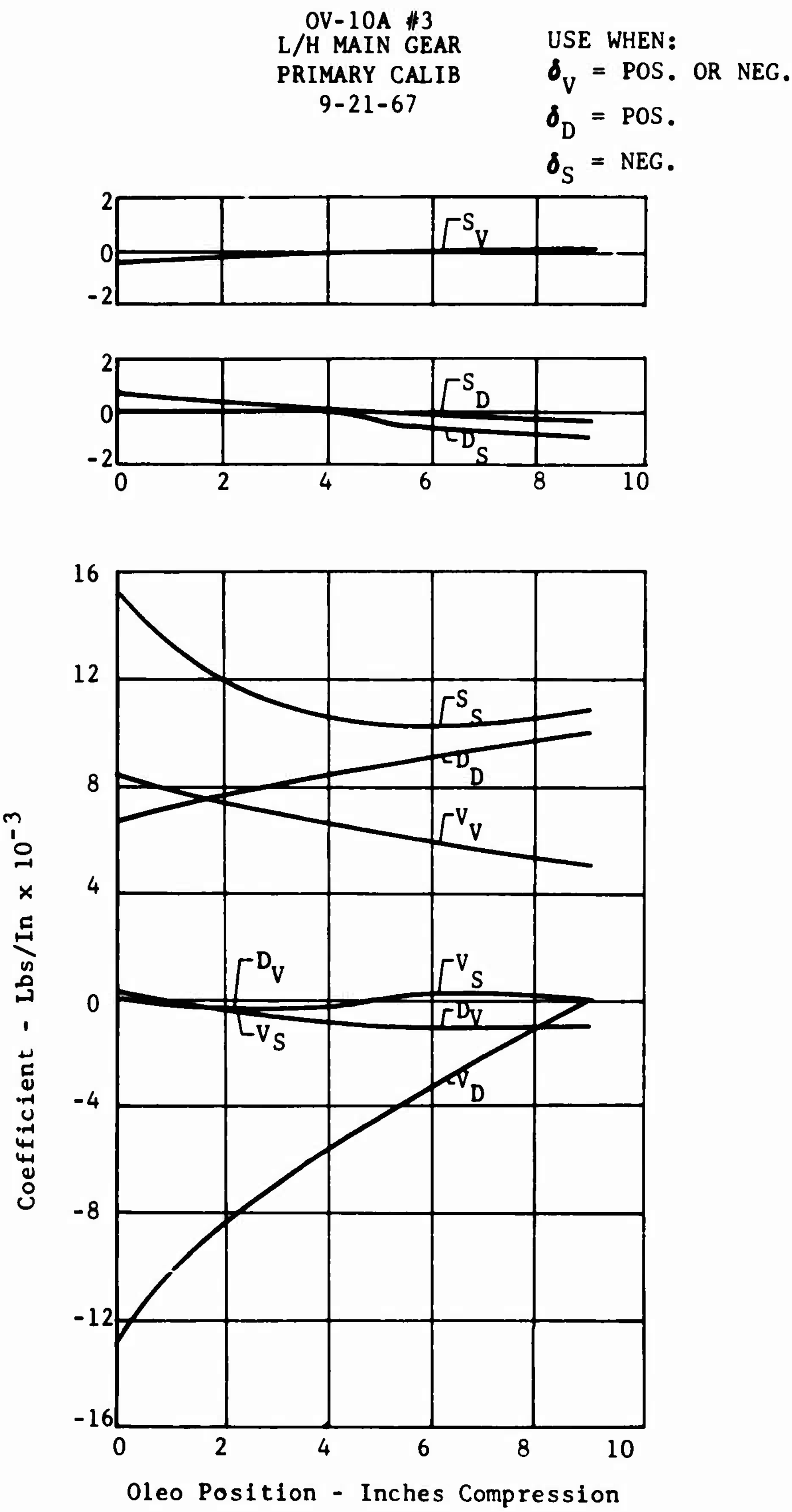
OV-10A #3
L/H MAIN GEAR
PRIMARY CALIB
9-21-67
USE WHEN:
δV = POS. OR NEG.
δD = POS.
δS = NEG.
SV
SD
DS
SS
DD
VV
DV
VS
VD
2
0
-2
16
12
8
4
-4
-8
-12
-16
10
6
Coefficient - Lbs/In x 10^-3
Oleo Position - Inches Compression

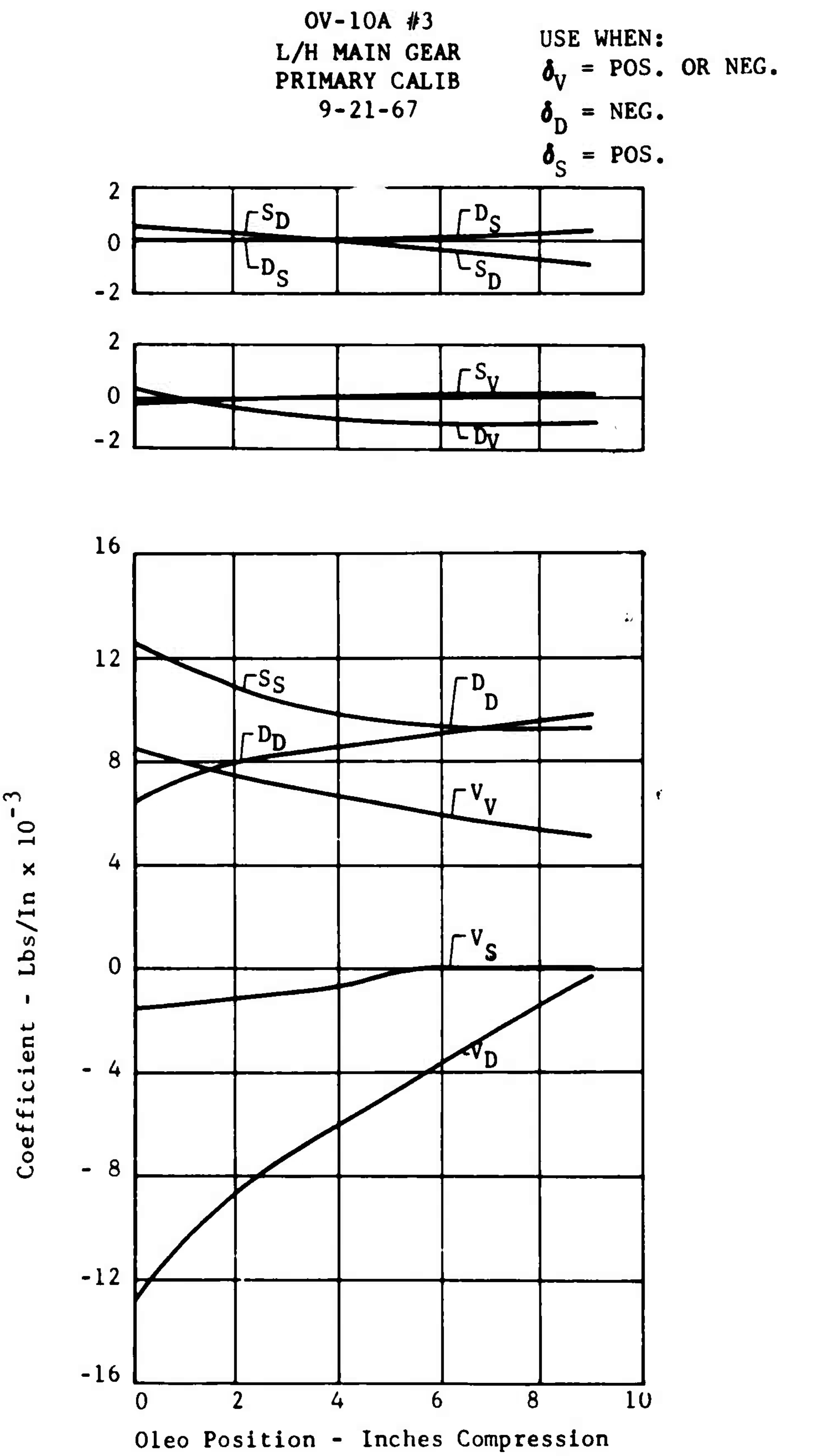
OV-10A #3
L/H MAIN GEAR
PRIMARY CALIB
9-21-67
USE WHEN:
δ_V = POS. OR NEG.
δ_D = NEG.
δ_S = POS.
2
0
-2
S_D
D_S
D_S
S_D
2
0
-2
S_V
D_V
16
12
8
4
0
- 4
- 8
-12
-16
S_S
D_D
D_D
V_V
V_S
V_D
0
2
4
6
8
10
Coefficient - Lbs/In x 10^{-3}
Oleo Position - Inches Compression

USE WHEN:
δ_V = POS. OR NEG.
δ_D = NEG.
δ_S = NEG.

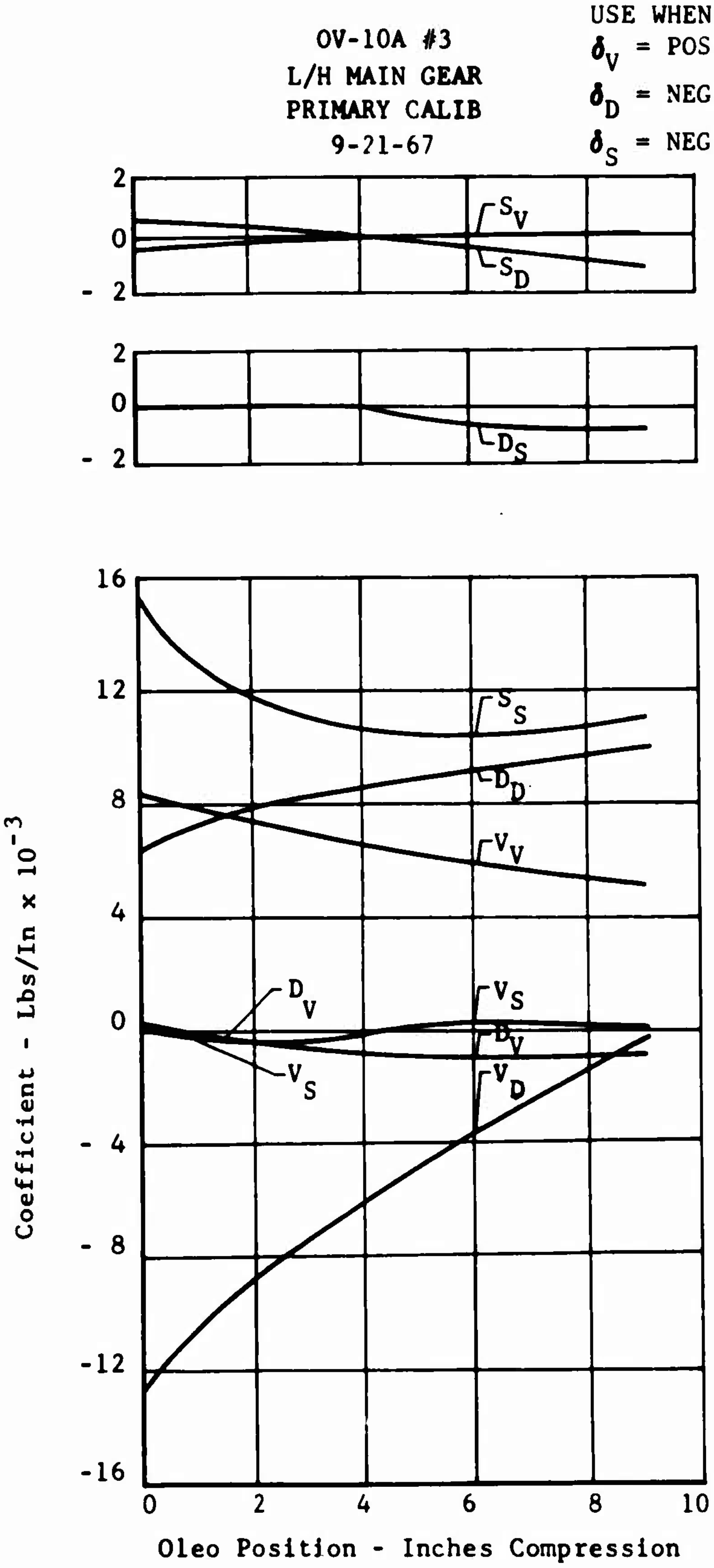

APPENDIX A3

AIRPLANE DATA

A

GENERAL ARRANGEMENT THREE VIEW OF THE OV-10A

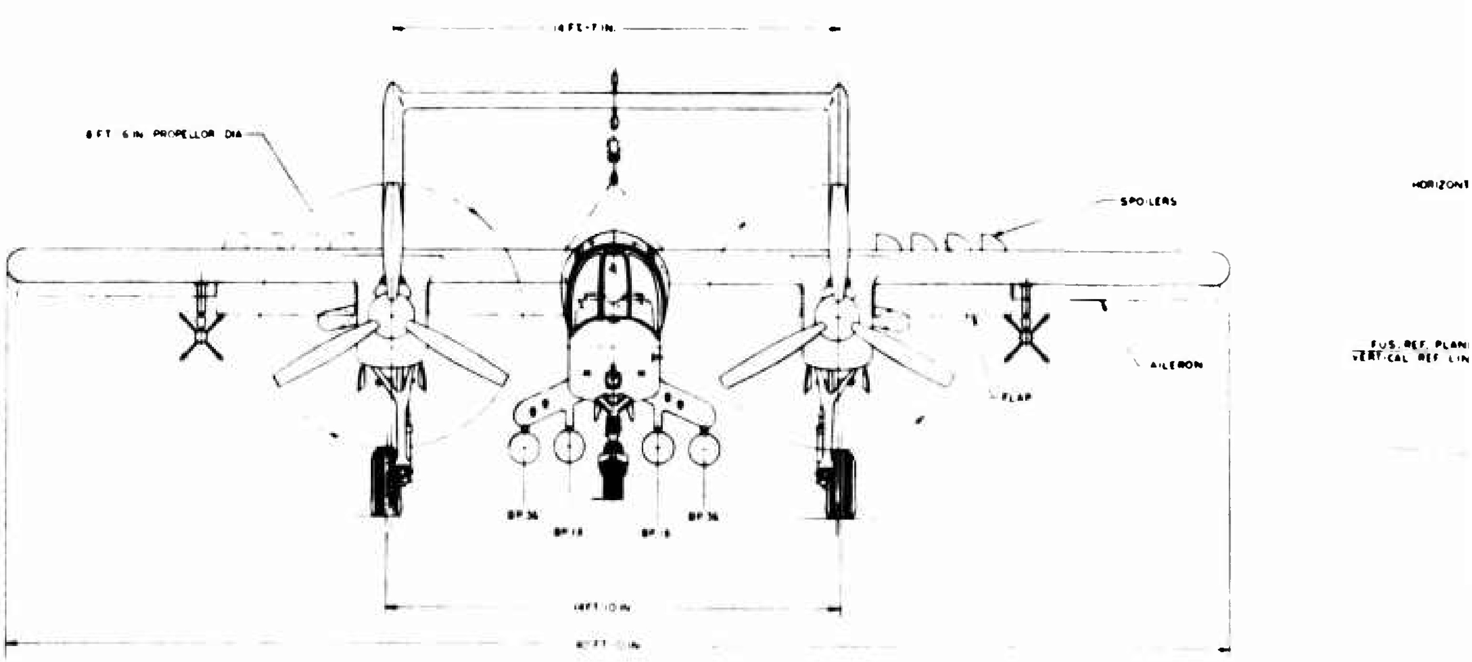

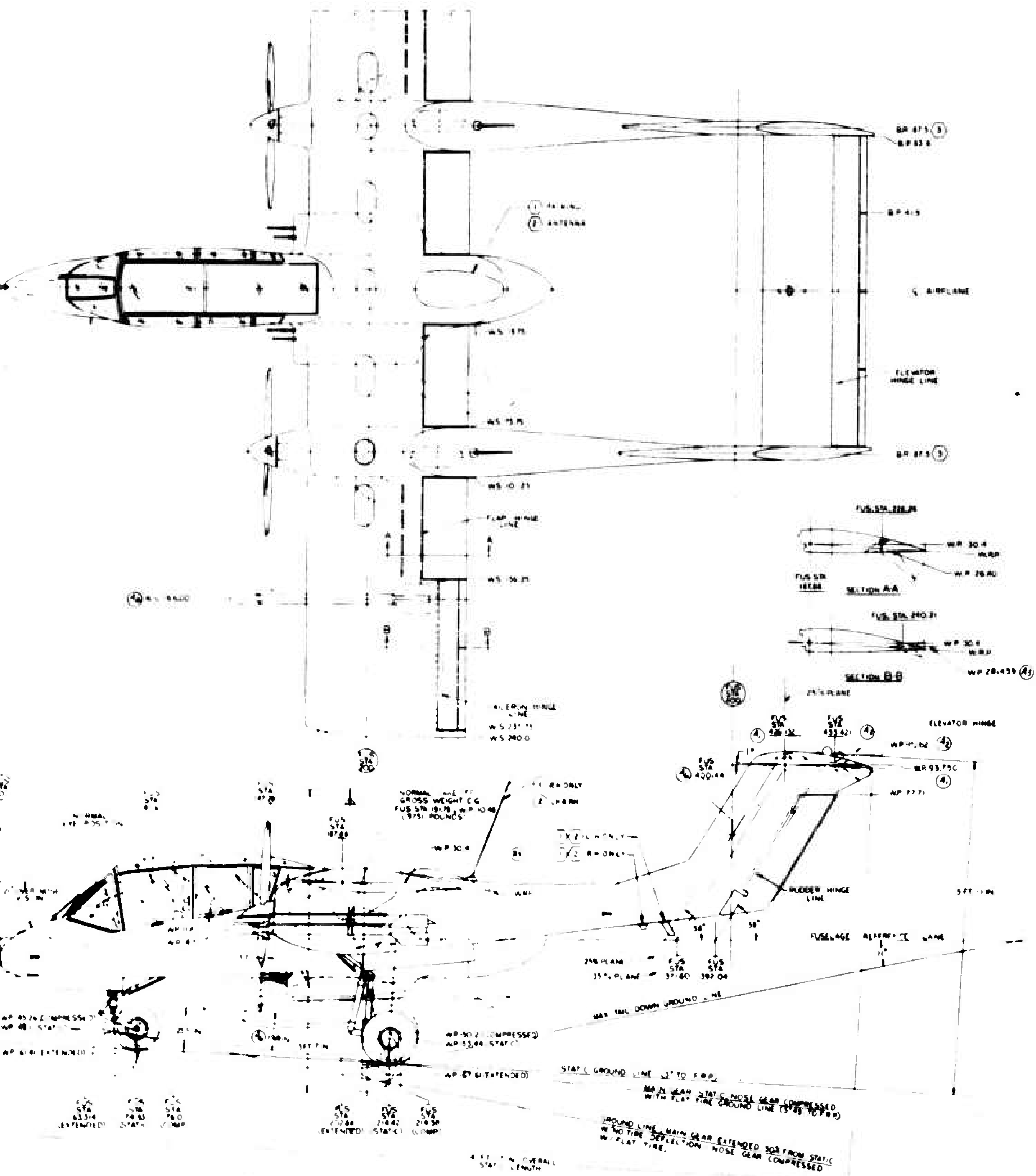

PRECEDING PAGE BLANK

OV-10A GENERAL DATA

WING

AREA (SQUARE FEET, TOTAL)	291
SWEEP (25% CHORD DEGREES)	0
ASPECT RATIO	5.51
TAPER RATIO	1.0
CHORD (INCHES)	87.25
AIRFOIL SECTION	NACA 64_2A-315 (MOD)
DIHEDRAL ANGLE (DEGREES)	0
INCIDENCE ANGLE TO F.R.P. (DEGREES)	+ 3.0
SPAN (FEET)	40.0
MEAN AERODYNAMIC CHORD (INCHES)	
VERTICAL DISTANCE FROM F.R.P. (25% CHORD)	30.4
FUSELAGE STA. (25% CHORD)	187.88
FLAP & VANE	
TYPE	NAA DOUBLE SLOTTED
AREA (TOTAL SQUARE FEET)	38.0
MAX DEFLECTION (DEGREES)	40
CHORD (PERCENT OF WING CHORD)	28.5

AILERONS

TYPE	SEALED INTERNAL BALANCE A7
AREA (TOTAL SQUARE FEET)	14.42
SPAN (INCHES)	79.25
CHORD (AFT OF H_L, PERCENT WING CHORD)	15
MAX DEFLECTION (UP/DOWN, DEGREES)	25/25 A7
SPRING TAB (OUTBOARD)	LEFT/RIGHT AILERON
SPAN/CHORD (INCHES)	42.75/4
MAX TAB DEFLECTION (UP/DOWN, DEGREES)	20/20
GEARED TAB (INBOARD)	LEFT/RIGHT AILERON
SPAN/CHORD (INCHES)	36.50/4
MAX TAB DEFLECTION (UP/DOWN DEGREES)	25/25 A7

A8 SPOILERS

TYPE	PLATE
SPAN (INCHES PER SIDE)	49.75
WING STATION (IN'BD TO OUT'BD, INCHES)	104.25 TO 154.0
CHORDWISE LOCATION (PERCENT WING CHORD)	58.7
MAX. PROJECTION (PERCENT WING CHORD)	7.625

MAIN LANDING GEAR TIRE

TYPE III	
SIZE	29 X 11-10 (11 X 10)
PLY RATING	8
ROLLING RADIUS (INCHES)	12.9
FLAT TIRE RADIUS (INCHES)	7.32

AUXILIARY LANDING GEAR TIRE

TYPE III	
SIZE	7.50 X 10
PLY RATING	8
ROLLING RADIUS (INCHES)	11.09
FLAT TIRE RADIUS (INCHES)	7.0

B1 HORIZONTAL TAIL

AREA (TOTAL SQUARE FEET)	70.48
SWEEP (25% CHORD, DEGREES)	0
ASPECT RATIO	3.02
TAPER RATIO	1.0
CHORD (INCHES)	58.0
AIRFOIL SECTION	NACA 66-012 (MO
INCIDENCE ANGLE TO F.R.P. (DEGREES)	1 A1
SPAN (INCHES)	175
MEAN AERODYNAMIC CHORD (INCHES)	
VERTICAL DISTANCE FROM F.R.P.	93.750 A1
FUSELAGE STA. (25% CHORD)	429.012
ELEVATOR	
AREA (TOTAL SQUARE FEET)	18.9
SPAN (INCHES)	167.622
CHORD (AFT OF HINGE LINE, PERCENT CHORD)	28.0
DEFLECTION (UP/DOWN, DEGREES)	35/25
TRAILING EDGE TABS	
SPRING TABS (OUTBOARD)	SYMMETRICAL ABOUT
SPAN/CHORD (INCHES)	83.8/3.75
UP-DOWN	20/28
GEARED TABS (INBOARD)	SYMMETRICAL ABOUT
SPAN/CHORD (INCHES)	83.8/3.75
B2 UP-DOWN % ELEVATOR TRAVEL	75

VERTICAL TAIL (TWIN)

AREA/SIDE (SQUARE FEET)	32.44 A6
SWEEPBACK (LEADING EDGE TO F.R.P., DEGREES)	32
ASPECT RATIO	1.37 A6
TAPER RATIO	1.0
ROOT CHORD (INCHES)	58.4
AIRFOIL SECTION	64A012
MEAN AERODYNAMIC CHORD	
VERTICAL DISTANCE FROM F.R.P. (25% CHORD)	55.5 A6
FUSELAGE STA. (25% CHORD)	400.44
HORIZONTAL DISTANCE FROM ℄ AIRPLANE	87.5
RUDDER/SIDE	
AREA (TOTAL SQUARE FEET)	11.16 A1
UPPER TIP CHORD W.P. (INCHES)	77.71
DEFLECTION, STREAM-WISE (RIGHT/LEFT DEGREES)	25/25

REVISIONS

	LTR	DESCRIPTION		DATE / APPROVED
	A	1 MAY BE REWORKED 3 RECORD CHANGE 2 CANNOT BE REWORKED 4 NOW SHOP PRACTICE 5 PARTS MADE OK		
8/11		1. 2°(WAS)0°; 93.635(WAS) 93.245; 429.059(WAS) 428.95; 11.16(WAS) 10.7	3	
11		2. 456.368(WAS) 456.21; 94.571 (WAS) 95.13	5	
11		3. 28.459 (WAS) 29.2	5	
14		4. WS 166.00(WAS) WS 162.6	3	
2/6		5. ADDED OV-10A-2. REV TITLE TO AGREE.	5	
3		6. 32.44(WAS) 34.88; 1.37(WAS) 1.4[illegible]; 55.5(WAS) 57.0; 400.44(WAS) 401.86; 13.9(WAS) 18.8	5	
6		7. "SEALED INTERNAL BAL" (WAS) "PLAIN BAL"; 25/25 (WAS) 20/20	5	
8		8. REMOVED LOWER SPOILERS & RELATED INFO.	5	BAROODY 6-25-68
5	B	1. HORIZ. TAIL INCIDENCE 1° WAS 2°; MAC VERT. DISTANCE 93.750 WAS 93.636 & FS 429.012 WAS 429.059.	8	[illegible] 5-14-68
5		2. ADDED GEARED TAB TRAVEL 75% OF ELEV. TRAVEL.	5	
12/5		3. ADDED DORSAL FAIRING & RELOC WHIP ANTENNA.	5	
	C	1. REVISE TO AGREE WITH [illegible]	8	F[illegible] 6-19-69

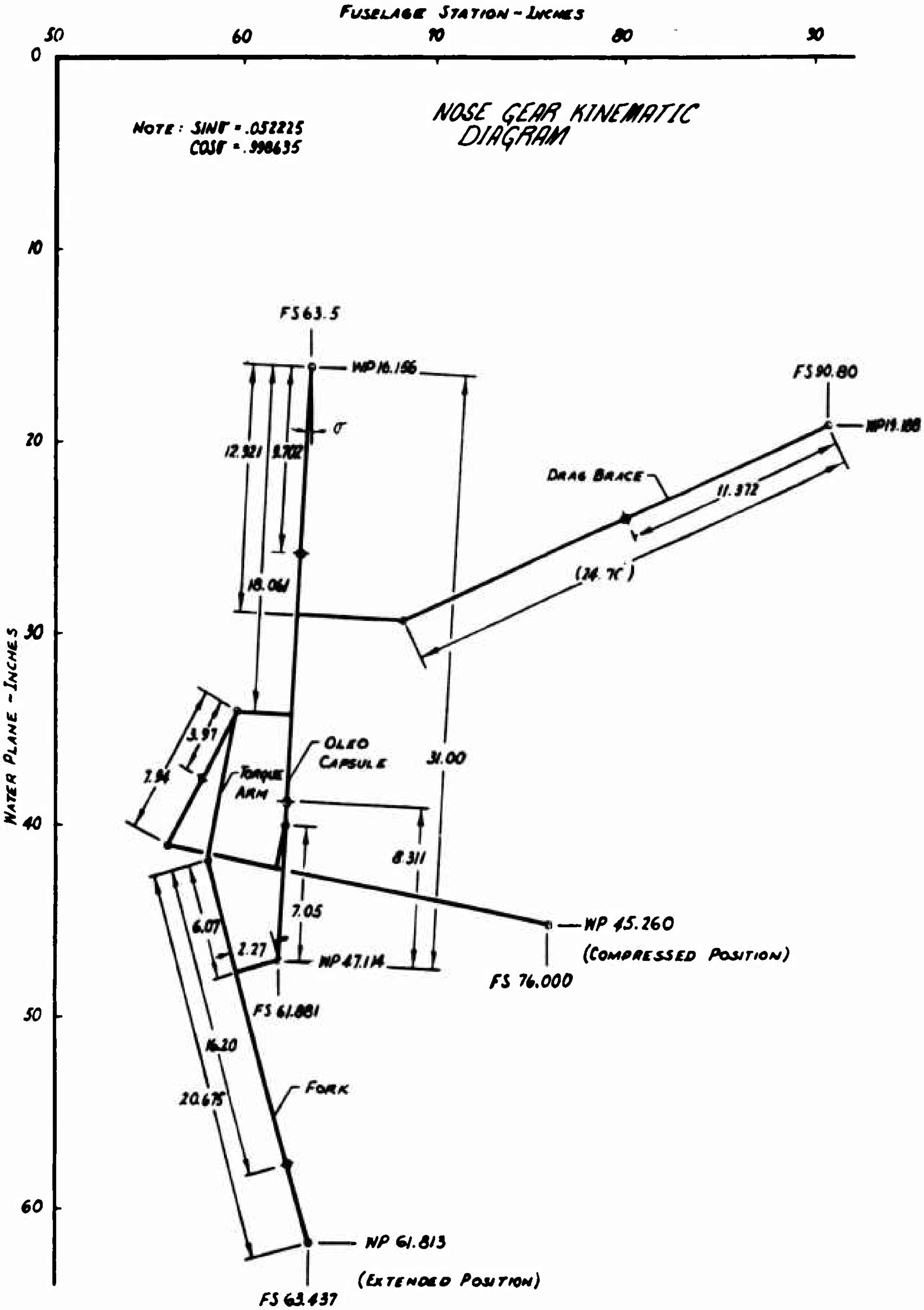

PRECEDING PAGE BLANK

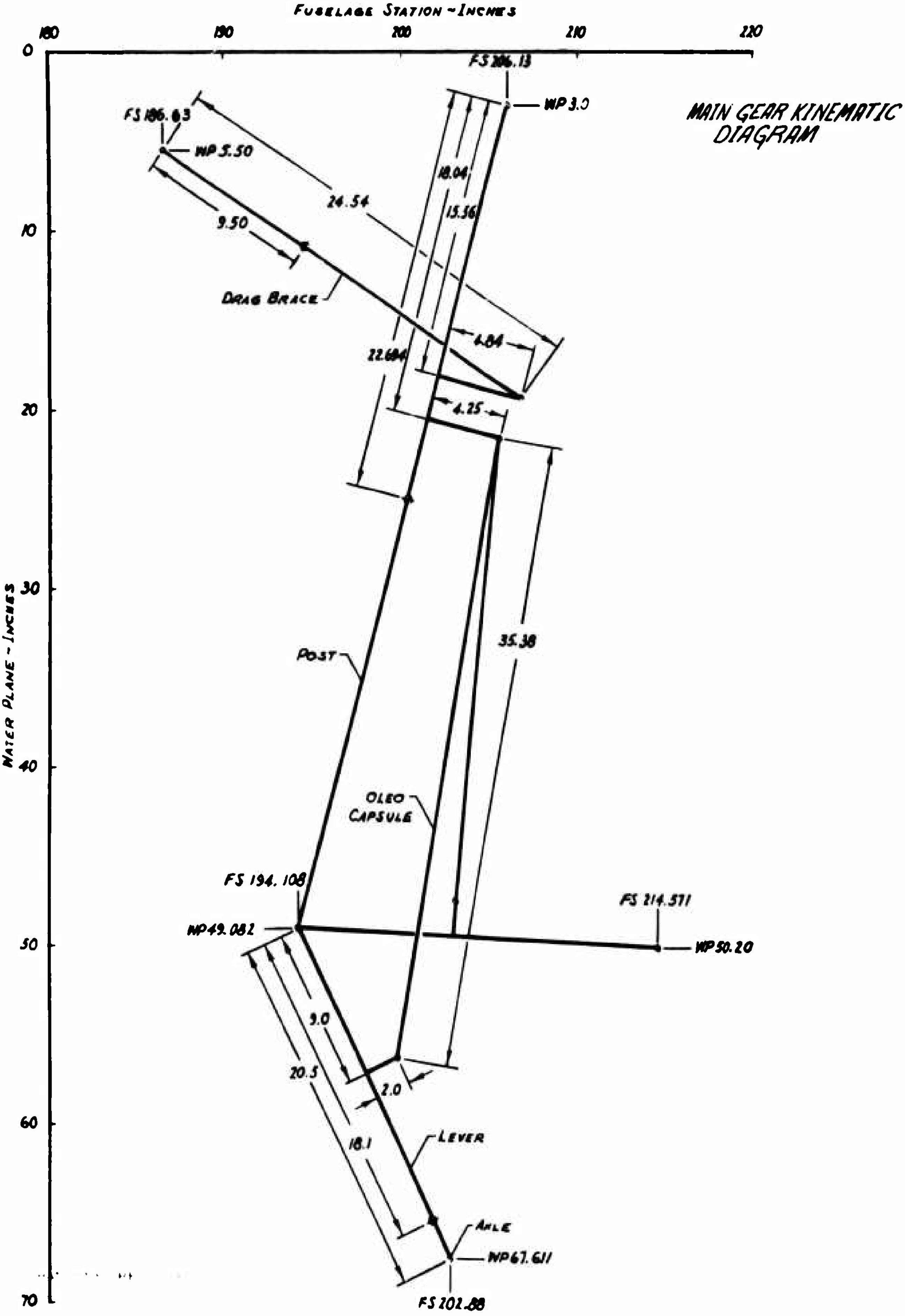
FUSELAGE STATION ~ INCHES
180
190
200
210
220
0
10
20
30
40
50
60
70
WATER PLANE ~ INCHES
MAIN GEAR KINEMATIC DIAGRAM
FS 206.13
WP 3.0
FS 186.63
WP 5.50
24.54
9.50
18.04
15.56
DRAG BRACE
4.84
22.684
4.25
35.38
POST
OLEO CAPSULE
FS 194.108
WP 49.082
FS 214.571
WP 50.20
9.0
20.5
2.0
18.1
LEVER
AXLE
WP 67.611
FS 202.88

NOSE GEAR RELIEF VALVE SCHEMATIC

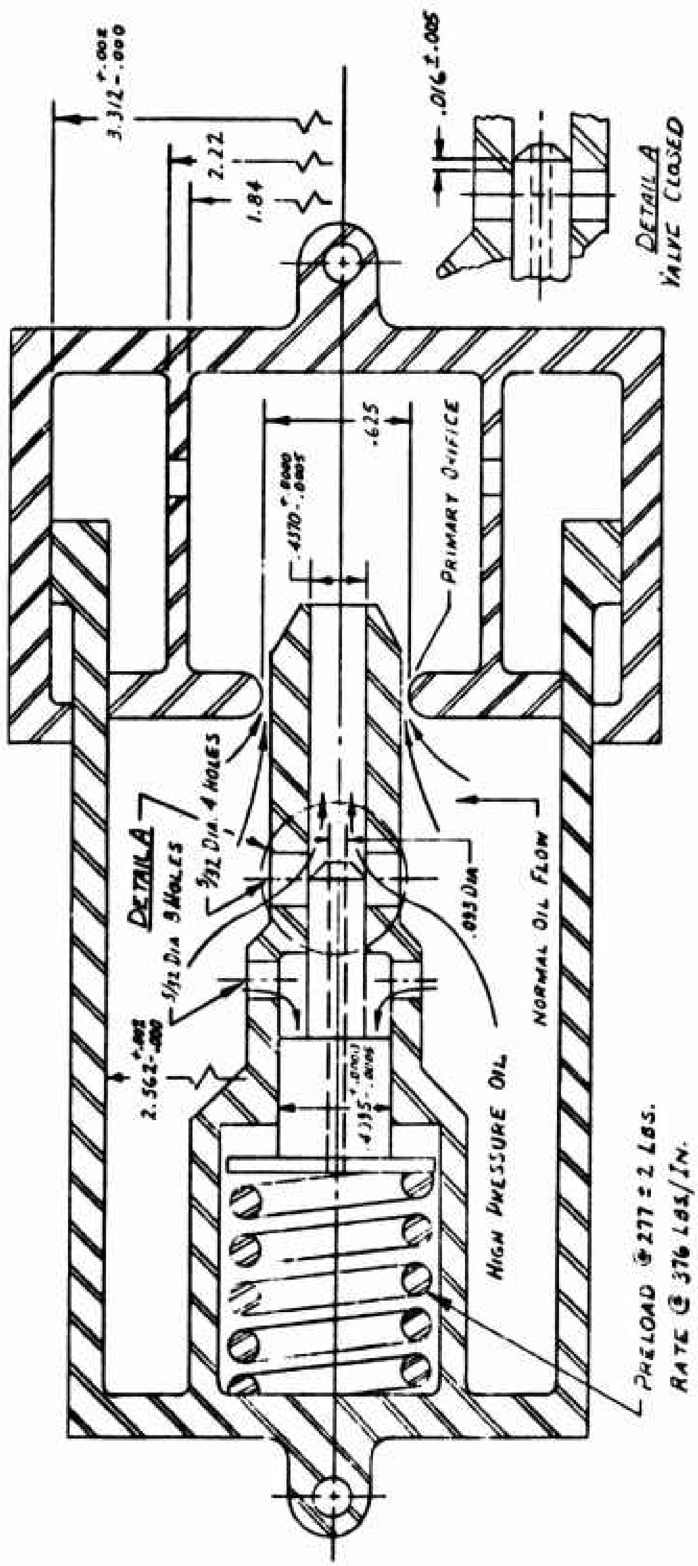

MAIN GEAR RELIEF VALVE SCHEMATIC

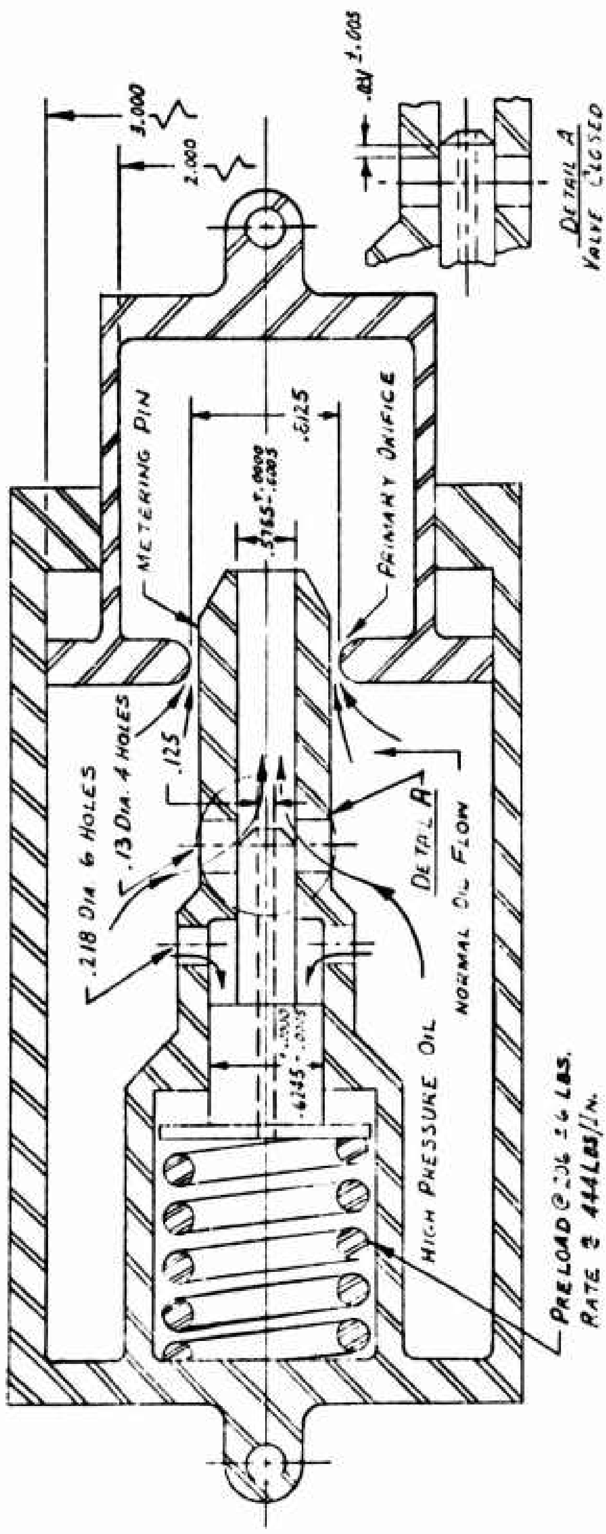

METERING PIN DIAMETER VS. OLEO STROKE

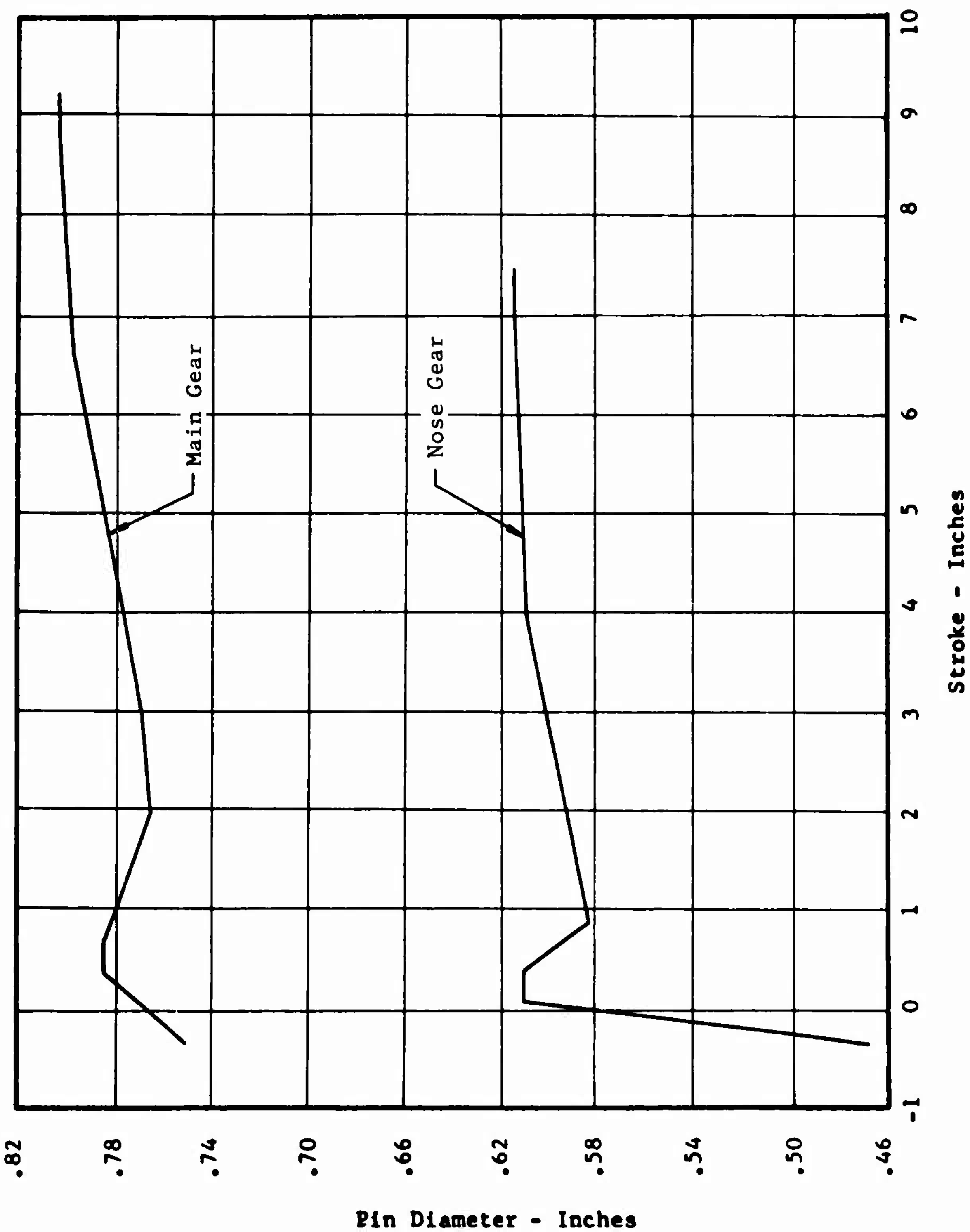

NOSE GEAR TIRE
FORCE-DEFLECTION CURVE
(Data by B. F. Goodrich Tire Co.)

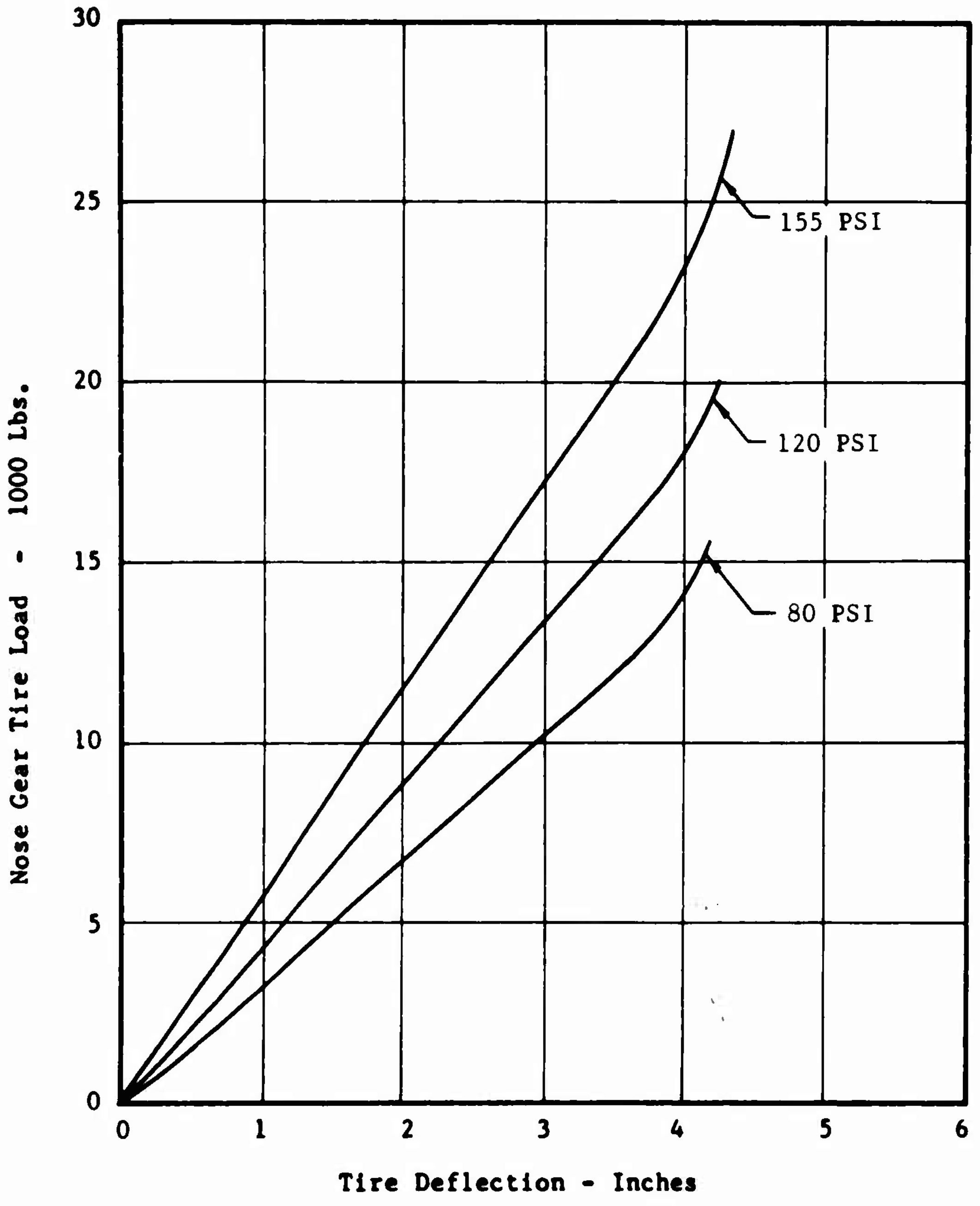

NOSE GEAR TIRE
FOOTPRINT AREA-DEFLECTION CURVE
(Data by B. F. Goodrich Tire Co.)

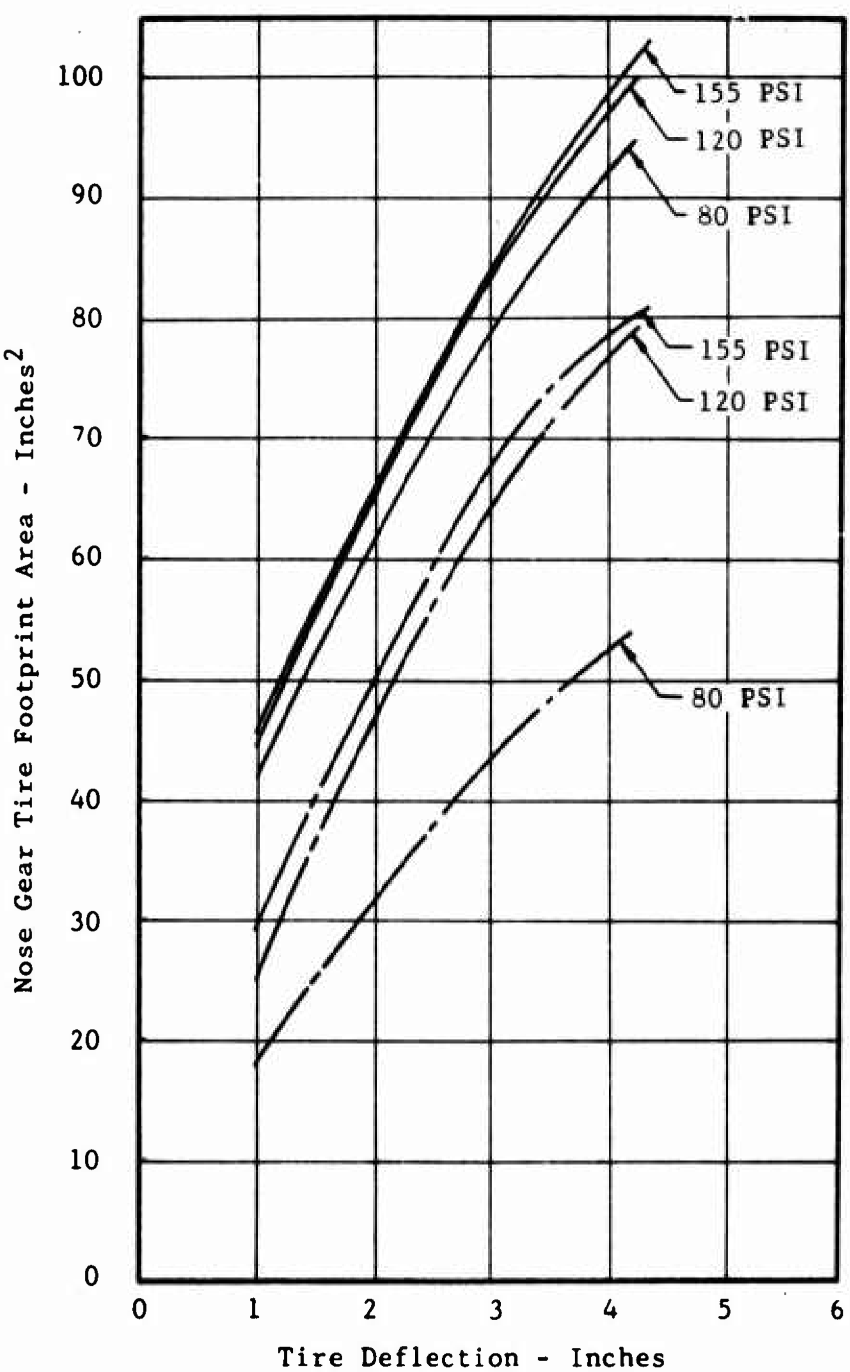

Notes: 1.—Implies Gross Area
2.–·–Implies Net Area

MAIN GEAR TIRE
FORCE-DEFLECTION CURVE
(Data by B. F. Goodrich Tire Co.)

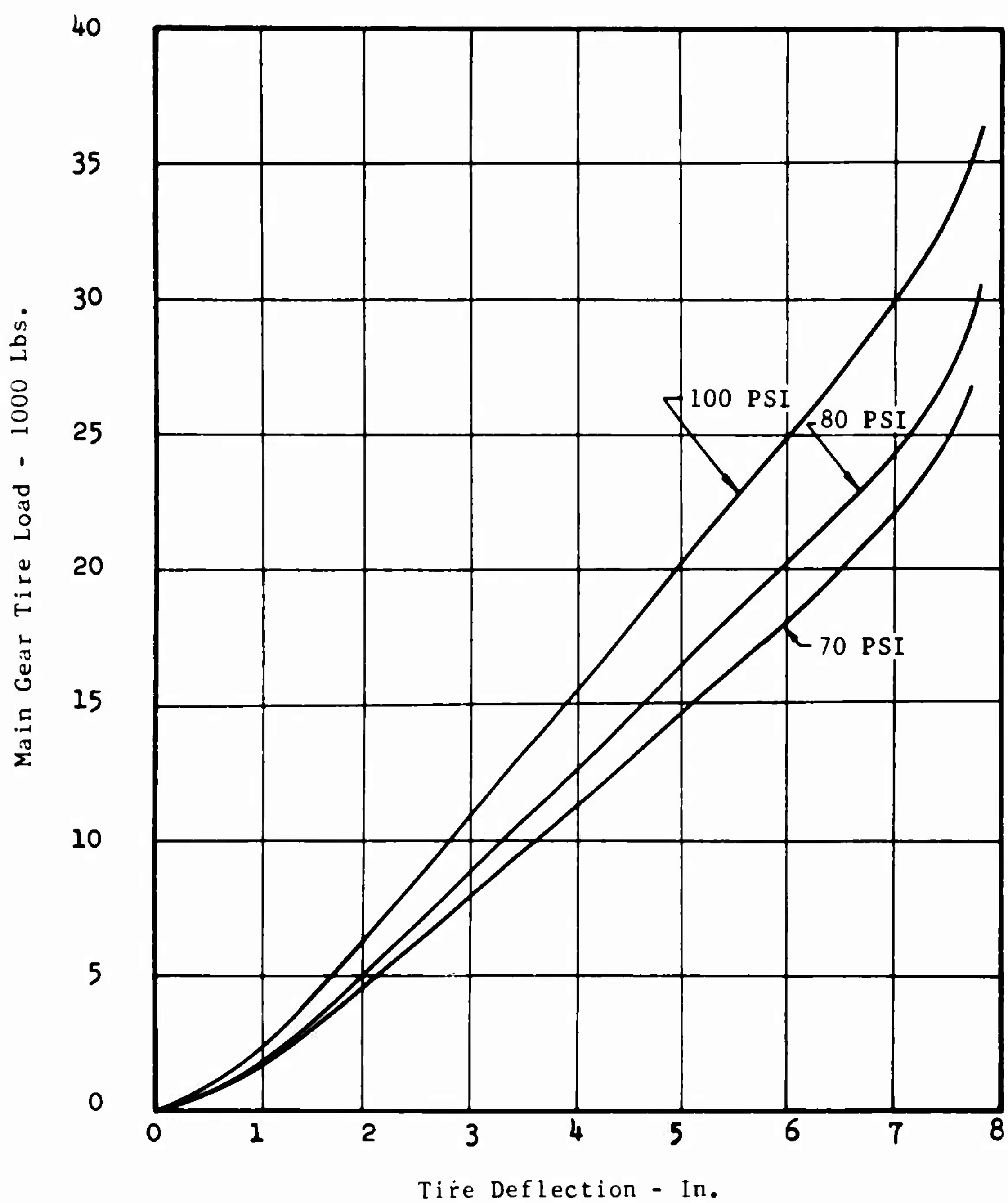

MAIN GEAR TIRE
FOOTPRINT AREA-DEFLECTION CURVE
(Data by B. F. Goodrich Tire Co.)

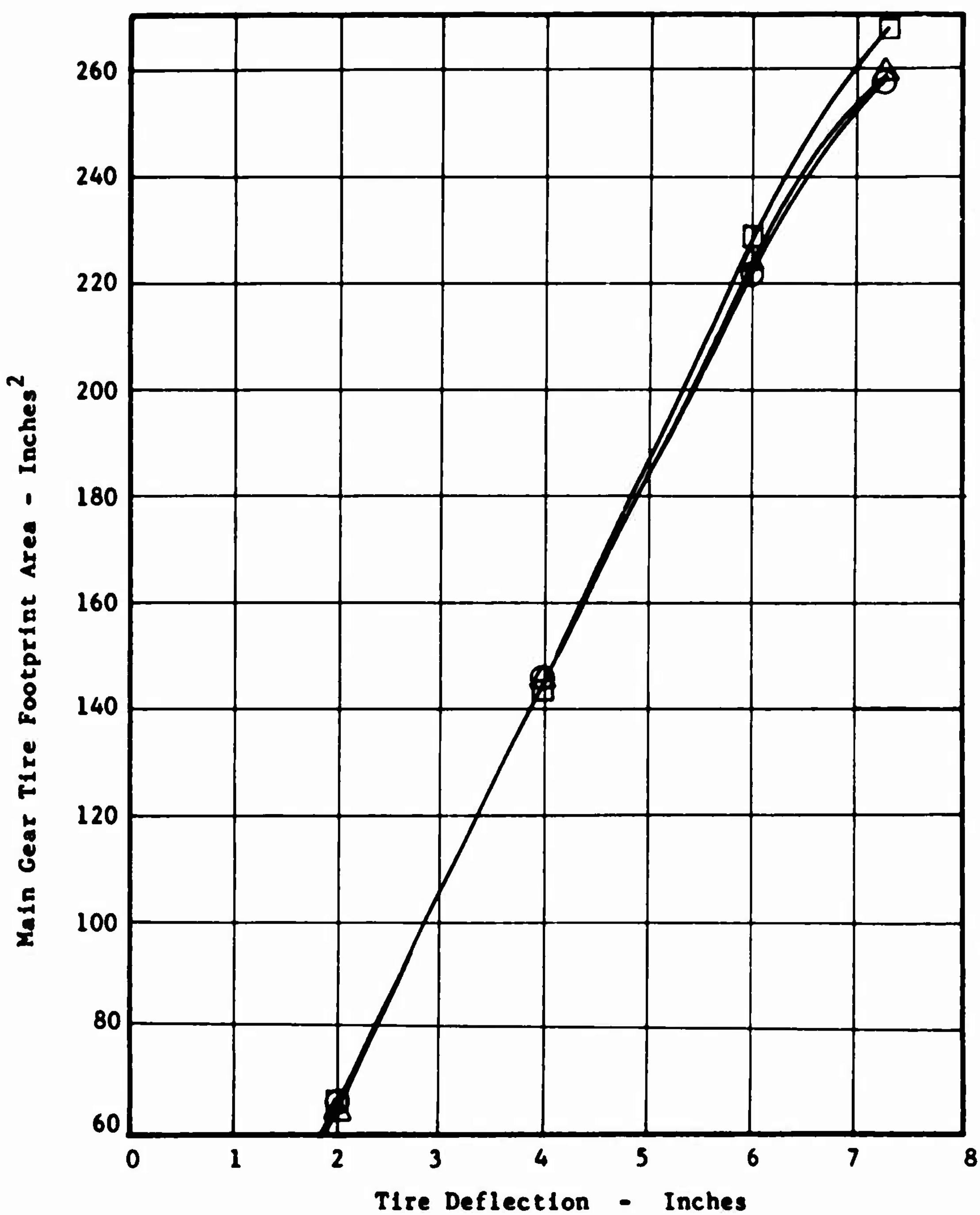

Notes: ○ Implies 70 PSI
△ Implies 80 PSI
□ Implies 100 PSI

LANDING GEAR INERTIA

Nose Gear Inertia											
Item	Wt. (lbs.)	X (in.)	Y (in.)	Z (in.)	I_{XX} (lb-in2)	I_{YY} (lb-in2)	I_{ZZ} (lb-in2)	I_{XY} (lb-in2)	I_{YZ} (lb-in2)	I_{XZ} (lb-in2)	$I_{O_{WTT}}$ (lb-in2)
Upper Cyl.	31.5	0.2	0	9.7	4400	4250	270	0	0	115	
Drag Brace	10.1	FS 80.1	0	WP -24.0	372	2031	1683	0	0	673	
Torque Arm	3.7	-3.9	0	0	11	45	56	0			
Fork, Wheel, Tire, & Tube	65.4	17.1	0	-0.1	2641	24891	23880	0			
Wheel, Tire, & Tube Only	42.0										3187
Lower Cyl. (Piston)	20.1	-0.2		-8.3	2130	2130	35				

Main Gear Inertia											
Item	Wt. (lbs.)	X (in.)	Y (in.)	Z (in.)	I_{XX} (lb-in2)	I_{YY} (lb-in2)	I_{ZZ} (lb-in2)	I_{XY} (lb-in2)	I_{YZ} (lb-in2)	I_{XZ} (lb-in2)	$I_{O_{WTT}}$ (lb-in2)
Post & Upper Cyl.	89.2	4.94	-0.45	22.15	61015	61624	3743	-156	-1214	10581	
Drag Brace	11.5	FS 193.8	BP 84.2	WP -10.3	655	2055	1410	0	0	932	
Fork, Wheel, Tire, Tube and Brake	94.6	18.5	3.1	-0.1	5347	39287	40525	6264			
Wheel, Tire, Tube, & Brake	54.5	20.3	5.8	0							4102
Lower Cyl. With Oil	11.35	9.15			23	1400	1400				

OLEO AIRSPRING vs. STROKE

NOTES: $G_A = p_o A_A \left(\frac{K}{K-S}\right)^{\gamma}$

FOR NOSE GEAR: p_o = 235 PSI
A_A = 7.068582 IN.^{2}
K = 7.701818 IN.
FOR MAIN GEAR: p_o = 690 PSI
A_A = 4.908738 IN.^{2}
K = 10.872 IN.

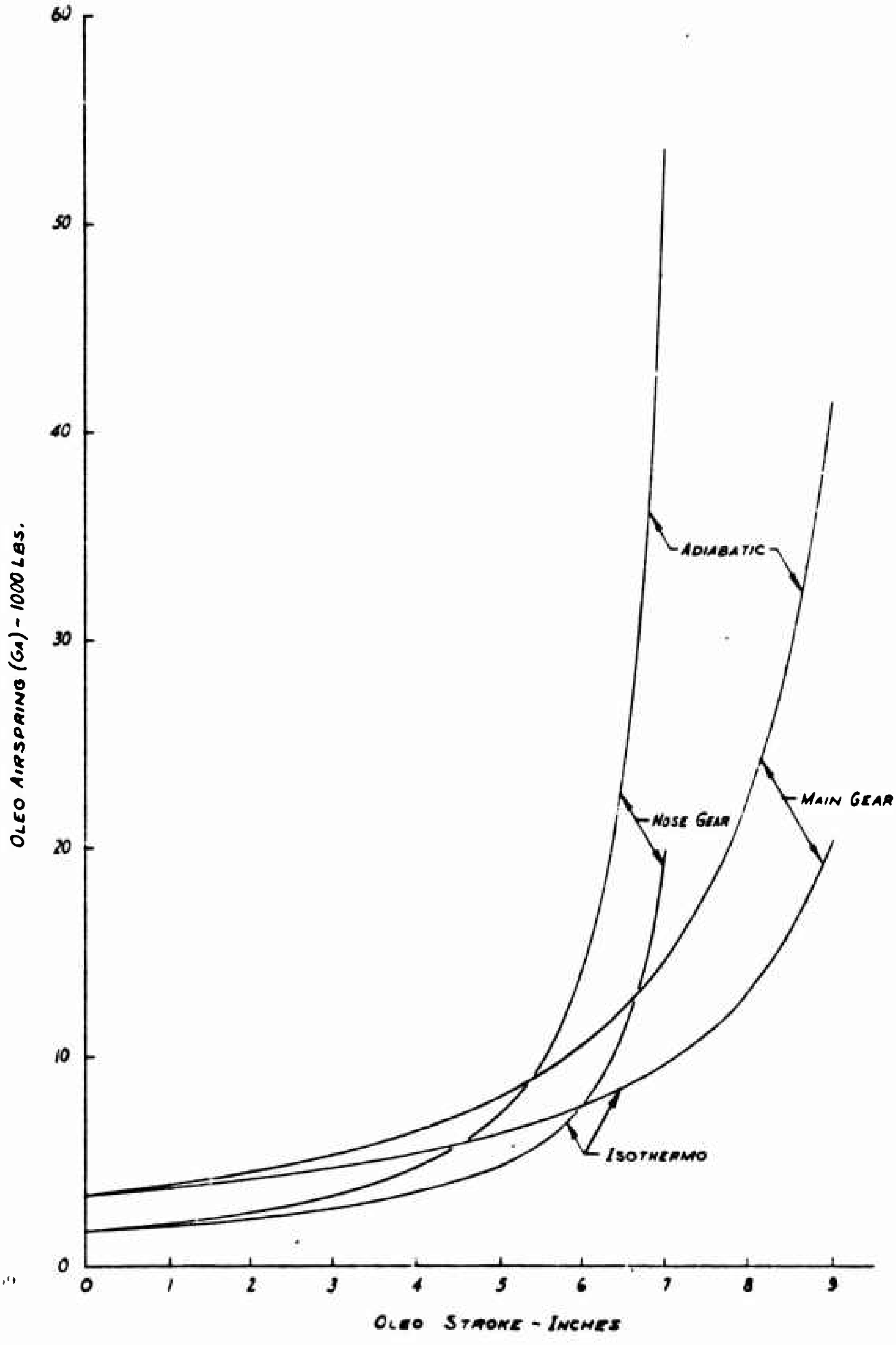

LANDING GEAR FLEXIBILITY DATA

ALL CURVES BELOW ARE FORE & AFT BENDING

ALL CURVES BELOW ARE LATERAL BENDING

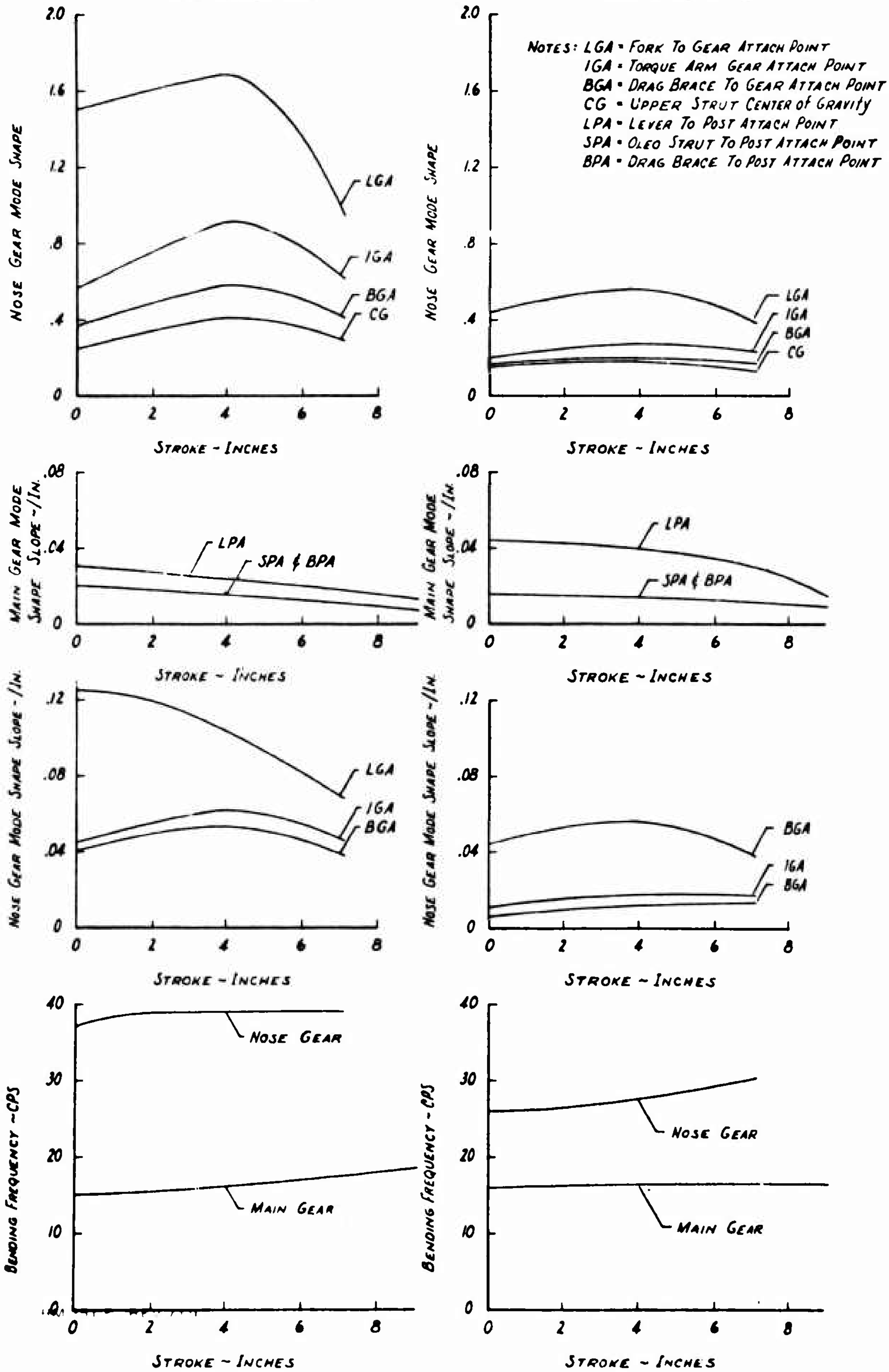

LANDING GEAR FLEXIBILITY DATA (CONT'D)

NOTES: LPA = LEVER TO POST ATTACH POINT
SPA = OLEO STRUT TO POST ATTACH POINT
BPA = DRAG BRACE TO POST ATTACH POINT

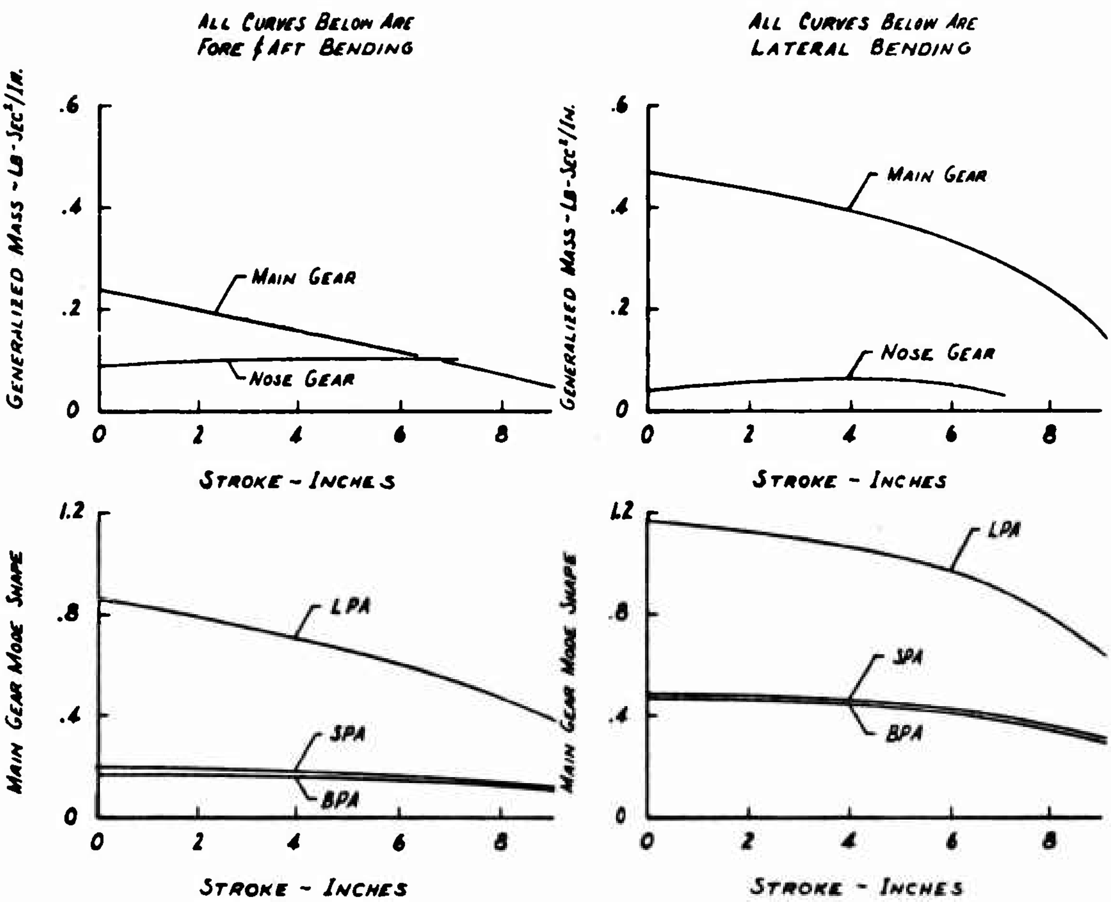

AIRPLANE FLEXIBILITY VALUES

PARAMETER	UNITS	MODE NUMBER 1	2	3	4
ϕZ_{NG} (Nose Gear)	--	-.536828	-.142938	.204473	-.018618
ϕZ_{MG} (Main Gear)	--	.169980	-.006477	.015131	-.131853
ϕZ_{NB} (Nose Brace)	--	-.378760	-.042109	.104360	.040145
ϕZ_{MB} (Main Brace)	--	.169648	-.025898	-.138563	-.171650
$\frac{d\phi}{dX} Z_{NG}$	/INCH	.005888	.003769	-.003897	.002337
$\frac{d\phi}{dX} Z_{MG}$	/INCH	-.000138	.000930	.007727	.001326
$\frac{d\phi}{dX} Z_{NB}$	/INCH	.005659	.003601	-.003374	.001962
$\frac{d\phi}{dX} Z_{MB}$	/INCH	.000110	.001045	.008110	.002724
ϕY_{NG}	--	0	0	0	0
ϕY_{MG}	--	-.039648	.196510	.012275	.173410
ϕY_{NB}	--	0	0	0	0
ϕY_{MB}	--	-.042674	.193656	.019082	.164904
$\frac{d\phi}{dY} Z_{NG}$	/INCH	0	0	0	0
$\frac{d\phi}{dY} Z_{MG}$	/INCH	.001401	-.006883	-.000484	-.006586
$\frac{d\phi}{dY} Z_{NB}$	/INCH	0	0	0	0
$\frac{d\phi}{dY} Z_{MB}$	/INCH	.001481	-.006630	-.000687	-.005524
$\frac{d\phi}{dX} Y_{NG}$	/INCH	0	0	0	0
$\frac{d\phi}{dX} Y_{MG}$	/INCH	-.000049	-.000012	.000101	-.000390
$\frac{d\phi}{dX} Y_{NB}$	/INCH	0	0	0	0
$\frac{d\phi}{dX} Y_{MB}$	/INCH	-.000163	-.000006	.000357	.000307
	CPS	6.461	9.301	14.613	24.074
c	--	.02	.03	.04	.05
m	LB-SEC^2/INCH	2	2	2	2

APPENDIX A4

TIME HISTORIES OF LANDING GEAR

LOADS AND RESPONSE

TABLE OF CONTENTS

Discussion

This Appendix, A4 contains the experimental data obtained from the takeoffs and landings of OV-10A No. 3, BuNo 155392 at Blackstone Army Air Base, Virginia during May of 1969. This aircraft was selected because it was fully instrumented. The instrumentation is listed in paragraph 4.1.2 of the main text.

The flight test program required by Reference (4) and reiterated in paragraph 2.0 (4) was flown as a series of 16 flights. The actual flight conditions for these flights are listed in the table on Page A4- 4. Sink speeds and longitudinal speeds were determined by TRODI (Touchdown Rate-of-Decent Indicator), SODI (Speed Over-the-Deck Indicator), SPN 12, and a high speed, 35 mm cinerama (Cine) camera. In addition, compatible sink speeds, touchdown times, pitch attitudes and roll angles were determined geometrically by the contractor.

A total of 105 parameters were recorded during each landing. Those parameters directly associated with the landing gear characteristics; i.e. loads, accelerations, strokes and pressures, have been selected for inclusion in this appendix. In addition, the aircraft accelerations are presented. A table of the parameters presented is given on Page A4- 5. Time histories have been produced directly from the oscilligraph records for Flights 212 through 226. Landing gear axle loads were calculated from the strain gage data using the equations presented in Appendix A2. This data is presented for Flights 217 through 226. The original time histories were produced through computer graphs and were difficult to read as well as volumnious. Therefore, the pertinent portion of the time history was replotted excluding the landing runout. The axle loads and gear strokes for Flight 221 were replotted for the entire time history. The computer plots are presented for Flight 225 for information.

Flights 209 through 214 were basically practice flights. Flight 209 included practice takeoffs and Flight 210 included practice landings with no data being recorded. Flights 211 and 222 were not relevent to this study. Partial data was recorded for Flights 212, 213 and 214. This data is presented on pages A4-8 through A4-12, A4-13 through A4-18, and A4-19 through A4-26, respectively. Flights 215 through 221 were tail down landings with sink speeds varying from 10.11 to 16.69 feet per second. The sink speed was controlled using a mirror landing aid. Pitch attitudes varied from 2.92 to 6.97 degrees. The maximum design attitude for the aircraft is 7.5 degrees. Data for this series of landings is presented on Pages A4-27 through A4-82.

Flights 223, 224, 225 and 226 were nose down flights. Flights 223 and 224 resulted in touchdown pitch attitudes of -0.07 and 0.52 degrees, respectively. The mean pitch attitude for the aircraft is 1.5 degrees. The data for these flights is given on Pages A4-83 through A4-101. A pitch attitude of -5.16 was attained on Flight 225 with a corresponding sink speed of 17.27 feet per second. The time histories for Flight 225 are given on Pages A4-102 through A4-116.

Flight 226 resulted in a failure of the nose gear fork. The conditions for the landing were derived from several independent readings with readings of sink speed varying from 17.46 to 20.53 as shown on Page A4-4. To provide compatibility between the touchdown times, pitch angle, roll angle and sink speed, a nomograph was constructed employing the aircraft geometry. The values determined for pitch angle, roll angle and sink speed were -6.48 degrees, 0.93 degrees, and 20.38 feet per second, respectively. The extreme 3σ design value for pitch attitude is -4.5. The design sink speed over rough terrain is 18.8 feet per second. Flight 226, therefore, exceeded the design strength of the aircraft. The time histories for Flight 226 are given on Pages A4-117 through A4-128.

LANDING TOUCHDOWN CONDITIONS

Date	Flight No.	Take-Off Time	Mirror Setting Degrees	Wind Velocity Knots @ Deg	TRODI Vv Ft/Sec	SODI V_ε Knots	SPN V_ε Knots	Cine Vv Ft/Sec By NATC	Cine Vv Knots By NR	θ Degrees By NR	φ Degrees By NR	A/P Wt. Lbs	A/P C.G. % MAC
May 7	209	1105-1135		TAKEOFF									
	210	1400-1450	5	PRACTICE LANDING									
May 8	212	1130-1155	5	8 @ 325	6.6	-	VALUES NOT RECORDED	7.91	VALUES NOT OBTAINED	-	-	10547	27.0
	213	1517	5½	8 @ 270	-	76.1		10.32		-	-	10415	26.9
	214	1550	5½	8@270-325	-	78.6		11.48		2.92	1.30	10283	26.7
May 10	215	0955	6	7-9@225	-	53.4		11.48		2.92	1.30	10547	27.0
	216	1045	6¼	6 @ 225	9.8	67.7		10.11		-	-	10415	26.9
	217	1115	6¼	8 @ 270	10.0	-		11.81		6.97	0.35	10283	26.7
	218	1404	6½	10-14@250	11.6	-		12.57		4.43	4.00	10151	26.6
	219	1425	7	10-14@263	12.5	75.0		13.56		3.53	1.00	10019	26.4
	220	1455	7½	8 @ 270	14.4	-		14.77		4.76	0.10	9887	26.3
	221	1525	7½	16 @ 270	15.7	79.8		16.69		3.76	1.00	9755	26.1
May 11	223	1056	5	5-7@270	9.5	-		9.63		-0.07	0.60	10547	27.0
	224	1117	6	-	13.0	-		11.32		.52	0.70	10415	26.9
	225	1141	6-3/4	10-12@255	13.7	-		13.40	17.27	-5.16	0.30	10283	26.7
	226*	1205	7	8-10@245-255	18.5	-	86	17.46	20.38	-6.48	0.93	10150	26.6
	226	1205						18.69	20.53				
	226	1205						18.38	19.81				

Notes: V_ε = Longitudinal Speed
Vv = Sink Speed
θ = Pitch Angle
φ = Roll Angle

NATC = Naval Air Test Center Personnel
NR = North American Rockwell Personnel
* Three Independent Reading of Vv Taken For Flight No. 226
Dashs Imply Data Inoperative

EXPERIMENTAL TIME HISTORY PARAMETERS

Curve Title	Units		Comments
<u>Tire Pressure</u> NG -Nose Gear RMG-Right Main Gear LMG-Left Main Gear	Pressure Time	pounds per sq. inch seconds	Curves present oscillograph traces of measured tire internal air pressure.
<u>Drag Brace Loads</u> NLG-Nose Landing Gear LMG-Left Main Gear RMG-Right Main Gear	Load Time	pounds seconds	The curves present oscillograph traces of measured drag brace loads. The nose gear drag brace values are positive when in compression while the main gear values are positive when in tension.
<u>Oleo Axial Loads</u> NLG-Nose Landing Gear LMG-Left Main Gear RMG-Right Main Gear	Load Time	pounds seconds	The curves present oscillograph traces of measured oleo axial loads. Loads are measured below the oleo for the nose gear and above the oleo for the main gear.
<u>Oleo Oil Pressure</u> NLG-Nose Landing Gear LMG-Left Main Gear RMG-Right Main Gear	Pressure Time	pounds per sq. inch seconds	The pressure curves present oscillograph traces of measured oleo internal oil pressure.
<u>Oleo Stroke</u> NLG-Nose Landing Gear LMG-Left Main Gear RMG-Right Main Gear	Stroke Time	inches seconds	The curves present oscillograph traces of measured oleo stroke. Zero stroke corresponds to the oleo fully extended.

Curve Title	Units		Comments
Torque Link Load NLG-Nose Landing Gear	Load Time	pounds seconds	The curve presents oscillograph traces of the measured axial load in the torque link. This link connects the nose gear strut to the fork arm.
Axle Accelerations NLG-Nose Landing Gear LMG-Left Main Gear RMG-Right Main Gear	Accelerations Time	g's seconds	These curves present oscillograph traces of the measured axle accelerations. The nose gear accelerations are measured in directions normal and parallel to the fork link. The main gear accelerations are measured in directions normal and parallel to the lever arm.
Airplane C.G. Accelerations	Accelerations Time	g's seconds	These curves present oscillograph traces of measured accelerations at the airplane C.G. in the vertical direction (normal to a water plane), longitudinal direction (parallel to the FRL), and the lateral direction (normal to a butt plane).
Stroke Curves NG -Nose Gear LMG-Left Main Gear RMG-Right Main Gear	Stroke Time	inches seconds	These stroke curves are the same as those labeled Oleo Stroke. The time scale is changed to coincide with that of the Side, Drag, and Vertical Load curves so that load-stroke relationships can be observed.

Curve Title	Units		Comments
Side Load NG -Nose Gear LMG-Left Main Gear RMG-Right Main Gear	Load Load Time	pounds (NG) 1000 pounds (LMG, RMG) seconds	These curves present the load acting at the axle in a direction normal to a butt plane. Positive loads act to the right. Loads are determined from strain gages on the gear.
Drag Load NG -Nose Gear LMG-Left Main Gear RMG-Right Main Gear	Load Load Time	pounds (NG) 1000 pounds (LMG, RMG) seconds	These curves present the load acting at the axle in a direction parallel to the FRL. Positive loads act aft. Loads are determined from strain gages on the gear.
Vertical Load NG -Nose Gear LMG-Left Main Gear RMG-Right Main Gear	Load Load Time	pounds (NG) 1000 pounds (LMG, RMG) seconds	These curves present the load acting at the axle in a direction normal to a water plane. Positive loads act up. Loads are determined from strain gages on the gear.
Loads At The Axle NG -Nose Gear LMG-Left Main Gear RMG-Right Main Gear	Load Time	pounds seconds	These curves are digital computer plots of the loads at the axle determined from strain gages on the landing gear. Vertical (V), Side (S), and Drag (D) loads are presented.

TIME HISTORIES OF LANDING GEAR
LOADS AND RESPONSE

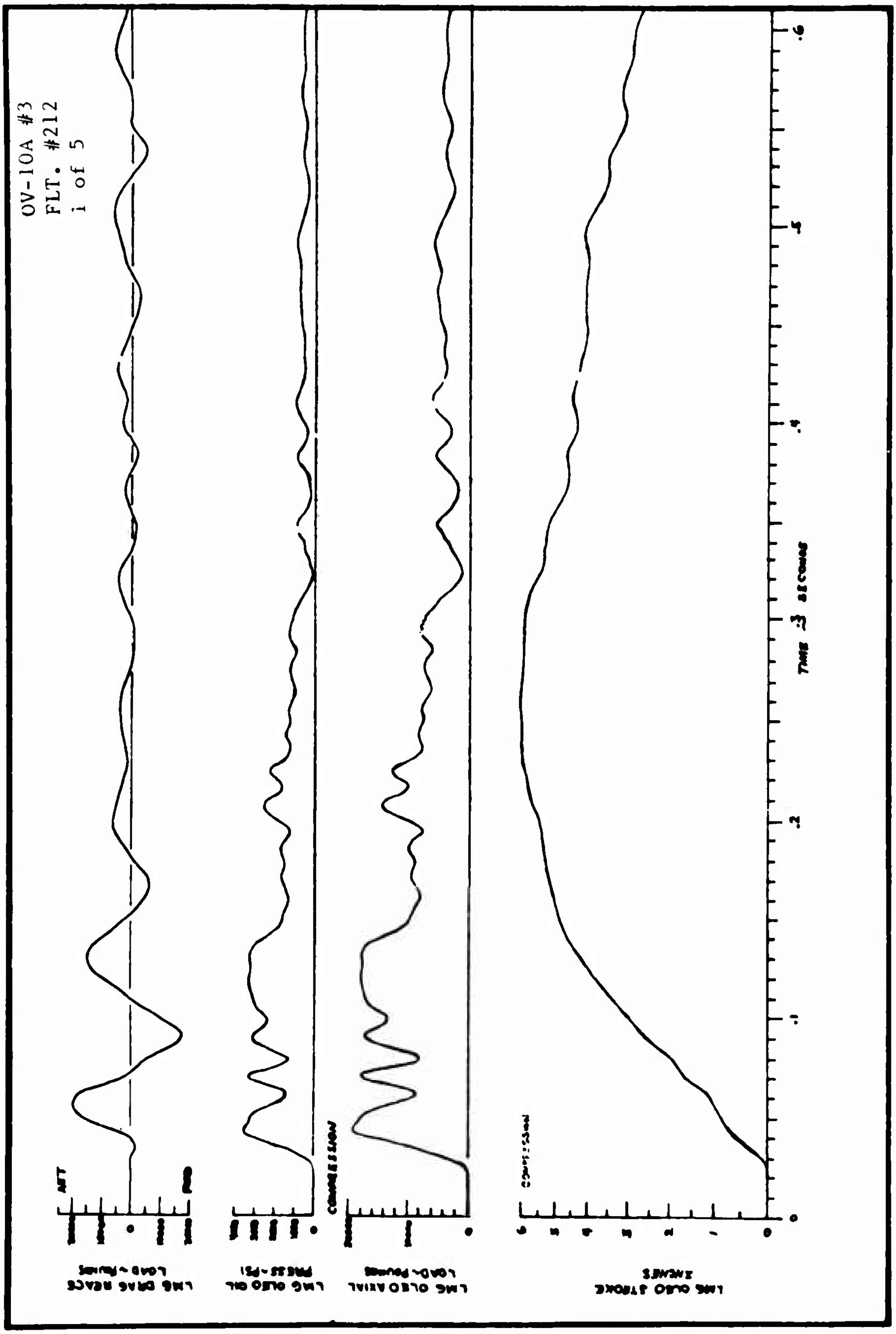

TIME HISTORIES OF LANDING GEAR LOADS AND RESPONSE

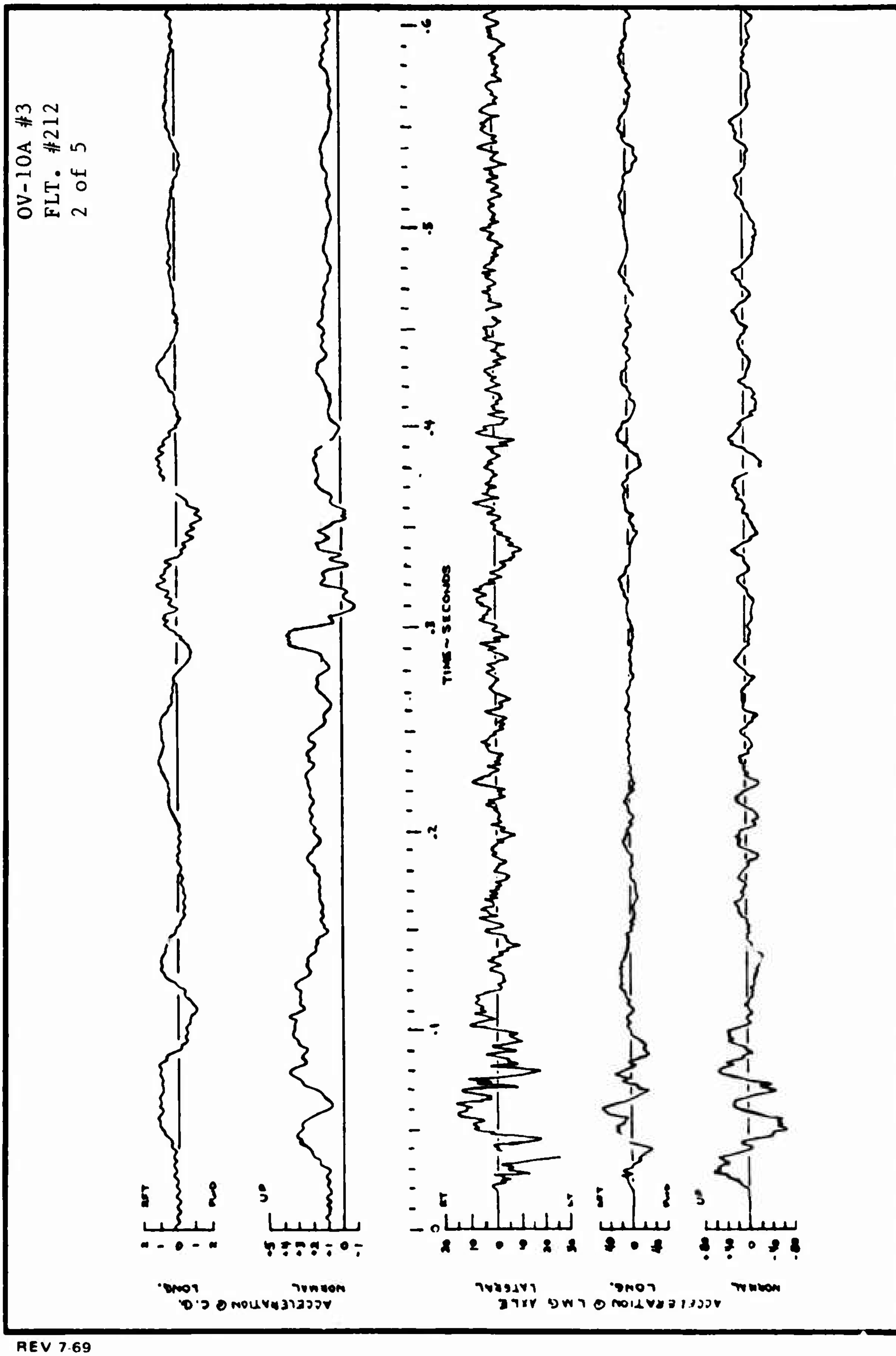

TIME HISTORIES OF LANDING GEAR LOADS AND RESPONSE

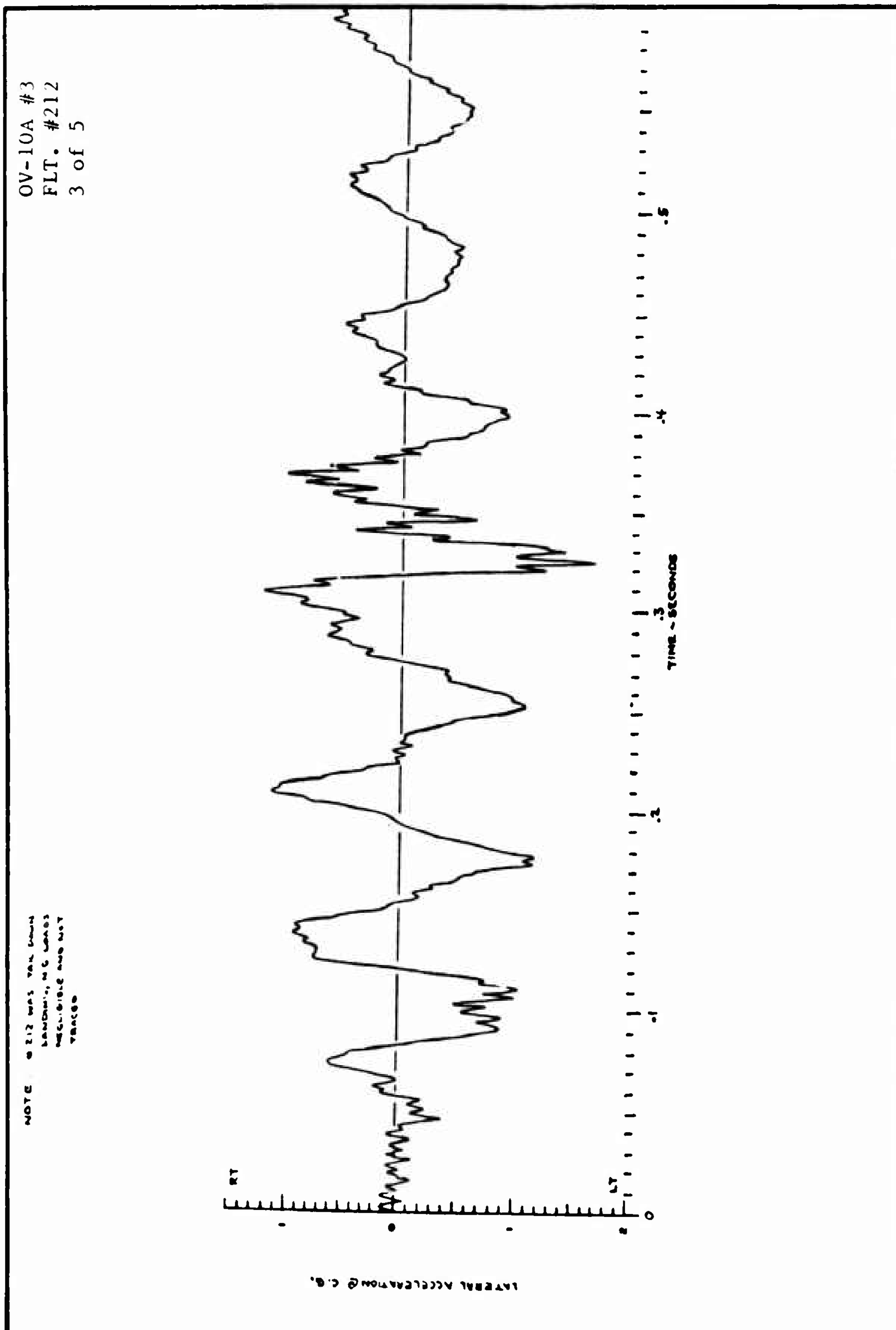

TIME HISTORIES OF LANDING GEAR LOADS AND RESPONSE

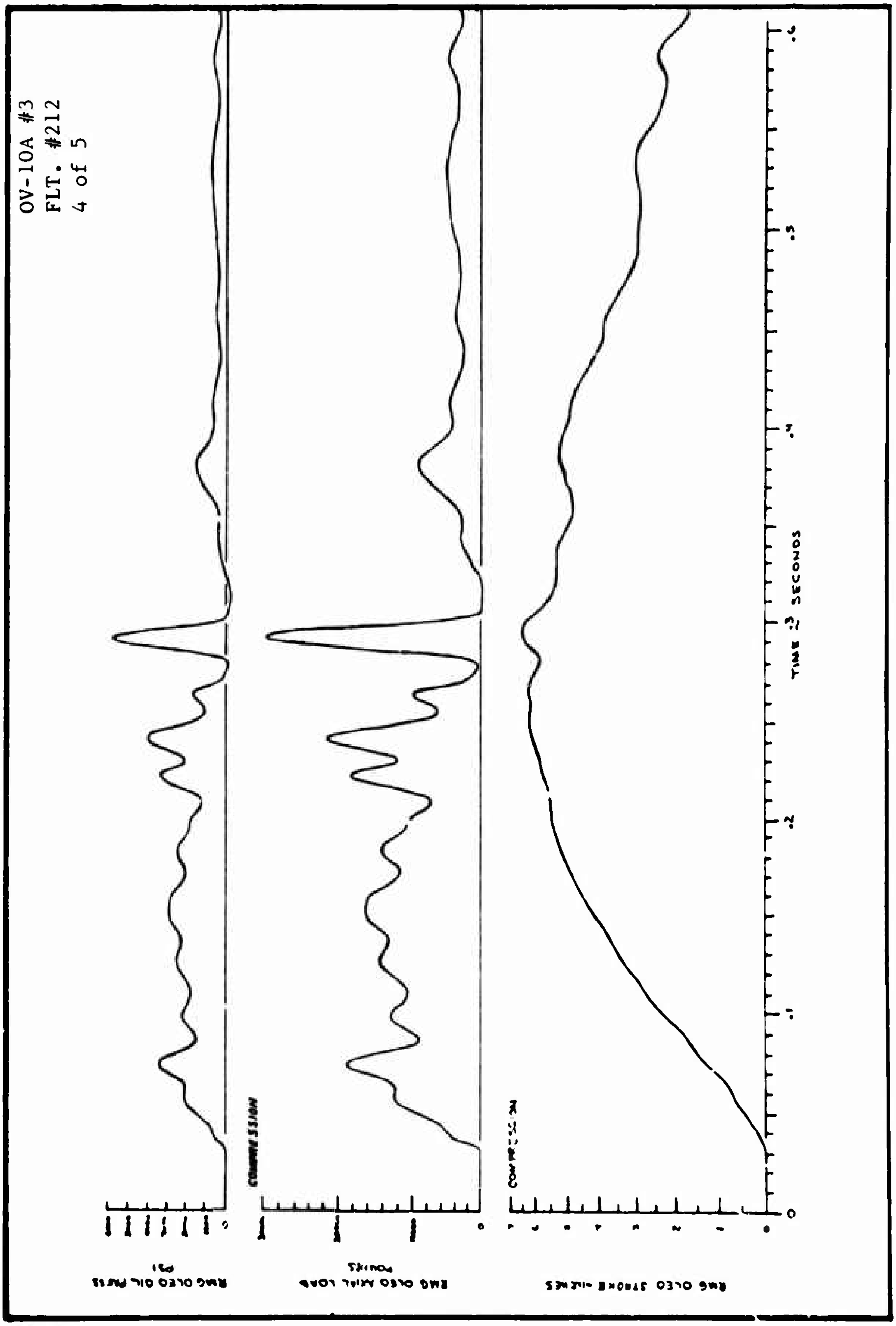

TIME HISTORIES OF LANDING GEAR LOADS AND RESPONSE

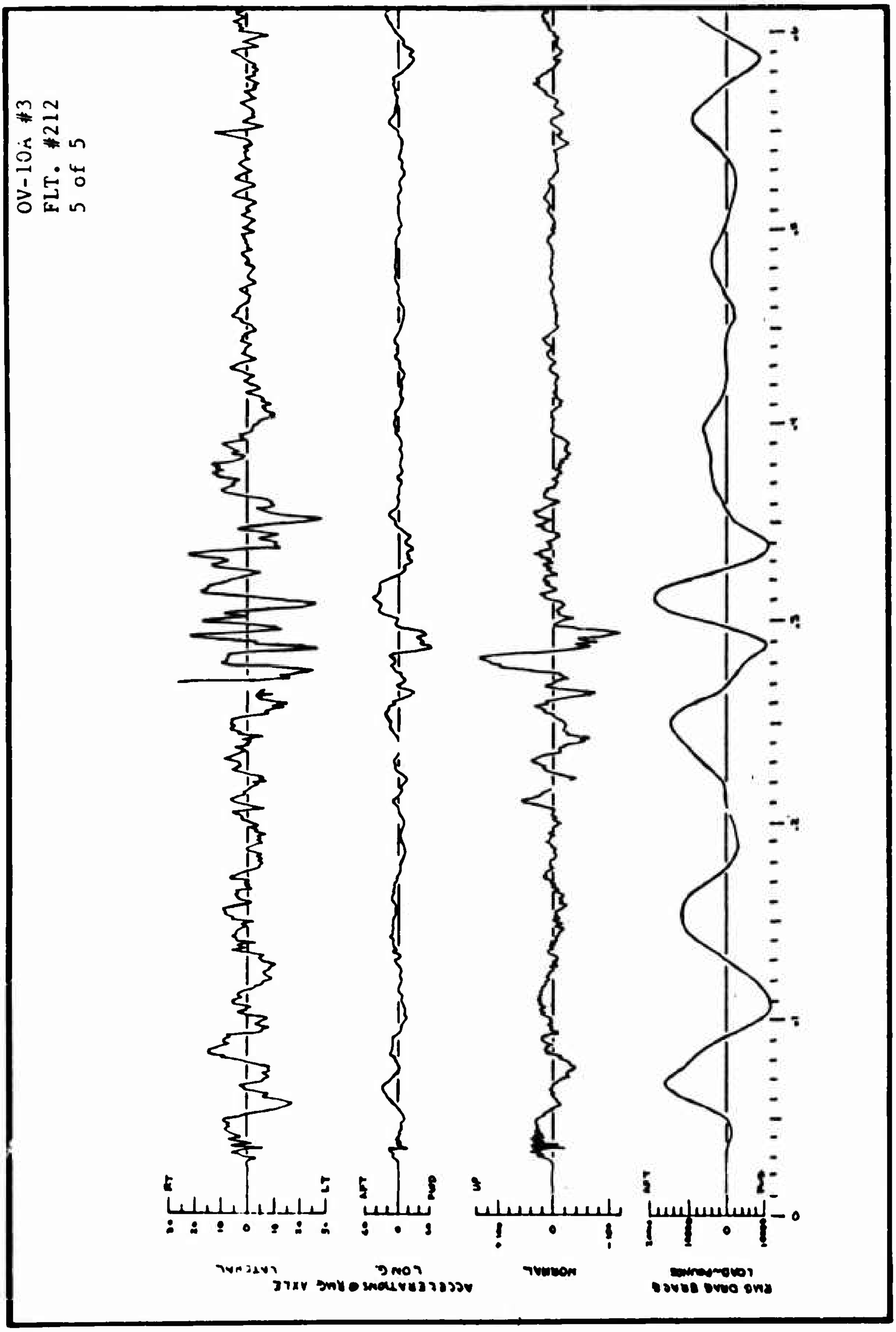

TIME HISTORIES OF LANDING GEAR LOADS AND RESPONSE

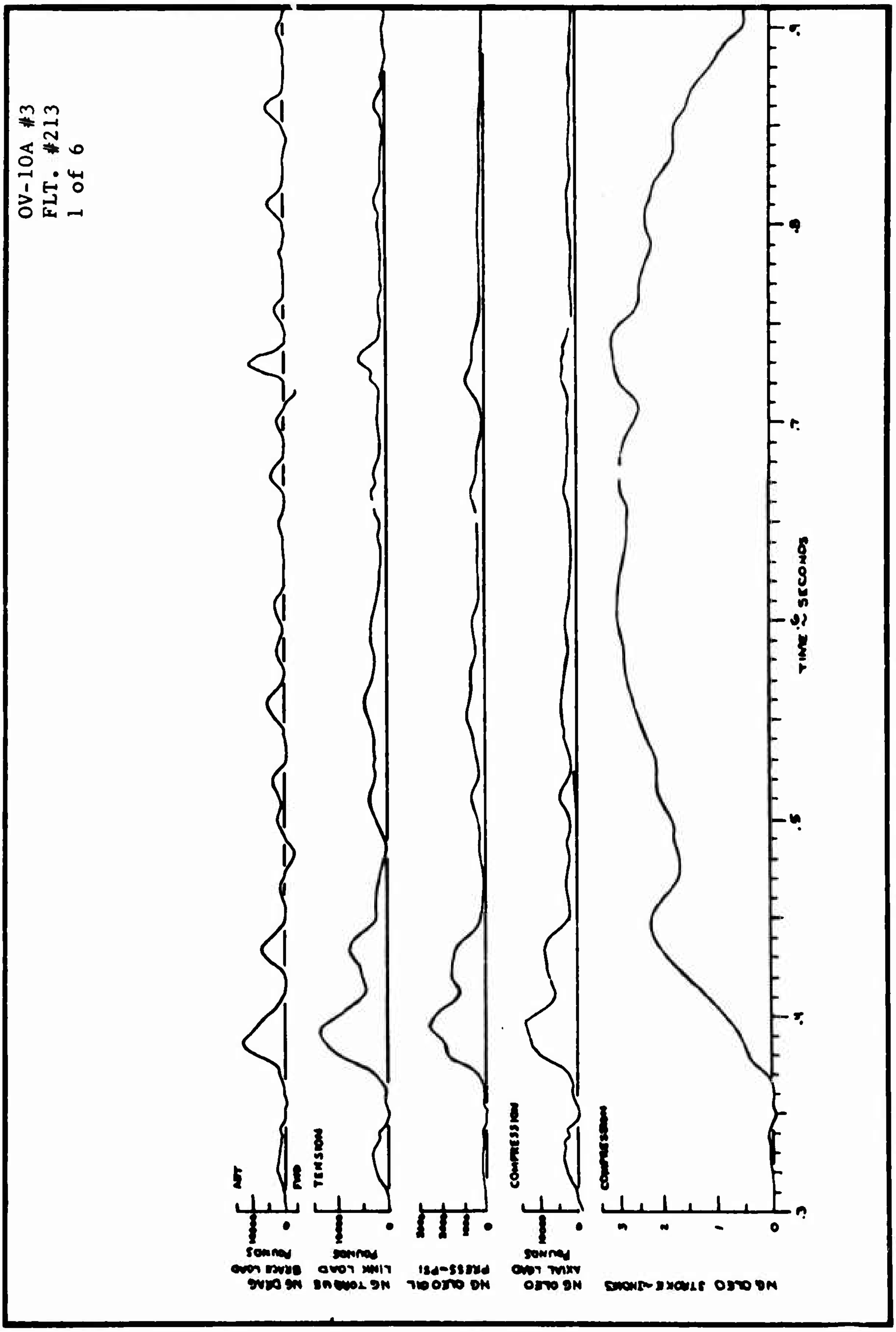

TIME HISTORIES OF LANDING GEAR
LOADS AND RESPONSE

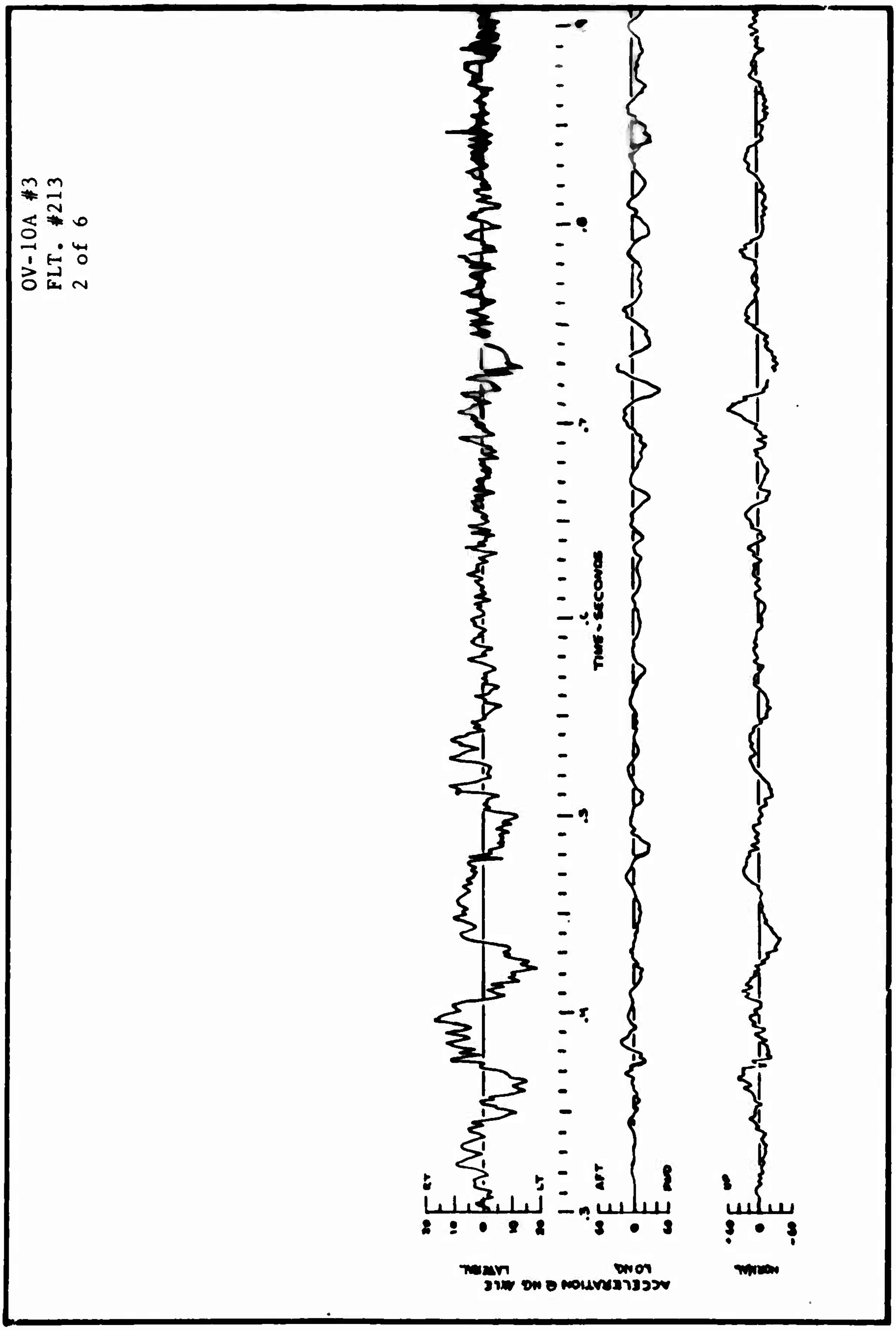

North American Aviation/Columbus
North American Rockwell

TIME HISTORIES OF LANDING GEAR LOADS AND RESPONSE

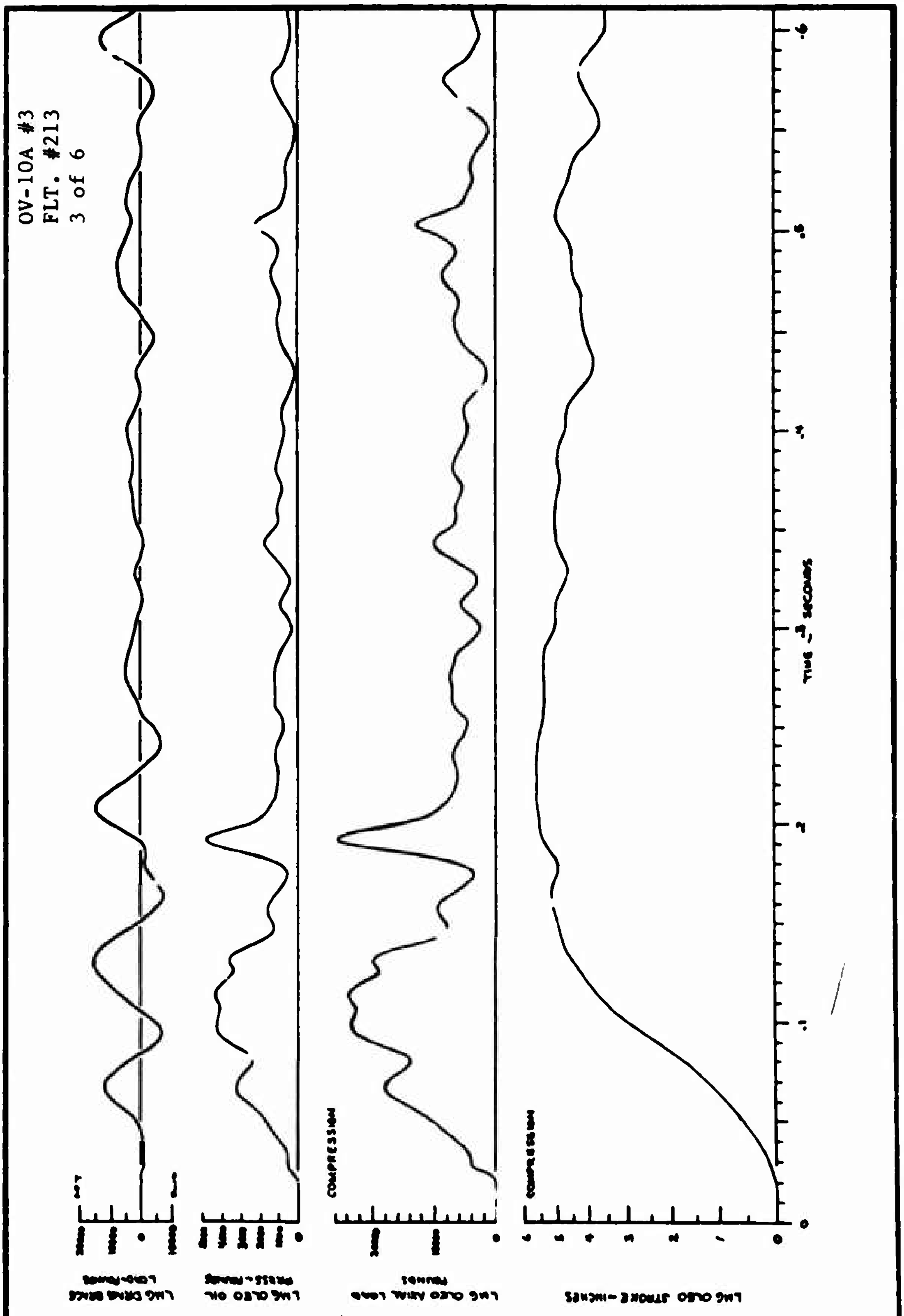

TIME HISTORIES OF LANDING GEAR LOADS AND RESPONSE

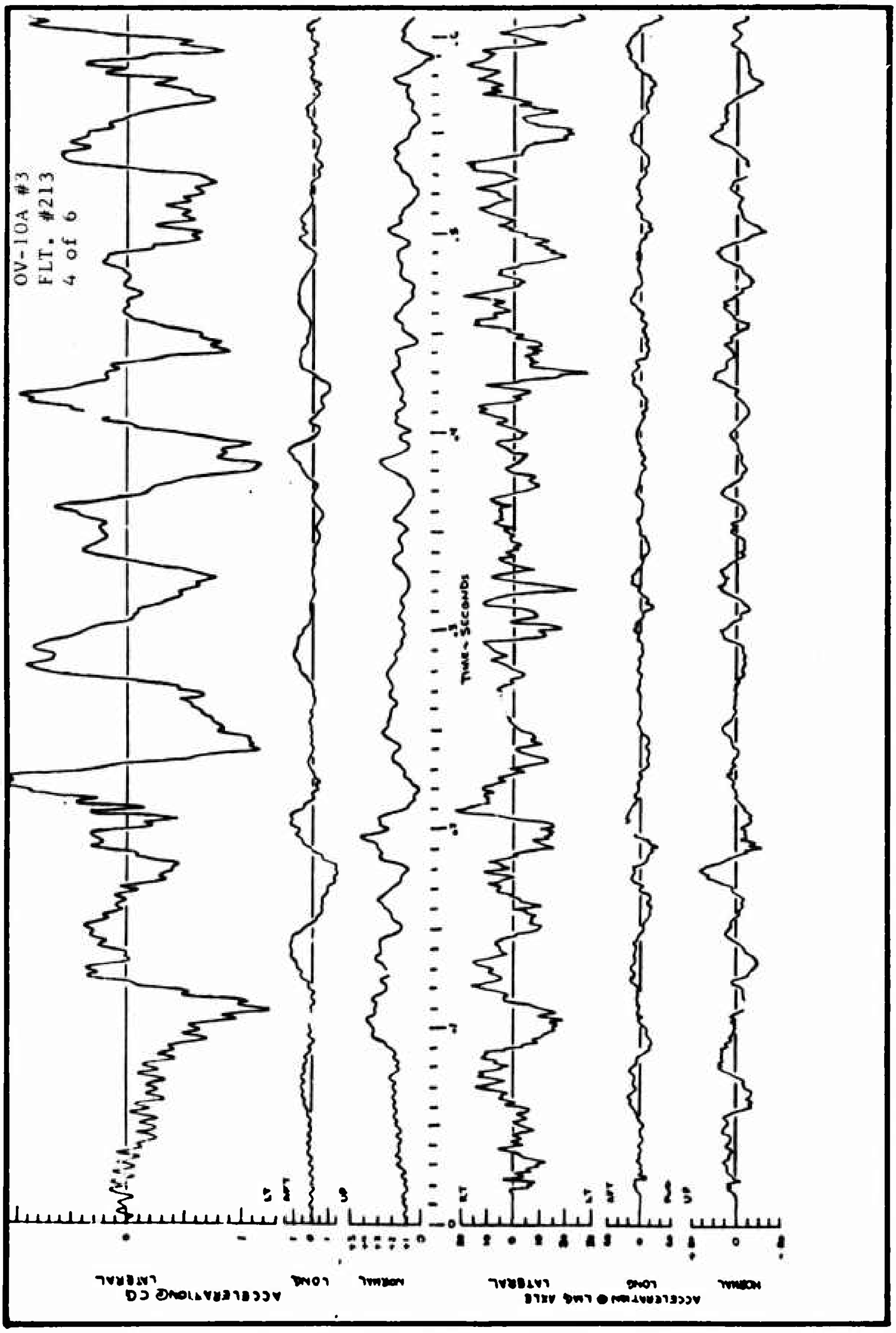

TIME HISTORIES OF LANDING GEAR
LOADS AND RESPONSE

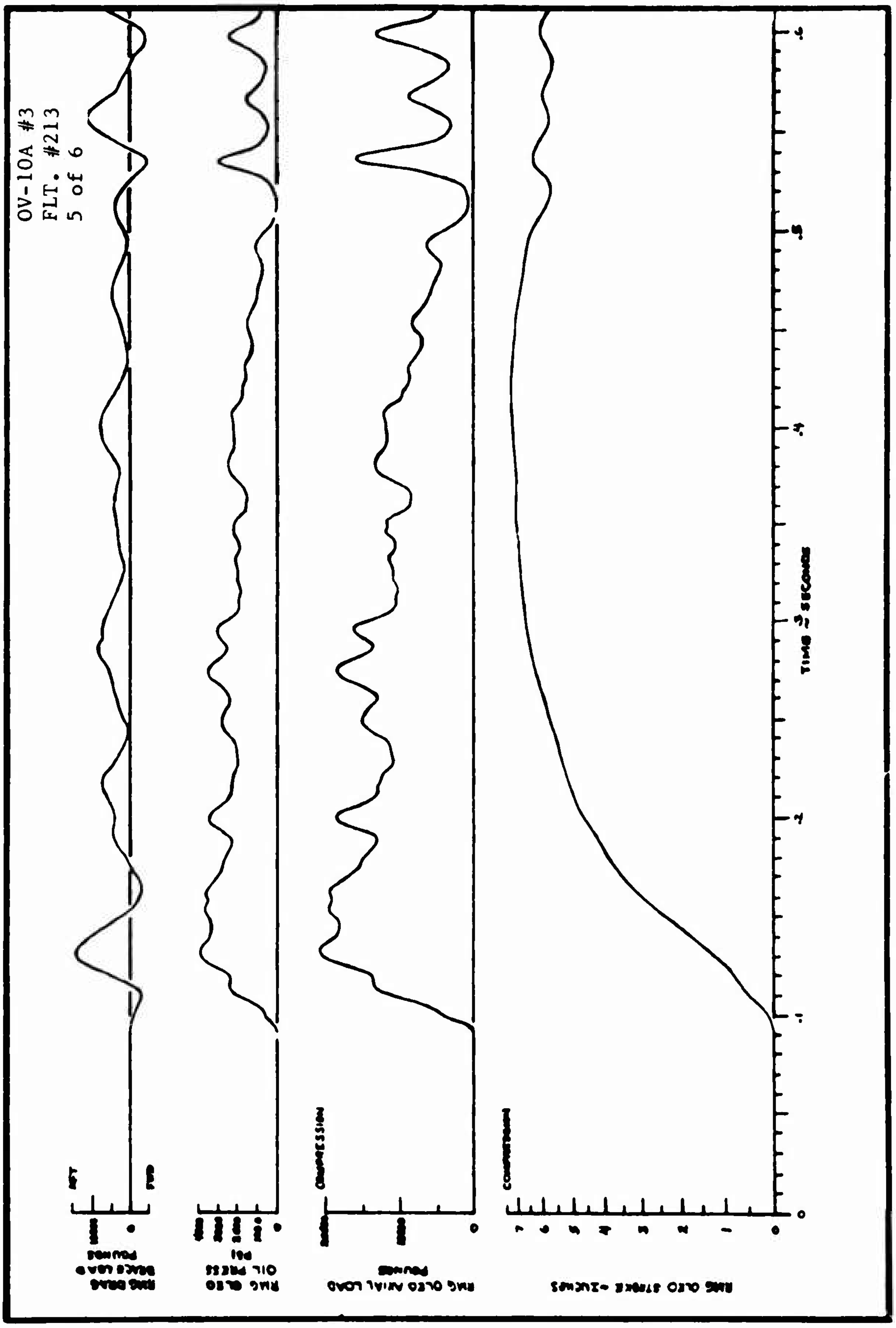

TIME HISTORIES OF LANDING GEAR
LOADS AND RESPONSE

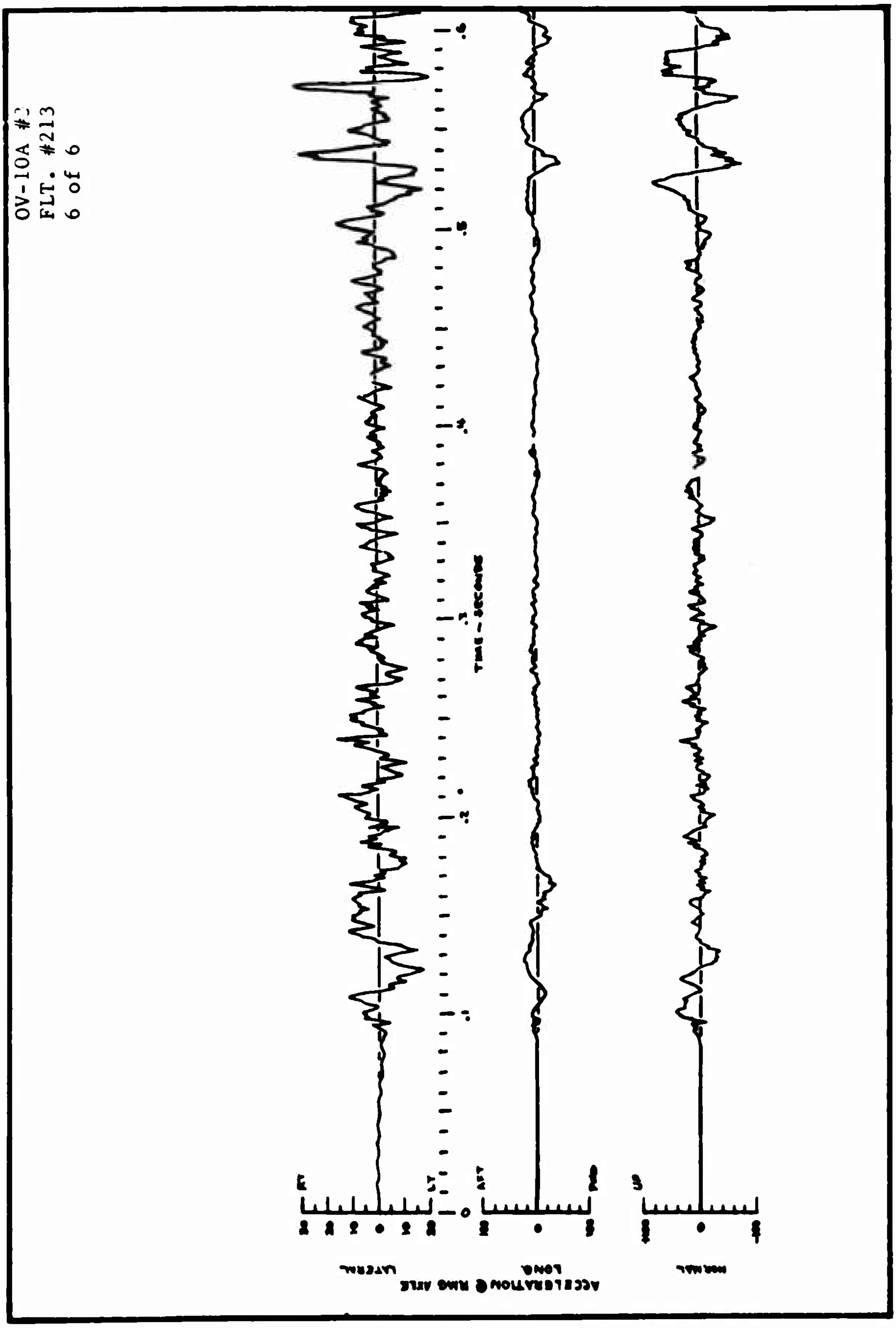

TIME HISTORIES OF LANDING GEAR LOADS AND RESPONSE

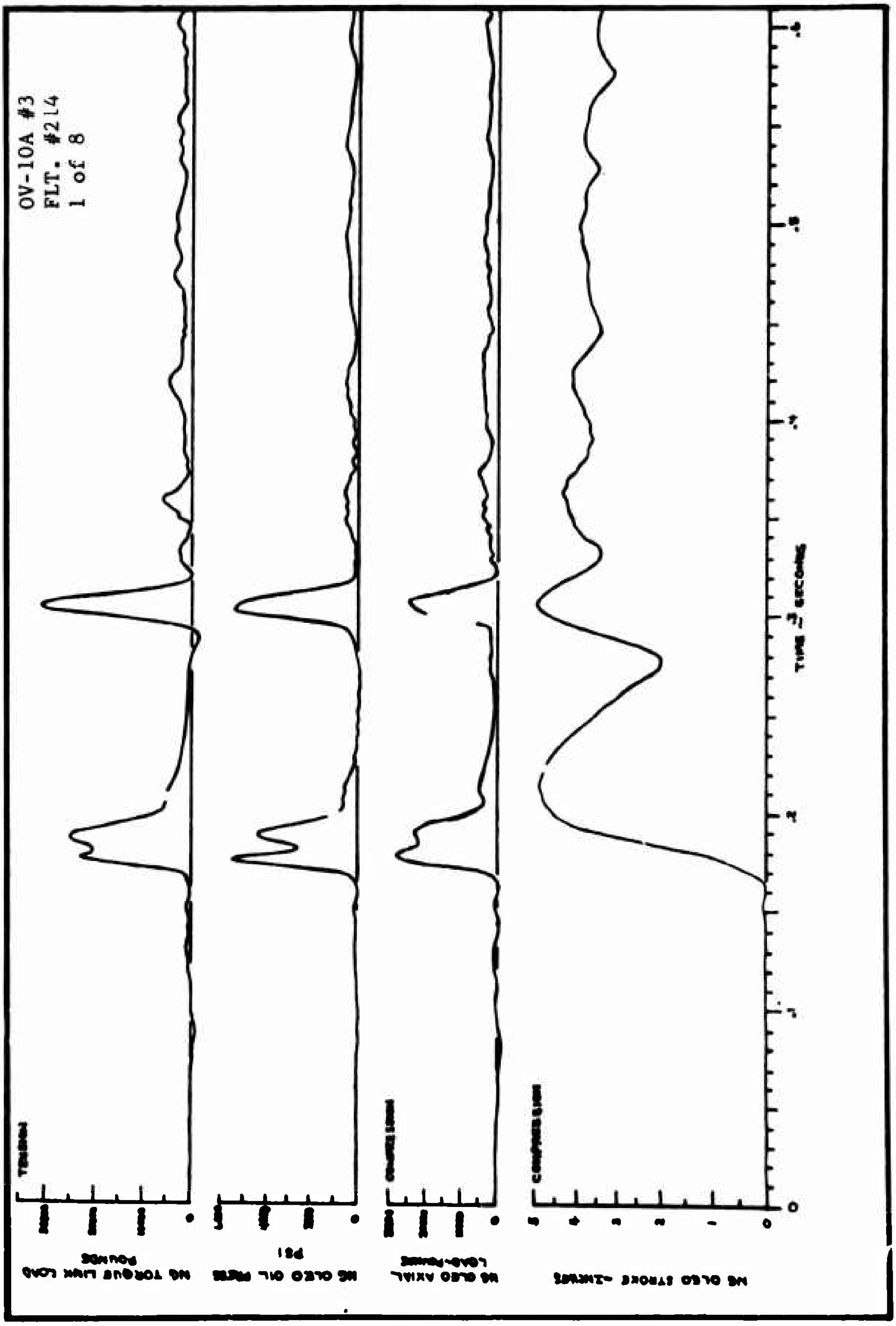

TIME HISTORIES OF LANDING GEAR LOADS AND RESPONSE

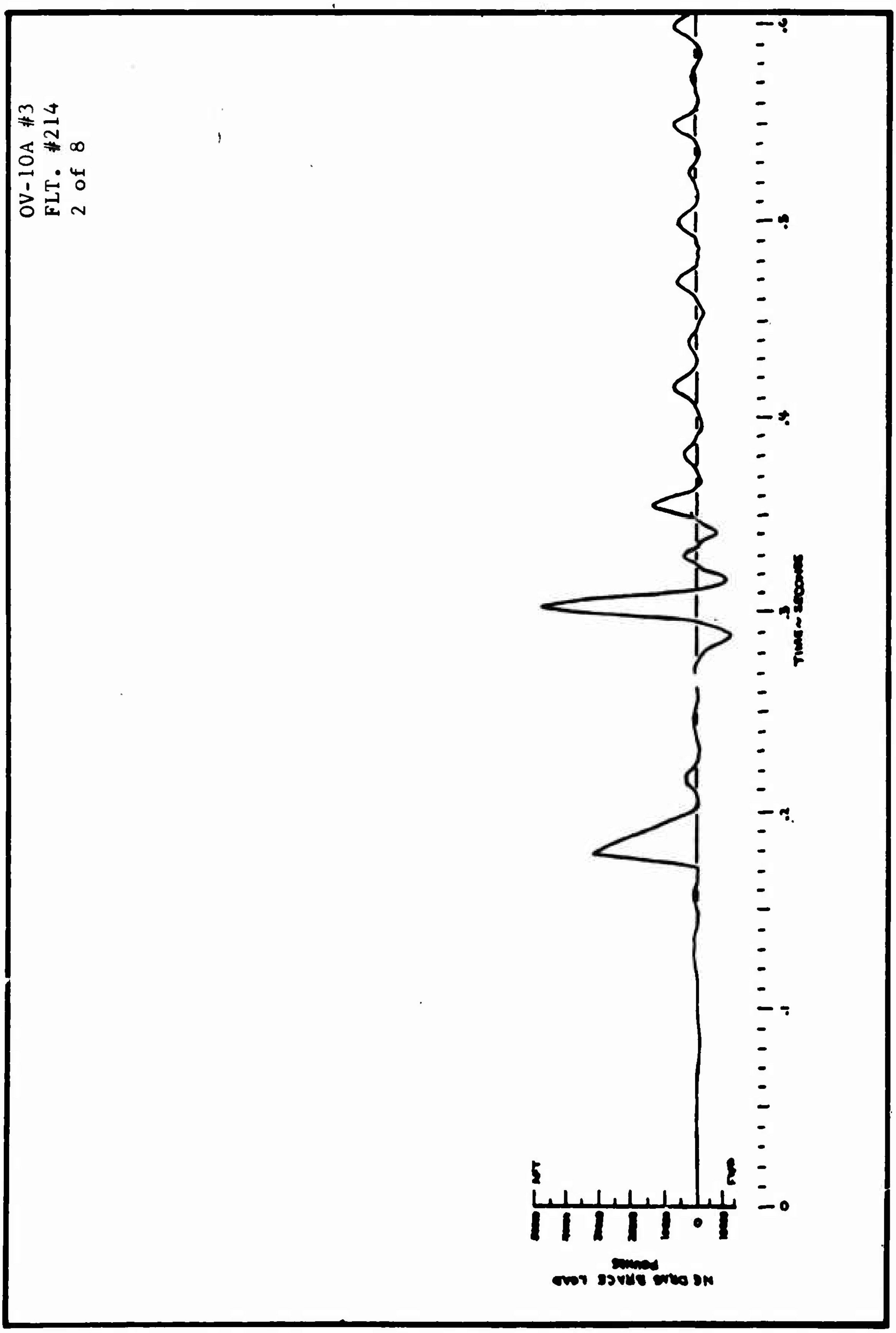

TIME HISTORIES OF LANDING GEAR
LOADS AND RESPONSE

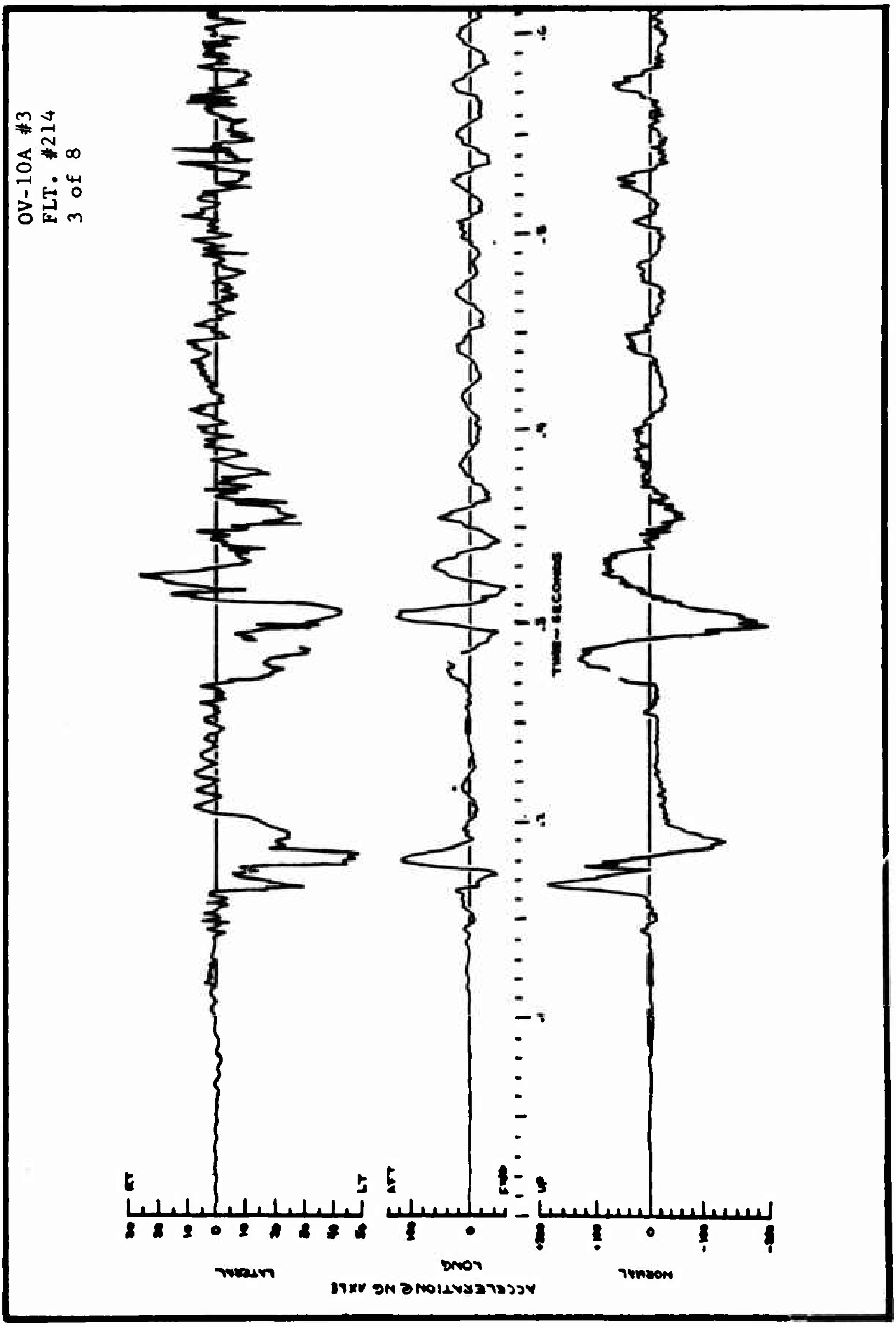

TIME HISTORIES OF LANDING GEAR
LOADS AND RESPONSES

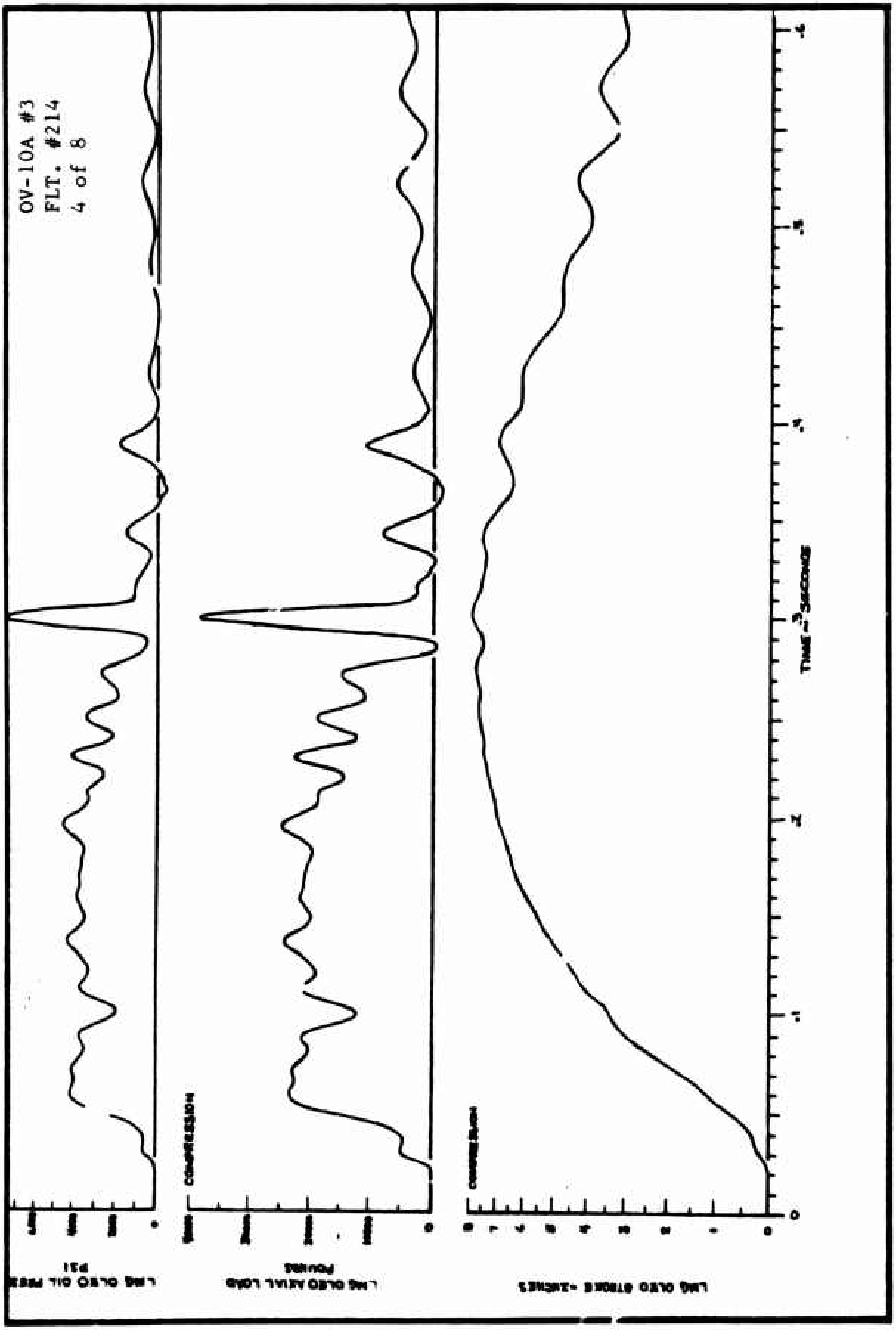

TIME HISTORIES OF LANDING GEAR
LOADS AND RESPONSES

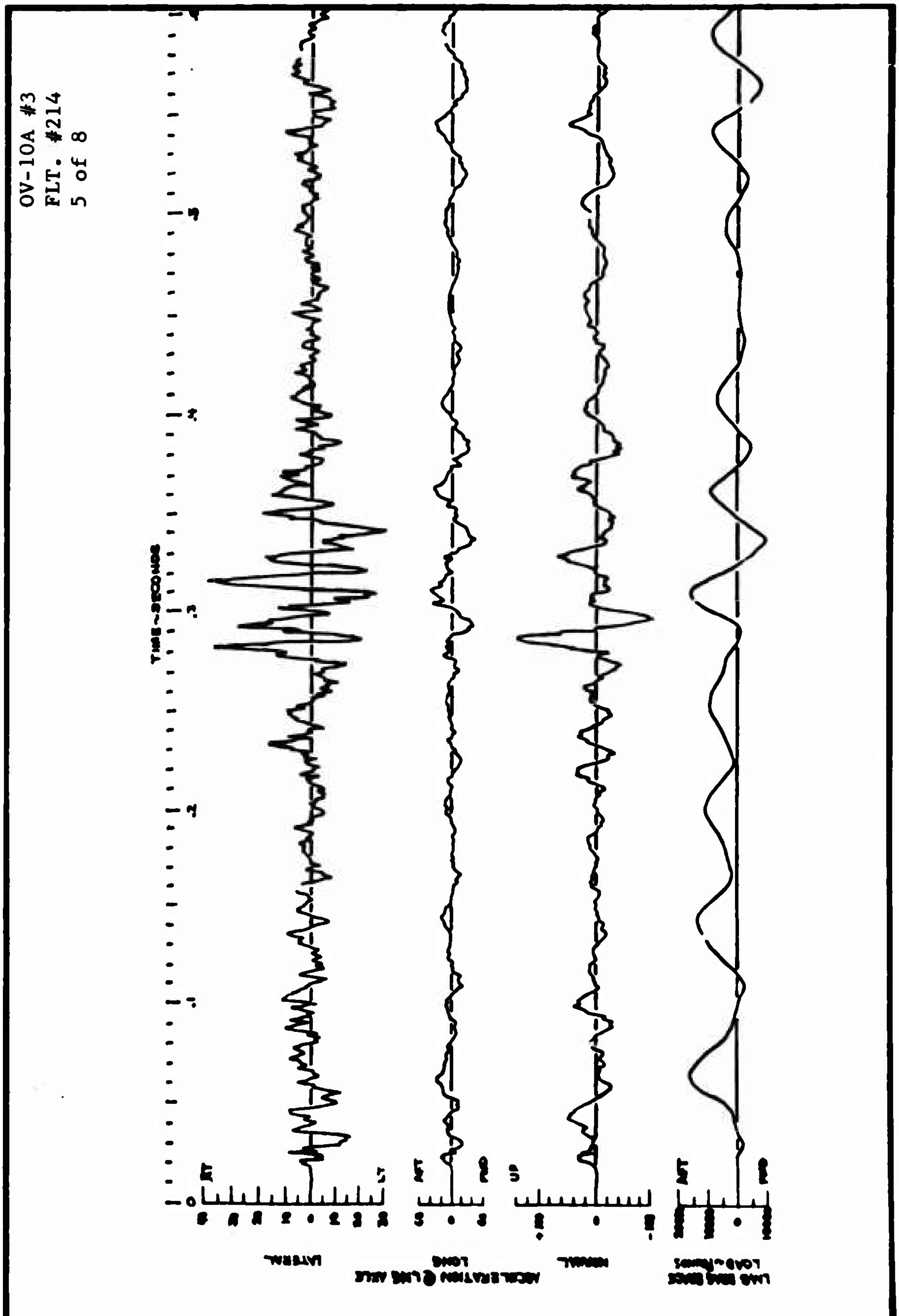

TIME HISTORIES OF LANDING GEAR
LOADS AND RESPONSE

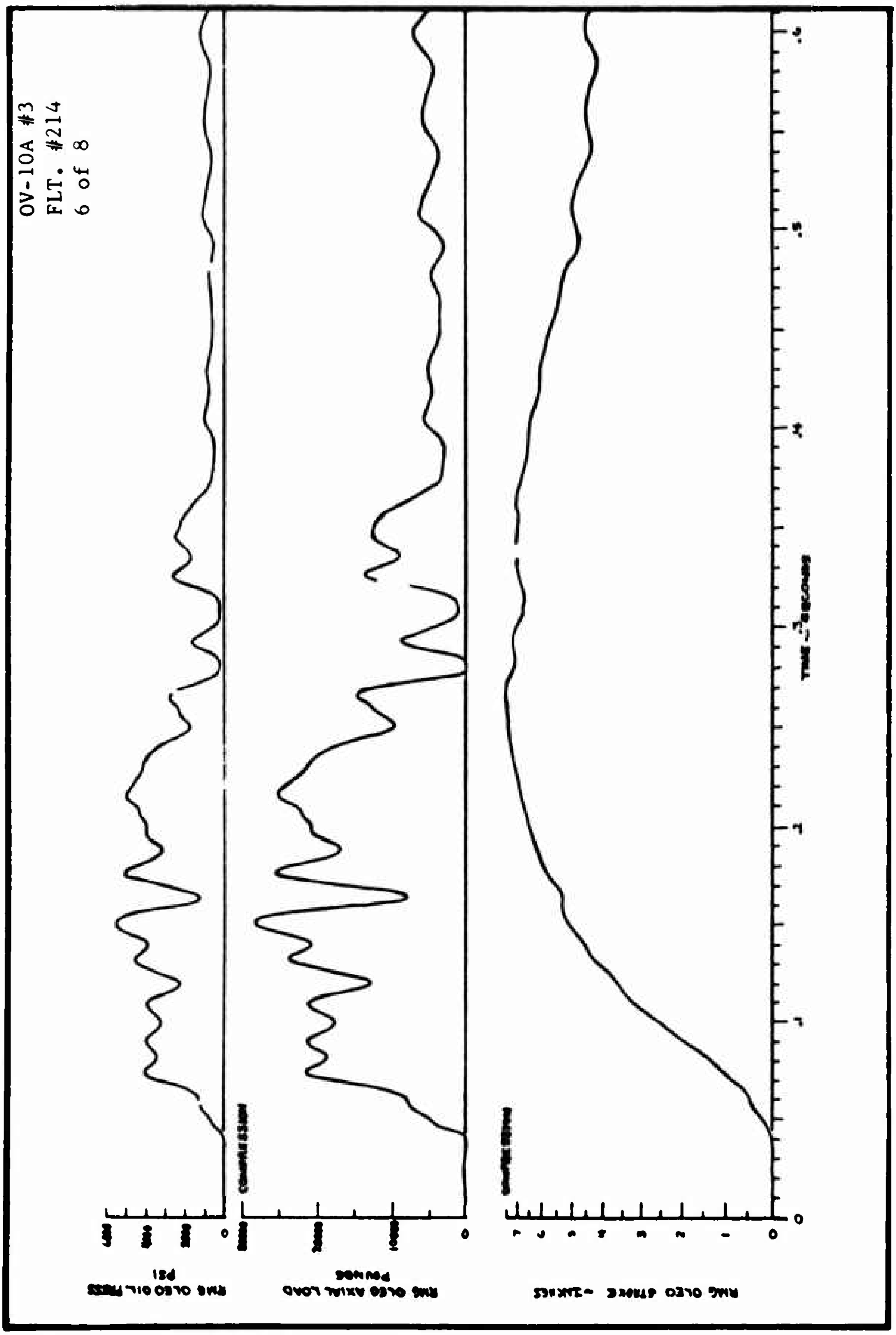

TIME HISTORIES OF LANDING GEAR
LOADS AND RESPONSE

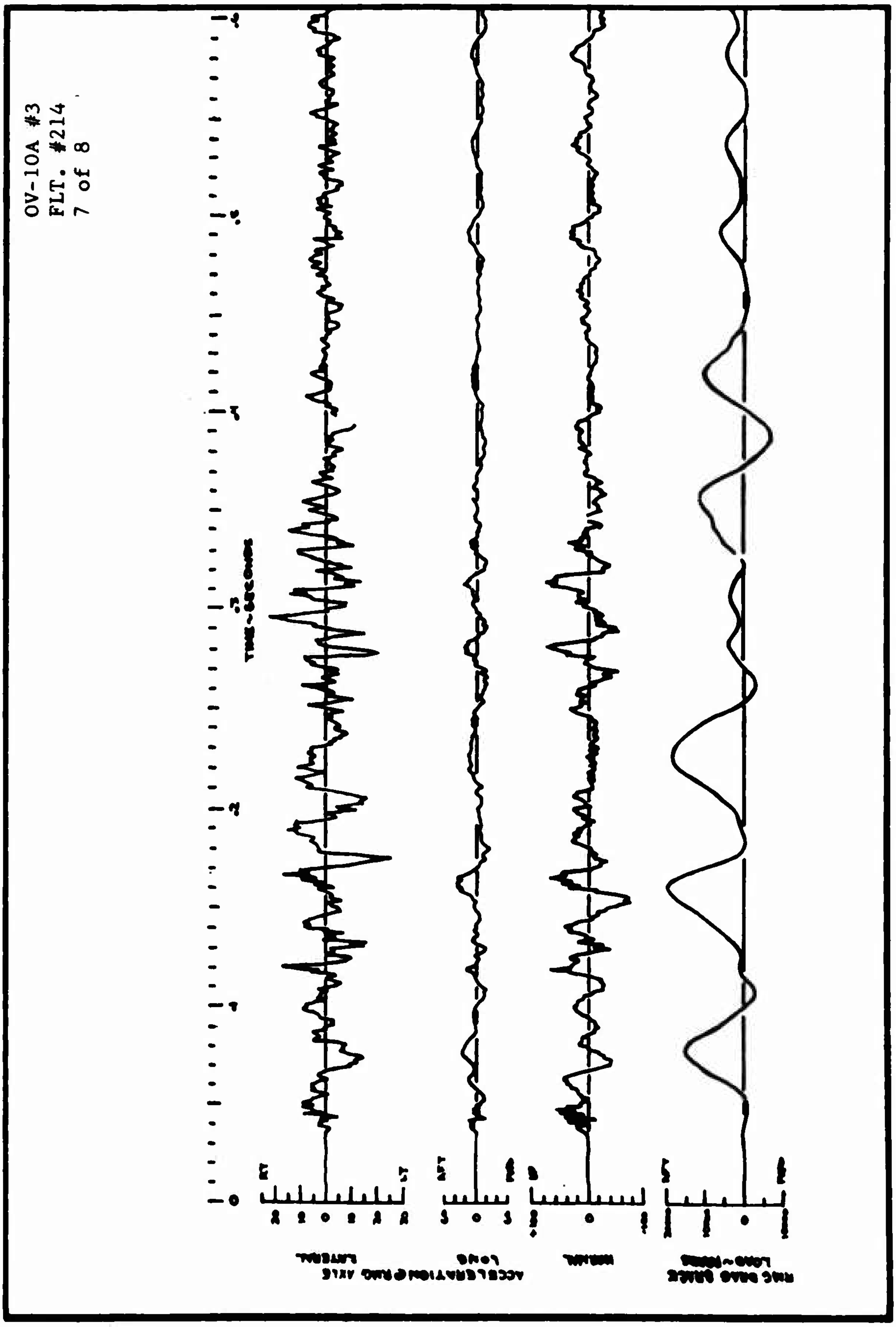

TIME HISTORIES OF LANDING GEAR
LOADS AND RESPONSE

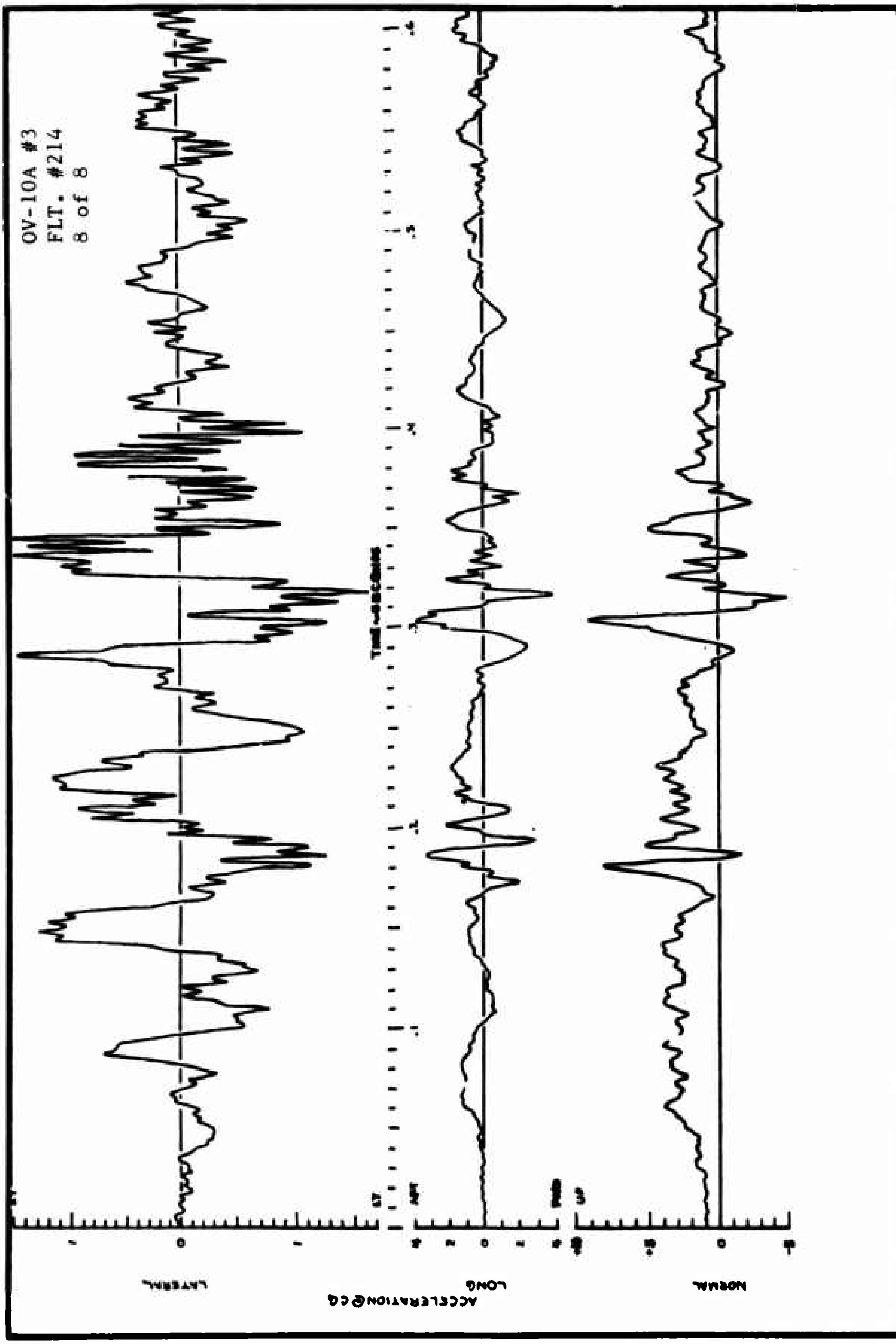

TIME HISTORIES OF LANDING GEAR
LOADS AND RESPONSE

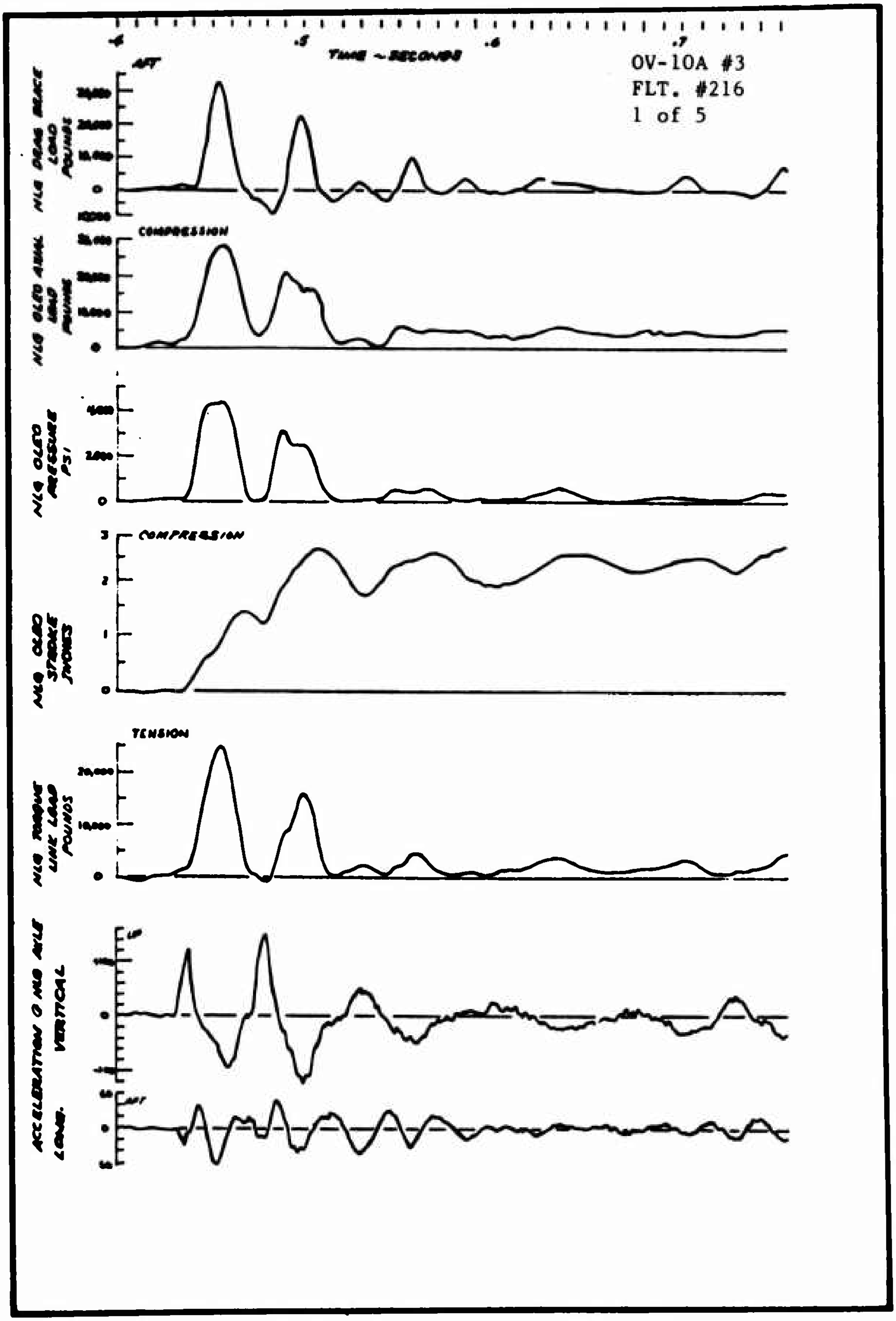

TIME HISTORIES OF LANDING GEAR
LOADS AND RESPONSE

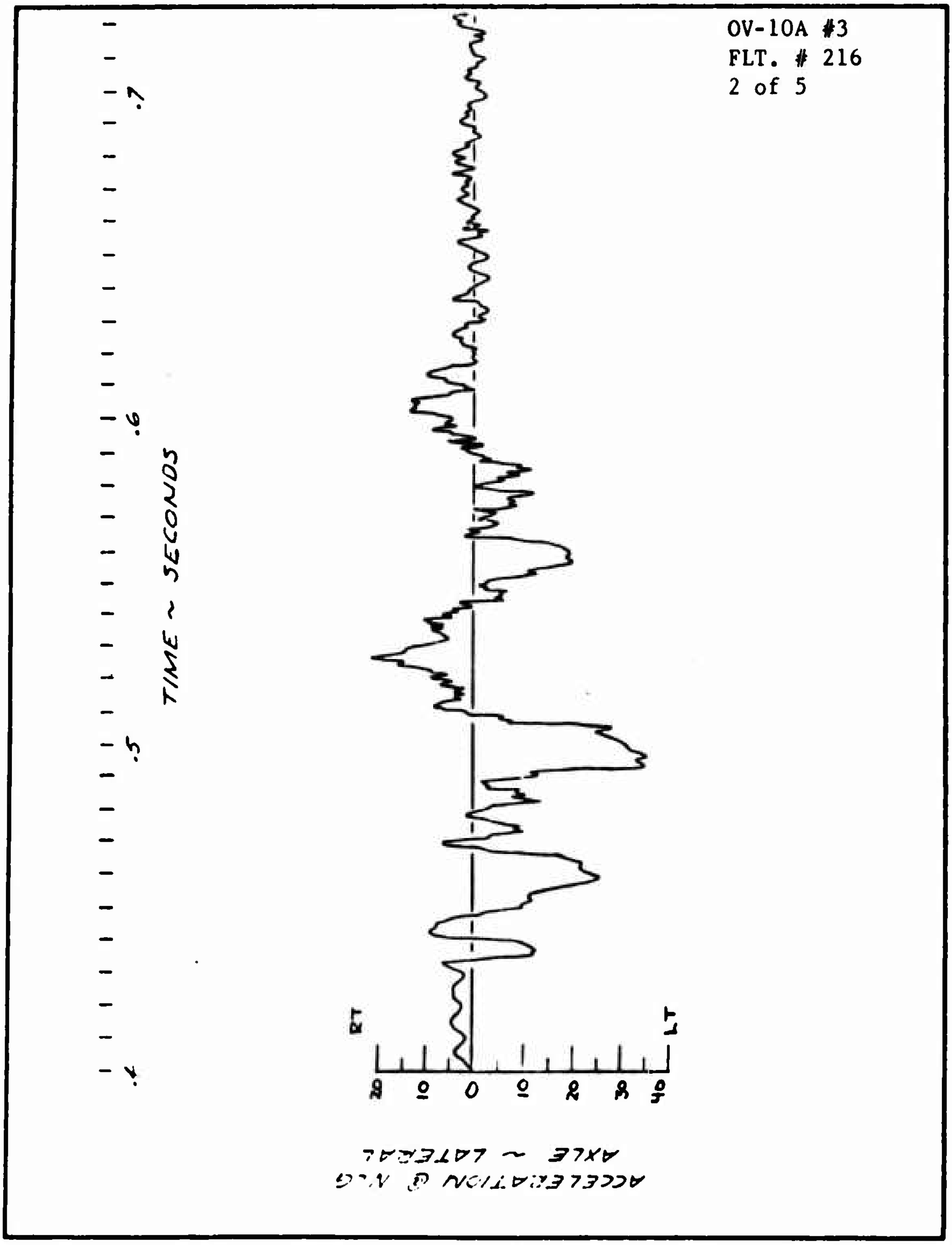

TIME HISTORIES OF LANDING GEAR
LOADS AND RESPONSES

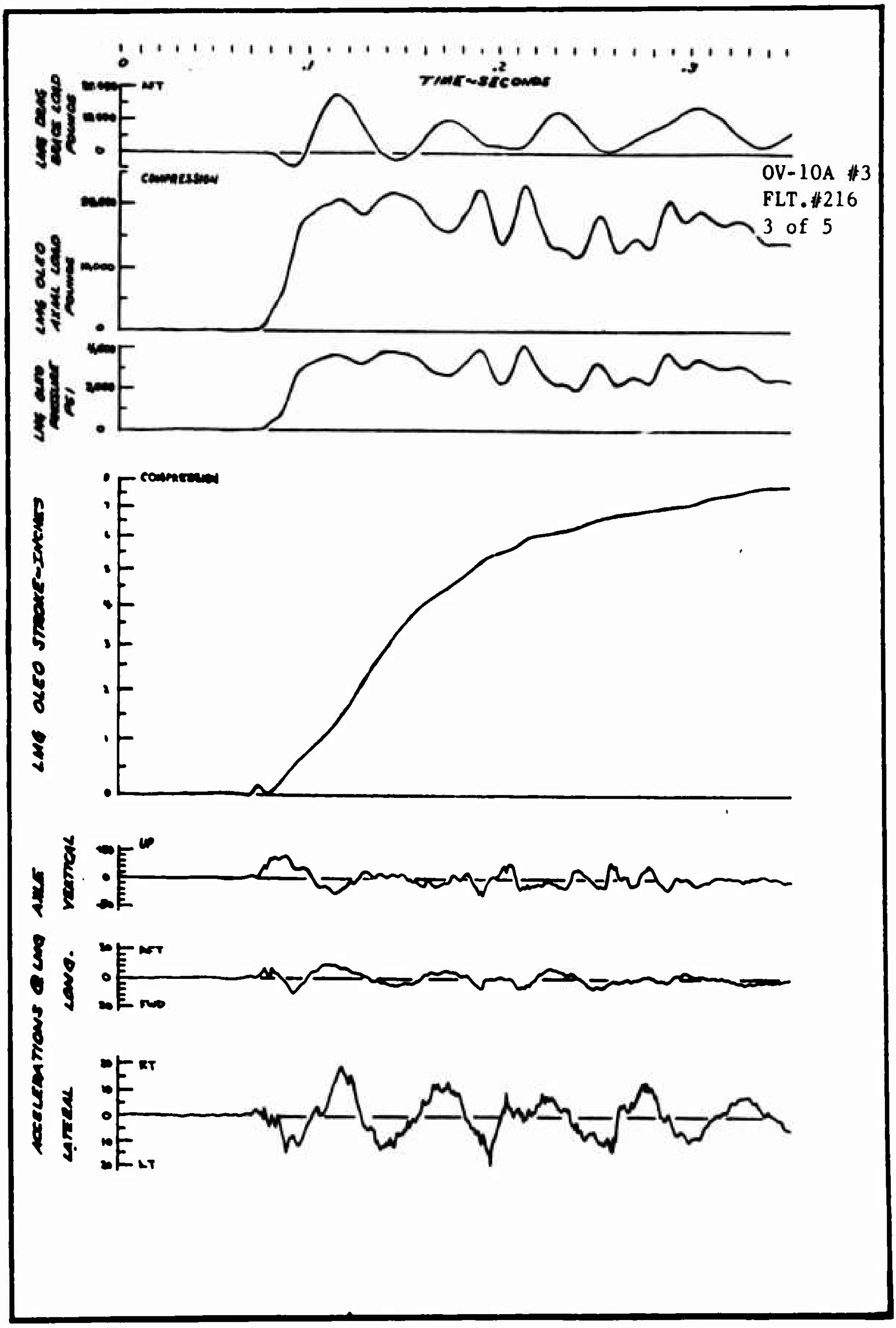

OV-10A #3
FLT.#216
3 of 5

TIME HISTORIES OF LANDING GEAR
LOADS AND RESPONSE

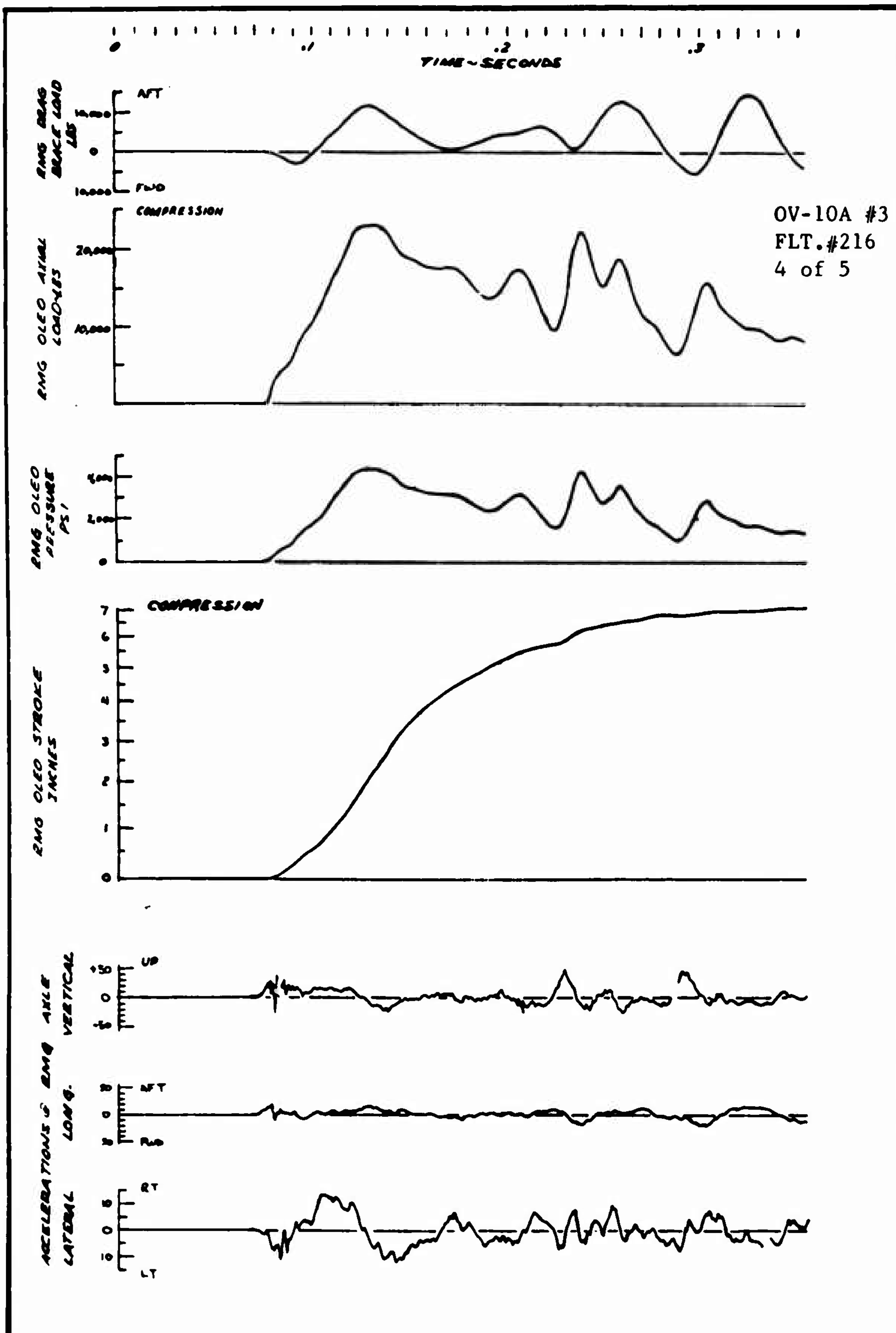

TIME HISTORIES OF LANDING GEAR
LOADS AND RESPONSE

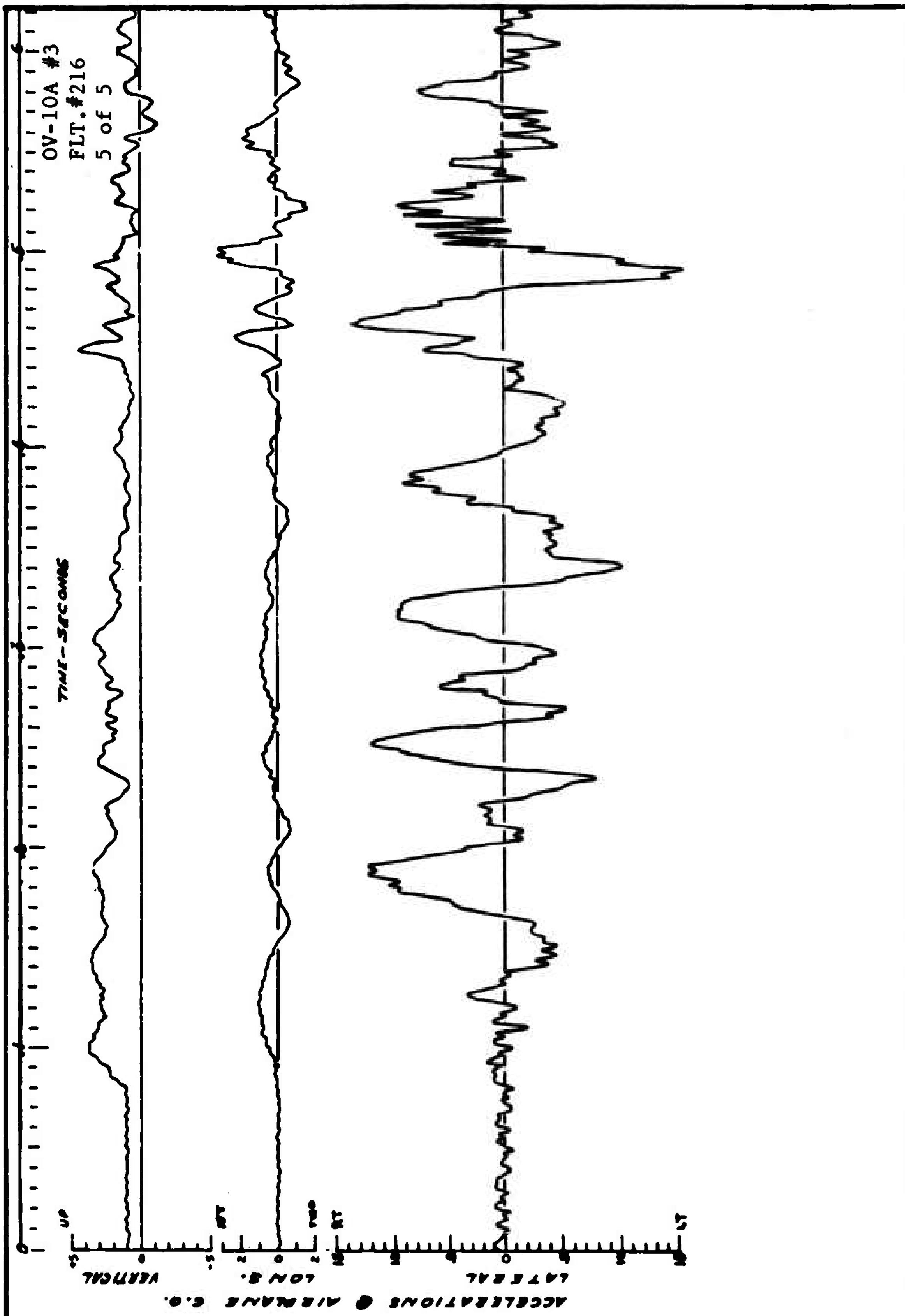

TIME HISTORIES OF LANDING GEAR
LOADS AND RESPONSE

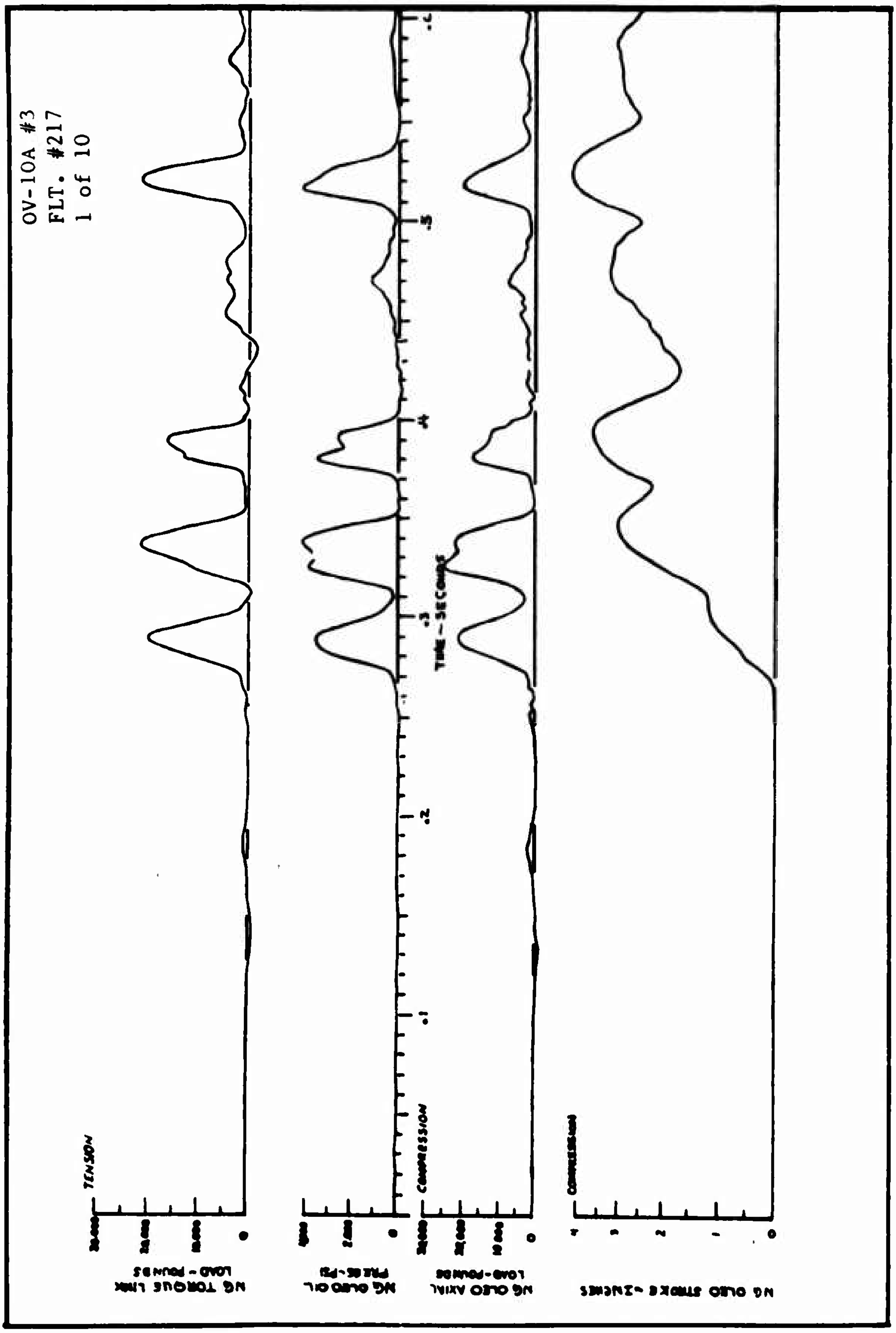

TIME HISTORIES OF LANDING GEAR
LOADS AND RESPONSE

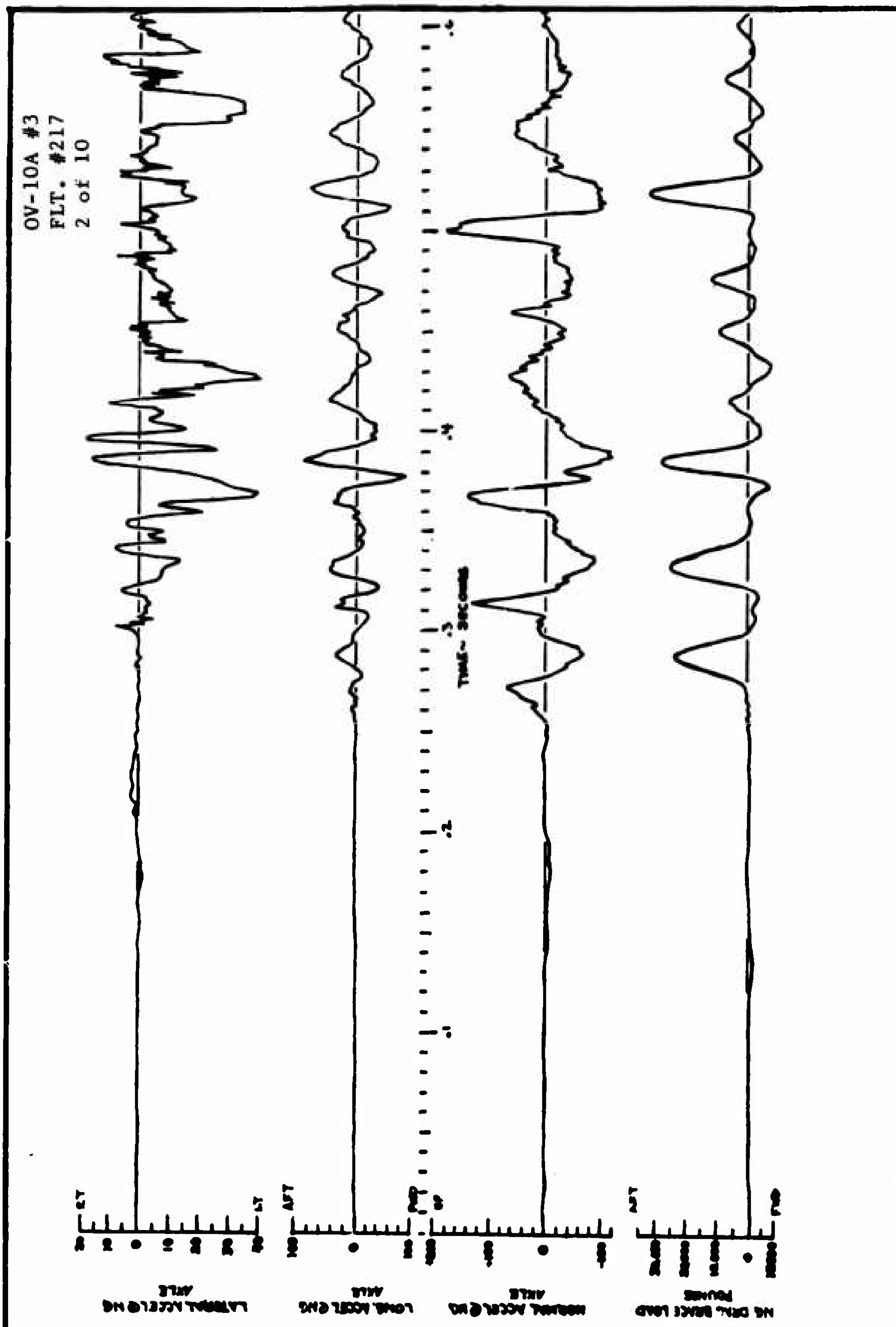

TIME HISTORIES OF LANDING GEAR
LOADS AND RESPONSE

OV-10A #3
FLT. #217
3 of 10

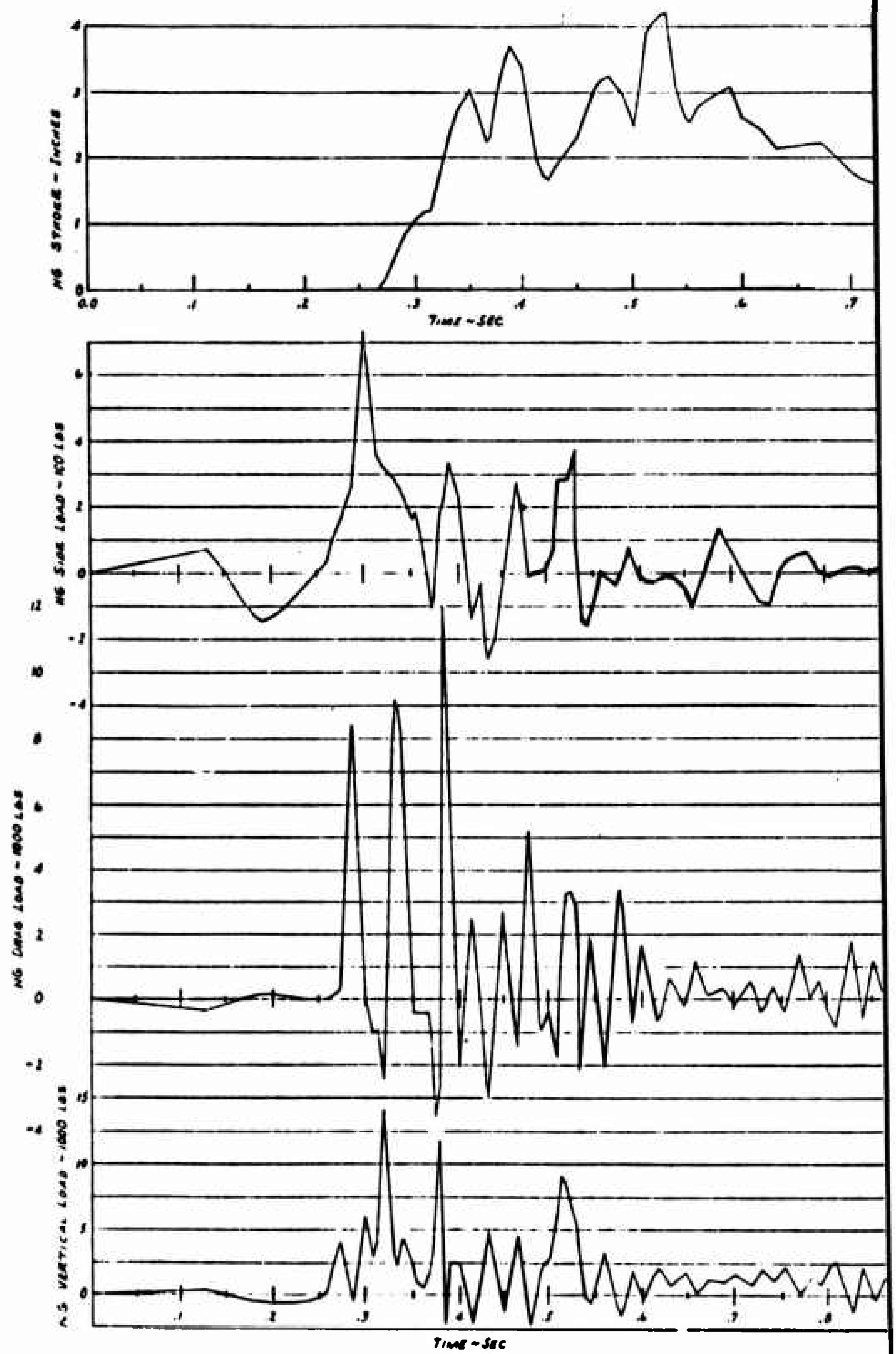

TIME HISTORIES OF LANDING GEAR
LOADS AND RESPONSE

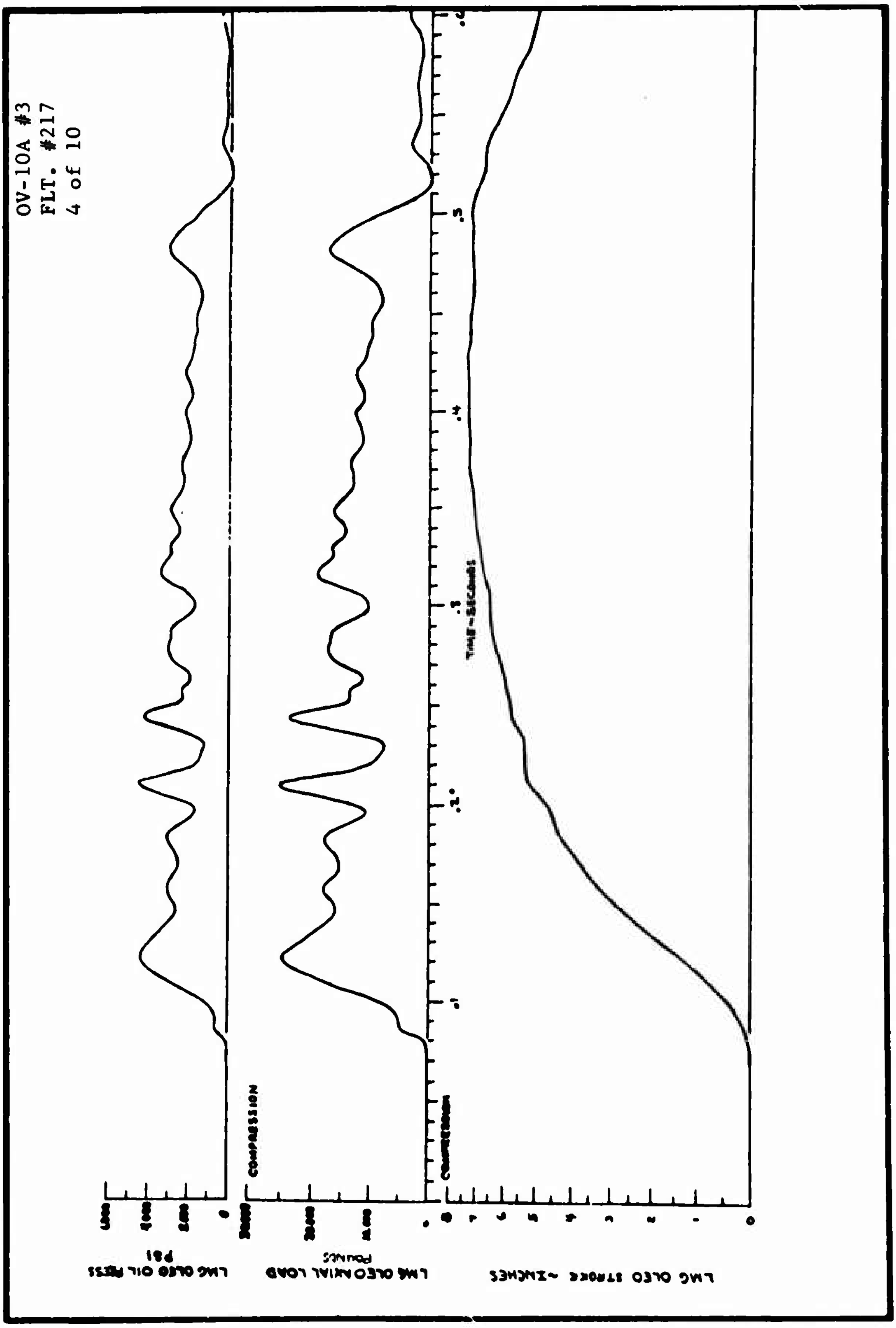

TIME HISTORIES OF LANDING GEAR
LOADS AND RESPONSE

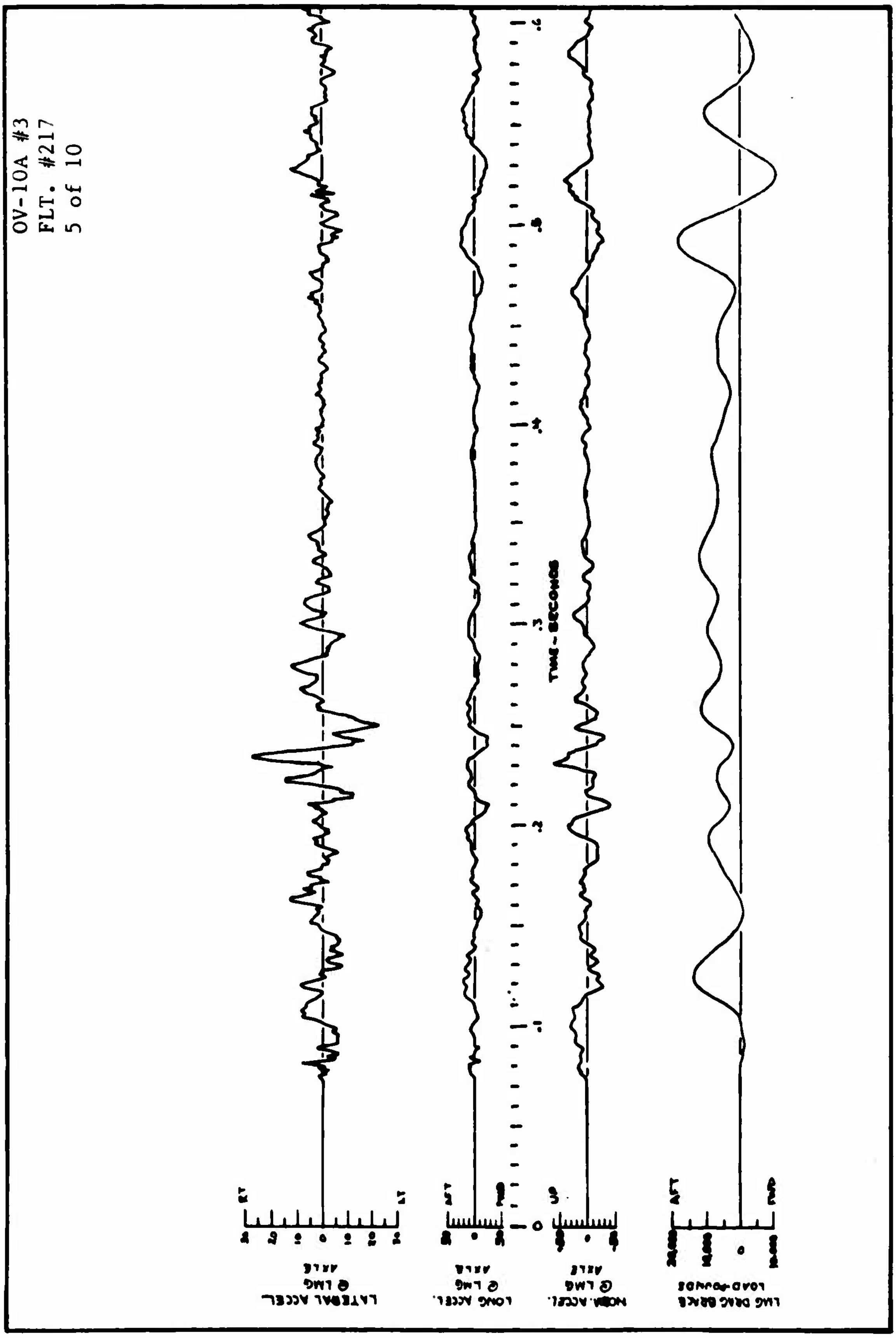

TIME HISTORIES OF LANDING GEAR LOADS AND RESPONSE

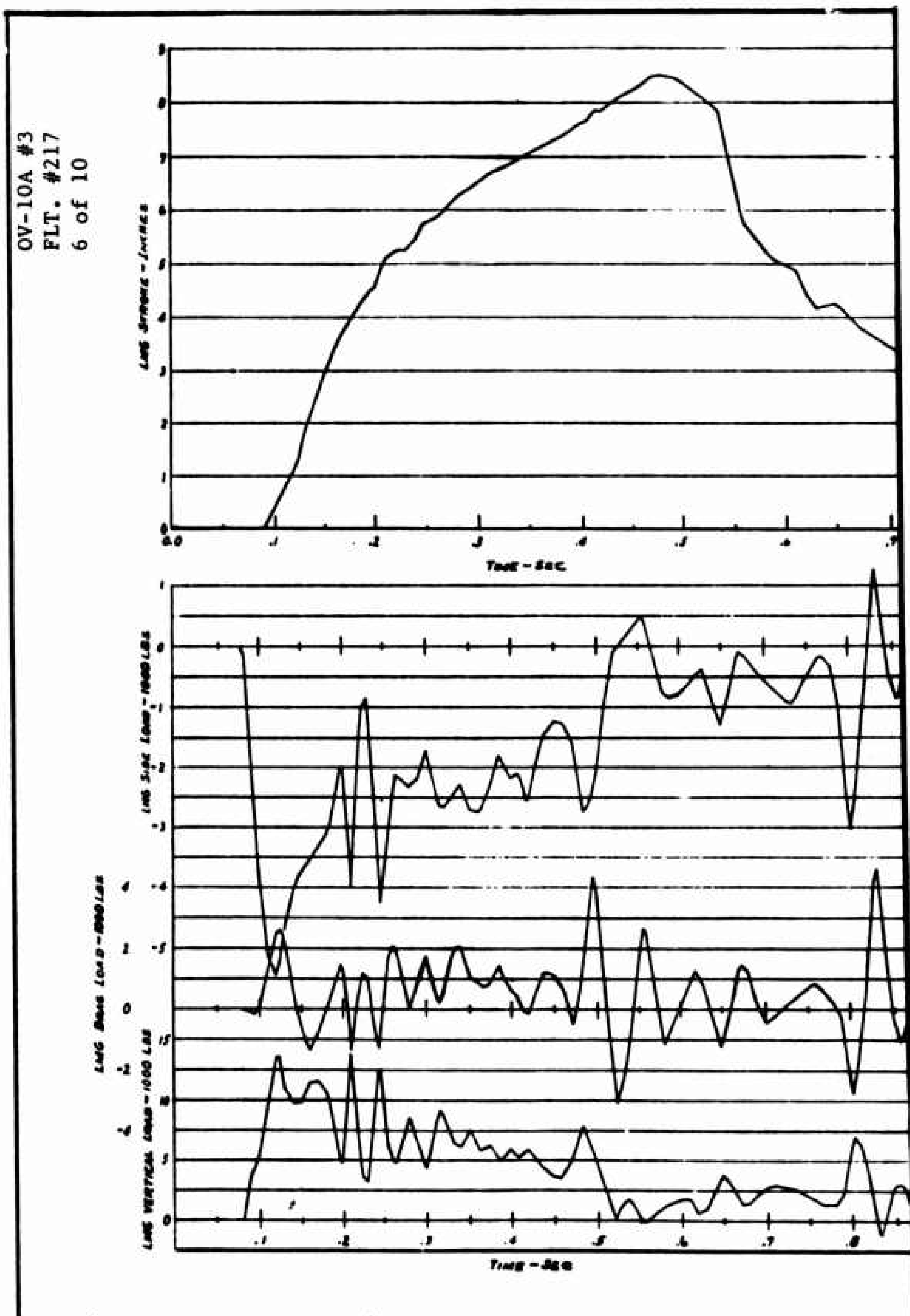

TIME HISTORIES OF LANDING GEAR
LOADS AND RESPONSE

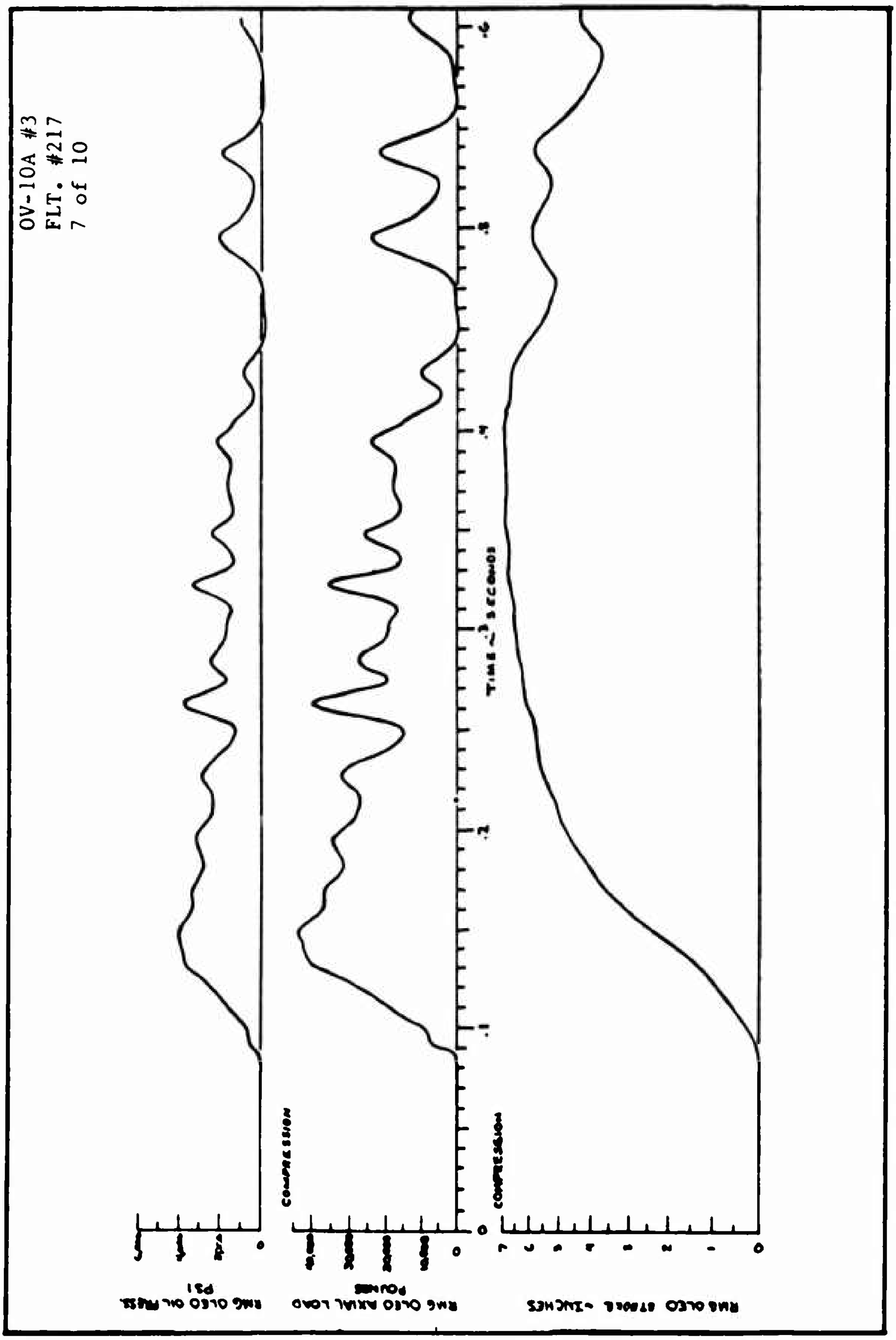

TIME HISTORIES OF LANDING GEAR
LOADS AND RESPONSE

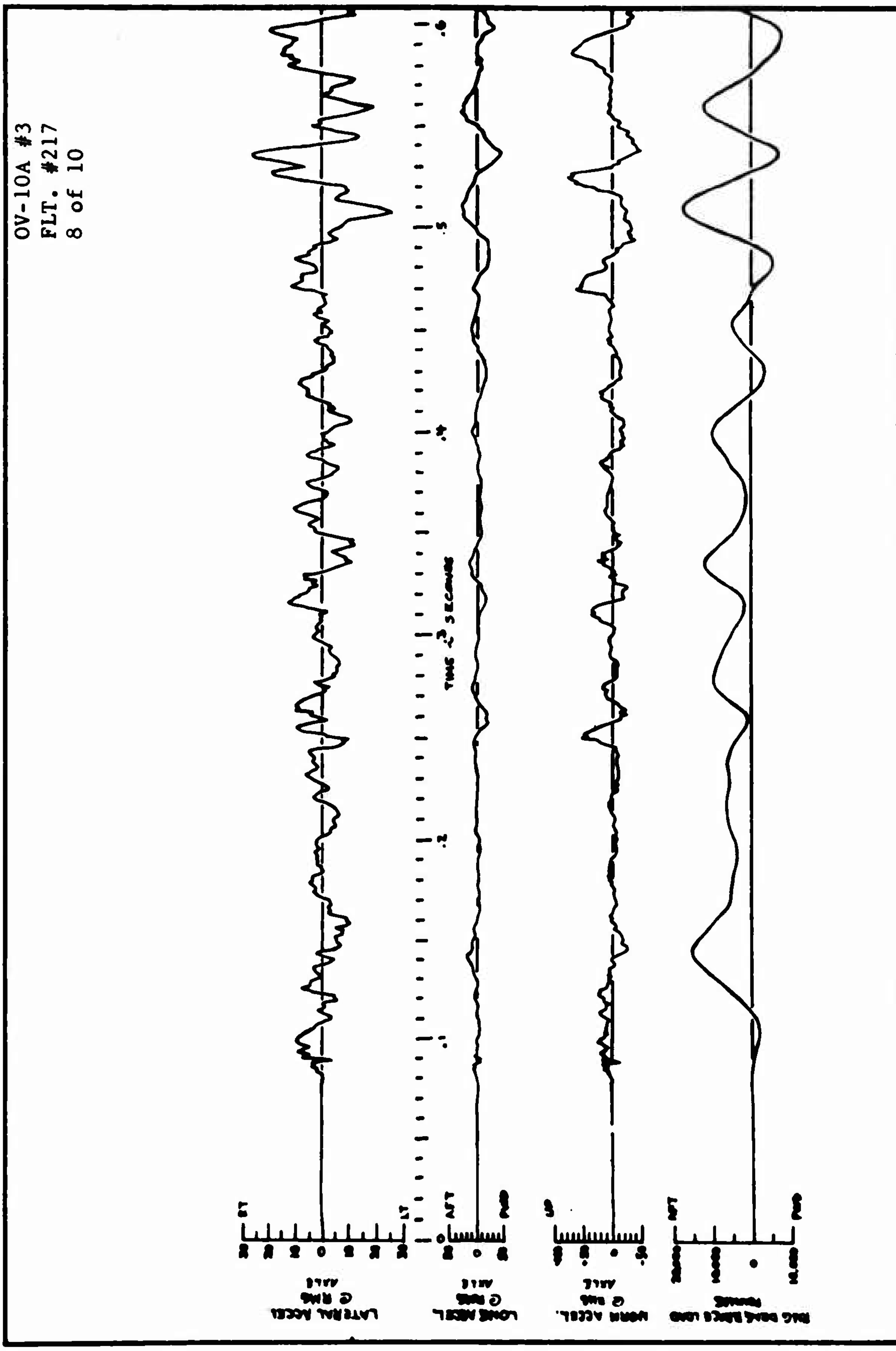

TIME HISTORIES OF LANDING GEAR
LOADS AND RESPONSE

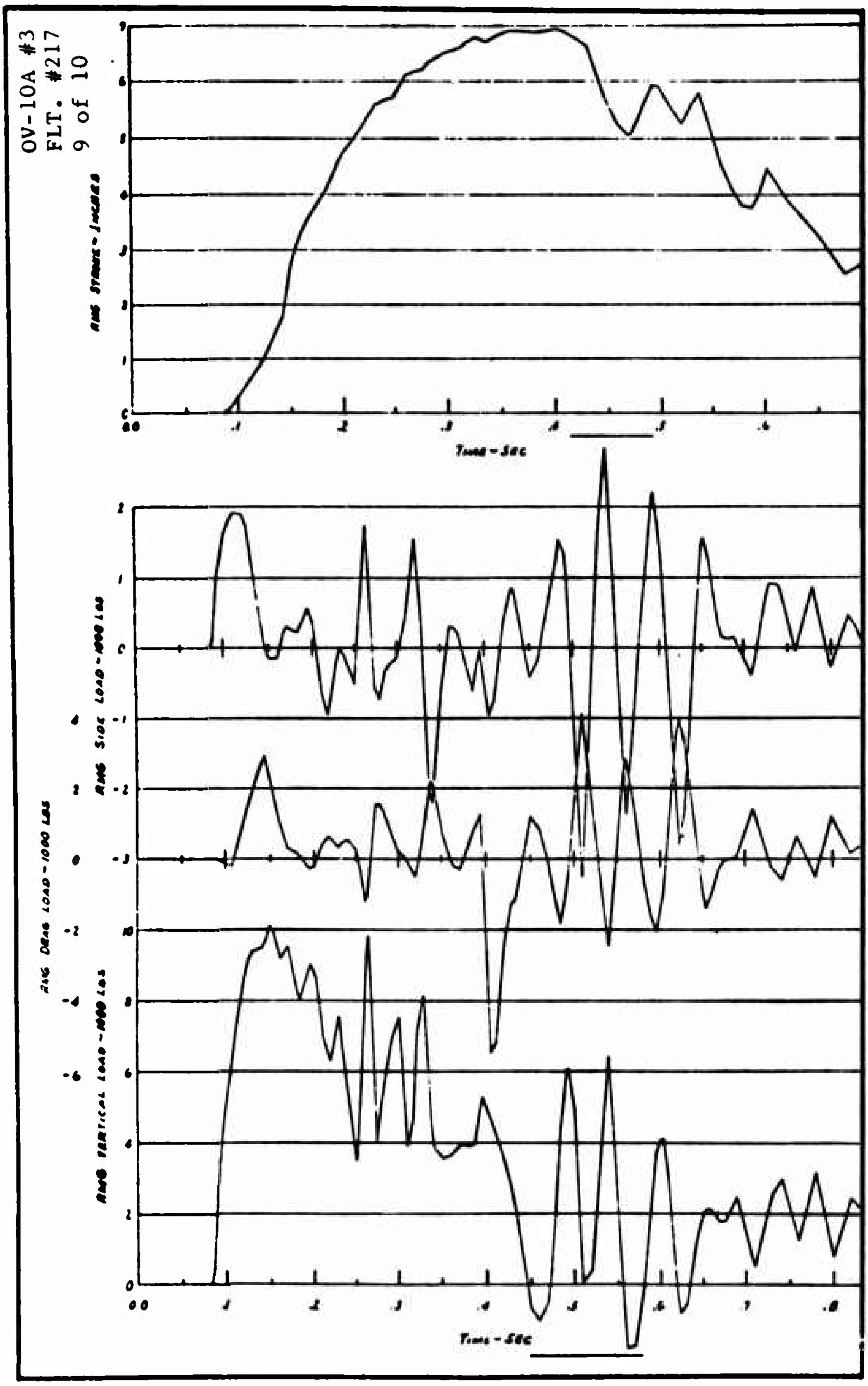

North American Aviation/Columbus
North American Rockwell

TIME HISTORIES OF LANDING GEAR
LOADS AND RESPONSE

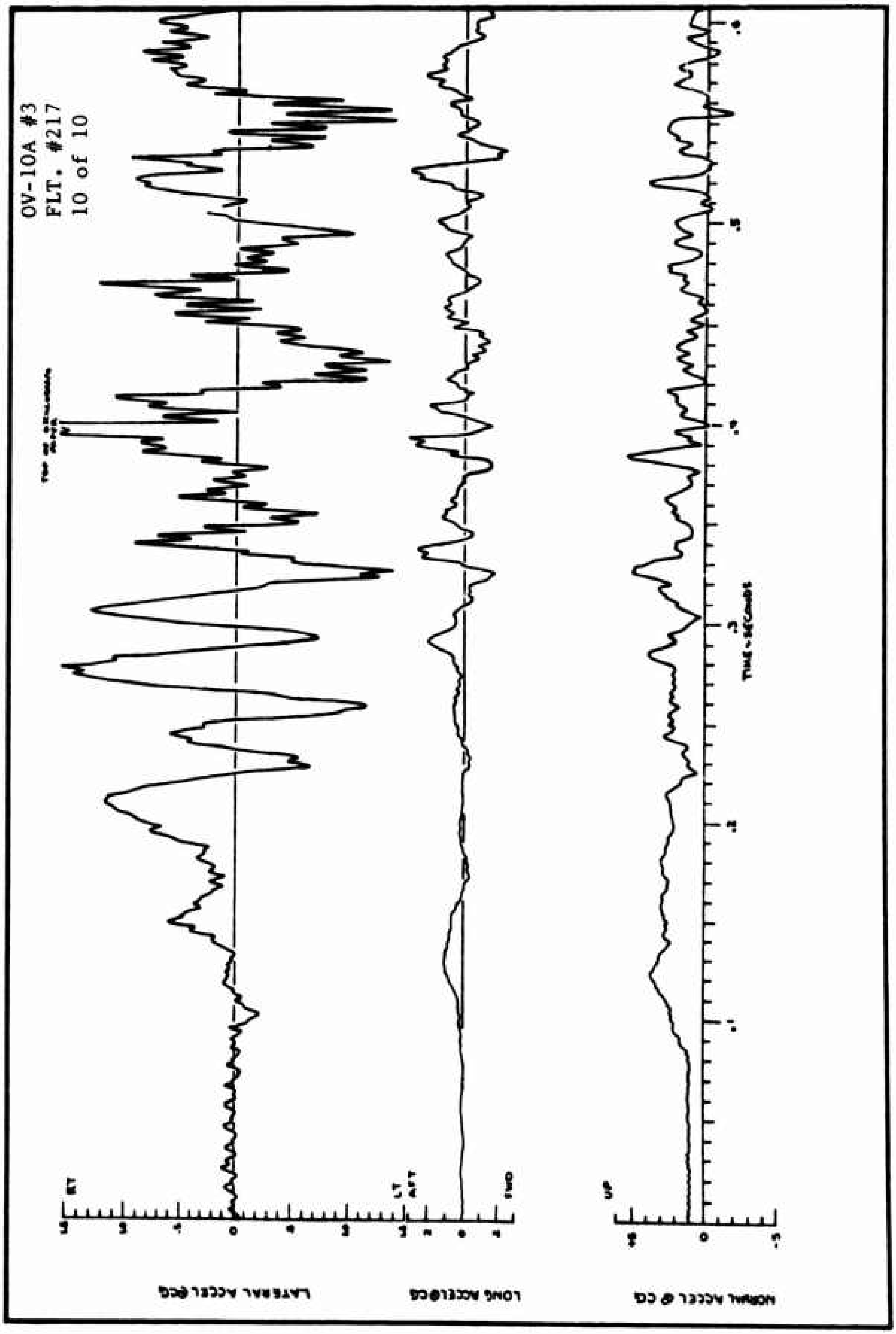

TIME HISTORIES OF LANDING GEAR
LOADS AND RESPONSE

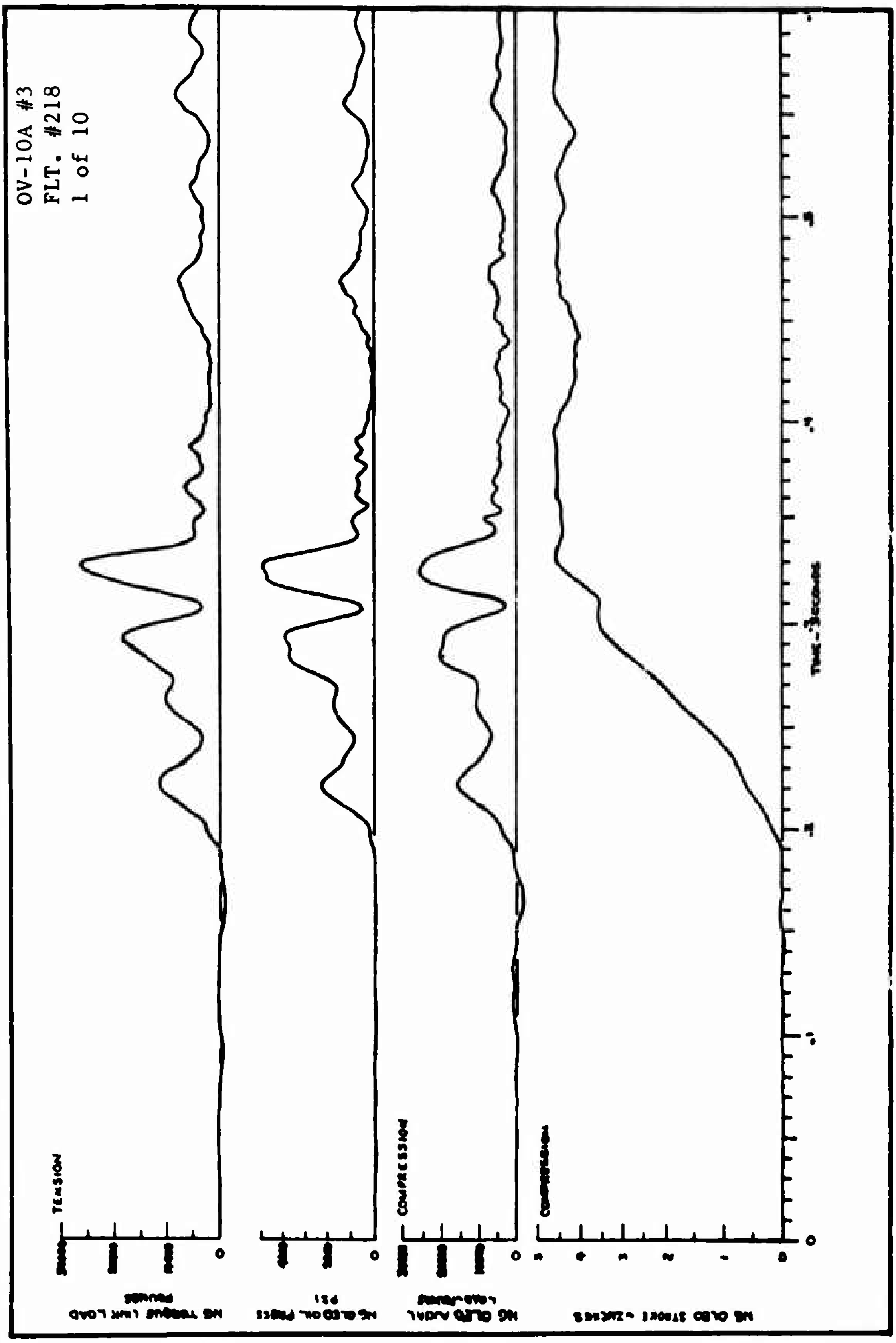

TIME HISTORIES OF LANDING GEAR
LOADS AND RESPONSE

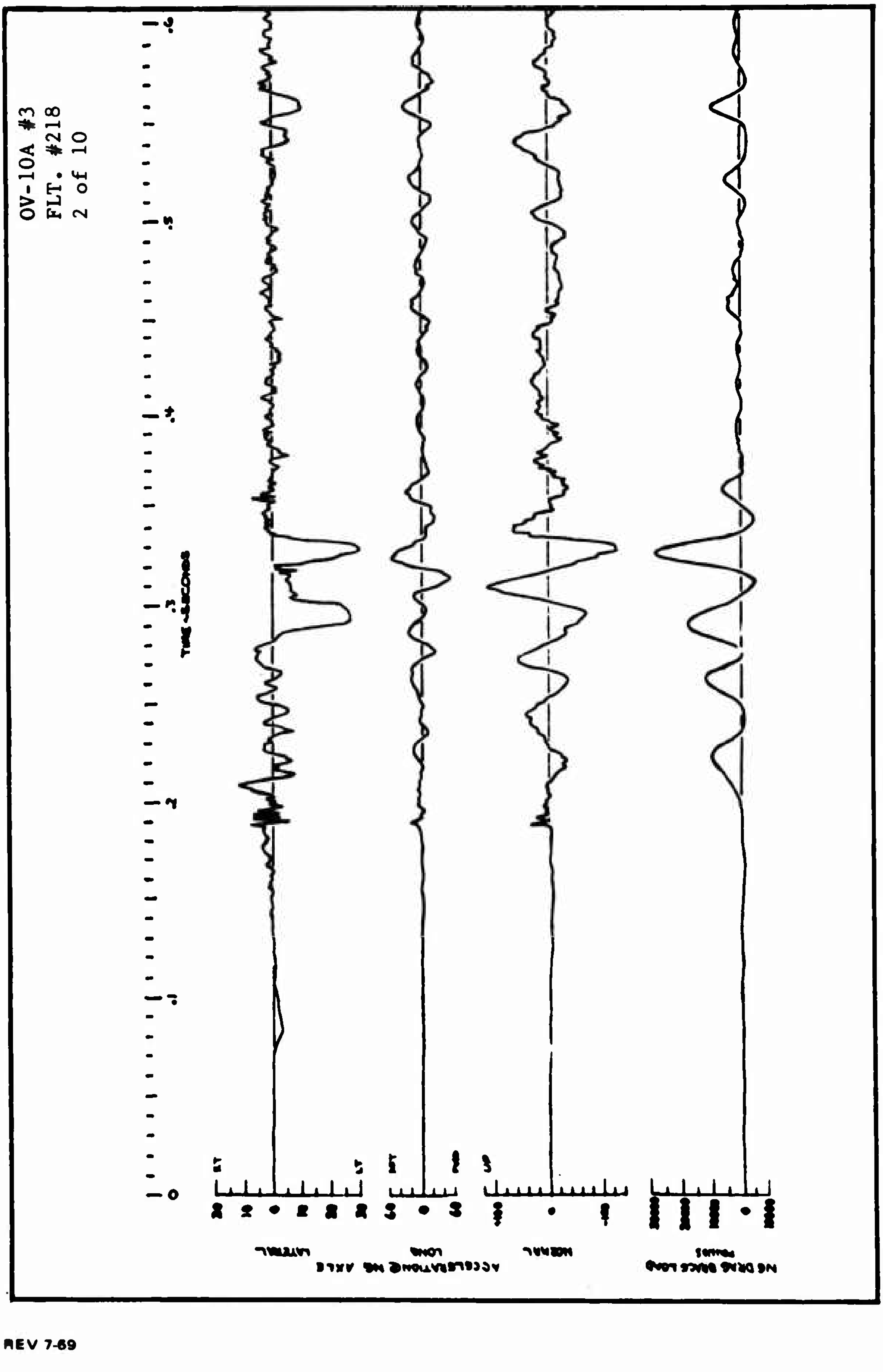

TIME HISTORIES OF LANDING GEAR
LOADS AND RESPONSE

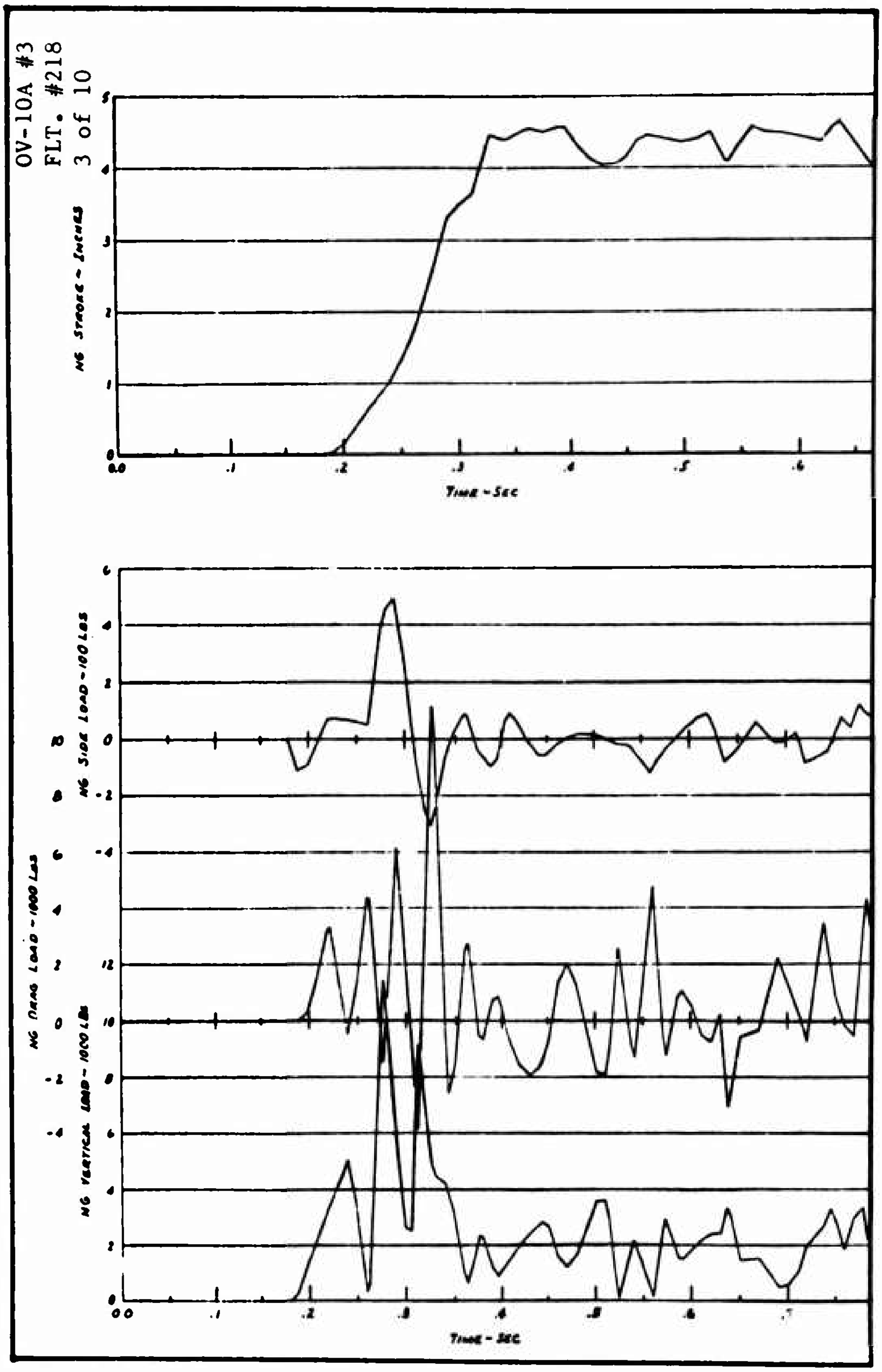

TIME HISTORIES OF LANDING GEAR
LOADS AND RESPONSE

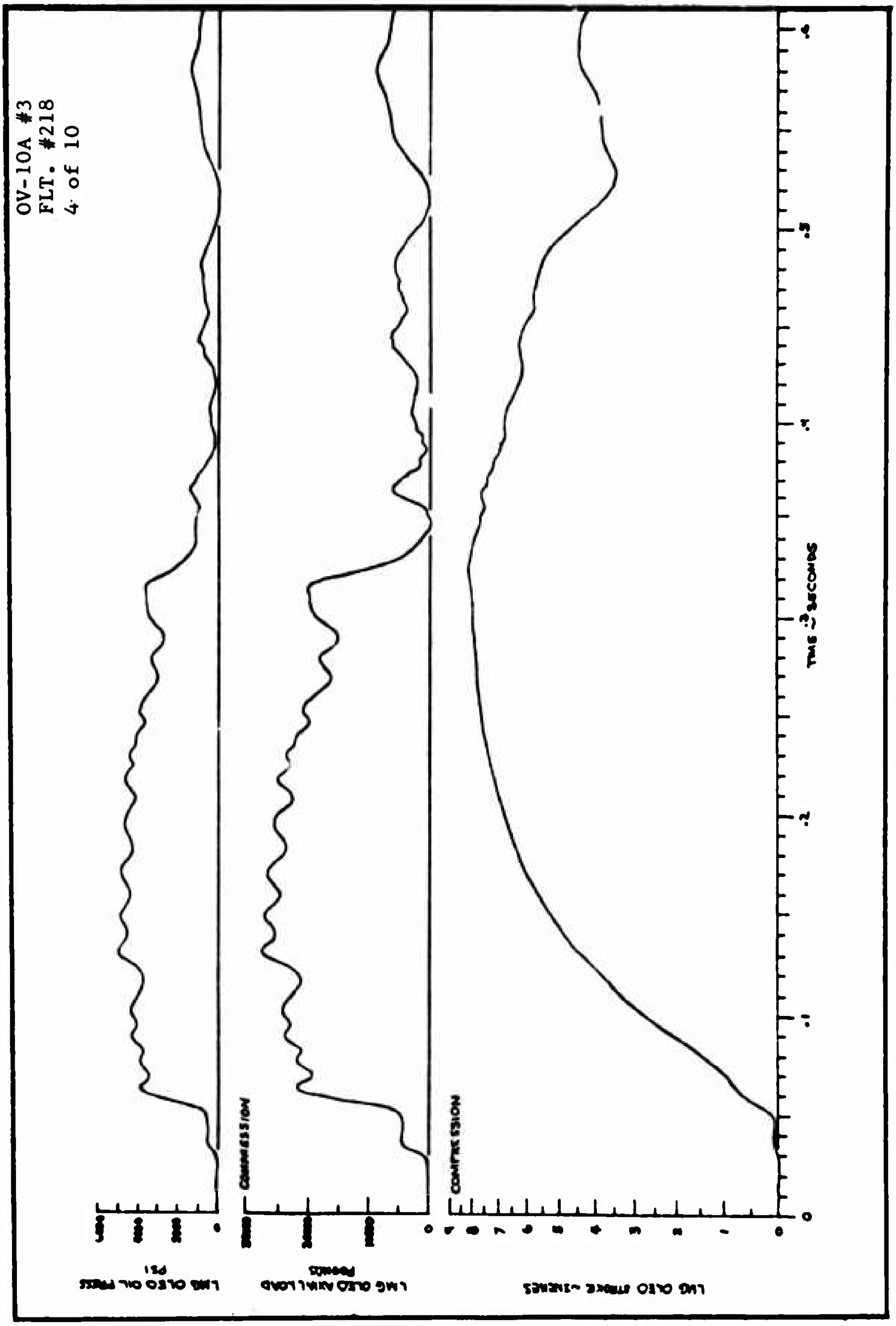

TIME HISTORIES OF LANDING GEAR
LOADS AND RESPONSE

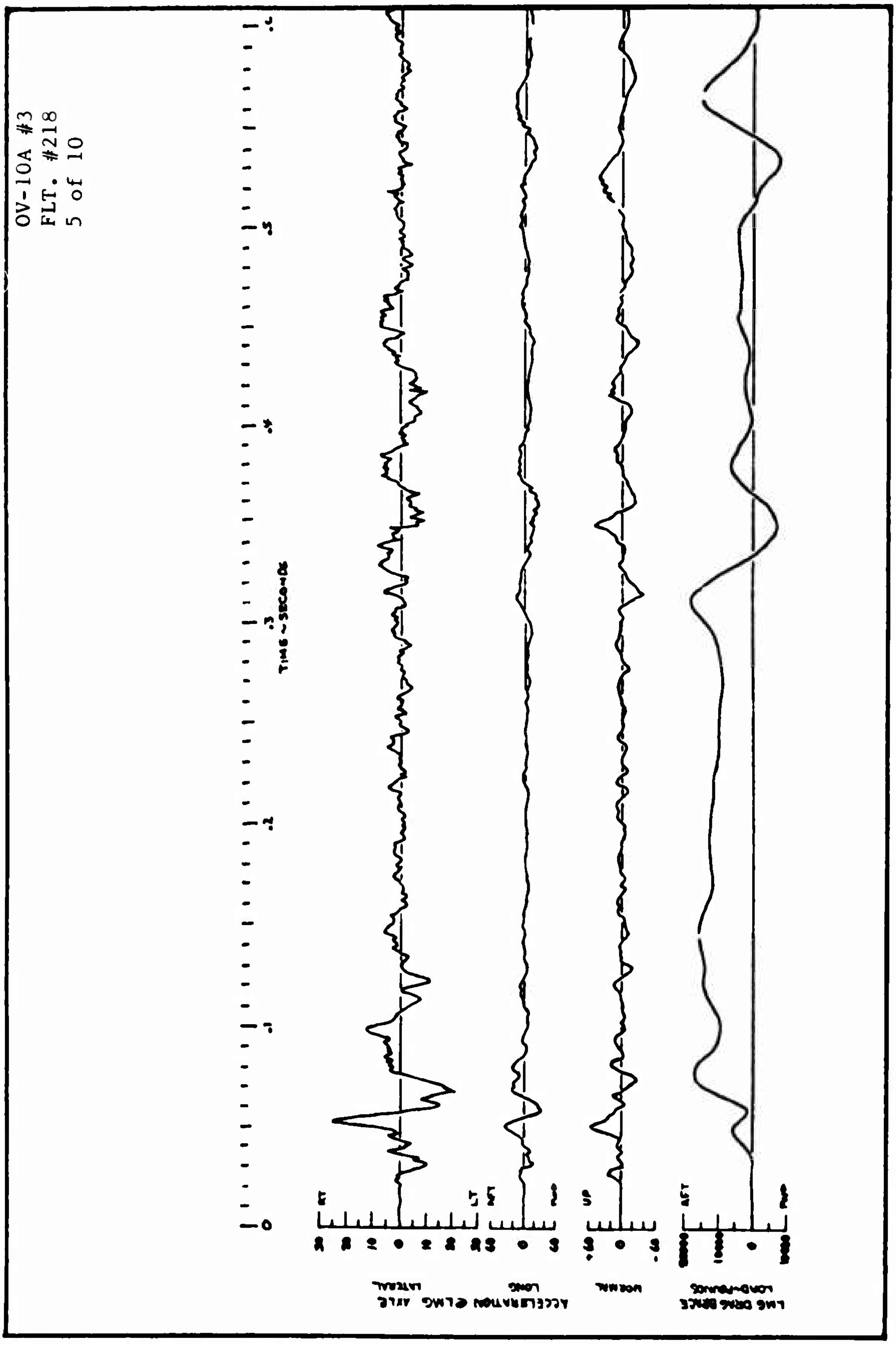

TIME HISTORIES OF LANDING GEAR
LOADS AND RESPONSE

OV-10A #3
FLT. #218
6 of 10

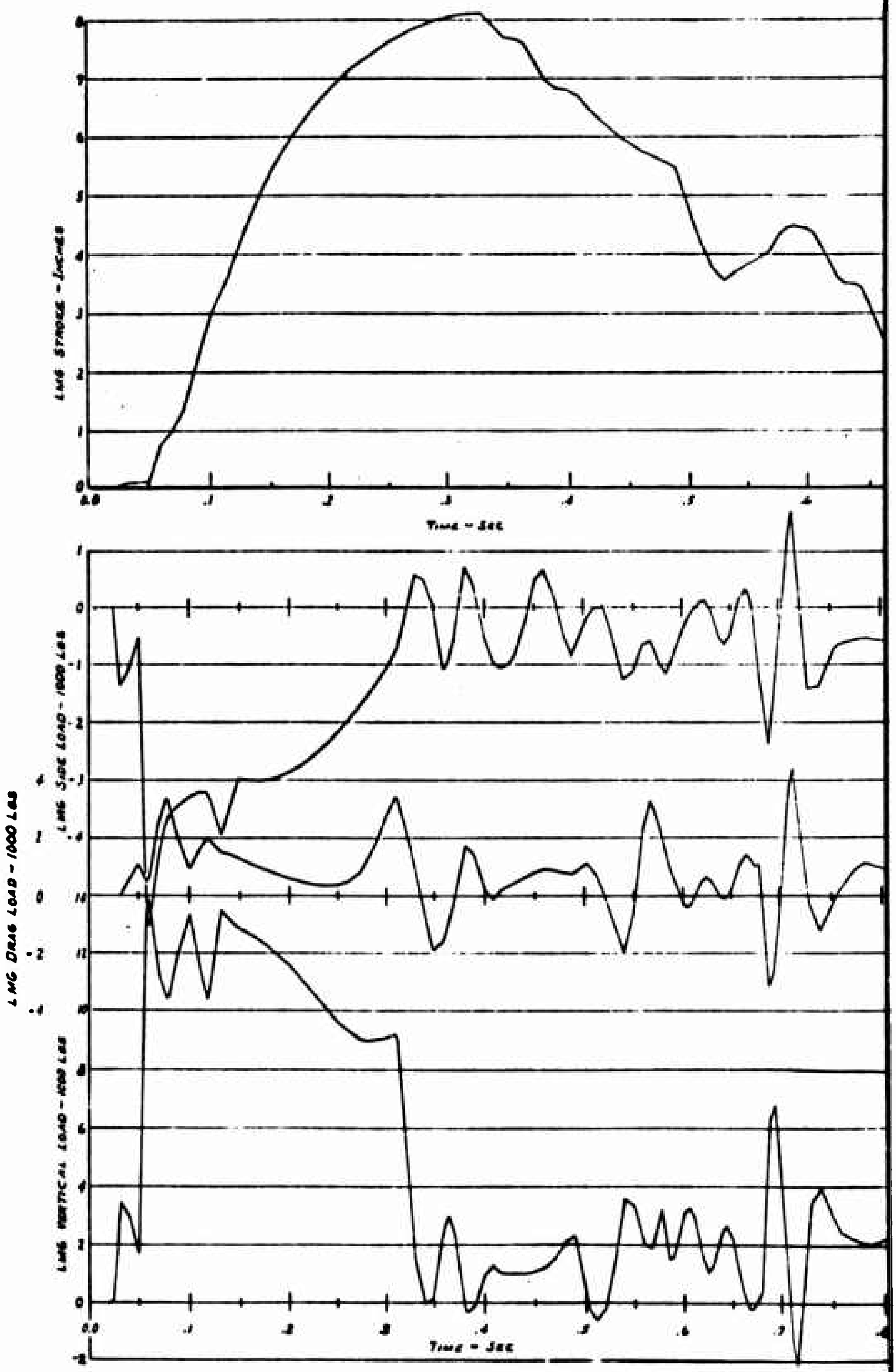

TIME HISTORIES OF LANDING GEAR
LOADS AND RESPONSE

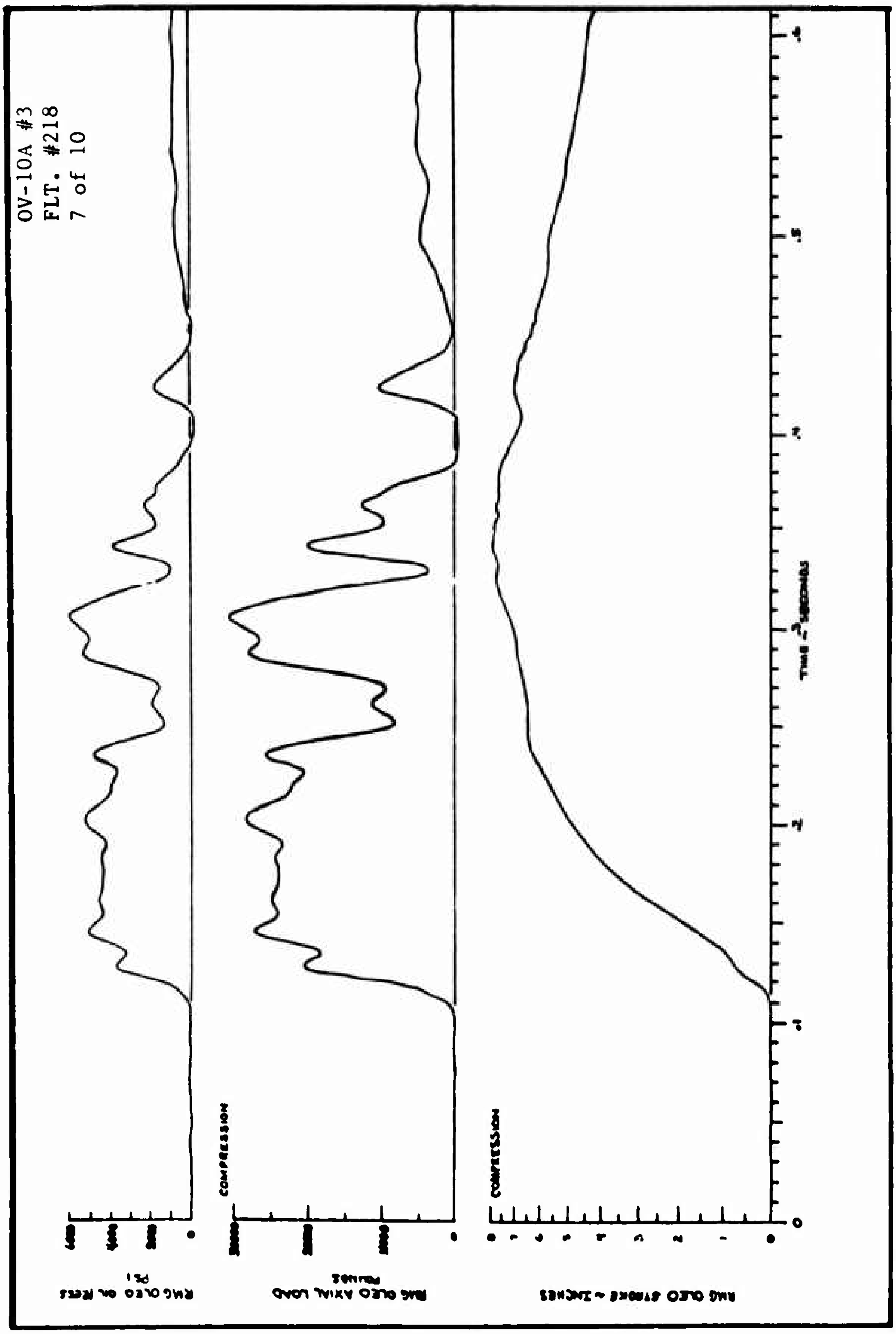

TIME HISTORIES OF LANDING GEAR
LOADS AND RESPONSE

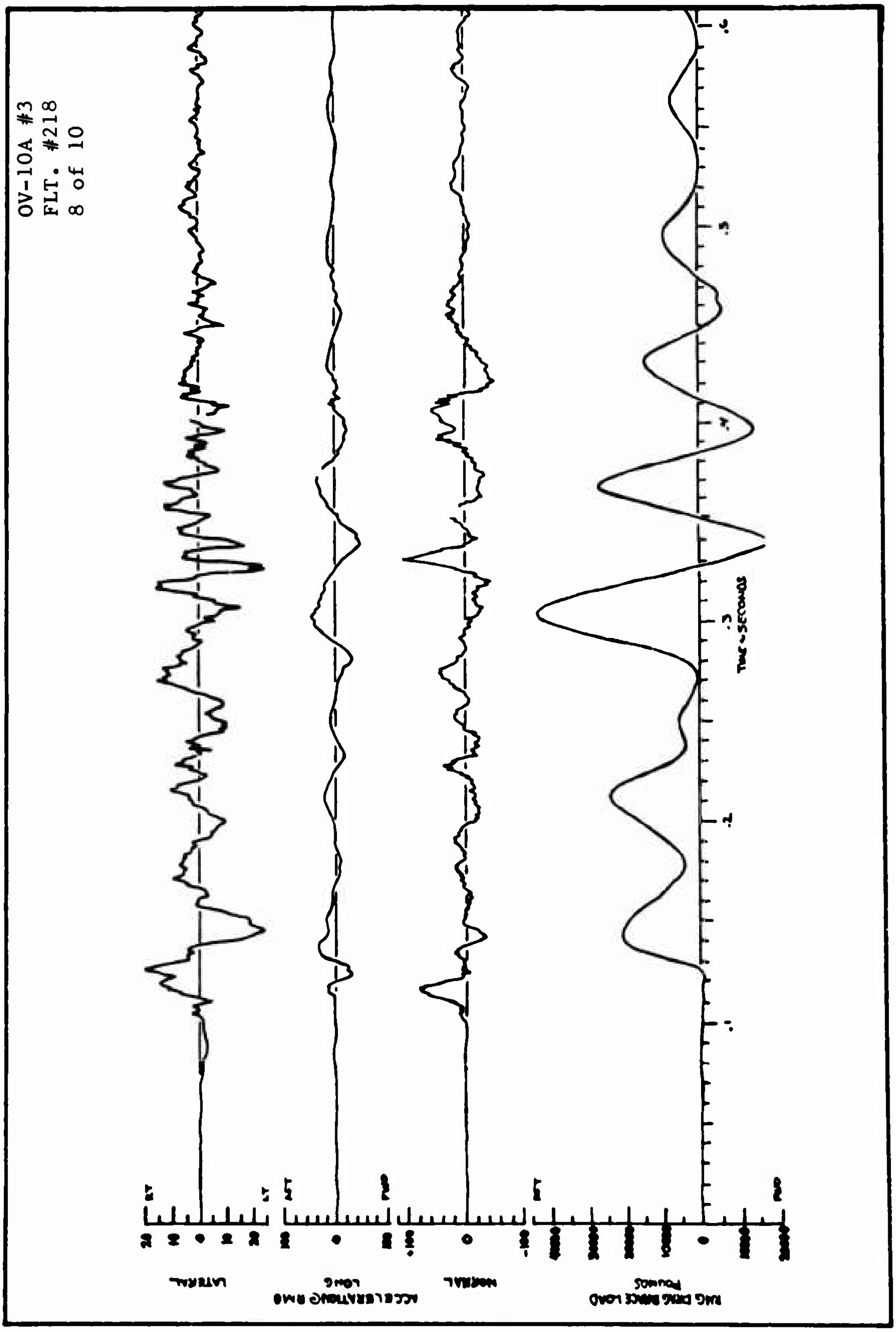

TIME HISTORIES OF LANDING GEAR
LOADS AND RESPONSE

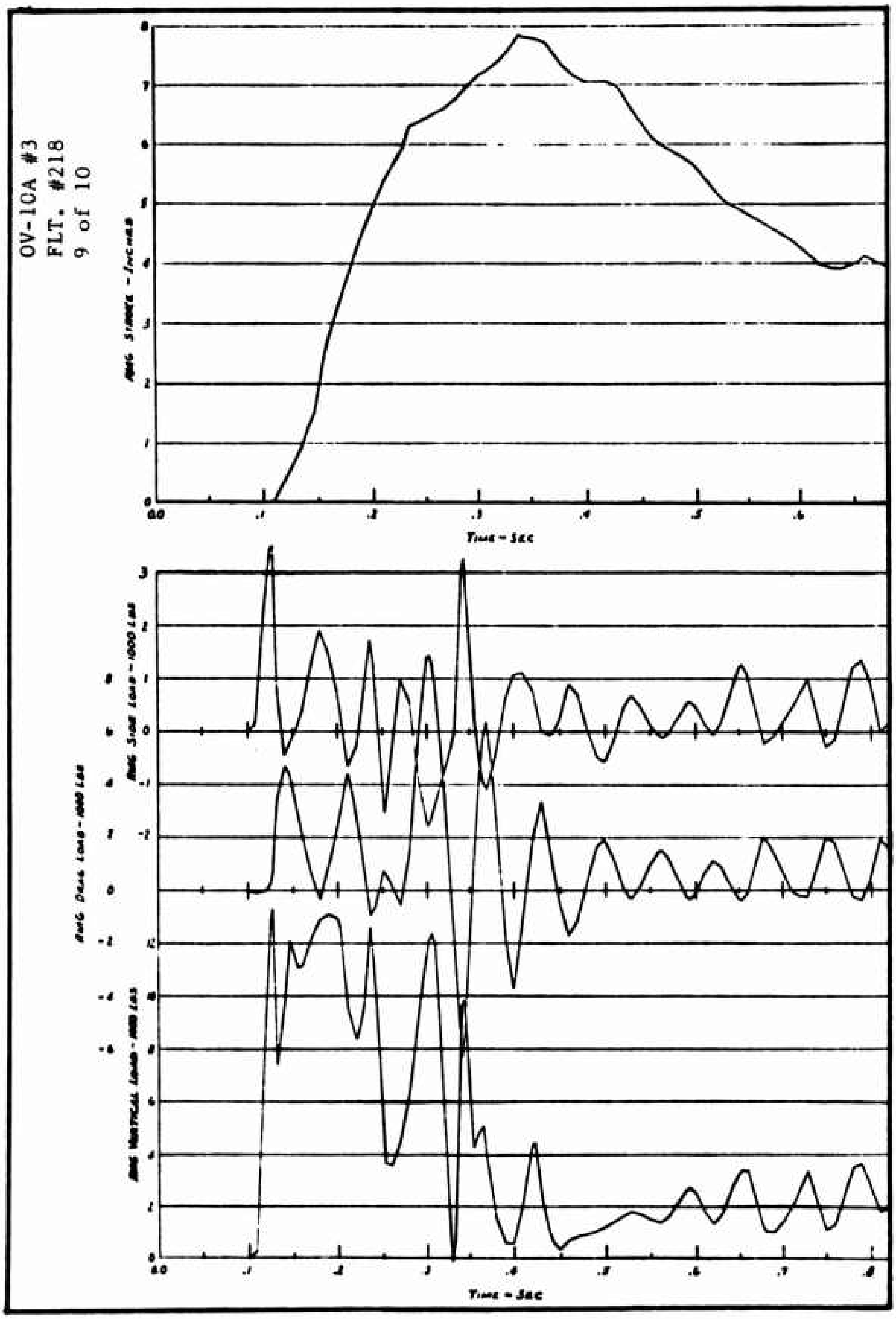

TIME HISTORIES OF LANDING GEAR
LOADS AND RESPONSE

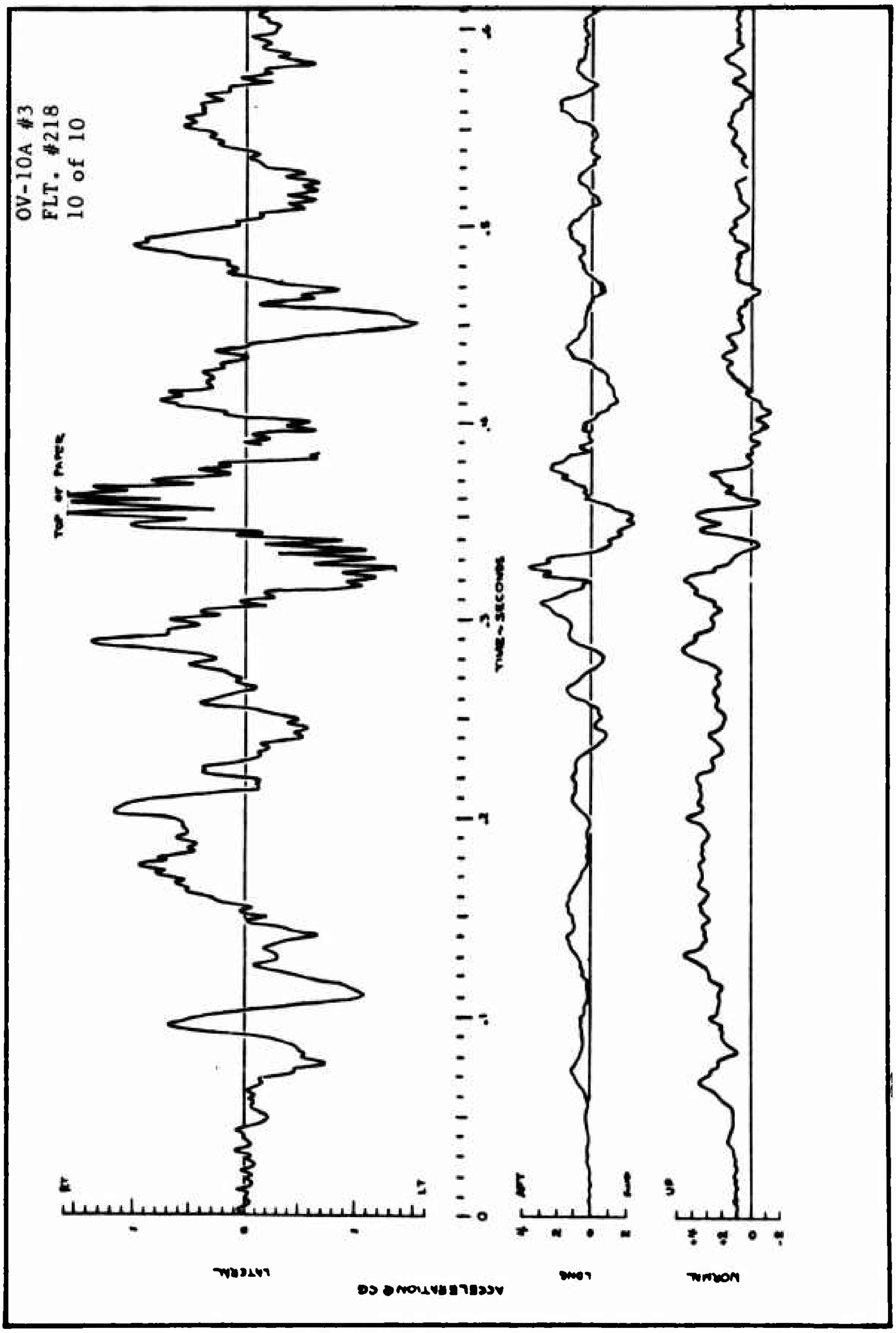

TIME HISTORIES OF LANDING GEAR
LOADS AND RESPONSE

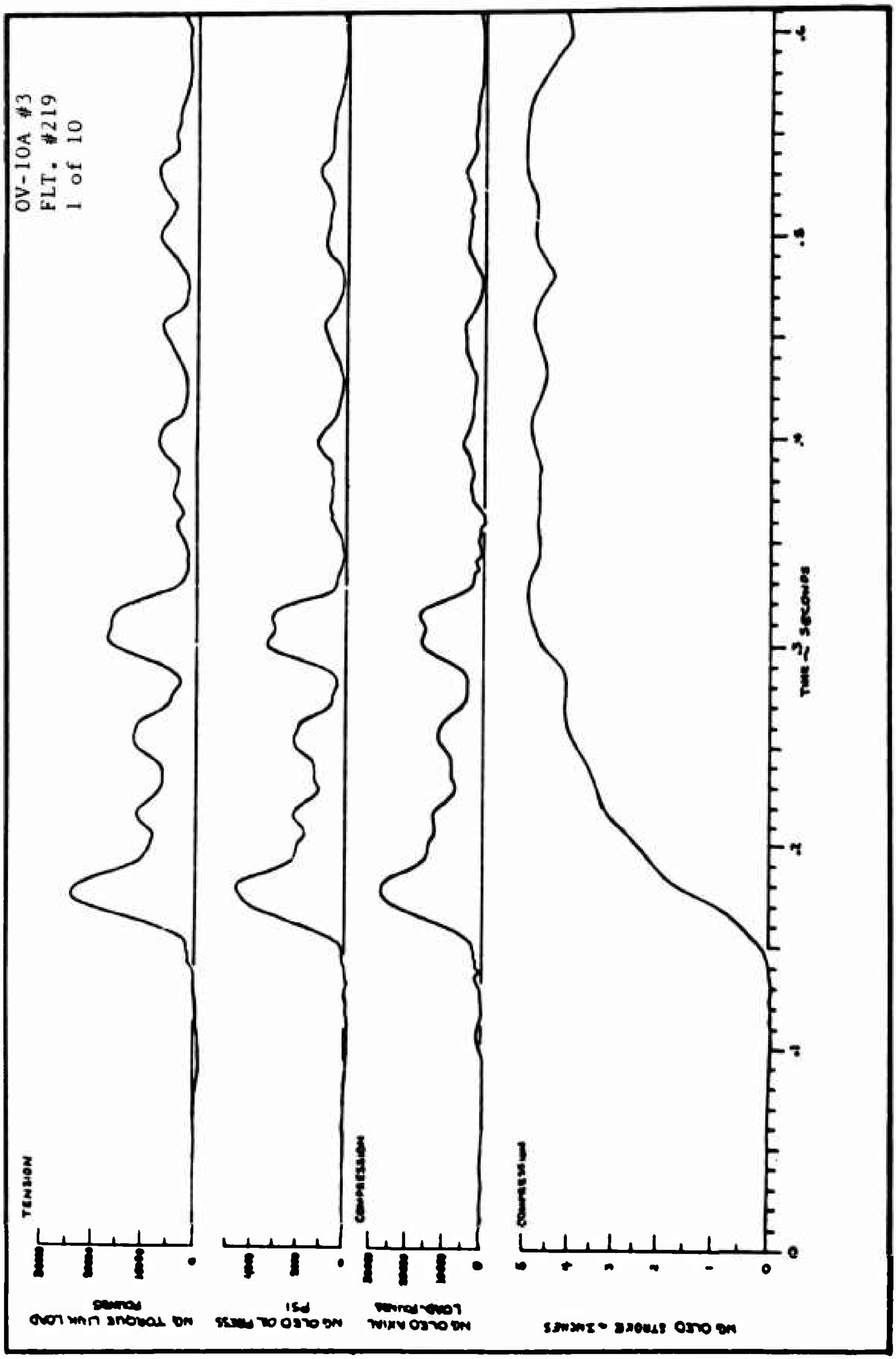

TIME HISTORIES OF LANDING GEAR
LOADS AND RESPONSE

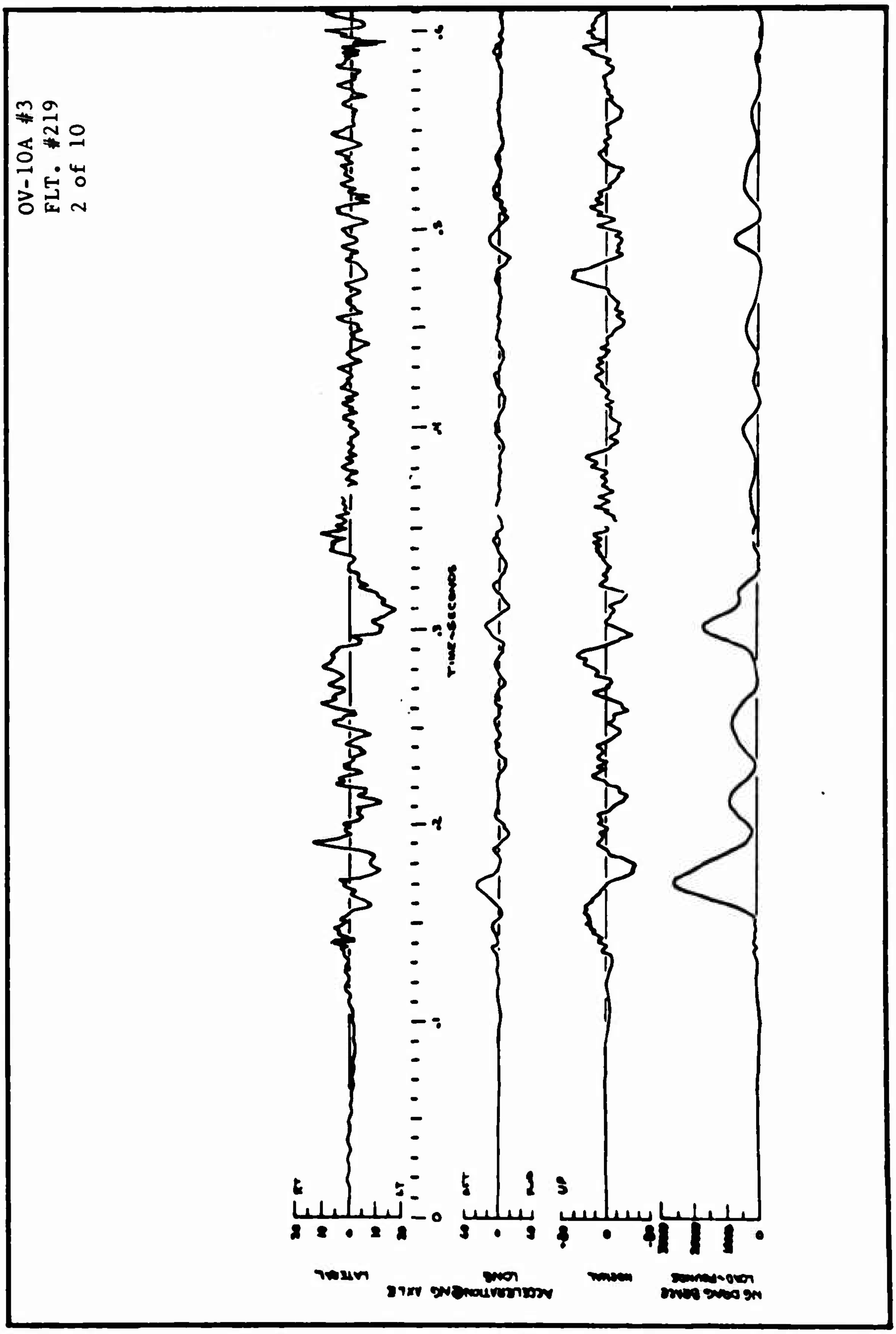

TIME HISTORIES OF LANDING GEAR
LOADS AND RESPONSE

OV-10A #3
FLT. #219
3 of 10

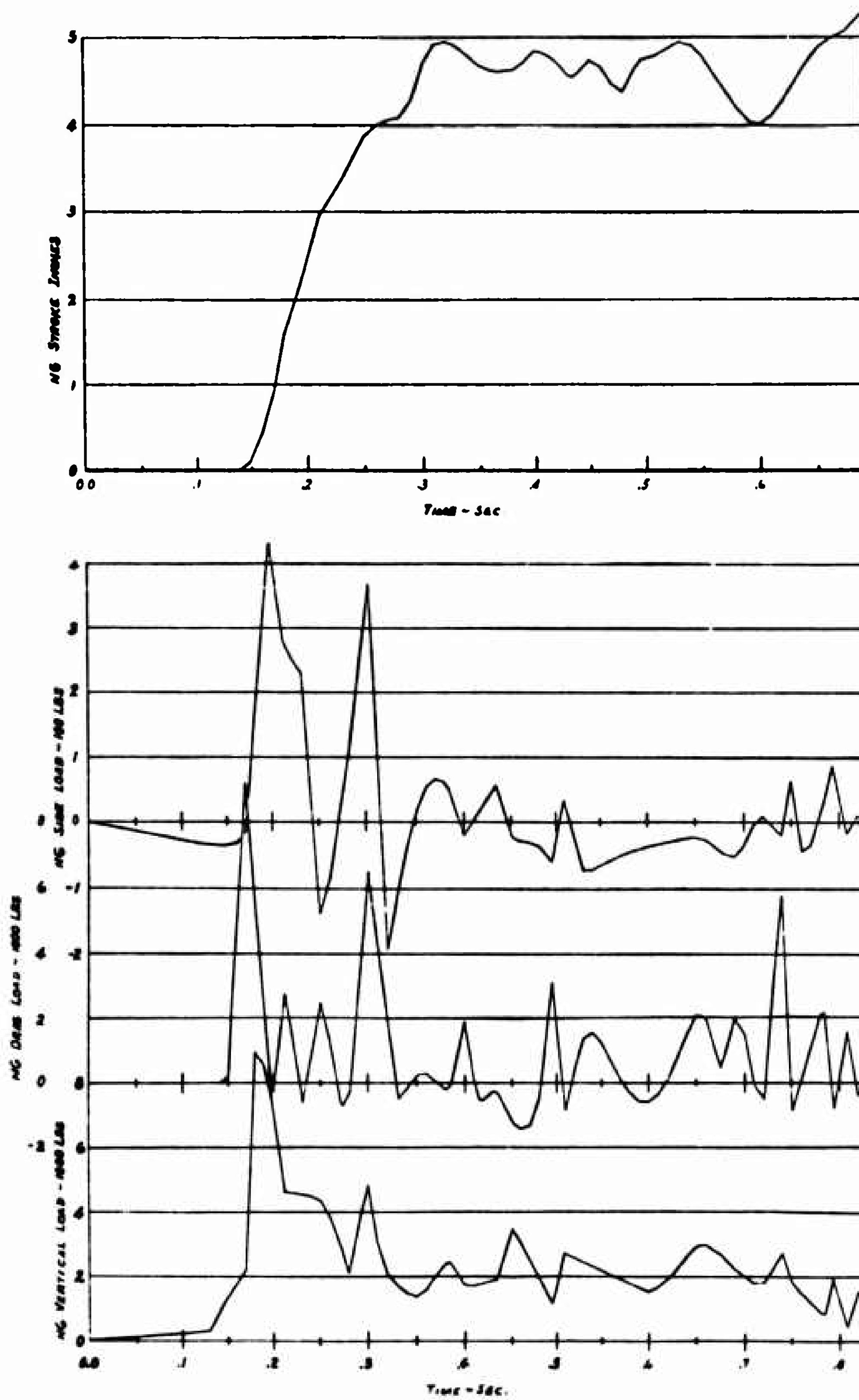

TIME HISTORIES OF LANDING GEAR
LOADS AND RESPONSE

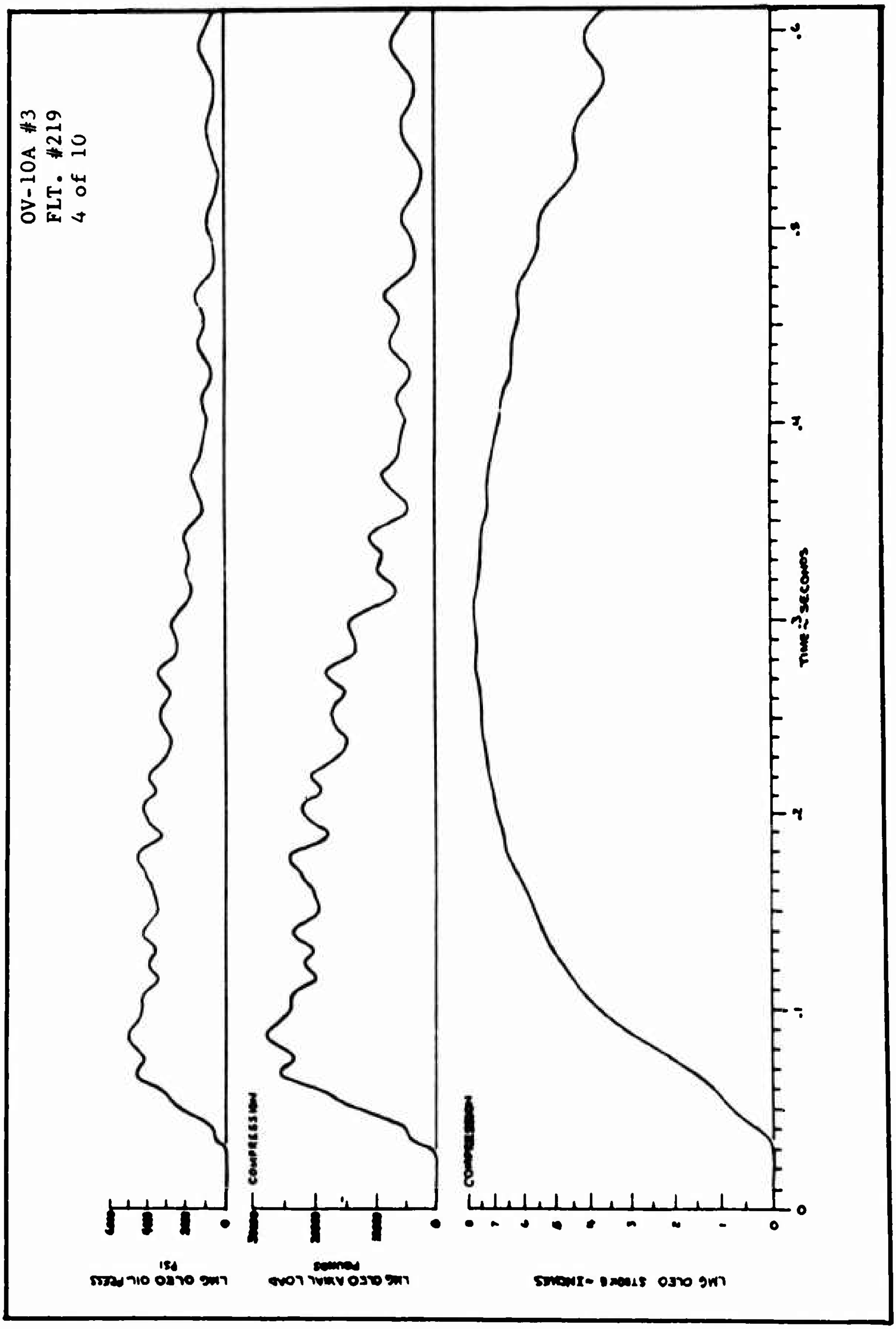

TIME HISTORIES OF LANDING GEAR
LOADS AND RESPONSE

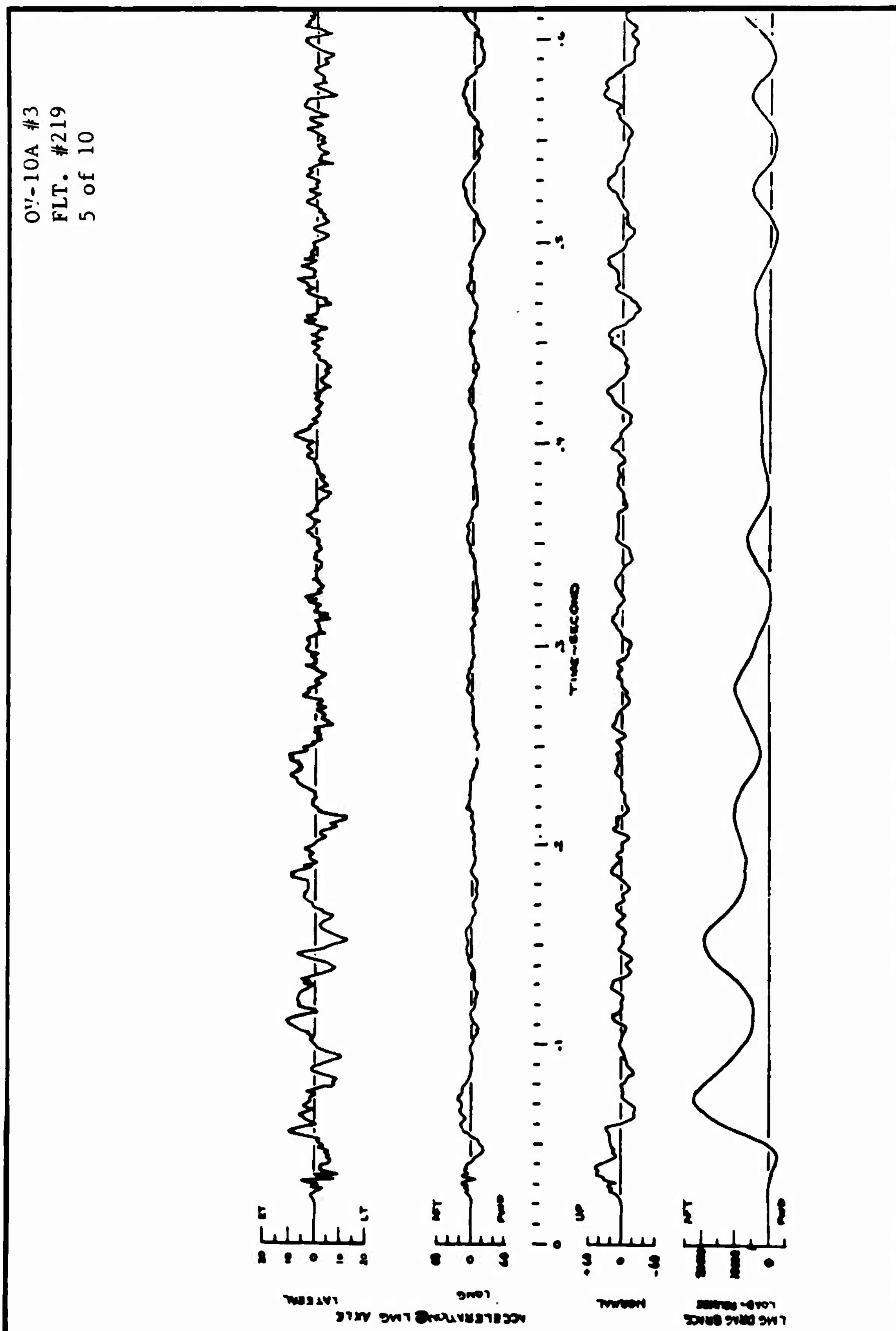

TIME HISTORIES OF LANDING GEAR
LOADS AND RESPONSE

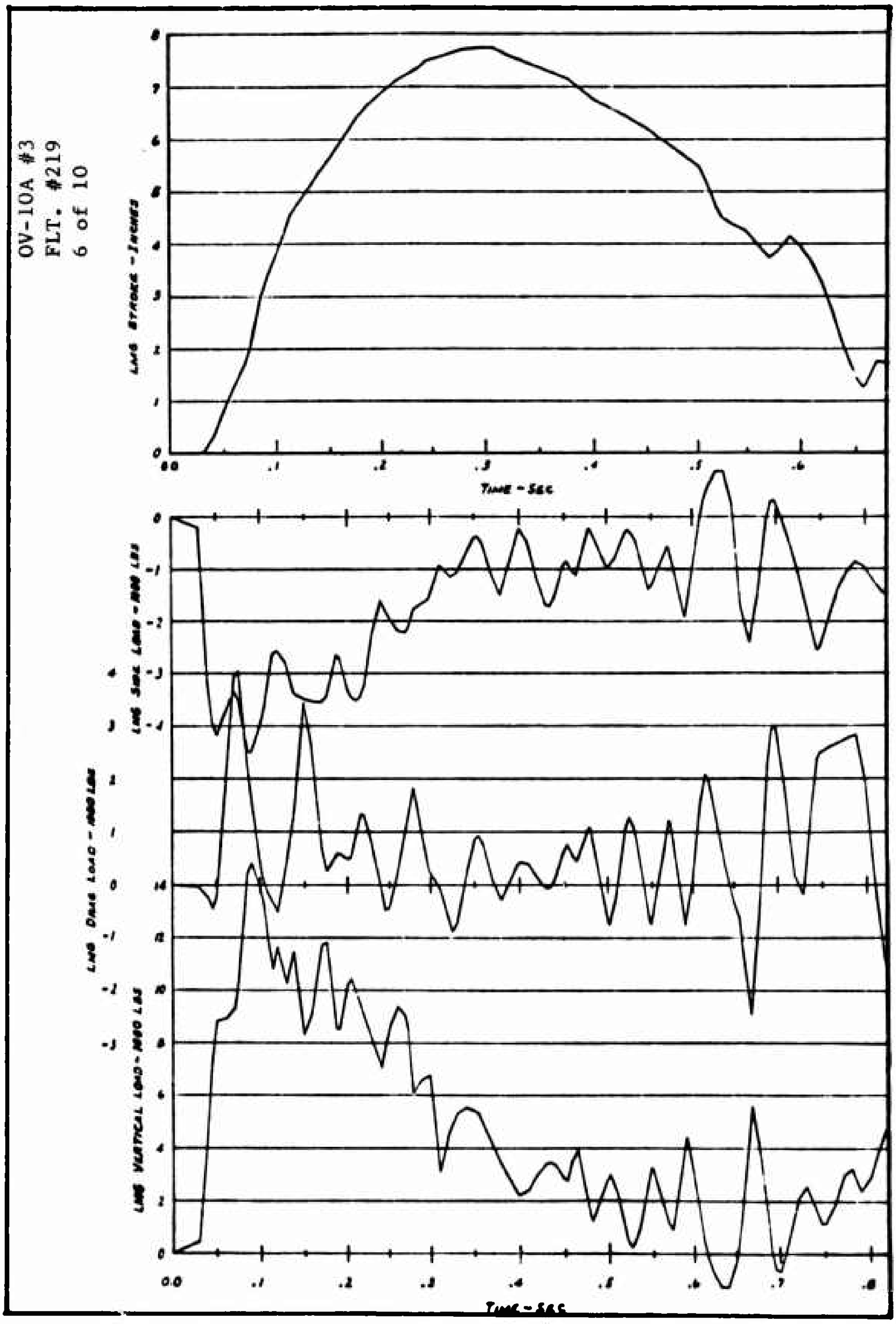

North American Aviation/Columbus
North American Rockwell

TIME HISTORIES OF LANDING GEAR
LOADS AND RESPONSE

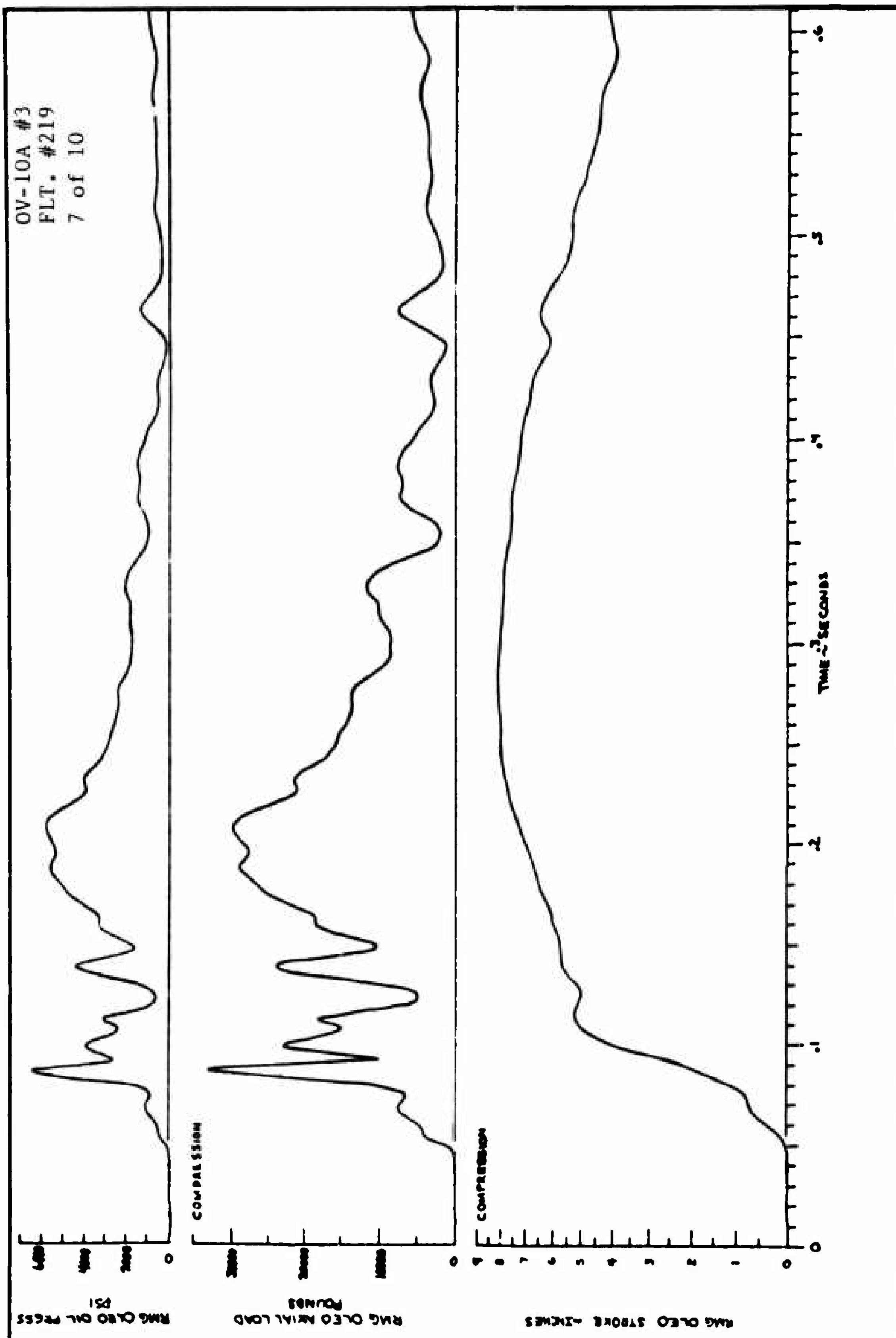

FORM 351-F REV 7-69

TIME HISTORIES OF LANDING GEAR
LOADS AND RESPONSE

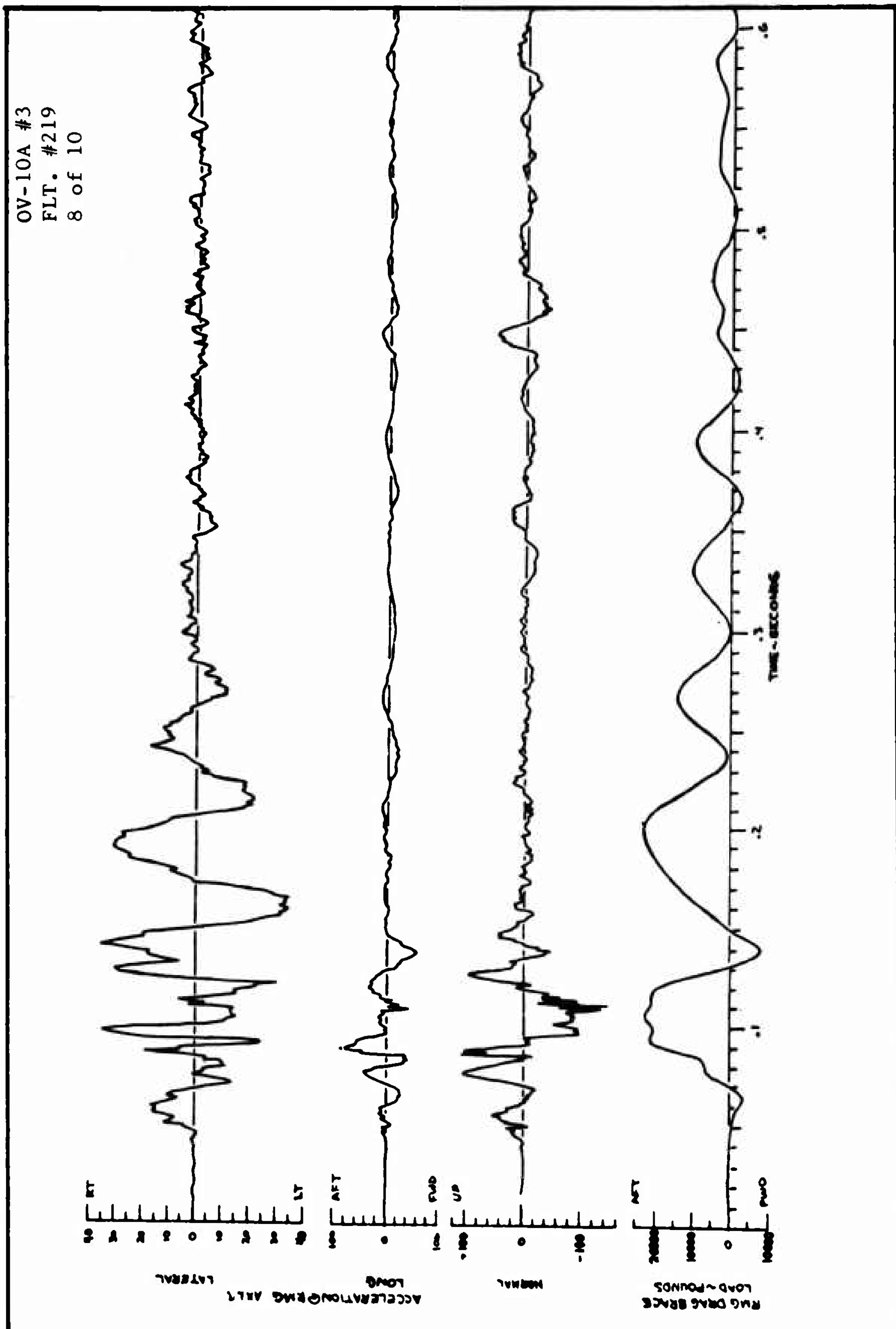

TIME HISTORIES OF LANDING GEAR
LOADS AND RESPONSE

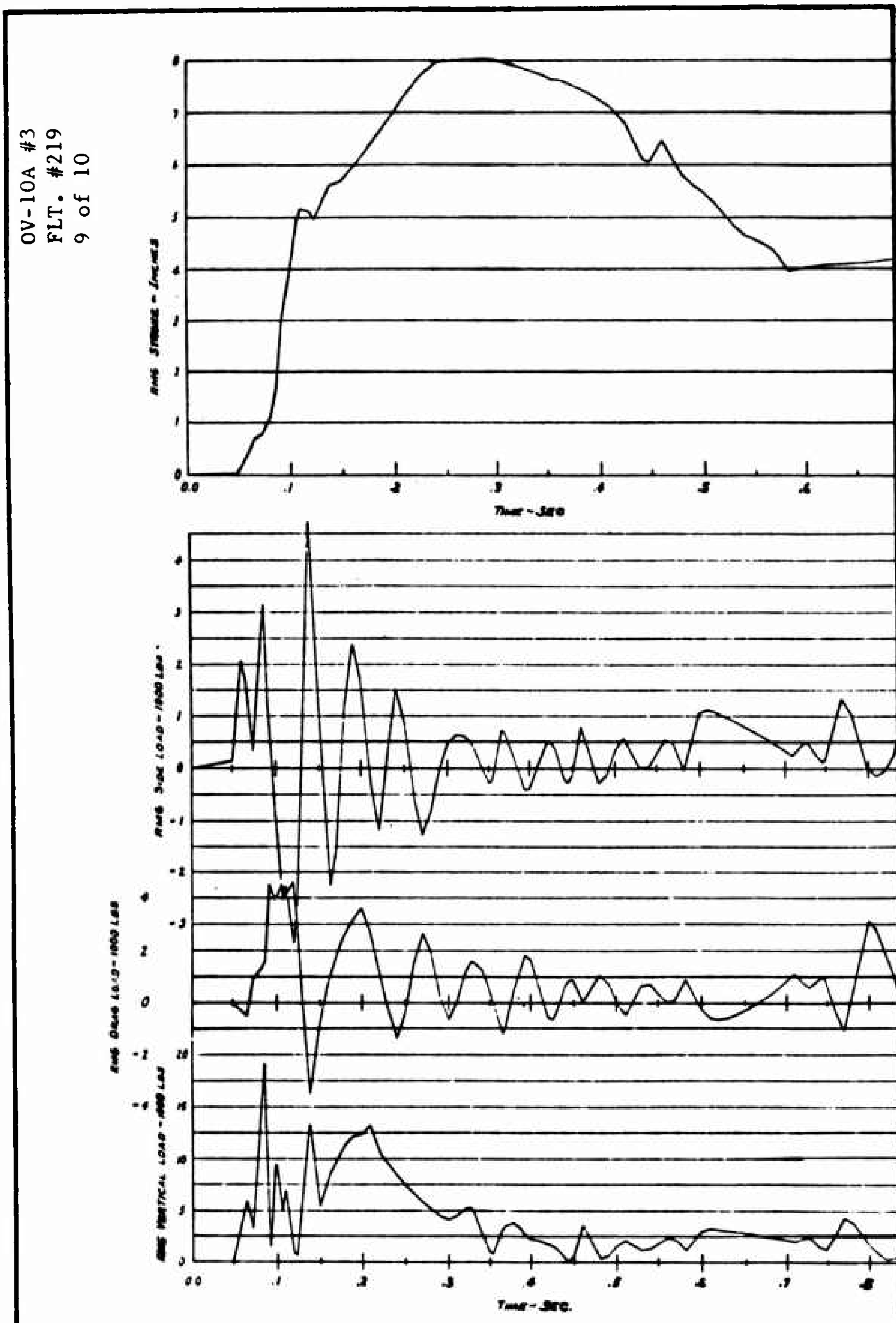

TIME HISTORIES OF LANDING GEAR
LOADS AND RESPONSE

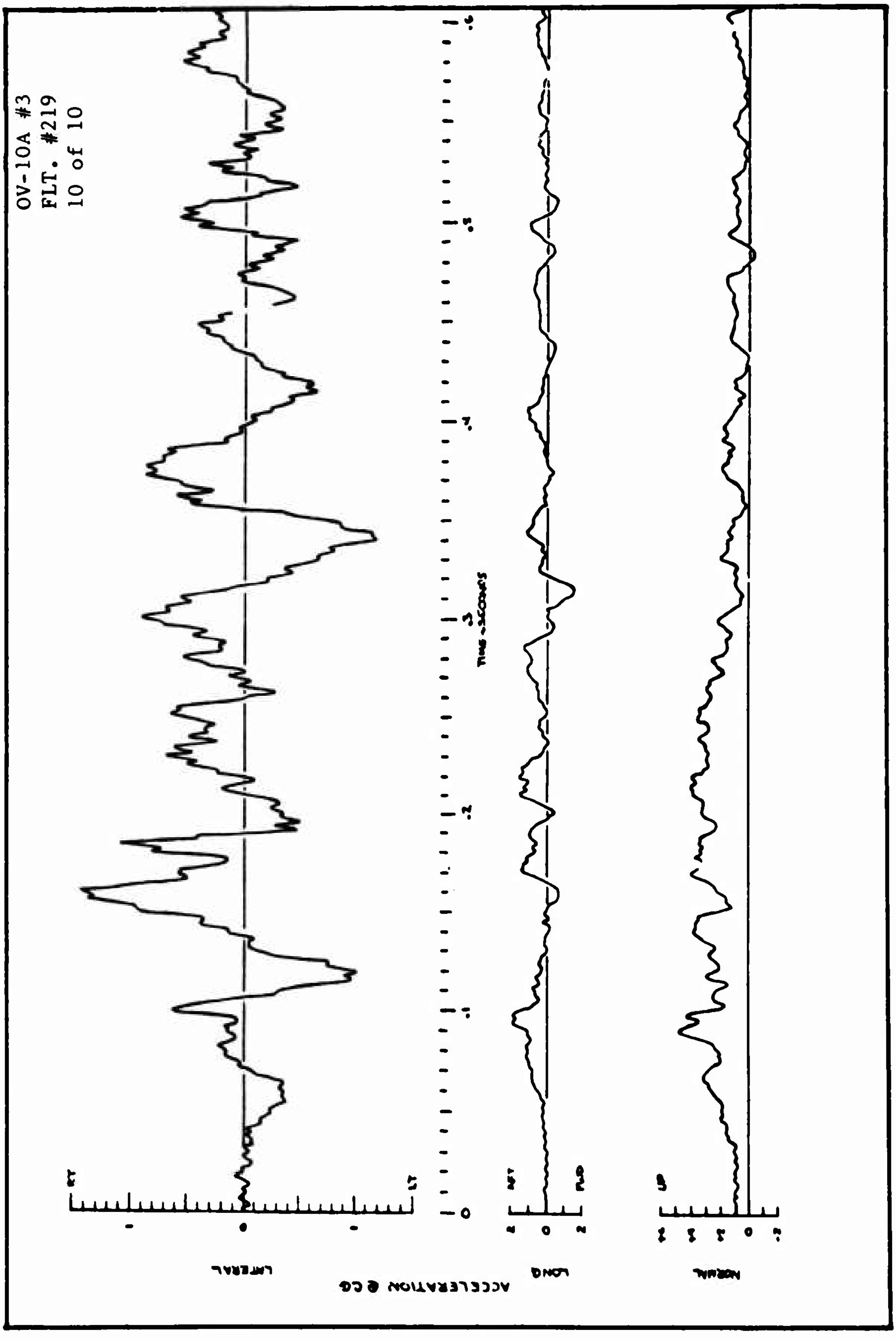

North American Aviation/Columbus
North American Rockwell

TIME HISTORIES OF LANDING GEAR
LOADS AND RESPONSE

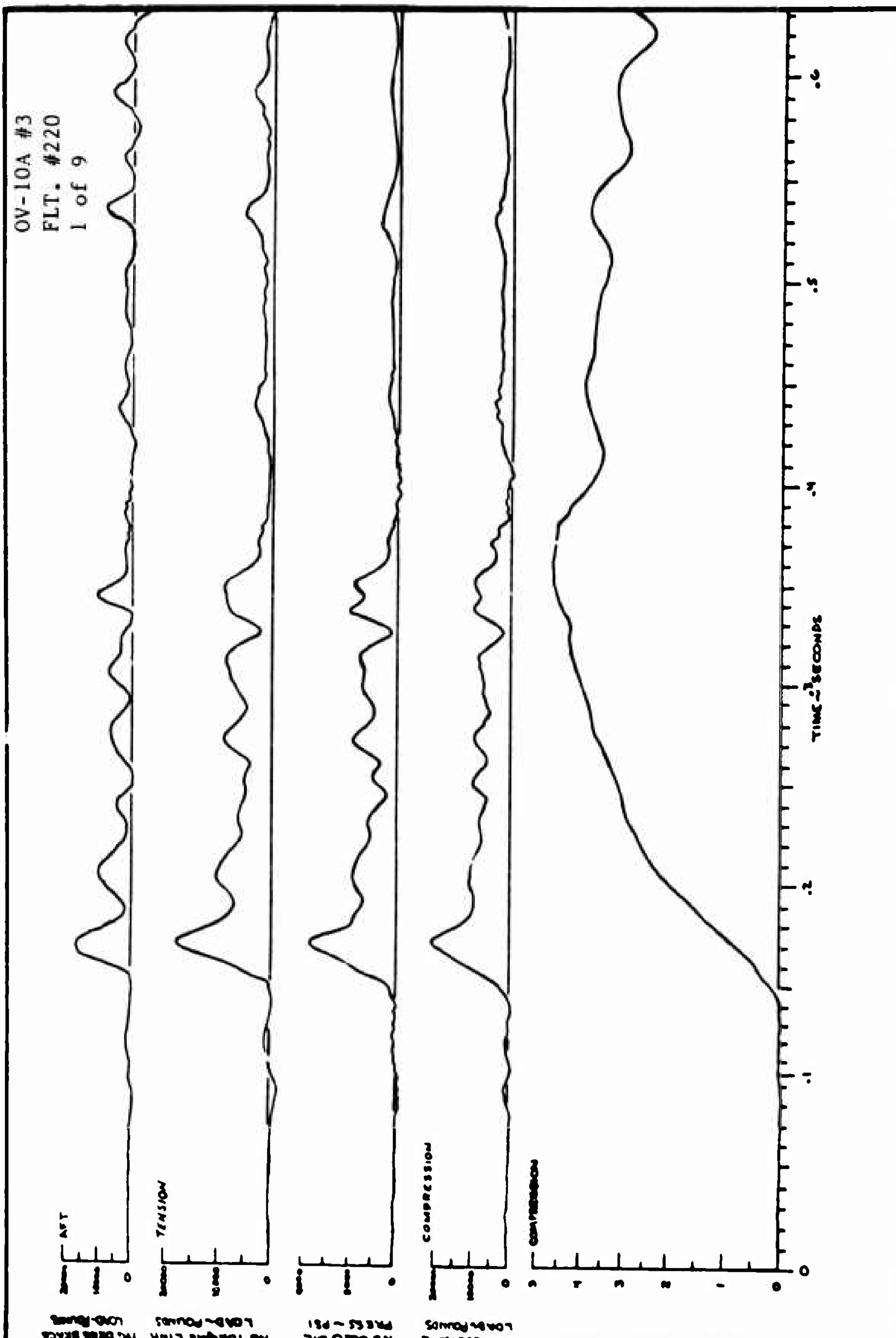

TIME HISTORIES OF LANDING GEAR
LOADS AND RESPONSE

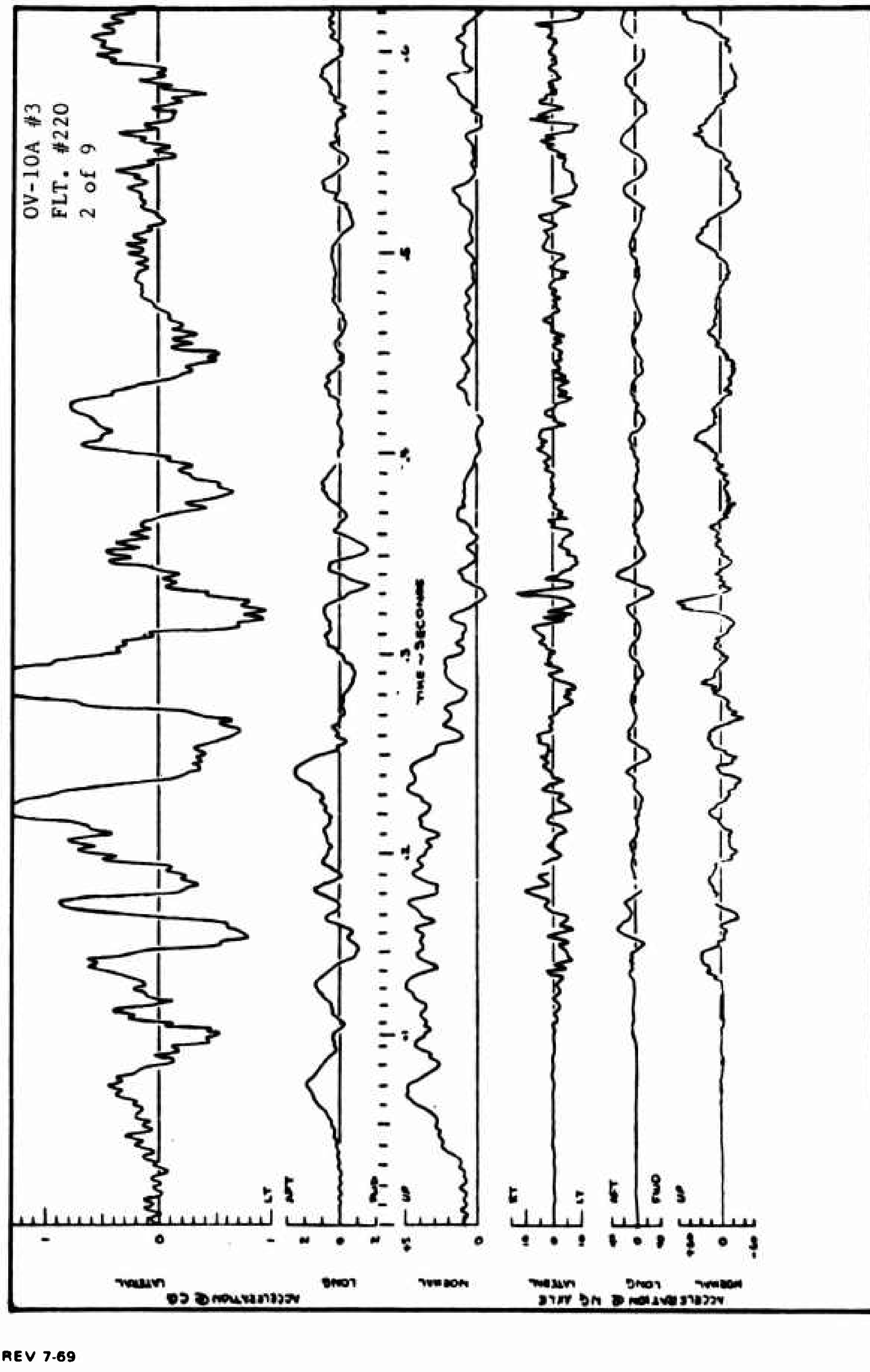

TIME HISTORIES OF LANDING GEAR
LOADS AND RESPONSE

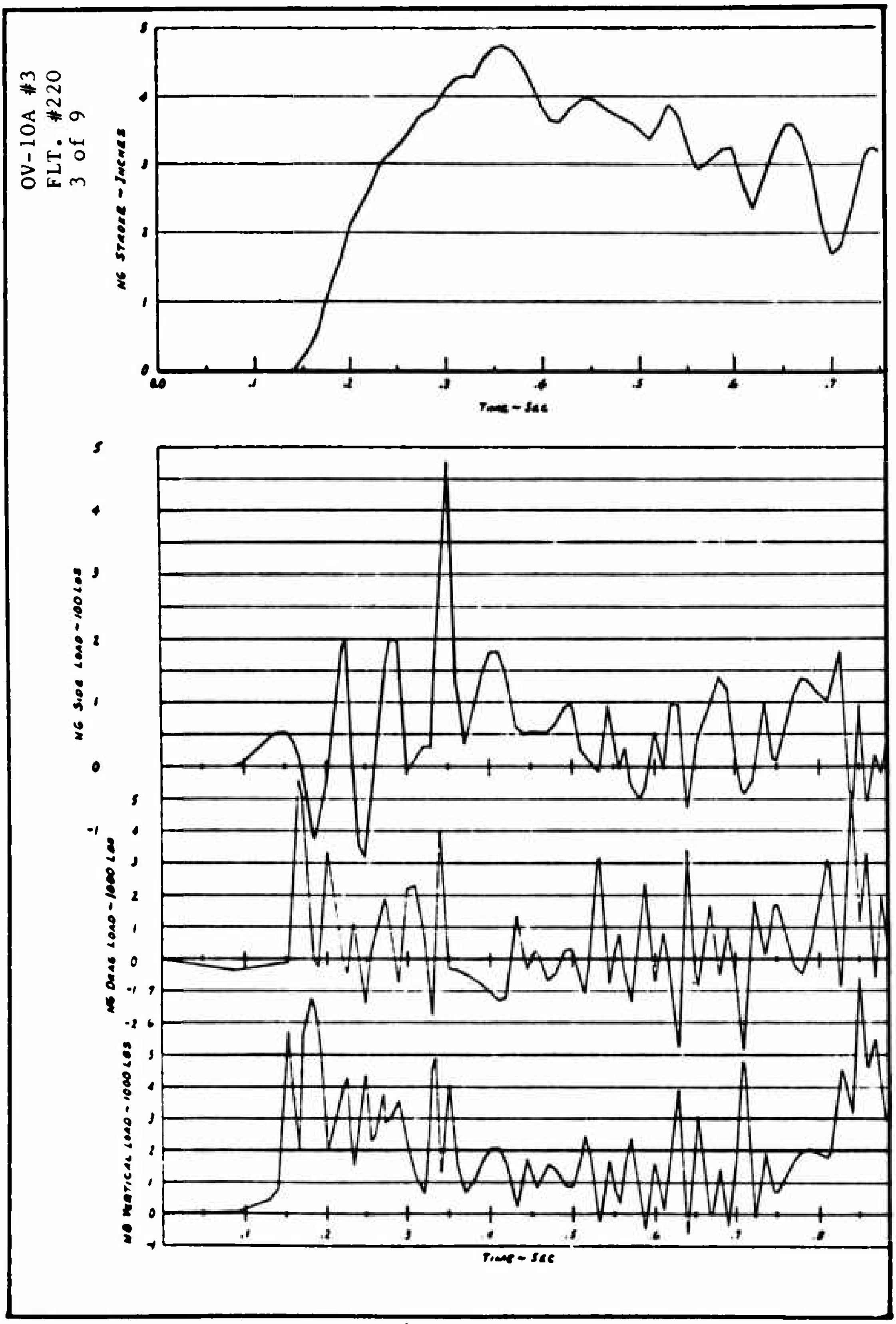

TIME HISTORIES OF LANDING GEAR
LOADS AND RESPONSE

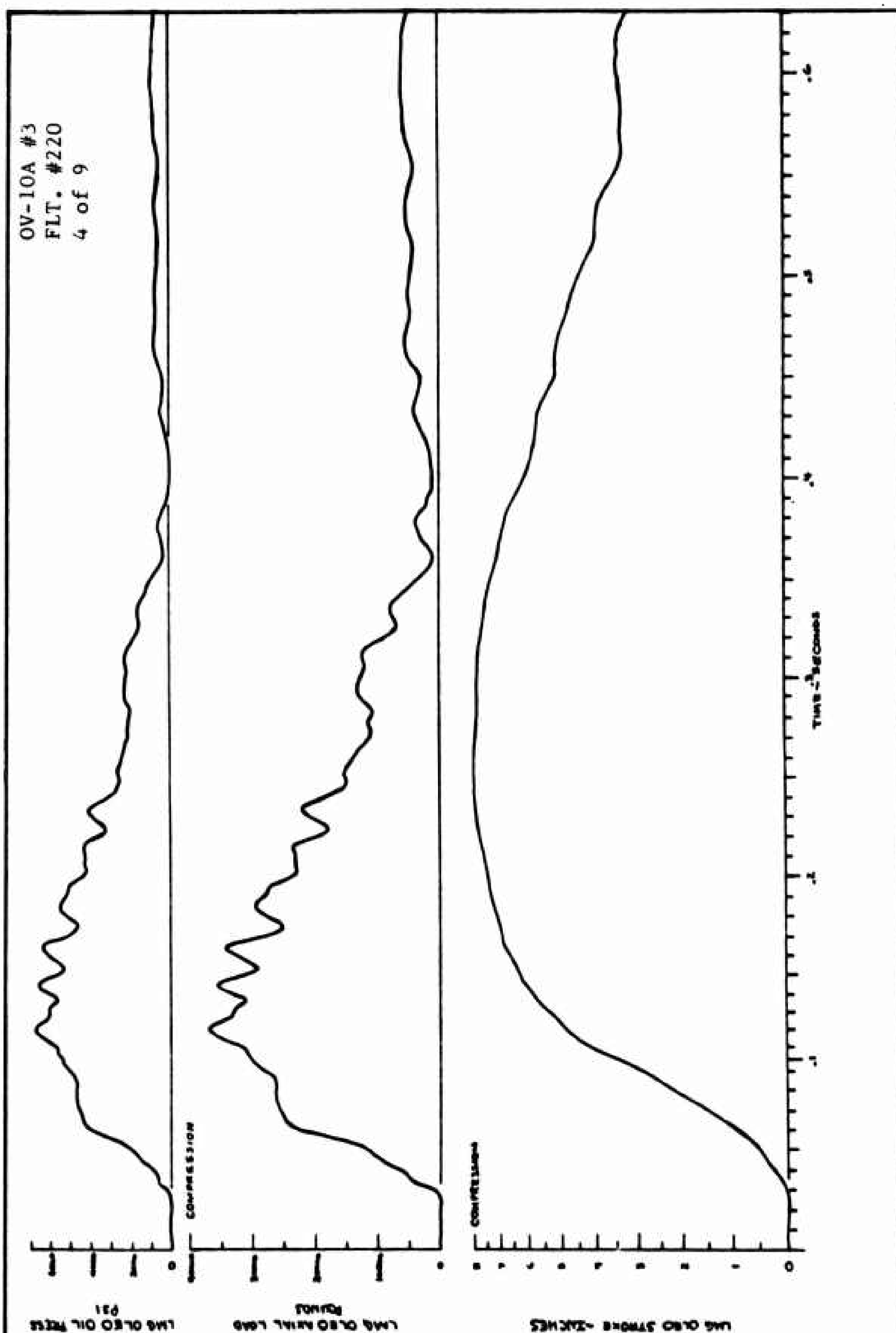

TIME HISTORIES OF LANDING GEAR
LOADS AND RESPONSE

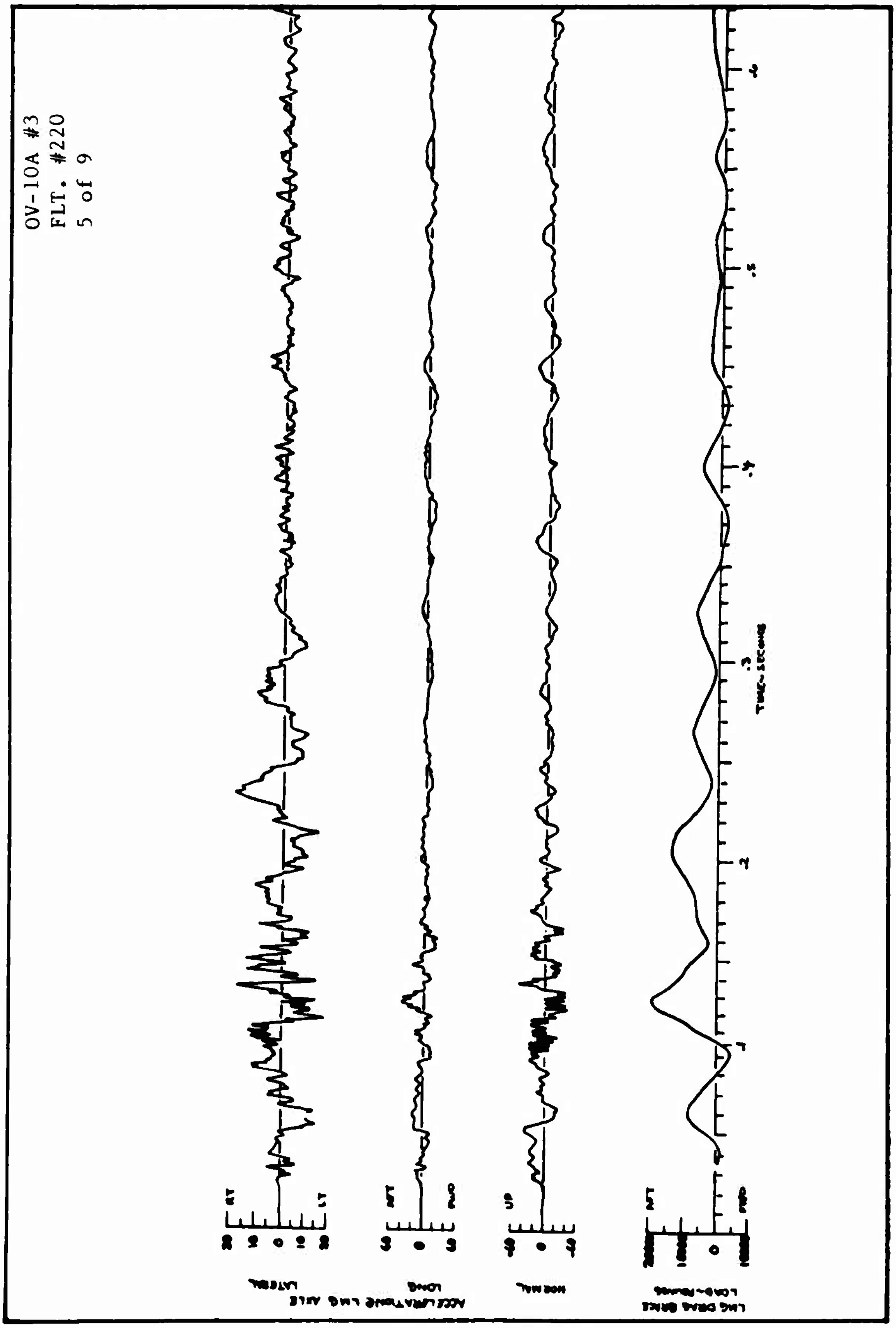

TIME HISTORIES OF LANDING GEAR
LOADS AND RESPONSE

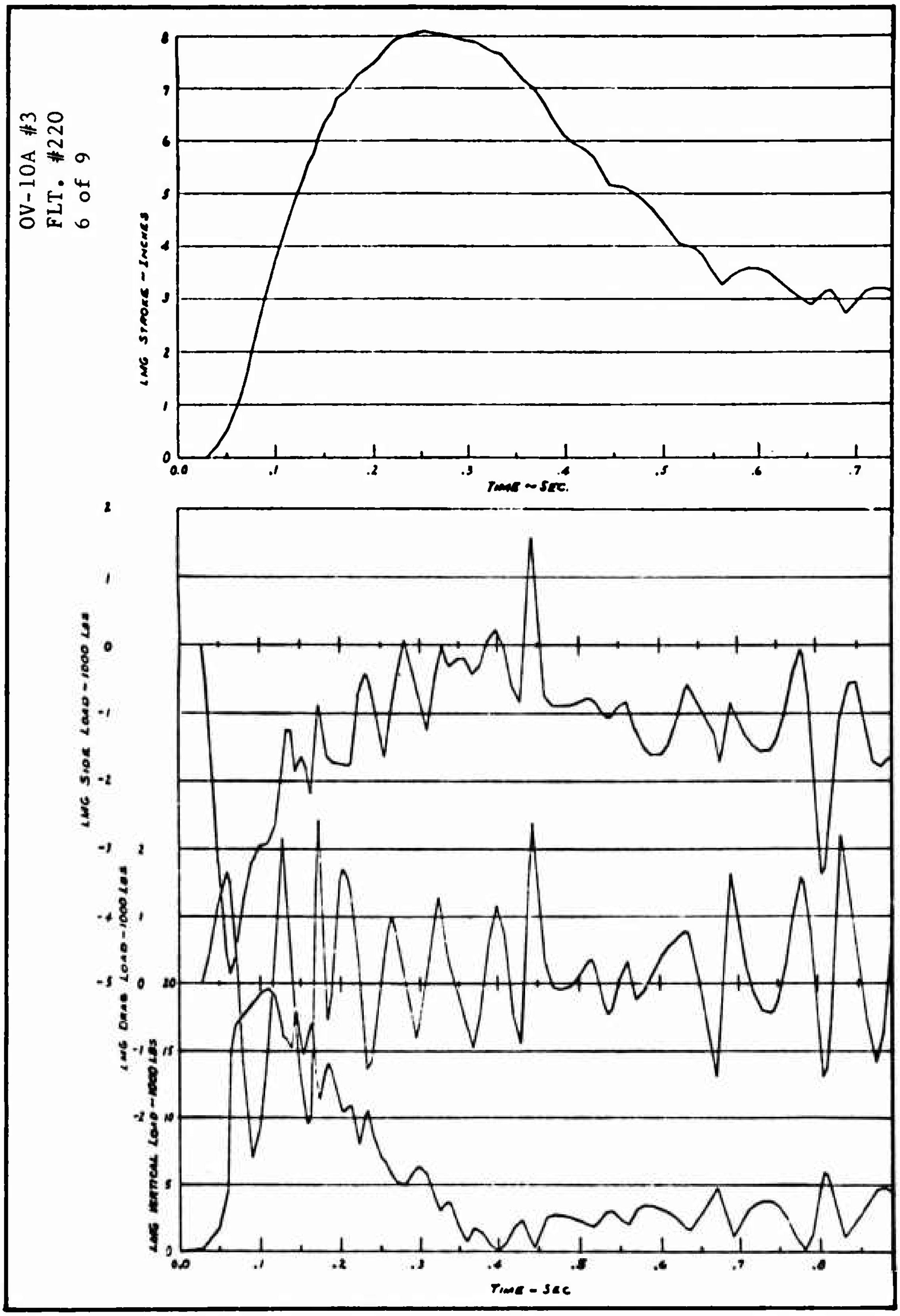

TIME HISTORIES OF LANDING GEAR
LOADS AND RESPONSE

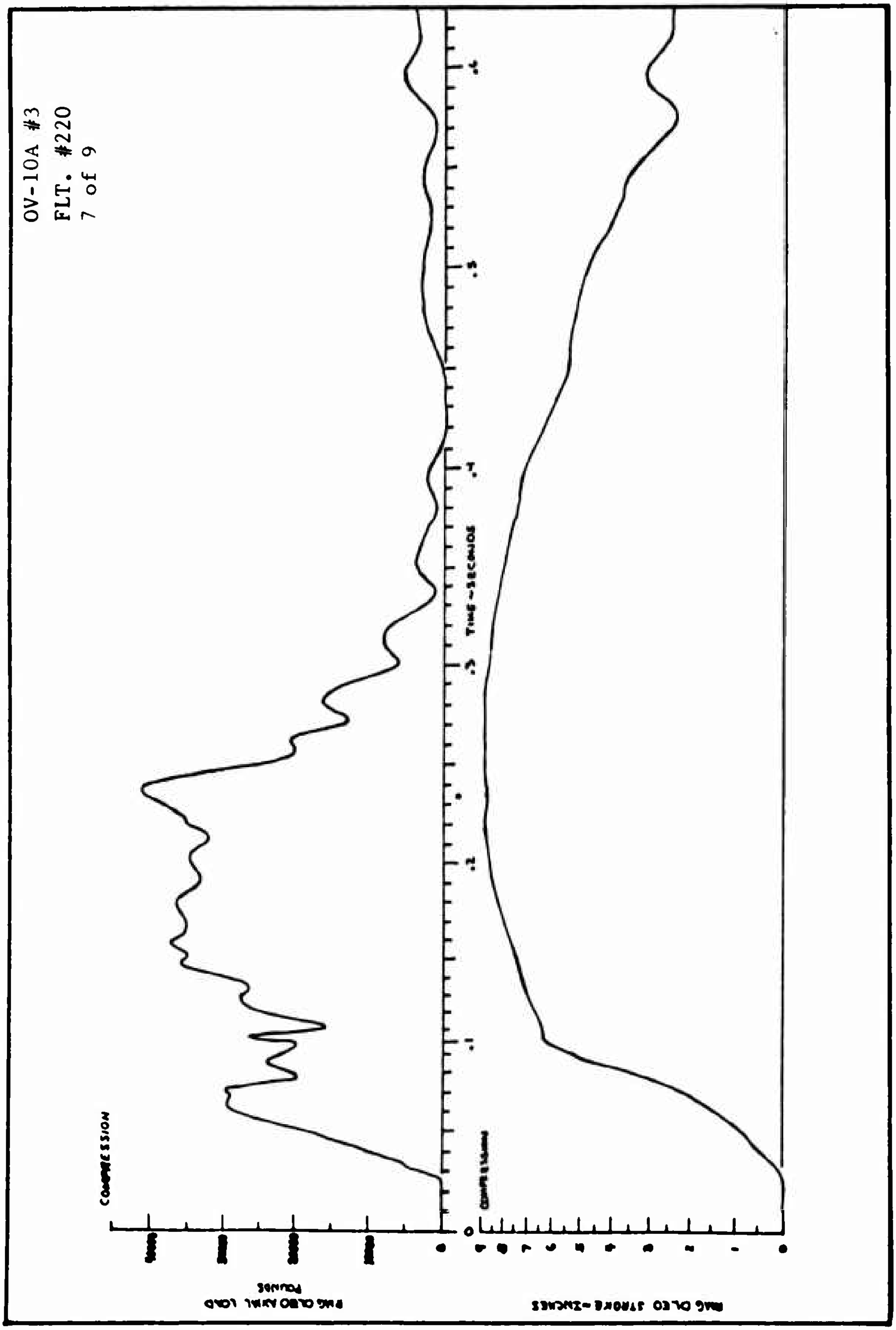

TIME HISTORIES OF LANDING GEAR
LOADS AND RESPONSE

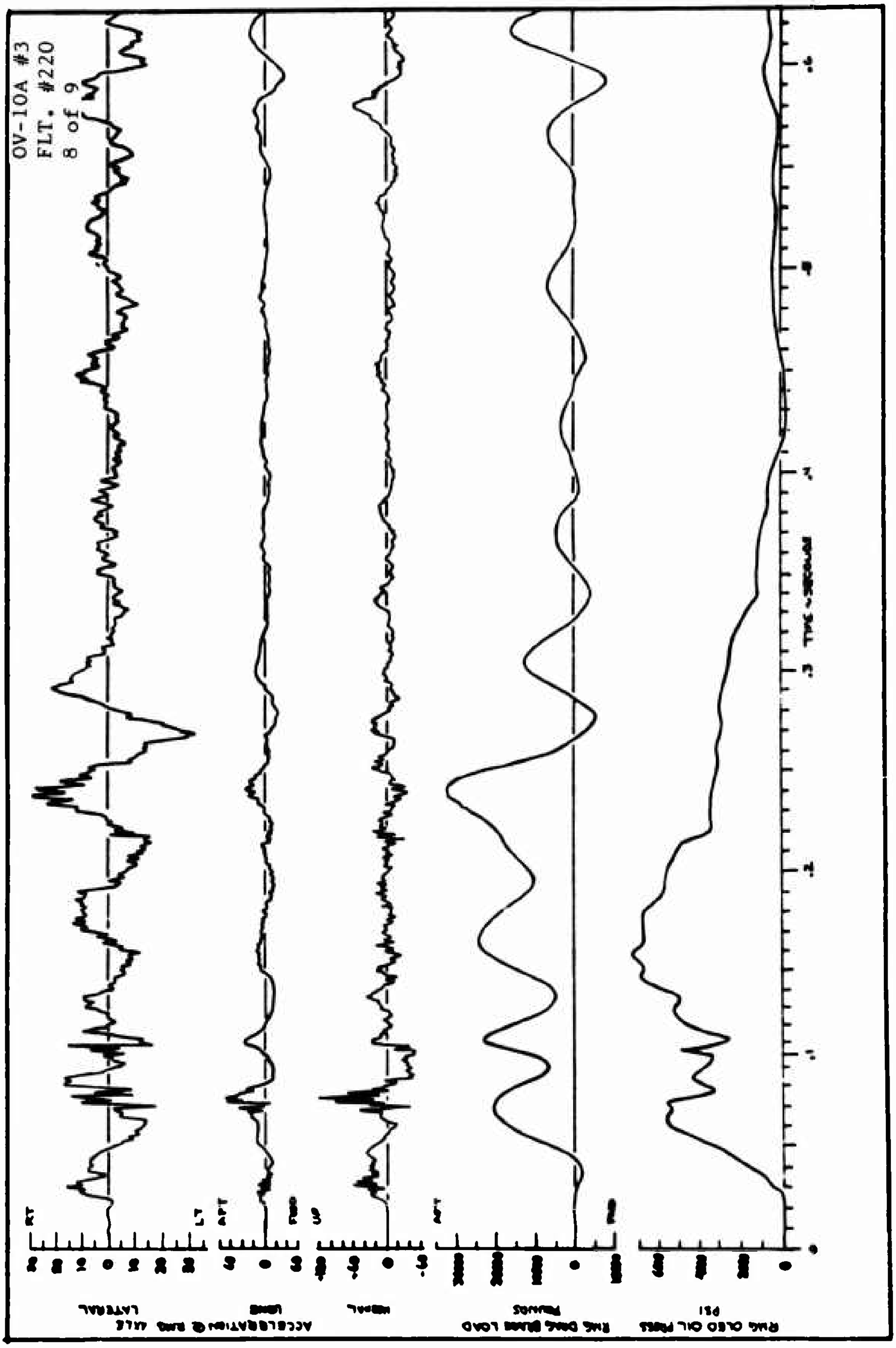

TIME HISTORIES OF LANDING GEAR
LOADS AND RESPONSE

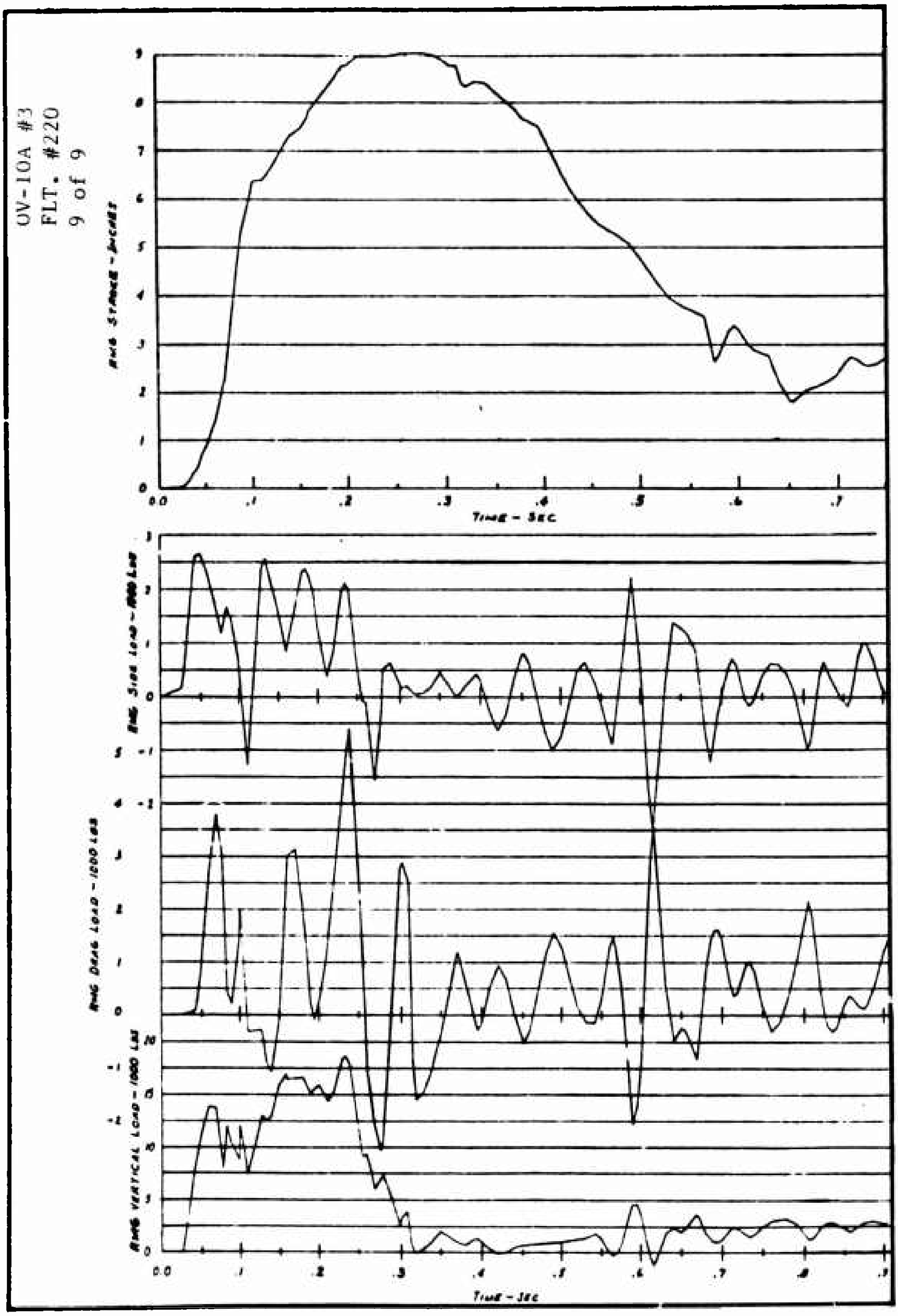

North American Aviation/Columbus
North American Rockwell

NR70H-570
A4-71

TIME HISTORIES OF LANDING GEAR
LOADS AND RESPONSE

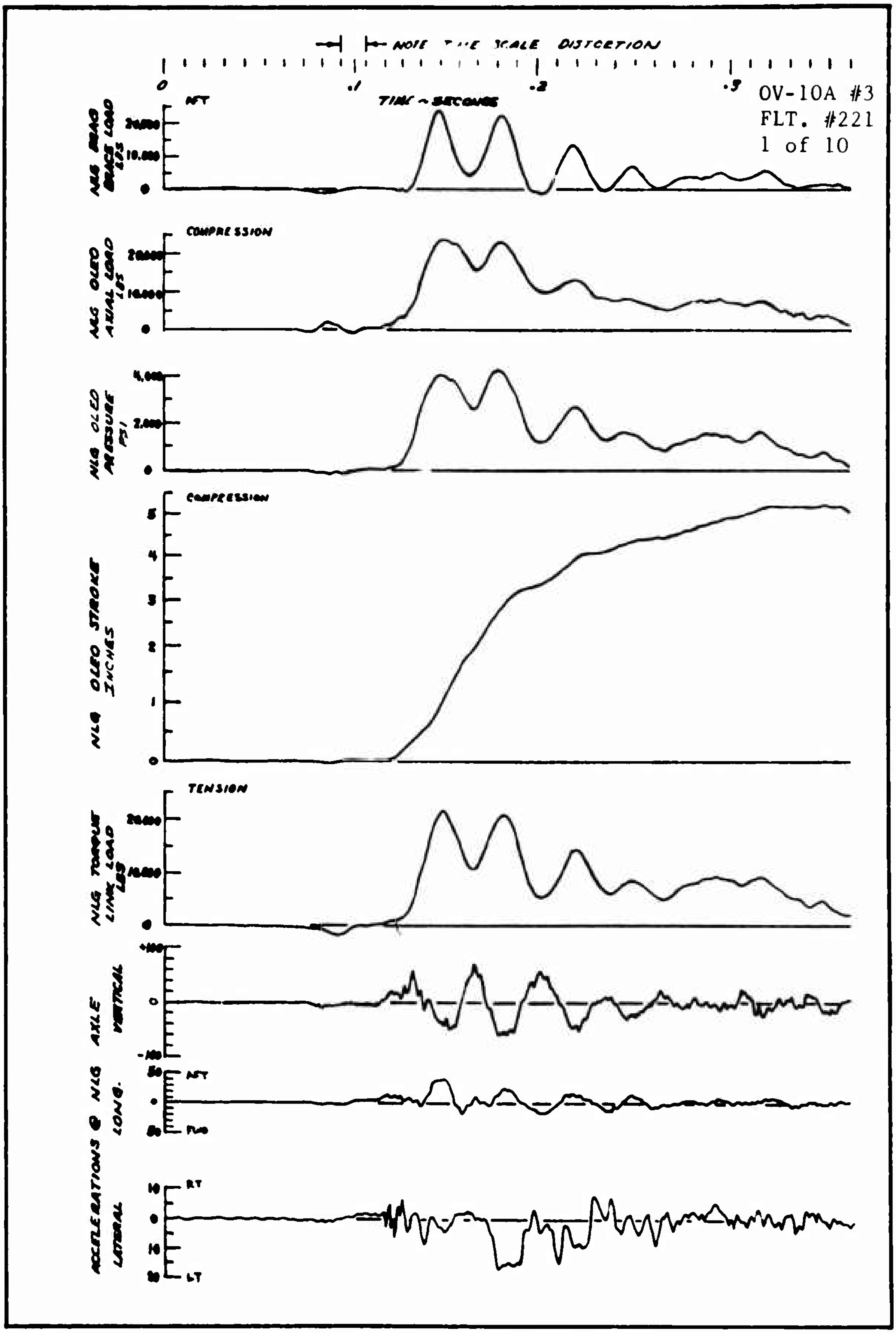

A

TIME H

L

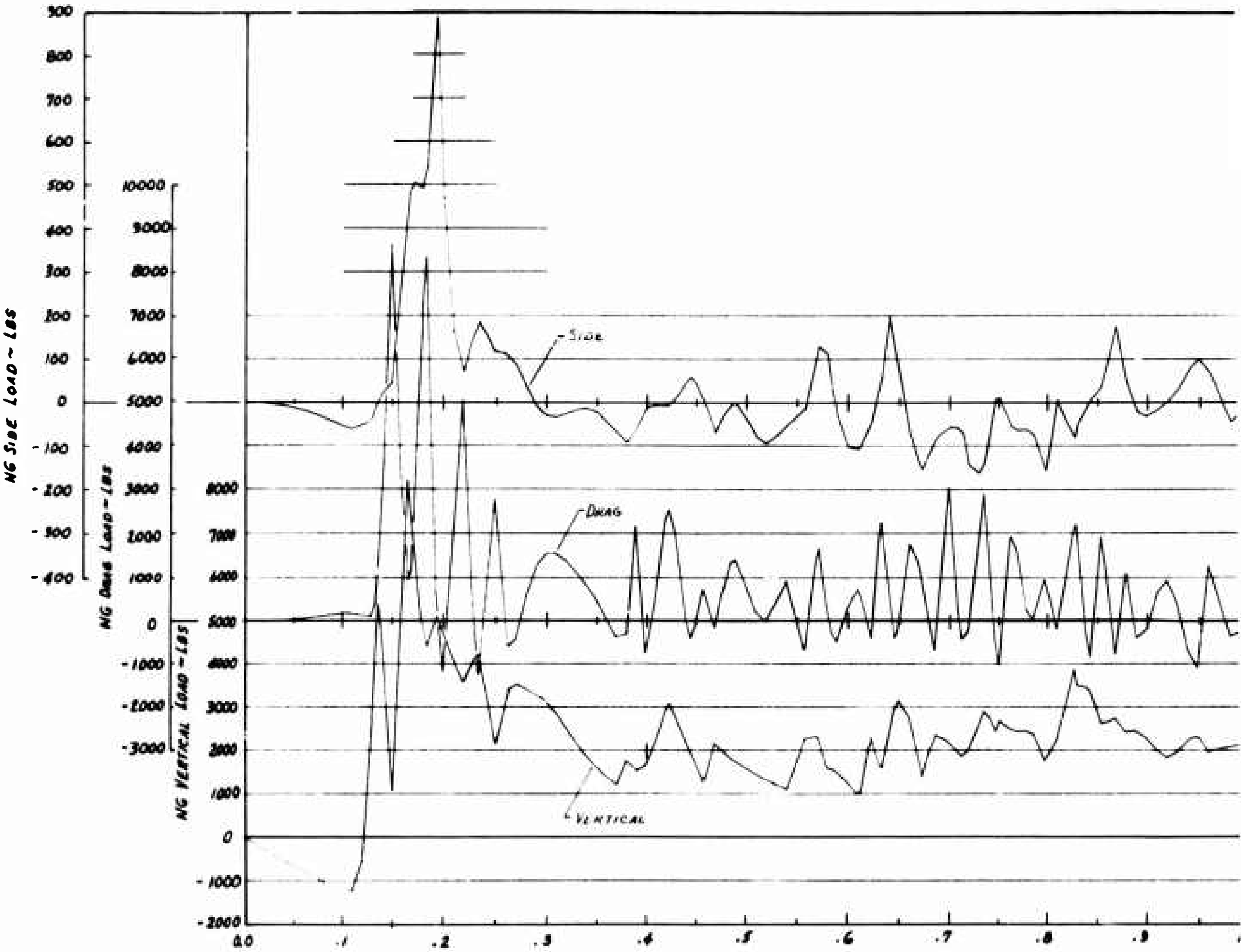

NG SIDE LOAD ~ LBS
NG DRAG LOAD ~ LBS
NG VERTICAL LOAD ~ LBS
SIDE
DRAG
VERTICAL
900
800
700
600
500
400
300
200
100
0
-100
-200
-300
-400
10000
9000
8000
7000
6000
5000
4000
3000
2000
1000
0
-1000
-2000
-3000
8000
7000
6000
5000
4000
3000
2000
1000
0
-1000
-2000
0.0
.1
.2
.3
.4
.5
.6
.7
.8
.9

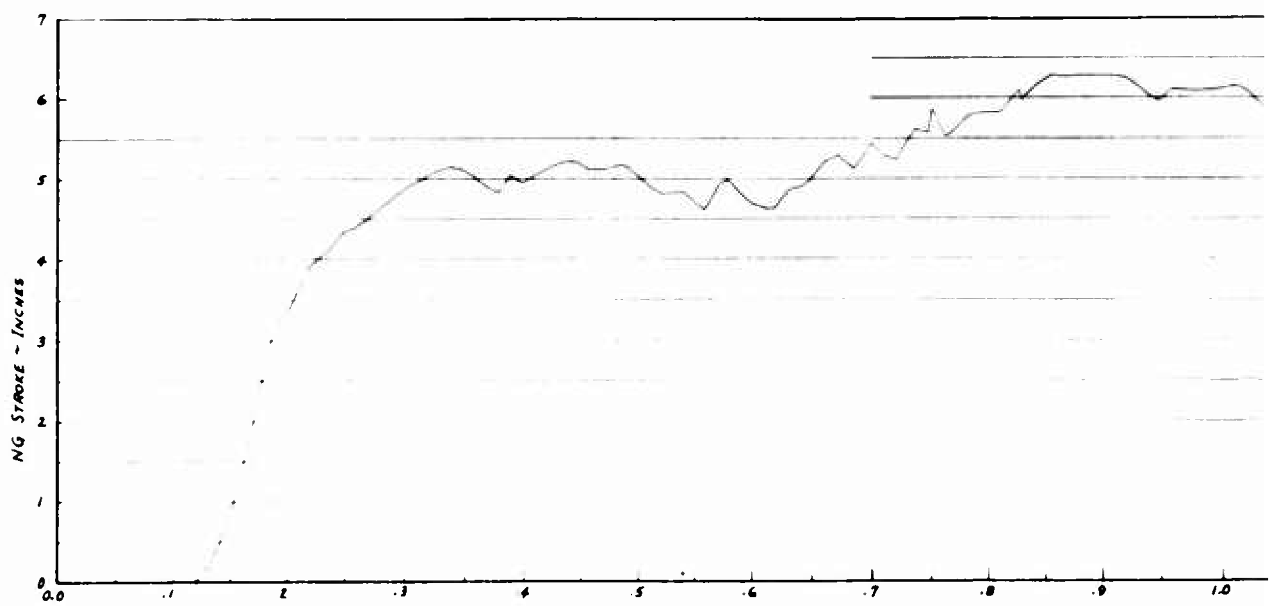

NG STROKE ~ INCHES
7
6
5
4
3
2
1
0
0.0
.1
.2
.3
.4
.5
.6
.7
.8
.9
1.0

1 B

OF LANDING GEAR
RESPONSE

OV-10A #3
FLT. #221
2 of 10

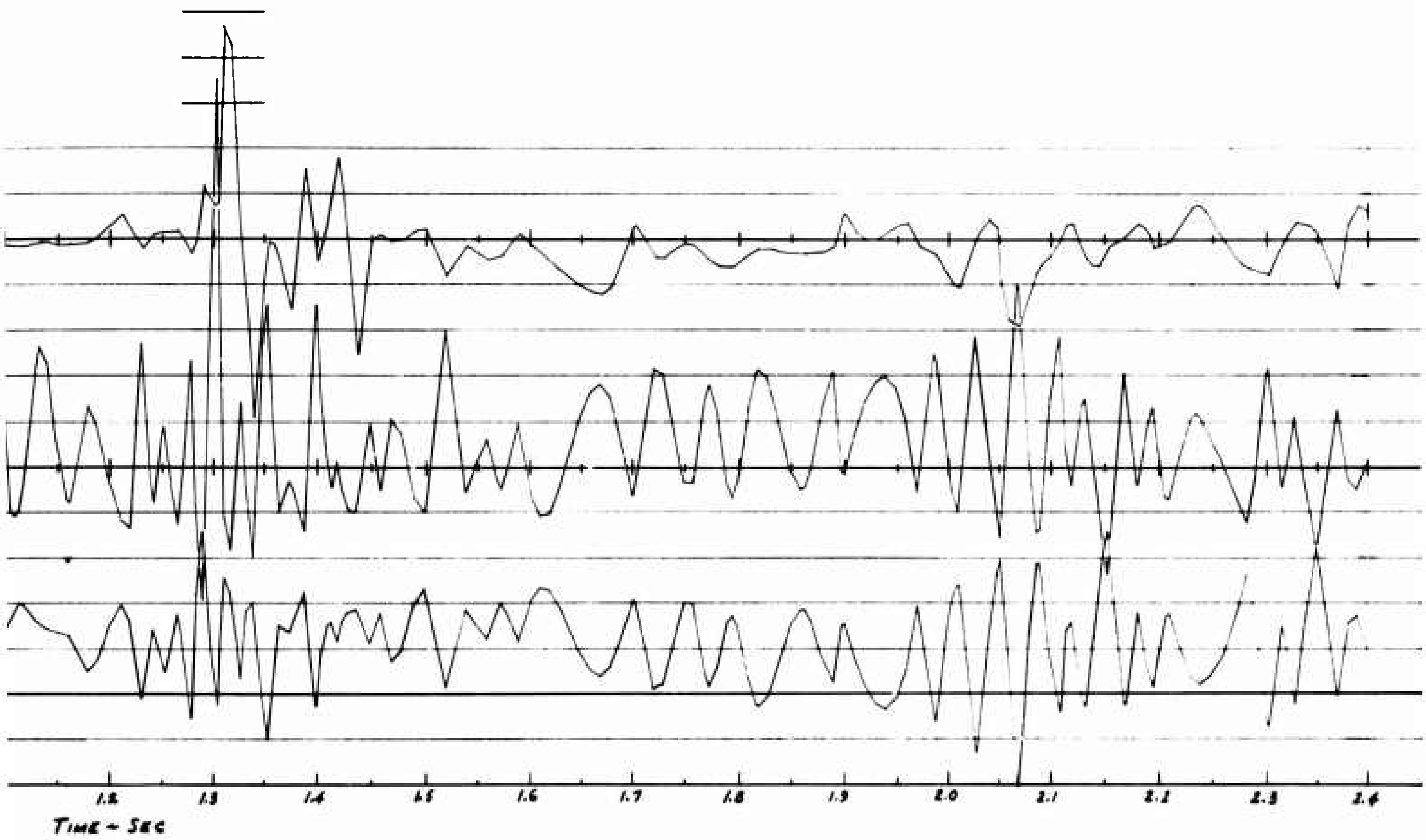

OV-10A #3
FLT. #221
3 of 10

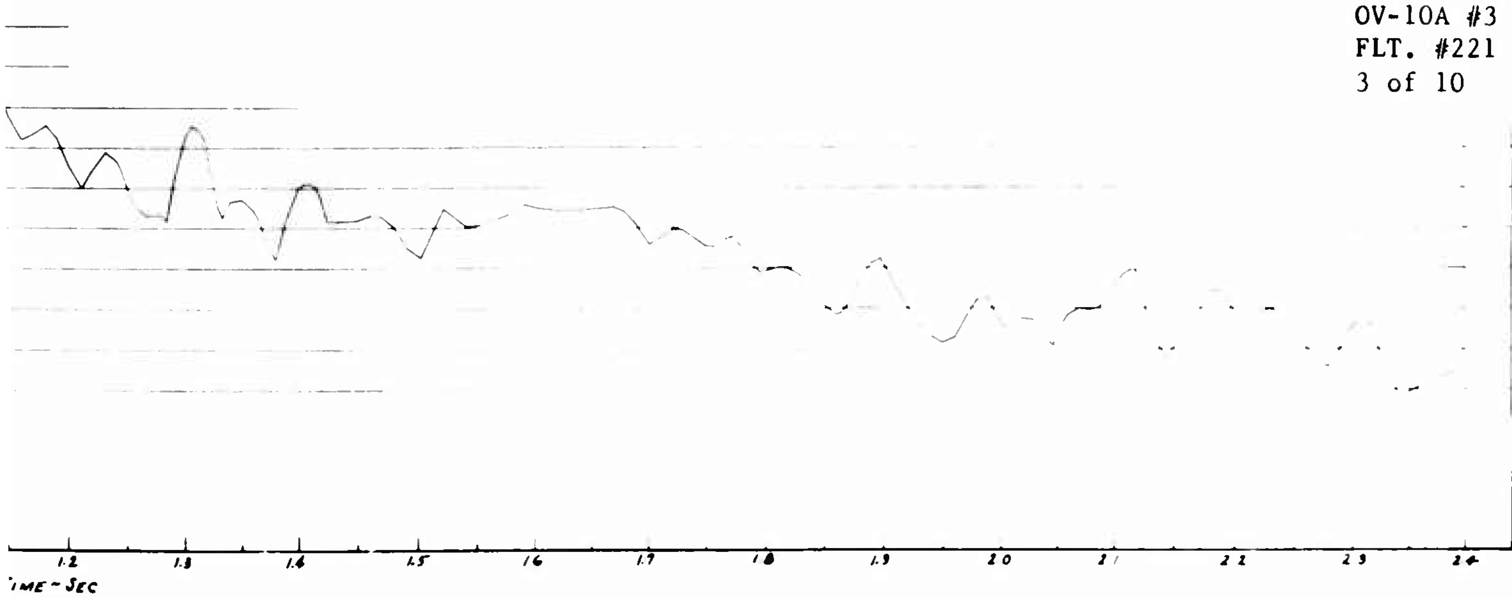

PRECEDING PAGE BLANK

TIME HISTORIES OF LANDING GEAR
LOADS AND RESPONSE

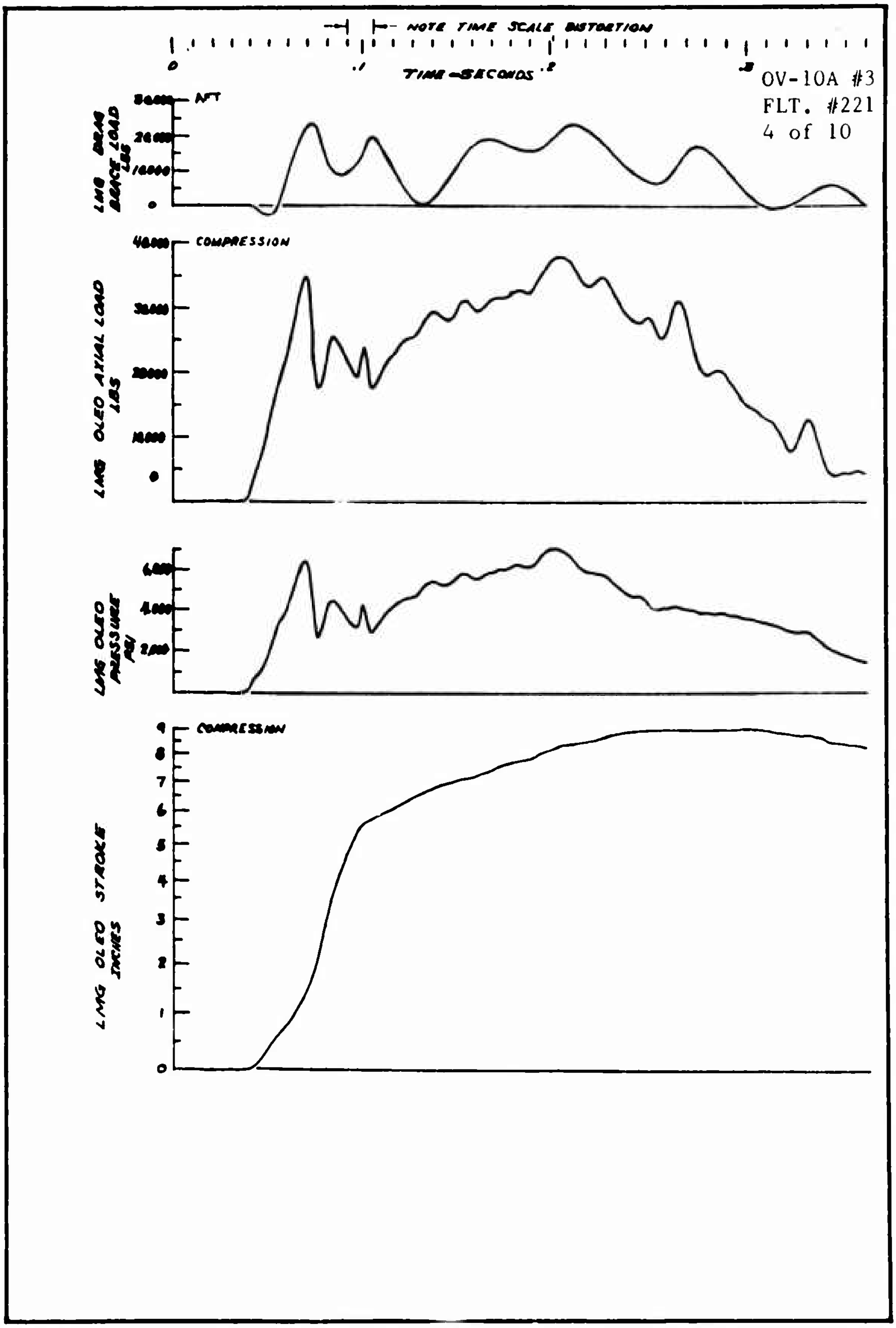

PRECEDING PAGE BLANK

TIME HISTORIES OF LANDING GEAR
LOADS AND RESPONSE

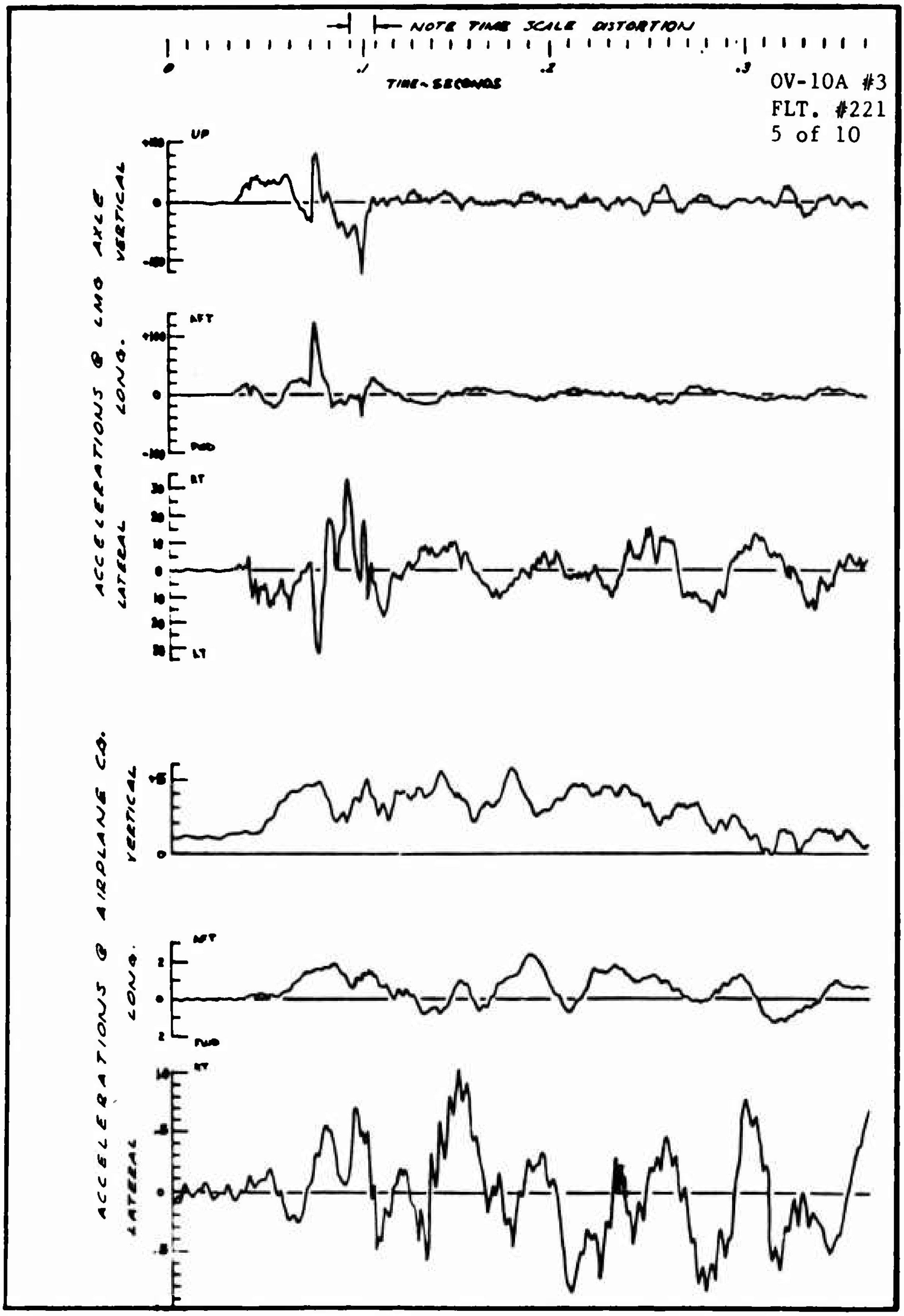

A

TIME HIS
LOA

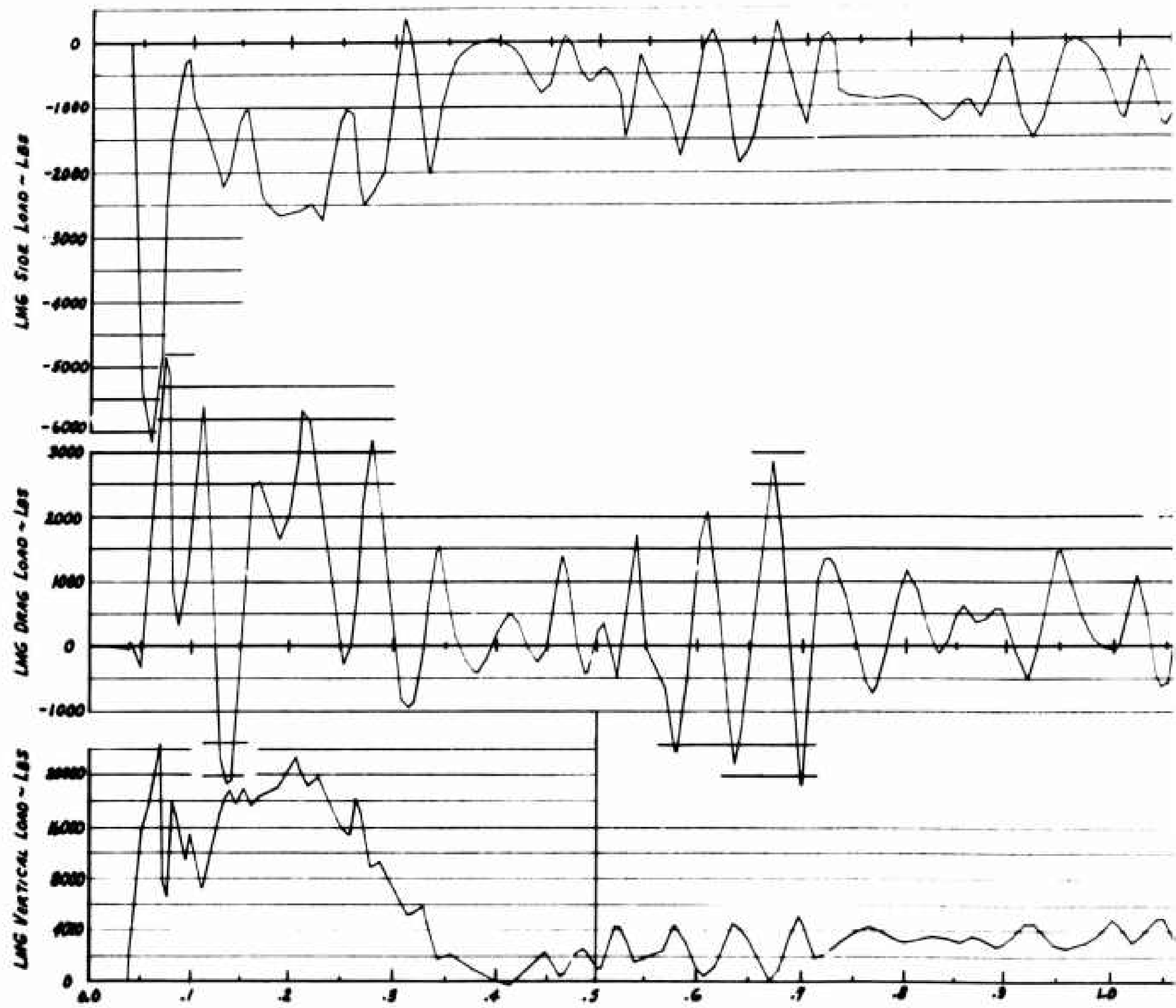

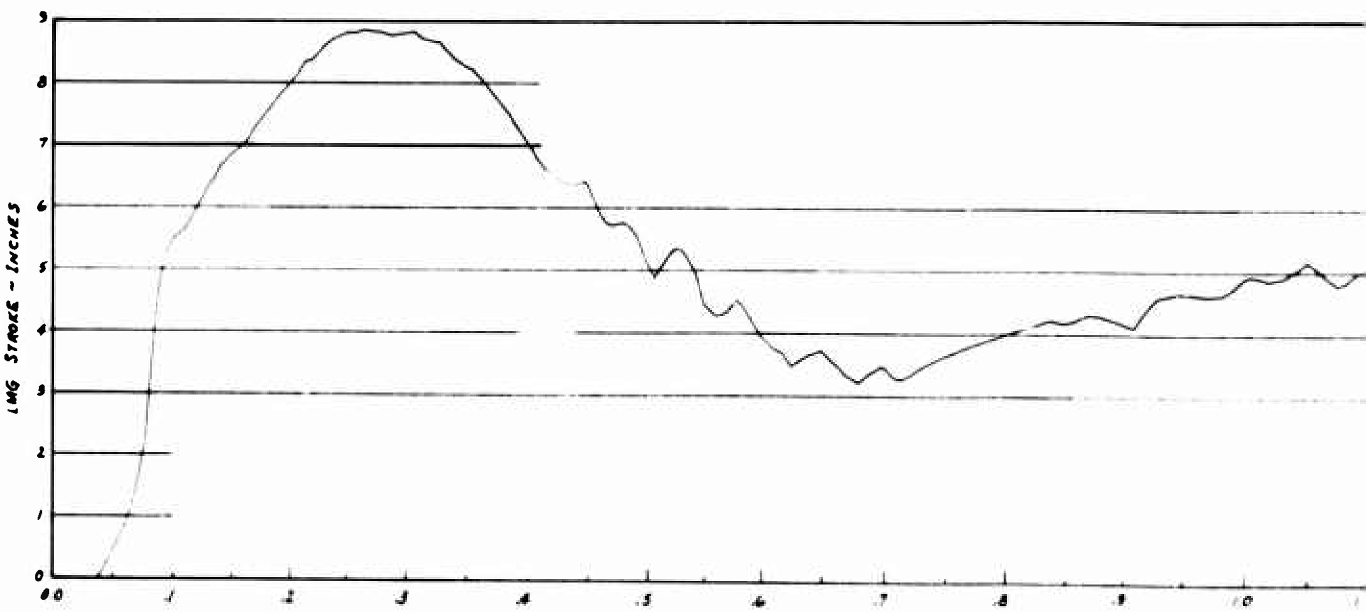

B

OF LANDING GEAR
RESPONSE

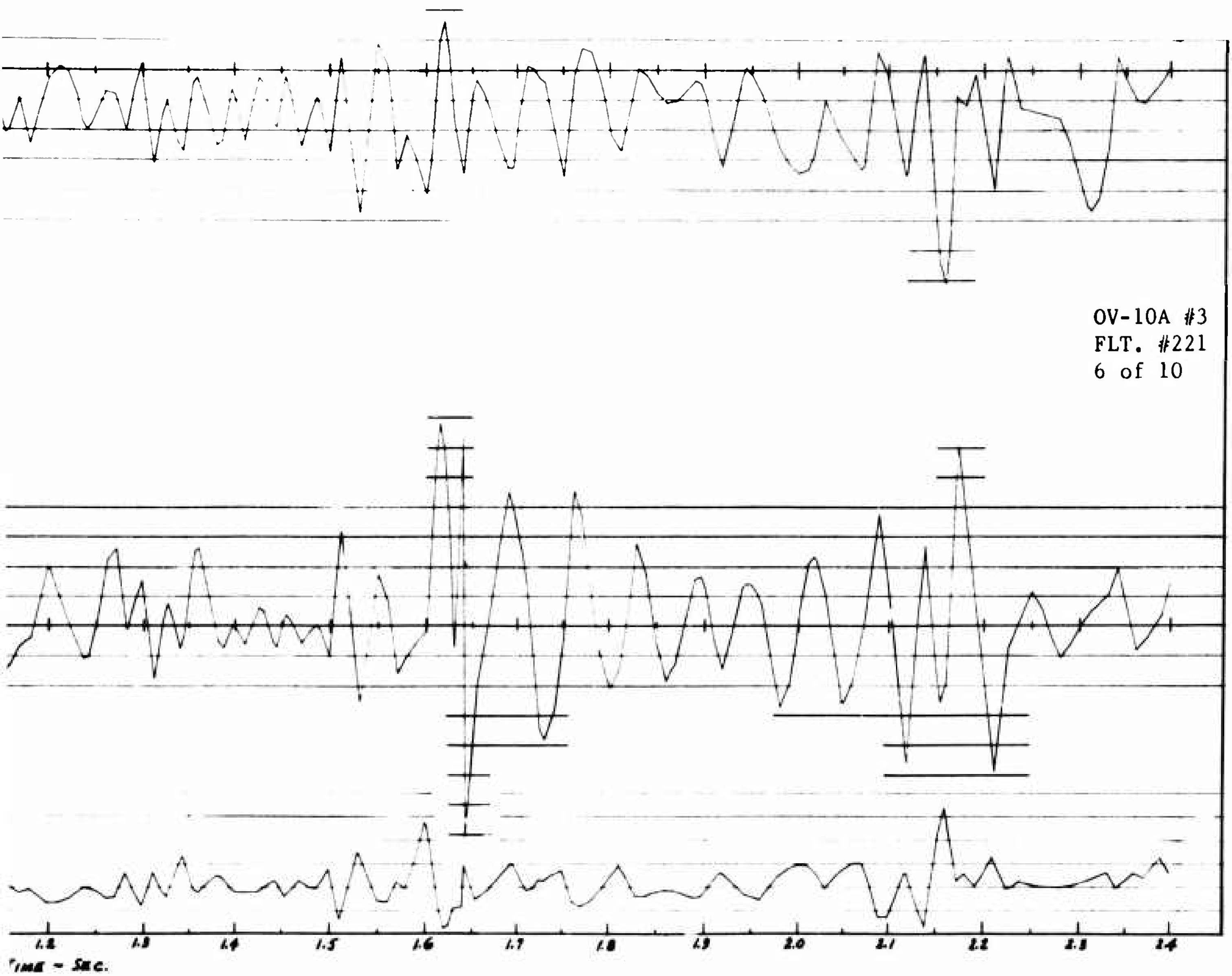

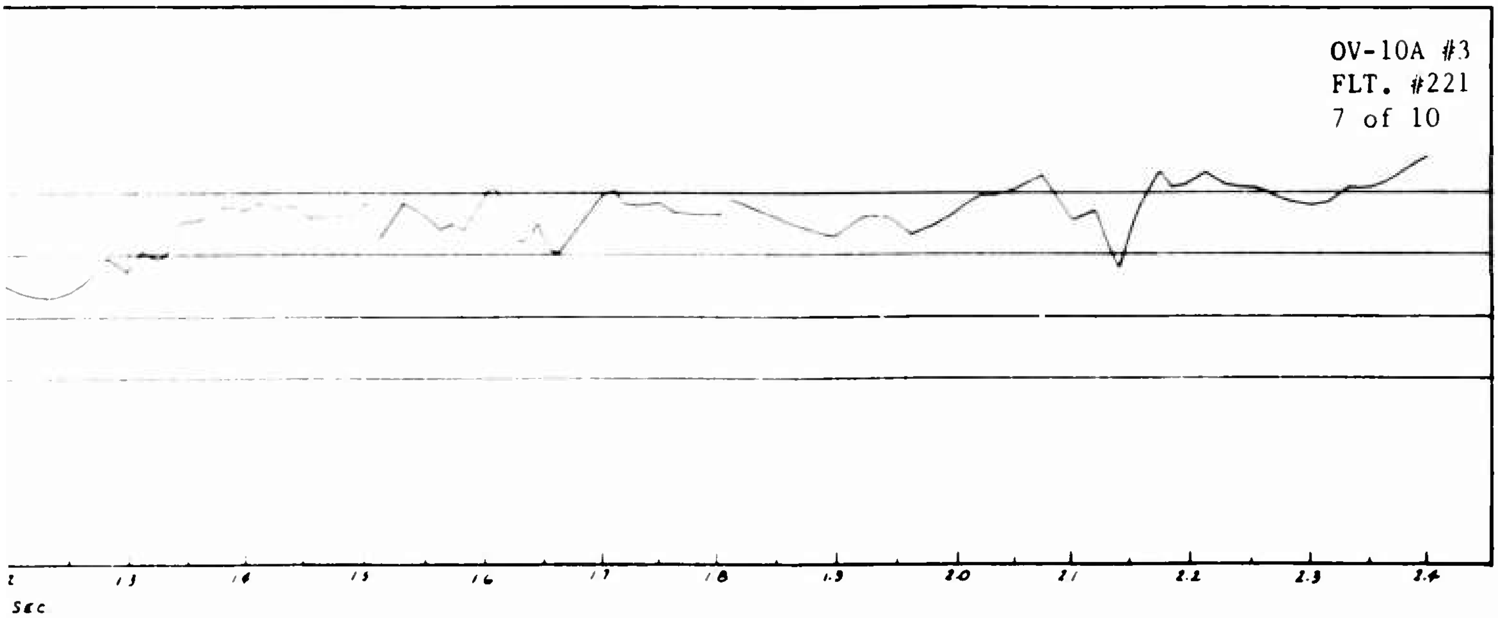

TIME HISTORIES OF LANDING GEAR
LOADS AND RESPONSE

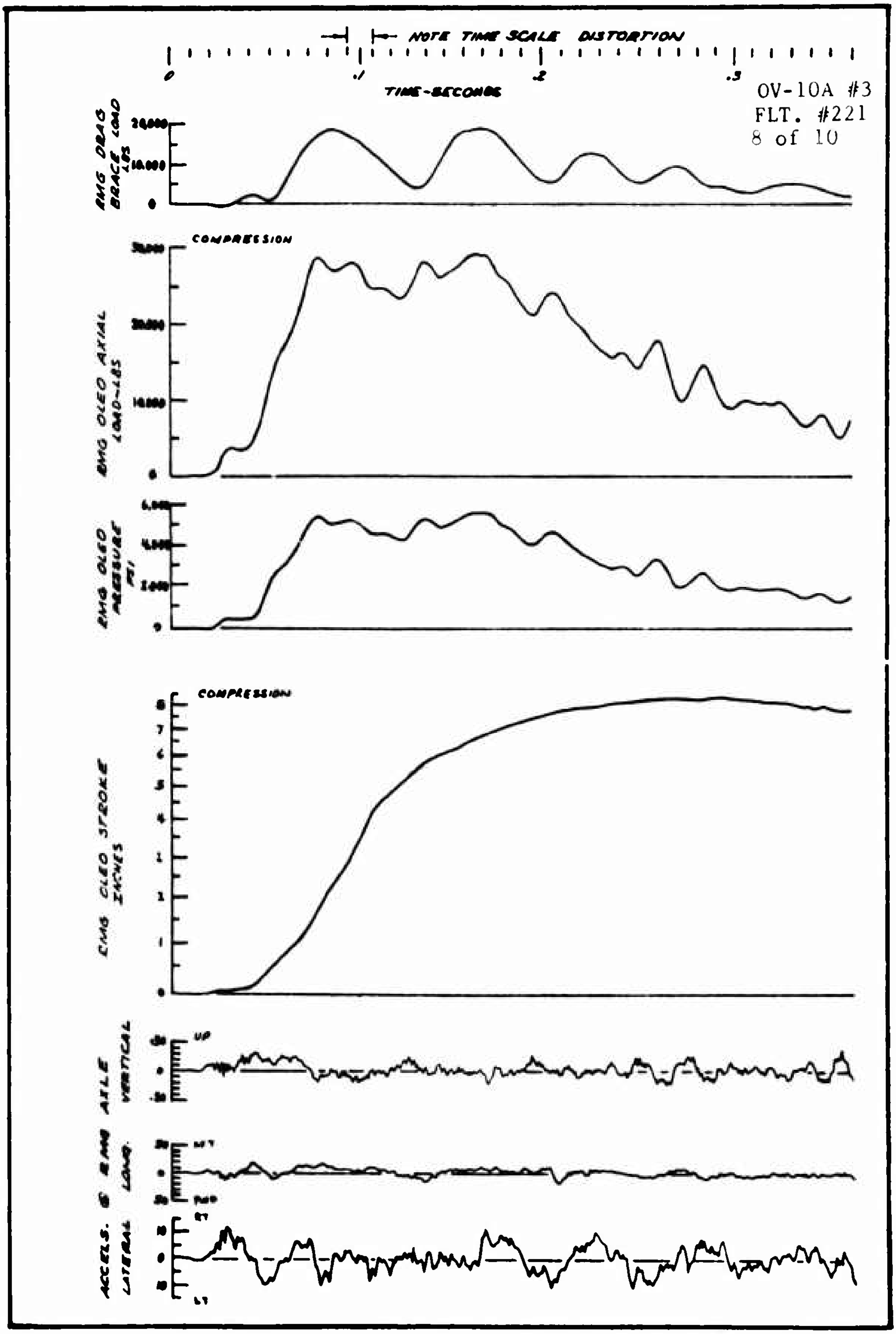

TIME HISTORIES
LOADS AND

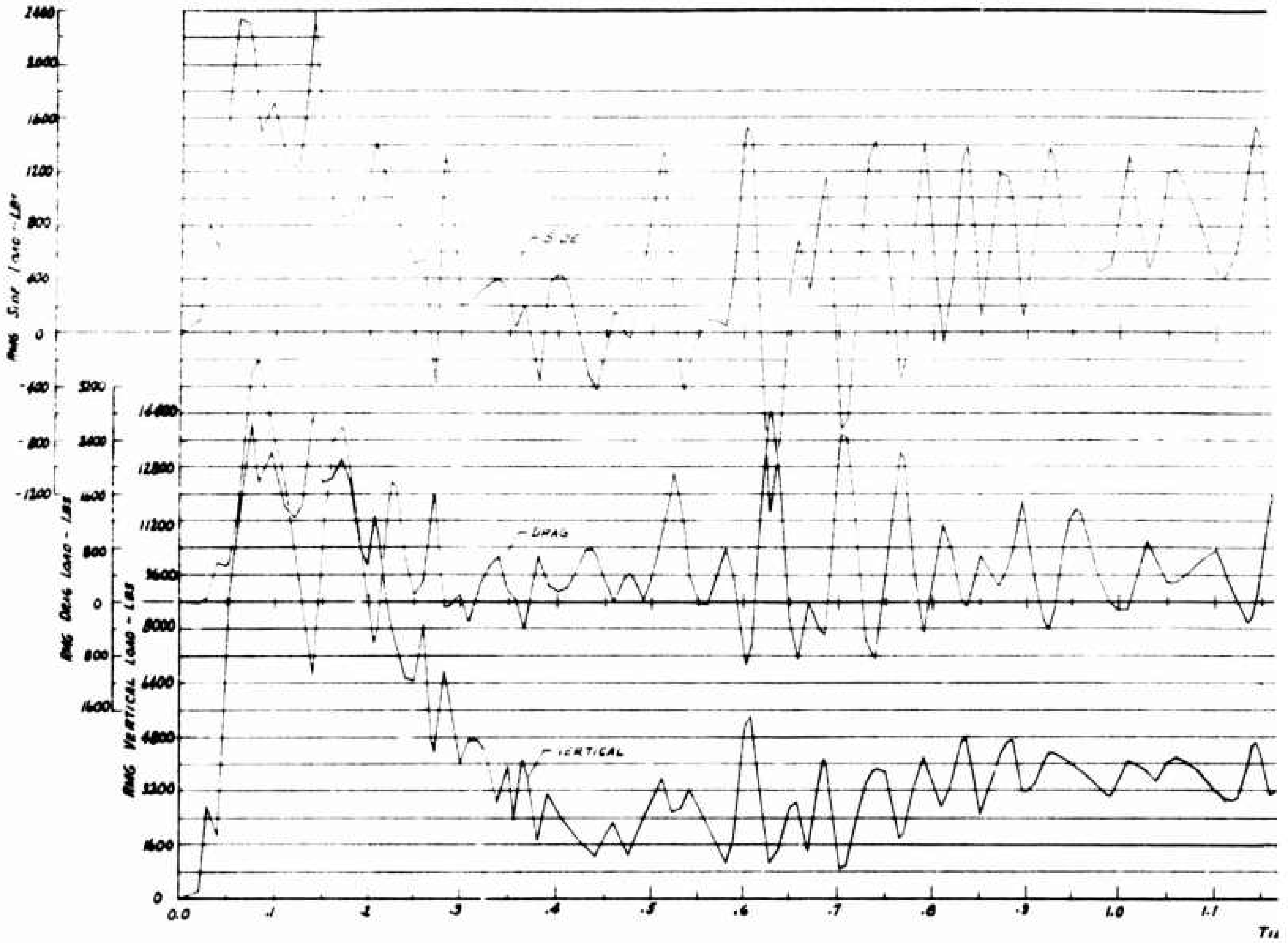

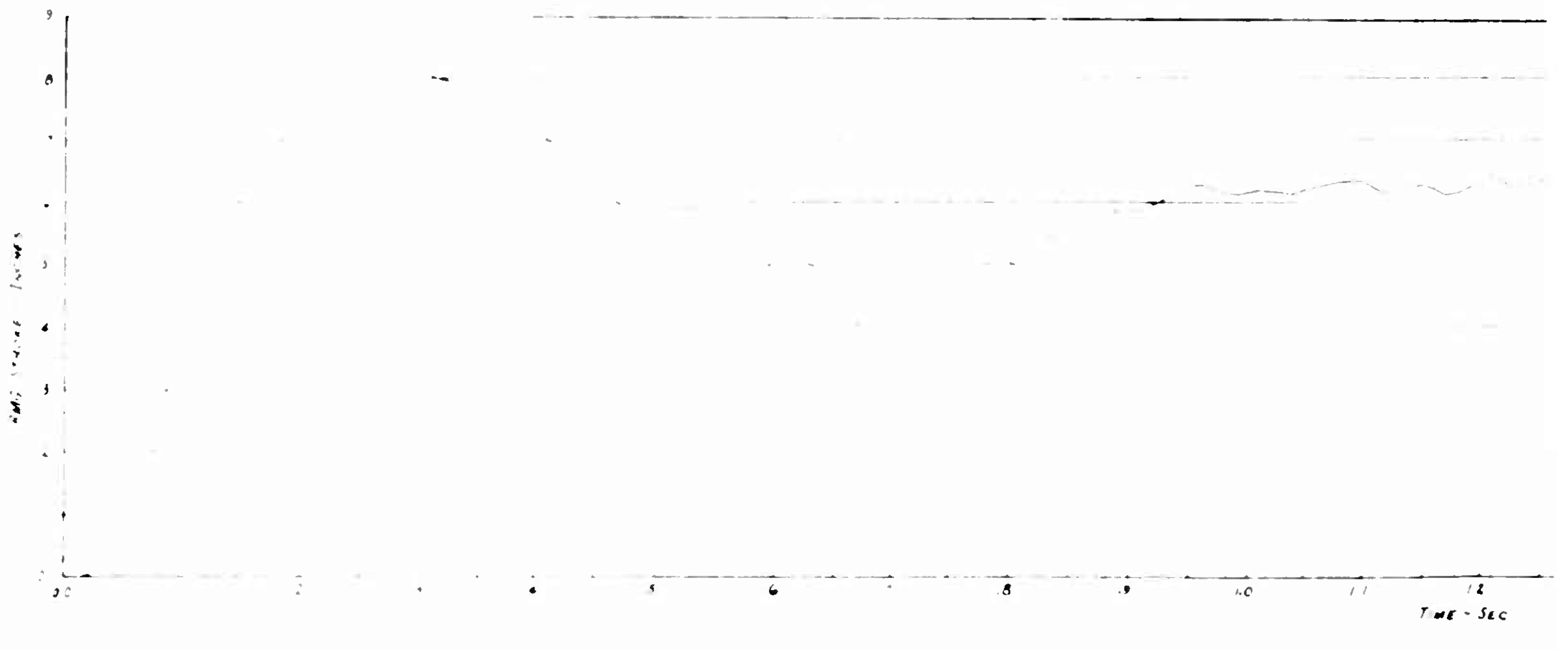

1 B

RIES OF LANDING GEAR
AND RESPONSE

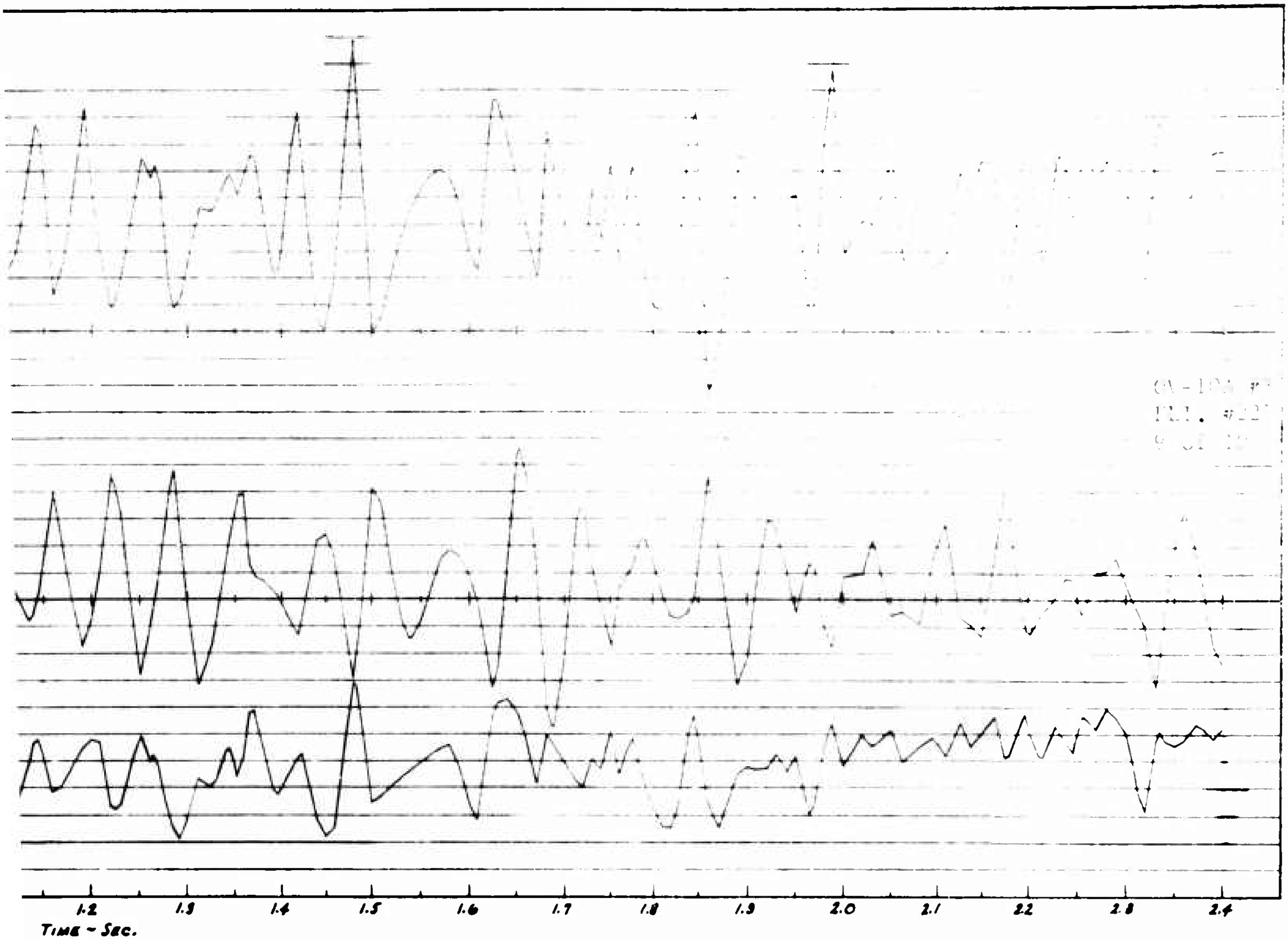

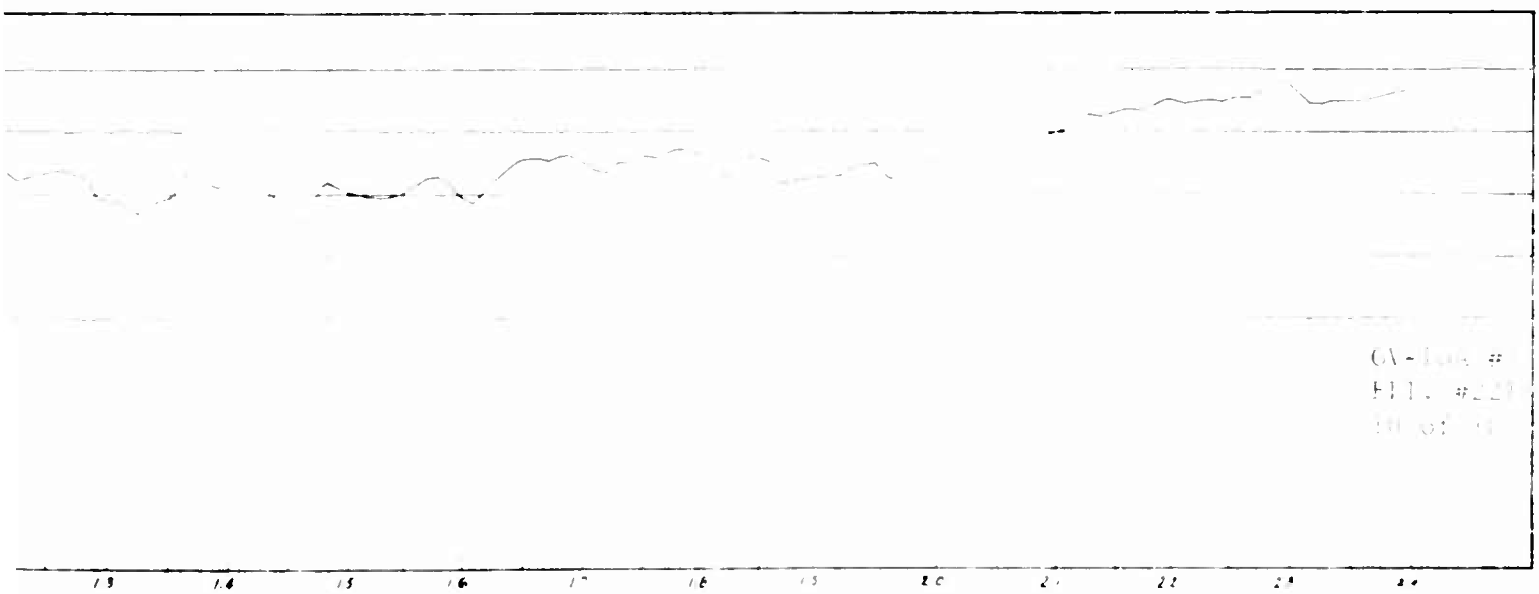

PRECEDING PAGE BLANK

TIME HISTORIES OF LANDING GEAR
LOADS AND RESPONSE

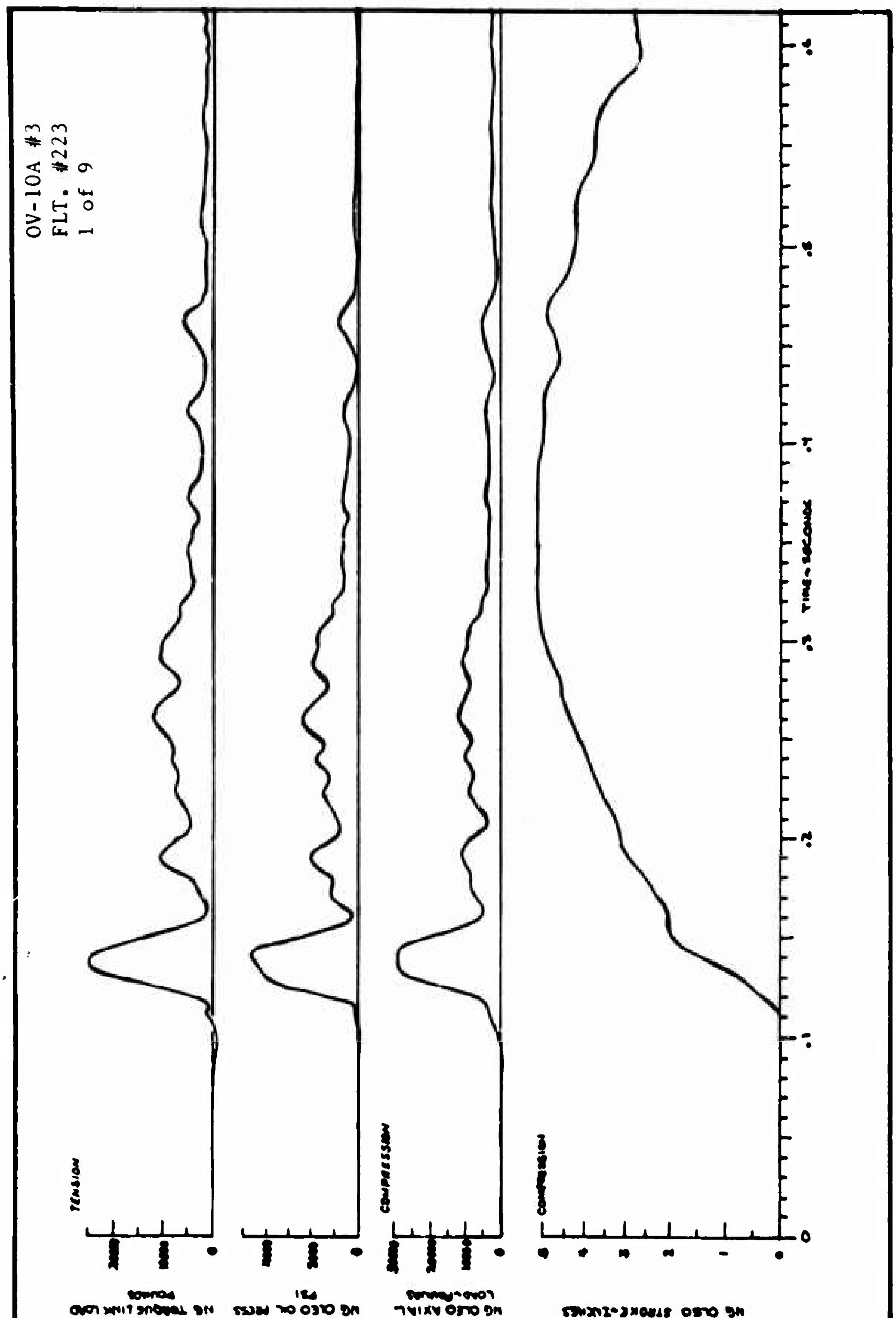

TIME HISTORIES OF LANDING GEAR
LOADS AND RESPONSE

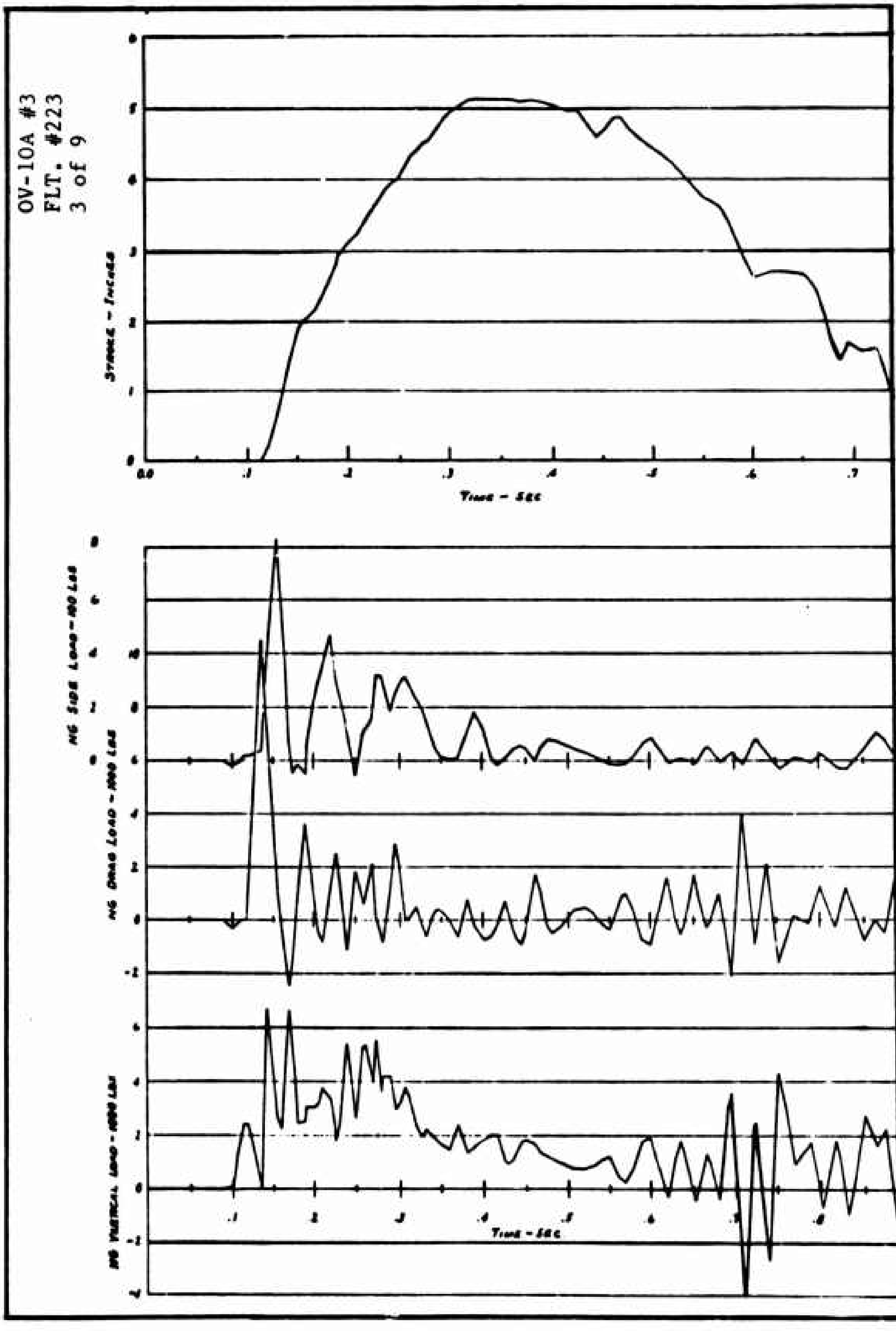

TIME HISTORIES OF LANDING GEAR
LOADS AND RESPONSE

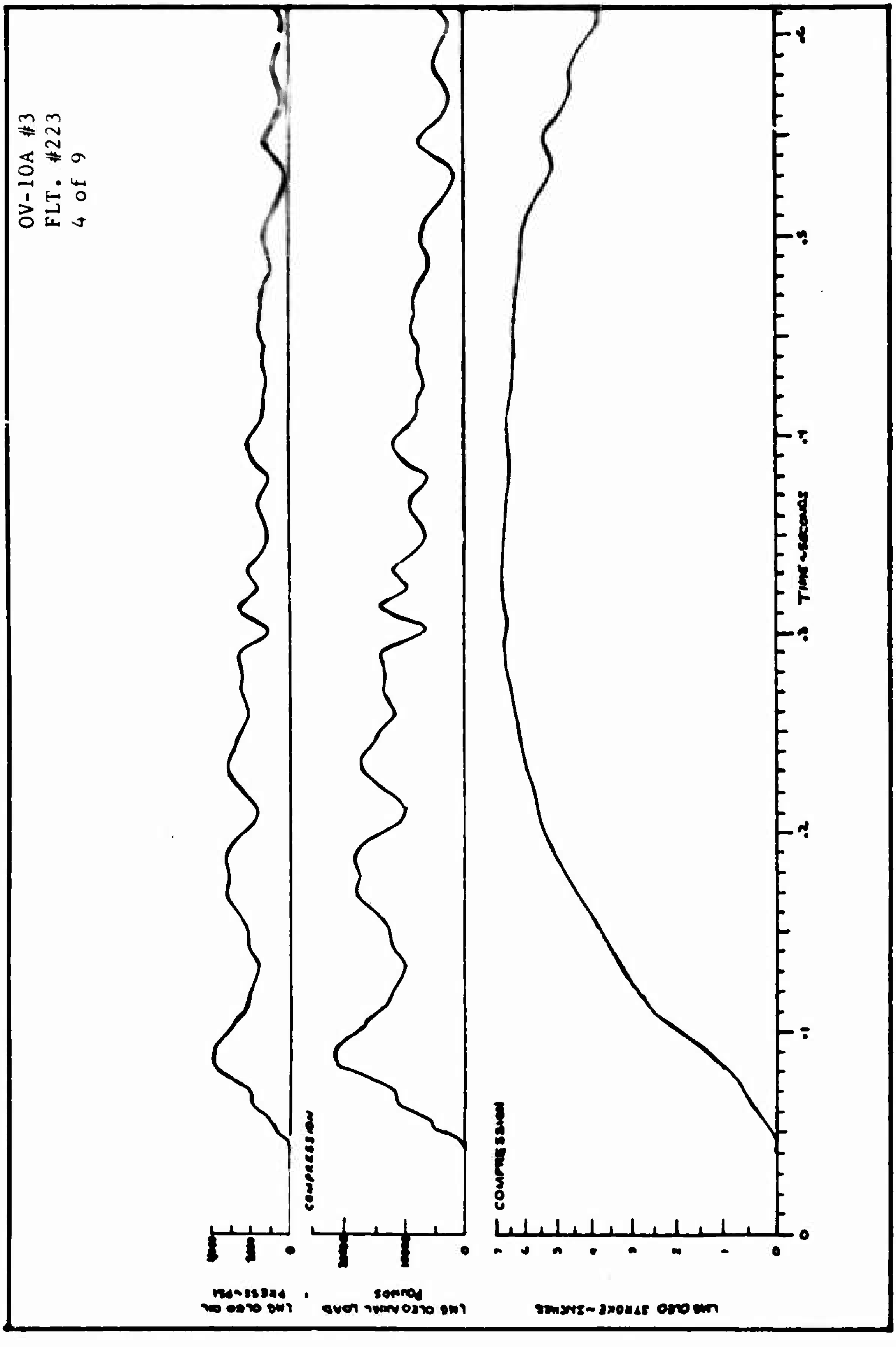

TIME HISTORIES OF LANDING GEAR
LOADS AND RESPONSE

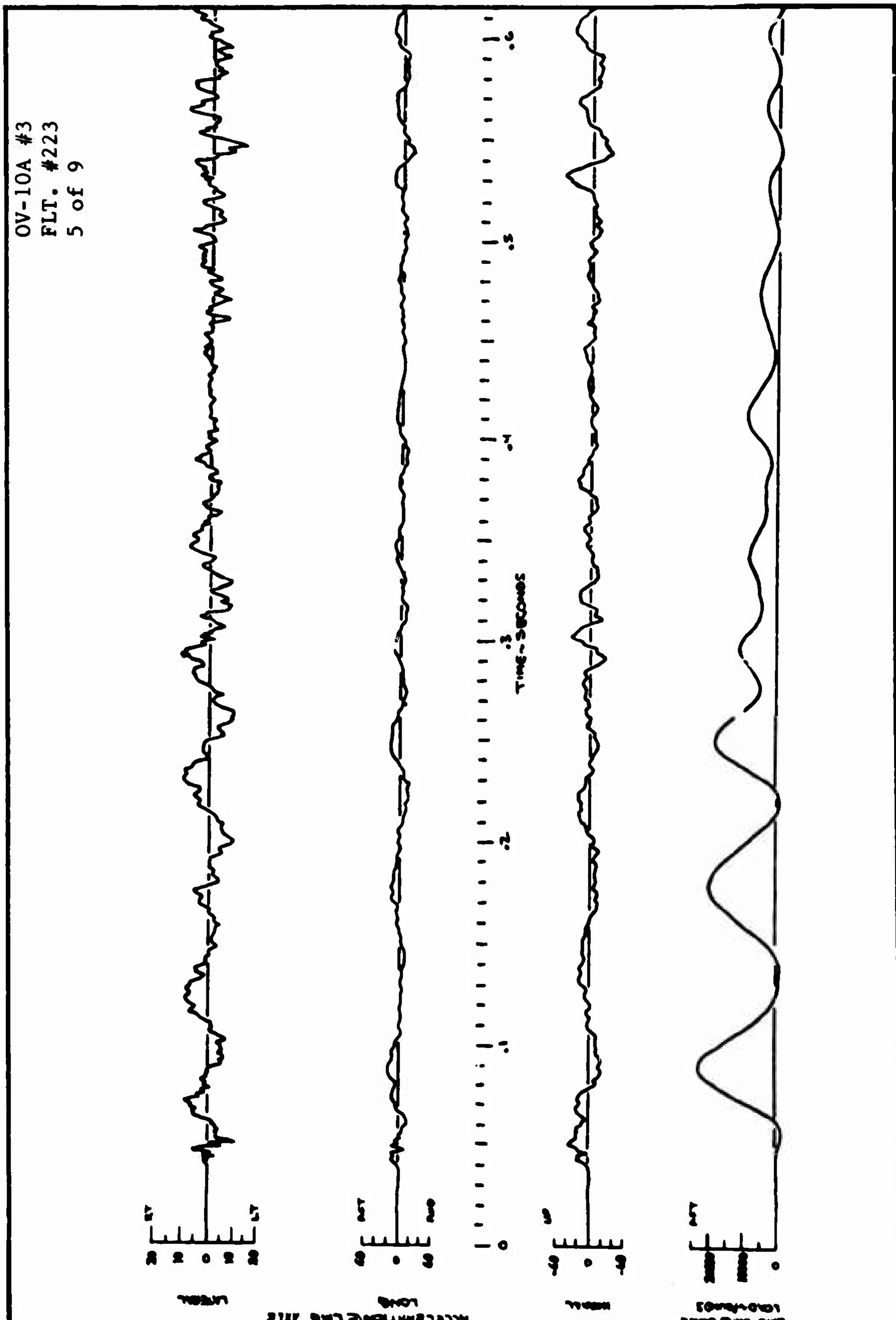

TIME HISTORIES OF LANDING GEAR
LOADS AND RESPONSE

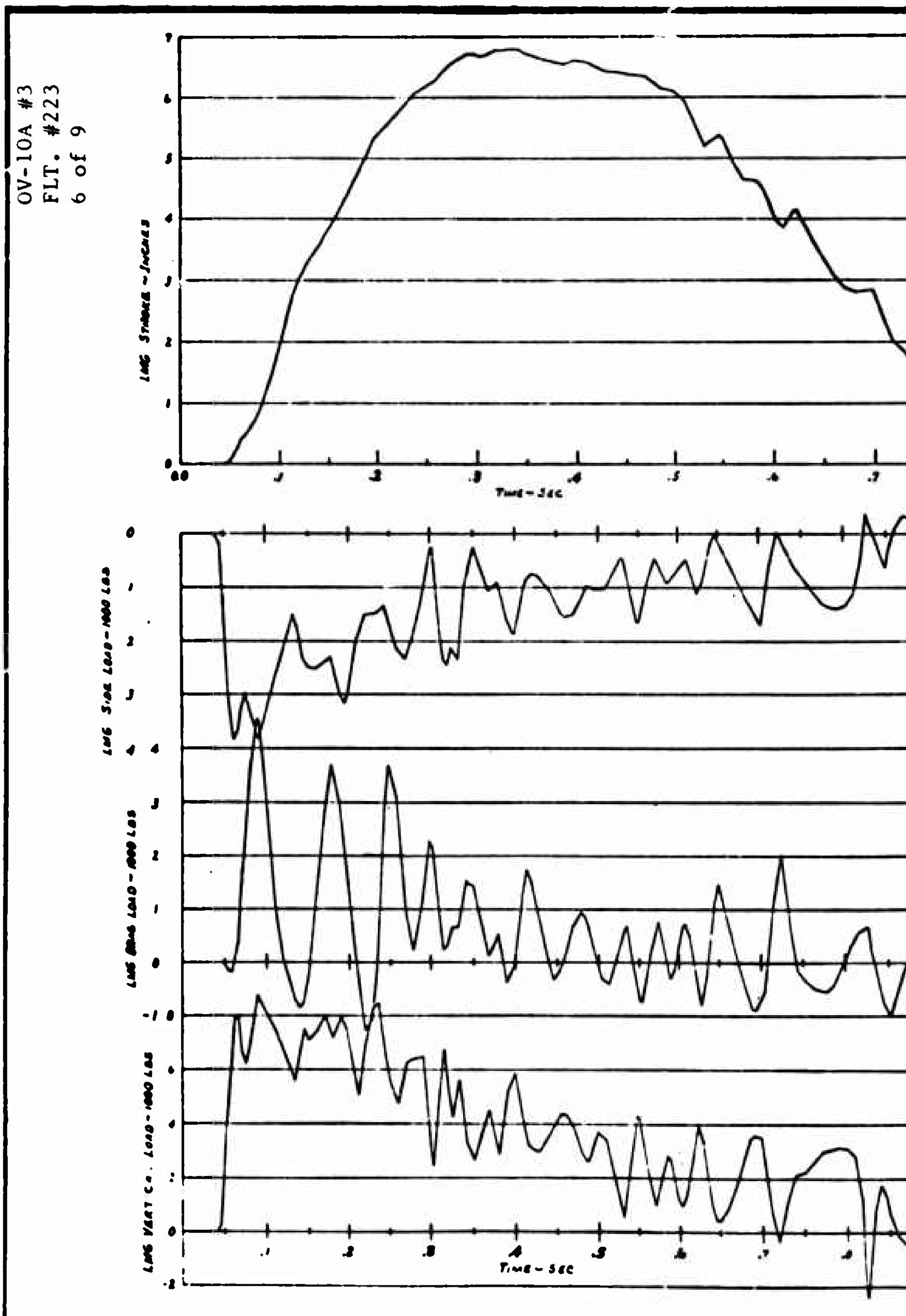

TIME HISTORIES OF LANDING GEAR
LOADS AND RESPONSE

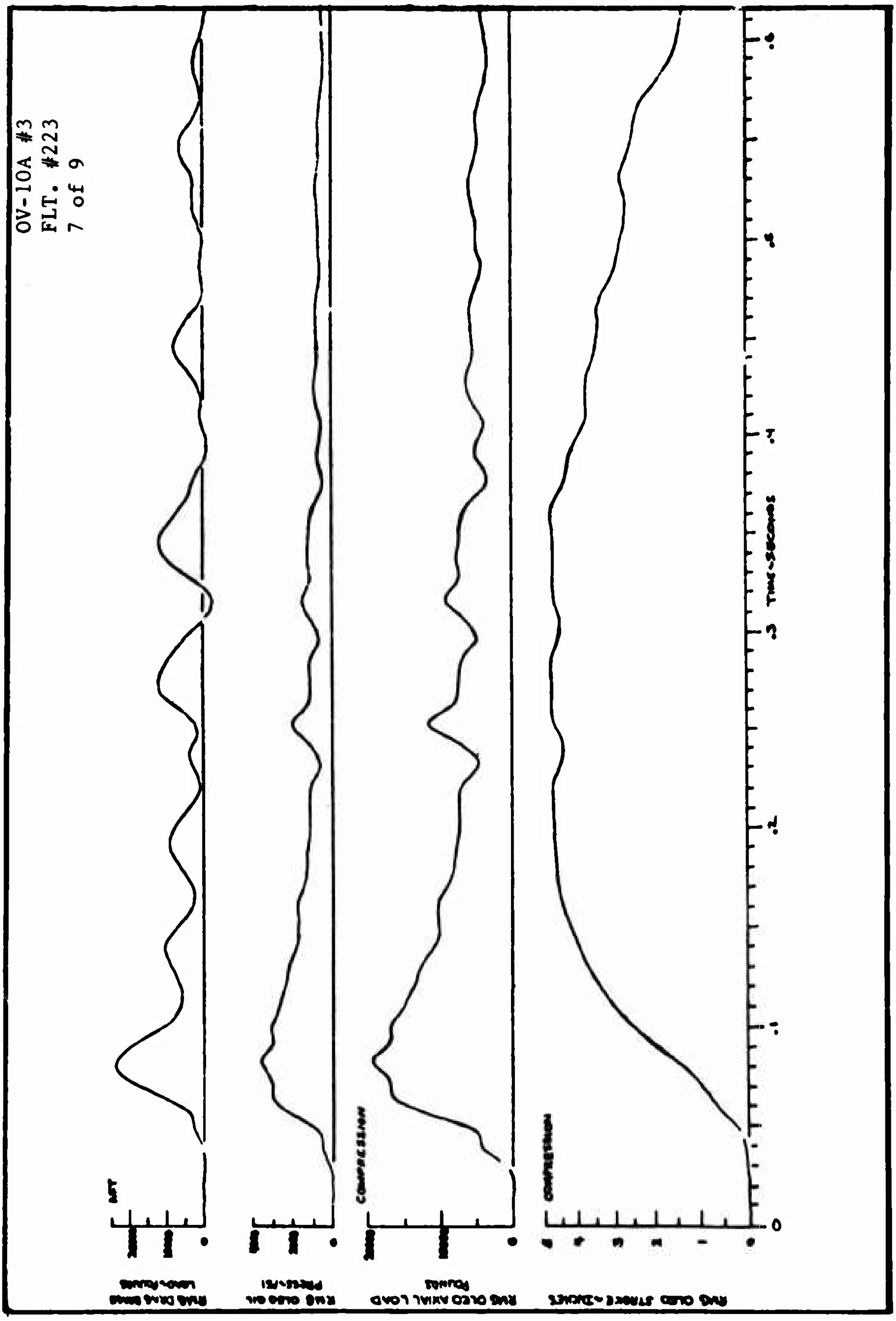

TIME HISTORIES OF LANDING GEAR
LOADS AND RESPONSE

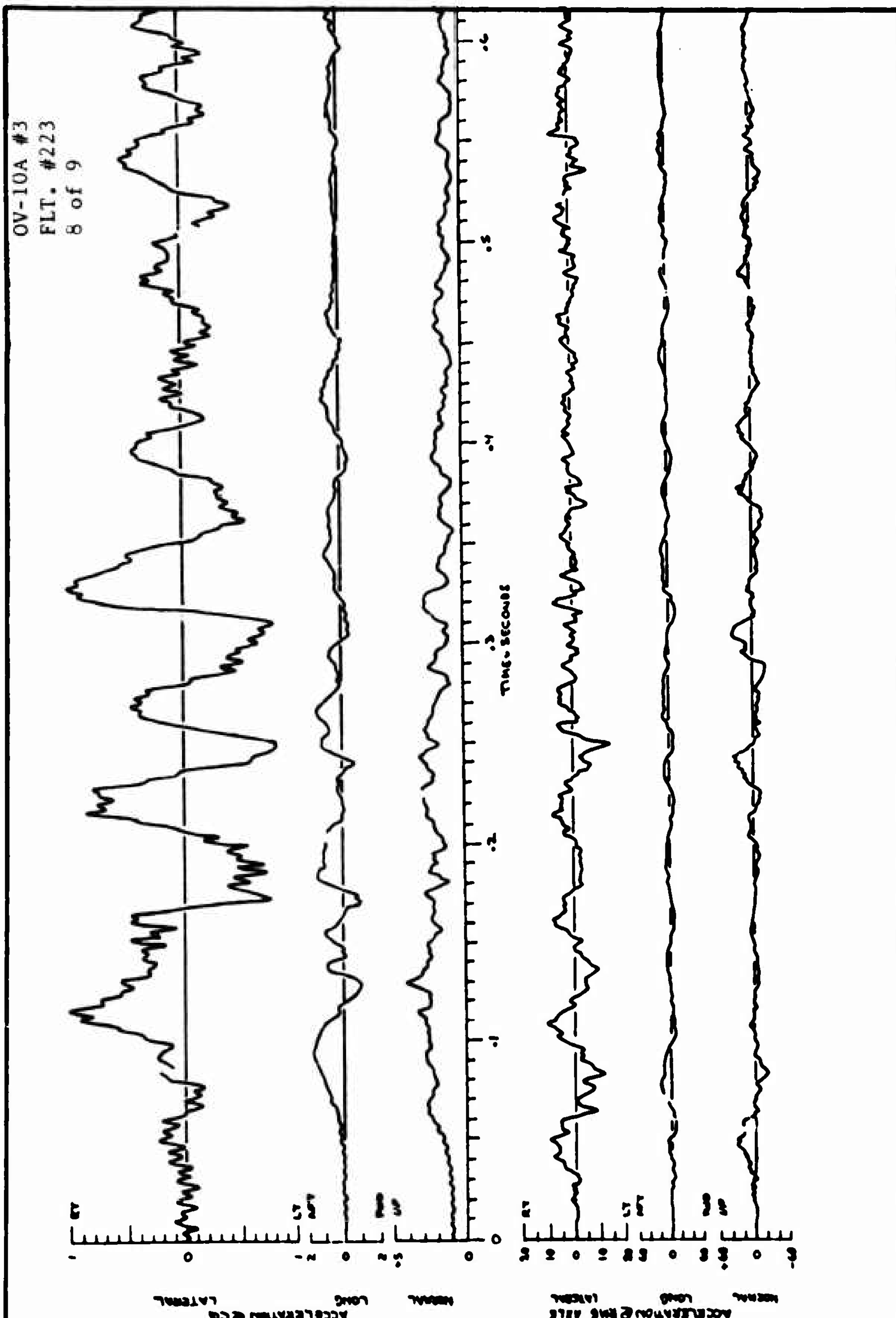

TIME HISTORIES OF LANDING GEAR
LOADS AND RESPONSE

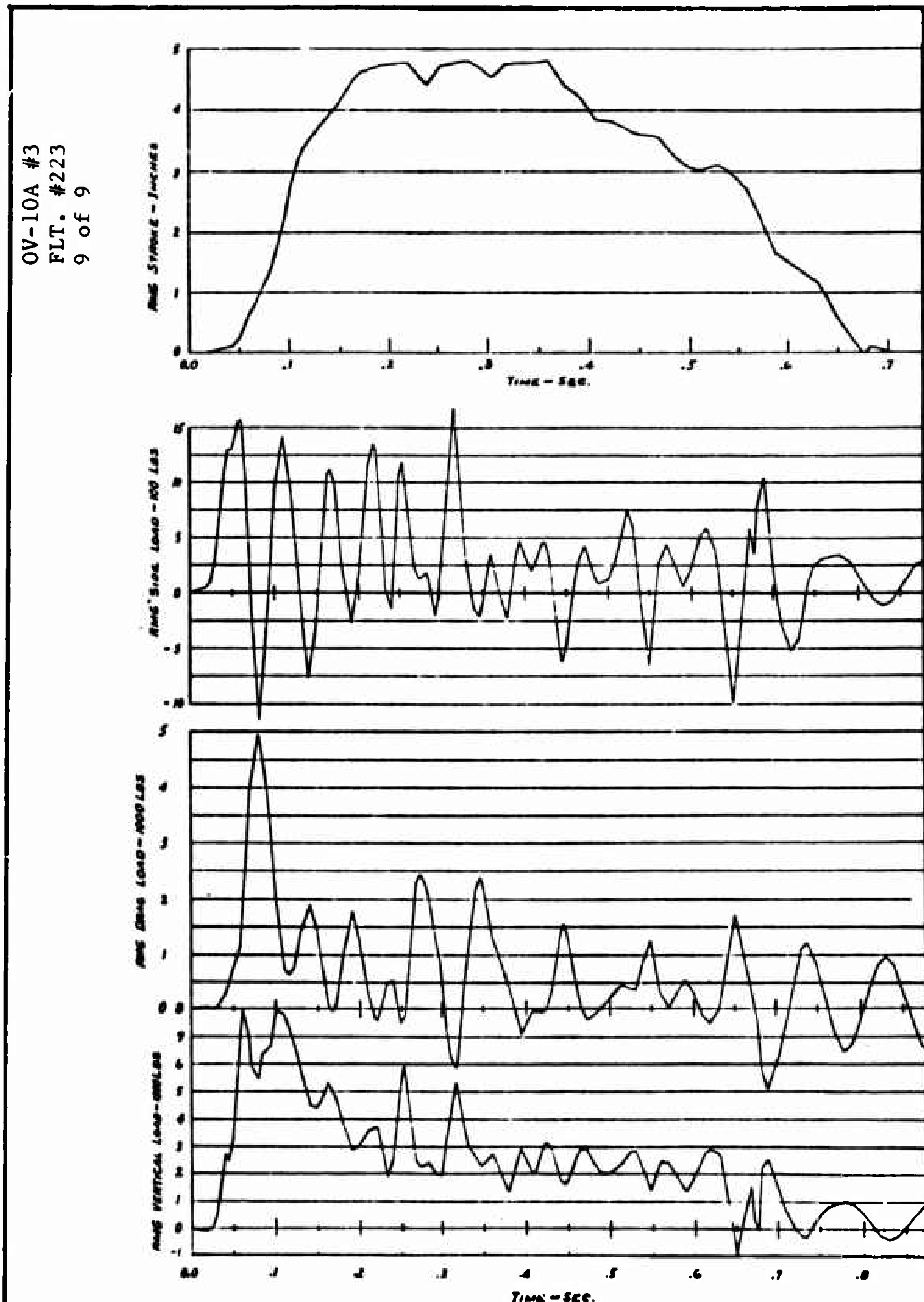

TIME HISTORIES OF LANDING GEAR
LOADS AND RESPONSE

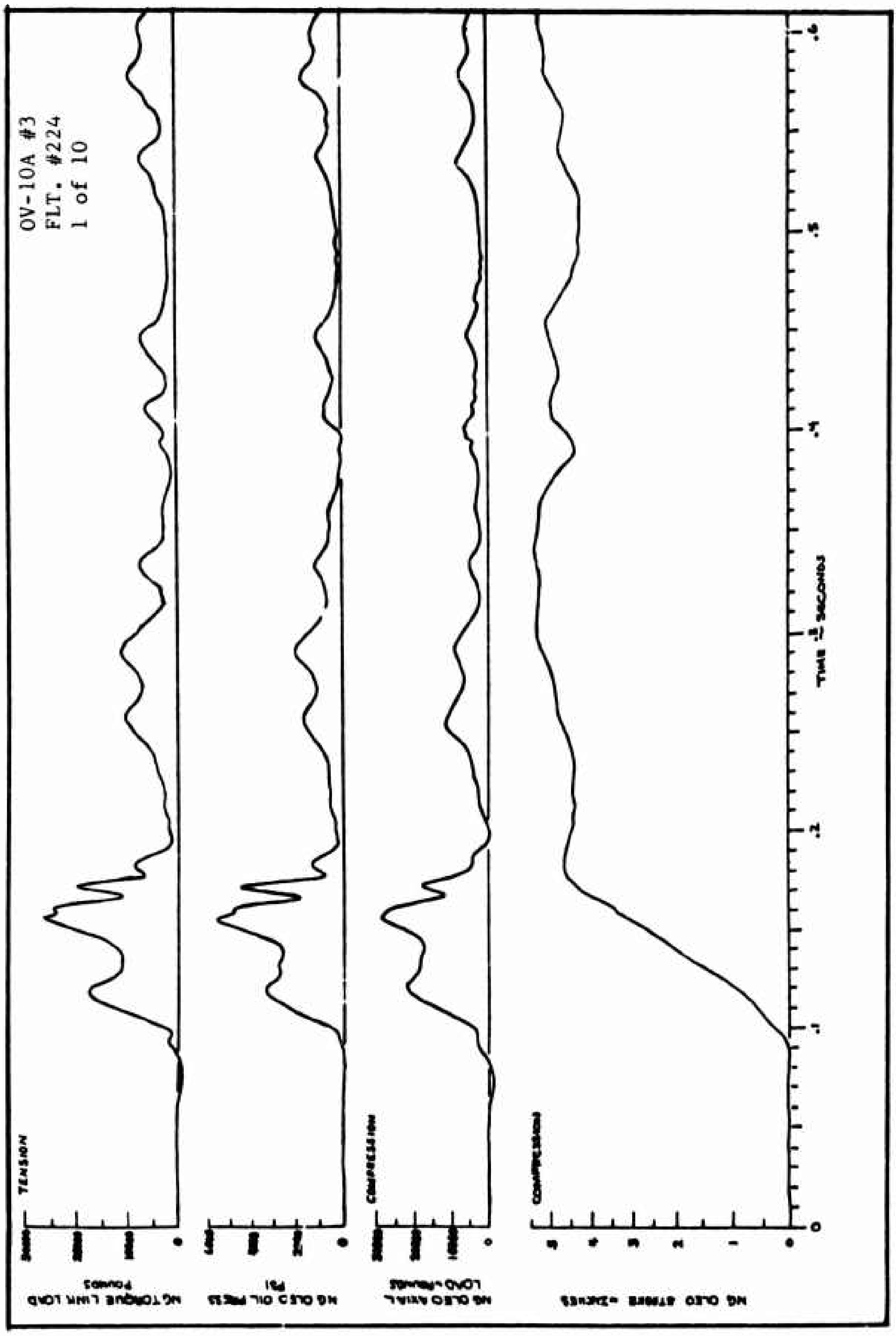

TIME HISTORIES OF LANDING GEAR
LOADS AND RESPONSE

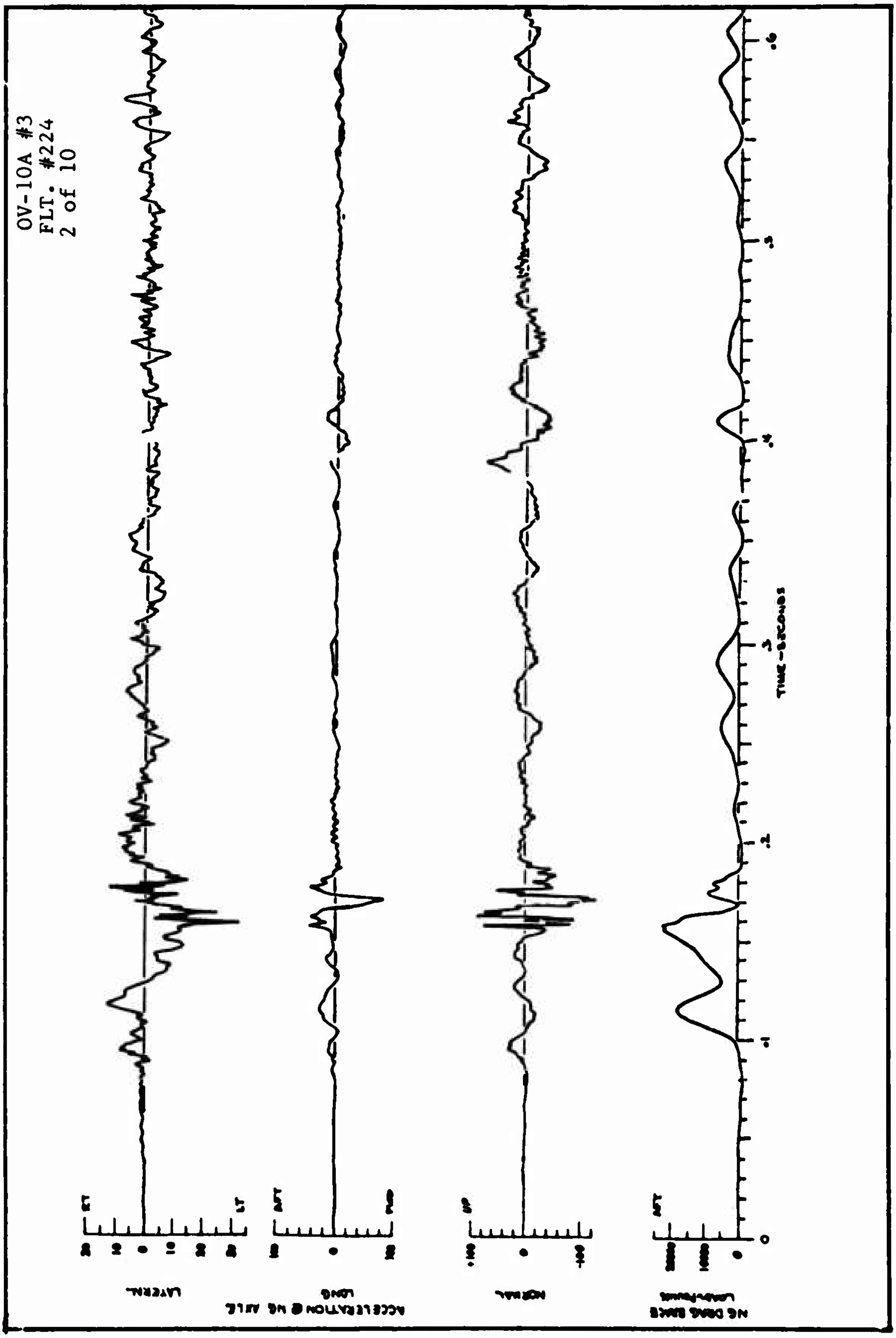

TIME HISTORIES OF LANDING GEAR
LOADS AND RESPONSE

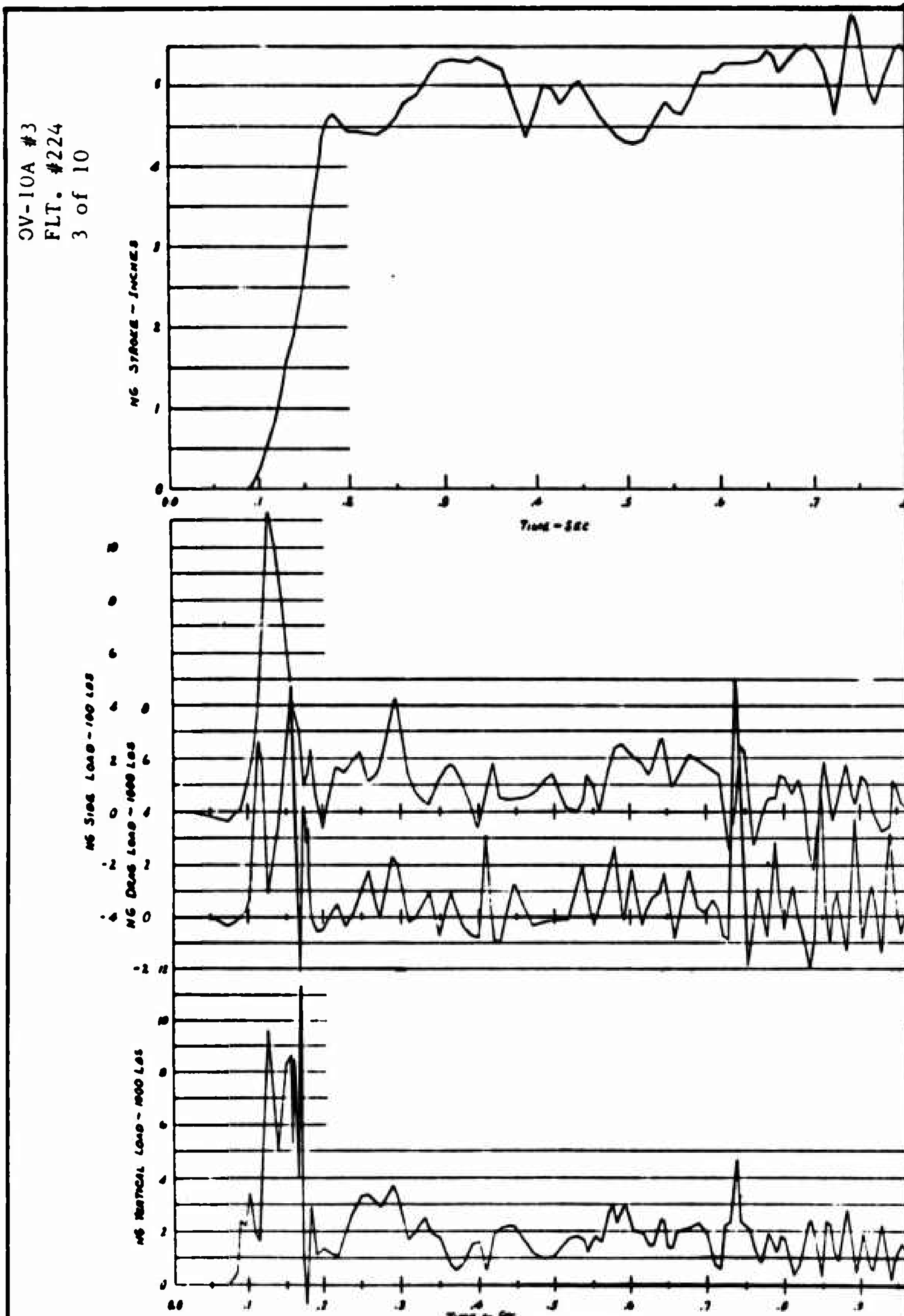

TIME HISTORIES OF LANDING GEAR
LOADS AND RESPONSE

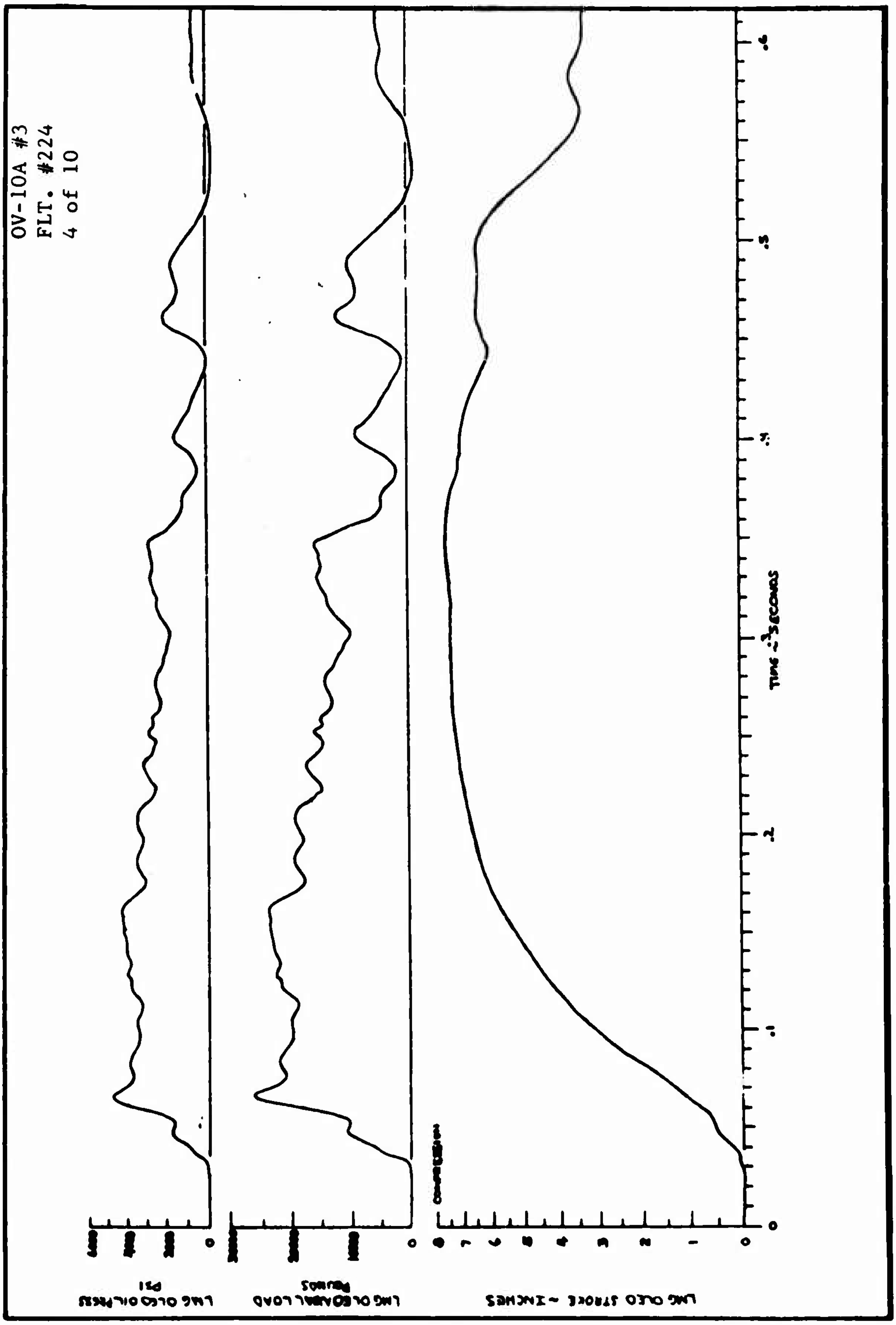

TIME HISTORIES OF LANDING GEAR
LOADS AND RESPONSE

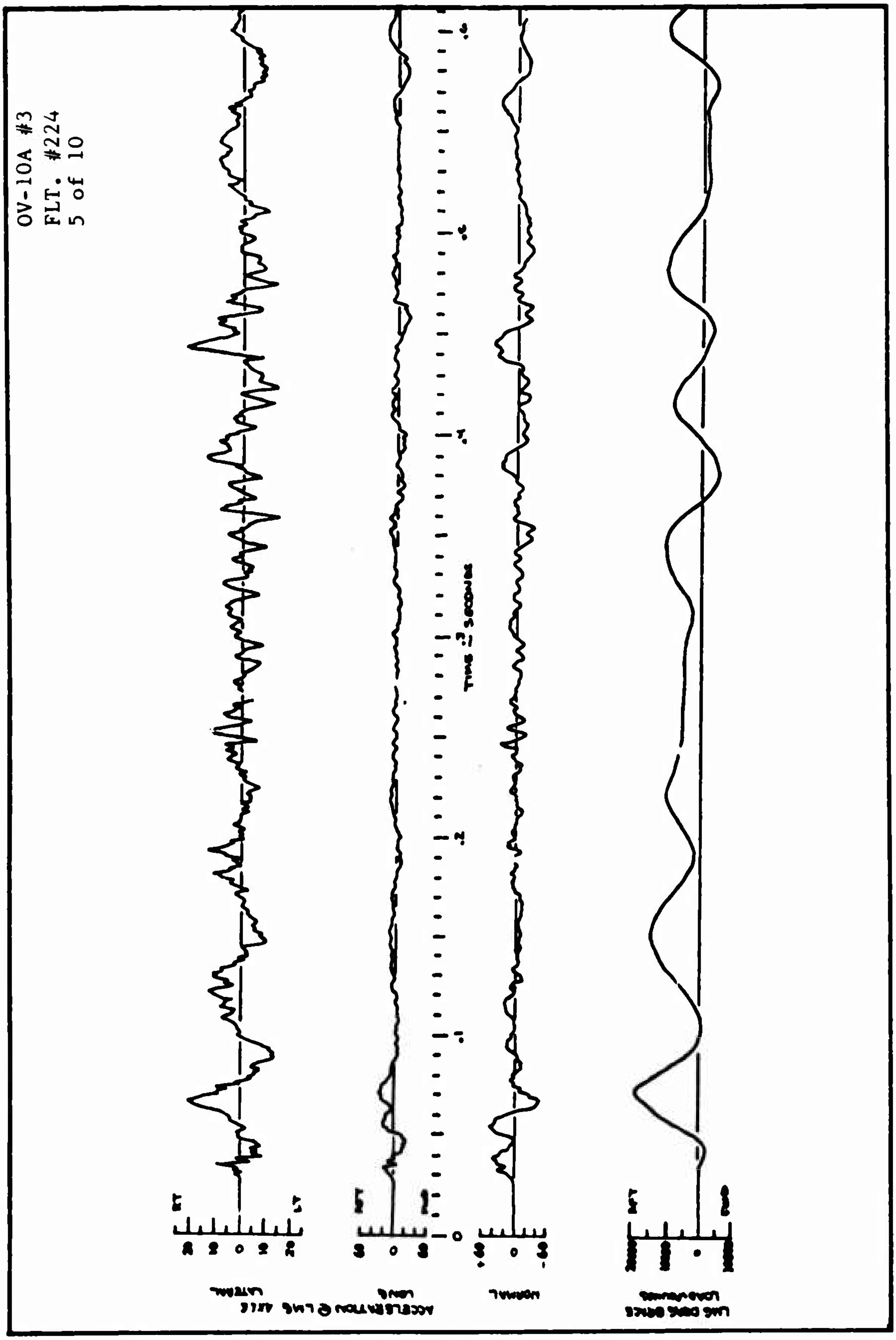

TIME HISTORIES OF LANDING GEAR
LOADS AND RESPONSE

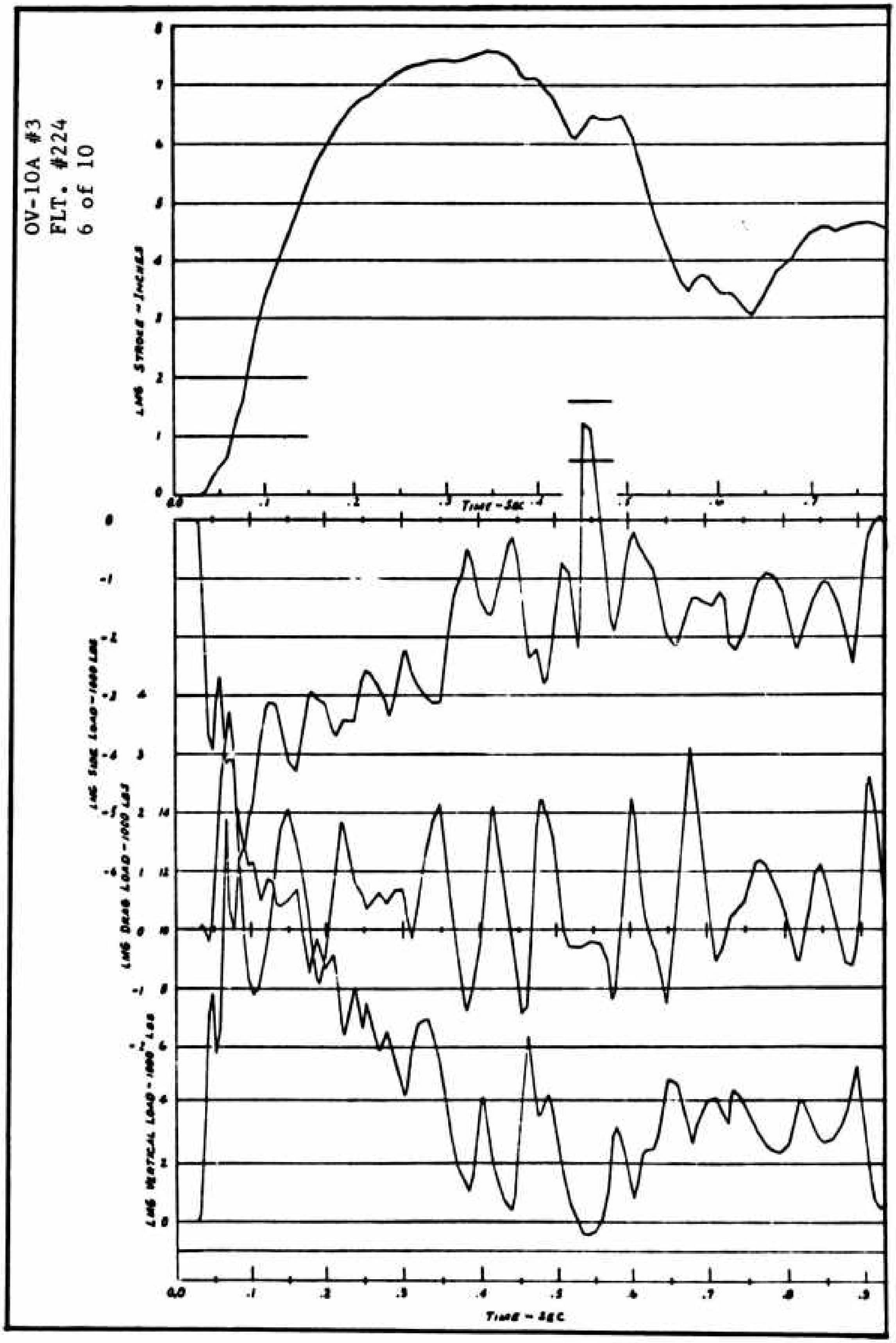

TIME HISTORIES OF LANDING GEAR
LOADS AND RESPONSE

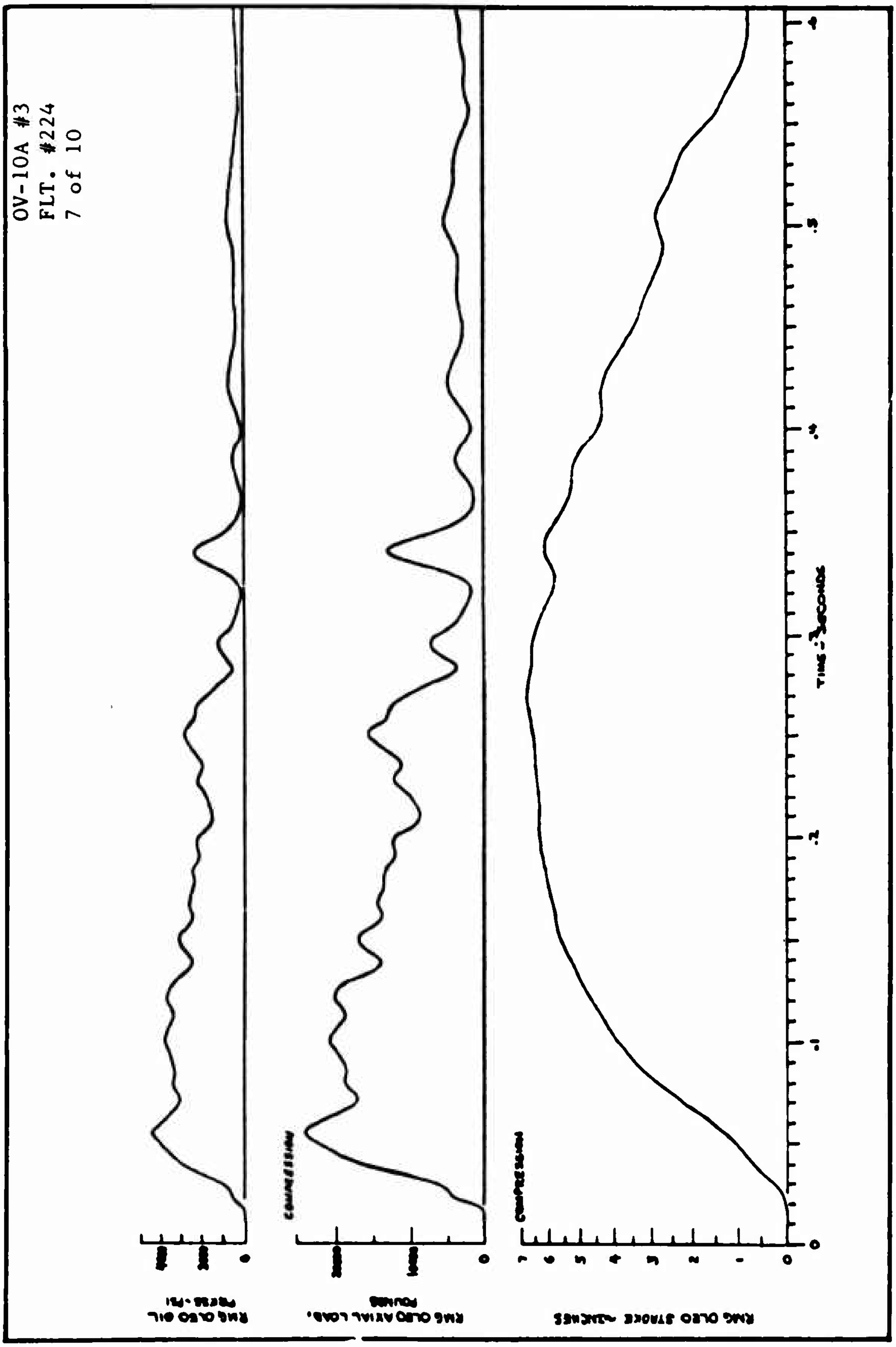

TIME HISTORIES OF LANDING GEAR
LOADS AND RESPONSE

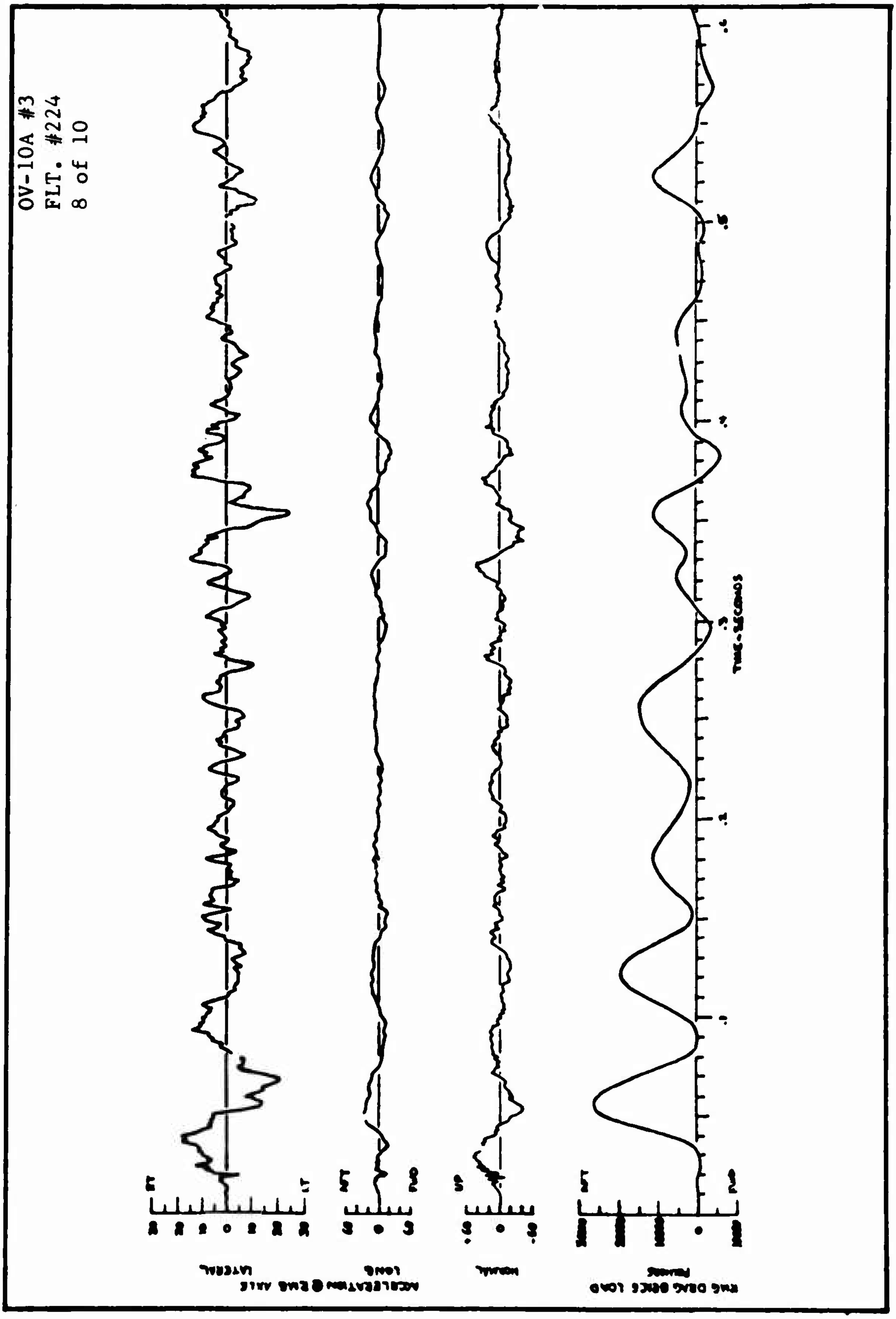

TIME HISTORIES OF LANDING GEAR
LOADS AND RESPONSE

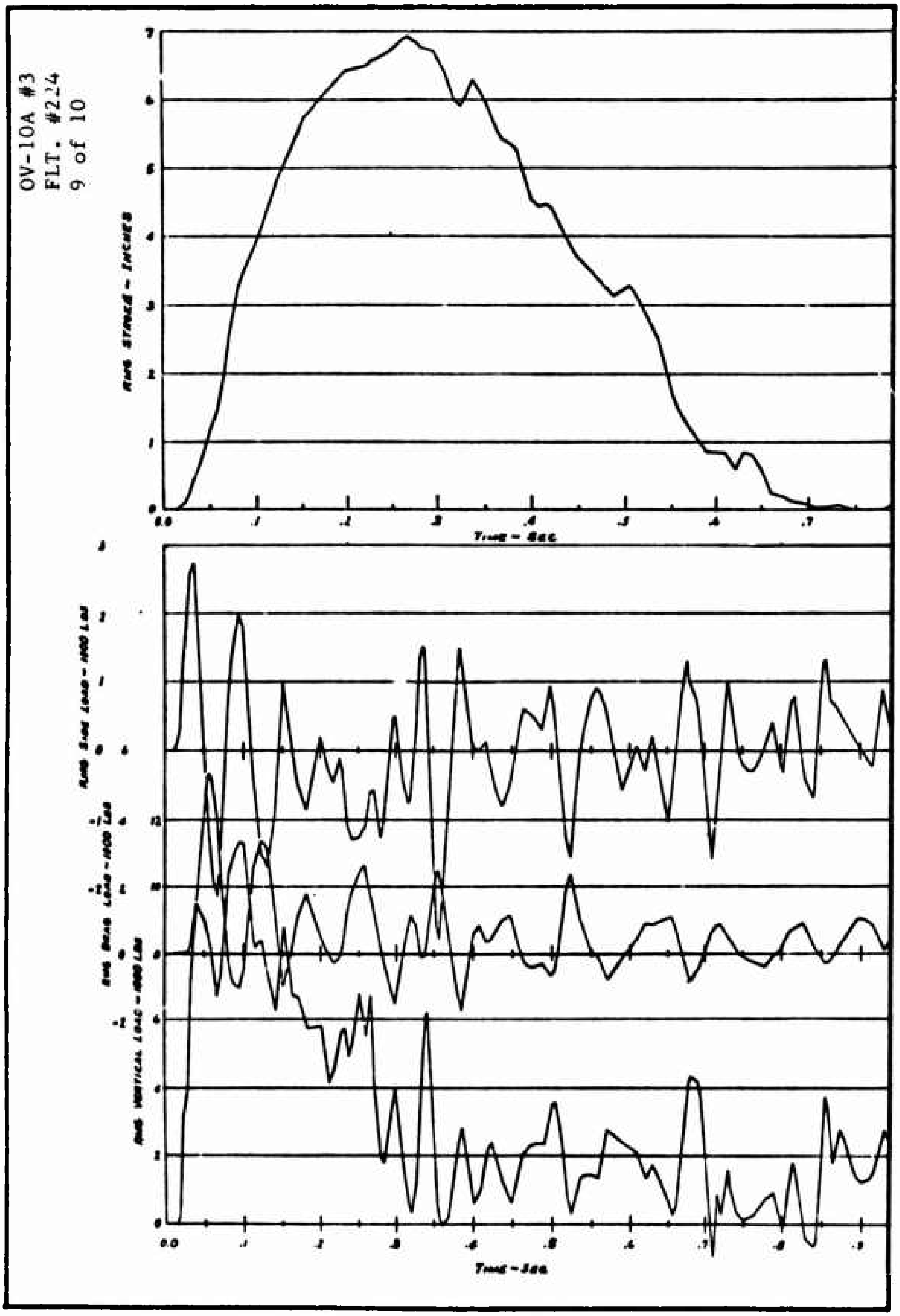

TIME HISTORIES OF LANDING GEAR
LOADS AND RESPONSE

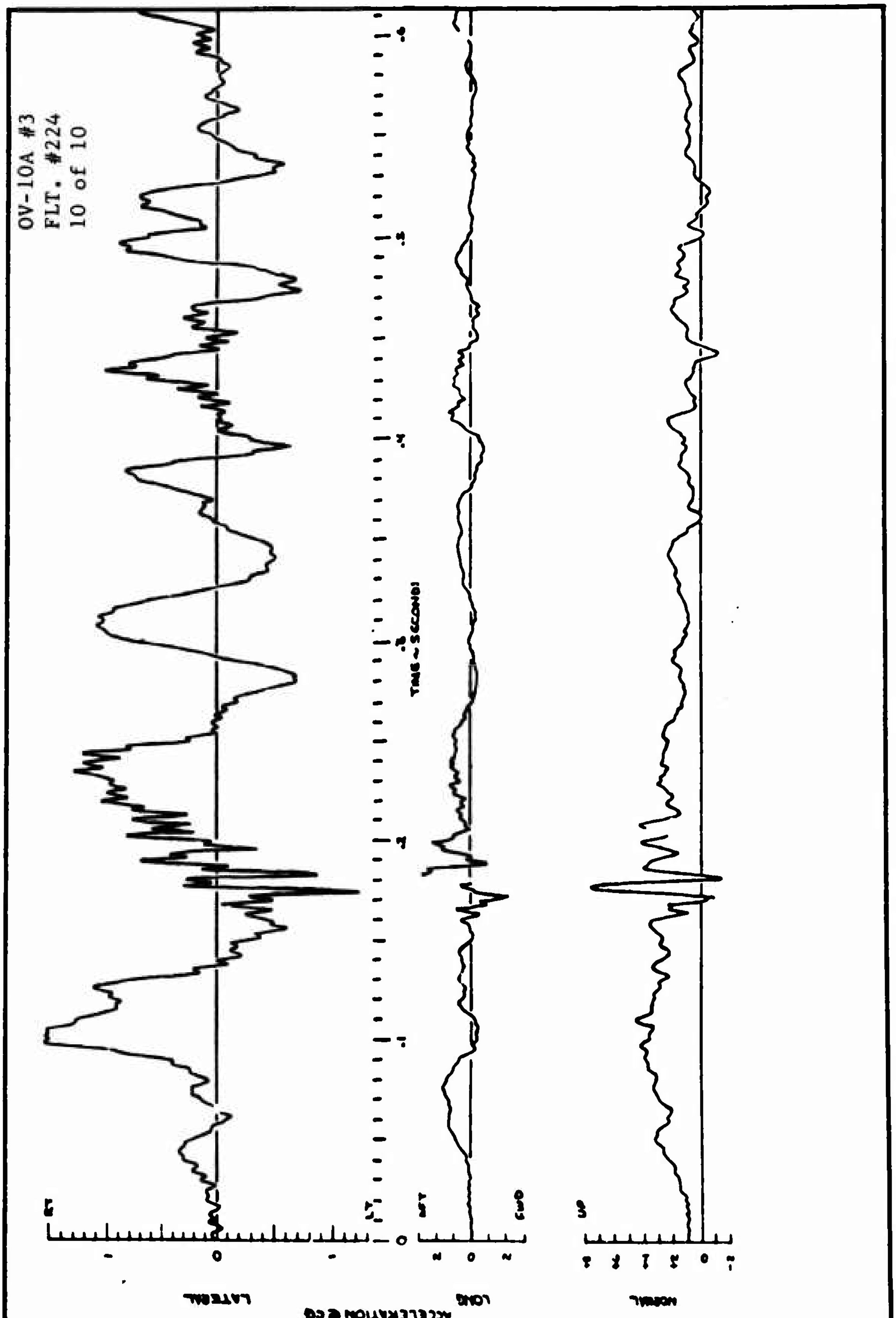

TIME HISTORIES OF LANDING GEAR
LOADS AND RESPONSE

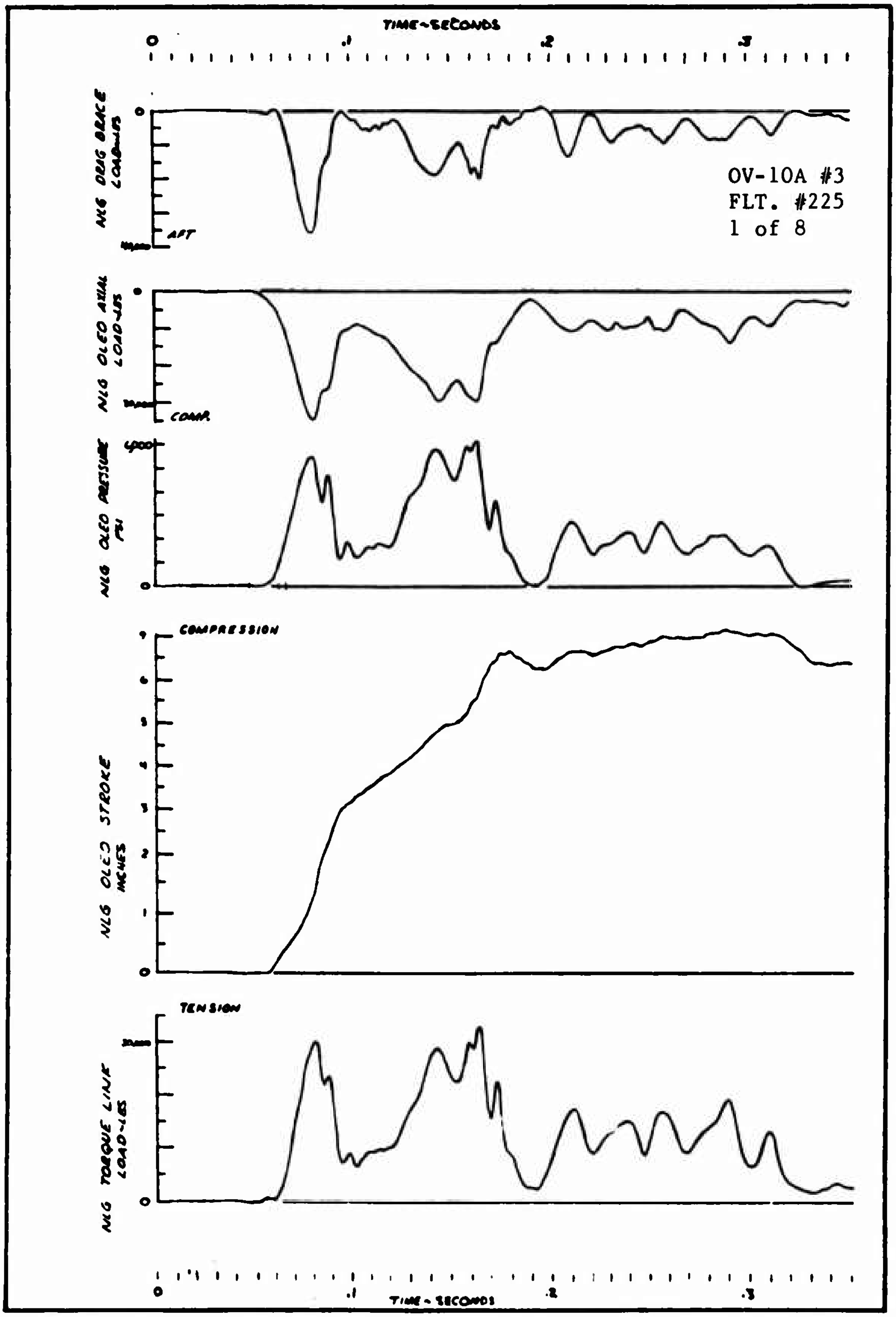

TIME HISTORIES OF LANDING GEAR
LOADS AND RESPONSE

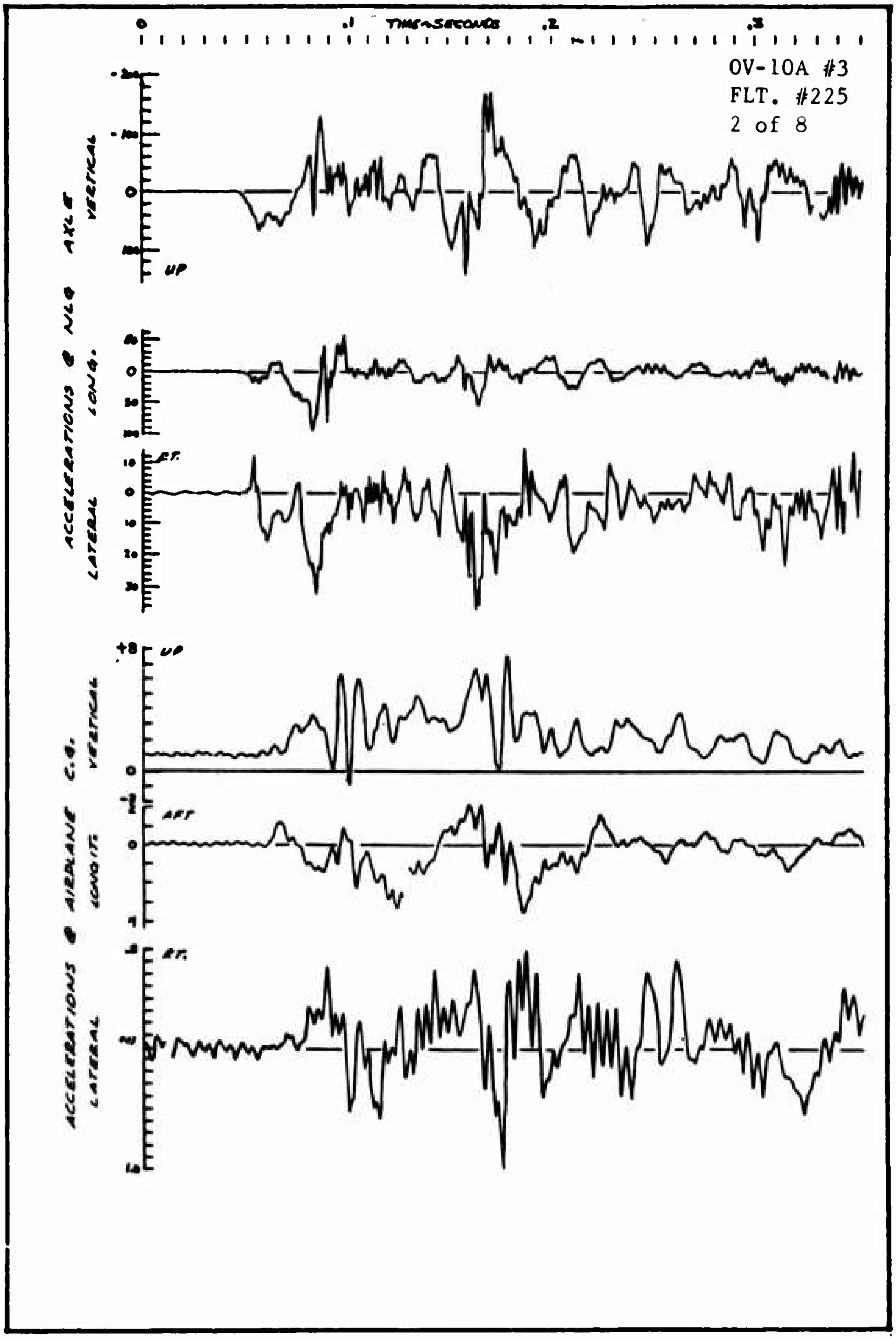

TIME HISTORIES OF LANDING GEAR
LOADS AND RESPONSE

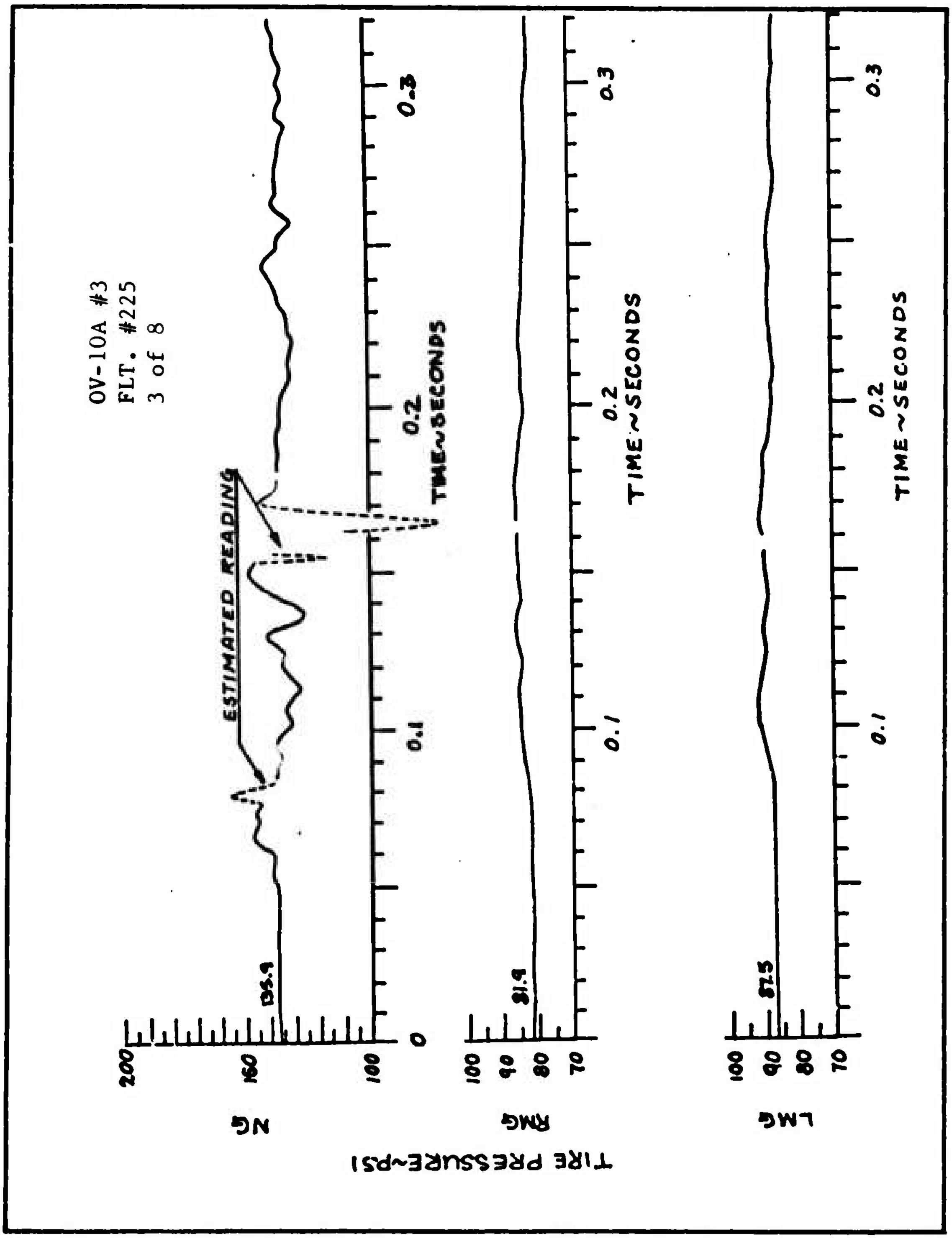

TIME HISTORIES OF LANDING GEAR
LOADS AND RESPONSE

OV-10A #3
FLT. #225
4 of 8

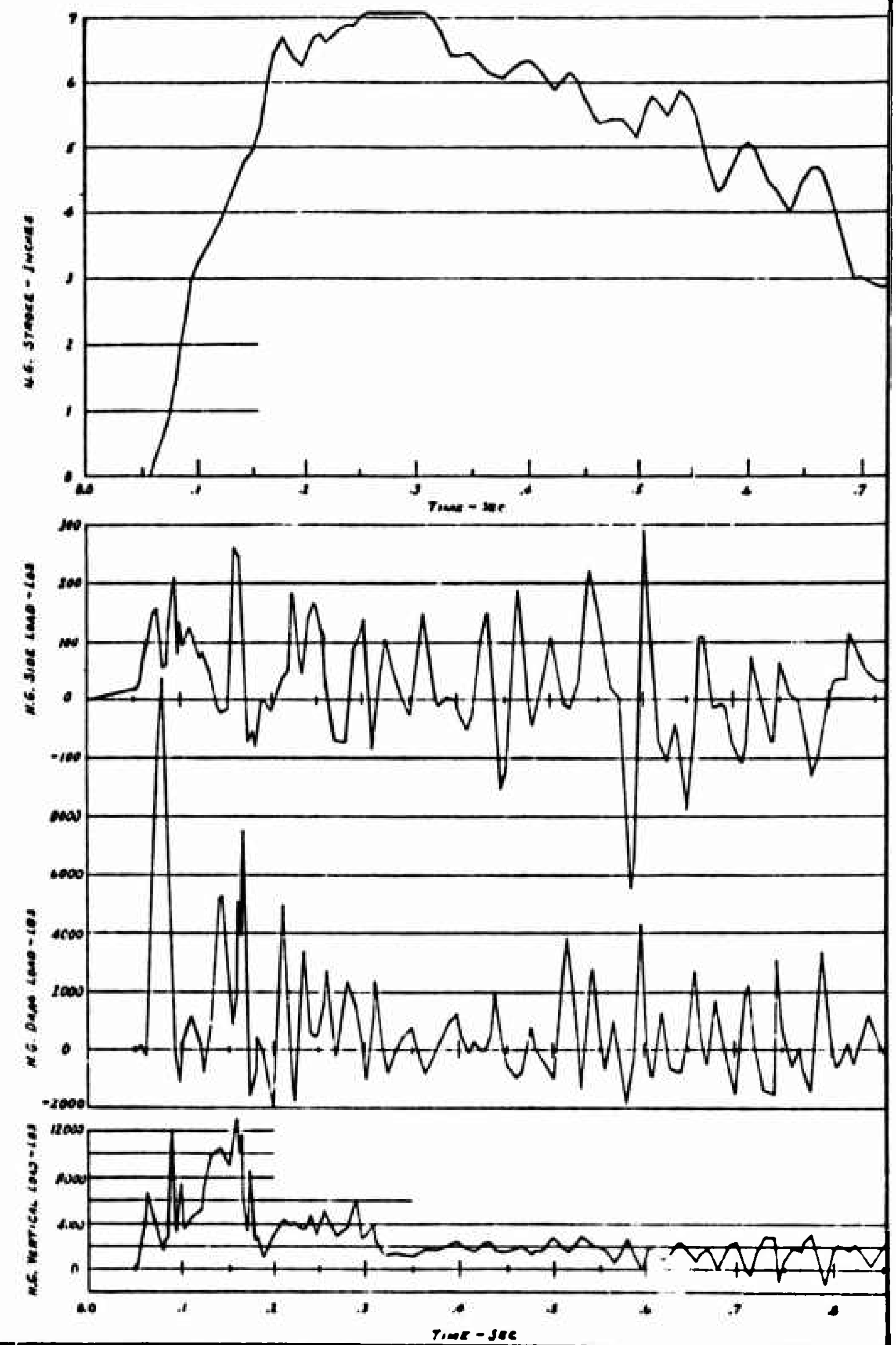

TIME HISTORIES OF LANDING GEAR
LOADS AND RESPONSE

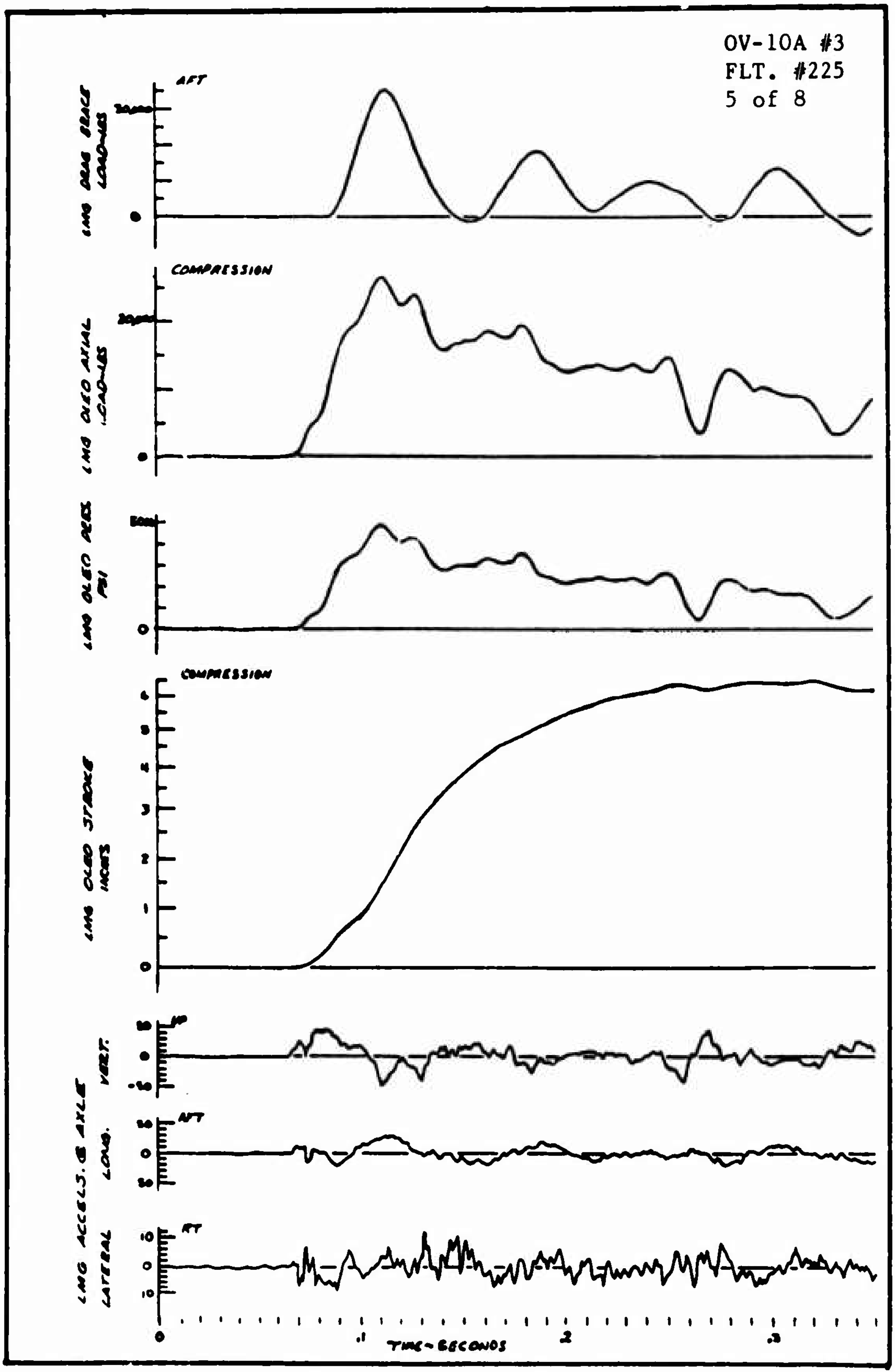

TIME HISTORIES OF LANDING GEAR
LOADS AND RESPONSE

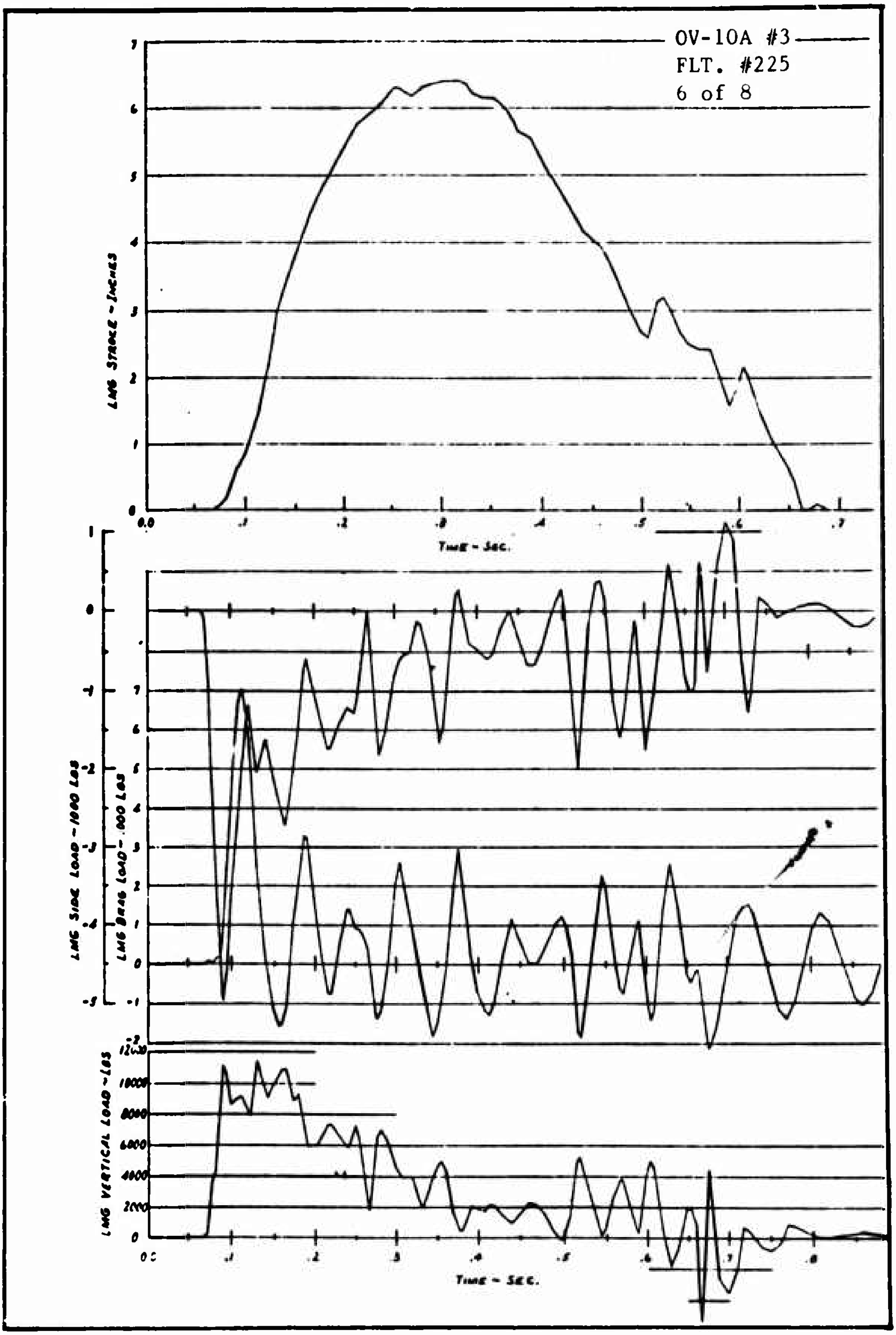

TIME HISTORIES OF LANDING GEAR
LOADS AND RESPONSE

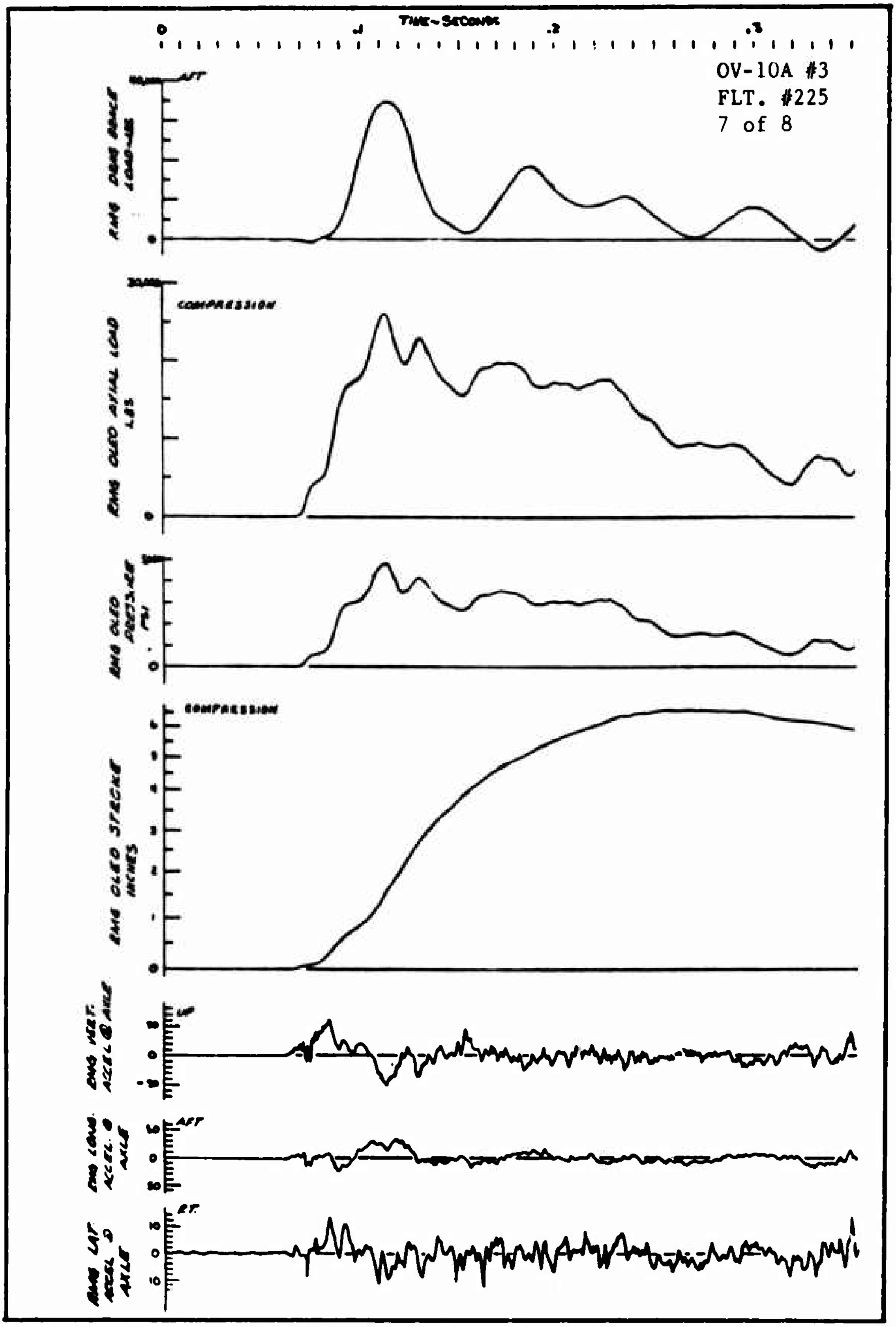

TIME HISTORIES OF LANDING GEAR
LOADS AND RESPONSE

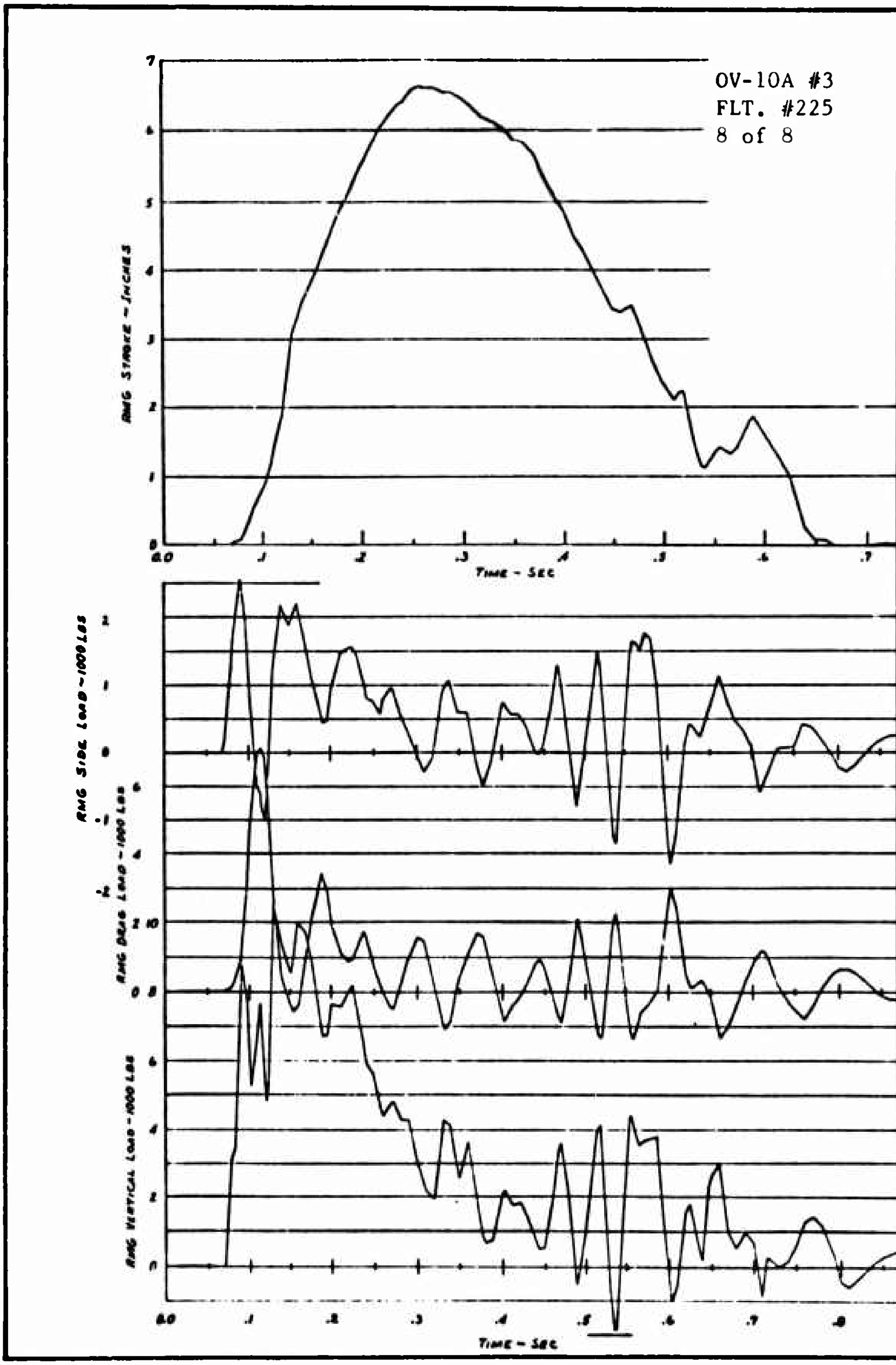

A

OV1(

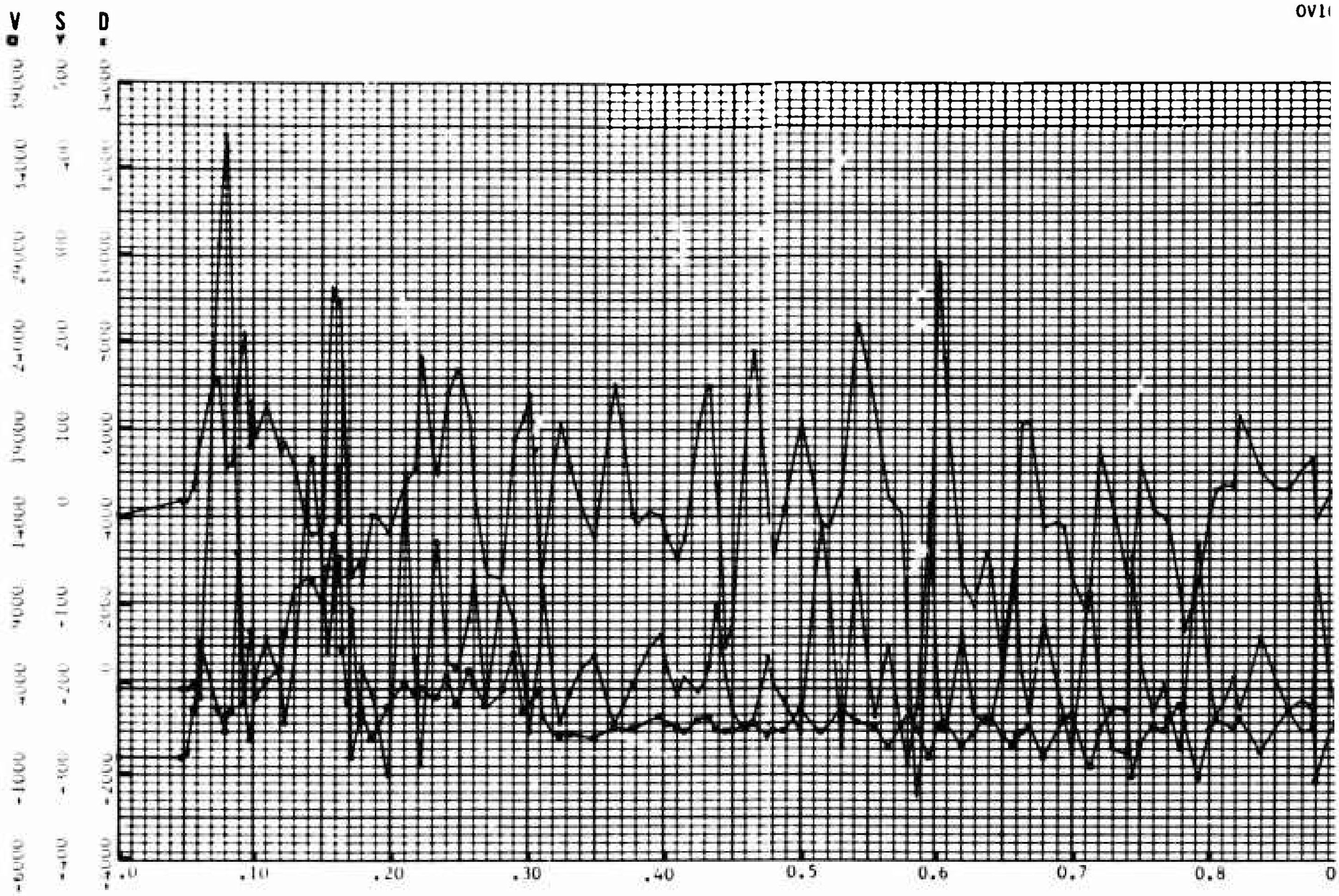

OV10A NG LOADS,

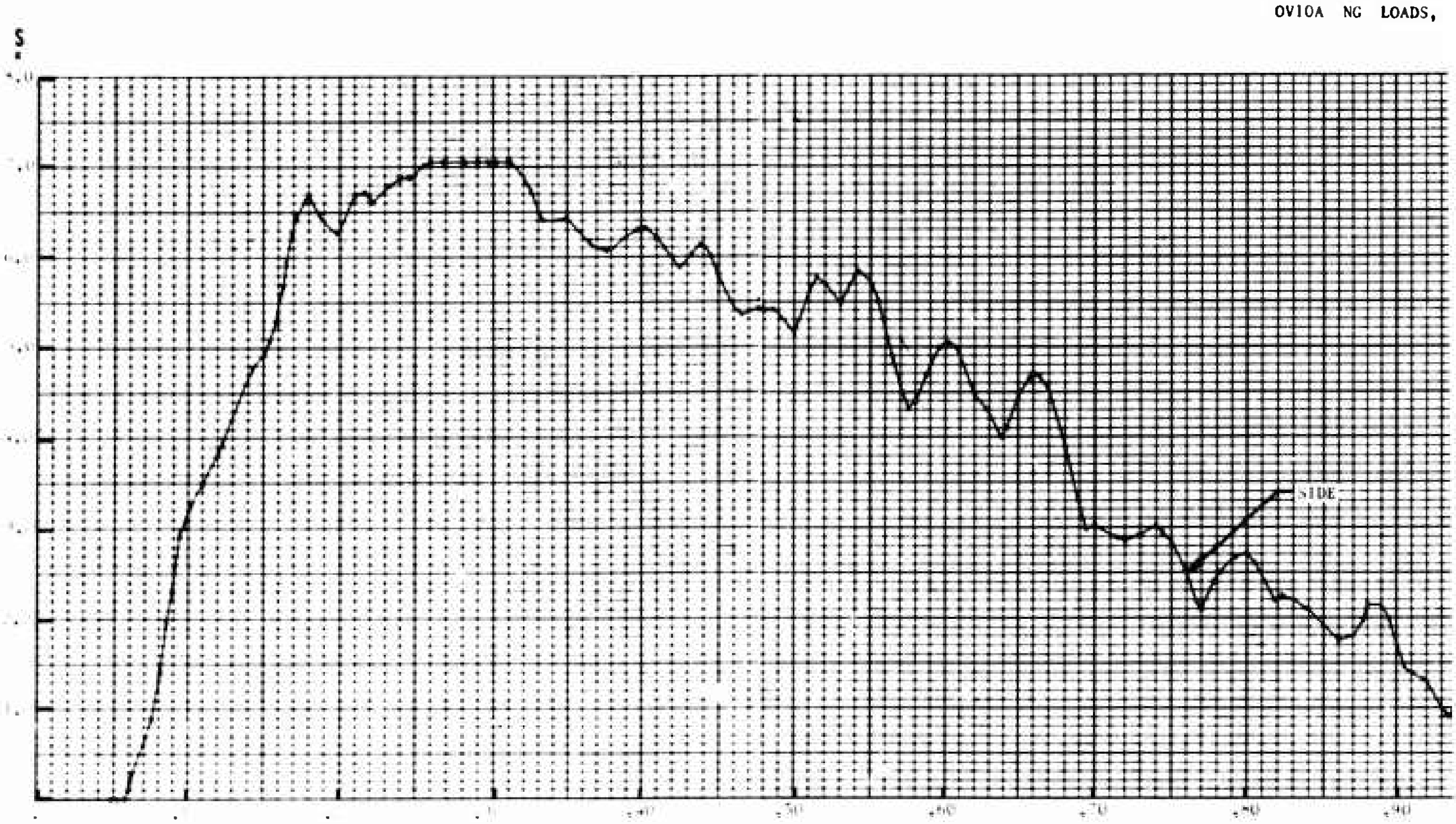

1 B

A NG LOADS, POUNDS FLIGHT NO. 225 RUN NO. 2

LOADS AT THE AXLE

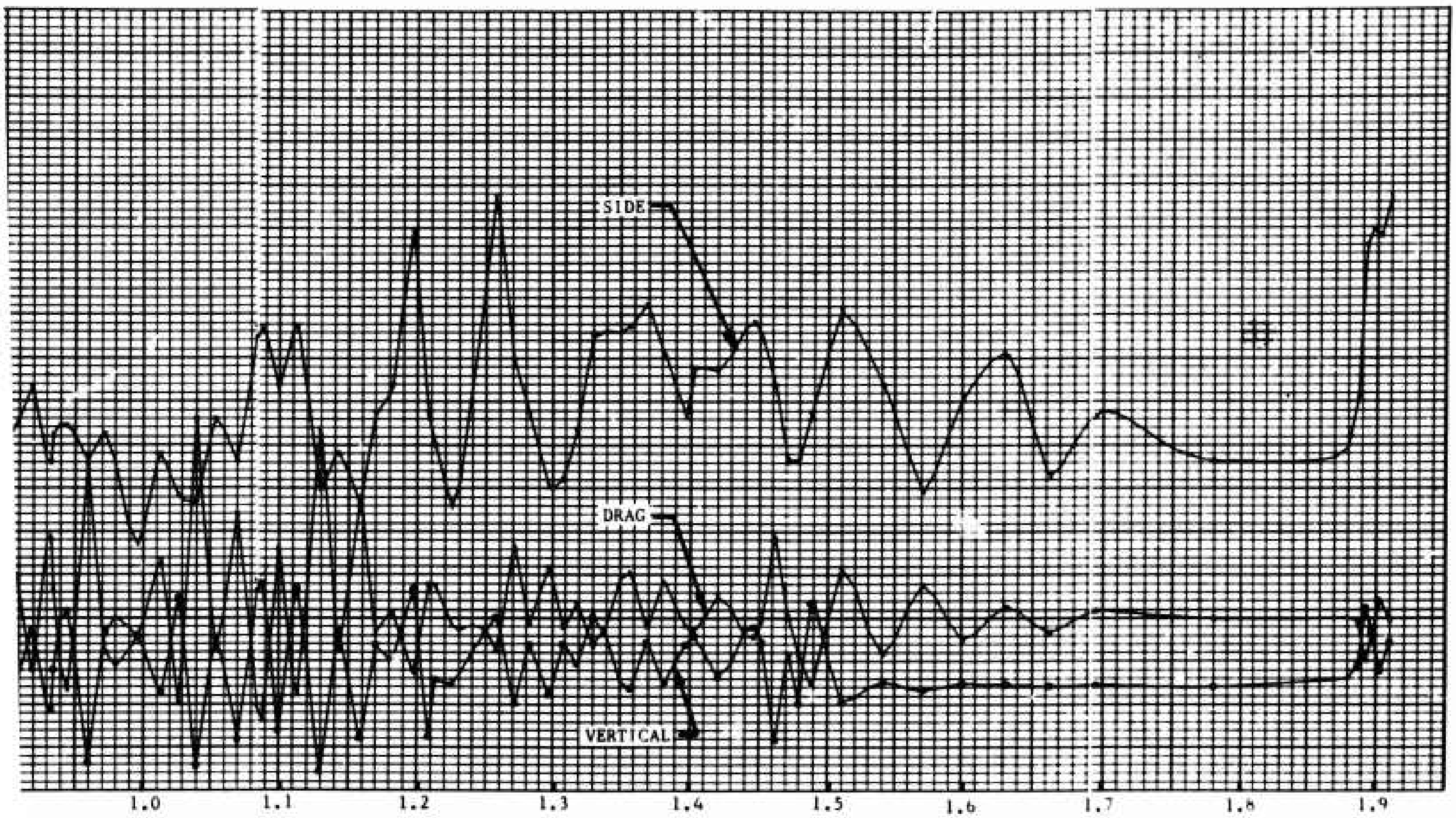

TIME, SECONDS

UNDS FLIGHT NO. 225 RUN NO. 2

LEO STROKE TIME HISTORY

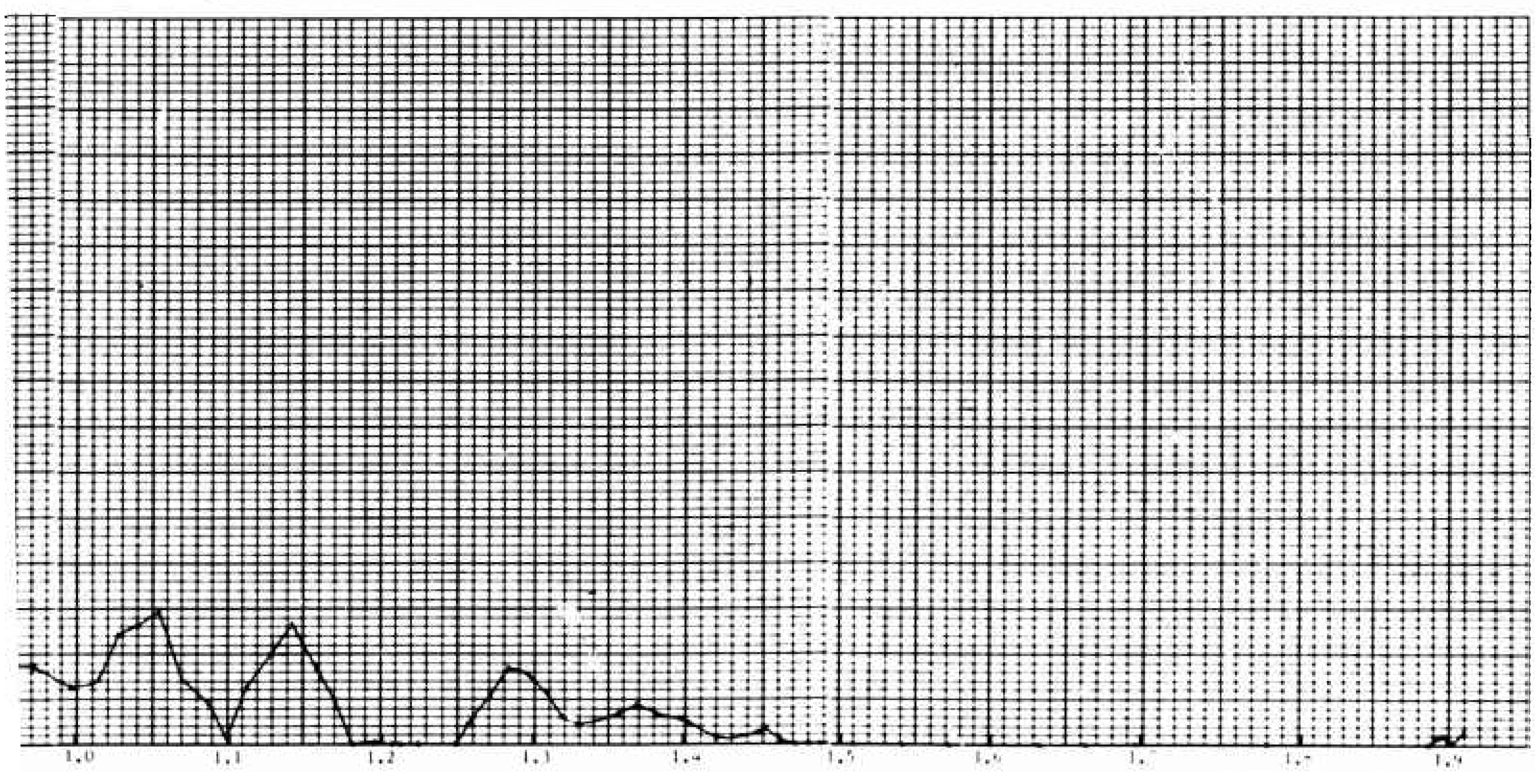

ME, SECONDS

PRECEDING PAGE BLANK

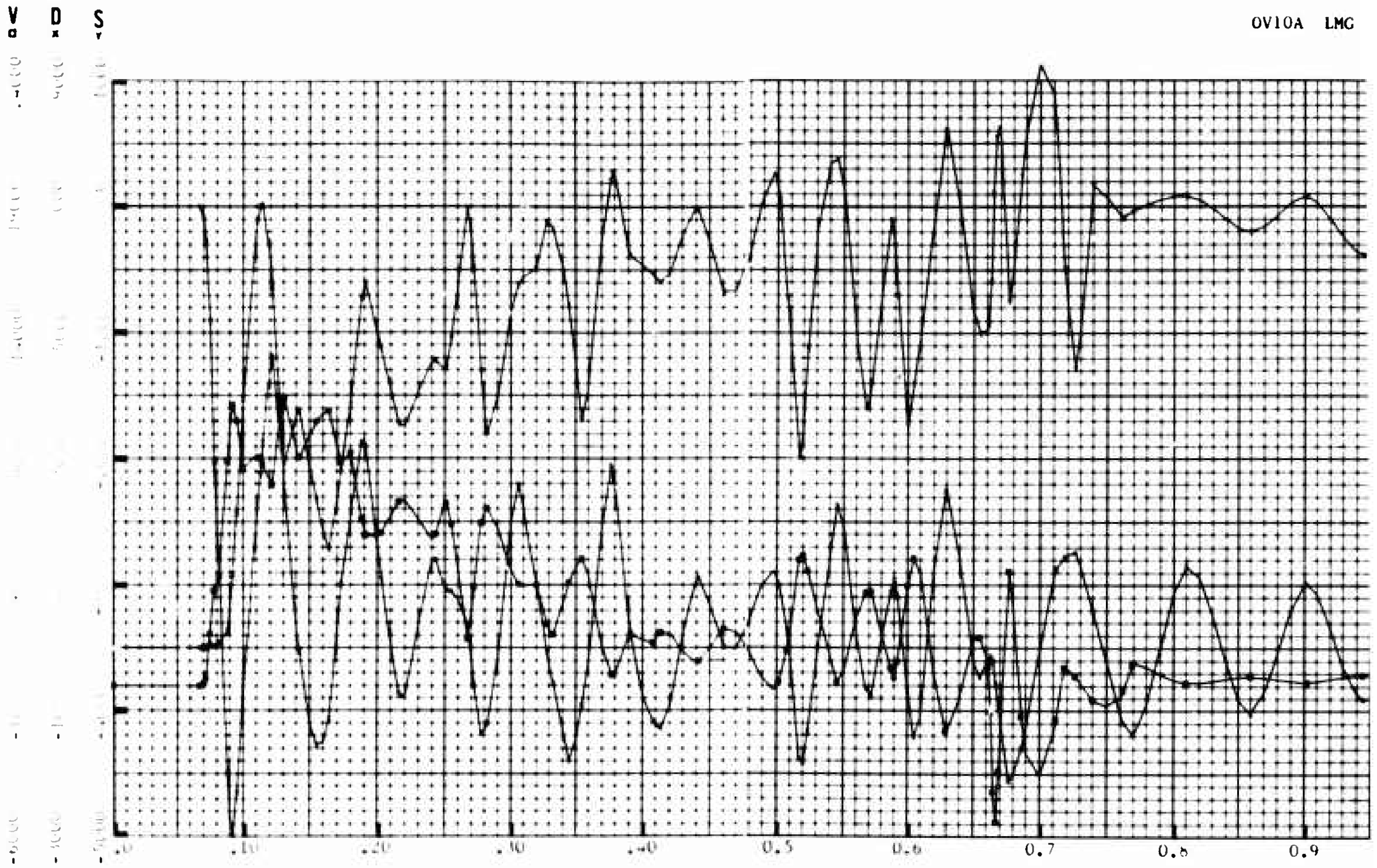

OV10A LMG LOADS, POUNDS

OLEO

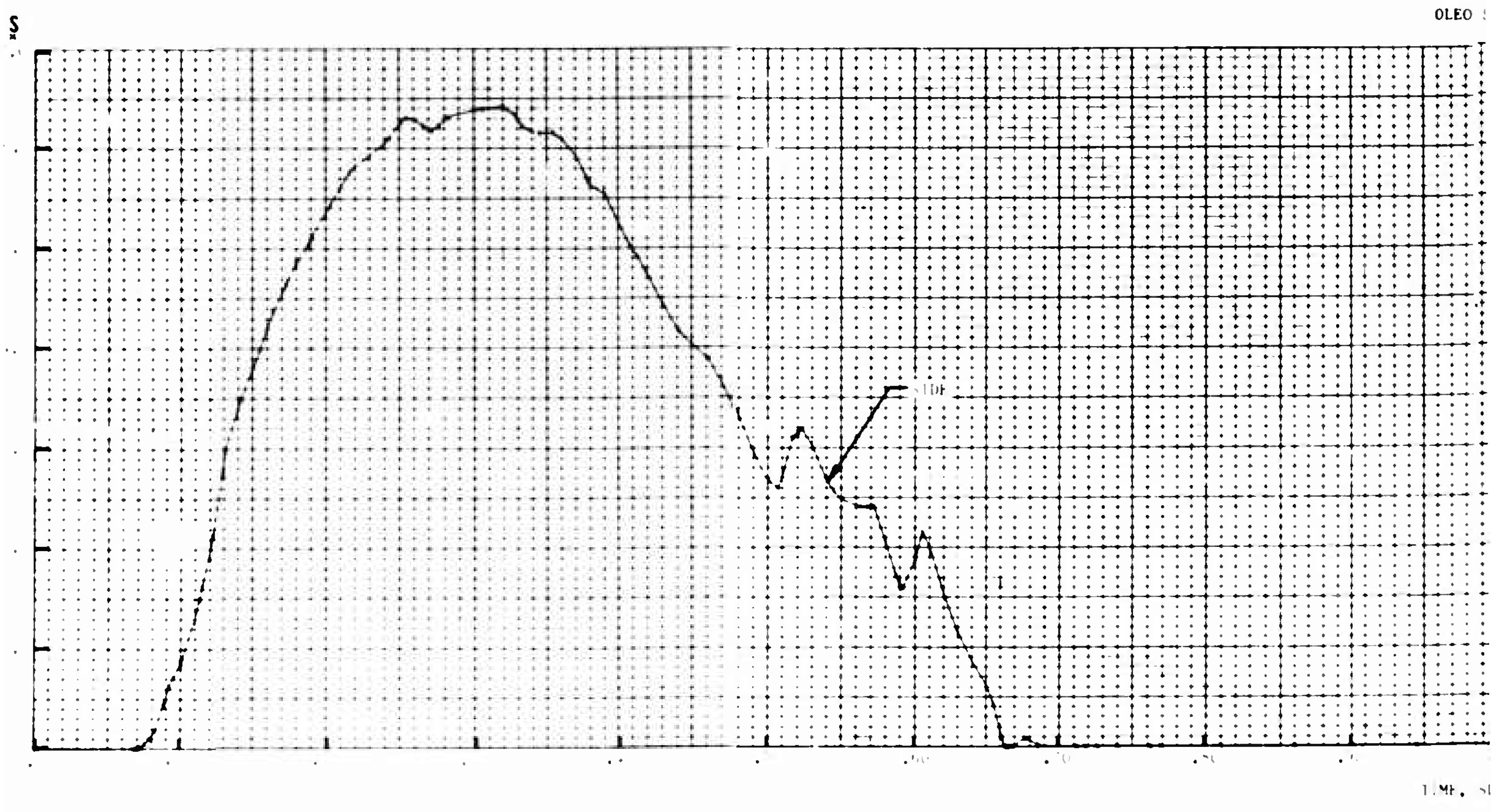

1 B

LMG LOADS, POUNDS FLIGHT NO. 225 RUN NO. 2
LOADS AT THE AXLE

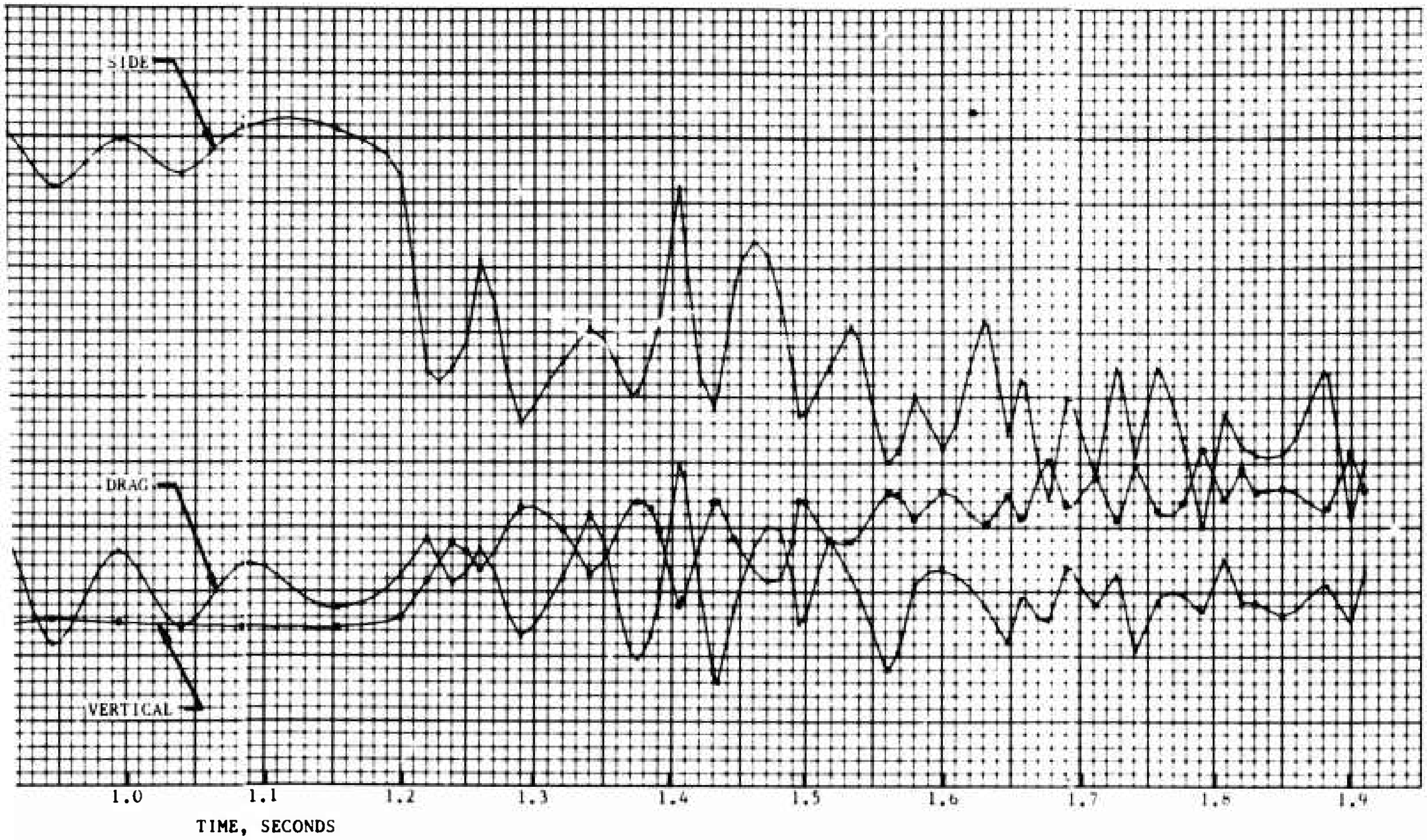

)UNDS FLIGHT NO. 225 RUN NO. 2
)LEO STROKE TIME HISTORY

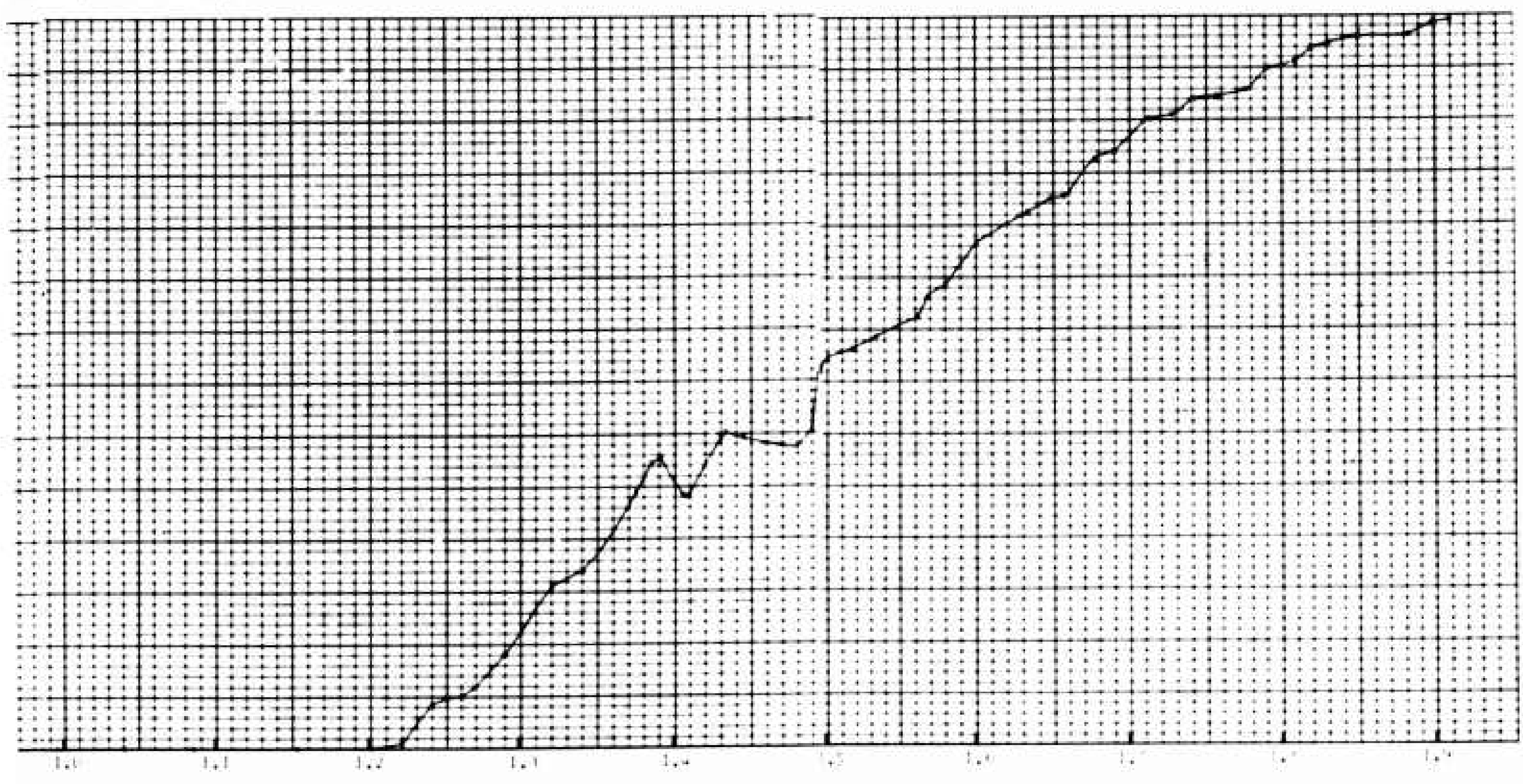

PRECEDING PAGE BLANK

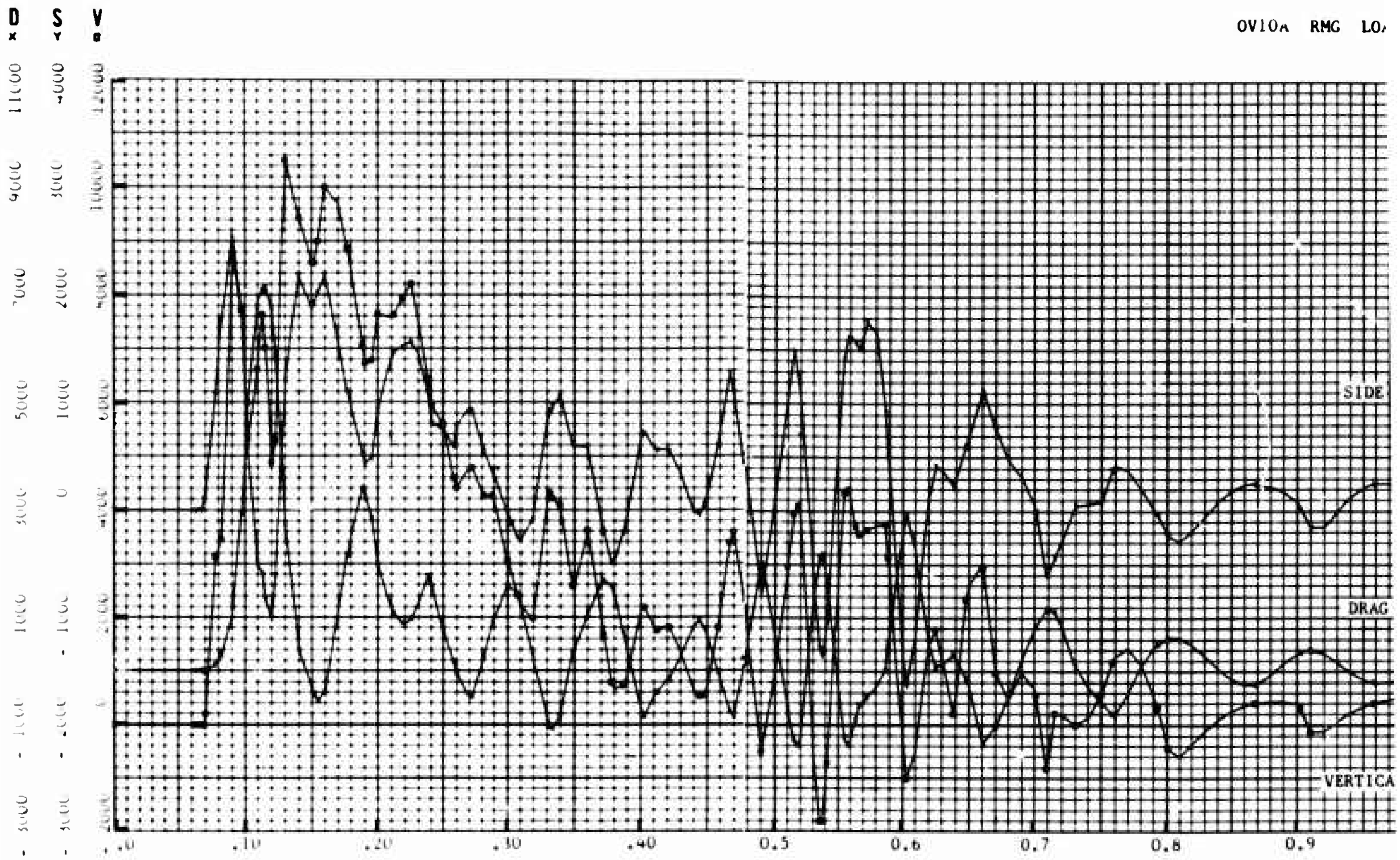

OV10A RMG LO
SIDE
DRAG
VERTICA
0.5
0.6
0.7
0.8
0.9

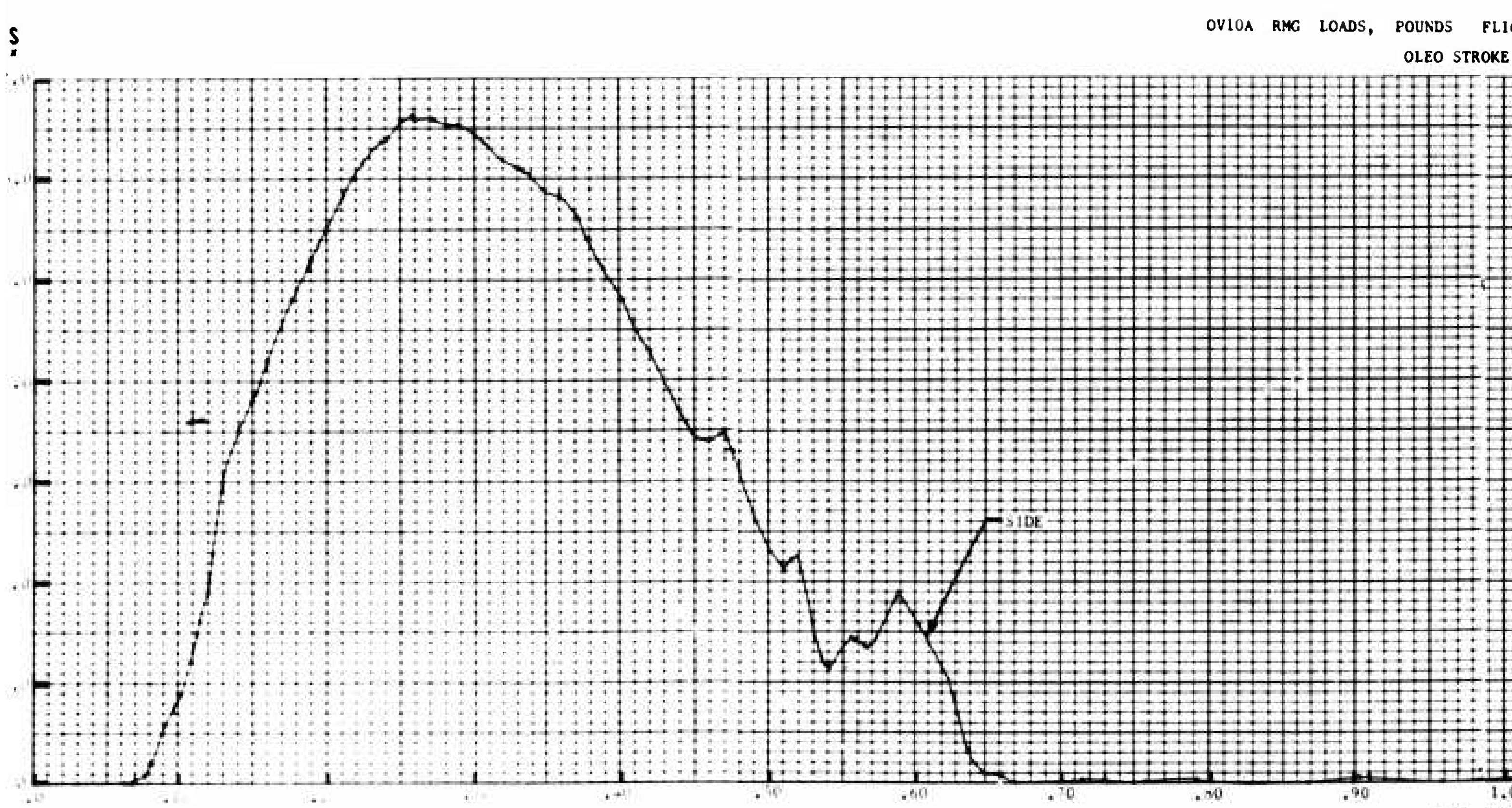

OV10A RMG LOADS, POUNDS FLIC
OLEO STROKE
SIDE
.70
.80
.90
1.0
TIME, SECC

1 B

G LOADS, POUNDS FLIGHT NO. 225 RUN NO. 2

LOADS AT THE AXLE

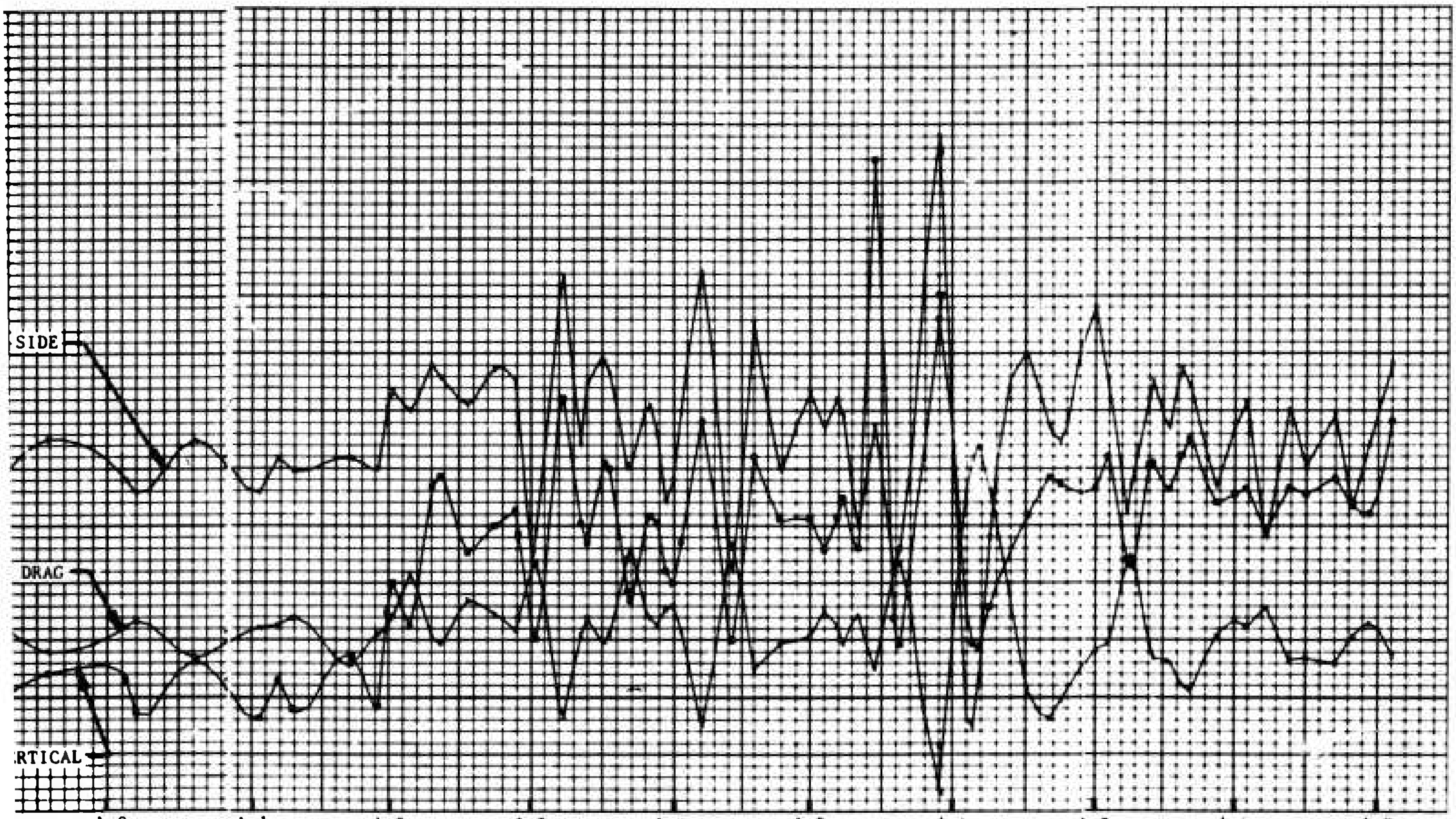

TIME, SECONDS

FLIGHT NO. 225 RUN NO. 2

STROKE TIME HISTORY

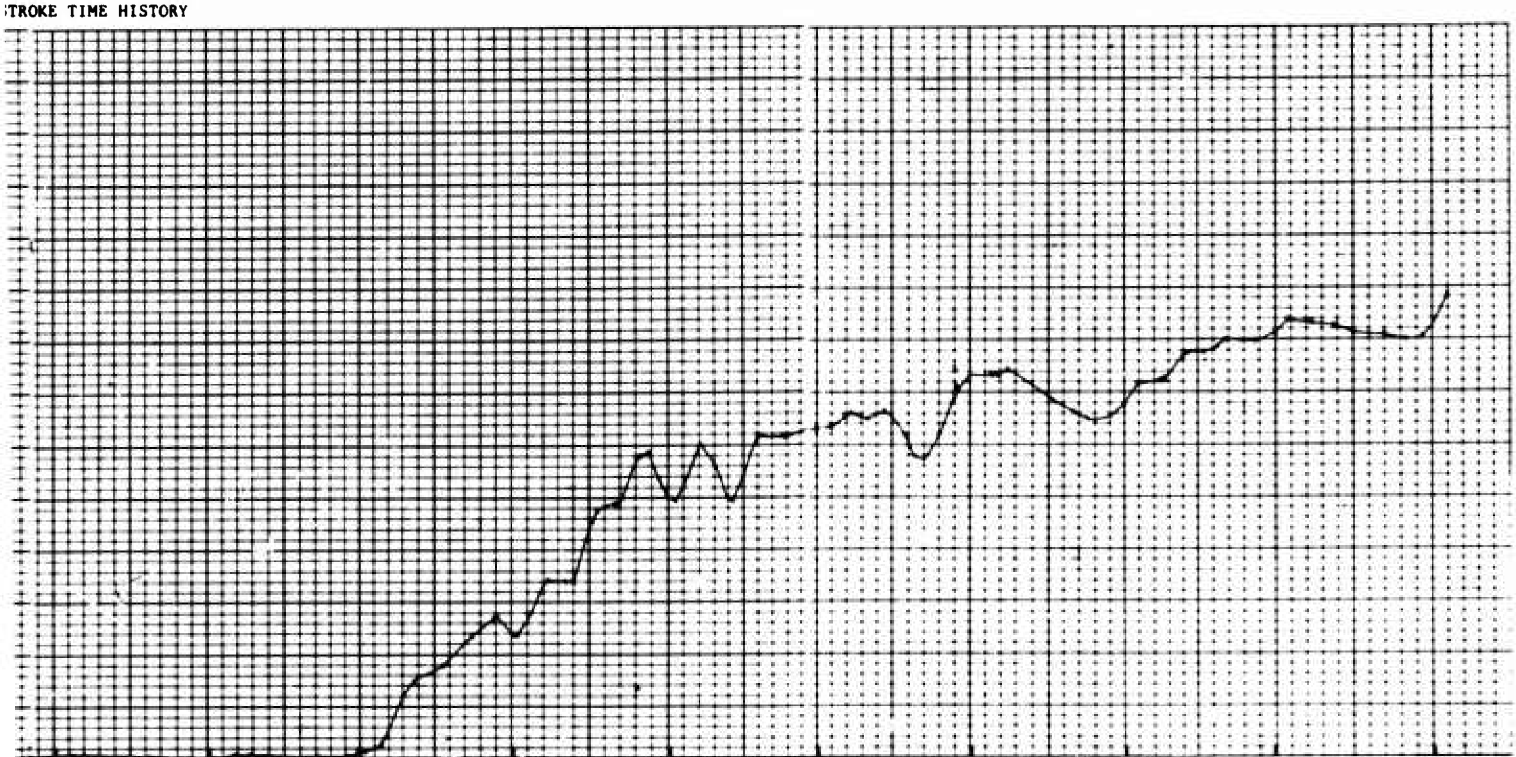

, SECONDS

PRECEDING PAGE BLANK

TIME HISTORIES OF LANDING GEAR
LOADS AND RESPONSE

OV-10A #3
FLT. #226
1 of 12

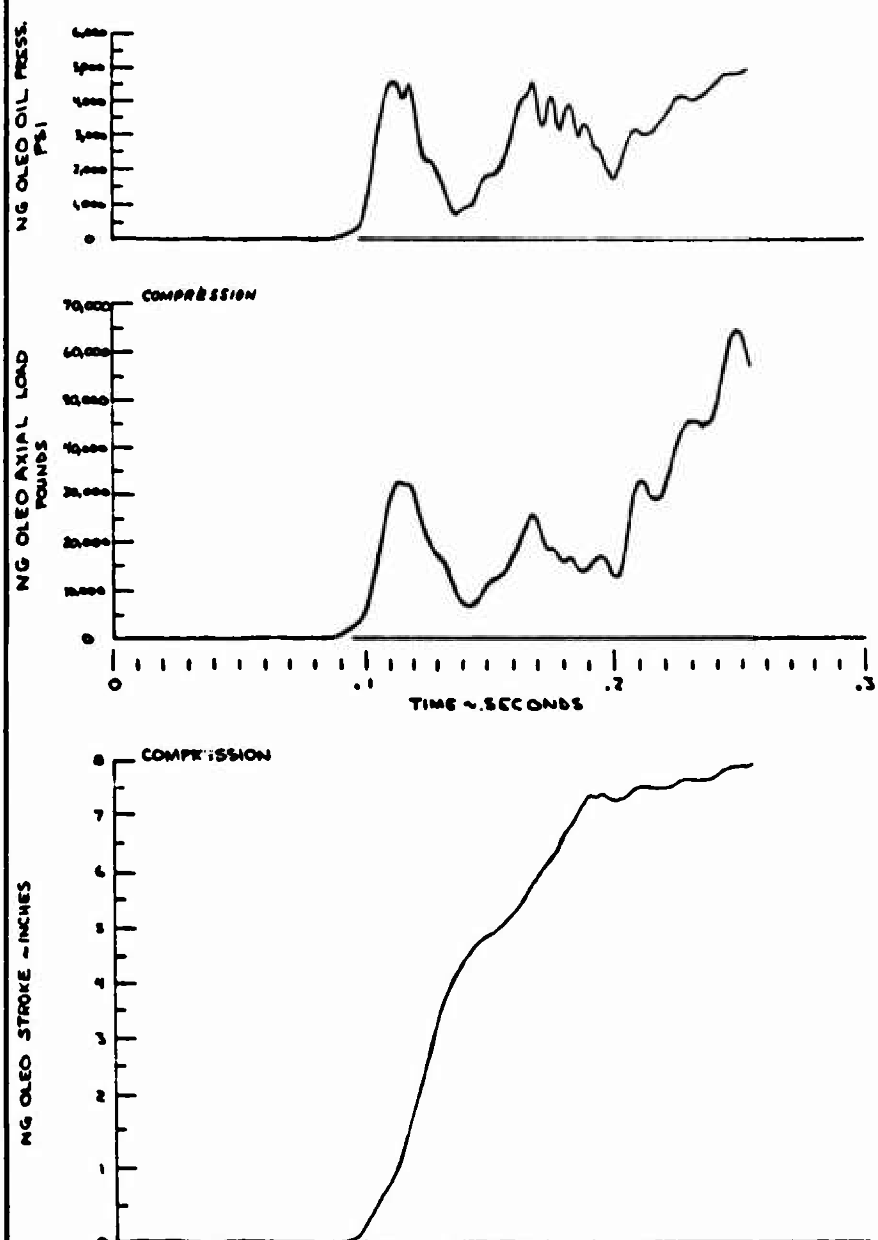

PRECEDING PAGE BLANK

TIME HISTORIES OF LANDING GEAR LOADS AND RESPONSE

OV-10A #3
FLT. #226
2 of 12

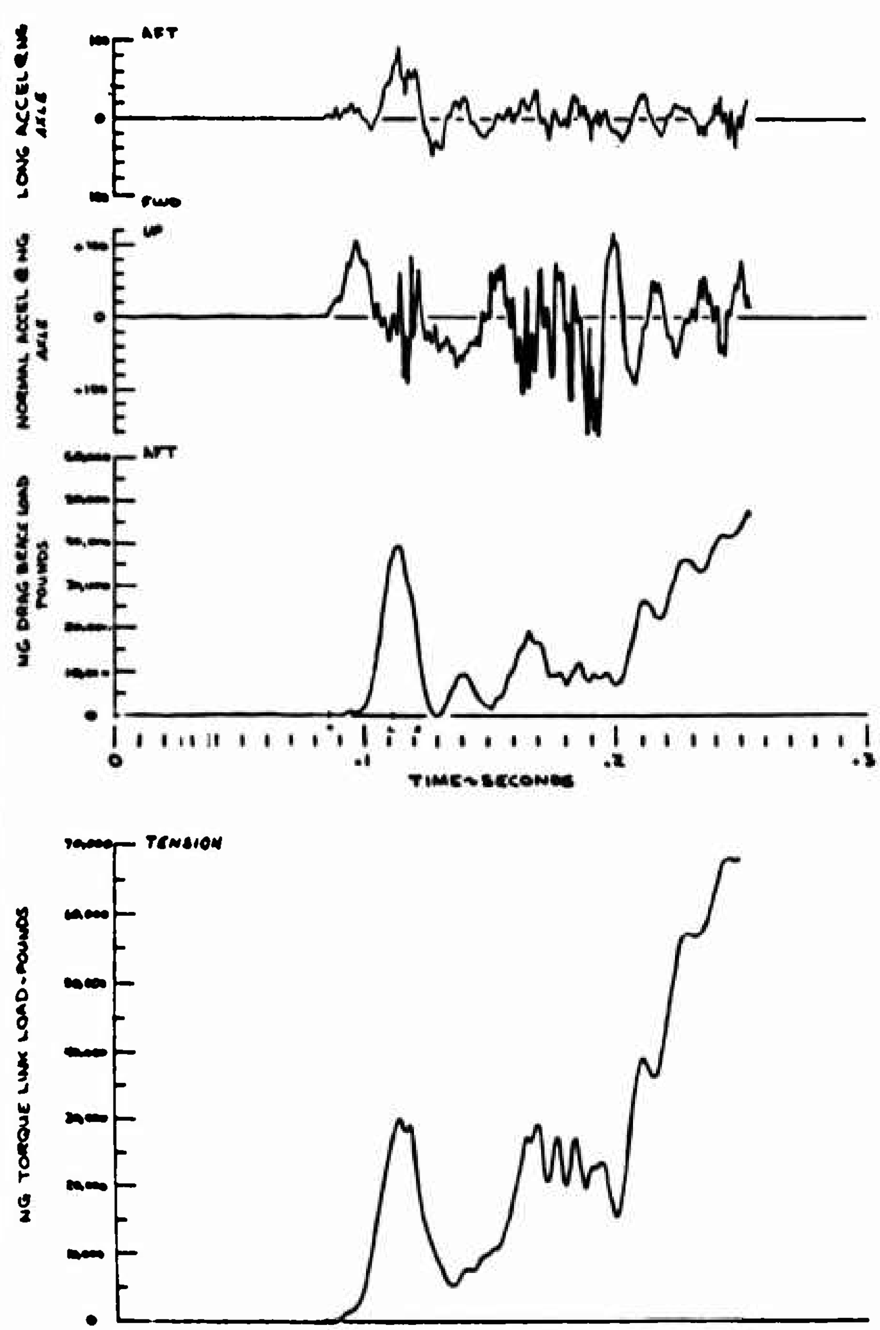

TIME HISTORIES OF LANDING GEAR
LOADS AND RESPONSE

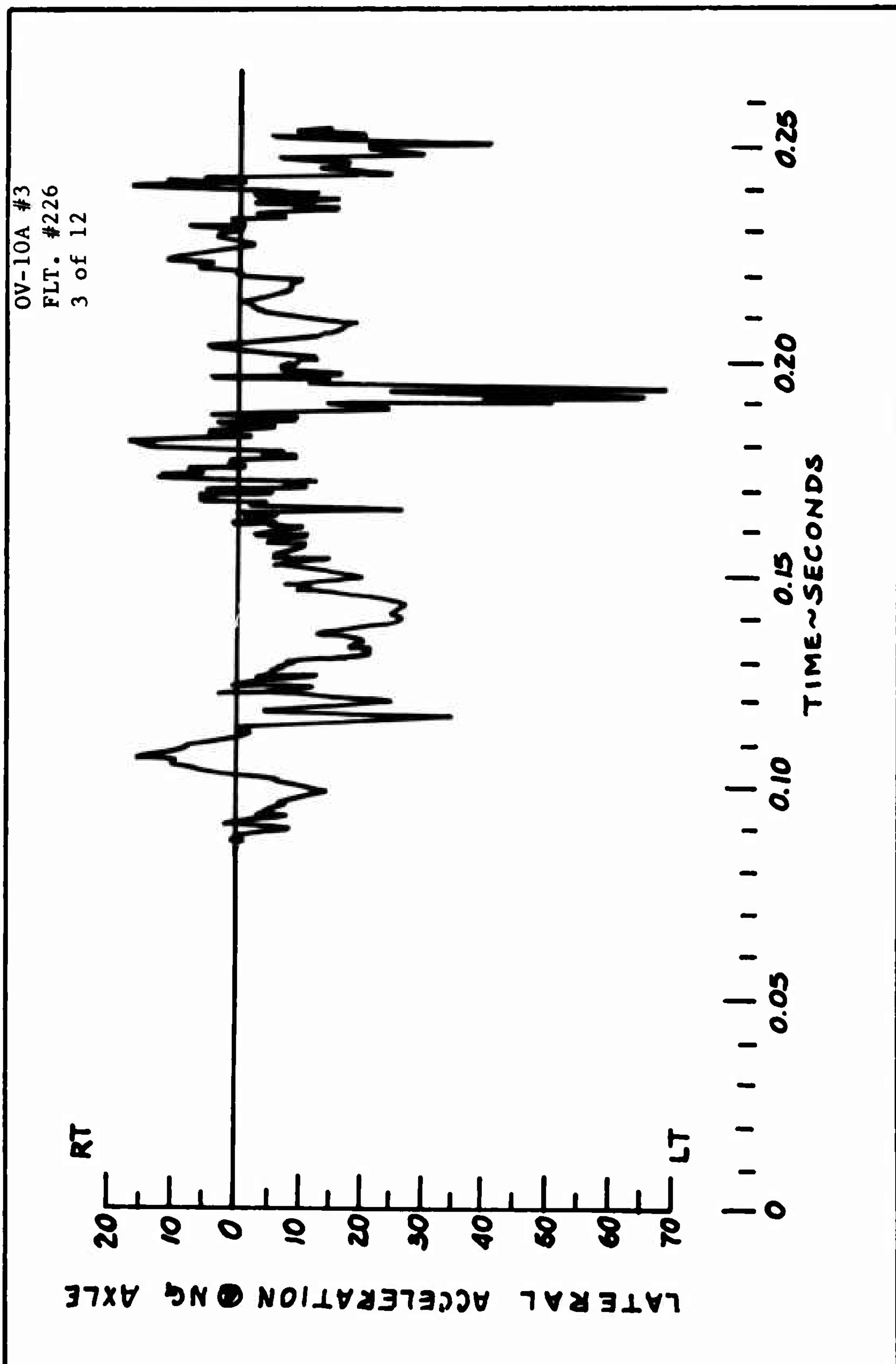

TIME HISTORIES OF LANDING GEAR
LOADS AND RESPONSE

OV-10A #3
FLT. #226
5 of 12

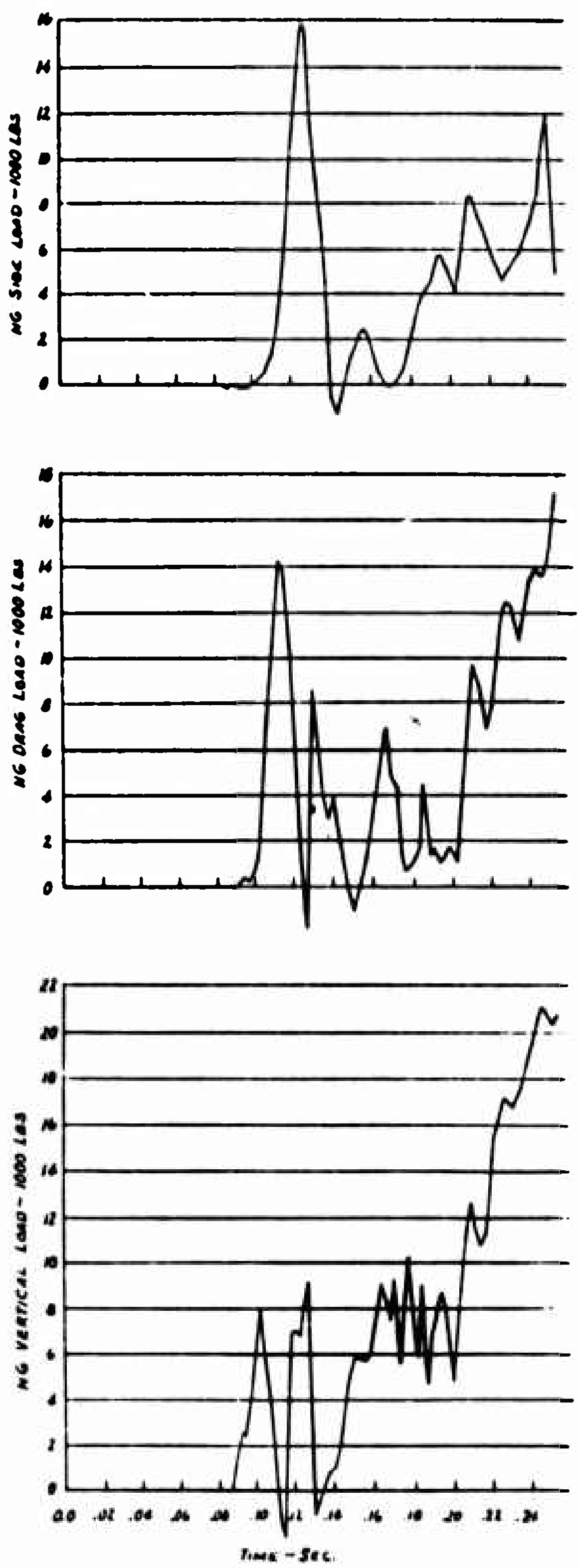

TIME HISTORIES OF LANDING GEAR
LOADS AND RESPONSE

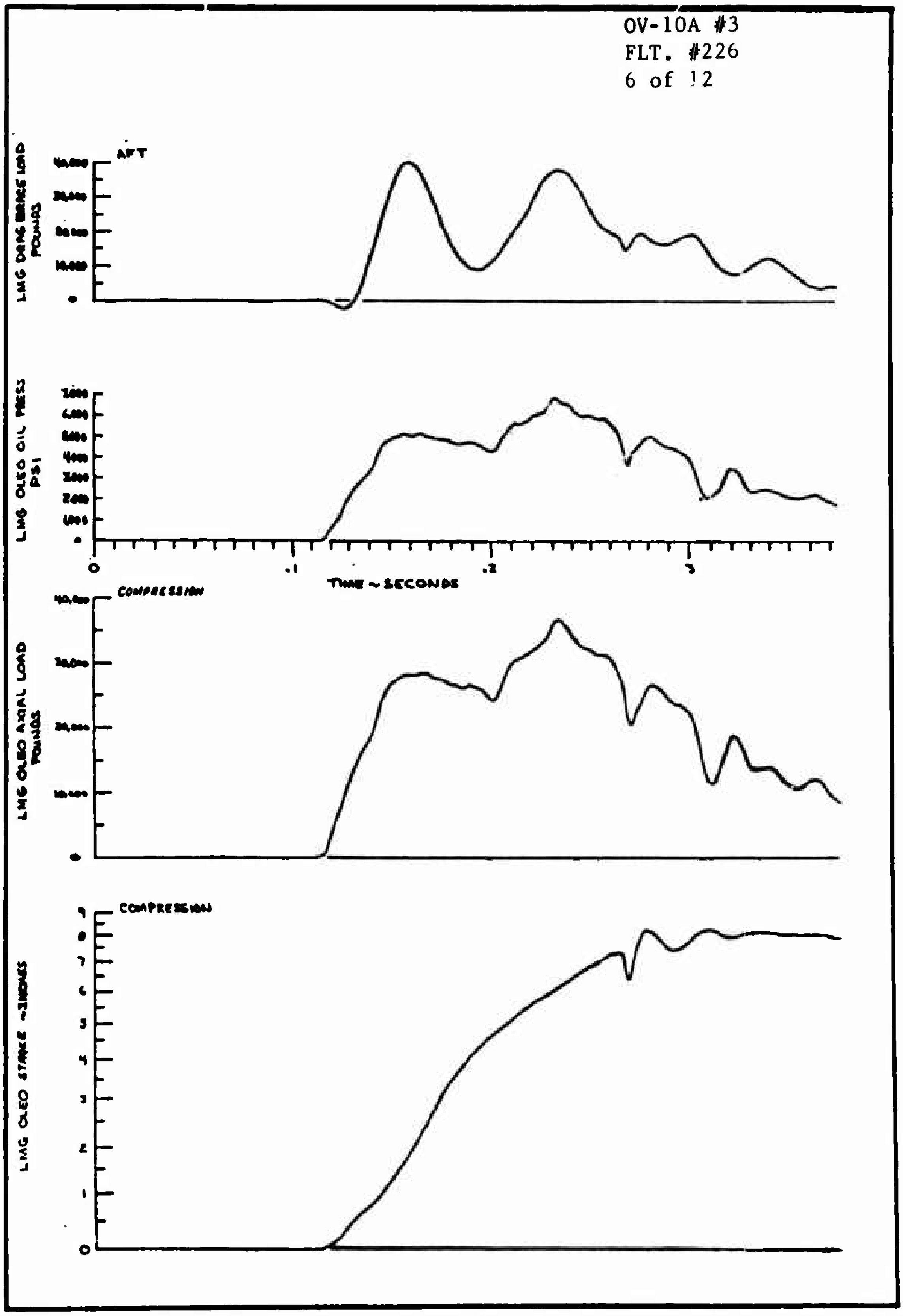

TIME HISTORIES OF LANDING GEAR
LOADS AND RESPONSE

OV-10A #3
FLT. #226
8 of 12

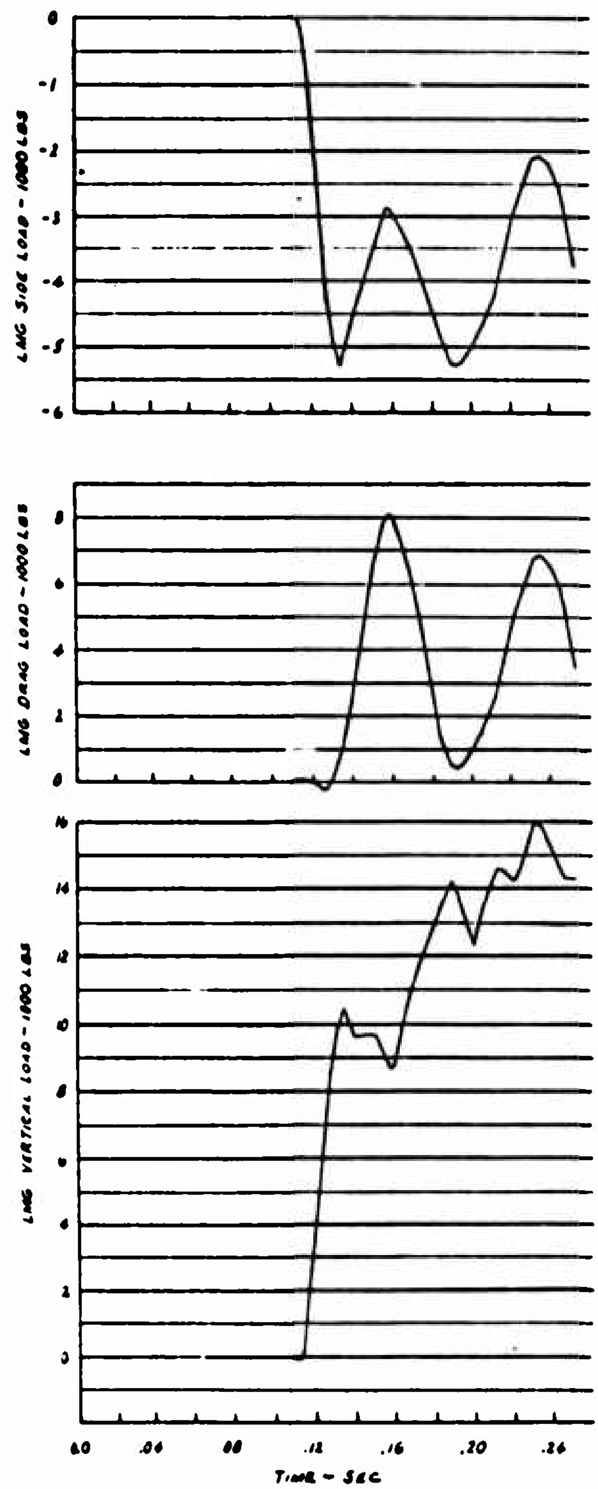

TIME HISTORIES OF LANDING GEAR
LOADS AND RESPONSE

OV-10A #3
FLT. #226
9 of 12

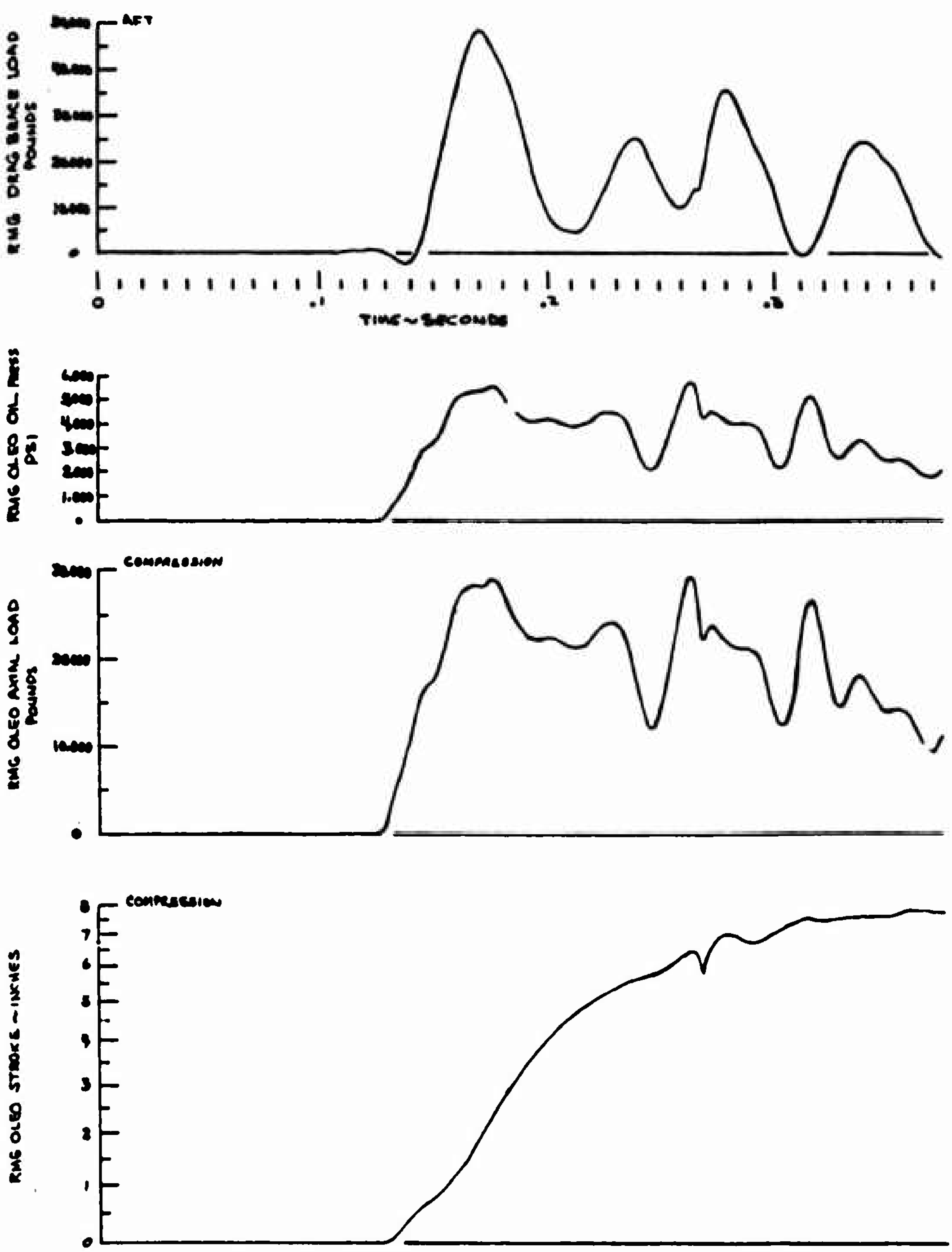

North American Aviation/Columbus
North American Rockwell

TIME HISTORIES OF LANDING GEAR
LOADS AND RESPONSE

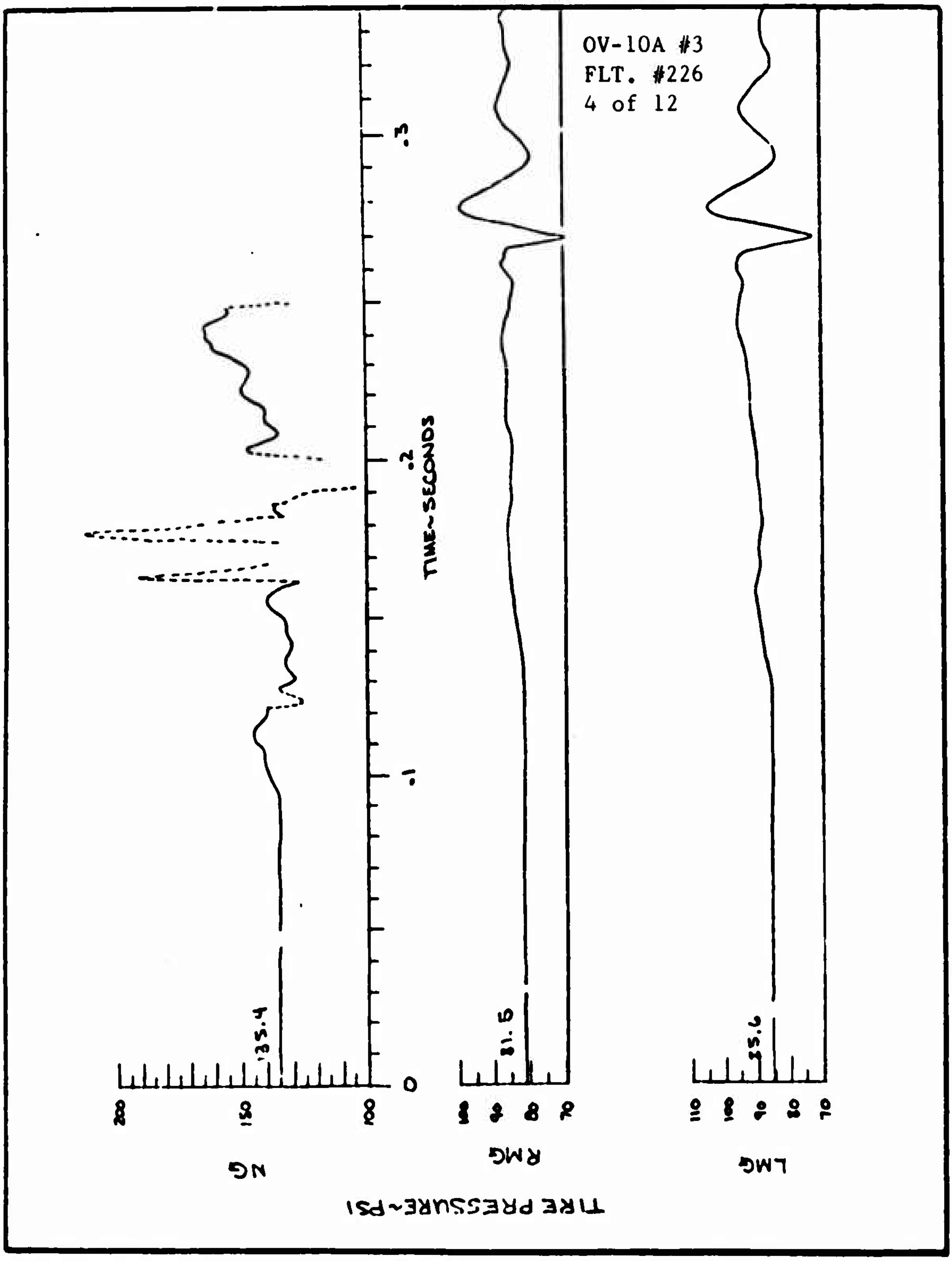

TIME HISTORIES OF LANDING GEAR LOADS AND RESPONSE

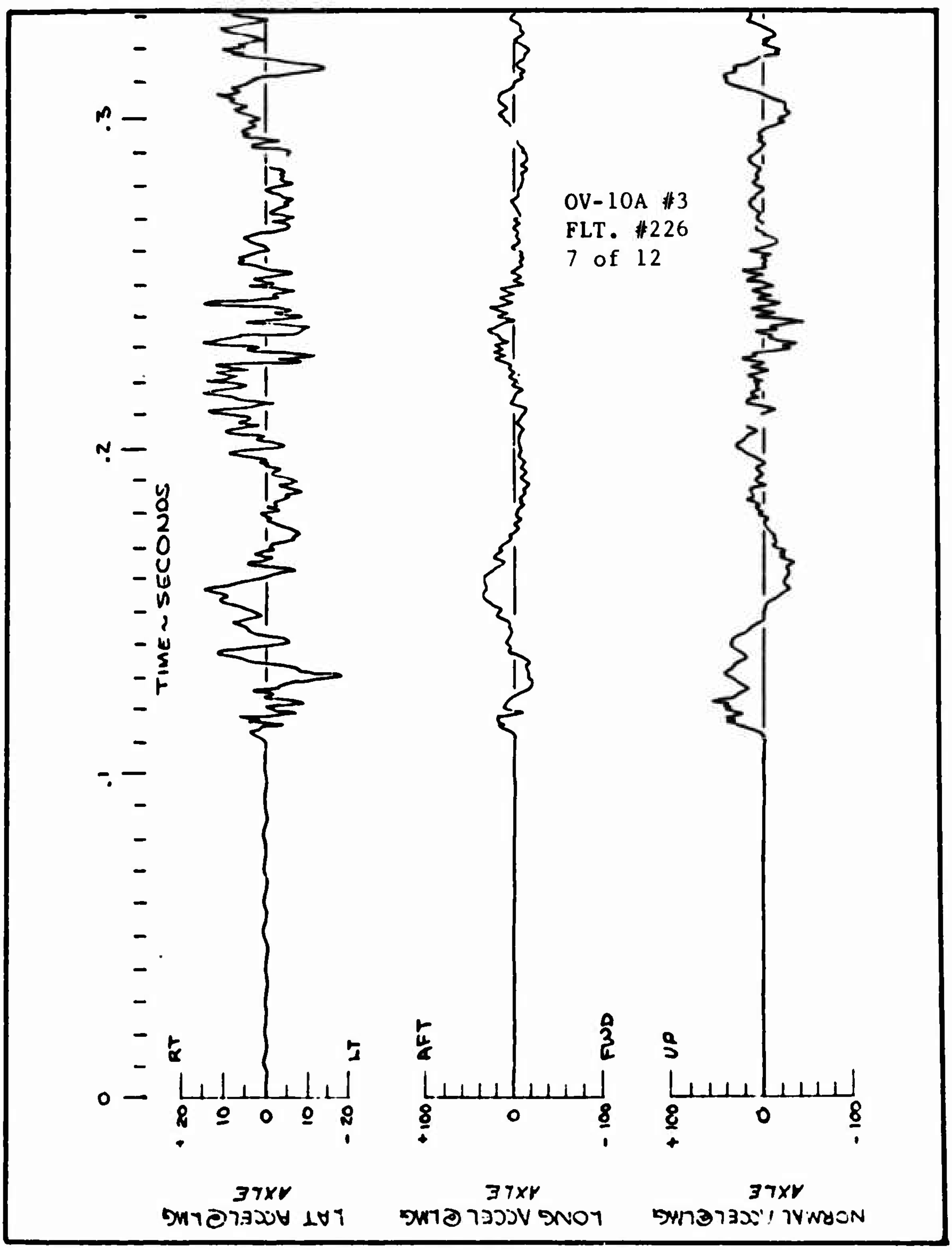

TIME HISTORIES OF LANDING GEAR
LOADS AND RESPONSE

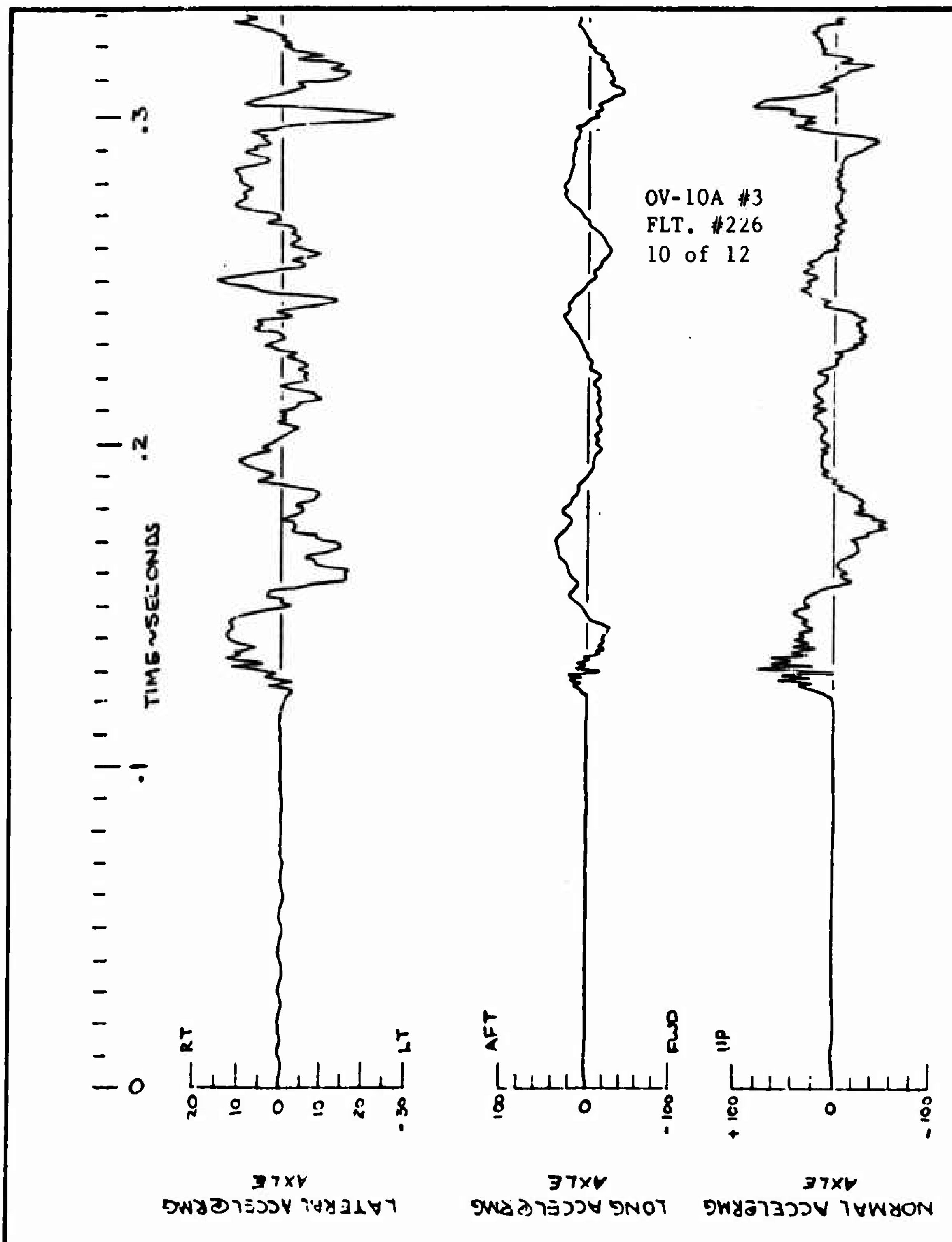

North American Aviation/Columbus
North American Rockwell

TIME HISTORIES OF LANDING GEAR
LOADS AND RESPONSE

OV-10A #3
FLT. #226
11 of 12

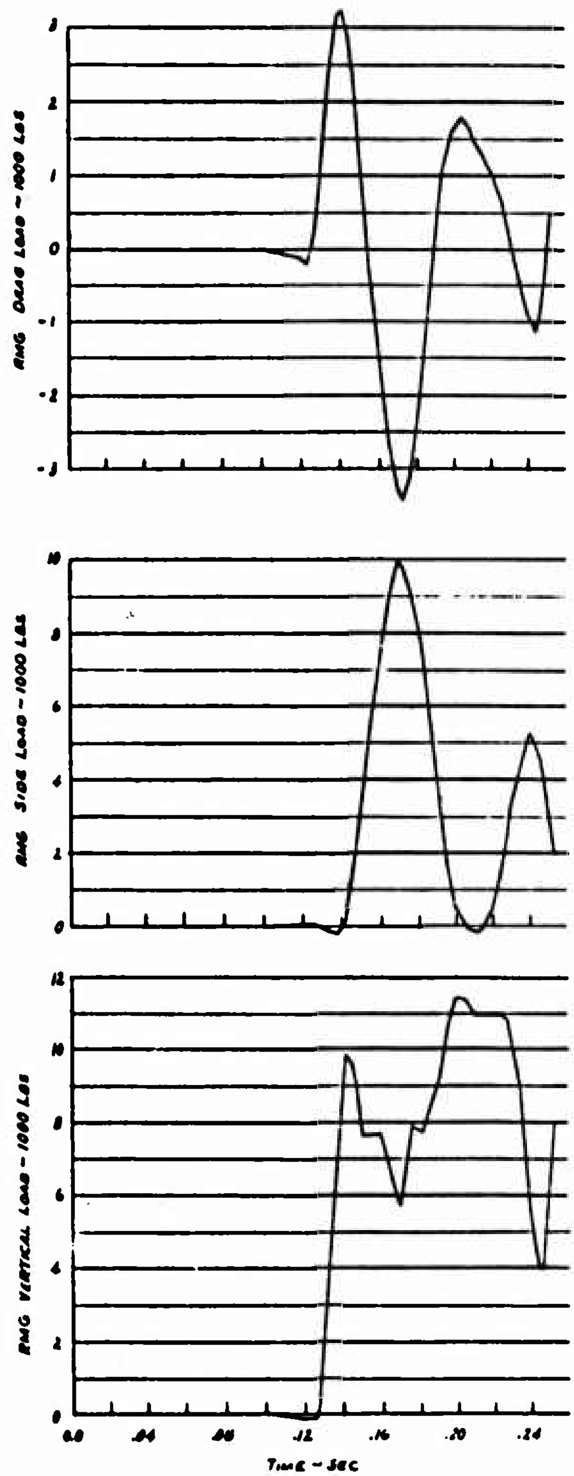

FORM 351-F REV 7-69

TIME HISTORIES OF LANDING GEAR
LOADS AND RESPONSE